

Final Report TWDB #1148301233

Hydrogeochemical Evaluation of the Texas Gulf Coast Aquifer System and Implications for Developing Groundwater Availability Models

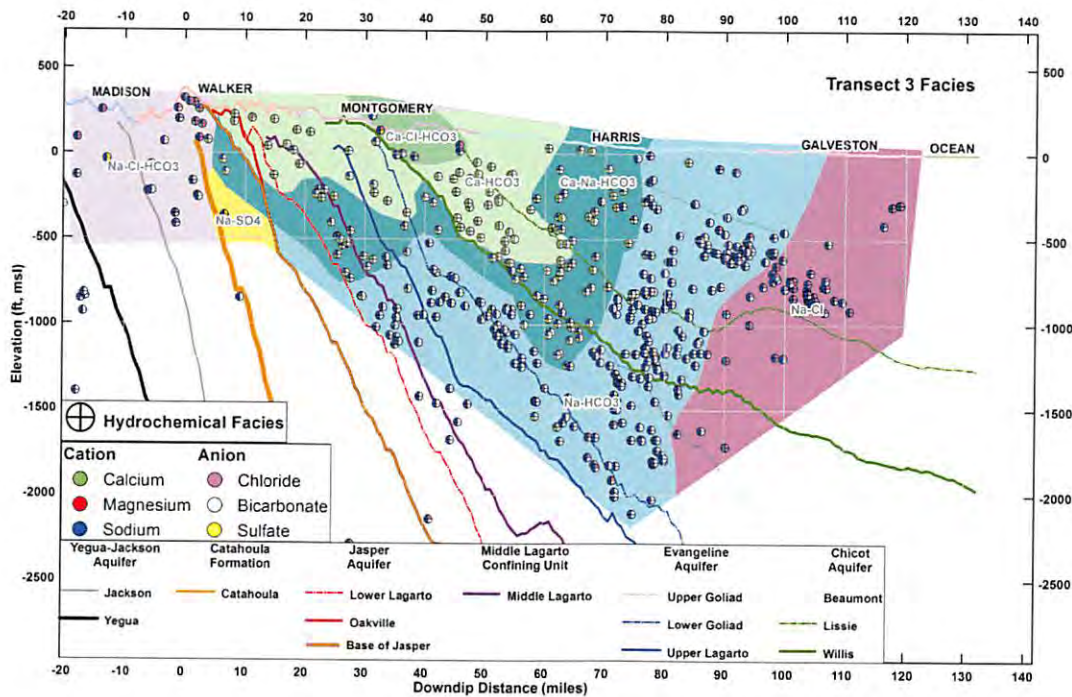
Prepared by

Steven C. Young, Ph.D., P.E., P.G.

James Pinkard

R.L. Bassett, Ph.D.

Ali H. Chowdhury, Ph.D., P.G.



Prepared for:

Texas Water Development Board

P.O. Box 13231, Capitol Station

Austin, Texas 78711-3231

Texas Water
Development Board

2014 APR - 7 AM 9:16

April 2014

ADMINISTRATIVE

Final Hydrogeochemical Evaluation of the Texas Gulf Coast Aquifer System and Implications for Developing Groundwater Availability Models

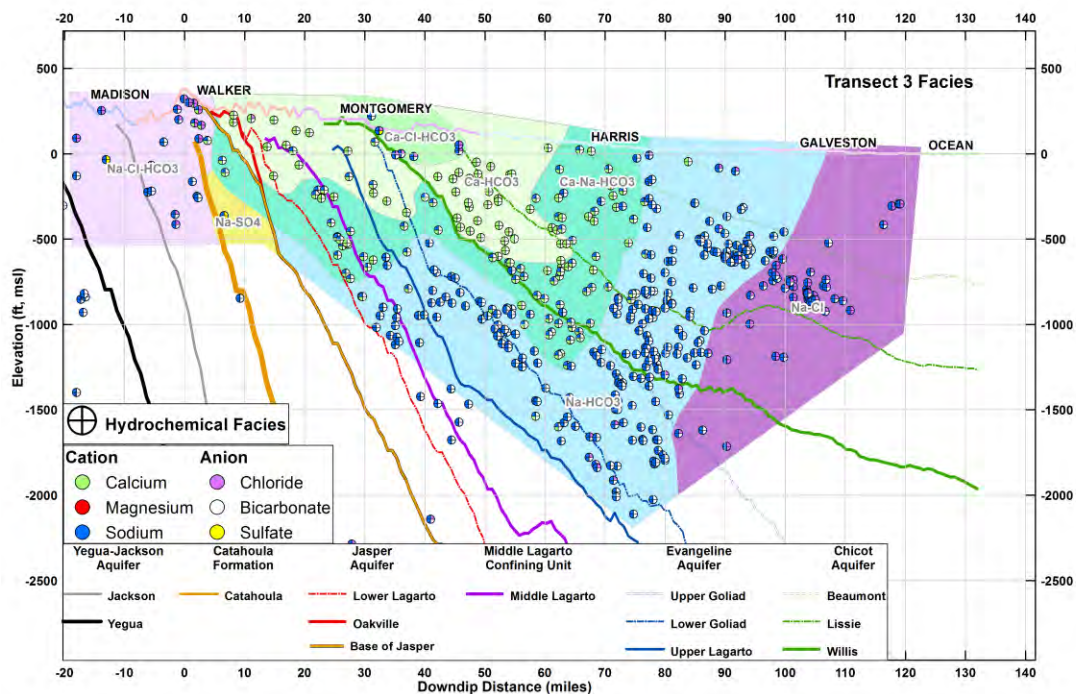
Prepared by

Steven C. Young, Ph.D., P.E., P.G.

James Pinkard

R.L. Bassett, Ph.D.

Ali H. Chowdhury, Ph.D., P.G.



Prepared for:

Texas Water Development Board

P.O. Box 13231, Capitol Station
Austin, Texas 78711-3231



April 2014



Texas Water Development Board

**Final
Hydrogeochemical Evaluation of the
Texas Gulf Coast Aquifer System and
Implications for Developing
Groundwater Availability Models**

**Steven C. Young, Ph.D., P.E., P.G.
James Pinkard
INTERA Incorporated**

**R.L. Bassett, Ph.D.
Tetra Tech**

Ali H. Chowdhury, Ph.D., P.G.

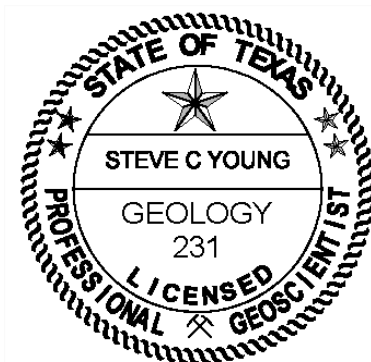
April 2014

This page intentionally blank.

Geoscientist Seal

This report documents the work of the following Licensed Texas Geoscientists.

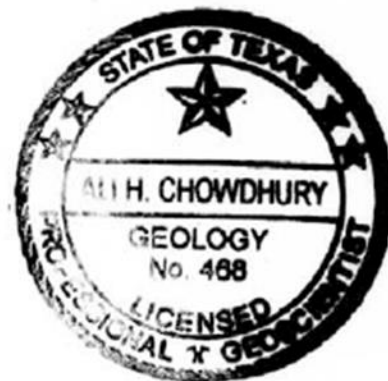
Dr. Young was the Project Manager for the work and was responsible for oversight on the project, for selecting the wells for sampling, the writing of the report, the flow modeling, and the final interpretation of all data. Dr. Young was the principal author of all sections of the report except for the discussion of the NETPATH simulation and the potential sources of groundwater salinity. The NETPATH simulations were set up, performed, and documented by Dr. Randy Bassett. The majority of the figures were generated by Mr. James Pinkard.




The seal appearing on this document was authorized on December 30, 2013 by :

Steven C. Young, P.G. 

Dr. Chowdhury worked on the project from September 2012 to February 2013. He was the principal author of the report section discussing the potential sources of groundwater salinity and contributed to the writing of report sections 6 and 7. Dr. Chowdhury also assisted with the analysis and interpretation of the stable isotope and carbon 14 data.



The seal appearing on this document was authorized on December 30, 2013 by:

Ali H. Chowdhury, P.G. 

This page intentionally left blank.

Acknowledgements

Considerable effort was required to identify prospective wells and secure permission to sample the wells. Through the project, we were well supported by groundwater conservation districts. In GMA 14, Ms. Kathy Jones from the Lone Star GCD, Mr. Tom Michel from the Houston-Galveston Subsidence District, and Mr. Zach Holland from the Bluebonnet GCD helped support our groundwater sampling efforts. In GMA 15, Mr. Tim Andruss from the Texana GCD helped with our sampling efforts. In GMA 16, Mr. Felix Saenz from Brush County GCD, Mr. Andy Garza from Kenedy County GCD, and Mr. Alberto Garcia from Duval County GCD helped with our samplings efforts. In addition to assistance from GCDs, we also received assistance from Mr. Mike Turco from the U.S. Geological Survey in Houston, TX; Mr. Robert Schmidt from the U.S. Department of Agriculture in Kleberg, TX; and Janie Hopkins from the TWDB in Austin, TX.

All groundwater sampling was performed by Michael Johnson with Baer Engineering and Environmental Consulting, Inc.. Michael often worked long hours to collect, document, package, and send samples each day in the field. In addition, the authors appreciate support from the Lone Star Groundwater District who provided financial assistance with the sampling and analysis of groundwater samples in the Catahoula and Jasper wells in Transect 3.

Final – Hydrogeochemical Evaluation of the Texas Gulf Coast Aquifer System and
Implications for Developing Groundwater Availability Models

This page intentionally left blank.

Table of Contents

Acronyms and Abbreviations	xxiii
Executive Summary	xxv
1.0 Introduction	1-1
1.1 The Texas Gulf Coast Aquifer System and the Brazos Alluvium Aquifer	1-2
1.1.1 Stratigraphy of the Gulf Coast Aquifer System	1-2
1.1.2 Stratigraphy of the Yegua-Jackson Aquifer	1-4
1.1.3 The Brazos River Alluvium Aquifer	1-5
1.2 Groundwater Availability Models	1-6
1.3 Technical Approach	1-7
2.0 Gulf Coast Aquifer System	2-1
2.1 Depositional History	2-2
2.2 Faults	2-4
2.3 Sea-Level History	2-6
2.4 Meteoric and Formation Waters	2-7
2.5 HydroPressured and Geopressed Zones	2-8
2.6 Paleohydrology	2-9
2.7 Salt Domes	2-11
3.0 Groundwater Models for GMA 14, GMA 15, and GMA 16	3-1
3.1 Conceptual Groundwater Model of the Gulf Coast Aquifer System	3-1
3.2 Simulated Groundwater Fluxes For Predevelopment Conditions	3-7
3.2.1 Estimated Groundwater Age	3-7
3.2.2 Components of Groundwater Flow	3-10
4.0 Geochemical Data	4-1
4.1 Database	4-1
4.2 Well Data for Transects 3, 5, and 8	4-4
5.0 Potential Sources of Groundwater Salinity	5-1
5.1 Groundwater Salinity	5-1
5.2 Sea Salt Spray	5-2
5.3 Saltwater Intrusion	5-2
5.4 Connate Water and the Effects of Pumping	5-4
5.5 Formation Brine Upwelling from Geopressed Zone	5-5
5.6 Bedded Halite and Evaporites	5-7
5.7 Salt Domes	5-7
5.8 Agriculture and Irrigation	5-9
5.9 Oil and Gas Activities	5-10
6.0 Cations and Anions	6-1
6.1 Overview of Geochemical Reactions	6-1
6.1.1 Redox Reactions	6-2

Table of Contents, continued

6.1.2	Dissolution-Precipitation Reactions	6-3
6.1.3	Ion Exchange Reactions	6-4
6.1.4	Chemical Evolution of Groundwater	6-6
6.2	Geochemistry Characterization	6-9
6.2.1	Ocean Water	6-9
6.2.2	Formation Water (Brines)	6-10
6.2.3	Groundwater Characterization.....	6-12
6.3	Regional Groundwater Flow and Geochemistry	6-13
6.3.1	Evidence for Salt Domes Contributing to Evaluated TDS Concentrations.....	6-20
6.3.2	Evidence for Geopressure Zones Contributing to Elevated TDS Concentrations.....	6-21
6.3.3	Evidence for Significant Difference in Recharge Rates between the Outcrops for the Jackson and the Catahoula Outcrops.....	6-23
6.3.4	Evidence for Recharge Occurring Across most of the Gulf Coast.....	6-24
6.4	Hydrochemical Facies and Concentration Contours Along Transects	6-25
6.4.1	Factors Affecting the Interpretation of Transect Data.....	6-25
6.4.1.1	Spatial Variability	6-26
6.4.1.2	Temporal Variability.....	6-26
6.4.1.3	Sampling Bias	6-27
6.4.2	Transect Data.....	6-27
6.4.2.1	GMA 14	6-30
6.4.2.2	GMA 15	6-33
6.4.2.3	GMA 16	6-35
6.4.3	Implication of the Transect Data to Mixing, Flow Paths, and Age from the Transect Data	6-36
6.5	Brazos River Alluvium	6-38
7.0	Stable Isotopes.....	7-1
7.1	Basic Concepts and Definitions.....	7-1
7.2	$\delta^2\text{H}$ and $\delta^{18}\text{O}$ in Precipitation	7-2
7.3	$\delta^2\text{H}$ and $\delta^{18}\text{O}$ in Groundwater.....	7-4
7.3.1	Measured Values of $\delta^2\text{H}$ and $\delta^{18}\text{O}$ in the Texas Gulf Coast	7-6
7.3.2	Evidence for Mixing, Flow Paths, and/or Age.....	7-8
7.4	$\delta^2\text{H}$ and $\delta^{13}\text{C}$ in Methane	7-8
7.4.1	Transect 3 (GMA 14)	7-10
7.4.2	Transect 5 (GMA 15)	7-10
7.4.3	Transect 8 (GMA 16)	7-11
7.4.4	Evidence for Mixing, Flow Paths, and Age	7-11
8.0	Carbon 14	8-1
8.1	Estimating Groundwater Age from ^{14}C	8-1
8.1.1	Half-life Calculation Approach Using Uncorrected ^{14}C	8-1
8.1.1.1	Consideration for “Dead” Carbon.....	8-2

Table of Contents, continued

8.1.1.2	Consideration for Mixing.....	8-4
8.1.2	NETPATH Mass Balance Approach.....	8-5
8.1.3	Pearson Correction Approach	8-10
8.2	¹⁴ C Ages Based on NETPATH Mass Balance Approach.....	8-12
8.2.1	Transect 3 in GMA 14.....	8-12
8.2.1.1	Chicot Aquifer Segment	8-15
8.2.1.2	Jasper/Lagarto Flow Segment.....	8-18
8.2.1.3	Sulfur and Chlorine Isotopes	8-18
8.2.1.4	Application of the Pearson Correction for ¹⁴ C Age Estimates.....	8-21
8.2.2	Transect 5 in GMA 15.....	8-21
8.2.2.1	Shallow Wells with NETPATH Solution.....	8-23
8.2.2.2	Shallow Wells with No NETPATH Solution	8-25
8.2.2.3	Sulfur Isotope.....	8-26
8.2.2.4	Region of Groundwater with Measured and Pearson Corrected Old ¹⁴ C Dates	8-26
8.2.3	Transect 8 in GMA 16.....	8-27
8.2.3.1	Well Cluster in Webb County.....	8-29
8.2.3.2	Wells 8-4 and 8-9.....	8-32
8.2.3.3	Region of Elevated TDS in the Evangeline Aquifer.....	8-33
8.2.3.4	Upper Evangeline Flow	8-34
8.2.3.5	Sulfur Isotopes	8-36
8.3	¹⁴ C Ages Based on Pearson Method.....	8-37
8.3.1	Factors affecting the Relationship between Groundwater Ages with Depth.....	8-37
8.3.2	Relationship between Measured and Predicted Groundwater Age and Geological Unit.....	8-39
8.4	Evidence for Groundwater Mixing, Flow Paths, and Age.....	8-41
9.0	Summary	9-1
9.1	Review of the Gulf Coast Aquifer System and Key Findings.....	9-1
9.2	Implications for the Conceptual Flow Model.....	9-5
9.3	Considerations for Implementing the Conceptual Model in a Numerical Model.....	9-10
10.0	Recommendation.....	10-1
10.1	Water Quality Investigations in the Gulf Coast.....	10-1
10.2	Groundwater Availability Program Guidelines	10-2
10.3	Development of Management Groundwater Models for the Gulf Coast	10-3
11.0	References.....	11-1
Appendix A	Analytical Results from San Antonio Testing	
Appendix B	Analytical Results from Beta Analytic Inc.	
Appendix C	Analytical Results from ZymaX Forensics Isotope	

Table of Contents, continued

Appendix D	Analytical Results from University of Arizona
Appendix E	Analytical Results from Ana-Lab Corp.
Appendix F	Well Sampling and Analysis Plan For GMA 14, 15, and 16 Geochemical Evaluation
Appendix G	TWDB Comments on Draft Report and Response to Comments

List of Figures

Figure 1	Map of the Texas Gulf Coast showing the outcrops of the Yegua-Jackson Aquifer, the Gulf Coast Aquifer System and the Brazos Alluvium Aquifer.....	xxxii
Figure 1-1	Map of the Texas Gulf Coast showing the outcrops of the Yegua-Jackson Aquifer, the Gulf Coast Aquifer System and the Brazos Alluvium Aquifer.....	1-11
Figure 1-2	Model Domains of the groundwater models used for joint planning in GMAs 14, 15, and 16 and the LCRA-SAWS Water Project.....	1-12
Figure 1-3	Location of the nineteen transects used to develop vertical cross-sections of geochemistry and the major rivers of Texas.....	1-13
Figure 2-1	Chronostratigraphic chart, Eustatic sea level, lithostratigraphic, and hydrostratigraphic chart of the Miocene to Holocene depositional episodes.....	2-13
Figure 2-2	Positions of principal fluvial-deltaic depocenters and interdeltic shorelines for selected depositional episodes, northwest Gulf of Mexico. Modified from Galloway (1989) and Galloway and others (2000).....	2-14
Figure 2-3	Geologic cross-sections through Transects 1 and 8. (Note: surfaces represent the bottom of each geological formation).	2-15
Figure 2-4	Lineation map of the Texas coastal zone in the Houston Embayment area. Lineations are the surface expressions of faults or fractures (Kreitler, 1976). The entire Texas coastal plain is covered by lineations, although only the more coastward lineations are mapped here. Modified from Fisher and others (1972, 1973) and McGowen and others (1976a,b).....	2-16
Figure 2-5	Schematic of a cross-section along the central part of the Texas Gulf Coast and northern Gulf of Mexico basin showing depositional and structural styles exhibited by fluvial deltas (from Bruce, 1973 and Solis, 1981). Deposition of coarse-grain deposits is shown by the triangular wedges along the down-dip face of the fault.....	2-16
Figure 2-6	Map showing major growth fault zones and shallow salt domes in the onshore part of the Texas coastal zone. (Fault locations from Ewing, 1990).	2-17
Figure 2-7	Cross-section showing hydrochemical facies of an aquifer and depth to base of fresh water. Cross-section through eastern Liberty, Harris, and Galveston counties (from Kreitler and others, 1977).....	2-18
Figure 2-8	A 7-point floating average curve to predict sea-level change during the last 20,000 years fitted to Gulf of Mexico radiodated shoreline markers by Balsillie and Donoghue (2004).	2-18
Figure 2-9	Estimated shoreline along the Texas Gulf Coast during the last 20,000 years based on historical sea-level data from Balsillie and Donoghue (2004) with topographic and bathymetry elevations measured relative to current sea level.	2-19

List of Figures, continued

Figure 2-10 General pattern of fluid pressures for Gulf of Mexico basin sediments from Sharp and others, 1988. 2-20

Figure 2-11 Meteoric and compactional circulation pathways in sand-rich progradational packages and growth fault zones beneath the Texas coastal plan (from Dutton and others, 2006). 2-21

Figure 2-12 Effect of a 200m sea level all at 31 Ma on the distribution of meteoric water entering the basin through topographic drive. Light stippled area shows strata in which compactional water has been replaced by meteoric water. Water of meteoric origin is predicted to move 75km further downdip in the Wilcox Formation as a result of the additional topography (from Harrison and Summa, 1991). 2-21

Figure 2-13 Cross section of Barbers Hill salt dome in Chambers County showing the salt stock, cap rock mineralogical zones, and enclosing hydrostratigraphic intervals (modified from Hamlin and others, 1988). This cross section has no vertical exaggeration (vertical and horizontal scales are equal). Cap-rock layering is generally more complicated than shown here and varies widely among domes. 2-22

Figure 3-1 Conceptual flow model of gravity driven groundwater flow in the Texas Gulf Coast Aquifer System based on the local, intermediate, and regional flow systems. 3-14

Figure 3-2 Texas Gulf Coast Area underlain by aquifers with artesian pressures (above land surface) in the early 1900’s (from Hill, 1901). 3-15

Figure 3-3 Mean annual precipitation in the Texas Gulf Coast region (1971 – 2000; PRISM www.prism.oregonstate.edu). Points represent locations of weather stations used in the study by Scanlon and others (2012). Black lines represent extent of the Gulf Coast Aquifer System study area regions bounded by the Rio Grande and Nueces Rivers, the Nueces and Brazos Rivers and the Brazos and Sabine Rivers (from Scanlon and others, 2012). 3-16

Figure 3-4 Distribution of groundwater chloride mass balance (CMB) recharge rates based on groundwater chloride concentrations and chloride concentration in bulk precipitation in the Gulf Coast Aquifer System. Blue line delineates northern region where Cl/Br > 300. Black lines represent extent of the Gulf Coast Aquifer System study area subdivided into southern, central, and northern regions (from Scanlon and others, 2012). 3-17

Figure 3-5 Conceptual water budget for the Lower Colorado River Basin Model (Young and others, 2006). Note that the shallow recharge includes enhanced recharge induced by the large amount of flooding that occurs with rice production in the Lower Colorado River Basin. 3-18

Figure 3-6 Comparison of the location of the down-dip boundary condition at Transect 4 for the Northern Gulf Coast Aquifer System GAM, Central Gulf Coast Aquifer System GAM, and the LCRB Model, and at Transect 8 for the GMA 16 AGM. 3-18

List of Figures, continued

Figure 3-7 Three dimensional view of: (a) Transects 1, 2, 3, and 4 for the Northern Gulf Coast Aquifer System GAM; and (b) Transects 4, 5, 6, 7 and 8 for the Central Gulf Coast Aquifer System GAM. The shaded areas in each model represent domain of the groundwater model. The model domain is represented by the shaded area..... 3-19

Figure 3-8 Three dimensional view of: (a)Transects 34, 4, 45, and 5 for the LCRB Model; and (b) Transects 6, 7, 8, and 9 for the GMA 16 AGM. The shaded areas in each model represent domain of the groundwater model. The model domain is represented by the shaded area..... 3-20

Figure 3-9 Schematic showing the groundwater fluxes through the six faces of a grid cell (from Pollock, 1994)..... 3-21

Figure 3-10 Schematic showing the computation of exit point and travel time for the case of a two-dimensional flow in the x-y plane (from Pollock, 1994). 3-21

Figure 3-11 Starting locations of the particle seeds used for reverse particle tracking with MODPATH to estimate groundwater age. 3-22

Figure 3-12 Locations of the polygons used to define the blocks of cells used to calculate the water balances of different sections of the Gulf Coast Aquifer System along the transects..... 3-23

Figure 3-13 Transect 1 groundwater ages and groundwater fluxes calculated using the Northern Gulf Coast Aquifer System GAM. (negative values indicate flow in the opposite directions and are highlighted in yellow). 3-24

Figure 3-14 Transect 3 groundwater ages and groundwater fluxes calculated using the Northern Gulf Coast Aquifer System GAM (negative values indicate flow in the opposite directions and are highlighted in yellow). 3-25

Figure 3-15 Transect 34 groundwater ages and groundwater fluxes calculated using the Northern Gulf Coast Aquifer System GAM (negative values indicate flow in the opposite directions and are highlighted in yellow). 3-26

Figure 3-16 Transect 34 groundwater ages and groundwater fluxes calculated using the LCRB Model (negative values indicate flow in the opposite directions and are highlighted in yellow)...... 3-27

Figure 3-17 Transect 45 groundwater ages and groundwater fluxes calculated using the Northern Gulf Coast Aquifer System GAM (negative values indicate flow in the opposite directions and are highlighted in yellow). 3-28

Figure 3-18 Transect 45 groundwater ages and groundwater fluxes calculated using the LCRB Model (negative values indicate flow in the opposite directions and are highlighted in yellow)...... 3-29

Figure 3-19 Transect 45 groundwater ages and groundwater fluxes calculated using the Central Gulf Coast Aquifer System GAM (negative values indicate flow in the opposite directions and are highlighted in yellow)...... 3-30

Figure 3-20 Transect 5 groundwater ages and groundwater fluxes calculated using the LCRB Model (negative values indicate flow in the opposite directions and are highlighted in yellow)...... 3-31

List of Figures, continued

Figure 3-21	Transect 5 groundwater ages and groundwater fluxes calculated using the Central Gulf Coast Aquifer System GAM (negative values indicate flow in the opposite directions and are highlighted in yellow).....	3-32
Figure 3-22	Transect 6 groundwater ages and groundwater fluxes calculated using the Central Gulf Coast Aquifer System GAM (negative values indicate flow in the opposite directions and are highlighted in yellow).....	3-33
Figure 3-23	Transect 6 groundwater ages and groundwater fluxes calculated using the GMA 16 AGM (negative values indicate flow in the opposite directions and are highlighted in yellow).....	3-34
Figure 3-24	Transect 78 groundwater ages and groundwater fluxes calculated using the Central Gulf Coast Aquifer System GAM (negative values indicate flow in the opposite directions and are highlighted in yellow).....	3-35
Figure 3-25	Transect 78 groundwater ages and groundwater fluxes calculated using the GMA 16 AGM (negative values indicate flow in the opposite directions and are highlighted in yellow).....	3-36
Figure 3-26	Transect 8 groundwater ages and groundwater fluxes calculated using the Central Gulf Coast Aquifer System GAM (negative values indicate flow in the opposite directions and are highlighted in yellow).....	3-37
Figure 3-27	Transect 8 groundwater ages and groundwater fluxes calculated using the GMA 16 Groundwater AGM (negative values indicate flow in the opposite directions and are highlighted in yellow).....	3-38
Figure 3-28	Composite averages for groundwater ages for the four groundwater models and the eight transects.	3-39
Figure 4-1	Wells with water quality measurements in GMA 14.....	4-20
Figure 4-2	Wells with water quality measurements in GMA 15.....	4-21
Figure 4-3	Wells with water quality measurements in GMA 16.....	4-22
Figure 4-4	Aerial view of the wells with isotope data that are associated with Transect 3. Wells that were sampled as part of this project are labeled as INTERA wells.	4-23
Figure 4-5	Cross-sectional view of the wells with isotope data associated with Transect 3. (Note: surfaces represent the bottom of each geological formation).	4-24
Figure 4-6	Aerial view of the wells with isotope data that are associated with Transect 5. Wells that were sampled as part of this project are labeled as INTERA wells.	4-25
Figure 4-7	Cross-sectional view of the wells with isotope data associated with Transect 5. (Note: surfaces represent the bottom of each geological formation).	4-26
Figure 4-8	Aerial view of the wells with isotope data that are associated with Transect 8. Wells that were sampled as part of this project are labeled as INTERA wells.	4-27
Figure 4-9	Cross-sectional view of the wells with isotope data associated with Transect 8. (Note: surfaces represent the bottom of each geological formation).	4-28

List of Figures, continued

Figure 5-1 Model proposed by Losh and others (1999) of vertical transport of fluids into reservoirs along the trace of a fault (from Kuecher and others, 2001). 5-12

Figure 5-2 Resistivity map of the lower Chicot aquifer at Barbers Hill salt dome (modified from Hamlin and others, 1988). Water wells completed in this lower Chicot sand are also shown along with total dissolved solids measurements. Low resistivities around the southern and southwestern dome flanks delineate a high-salinity plume extending away from the salt dome in the down-flow direction. 5-13

Figure 6-1 Conceptualized groundwater flow system incorporating hydrochemical processes that affect reactions and transport involving major ions (modified after Back and others, 1983; Herczeg and Edmunds, 2000). The distinction between an open and closed system is based on whether the aquifer is connected to atmospheric gases such as CO₂ and O₂. 6-40

Figure 6-2 Estimated distribution of mean annual chloride concentrations in bulk precipitation in the study area based on mass deposition and the distribution of mean annual precipitation. Wet chloride deposition from NADP was multiplied by two to account for dry deposition. Points represent locations of open (bulk) precipitation collectors at the NADP sites (circles), and at sites hosted by the Lavaca-Navidad River Authority (LNRA, squares) and by the TexasET Network (Texas A&M University, triangles) (from Scanlon and others, 2012). 6-41

Figure 6-3 Relationship between flow regimes, hydrochemical facies, and geochemical processes in a coastal aquifer (modified after Back, 1966 and Custodio, 1987)..... 6-42

Figure 6-4 Measured Total Dissolved Solids concentration in the Catahoula Formation for GMA 14 , GMA 15, and GMA 16 and a bivariate plot of bromide concentrations versus chloride concentrations for groundwater samples from the Catahoula Formation. (Note that bgs stands for below ground surface). 6-43

Figure 6-5 Classification diagram for anion and cation facies in terms of major-ion percentages. Water types are designated according to the domain in which they occur on the diagram segments (after Morgan and Winner, 1962; Back, 1966) (from Freeze and Cherry, 1979). 6-44

Figure 6-6 Piper Diagram for the Chicot, Evangeline, Middle Lagarto, Jasper, Catahoula, and Yegua-Jackson Units in GMA 14. 6-45

Figure 6-7 Piper Diagram for the Chicot, Evangeline, Middle Lagarto, Jasper, Catahoula, and Yegua-Jackson Units in GMA 15. 6-46

Figure 6-8 Piper Diagram for the Chicot, Evangeline, Middle Lagarto, Jasper, Catahoula, and Yegua-Jackson Units in GMA 16. 6-47

Figure 6-9 Total Dissolved Solids concentrations as a function of depth estimated by kriging point measurements from the TWDB groundwater database. 6-48

List of Figures, continued

Figure 6-10 Chloride concentrations as a function of depth estimated by kriging point measurements from the TWDB groundwater database. 6-49

Figure 6-11 Sulfate concentrations as a function of depth estimated by kriging point measurements from the TWDB groundwater database. 6-50

Figure 6-12 Calcium concentrations as a function of depth estimated by kriging point measurements from the TWDB groundwater database. 6-51

Figure 6-13 Sodium concentrations as a function of depth estimated by kriging point measurements from the TWDB groundwater database. 6-52

Figure 6-14 Ratio of chloride to bromide milliequivalents as a function of depth estimated by kriging point measurements from the TWDB groundwater database. 6-53

Figure 6-15 Ratio of chloride to sulfate milliequivalents as a function of depth estimated by kriging point measurements from the TWDB groundwater database. 6-54

Figure 6-16 Ratio of sodium to calcium milliequivalents as a function of depth estimated by kriging point measurements from the TWDB groundwater database. 6-55

Figure 6-17 Ratio of sodium to chloride milliequivalents as a function of depth estimated by kriging point measurements from the TWDB groundwater database. 6-56

Figure 6-18 Selected Ion Concentrations and Ion Ratios as a function of depth and down dip distance for GMA 14, GMA 15, and GMA 16. 6-57

Figure 6-19 Concentration Maps for Cl for Transect 3 in GMA 14. (Note Lake Conroe is located at approximately downdip distances of 24 miles to 32 miles). (Note: surfaces represent the bottom of each geological formation). 6-58

Figure 6-20 Concentration Maps for Ca for Transect 3 in GMA 14. (Note Lake Conroe is located at approximately downdip distances of 24 miles to 32 miles). (Note: surfaces represent the bottom of each geological formation). 6-59

Figure 6-21 Concentration Maps for Na for Transect 3 in GMA 14. (Note Lake Conroe is located at approximately downdip distances of 24 miles to 32 miles). (Note: surfaces represent the bottom of each geological formation). 6-60

Figure 6-22 Hydrochemical facies for Transect 3 in GMA 14. (Note Lake Conroe is located at approximately downdip distances of 24 miles to 32 miles). (Note: surfaces represent the bottom of each geological formation). 6-61

Figure 6-23 Concentration Maps for Cl for Transect 34 in GMA 14. (Note: surfaces represent the bottom of each geological formation). 6-62

Figure 6-24 Concentration Maps for Ca for Transect 34 in GMA 14. (Note: surfaces represent the bottom of each geological formation). 6-63

Figure 6-25 Concentration Maps for Na for Transect 34 in GMA 14. (Note: surfaces represent the bottom of each geological formation). 6-64

List of Figures, continued

Figure 6-26	Hydrochemical facies for Transect 34 in GMA 14. (Note: surfaces represent the bottom of each geological formation).	6-65
Figure 6-27	Hydrochemical facies for Transect 23 in GMA 14. (Note: surfaces represent the bottom of each geological formation).	6-66
Figure 6-28	Bivariate plots of Na/Cl ratio versus chloride and SO ₄ versus chloride for transects in GMA 14, 15, & 16.	6-67
Figure 6-29	Concentration Maps for Cl for Transect 5 in GMA 15. (Note: surfaces represent the bottom of each geological formation).	6-68
Figure 6-30	Concentration Maps for Ca for Transect 5 in GMA 15. (Note: surfaces represent the bottom of each geological formation).	6-69
Figure 6-31	Concentration Maps for Na for Transect 5 in GMA 15. (Note: surfaces represent the bottom of each geological formation).	6-70
Figure 6-32	Hydrochemical facies for Transect 5 in GMA 15. (Note: surfaces represent the bottom of each geological formation).	6-71
Figure 6-33	Concentration Maps for Cl for Transect 56 in GMA 15. (Note: surfaces represent the bottom of each geological formation).	6-72
Figure 6-34	Concentration Maps for Ca for Transect 56 in GMA 15. (Note: surfaces represent the bottom of each geological formation).	6-73
Figure 6-35	Concentration Maps for Na for Transect 56 in GMA 15. (Note: surfaces represent the bottom of each geological formation).	6-74
Figure 6-36	Hydrochemical facies for Transect 56 in GMA 15. (Note: surfaces represent the bottom of each geological formation).	6-75
Figure 6-37	Hydrochemical facies for Transect 4 in GMA 15. (Note: surfaces represent the bottom of each geological formation).	6-76
Figure 6-38	Concentration Maps for Cl for Transect 8 in GMA 16. (Note: surfaces represent the bottom of each geological formation).	6-77
Figure 6-39	Concentration Maps for Ca for Transect 8 in GMA 16. (Note: surfaces represent the bottom of each geological formation).	6-78
Figure 6-40	Concentration Maps for Na for Transect 8 in GMA 16. (Note: surfaces represent the bottom of each geological formation).	6-79
Figure 6-41	Hydrochemical facies for Transect 8 in GMA 16. (Note: surfaces represent the bottom of each geological formation).	6-80
Figure 6-42	Concentration Maps for Cl for Transect 910 in GMA 16. (Note: surfaces represent the bottom of each geological formation).	6-81
Figure 6-43	Concentration Maps for Ca for Transect 910 in GMA 16. (Note: surfaces represent the bottom of each geological formation).	6-82
Figure 6-44	Concentration Maps for Na for Transect 910 in GMA 16. (Note: surfaces represent the bottom of each geological formation).	6-83
Figure 6-45	Hydrochemical facies for Transect 910 in GMA 16. (Note: surfaces represent the bottom of each geological formation).	6-84
Figure 6-46	Hydrochemical facies for Transect 89 in GMA 16. (Note: surfaces represent the bottom of each geological formation).	6-85

List of Figures, continued

Figure 6-47	Calcium/Magnesium ratios for wells intersecting the Brazos River Alluvium and for wells that intersect deposits surrounding the Brazos River Alluvium.	6-86
Figure 6-48	Calcium concentrations for wells intersecting the Brazos River Alluvium and for wells that intersect deposits surrounding the Brazos River Alluvium.	6-87
Figure 6-49	Magnesium concentrations for wells intersecting the Brazos River Alluvium and for wells that intersect deposits surrounding the Brazos River Alluvium.	6-88
Figure 7-1	The meteoric relationship between $\delta^{18}\text{O}$ and $\delta^2\text{H}$ in precipitation. Data are weighted average annual values for precipitation monitored at stations in the International Atomic Energy Agency global network as compiled by Rozanski and others (1993) (modified from Figure 2-1 from Clark and Fritz (1997)).	7-13
Figure 7-2	Isotope exchange processes that can modify the isotopic composition of meteoric water (after Clark and Fritz, 1997).	7-13
Figure 7-3	Comparison of the relationship between $\delta^{18}\text{O}$ and $\delta^2\text{H}$ for groundwater samples compiled as part of this study, from the deep Catahoula study by Kreitler and others (1988), and from a very deep Catahoula study by the EPA.	7-14
Figure 7-4	Location of the groundwater samples with $\delta^{18}\text{O}$ and $\delta^2\text{H}$ relationships that plot above ($\delta^{18}\text{O}$ depleted), very close to, and below ($\delta^{18}\text{O}$ enriched) the meteoric line.	7-15
Figure 7-5	$\delta^2\text{H}_{\text{CH}_4}$ and $\delta^{13}\text{C}_{\text{CH}_4}$ compositions of methane gas of multiple origins. Note that thermogenic methane is more enriched in $\delta^{13}\text{C}_{\text{CH}_4}$ than methane of bacterial origin. Most of the methane gas from the Gulf Coast Aquifer System falls within the thermogenic field. The grey shaded area within the thermogenic field is for methane associated with oil and the dark-shaded area is non-associated. Methane of bacterial origin could form either by reduction or fermentation (see text). Note small overlap areas between bacterial fermentation and thermogenic fields. Dashed areas outline fields of methane by their origin (Schoell, 1988). Arrow shows possible oxidation of bacterial methane that can transform its isotopic compositions similar to thermogenic methane.	7-16
Figure 7-6	A cross-plot of $\delta^2\text{H}_{\text{CH}_4}$ and $\delta^2\text{H}_{\text{H}_2\text{O}}$ of groundwater samples from wells sampled along transects 3 and 5. Note random scatter in the data and an absence of any preferential trend.	7-17
Figure 8-1	Vertical cross-section of Transect 3 showing sampled groundwater wells, geologic formations, average sand percentages, and sand beds identified from geophysical logs. (Note: surfaces represent the bottom of each geological formation).	8-45

List of Figures, continued

Figure 8-2	Vertical cross-section of Transect 3 showing uncorrected ¹⁴ C dates for wells. (Note: surfaces represent the bottom of each geological formation).	8-46
Figure 8-3	Carbon isotopic data for the Chicot Aquifer segment along Transect 3.	8-47
Figure 8-4	Anion composition for Chicot Aquifer segment along Transect 3.	8-48
Figure 8-5	TDS composition for Chicot Aquifer segment along Transect 3.	8-49
Figure 8-6	Sulfur isotopic sulfate for Transect 3 with respect to a) sulfate concentration and b) distance along Transect 3 from the Catahoula outcrop.	8-50
Figure 8-7	³⁶ Chlorine to Chloride as function of transect distance along Transect 3.	8-51
Figure 8-8	Vertical cross-section of Transect 5 showing sampled groundwater wells, geologic formations, average sand percentages, and sand beds identified from geophysical logs. (Note: surfaces represent the bottom of each geological formation).	8-52
Figure 8-9	Vertical cross-section of Transect 5 showing uncorrected ¹⁴ C dates for wells. (Note: surfaces represent the bottom of each geological formation).	8-53
Figure 8-10	Vertical cross-section of Transect 8 showing sampled groundwater wells, geologic formations, average sand percentages, and sand beds identified from geophysical logs. (Note: surfaces represent the bottom of each geological formation).	8-54
Figure 8-11	Vertical cross-section of Transect 8 showing uncorrected ¹⁴ C dates for wells. (Note: surfaces represent the bottom of each geological formation).	8-55
Figure 8-12	δ ³⁴ S plotted as a function of sulfate concentration and well depth for Transect 8.	8-56
Figure 8-13	Environmental isotope data for Transect 8 wells.	8-57
Figure 8-14	Distribution of groundwater age versus depth for ¹⁴ C values that are uncorrected and for ¹⁴ C values that are corrected using the Pearson method.	8-58
Figure 8-15	Groundwater ages based on the Pearson Method for the entire Gulf Coast Aquifer System.	8-59
Figure 8-16	Groundwater ages based on the Pearson Method for the Chicot and the Evangeline Aquifers.	8-60
Figure 8-17	Groundwater ages based on the Pearson Method for the Middle Lagarto, Jasper Aquifer, the Catahoula, and the Jackson Formation.	8-61
Figure 8-18	¹⁴ C ages corrected using the Pearson Method versus depth for samples from the Beaumont, Lissie, and Willis formations.	8-62
Figure 8-19	¹⁴ C ages corrected using the Pearson Method versus depth for samples from the Upper Goliad, Lower Goliad, and Upper Lagarto formations.	8-63
Figure 8-20	¹⁴ C ages corrected using the Pearson Method versus depth for samples from the Middle Lagarto, Lower Lagarto, and Oakville formations.	8-64

List of Figures, continued

Figure 8-21	¹⁴ C ages corrected using the Pearson Method versus depth for samples from the Catahoula and Jackson formations.	8-65
Figure 9-1	Distribution of the percent of the Catahoula Formation in the vicinity of Montgomery County with TDS concentrations below 1,000 ppm based on the analysis of geophysical logs (modified from LGB Guyton and INTERA, 2012).	9-14
Figure 9-2	Distribution of the percent of the Catahoula Formation in the vicinity of Montgomery County with TDS concentrations below 3,000 ppm based on the analysis of geophysical logs (modified from LGB Guyton and INTERA, 2012).	9-14
Figure 9-3	Distribution of recharge rates from Scanlon and other (2012) previous shown in Figure 3-4 but replotted to show a different symbology for the recharge rate and to show the location of four groundwater flow models.	9-15
Figure 9-4	Calculation of net flux across the top layer of the Northern Gulf Coast Aquifer System GAM based on the water budget developed for the steady-state condition representing predevelopment (no pumping) conditions. (Note: positive fluxes represent recharge into the aquifer and negative fluxes represent discharge out of the aquifer).	9-16
Figure 9-5	Calculation of net flux across the top layer of the Central Gulf Coast Aquifer System GAM based on the water budget developed for the steady-state condition representing predevelopment (no pumping) conditions. (Note: positive fluxes represent recharge into the aquifer and negative fluxes represent discharge out of the aquifer).	9-17
Figure 9-6	Calculation of net flux across the top layer of the LCRB Model based on the water budget developed for the steady-state condition representing predevelopment (no pumping) conditions. (Note: positive fluxes represent recharge into the aquifer and negative fluxes represent discharge out of the aquifer).	9-18
Figure 9-7	Calculation of net flux across the top layer of the GMA 16 AGM based on the water budget developed for the steady-state condition representing predevelopment (no pumping) conditions. (Note: positive fluxes represent recharge into the aquifer and negative fluxes represent discharge out of the aquifer).	9-19
Figure 10-1	Table of contents from the TWDB groundwater Availability Modeling Program Guidelines for the Brazos River Alluvium Aquifer GAM (TWDB, unpublished correspondence with Cindy Ridgeway).	10-4

List of Tables

Table 1	Simplified stratigraphic and hydrogeologic chart of the northwestern Gulf of Mexico basin, Texas coastal zone (Galloway and others, 1991; Sharp and others, 1991).	xxvi
Table 2	Options for numerically representing conceptualization of groundwater flow of the Gulf Coast Aquifer System for GMAs 14, 15, and 16.	xxvii
Table 3	Analysis of geochemical and isotopic signatures that may provide insight into the conceptual groundwater flow model for GMAs 14, 15, and 16.	xxvii
Table 1-1	Simplified stratigraphic and hydrogeologic chart of the northwestern Gulf of Mexico basin, Texas coastal zone (Galloway and others, 1991; Sharp and others, 1991).	1-3
Table 1-2	Options for numerically representing conceptualization of groundwater flow of the Gulf Coast Aquifer System for GMAs 14, 15, and 16.	1-8
Table 1-3	Analysis of geochemical and isotopic signatures that may provide insight into the conceptual groundwater flow model for GMAs 14, 15, and 16.	1-9
Table 1-4	The cross-sections for which reverse particle tracks and water mass balances were calculated for groundwater availability models.	1-10
Table 2-1	Salt Domes Located Within 15,000 feet of the Land Surface in the Texas Gulf Coast. (data from Ewing, 1990)	2-12
Table 3-1	Spatial Distribution of Average Annual Recharge Values for GMA 14, 15, and 16.	3-5
Table 4-1	Spatial Distribution of Wells Among GMAs 14, 15, and 16.	4-3
Table 4-2	Analytes collected by INTERA at Gulf Coast Aquifer System Wells.	4-6
Table 4-3	Geochemistry Measurements for Transect 3.	4-7
Table 4-4	Geochemistry Measurements for Transect 5.	4-13
Table 4-5	Geochemistry Measurements for Transect 8.	4-16
Table 4-6	State Well Numbers and Secondary Well IDs for the Wells in Transects 3, 5, and 8.	4-19
Table 6-1	Reported constituent concentration ranges for precipitation (from Hem, 1985).	6-6
Table 6-2	Composition of Ocean Water with a Salinity of 35,000 ppm (Anthoni, 2006).	6-9
Table 6-3	Ion Ratios for Ocean Water (Anthoni, 2006).	6-10
Table 6-4	Ion Concentrations for Formation Water in the Deep Catahoula.	6-11
Table 6-5	Ion Ratios for Formation Water in the Deep Catahoula.	6-12
Table 6-6	Average and Median Values for Chemical Concentrations and Ion Ratios for GMA 14. (note the ion ratios are dimensionless)	6-15
Table 6-7	Average and Median Values for Chemical Concentrations and Ion Ratios for GMA 15. (note the ion ratios are dimensionless)	6-16
Table 6-8	Average and Median Values for Chemical Concentrations and Ion Ratios for GMA 16. (note the ion ratios are dimensionless)	6-17
Table 6-9	Comparison of Major Ion and TDS Concentrations among GMA 14, GMA 15, and GMA 16.	6-18

List of Tables, continued

Table 6-10	Factors that increase spatial variability in an aquifer’s concentration distribution.	6-26
Table 6-11	Sources of Sampling Bias.	6-28
Table 6-12	Stable Isotope concentration for the wells in the Brazos River Alluvium and the Evangeline Aquifer (from Chowdhury and others, 2012).	6-39
Table 7-1	Abundance of hydrogen and oxygen isotopes (from Cook and Herczeg, 2000).	7-1
Table 7-2	Comparison of the Means and Medians for $\delta^{18}\text{O}$ and $\delta^2\text{H}$ value for isotope measurements in GMAs shown in Figure 7-4.	7-7
Table 8-1	Abundance of carbon isotopes (from Clark and Fritz, 1997).	8-1
Table 8-2	Calculated Ages for Mixtures of Groundwater with Different pMCs.	8-5
Table 8-3	Results of modeling groundwater evolution from recharge location through 3-15 and 3-17 in the Chicot aquifer, Transect 3.	8-9
Table 8-4	Comments Regarding the Evaluation of Wells in Transect 3 for NETPATH Simulations.	8-14
Table 8-5	Results of NETPATH modeling of groundwater evolution from recharge location through 3-15 and 3-17 to Well 43 in the Chicot Aquifer, Transect 3.	8-16
Table 8-6	Results of NETPATH modeling of groundwater evolution from one well to another down-gradient well for wells in the Middle Lagarto and the Jasper Aquifer along Transect 3.	8-19
Table 8-7	Application of Pearson Correction($^{14}\text{C}_{\text{cor}}$) to Measured ^{14}C ($^{14}\text{C}_{\text{meas}}$) along Transect 3.	8-22
Table 8-8	Comments Regarding the Evaluation of Wells in Transect 5 for NETPATH Simulations.	8-24
Table 8-9	Results of NETPATH modeling of groundwater evolution from one well to another down-gradient well for wells in the Chicot for Wells 5-1 and 5-3.	8-25
Table 8-10	Comparison of measured $^{14}\text{C}_{\text{MEAS}}$ to Pearson corrected ^{14}C values for “old” groundwater along Transect 5.	8-27
Table 8-11	NETPATH modeling results for Transect 8 Involving Wells 8-1, 8-2, and 8-3.	8-30
Table 8-12	Chemistry and ^{14}C Ages for the Upper Evangeline Flow System.	8-35
Table 8-13	Depths where Groundwater of Age 10,000 ybp occurs for Different Geologic Formations.	8-41
Table 8-14	Comparison of Measured and Predicted Depth Intervals for Groundwater that is 10,000 years old for the Lissie, Willis, and Upper Goliad Formations.	8-44

Acronyms and Abbreviations

‰	per thousand (one tenth of a percent)
%	percent(parts per hundred)
δ	delta, defined by equation 7.1
bls	below land surface
AGM	Alternative Groundwater Model
BFZ	Balcones Fault Zone
BRA	Brazos River Alluvium
CEC	cation exchange capacity
CMB	chloride mass balance
GMA	Groundwater Management Area
GAM	Groundwater Availability Model
GBDS	Gulf Basin Depositional Synthesis Project
GCD	Groundwater Conservation District
GHB	General Head Boundary
GWML	Global meteoric water line
Kg	kilograms
Km	kilometers
KPa/m	Kilopascals per meter
KPA/km	Kilopascals per kilometer
LCRB	Lower Colorado River Basin
LCRA-SAWS	Lower Colorado River Authority and San Antonio Water System
Ln	natural logarithm
log ₁₀	logarithm base 10
LNRA	Lavaca Navidad River Authority
LSWP	LCRA-SAWS Project
NADP	National Atmospheric Deposition Program
MAG	modeled available groundwater
Meq	milliequivalents
meq/L	milliequivalents per liter
mg/L	milligrams per liter
mm	millimeter
pMC	percent modern Carbon
ppm	parts per million
psi/ft	pounds per square foot
p _{co2}	Partial pressure of carbon dioxide
pH	the negative logarithm of the activity of the hydronium ion (measure of acidity or basicity)
pE	the negative logarithm of the activity of the electron (measure of redox potential)
SWAP	Source Water Protection Program
TCEQ	Texas Commission on Environmental Quality
TDS	Total Dissolved Solids
TWDB	Texas Water Development Board
USGS	United States Geological Survey
μS/cm	microsiemens per centimeter

Acronyms and Abbreviations, continued

X	exchange site in play during ion exchange reactions
Ybp	years before present

Chemical

Ar	argon gas
Br	bromide
C	carbon
C ₁ gas	methane
C ₂ gas	ethane
C ₃ gas	propane
C ₄ gas	butane
C ₅ gas	pentane
¹² C	stable carbon isotope with six neutrons
¹³ C	stable carbon isotope with seven neutrons
¹⁴ C	radiocarbon or carbon with eight neutrons
² H	hydrogen with two neutrons (deuterium)
¹⁸ O	oxygen with ten neutrons
Ca	calcium
CaCO ₃	calcite
Cl	chloride
CO	carbon monoxide
CO ₂	carbon dioxide
CO ₃	carbonate
CH ₄	methane
F	fluoride
Fe	iron
H ₂ O	water
HCO ₃	bicarbonate
H ₂ S	hydrogen sulfide
I	iodine
K	potassium
Mg	magnesium
Mn	manganese
Na	sodium
N ₂	nitrogen gas
NH ₄	ammonium
Na	sodium
NaCl	sodium chloride
O ₂	oxygen gas
Si	silicon
SiO ₂	silica
SO ₄	sulfate

Executive Summary

The project focused on reviewing the geochemical data in the Gulf Coast Aquifer System, the Yegua-Jackson Aquifer, and the Brazos River Alluvium Aquifer to identify relationships relevant for evaluating the conceptual flow model for the Gulf Coast Aquifer System. The geochemical database includes information from 13,000 wells that was assembled from TWDB and USGS databases, data tables from university theses, and from sampling events we conducted from September 2012 to February 2013. Detailed mapping of geochemical data was performed to help assess the conceptual flow model for the Gulf Coast Aquifer System by evaluating lines of evidence for groundwater mixing, flow paths, and ages. These maps consist of areal plots and vertical cross-sections of ions, ion ratios, hydrogeochemical facies, stable isotopes, and groundwater ages based on ^{14}C .

Table 1 provides a simplified stratigraphic and hydrogeological chart of the geological units for the study area, which is shown in Figure 1. As shown in Table 1, the Gulf Coast Aquifer System consists of the Catahoula Formation and younger formations. The primary aquifers that are associated with the Gulf Coast Aquifer System are the Chicot Aquifer, the Evangeline Aquifer, and the Jasper Aquifer.

The general conceptual flow models for the Gulf Coast have remained relatively the same for the last fifty years. In the Gulf Coast Aquifer System, the shallow flow zone controls the majority of flow to local springs and streams; in the intermediate flow systems, the intermediate flow zone controls the majority of flow in the large river basins and to the large rivers; and the regional flow system controls the majority of the flow to the ocean. Despite having the same general conceptual flow system, the regional groundwater flow models can vary substantially in their simulated groundwater flows because of differences in the groundwater models' numerical construction to represent the conceptual flow system. Table 2 lists some of the issues associated with the conceptualization and construction of a groundwater flow model.

This report reviews and analyzes the construction and conceptualization of the following four groundwater models: the Northern Gulf Coast Aquifer System GAM, the Central Gulf Coast Aquifer System GAM, the GMA 16 Alternative Groundwater Model and the Lower Colorado River Basin (LCRB) model. The analysis of these models include comparisons of their water

budgets, particle tracks, recharge rates, and aquifer properties for Transects where maps have been developed for ions, ion ratios, hydrogeochemical facies, stable isotopes, and groundwater ages based on ¹⁴C. Table 3 lists several of the insights and information sought by creating these maps and/or performing the analyses.

Table 1 Simplified stratigraphic and hydrogeologic chart of the northwestern Gulf of Mexico basin, Texas coastal zone (Galloway and others, 1991; Sharp and others, 1991).

Period		Epoch	Age (M.Y.)	Stratigraphic Unit	Hydrogeologic Unit		
Quaternary		Holocene	0.02	Brazos River Alluvium Aquifer and other Alluviums	Alluvium	Gulf Coast Aquifer System	
		Pleistocene		Beaumont	Chicot Aquifer		
Tertiary	Neogene		1.8	Lissie/Alta Loma			Chicot Aquifer
				Willis			
			Miocene	5.3	Goliad		Evangeline Aquifer
					Fleming/Lagarto		Burkeville Aquitard
	Paleogene	Oligocene		23.9	Fleming/Oakville		Jasper Aquifer
					Catahoula/Frio/Anahuac		aquifer and aquitard
		Eocene		33.9	Catahoula/Vicksburg		Aquitard and aquifer
					Jackson		Yegua-Jackson Aquifer
				Yegua			
				Sparta	Queen City-Sparta Aquifer		
	Queen City						
Paleocene		55.8	Reklaw	aquitard			
			Upper Wilcox/Carrizo	Carrizo-Wilcox Aquifer			
		Middle Wilcox					
		66.5	Lower Wilcox/Simsboro				
			66.5	Midway	aquitard		

Table 2 Options for numerically representing conceptualization of groundwater flow of the Gulf Coast Aquifer System for GMAs 14, 15, and 16.

Conceptualization Issue	Numerical Implementation in Model
Hierarchy of flow systems	Grid cell and model layer resolution
Predevelopment Flow Condition	Steady-state flow assumptions
Recharge	Recharge cells or general head boundary (GHB) cells
Up-dip & bottom boundary	Location of No-flow or GHB cells
Down-dip and ocean boundary	Location of No-flow or GHB cells
Surface water-groundwater boundary	River/Stream cells or GHB cells
Aquifer Structure	Model layers
Aquifer Hydraulic Properties	Scale of heterogeneity

Table 3 Analysis of geochemical and isotopic signatures that may provide insight into the conceptual groundwater flow model for GMAs 14, 15, and 16.

Analyses Method and/or Map	Desired Insight
Tabulated and plotted depth-average geochemical values for the Gulf Coast Aquifer System Region	Notable differences in the geochemistry of GMA 14, 15, and 16
Plotted geochemistry along vertical cross-sections	Mixing or lack of mixing between and within aquifers at a local and intermediate scale
Plots of hydrogeochemical facies, chloride values, and sand and salinity profiles along vertical cross-sections	Direction of groundwater flow and evidence of a “high-flow” region within or between aquifers
Analyses where changes occur with ion concentrations and ratios and with the locations for geological and anthropogenic features	Cause-and-effect relationships between the presences of some salt domes, growth faults, and anthropogenic contamination and changes in groundwater geochemistry
Analysis of the hydropressure and brine concentrations in the Catahoula and deeper deposits	Evidence that a source of the increased total dissolved solids (TDS) near the coast is upswelling of brine
Analysis of carbon and isotope of gases such as carbon dioxide and methane	Evidence of movement along growth faults
Analysis of stable isotopes of oxygen and hydrogen	Evidence of meteoric water
Analysis of carbon stable and radioactive isotopes	Estimate of groundwater age

While there is significant chemical variability at the local scale, regional groundwater flow paths could nevertheless be inferred from our geochemical analysis. Our analyses included examining the following: evolutionary development of the bicarbonate-sulfate-chloride anion sequence; the occurrence of high Ca and HCO₃ concentrations in recharge areas; the increase of Na concentrations and decrease of Ca concentrations along flow paths in a closed system environment as a result of exchange of Ca for Na on clays; and the general increase in salinity concentrations with depth and distance from the recharge source. These analyses indicate that

groundwater flows are consistently toward the coast and generally down-dip. Toward the coast, the down dip angle becomes less steep and more horizontal – a result that is consistent with the general smaller dip angle of the younger formations.

The flow paths inferred from our geochemical analysis are consistent with the flow paths inferred from the distribution of ^{14}C measurements. Our examination of the estimated age of groundwater based on ^{14}C measurements, we conclude that the current groundwater regional flow system is reflective of hydrogeological conditions that have existed since 7,000 to 10,000 ybp. Between 10,000 ybp and 30,000 ybp, significant changes in groundwater flow conditions occurred in response to continual changes in shoreline locations and sea levels. During the last 30,000 years, the important aspects of the paleohistory of the Texas Gulf Coast can be grouped into the following 10,000 year periods:

- 1) 30,000 to 20,000 years ago – Groundwater was part of a larger regional flow system than it is today because of a lower ocean level and more distant shore line. Also the base of the meteoric water was deeper than it is currently. Much of the Chicot footprint currently above sea level was being actively recharged and groundwater typically has a large vertical downward flow component.
- 2) 20,000 to 10,000 years ago – As ocean levels rose 400 feet and the shoreline moved inland from about 50 miles in GMA 16 and about 100 miles in GMA 14, the base of the meteoric water rose. Beneath the Chicot footprint that is above sea level today, the downward hydraulic gradients gradually lessen and even reversed as movement in the deep Gulf Coast Aquifer System began to slow as the regional flow system shrunk in response to the transgression of the coastline caused by a rise in sea level.
- 3) 10,000 years ago to present – The ocean level reached stability about 7,000 ybp and the Gulf Coast Aquifer System regional flow system achieved the current equilibrium with the current shore line, sea level and recharge condition. Groundwater with an age greater than 10,000 years is a mixture of waters that has been a part of regional flow systems that have changed with changes in sea levels and recharge conditions.

The overarching concept for groundwater flow in the majority of, if not all, Gulf Coast Aquifer System groundwater numerical models for GMAs 14, 15, and 16 is that basinal flow can be subdivided into local, intermediate, and regional flow regimes. The major driver for the local,

shallow flow system is the difference in topography between adjacent hills and valleys. Recharge to local flow regimes occurs in topographically high areas, and discharge occurs in nearby low areas, such as stream valleys. The shallow flow system occurs primarily in the outcrop or unconfined portion of the aquifer and is characterized by flow paths on the scale of a few miles, travel depths measured in tens of feet, and travel times that last between a month and several decades. Intermediate flow paths are longer and deeper than local flow paths and can underlie several local flow regimes. An example of an intermediate flow path would be the migration of groundwater from the perimeter of a watershed for a major river to a discharge location near the river. Regional flow regimes extend from regional recharge areas such as outcrops and discharge areas near the coastline. The regional system is composed of confined to semi-confined aquifers and is characterized by groundwater flow paths involving travel distances measured on a scale of tens of miles, travel depths in the range of 500 to 3,000 feet, and travel times that range between 50 and 40,000 years. The major topographic driver for the regional flow system is the difference between the water levels in the updip regions of the aquifer (e.g., in Colorado and Lavaca counties) and the downdip portion of the aquifer (e.g., near Matagorda and Brazoria counties). Thus, regional groundwater flow is primarily toward the coast and the groundwater movement tends to be much slower than in either the intermediate or shallow flow systems.

Important components of a conceptual model for the Gulf Coast Aquifer System flow system are inflows from other aquifer systems, distribution of recharge rates, groundwater interaction with rivers, groundwater interaction with the ocean, relative differences in permeability among the different geologic formations, and estimates of groundwater age. Listed below are implications for the conceptual flow model for GMAs 14, 15, and 16 based on the findings of this project:

- The up-dip boundary for the regional Gulf Coast Aquifer System flow should be the Catahoula Formation outcrop;
- The downdip boundary for the regional Gulf Coast Aquifer System flow should allow groundwater to discharge across a large area of the ocean bottom;
- The bottom boundary of the regional Gulf Coast Aquifer System flow should be based on where the TDS concentrations are not less than 10,000 ppm, and preferably greater;

- The numerical representation of the regional groundwater flow system should be constrained by estimates of groundwater age calculated from ^{14}C measurements;
- A conceptual water budget should be developed and be guided by recharge estimates by Scanlon and others (2012) after appropriate uncertainty estimates have been developed;
- Proper conceptualization and representation of groundwater mixing and flow paths requires vertical layering smaller than the thicknesses of the major aquifers; and the utility and accuracy of the GAMs could be improved if model layers represented the geological formations that comprised the Chicot, Evangeline, and Jasper Aquifers,
- General head boundaries do not accurately model recharge to an aquifer and should not be used for that purpose in any future GAMs for the Gulf Coast Aquifer System,
- A continuous, low permeability “Burkeville” Confining Unit does not exist up dip at the outcrop; and
- Groundwater from the Gulf Coast Aquifer System flows into the Brazos River Alluvium Aquifer but the relative magnitude of the inflows are unknown.

Our review of lithologic profiles along several transects suggests that groundwater flow through the geological units is not characterized by the bulk movement of large regional slugs of water but rather is largely controlled by sand rich sections that finger through lower permeability deposits. The lack of a bulk flow movement hinders the rigorous application of geochemical models such as NETPATH. In addition, the application of models such as NETPATH is complicated by the occurrence of numerous sources of TDS; for example, halite dissolution from salt domes, upward vertical flow of brines along growth faults, cross-flow through leaky abandoned wells, and contamination from former oil and gas surface pits.

Because halite contains very low concentrations of Br (much less than sea water or shallow groundwater), we used high Cl/Br ratios in groundwater as evidence for dissolution of halite from salt domes. Primarily in GMA 14, but also in GMAs 15 and 16, the dissolution of halite (NaCl) from salt domes and other salt formations can account for large differences in Cl, Na, and TDS concentrations over distances of a few miles or less. In addition to salt domes, upwelling of brines (TDS concentrations between 40,000 ppm and 80,000 ppm) along growth faults that intersect the geopressure zone is a significant source of Cl and Na in groundwater. One of the

indicators that was used to identify upwelling of brines as a source of elevated TDS and not sea water was low Cl/SO₄ ratios in the groundwater. Previous studies have documented the vertical migration of brines into meteoric groundwater along growth faults that intersect the geopressured zone. This study corroborates these findings. We estimate that only about 1.5% to 3% mixture of brines is sufficient to produce the TDS concentrations between 1,000 and 1,500 ppm that commonly exist within the down-gradient regions of the Chicot and Evangeline aquifers.

Thermogenic gases in groundwater also offer compelling evidence that upward migration is occurring along growth faults. Thermogenic gases are typically associated with coal bed and oil and gas formations and are formed at deeper depths by: (1) thermal cracking of sedimentary organic matter into hydrocarbon liquids and gas, and (2) thermal cracking of oil at high temperatures into gas. In GMA 14, 15, and 16, thermogenic methane was measured in groundwater samples. The methane was identified by mapping $\delta^2\text{H}_{\text{CH}_4}$ versus $\delta^{13}\text{C}_{\text{CH}_4}$ on a diagnostic plot for different types of methane. In the samples with higher concentrations of methane, ethane and propane gases were also present. The presence of ethane and propane with methane supports a thermogenic origin for the gases. The source of the thermogenic methane is the geopressured aquifers of the Texas Gulf Coast, where substantial quantities of methane are contained within Tertiary sediments that exhibit abnormally high temperature and pressure gradients.

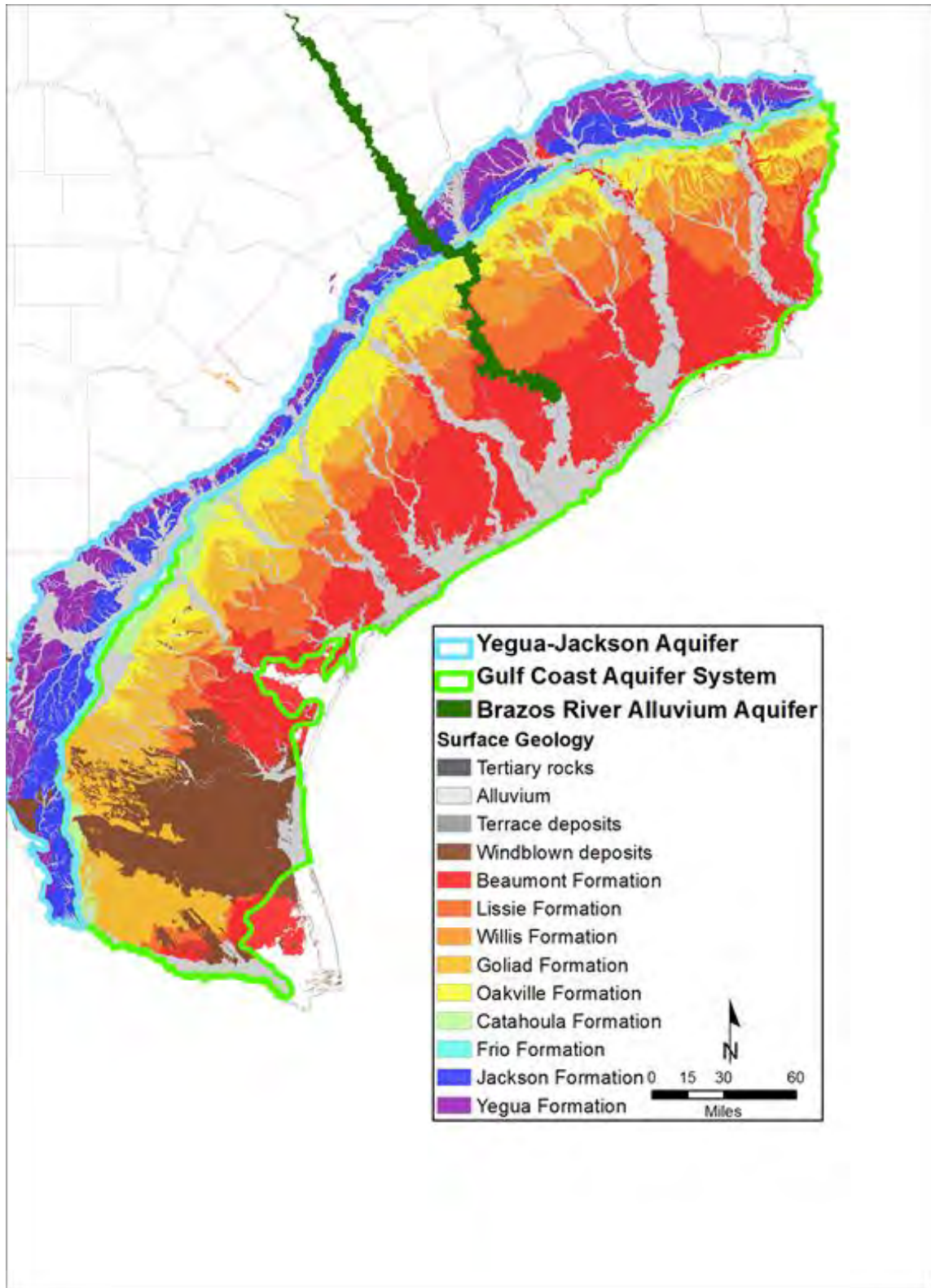


Figure 1 Map of the Texas Gulf Coast showing the outcrops of the Yegua-Jackson Aquifer, the Gulf Coast Aquifer System and the Brazos Alluvium Aquifer.

1.0 Introduction

The Texas Water Development Board (TWDB) staff began working on an initial prototype Groundwater Availability Model (GAM) in 1999 for the Hill County portion of the Trinity Aquifer. Funding for the GAM Program by the Texas Legislature began in 2001 due to the initial success of the Hill County Trinity Aquifer GAM. The objective of the GAM program is to provide reliable, timely data on groundwater availability to the citizens of Texas to ensure adequacy of water supplies. One of the goals of the GAM Program is to develop and update GAMs for the nine major and the 21 minor aquifers in Texas.

The Gulf Coast Aquifer System is one of the major aquifers in Texas. The aquifer system is the primary source of groundwater for three Groundwater Management Areas (GMAs) along the Gulf Coast: GMA 14 (northern Gulf Coast), GMA 15 (central Gulf Coast), and GMA 16 (southern Gulf Coast). In 2005, the 79th Texas Legislature mandated that the groundwater conservation districts (GCDs) evaluate and develop desired future conditions (DFCs) for aquifers within their groundwater management areas. After a GMA has adopted its DFCs, the TWDB uses the GAMs to estimate the modeled available groundwater (MAG) associated with the DFCs. According to Texas Administrative Code Section 36.108, MAG is the amount of water that may be produced on an average annual basis to achieve a desired future condition. In addition to being used to calculate MAG, the GAMs are also used by the TWDB to calculate water budgets for aquifers and the amount of groundwater volume that is recoverable storage. Furthermore, GCDs often use GAMs to help develop management plans, evaluate well permits, and develop long-term water management strategies. One of the purposes of updating each GAM as new information becomes available is to help ensure that the best science information, technology, and practices are available to GCDs and GMAs.

A key objective of this study is to collect, review, and analyze measurements of geochemistry in the Gulf Coast Aquifer System and the Brazos River Alluvium Aquifer with the purpose of evaluating and improving, where appropriate, the conceptual groundwater flow model for the Gulf Coast Aquifer System and for the GAMs used by GMA 14, 15, and 16.

1.1 The Texas Gulf Coast Aquifer System and the Brazos Alluvium Aquifer

The Texas Gulf Coast is a part of the Gulf of Mexico, which is a small semi-enclosed ocean basin surrounded by continental shelves and coastal plains (Bryant and others, 1991). The northwest portion of the Gulf of Mexico includes the major sand and sandstone aquifer systems that include the Texas Gulf Coast Aquifer System (Williamson and Grubb, 2001; Chowdhury and Turco, 2006). Table 1-1 provides a simplified stratigraphic and hydrogeologic chart of the Texas Gulf Coast Aquifer System.

As shown in Table 1-1, the Gulf Coast Aquifer System consists of the Catahoula Formation and younger formations. Underlying the Catahoula Formation is the Yegua-Jackson Aquifer. For this study, the stratigraphic boundary between the Jackson and Catahoula formations is defined by Knox and others (Knox and others, 2007). Figure 1-1 shows the outcrops of the two aquifers.

As shown in Figure 1-1, the Brazos River Alluvium Aquifer overlies the Gulf Coast Aquifer System in Waller, Austin, and Fort Bend counties. The Brazos River Alluvium Aquifer consists of fine to coarse sand, gravel, silt, and clay deposited by the Brazos River (Cronin and Wilson, 1967). The adjacent terrace alluvium is not an appreciable source of water and thus not considered part of the aquifer.

1.1.1 Stratigraphy of the Gulf Coast Aquifer System

Prior to the 1980s, lithofacies correlations were the most common technique to define stratigraphy. Lithostratigraphic correlations rely on the interpretation from well logs of formation lithologies and boundaries between different lithologies (e.g., mud on sand) and then correlating those boundaries between wells. Since the 1980's, an improved understanding of depositional processes has shown that lithostratigraphic correlations are less reliable for characterizing the continuity and size of a formation than are chronostratigraphic correlations.

Chronostratigraphic correlations focus on identifying clay-dominated flooding surfaces of the same age that form the boundaries of episodes that deposit the coarse sediment of an aquifer. The stratigraphic surfaces for this study will use the chronostratigraphic correlations developed by Young and others (2010, 2012a). Young and others (2010, 2012a) base their technical approach on the correlation and sequence stratigraphic concepts used by the Gulf Basin Depositional Synthesis Project (GBDS) and the LCRA-SAWS Water Project (LSWP).

Final – Hydrogeochemical Evaluation of the Texas Gulf Coast Aquifer System and Implications for Developing Groundwater Availability Models

Table 1-1 Simplified stratigraphic and hydrogeologic chart of the northwestern Gulf of Mexico basin, Texas coastal zone (Galloway and others, 1991; Sharp and others, 1991).

ERA	Period		Epoch	Age (M.Y.)	Stratigraphic Unit	Dominant Lithology	Hydrogeologic Unit		
Cenozoic	Quaternary		Holocene	0.02	Alluvium	sand	Alluvium	Gulf Coast Aquifer System	
			Pleistocene		Beaumont	sand	Chicot Aquifer		
	Tertiary	Neogene	Pliocene	1.8 5.3	Lissie/Alta Loma	sand			Evangeline Aquifer
			Miocene		Goliad	sand	Burkeville Aquitard		
			Paleogene	Oligocene	23.9	Fleming/Lagarto	mud		Jasper Aquifer
						Catahoula/Frio/Anahuac	sand and mud		aquifer and aquitard
		Eocene		33.9	Catahoula/Vicksburg	mud and sand	Aquitard and aquifer		
					Jackson	sand and mud	Yegua-Jackson Aquifer		
				Yegua	sand and mud				
				Sparta	sand	Queen City-Sparta Aquifer			
		Queen City	sand and mud						
		Paleocene	55.8	Reklaw	mud	aquitard			
	Upper Wilcox/Carrizo			sand	Carrizo-Wilcox Aquifer				
	Middle Wilcox			mud					
			Lower Wilcox/Simsboro	sand and mud					
		Midway	65.5	mud	aquitard				
Mesozoic	Cretaceous	Upper	145.5		carbonate				
		Lower		Edwards	carbonate	Edwards (BFZ) Aquifer			
	Jurassic	Upper	201.6		carbonate				
		Middle		Louann salt	evaporite	salt domes			
	Triassic								

The GBDS project was conducted by the Texas Bureau of Economic Geology and was funded by a consortium of petroleum companies to characterize the Cenozoic depositional history of the Gulf of Mexico Basin. Among the key papers that explain the concepts and methods used by the GBDS project are Galloway (1989), Galloway and others (2000), and Galloway (2005). The LCRA-SAWS Water Project (LSWP) was conducted by the Lower Colorado River Authority and it focused on modeling groundwater in the Chicot and Evangeline Aquifers across a 10-county region in the Lower Colorado River Basin. Among the key papers that describe the LSWP study are Knox and others (2006) and Young and Kelley (2006).

Young and others (2010, 2012a) defined 10 geological units in the Gulf Coast Aquifer System. The Chicot Aquifer includes, from the shallowest to deepest, the Beaumont and Lissie Formations of Pleistocene age and the Pliocene-age Willis Formation. The Evangeline Aquifer includes the upper Goliad Formation of earliest Pliocene and late Miocene age, the lower Goliad Formation of middle Miocene age, and the upper unit of the Lagarto Formation (a member of the Fleming Group) of middle Miocene age. The Jasper Aquifer includes the lower Lagarto unit of early Miocene age, the early Miocene Oakville sandstone member of the Fleming Group, and the portions of the Oligocene-age Catahoula Formation.

Young and others (2010, 2012a) did not define the Catahoula Formation for their study. In order to define their base of the Jasper Aquifer, they used the lower of the following two surfaces. One of these surfaces was the base of the Jasper Aquifer defined by the Source Water Assessment Program (Strom and others, 2003) and the other surface was the base of Oakville Formation. In addition, Young and others (2010, 2012a) did not explicitly define a Burkeville Confining Unit. As defined by Baker (1979) and the SWAP database (Strom and others, 2003), the Burkeville Confining Unit is a lithostratigraphic unit delineated by correlating clay units from different formations. Young and others (2010, 2012a) selected the Middle Lagarto Formation as the geologic unit that best represented the properties of a Burkeville confining unit for the entire Texas Gulf Coast. A review of the lithologic profiles of the Middle Lagarto reveals large areas, particularly in up-dip areas of the Gulf Coast, where sands are prevalent.

1.1.2 Stratigraphy of the Yegua-Jackson Aquifer

This report uses the nomenclature and surfaces for the Yegua-Jackson Aquifer developed by Knox and others (2007). Knox and others (2007) uses a chronostratigraphic approach for

delineating surfaces between geological formations that is consistent with those used by Young and others (2010, 2012a). From 2004 to 2010, Mr. Paul Knox was the primary stratigrapher responsible for developing the surfaces used to define the geological formations in the Gulf Coast Aquifer System for the LCRA-SAWS Project (LSWP) and for Young and others (2010).

Knox and others (2007) used the four chronostratigraphic units as the basis for defining four operational aquifer units within the Yegua-Jackson Aquifer: the Lower Yegua Layer, the Upper Yegua Unit, the Lower Jackson Layer, and the Upper Jackson Unit. For this study, the top of the Upper Jackson Unit is used to define the base of the Catahoula. A potential concern with this association is that for some regions of the Gulf Coast, Knox and others (2007) had sparse well control points near the down dip extent of their study. In the vicinity of Montgomery County, a study (LBG Guyton and INTERA, 2012) defined the chronostratigraphy of the Catahoula Formation using significantly more well logs than used by Knox and others (2007). The base of the Catahoula as determined by Guyton and INTERA was similar to that produced by Knox and others (2007) but it was often offset by several hundred feet. This comparison serves as a reminder that chronostratigraphic surfaces in this report for both the Yegua-Jackson and the Gulf Coast Aquifer System are dependent on the density of geophysical logs used for control points. As such, the surfaces should be considered as works in progress that should be continually reviewed and updated as new information becomes available.

1.1.3 The Brazos River Alluvium Aquifer

The Brazos River Alluvium Aquifer comprises floodplain alluvium that consists of fine to coarse sand, gravel, silt, and clay deposited by the Brazos River (Cronin and Wilson, 1967). The adjacent terrace alluvium is not an appreciable source of water and thus not considered part of the aquifer. Cronin and Wilson (1967) describe the composition of the floodplain alluvium as varying from place to place, with beds or lenses of sand and gravel that pinch out or grade laterally into vertically finer or coarser material. In general, the finer material is in the upper part of the aquifer, and the coarser material is in the lower part. The aquifer is under water-table conditions in most places and is used mainly for irrigation (HDR Engineering, Inc., 2001). The water table generally slopes toward the Brazos River, indicating that the river is a gaining stream in most places.

Figure 1-1 shows the areal extent of the Brazos River Alluvium Aquifer that overlies the Gulf Coast Aquifer System. The base of the aquifer is defined by the surface developed by Shah and others (2007). The thickness of the Brazos River Alluvium Aquifer ranges from negligible to 168 feet. Shah and others (2007) identified the contact between the alluvium and the underlying geologic units at well sites based on lithologic or geologic units picked from drillers' logs, geophysical logs, or published geologic sections.

For this study, the portion of the aquifer south of the updip extent of the Catahoula Formation is of interest. For much of this area, Shah and others (2007) report that the mapped thicknesses are less reliable than most of the other areas because of the sparseness of data. Shah and others (2007) identify areas east of the Brazos River in Grimes County and east of the Brazos River in Waller County as areas with few or no control points. For these areas, Shah and others (2007) expressed concerns that their analyses may have produced anomalously large aquifer thicknesses. Shah and others (2007) indicate that areas with less reliable thickness calculations include areas near the aquifer boundary and Fort Bend County. One of the difficulties cited by Shah and others (2007) in Fort Bend County is that they had difficulty using the driller's logs to differentiate the sand and gravel of the alluvium aquifer from that of the underlying Gulf Coast Aquifer System.

1.2 Groundwater Availability Models

Groundwater Availability Models (GAMs) include comprehensive information on aquifers such as recharge, geology and how that translates into the framework of the model, rivers, lakes, and springs; water levels; aquifer properties; and pumping. The TWDB uses groundwater availability models to estimate the Modeled Available Groundwater (MAG) for each aquifer for each groundwater conservation district, as appropriate and applicable. The application of groundwater availability models to calculate MAGs is a result of House Bill 1763, which became effective in September 2005.

This report will discuss four models that have been used to calculate groundwater availability, including the Northern Gulf Coast Aquifer System GAM (Kasmarek and Robinson, 2004), the Central Gulf Coast Aquifer System GAM (Chowdhury and others, 2004), the GMA 16 Alternative Groundwater Model (Hutchison and others, 2011) and the Lower Colorado River

Basin (LCRB) model (Young and others, 2009). Figure 1-2 shows the model domains for these four models. The Northern Gulf Coast Aquifer System GAM, Central Gulf Coast Aquifer System GAMs, and the GMA 16 Alternative Groundwater Model (AGM) were used by the TWDB to calculate the MAGs for GMAs 14, 15, and 16, respectively.

During the 2010 joint planning, GMA 16 used the GMA 16 AGM (Hutchison and others, 2011). The GMA 16 AGM was built toward the end of the 2010 planning session because the Southern Gulf Coast Aquifer System GAM (Chowdhury and Mace, 2004) and the Central Gulf Coast Aquifer System GAM (Chowdhury and others, 2004) had boundary issues and neither covered the entire groundwater management area. The LCRB model (Young and others, 2009) was built as part of the LCRA-SAW Water Project to estimate the impacts of pumping up to 90,000 AFY for irrigation in Colorado, Wharton, and Matagorda counties. The LCRB has not been used by any GMA for planning purposes but it continues to be used by the Colorado GCD, Coastal Plains GCD, and Coastal Bend GCD for evaluating pumping permits and supporting water management decisions.

1.3 Technical Approach

The technical approach focuses on deconstructing the spatial distribution of chemical signatures in the Gulf Coast Aquifer System to identify relationships relevant for evaluating the conceptual flow model for the Gulf Coast Aquifer System. Our approach requires an examination of four technical areas. The first technical area is the conceptual and numerical groundwater flow models for the Gulf Coast Aquifer System. The second technical area is the geochemical database for the Gulf Coast Aquifer System including the new groundwater quality measurements performed for this study. The third technical area is the sources, chemical process, and flow mechanisms that have produced the regions of high total dissolved solids (TDS) in the Gulf Coast. The fourth technical area includes the geochemical reactions and relationships that are useful for identifying groundwater flow direction, mixing, and age.

The general conceptual flow models for the Gulf Coast have remained relatively the same for the last fifty years since the reconnaissance investigation performed by Wood and others (1963). This general framework's foundation is built on the Toth (1962, 1963, 1970) and Freeze and Witherspoon (1966, 1967, 1968) concepts of hierarchy of shallow, intermediate, and deep flow

systems as applied to a Gulf Coast Aquifer System groundwater basin. In the Gulf Coast Aquifer System, the shallow flow zone controls the majority of flow to local springs and streams; in the intermediate flow systems, the intermediate flow zone controls the majority of flow in the large river basins and to the large rivers; and the regional flow system controls the majority of the flow to the ocean. Despite having the same general conceptual flow system, the regional groundwater flow models can vary substantially in their simulated groundwater flows because of the differences in the hydrogeological conditions and aquifer properties along the Texas Gulf Coast. In addition, differences occur in simulated groundwater flows because of differences in the groundwater models' numerical construction to represent the conceptual flow system. Table 1-2 lists some of the issues associated with the conceptualization and construction of a groundwater flow model. One of the goals of the study is to provide insight and information concerning these modeling issues is by examination of the measurements of geochemistry and isotopes.

Table 1-2 Options for numerically representing conceptualization of groundwater flow of the Gulf Coast Aquifer System for GMAs 14, 15, and 16.

Conceptualization Issue	Numerical Implementation in Model
Hierarchy of flow systems	Grid cell and model layer resolution
Predevelopment Flow Condition	Steady-state flow assumptions
Recharge	Recharge cells or GHBs cells
Up-dip & bottom boundary	Location of No-flow or GHB cells
Down-dip and ocean boundary	Location of No-flow or GHB cells
Surface water-groundwater boundary	River/Stream cells or GHB cells
Aquifer Structure	Model layers
Aquifer Hydraulic Properties	Scale of heterogeneity

In order to introduce the reader to the geochemistry in Gulf Coast Aquifer System, this report provides an overview of the TWDB geochemical data and discusses the analysis of several geochemical measurements of interest. Of special interest to this study are maps and analysis of hydrogeochemical facies, the cations and anions that determine hydrogeochemical facies, total dissolved solids (TDS), chloride-bromide ratios, stable isotopes (e.g., $\delta^2\text{H}$, $\delta^{18}\text{O}$, $\delta^{13}\text{C}$), and radiogenic isotopes (e.g., $\delta^{14}\text{C}$). Table 1-3 lists several of the insights and information sought by creating these maps and/or performing the analyses.

Table 1-3 Analysis of geochemical and isotopic signatures that may provide insight into the conceptual groundwater flow model for GMAs 14, 15, and 16.

Analyses Method and/or Map	Desired Insight
Tabulated and plotted depth-average geochemical values for the Gulf Coast Aquifer System Region	Notable differences in the geochemistry of GMA 14, 15, and 16
Plotted geochemistry along vertical cross-sections	Mixing or lack of mixing between and within aquifers at a local and intermediate scale
Plots of hydrogeochemical facies, chloride values, and sand and salinity profiles along vertical cross-sections	Direction of groundwater flow and evidence of a “high-flow” region within or between aquifers
Analyses where changes occur with ion concentrations and ratios and with the locations for geological and anthropogenic features	Cause-and-effect relationships between the presences of some salt domes, growth faults, and anthropogenic contamination and changes in groundwater geochemistry
Analysis of the hydropressure and brine concentrations in the Catahoula and deeper deposits	Evidence that a source of the increased total dissolved solids (TDS) near the coast is upswelling of brine
Analysis of carbon and isotope of gases such as carbon dioxide and methane	Evidence of movement along growth faults
Analysis of stable isotopes of oxygen and hydrogen	Evidence of meteoric water
Analysis of carbon stable and radioactive isotopes	Estimate of groundwater age

A key aspect of our technical approach is the ability to superimpose and visualize geochemical data, stratigraphic surfaces, lithologic profiles, and groundwater model output along the vertical cross-sections at the transect locations in Figure 1-3. The transects consist of primary and secondary groups. The primary group of transects are those numbered from 1 to 10. These transects were oriented to include isotope measurements made by the TWDB prior to 2010. The secondary group of transects were inserted between the original ten transects. Each of these nine transects were numbered according to the two original transects it lies between. Thus, transect 12 is between transects 1 and 2.

Table 1-4 lists the transects for which reverse particle tracking and water mass balances were performed using the four groundwater models previously discussed. Reverse particle tracking was performed using the USGS program MODPATH (Pollock, 1994) to estimate the groundwater age based on a quasi-steady state conditions associated with predevelopment. Water mass balances were performed using the USGS program ZONEBUDGET (Harbaugh, 1990) to estimate groundwater flow and mixing that occurs between and within the aquifers. The results of the MODPATH and ZONEBUDGET applications will be compared to estimates of groundwater age, flow direction, and mixing deduced from the analysis of the chemical data.

These types of comparisons will be one of the cornerstones for evaluation of the reasonableness of the Gulf Coast Aquifer System conceptual model and its numerical implementation manifested in the different models.

Table 1-4 The cross-sections for which reverse particle tracks and water mass balances were calculated for groundwater availability models.

GMA	Transect	Groundwater Availability Model
14	1	Northern GC GAM
	3	Northern GC GAM
	34	Northern GC GAM, LSWP Model
15	4	Northern GC GAM, Central GC GAM, LSWP Model
	45	Northern GC GAM, Central GC GAM, LSWP Model
	5	Central GC GAM, LSWP Model
	6	Central GC GAM, GMA 16 AGM
15 & 16	67	Central GC GAM, GMA 16 AGM
16	78	Central GC GAM, GMA 16 AGM
	8	Central GC GAM, GMA 16 AGM

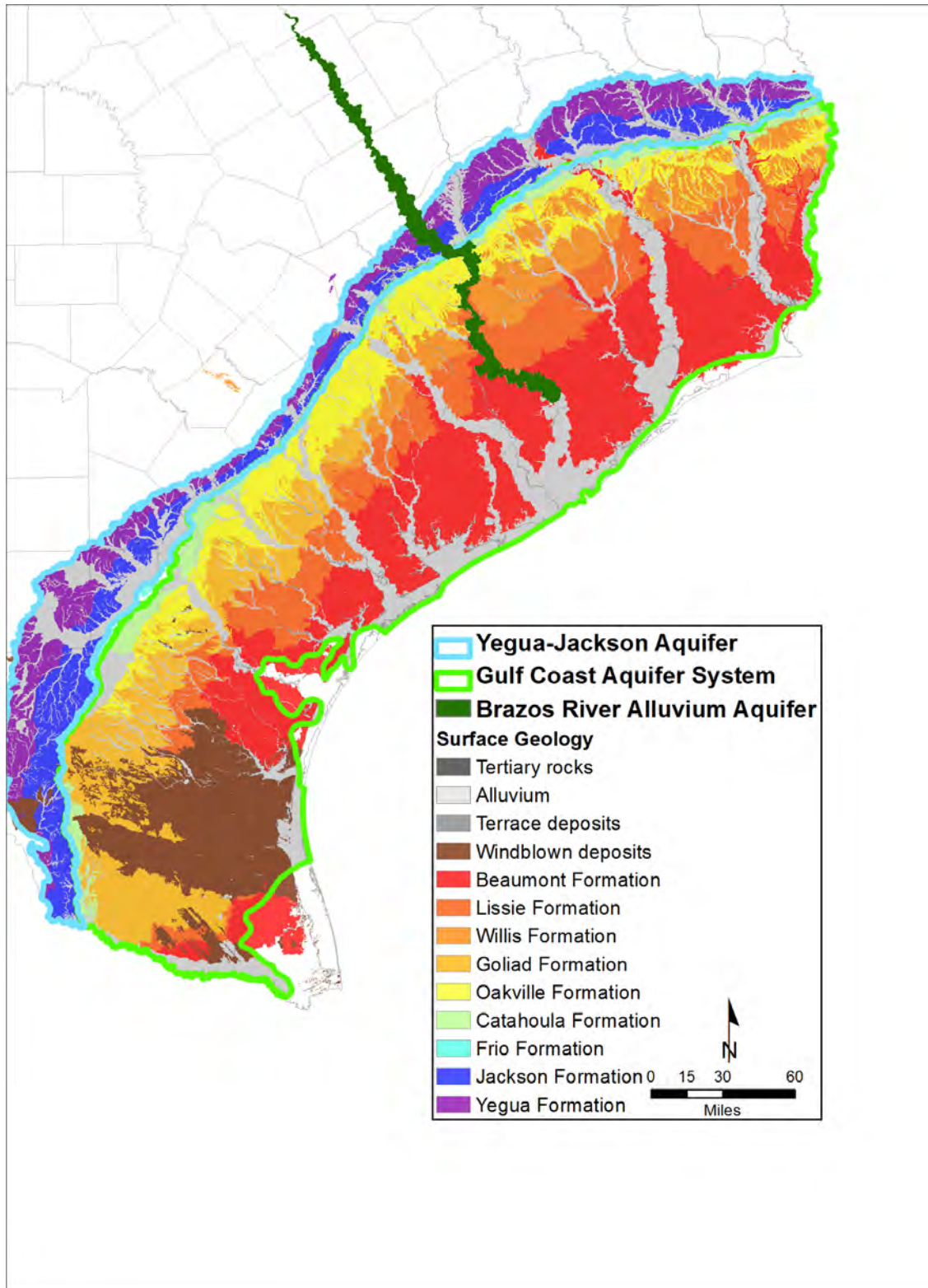


Figure 1-1 Map of the Texas Gulf Coast showing the outcrops of the Yegua-Jackson Aquifer, the Gulf Coast Aquifer System and the Brazos Alluvium Aquifer

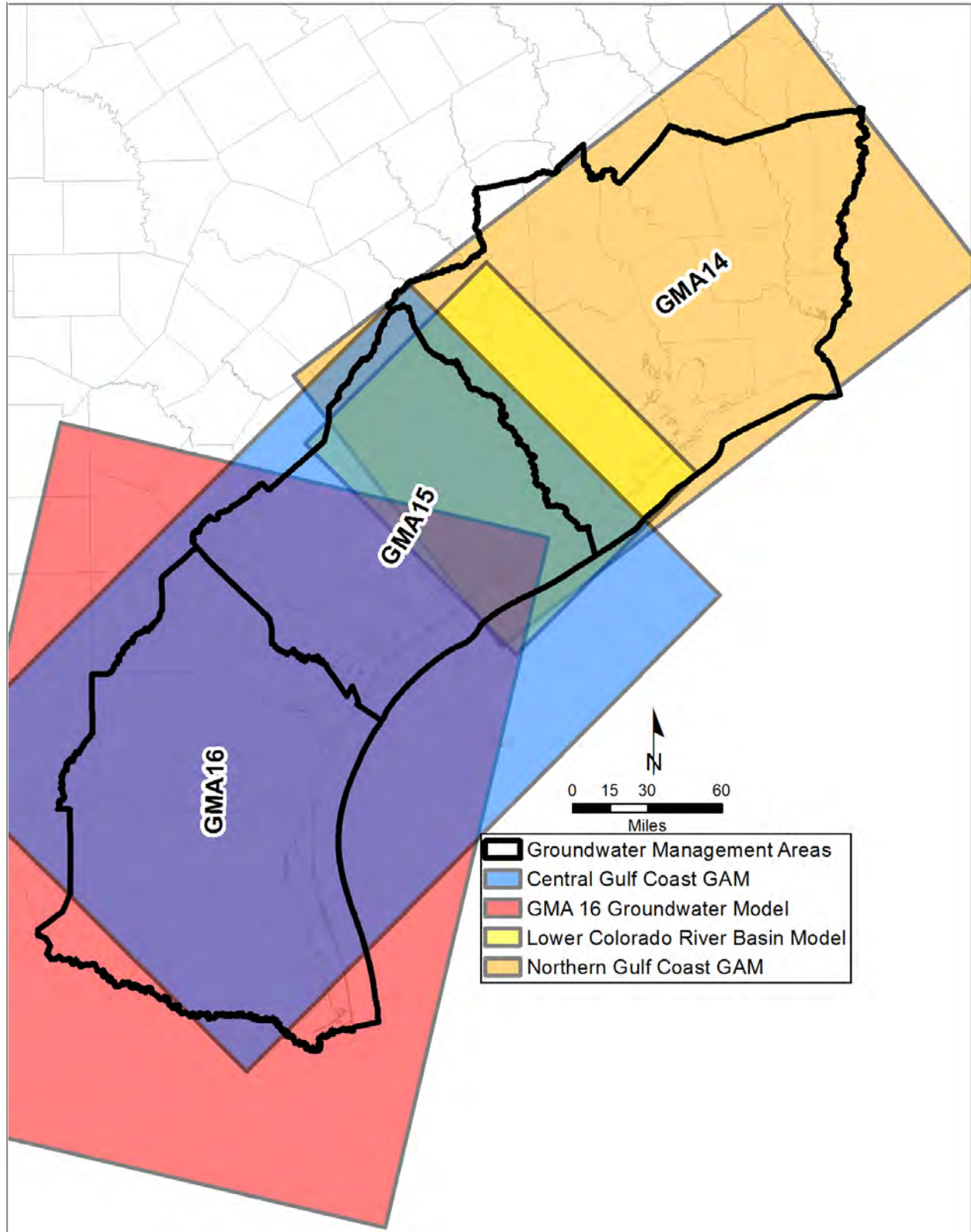


Figure 1-2 Model Domains of the groundwater models used for joint planning in GMAs 14, 15, and 16 and the LCRA-SAWS Water Project.

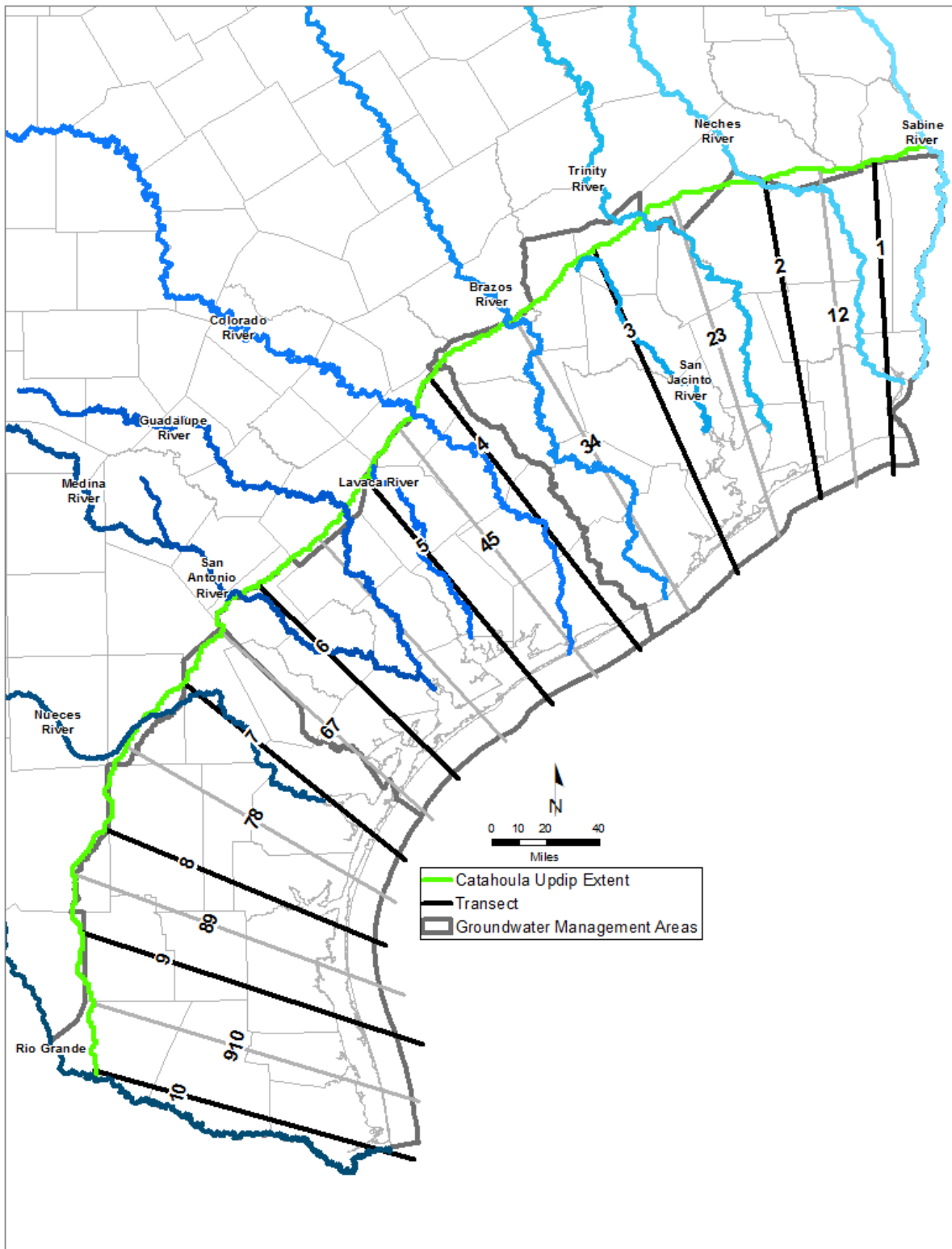


Figure 1-3 Location of the nineteen transects used to develop vertical cross-sections of geochemistry and the major rivers of Texas.

Final – Hydrogeochemical Evaluation of the Texas Gulf Coast Aquifer System and
Implications for Developing Groundwater Availability Models

This page intentionally left blank.

2.0 Gulf Coast Aquifer System

This section discusses aspects of the Gulf Coast Aquifer System hydrogeology relevant to interpreting geochemical and isotopic data to evaluate the conceptual groundwater flow model. These aspects include the following:

Depositional History – The aquifers and geologic units that comprise the Gulf Coast Aquifer System exhibit significant spatial variability in their size and composition relative to each other and themselves across the Texas coast. This spatial variability (both vertically and laterally), which can affect both groundwater flow and geochemical reactions, complicates and may prevent the transfer of findings from one area of the Gulf Coast Aquifer System to another.

Faults – Faults can hinder horizontal flow and/or provide an avenue for preferential vertical migration of gas and groundwater. If sufficient concentrations of solutes/gases move vertically along the faults, then the geochemistry of an aquifer can be altered. As a result, the potential impacts of faults on groundwater flow and the transfer of chemical mass needs to be considered as part of our chemical analyses.

Sea-level change – The conceptual model for the groundwater system presumes quasi-steady flow conditions prior to pumping in the late 1800's or early 1900's. If sea level has changed significantly over the time period in which we are interested in age dating groundwater (tens of thousands of years), then the predevelopment flow field simulated by the GAM may not adequately reflect the groundwater flow conditions under which the chemical system evolved. As such, an understanding of the timing and magnitude of sea-level change is paramount to proper comparison of groundwater age dates derived from the analyses of chemical/isotope measurements and of groundwater model output.

Meteoric and Formation Waters – The Gulf Coast Aquifer System has two primary types of groundwaters: meteoric, which are recharged by precipitation into shallow aquifers, and formation waters, which were incorporated into the strata when the sediments were originally deposited. Three hydrologic regimes occur for these two types of water in large sedimentary basins: (1) A fresh water regime comprised of meteoric water forms the uppermost groundwater regime, (2) Beneath the meteoric regime is the underlying hydrostatic regime characterized by

expulsion of formation water from sediments due to compaction. (3) In the underlying section, restricted drainage conditions at greater depths formation waters that would otherwise escape due to overburden pressures.

Hydropressure and Geopressure Zones – The occurrence of geopressure zones could cause the vertical migration of deep brines (total dissolved solids greater than 50,000 ppm) along fractures or faults to the Gulf Coast Aquifer System. Because of the high solute concentration in deep brines, the influx of a small portion into the shallow flow system is an important consideration. Moreover, because the location of the hydropressure and geopressure zones will impact the regional flow at some scale in the Gulf Coast, defining that scale of impact is important toward determining whether or not abnormal pressures should be considered as part of the conceptual flow model for the GAMs.

Paleohydrology – The use of paleohydrologic data provides the opportunity to better address issues and answer questions that cannot be satisfactorily resolved by only using information about the current hydrogeologic system.

Salt domes – Shallow salt domes have the potential to increase groundwater salinities in the Gulf Coast Aquifer System in two ways: first by direct dissolution and transport of soluble dome minerals and second by providing pathways for groundwater mixing between shallow freshwater and deep saline-water aquifers.

2.1 Depositional History

Sediments of the Gulf Coast Aquifer System were deposited in a fluvial-deltaic or shallow-marine environment (Sellards and others, 1932). Repeated sea level changes (Figure 2-1) and basin subsidence caused the development of cyclic sedimentary deposits comprised of discontinuous sand, silt, and gravel. Inland, closer to the sediment source areas, coarser fluvial and deltaic sand, silt, and clay sediments predominate, while in offshore areas they grade into mainly finer brackish and marine sediments. These deposits tend to progressively thicken toward the gulf because of subsidence of the Gulf Coast Aquifer System basin, which is caused by the weight of the sediment flow, and a sequential rise of the land surface.

The cyclic depositional processes are characterized by depositional episodes. These episodes represent periods of focused deposition and progradation of the shoreline followed by nondeposition and transgression (marine flooding) of the coastal plain (Galloway and others, 1991, 2000). The location of deposition (depocenter) shifts through time owing to geographic variations in sediment supply, which are controlled by tectonic events in the sediment source area (Winker, 1982). Figure 2-2 shows the location over time of the major depocenters from the later Eocene (the Yegua-Jackson Aquifer) to the present. The location and timing of the depocenters are potentially important to Gulf Coast Aquifer System geochemistry for two reasons. First, they control the source material and hence mineralogy of aquifer deposits. Second, they impact the overall thickness of the aquifer deposits and the size and distribution of sand and clay beds that comprise an aquifer.

Early Cenozoic (Paleogene, Table 1-1) depositional episodes in the Gulf Coast Aquifer System region were responses first to mountain building in the southern Rocky Mountains and later to explosive volcanism in West Texas and Mexico (Winker, 1982; Morton and Galloway, 1991; Galloway, 2005). In response to the large volumes of sand, silt, and clay that were delivered to the Gulf Coast Aquifer System from these regions, extrabasinal fluvial-deltaic systems developed in the Houston embayment and then in the Rio Grande embayment. Tectonic development of the Rio Grande Rift in New Mexico disrupted drainage systems feeding the Rio Grande and Houston embayments so that large extrabasinal fluvial systems began shifting northeast into the Mississippi embayment (Winker, 1982). Uplift of the Edwards Plateau along the Balcones Fault Zone in Central Texas supplied abundant Cretaceous calcareous detritus to smaller Miocene fluvial systems on the Texas Coastal Plain (Galloway and others, 1986; Morton and others, 1988). The principal middle-late Miocene fluvial-deltaic system in Texas was located on the San Marcos Arch (Figure 2-2). During the Plio-Pleistocene (Table 1-1), tectonic quiescence and high-frequency glacio-eustatic fluctuations (this time from northern hemisphere glaciation) resulted in multiple cross-cutting and superimposed alluvial valley fills and preservation of thin sequences on the Texas Coastal Plain (Blum and Price, 1998).

For this report, the structure of the Gulf Coast Aquifer System is based on Young and others (2010, 2012a). These studies were funded by the TWDB for the purpose of updating the GAMs. Figure 2-3 shows the major aquifer units and their geologic units for Transects 1 and 8 (for the

location of the transects see Figure 1-3). The Chicot Aquifer subaquifer layers include, from the shallowest to deepest, the Beaumont and Lissie Formations of Pleistocene age and the Pliocene-age Willis Formation. The Evangeline Aquifer subaquifer layers include the upper Goliad Formation of earliest Pliocene and late Miocene age, the lower Goliad Formation of middle Miocene age, and the upper unit of the Lagarto Formation (a member of the Fleming Group) of middle Miocene age. The Jasper Aquifer includes the lower Lagarto unit of early Miocene age, the early Miocene Oakville sandstone member of the Fleming Group, and a portion of the Oligocene-age Catahoula Formation. In Figure 2-3, and as for other figures in this report, the base of the Catahoula Formation and the Yegua-Jackson Aquifer are from Knox and others (2007).

Figures 2-3 illustrates the type of variability that exists among the hydrogeologic units in the Gulf Coast Aquifer System. One important type of variability is aquifer size and/or thickness. In Transect 1 the Chicot aquifer is about twice as thick as the Chicot aquifer in Transect 8. In Transect 1, the Catahoula Formation also comprises about 40% of the upper 1000 feet of the Jasper Aquifer, whereas in Transect 8, the Catahoula Formation occupies about 10% of the upper 1000 feet of the Jasper Aquifer. Another importance type of variability is outcropping and subcropping. In Transect 8, the Evangeline Aquifer outcrops for about 20 miles. In Transect 1, however, the Evangeline Aquifer does not outcrop because it was significantly truncated during the deposition of the Chicot Aquifer. As a result, the Evangeline Aquifer in Transect 8 subcrops into the base of the Chicot at elevations below -500 ft msl. As a result of the different thicknesses/depths and exposures to precipitation, atmospheric gases, and vegetation, the chemistry of the Evangeline at Transect 1 and 8 could be significantly different.

2.2 Faults

Active faults in the Gulf Coast Aquifer System typically display mappable surface expressions. Lineations are straight, lengthy surface features that, in part, represent the surface traces of faults and locally coincide with boundaries between zones of differential subsidence (Kreitler, 1976). Over 7,000 miles of lineations have been mapped on the Texas Coastal Plain (Fisher and others, 1972, 1973; McGowen and others, 1976a, 1976b). Lineations are identified by color variations on aerial photographs and are coincident with geomorphic features, such as rectilinear drainage patterns and vegetation changes (Kreitler, 1976). On the Texas Coastal Plain, the most detailed

investigations of shallow faulting have been conducted in the Houston area (Harris County). More than 300 active surface faults with a total length exceeding 300 miles have been mapped in the Houston metropolitan area (Holzer, 1984; Shah and Lanning-Rush, 2005) (Figure 2-4).

One of the most prevalent fault types in the Gulf Coast Aquifer System are growth faults. Growth faults are syndepositional normal faults that form mainly by gravitational failure during rapid sediment loading along an unstable shelf margin and upper slope (Winker and Edwards, 1983). Syndepositional means that sedimentation (deposition) is occurring at the same time as faulting. A consequence of syndeposition is that erosion of the upthrown block, which is typically on the landward side, provides coarse material that is deposited immediately adjacent to the fault on the downthrown side (see Figure 2-5) and thereby creating a preferential zone for vertical groundwater migration. Growth faults are not isolated surfaces but instead are zones of sediment deformation that commonly enhance vertical flow and impede horizontal groundwater flow. It is believed that growth faults propagate upward through thin sedimentary cover as a series of minor, en echelon, faults that constitute a single mapped fault (Crans and others, 1980; Durham, 1971; Roland and others, 1981).

Figure 2-6 shows the major faults mapped in the Gulf Coast Aquifer System by the Bureau of Economic Geology. Abundant growth faults at depth and lineations on the land surface suggest that most if not all of the sand bodies in the Gulf Coast Aquifer System are intersected by faults. Because the downthrown fault block is topographically lower than the upthrown block, greater thicknesses of sediment are deposited on the downthrown block. Maximum displacement (several thousand feet) on growth faults occurs in deep formations, such as the Wilcox and Frio, and decreases upward. In the Gulf Coast Aquifer System, maximum fault displacements are a few hundred feet, and surface expressions of active faults are generally only a few feet (Verbeek, 1979).

Coast-parallel growth fault zones mark shelf-margin positions of major Cenozoic depositional episodes, which get younger basinward (Figure 2-6). Antithetic faults having opposing sense of movement (downward displacement on the landward side) locally accompany down-to-the-coast growth faults forming complete fault-bounded blocks that are downthrown on all sides.

Faults in the Gulf Coast Aquifer System have the potential to impact groundwater flow in several ways. As discussed in Section 5, growth faults can enhance vertical flow by providing vertical pathways for preferential transport. In addition, growth faults and other faults can hinder horizontal flow by offsetting sand units and restricting the continuity of sands across the fault zone. Kreitler and others (1977) demonstrate the latter for an antithetic fault in Pasadena, Texas, south of the Houston Ship Channel. Closely spaced borings across the fault show that eight sand units have been offset by the fault. The percent offset (the ratio of displacement to bed thickness) varies from 40% to complete offset of the same bed. Kreitler and others (1977) show significant and abrupt changes in water quality and the base of fresh water across the fault. Figure 2-7 shows that the change in the base of fresh water is coincident with the faulting – the fault greatly reduces the flow and permitted the base of fresh water lens in Galveston County to rise to 1,000 feet. Kreitler and others (1977) conclude that the brackish waters on the down-dip side of the fault are either seawater or deep formation water that has recently intruded, but are not residual waters of deposition that have yet to be flushed from the sediments.

Galloway and others (1977) also provides detailed water quality and lithology parameters derived from numerous logs in the Catahoula Formation to demonstrate that a fault zone is significantly restricting horizontal flow. Galloway and others (1977) conclude that the fault is affecting water quality and groundwater flow several miles up dip of the fault zone.

2.3 Sea-Level History

The location of the shore line and the elevation of the sea level in the Gulf Coast Aquifer System has been the subject of several papers (Shepard, 1960; Redfield, 1967; Emery and Garrison, 1967; McFarland, 1961; Balsillie and Donoghue, 2004; Donoghue, 2011). Among the reasons for the continued research are the unknowns associated with the Earth's differential isostatic response to the waxing and waning of the ice sheets since the last maximum glaciation. As ice sheets grew and melted during the last glaciation cycle, the effective sea-level change at any one point on the globe is not simply a function of the volume of meltwater added or taken away from the ocean (Bloom, 1967; Walcott, 1972; Milne and others, 2002). As a result, there is a need to account for the Earth landscape shifts in response to the migration of mass from the polar caps to the oceans. Some researchers have tried to model numerically this change (Peltier and others,

1978; Lambeck and others, 2003), while others have attempted to map carefully shoreline markers (Simms and others, 2007; Balsillie and Donoghue, 2004).

Balsillie and Donoghue (2004) were among the first to use geologic indicators and statistics to quantify the magnitude and uncertainty of the sea-level change in the Gulf of Mexico during the last 20,000 years. They integrated twenty-three databases of paleo-shoreline markers based on ^{14}C dating. The analysis produced 353 ^{14}C -date sea-level indicators to produce a 7-point floating average curve shown in Figure 2-8 that reflects the historical change in sea level. By using this curve and the bathymetry of the Gulf Coast of Mexico, the approximate location of the Texas shoreline during the last 20,000 years in Figure 2-9 was created.

Figures 2-8 and 2-9 show that although the shoreline and sea level have been relatively constant the last 6,000 years, the sea level was very different 20,000 years ago. At 20,000 years ago, the sea-level was approximately 400 feet lower than it is currently and the shoreline location was between 100 miles to 150 miles offshore from its present day location. This amount of sea level change would significantly impact groundwater flow in the Gulf Coast Aquifer System by increasing the travel distance required before groundwater can be discharged to the ocean, by changing the land area that provides recharge to the aquifer, and by altering the direction and magnitude of the hydraulic gradient.

2.4 Meteoric and Formation Waters

The Gulf Coast Aquifer System has two primary types of groundwaters: meteoric, which are recharged by precipitation into shallow aquifers, and formation waters, which were incorporated into the strata when the sediments were originally deposited (Kreitler, 1979). Three hydrologic regimes occur for these two types of water in large sedimentary basins (Kreitler and Richter, 1986): (1) A fresh water regime comprised of meteoric water (which is water derived from precipitation) forms the uppermost groundwater regime. Within this regime, surface waters infiltrate permeable strata and groundwater flow is directed toward the basin center. In the Gulf Coast, depths to the lower boundary of the meteoric water varies from a few hundred feet to a few thousand feet below land surface. (2) Beneath the meteoric regime is the underlying hydrostatic regime characterized by expulsion of water from sediments due to compaction. Hydraulic connection between the hydrostatic and meteoric sections prevents excessive pressure buildups within the hydrostatic zones. The waters within the saline hydrostatic zone generally

have been assumed to be original formation waters or at least several million years old and hydrologically static (Kreitler and Richter, 1986). (3) In the underlying section, restricted drainage conditions at greater depths hold fluids that would otherwise escape due to overburden pressures. This regime is oftentimes called the overpressured or geopressured zone. In the Gulf Coast, the overpressured system includes sequences of thick shales. These overpressured shales are slowly compacting as a result of continuous sedimentation, thereby expelling pore fluids in to shallower hydrostatic section. Extensive growth faulting and deltaic sedimentation have compartmentalized sand body distribution; lateral fluid movement in the basin is restricted. Growth faults are likely pathways for upward migration of saline waters into the shallower section (Kreitler, 1989).

2.5 HydroPressured and Geopressured Zones

Hydrostatic fluid pressures are those in which the fluid pressure at any depth is due to the overburden weight of the overlying fluid. Hydrostatic fluid-pressure gradients range between 9.8 and 10.5 KPa/m, (0.433 to 0.465 psi/ft) and increase with depth according to the specific weight of water, whose density increases in increases with salinity. Lithostatic pressure is the pressure due to the weight of the entire overburden (fluid plus subsurface matrix). Fluid pressures generally cannot exceed lithostatic, as fluid pressures in excess of lithostatic cannot be contained by the total overburden weight. Fluid pressures in excess of hydrostatic are termed overpressured or geopressured.

Figure 2-10 shows a generalized pattern of fluid pressure for the Gulf of Mexico basin sediments. The figure shows that the hydrostatic zone ends at depths of 6,000 feet and that after a transition zone of a few thousand feet, a geopressure zone begins at 9,000 to 10,000 feet. The hydrogeologic characteristics of the geopressured zone include: (1) fluid-pressure/depth ratios $> \sim 16$ MPa/km that can approach the ratio for lithostatic load; (2) formation water with salinity typically much greater than that of seawater; and (3) major oil and gas fields (Galloway and others, 1983; Bethke and others, 1988; Land and Macpherson 1992; Kosters and others, 1989).

The existence of an overpressured system is an indication that the rate of pressure generation is sufficiently high so as to maintain abnormal pressures in the pressures of low-permeability rocks for substantial periods of geologic time. Along the Texas Gulf Coast, geopressure is thought to

result from a combination of: (1) rapid burial of uncompacted sediments; (2) conversion of bound water to pore water from the temperature-controlled mineralogic phase change of smectite to illite; and (3) presence of low-permeability seals that prevent discharge of fluid and dissipation of fluid pressure (Bethke 1986; Harrison and Summa 1991).

Regional variations exist in the pressure pattern. Onshore, the transitional zone from the normally pressured to geopressured sediments is abrupt, often occurring over a depth interval of few hundred meters. Onshore geopressured sediments may not be encountered at depths shallower than 3 to 4 kilometers. Offshore sediments may be found in sediments as shallow as 1.5 kilometers. Facies distribution also tends to control hydrostatic and geopressured zones. Massive fluvial sands commonly have near normal fluid pressure as sands have good lateral continuity allowing pressures to be dissipated rapidly updip. Interbedded sands and shales typical of nearshore marine, deltaic coastal plain environments often show normally pressured sands and overpressured shale. Growth faults may further impede pressure dissipation and thus cause fluvial and marine sands downdip of the faults to be overpressured (Harrison and Summa, 1991). Even in sand-rich sections fault movement can further create shale smear zones that laterally confine geopressured blocks. The low-permeability seal of shale-bounded or shale-smear growth faults is critical for development and preservation of geopressured conditions in the Gulf of Mexico Basin; geopressure would have bled off without bounding seals (Bethke 1986). The updip limit of the geopressured zone in each Cenozoic progradational package generally occurs in shale-bounded growth faults and thick shale sections (Fig. 2-11).

2.6 Paleohydrology

Harrison and Summa (1991) use two-dimensional numerical modeling of groundwater from Jurassic to present time to demonstrate that geopressures in the Gulf Coast Aquifer System basin are primarily a result of compaction disequilibrium. Their modeling shows that the requirements for compactional geopressures to be developed are: (1) low permeability sediments, (2) thick shale sequences, and (3) sedimentation rates of >1 mm/yr for pressures approaching lithostatic gradients and >0.1 mm/yr for moderate overpressure developments. Harrison and Summa (1991) state that the paleohydrology of the Gulf of Mexico basin and the evolution of geopressures can be divided into three stages.

In the first stage from the Jurassic to the early Tertiary times, the basin was characterized by circulating waters of meteoric origin, driven into the basin by topographic drive and re-enhanced by eustatic falls in sea levels. During these times, low sedimentation rates (less than 0.1 mm/yr) were prevalent. Abnormal pressures were restricted to the very deepest parts of the basin beyond the shelf margin. In the second stage, beginning in the Eocene and continuing through the Oligocene, sediment accumulations rates increased, due in part to the Oligocene fall in sea level (Haq and others, 1987). As a result, geopressures developed beneath the major depocenters related to the positions of the ancestral Mississippi and the Rio Grande river systems. Sediments overlying these cores had only slight amounts of overpressuring, which was, however, adequate to begin to restrict the migration of topographically driven water, reducing the basinward extent of the meteoric regime. The third stage began in the late Miocene times and continues to the present day. A sharp increase in the rate of sediment accumulation in the northern Gulf basin resulted in widespread development of geopressed sediments and the concomitant restriction in the distribution of near normally-pressured sediments and water of meteoric origin.

Harrison and Summa (1991) correctly predict the distribution of meteoric water and geopressures in the Gulf Coast Aquifer System basin for present day conditions. The predicted depth of freshwater incursion, based on the calculated limit of flow in the basinward direction, matches the distribution of salinities less than 35,000 mg/L total dissolved solids (TDS) provided by Wesselman (1985). Using their model, Harrison and Summa (1991) show that falls in sea level effectively enhance topographic drive to groundwater flow, allowing meteoric water to infiltrate greater depth. For example, Figure 2-12 shows the change in the location of the meteoric water that occurs in the Miocene with a 200 meter drop in sea level. The figure shows that water of meteoric origin is predicted to move 75 km (45 miles) for both the Wilcox and the base of the Vicksburg (Catahoula Formation).

By analogy to their results in Figure 2-12, Harrison and Summa (1991) state basin incursion of meteoric water should occur for every sea level fall during the sedimentary history of the Gulf Basin. Similar studies to of Harrison and Summa (1991), have been performed by Meisler and others (1985) who show that along the Atlantic Coast of the United States, the lowering of the sea level during the last glaciation increased the downward migration rate of meteoric water toward the coast. As a result of this migration thousands of years ago, the current salinity

distribution in the transition zone between meteoric and sea-water is not in equilibrium and is reflective of a sea-level that is 50 to 100 feet lower. In addition Meisler and others (1985) show that the relatively thick transition zone between fresh and seawater is largely due to the changes in sea-level elevations.

2.7 Salt Domes

Salt domes are common geologic features along the upper Texas Coast and in southwest Louisiana. In the Texas part of the northern Gulf Coast Aquifer System, there are 63 salt domes that are less than 15,000 feet deep (Figure 2-6). An additional 17 salt domes at similar depths are located in southwest Louisiana within 60 miles of the Texas border. Shallow salt domes have the greatest potential to affect groundwater quality. There are 38 shallow salt domes in the Gulf Coast Aquifer System in Texas that range in depth from 0 (land surface) to 1,500 feet (Figure 2-6, Table 2-1). The average depth of these shallow Texas salt domes is 585 feet.

Salt domes typically include three elements: salt stock, cap rock, and surrounding uplifted sediments. The core of a salt dome forms a vertically elongate, cylindrical stock, consisting of 90 to 99 percent crystalline rock salt (halite). Salt-dome crests are generally one to three miles in diameter. Cap rock composed of sulfate and carbonate minerals commonly overlies the crest of the salt stock and drapes down the uppermost flanks (Figure 2-13). Cap rock formation results from salt dissolution. Anhydrite (calcium sulfate), the main impurity in the salt stock, forms a residual accumulation at the dome crest. Commonly, a thin layer of loose, sand-size anhydrite crystals directly overlies the top of the salt. As salt continues to dissolve and more anhydrite accumulates, it compacts and recrystallizes, forming the lower part of the cap rock (Figure 2-13). Circulating groundwater converts anhydrite into gypsum (hydrous calcium sulfate), and sulfate-reducing bacteria convert anhydrite into calcite (calcium carbonate), and to a lesser extent, native sulfur and metallic sulfides (Bodenlos, 1970; Kyle and Price, 1986). Thus, the upper part of the cap rock is typically composed of gypsum and calcite. Cap rocks are direct evidence for dissolution of salt by groundwater.

Final – Hydrogeochemical Evaluation of the Texas Gulf Coast Aquifer System and
Implications for Developing Groundwater Availability Models

**Table 2-1 Salt Domes Located Within 15,000 feet of the Land Surface in the Texas Gulf Coast.
(data from Ewing, 1990)**

Salt Dome Name	Land Surface (ft, msl)	Depth(ft) to Cap	Depth (ft) to Salt	Aquifer at Dome Top	Salt Dome Name	Land Surface (ft, msl)	Depth (ft) to Cap	Depth (ft) to Salt	Aquifer at Dome Top
ALLEN	5	760	1380	Chicot	LONG POINT	75	550	930	Chicot
ARRIOLA	40	3930	3930	Deep	LOST LAKE	5	3275	5430	Evangelina
BARBERS HILL	75	350	1000	Chicot	MANVEL	55	11400	11400	Deep
BATSON	80	1080	1400	Evangelina	MARKHAM	55	1350	1420	Chicot
BIG CREEK	80	450	600	Chicot	MCFADDIN BEACH	0	1410	2600	Chicot
BIG HILL	30	200	1300	Chicot	MILLICAN	300	4890	5170	Deep
BLUE RIDGE	85	143	230	Chicot	MOCA	500	6365	6365	Deep
BOLING	75	380	975	Chicot	MOSS BLUFF	35	625	1100	Chicot
BRENHAM	300	700	1834	Jasper	MYKAWA	50	7100	7100	Deep
BRYAN MOUND	10	680	1067	Chicot	NASH	55	620	950	Chicot
CEDAR POINT	0	10300	10300	Deep	NORTH DAYTON	85	580	800	Chicot
CLAM LAKE	0	8200	8200	Deep	ORANGE	10	7120	7120	Deep
CLAY CREEK	250	1400	2400	Deep	ORCHARD	110	285	369	Chicot
CLEMENS	13	600	1400	Chicot	PALANGANA	430	120	420	Evangelina
DAMON MOUND	110	0	530	Chicot	PESCADITO	680	14500	14500	Deep
DANBURY	20	5000	5000	Jasper	PIEDRAS PINTAS	375	830	830	Evangelina
DAVIS HILL	100	800	1200	Evangelina	PIERCE JUNCTION	60	730	950	Chicot
DAY	250	2710	3200	Deep	PORT NECHES	5	6950	6950	Deep
DILWORTH RANCH	290	7650	7650	Deep	RACCOON BEND	150	11000	11000	Deep
ESPERSON	55	6000	6000	Deep	RED FISH REEF	0	15200	15200	Deep
FANNETT	15	740	2000	Chicot	SAN FELIPE	120	3160	4200	Deep
FERGUSON XING	220	3820	4040	Deep	SAN LUIS PASS	0	193	400	Chicot
GULF	20	825	1100	Chicot	SARATOGA	90	1500	1900	Evangelina
GYP HILL	130	0	986	Chicot	SOUR LAKE	50	500	720	Chicot
HANKAMER	35	7535	7580	Deep	SOUTH HOUSTON	35	4406	4406	Jasper
HAWKINSVILLE	10	95	600	Chicot	SOUTH LIBERTY	20	320	480	Chicot
HIGH ISLAND	20	150	1100	Chicot	SPINDLETOP	20	700	1200	Chicot
HOCKLEY	170	76	1000	Chicot	STRATTON RIDGE	10	850	1308	Chicot
HOSKINS MOUND	20	574	1070	Chicot	SUGARLAND	65	3450	4280	Jasper
HULL	75	260	600	Chicot	THOMPSON	55	9315	9315	Deep
HUMBLE	75	700	1200	Chicot	WEBSTER	30	10500	10500	Deep
KITTRELL	300	2990	3855	Deep	WEST COLUMBIA	30	740	790	Chicot

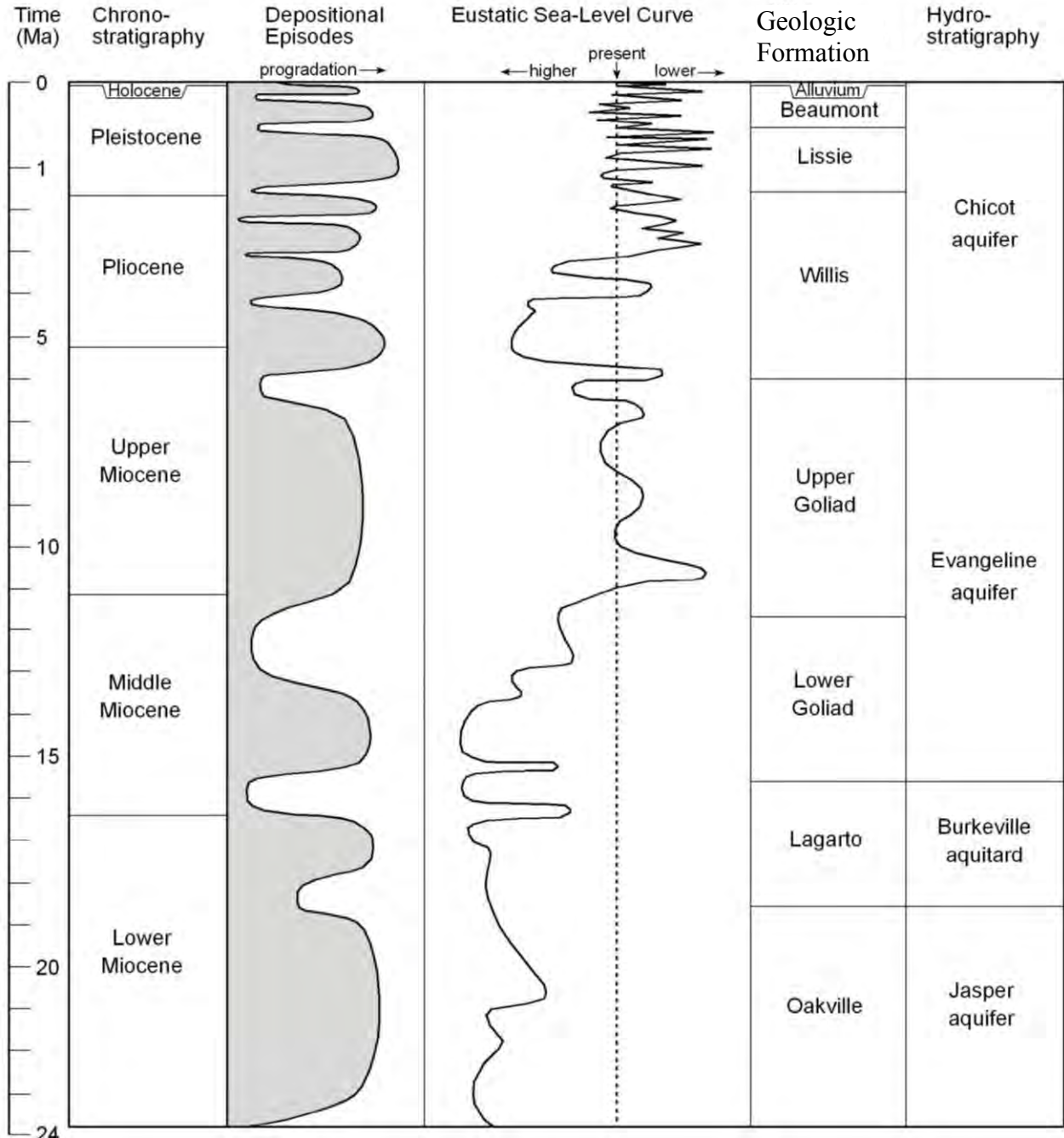


Figure 2-1 Chronostratigraphic chart, Eustatic sea level, lithostratigraphic, and hydrostratigraphic chart of the Miocene to Holocene depositional episodes. Hydrostratigraphy boundaries are approximate. Depositional episodes from Galloway and others (2000) and sea-level curve from Haq and others (1987). Geologic ages in millions of years ago (Ma) from Berggren and others (1995).

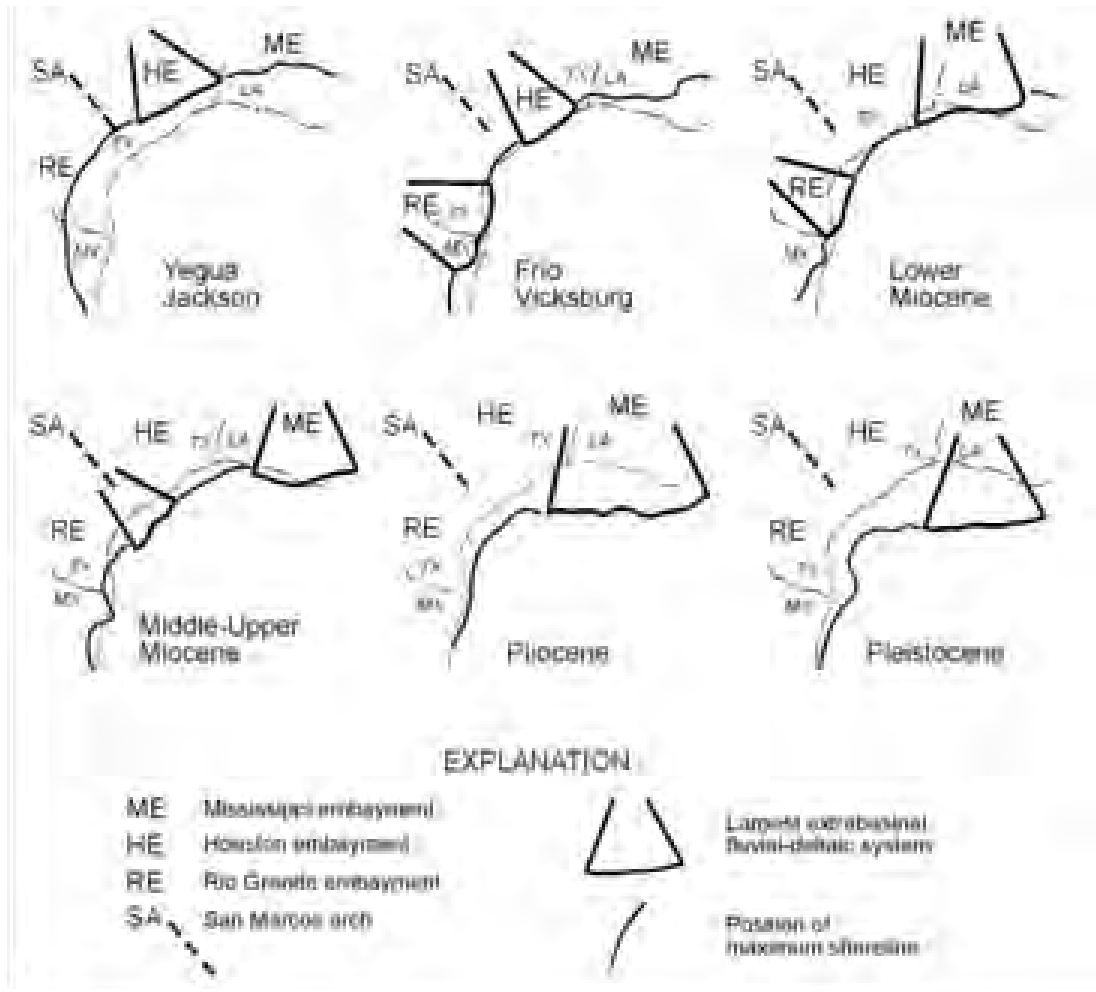


Figure 2-2 Positions of principal fluvial-deltaic depocenters and interdeltic shorelines for selected depositional episodes, northwest Gulf of Mexico. Modified from Galloway (1989) and Galloway and others (2000).

Final – Hydrogeochemical Evaluation of the Texas Gulf Coast Aquifer System and Implications for Developing Groundwater Availability Models

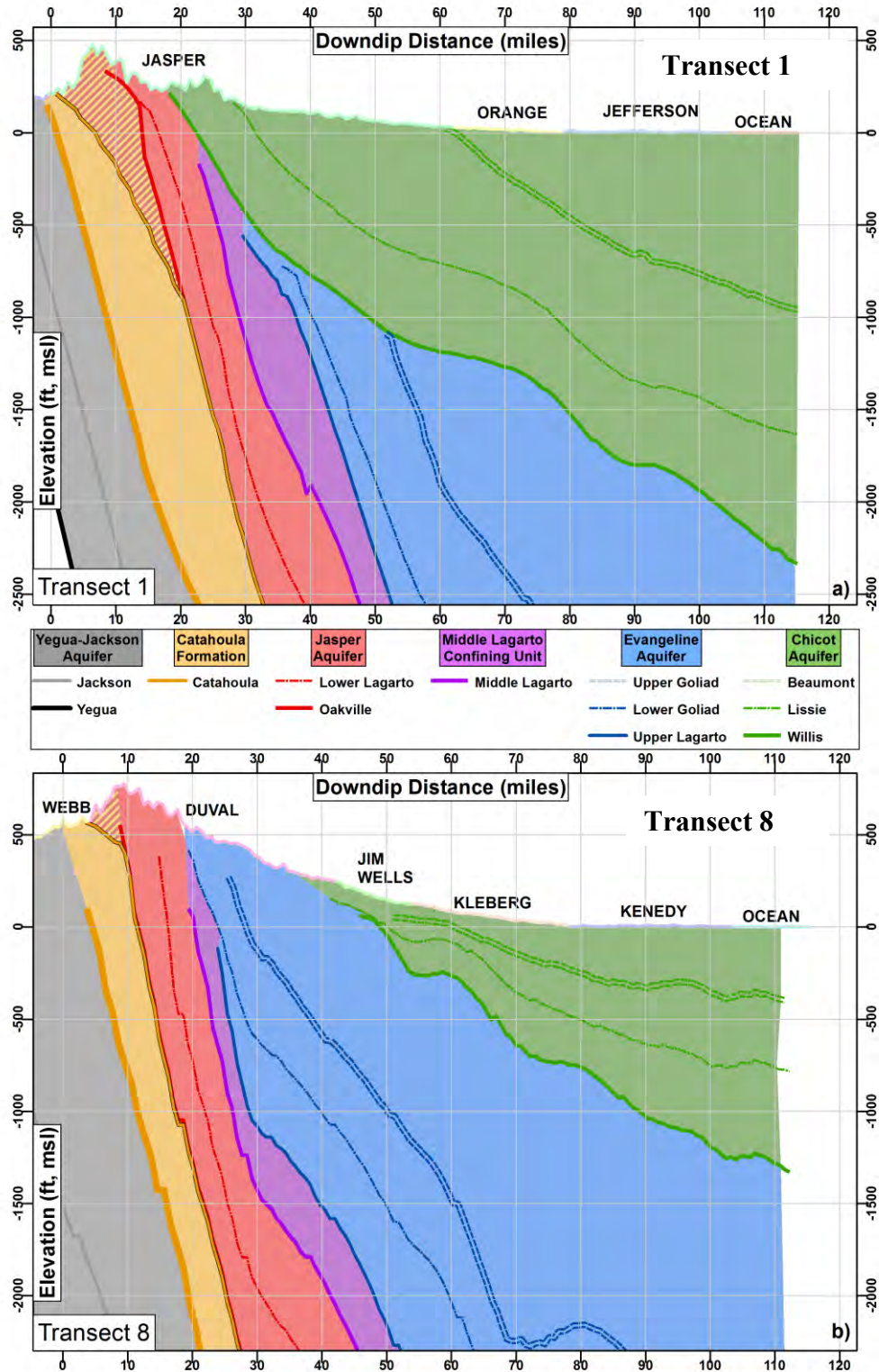


Figure 2-3 Geologic cross-sections through Transects 1 and 8. (Note: surfaces represent the bottom of each geological formation).

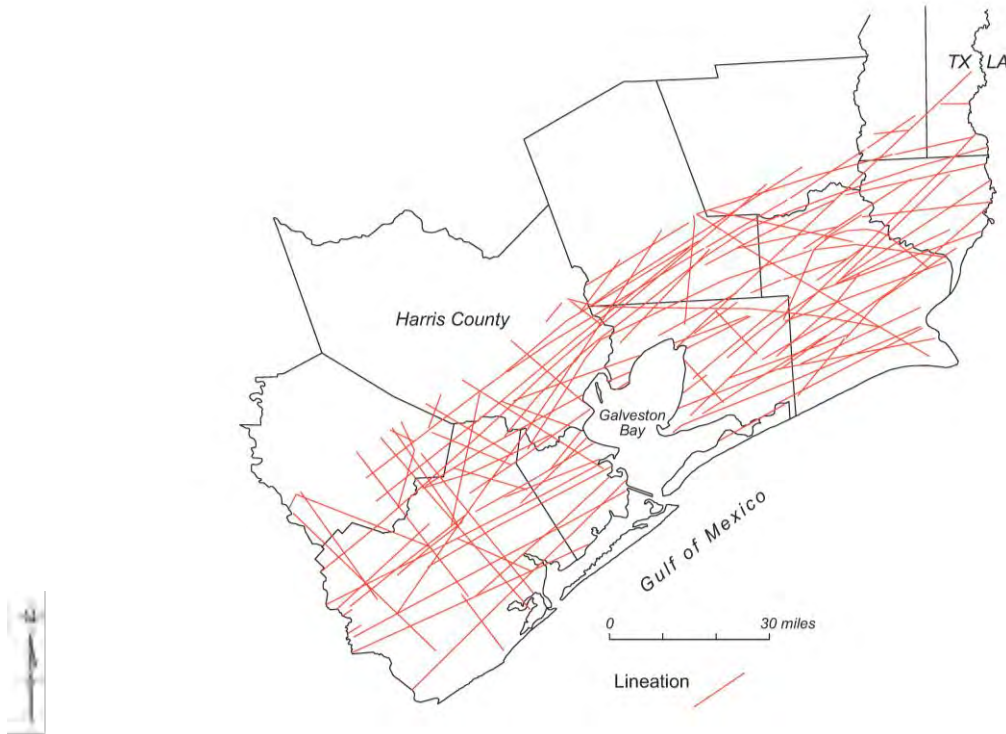


Figure 2-4 Lination map of the Texas coastal zone in the Houston Embayment area. Lineations are the surface expressions of faults or fractures (Kreitler, 1976). The entire Texas coastal plain is covered by lineations, although only the more coastward lineations are mapped here. Modified from Fisher and others (1972, 1973) and McGowen and others (1976a,b).

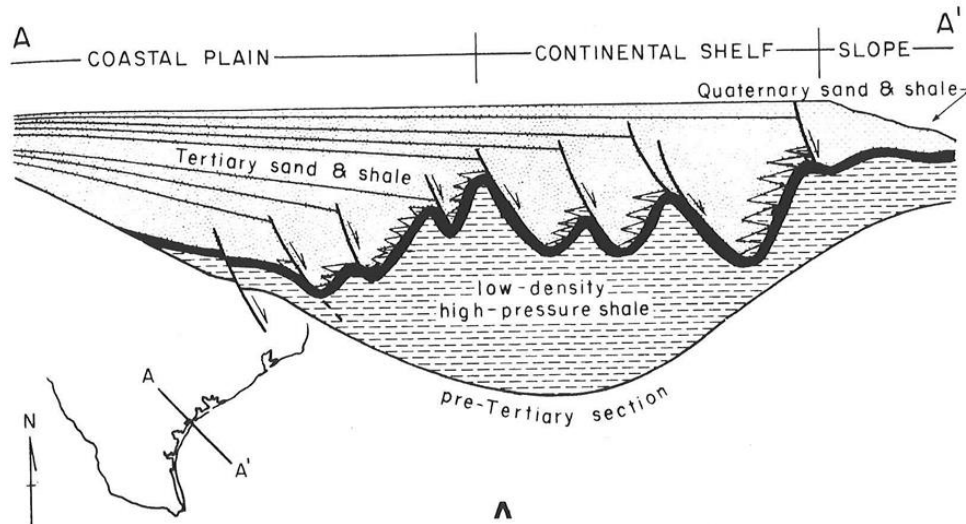


Figure 2-5 Schematic of a cross-section along the central part of the Texas Gulf Coast and northern Gulf of Mexico basin showing depositional and structural styles exhibited by fluvial deltas (from Bruce, 1973 and Solis, 1981). Deposition of coarse-grain deposits is shown by the triangular wedges along the down-dip face of the fault.

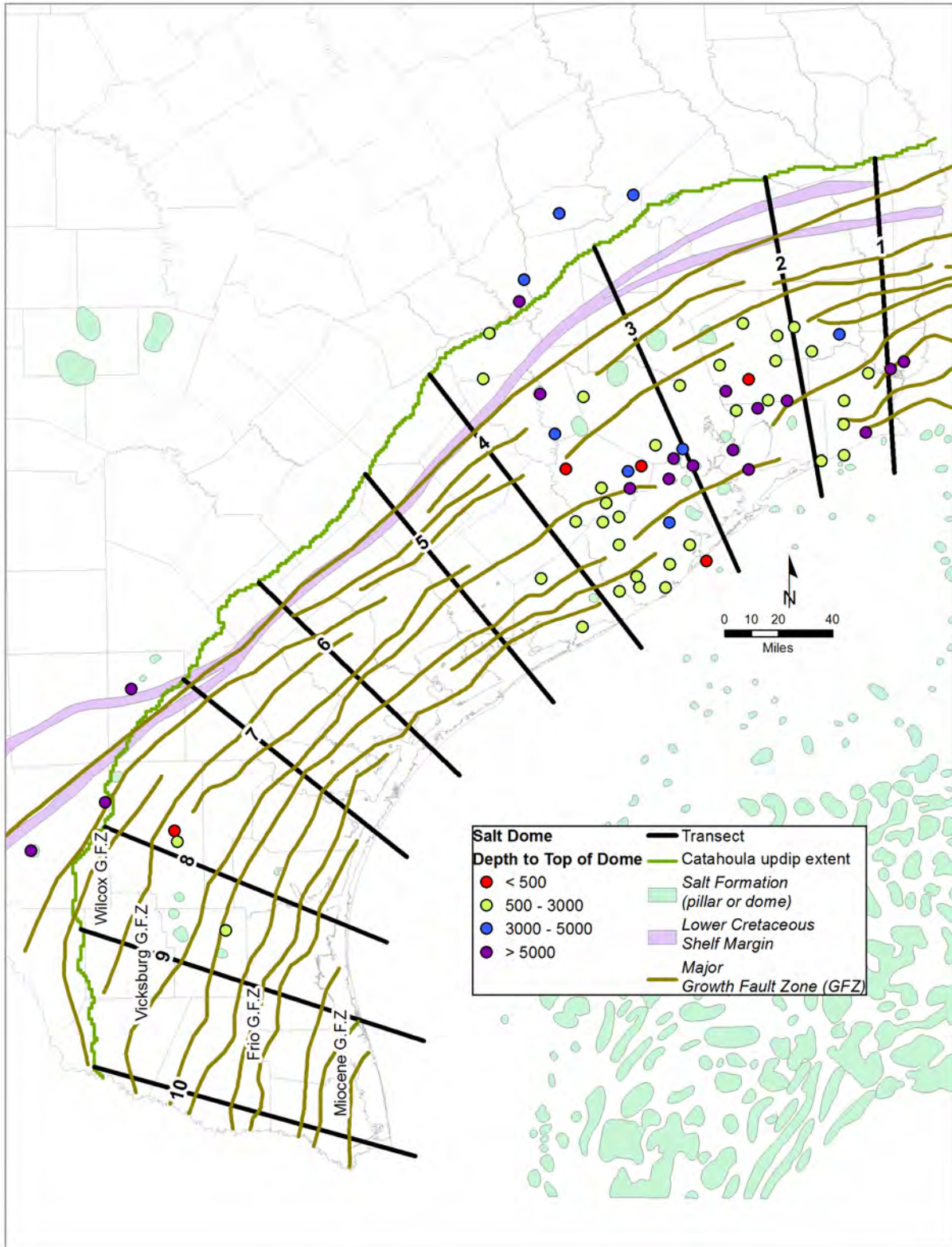


Figure 2-6 Map showing major growth fault zones and shallow salt domes in the onshore part of the Texas coastal zone. (Fault locations from Ewing, 1990).

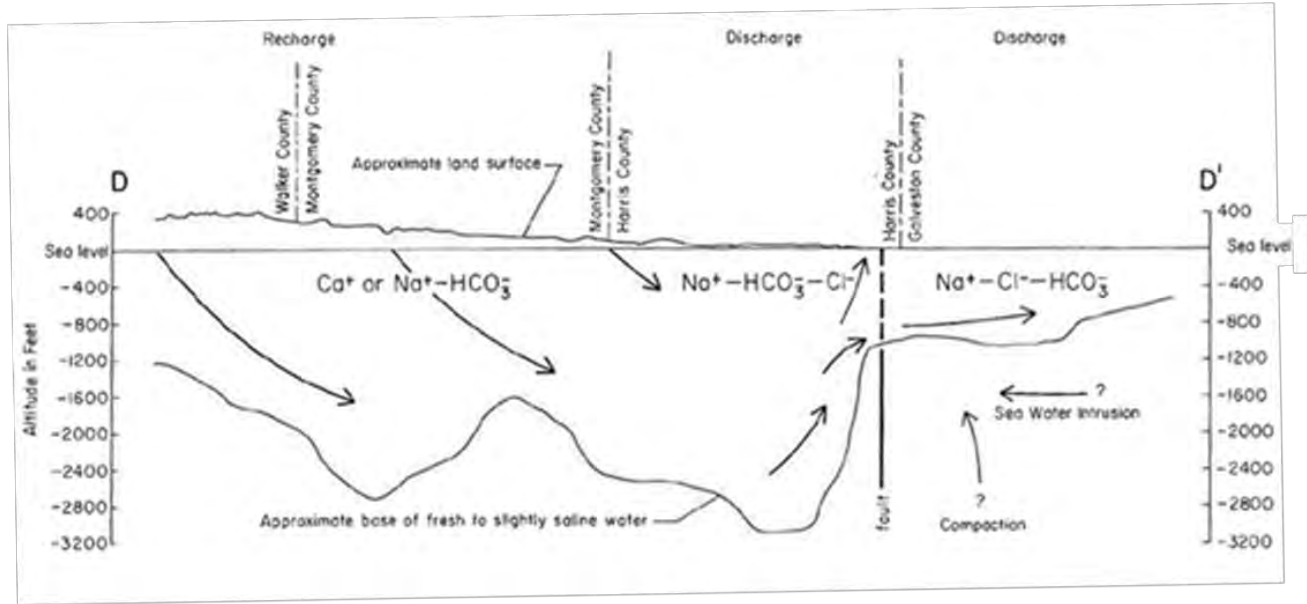


Figure 2-7 Cross-section showing hydrochemical facies of an aquifer and depth to base of fresh water. Cross-section through eastern Liberty, Harris, and Galveston counties (from Kreitler and others, 1977).

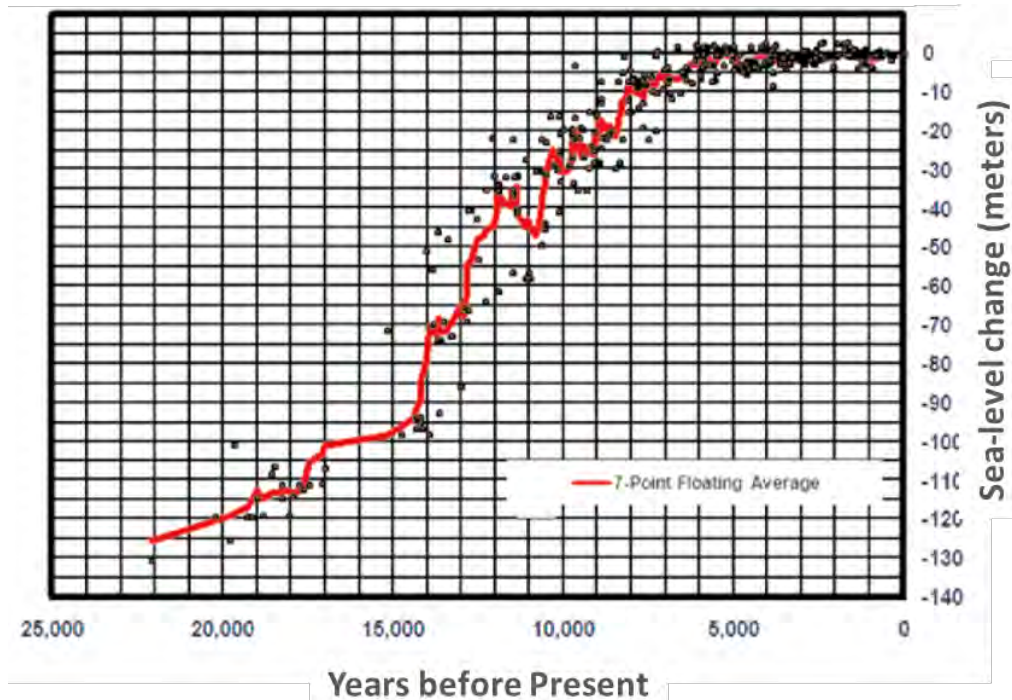


Figure 2-8 A 7-point floating average curve to predict sea-level change during the last 20,000 years fitted to Gulf of Mexico radiodated shoreline markers by Balsillie and Donoghue (2004).

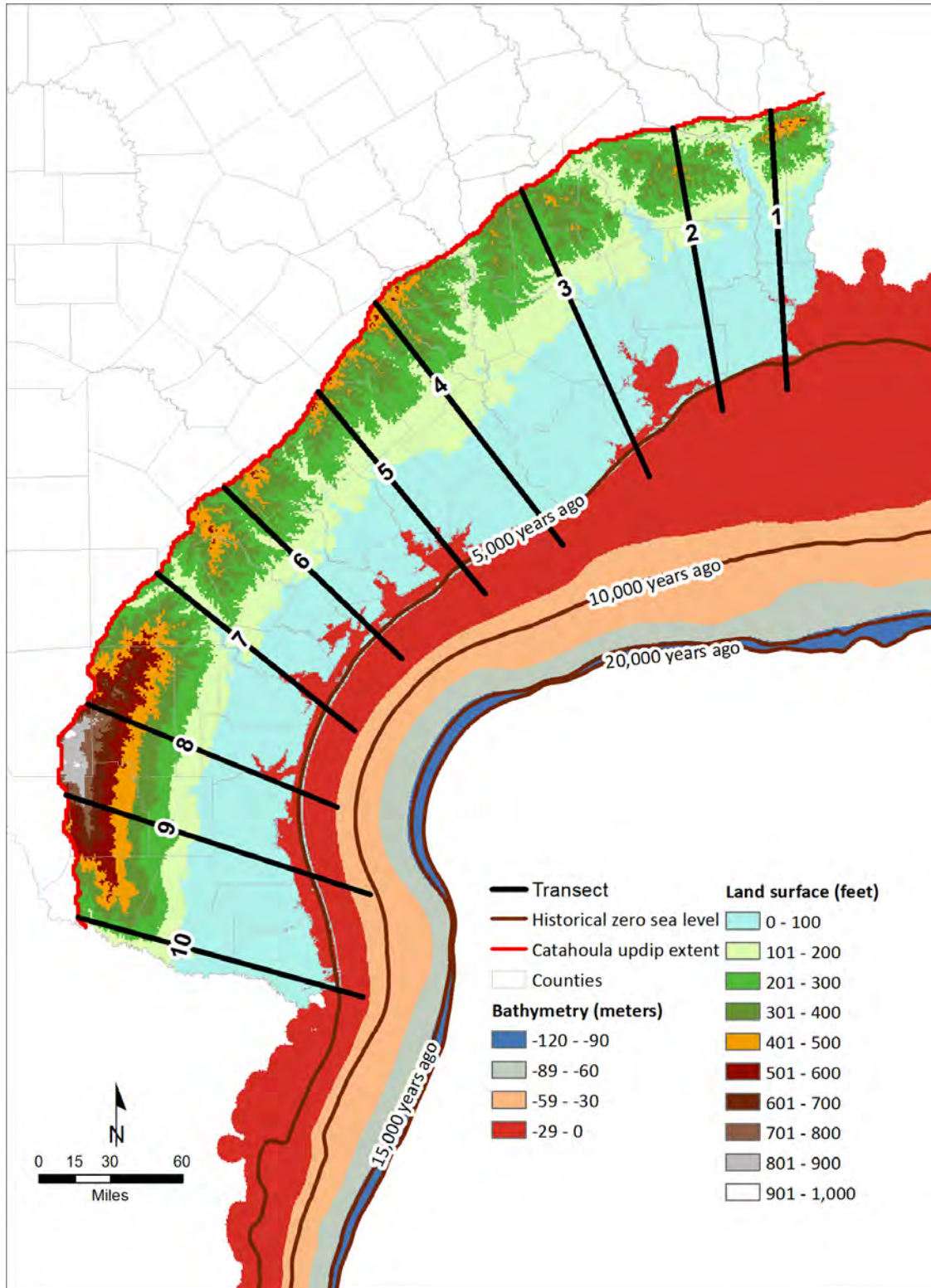


Figure 2-9 Estimated shoreline along the Texas Gulf Coast during the last 20,000 years based on historical sea-level data from Balsillie and Donoghue (2004) with topographic and bathymetry elevations measured relative to current sea level.

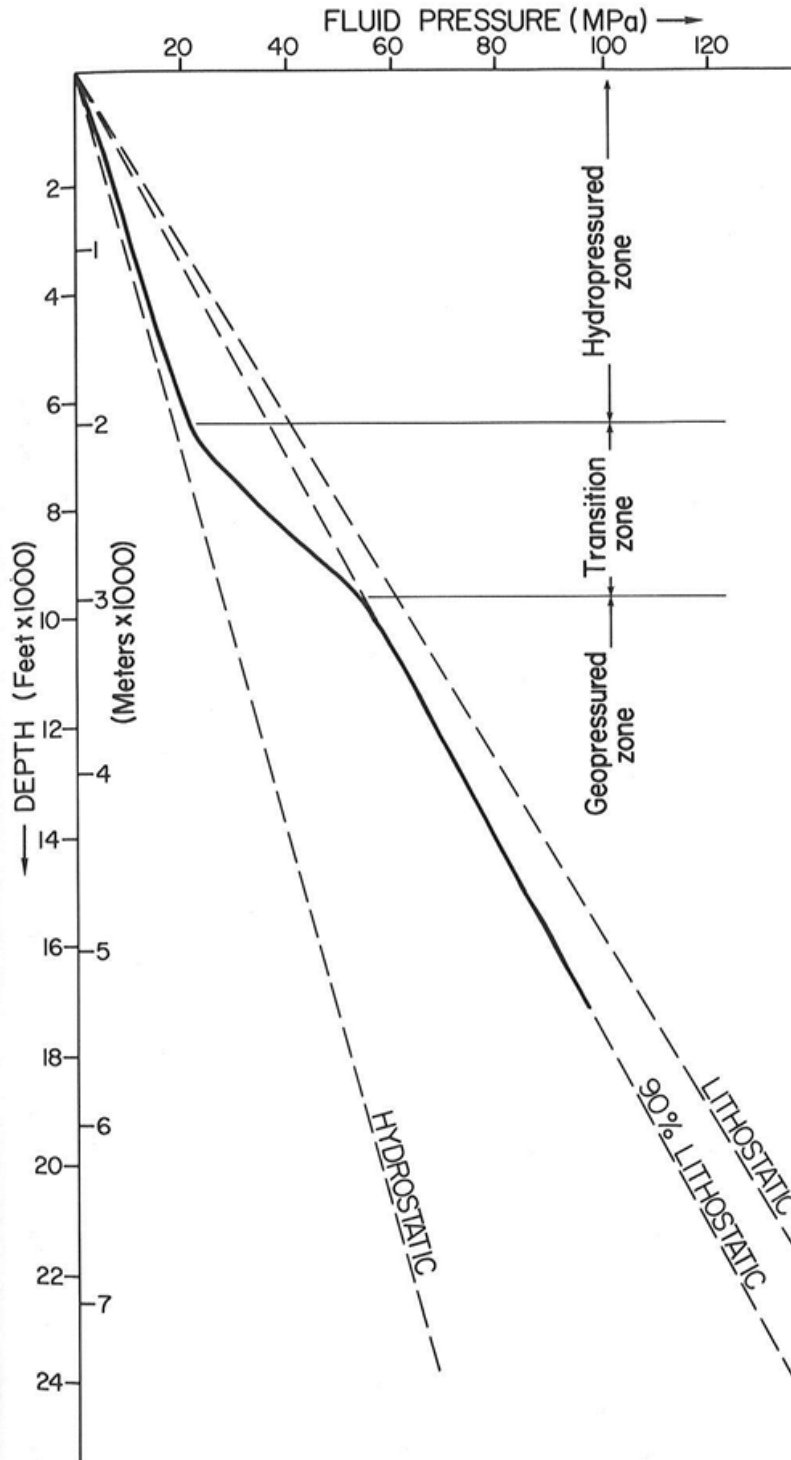


Figure 2-10 General pattern of fluid pressures for Gulf of Mexico basin sediments from Sharp and others, 1988. Note sediments are geopressured at depths below 3 km and that the transition interval is a narrow abrupt interval between hydrostatic and geopressured sections.

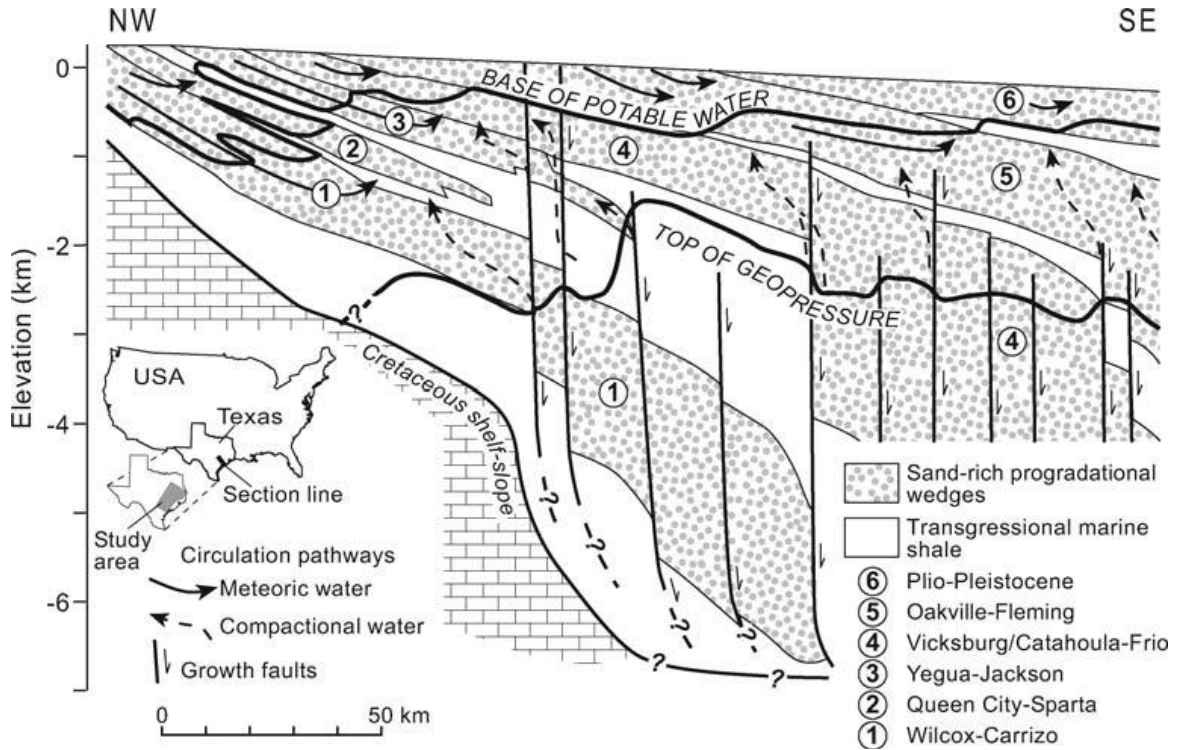


Figure 2-11 Meteoric and compactional circulation pathways in sand-rich progradational packages and growth fault zones beneath the Texas coastal plan (from Dutton and others, 2006).

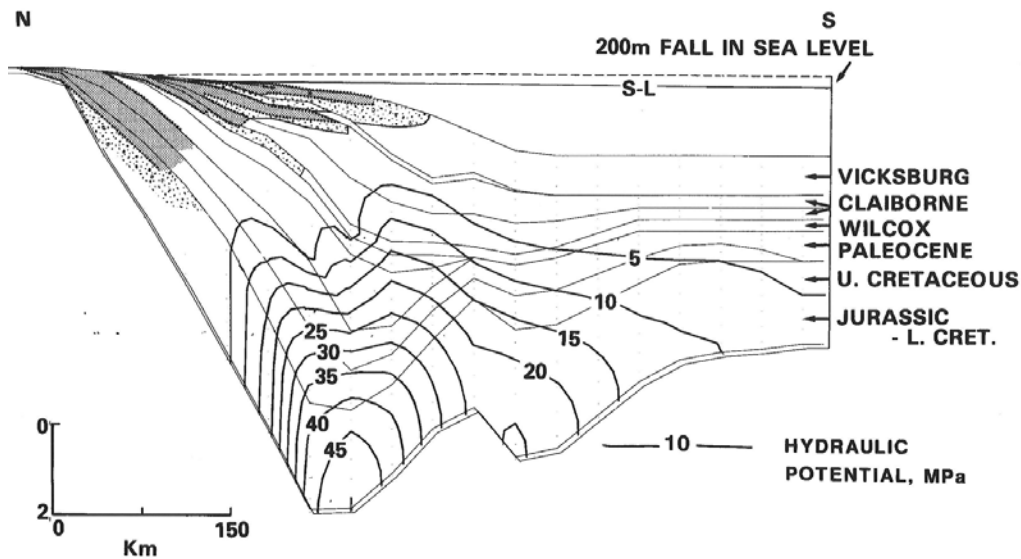


Figure 2-12 Effect of a 200m sea level all at 31 Ma on the distribution of meteoric water entering the basin through topographic drive. Light stippled area shows strata in which compactional water has been replaced by meteoric water. Water of meteoric origin is predicted to move 75km further downdip in the Wilcox Formation as a result of the additional topography (from Harrison and Summa, 1991).

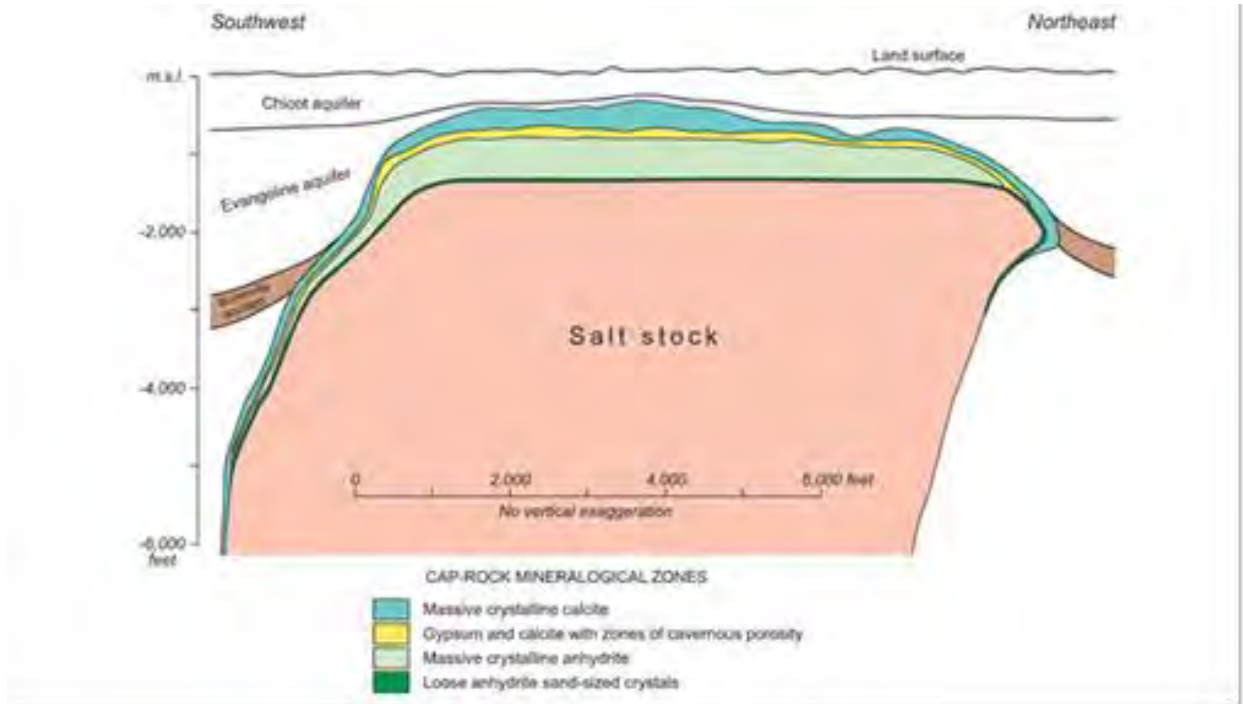


Figure 2-13 Cross section of Barbers Hill salt dome in Chambers County showing the salt stock, cap rock mineralogical zones, and enclosing hydrostratigraphic intervals (modified from Hamlin and others, 1988). This cross section has no vertical exaggeration (vertical and horizontal scales are equal). Cap-rock layering is generally more complicated than shown here and varies widely among domes.

3.0 Groundwater Models for GMA 14, GMA 15, and GMA 16

This report section presents a conceptual site groundwater model that has served as the framework for the majority of the numerical models built for the Gulf Coast Aquifer System. In order to help evaluate the site conceptual groundwater model, groundwater fluxes were generated for predevelopment conditions by running the groundwater availability models for (1) the northern portion of the Gulf Coast Aquifer System (Northern Gulf Coast GAM), (2) the central portion of the Gulf Coast Aquifer System (the Southern Gulf Coast GAM), and (3) the alternative groundwater flow model for Groundwater Management Area 16 (the GMA 16 Alternative Groundwater Model (AGM)), and the Lower Colorado River Basin (LCRB) model. These groundwater fluxes are used to develop estimates for groundwater ages and to develop water budgets.

3.1 Conceptual Groundwater Model of the Gulf Coast Aquifer System

A conceptual model of groundwater flow can be defined as an interpretation or working description of the characteristics and dynamics of a physical hydrogeologic system (ASTM, 1999). The purpose of the conceptual flow model is to integrate hydrogeological data into a set of assumptions that can be evaluated quantitatively. The conceptual model identifies and describes important aspects of the physical hydrogeologic system, including: geologic and hydrologic framework, media type, physical and chemical processes, hydraulic properties, and sources and sinks (water budget).

A consistent tenet for the majority, if not all, Gulf Coast Aquifer System groundwater models is that basinal flow can be subdivided into local, intermediate, and regional flow regimes, as described by Toth (1963) and as illustrated in Figure 3-1. The major driver for the local, shallow flow system is the difference in topography between adjacent hills and valleys. Recharge to local flow regimes occurs in topographically high areas, and discharge occurs in nearby low areas, such as stream valleys. The shallow flow system occurs primarily in the outcrop or unconfined portion of the aquifer and is characterized by flow paths on the scale of a few miles, travel depths measured in tens of feet, and travel times that lasting between a month and a several decades. Intermediate flow paths are longer and deeper than local flow paths and underlie several local flow regimes. An example of an intermediate flow path would be the

migration of groundwater from the perimeter of a watershed of one Texas's major rivers to a discharge location near the river. Regional flow regimes extend from regional recharge areas such as outcrops and discharge to near the coastline. The regional system is composed of confined to semi-confined aquifers and is characterized by groundwater flow paths involving travel distances measured on a scale of tens of miles, travel depths in the range of 500 to 3,000 feet, and travel times that range between 50 and 40,000 years. The major topographic driver for the regional flow system is the difference between the water levels in the updip regions of the aquifer (e.g., in Colorado and Lavaca counties) and the downdip portion of the aquifer (e.g., near Matagorda and Brazoria counties). Thus, regional groundwater flow is primarily toward the coast and the groundwater movement tends to be much slower than in either the intermediate and shallow flow systems.

Figure 3-1 shows piezometers intersecting the local (shallow) and regional (deep) aquifer flow systems. In the updip region (a.k.a., high topographic elevations), the hydraulic head is greater in the shallow aquifer than in the deep aquifer. Thus, the vertical hydraulic gradient and groundwater flow are downward. In the downdip region (e.g., low topographic elevations), the reverse occurs; the hydraulic head is greater in the deep aquifer than in the shallow aquifer. Thus, the vertical hydraulic gradient and groundwater flow are upward. Across the Gulf Coast, several investigators (Hammond, 1969; Sandeen and Wesselman, 1973; and Loskot and others, 1982) have documented that upward hydraulic gradients from the Evangeline aquifer to the Chicot aquifer were prevalent across much of the downdip region of the model area during the early period of pumping. In fact, Hill (1901) estimates that prior to pumping the majority of the deep aquifers (see Figure 3-2) in the Coastal plains of Texas were under artesian pressure, meaning that at an open well would flow freely at land surface if exposed to the atmosphere.

The flow lines in Figure 3-1, and those associated with Toth's (1963) original conceptualization of a hierarchical system of groundwater flows, assume that aquifers are homogenous and isotropic. Consequently, any geologic feature or condition that introduces heterogeneity on a moderately large scale can distort or modify this concept. A review of the previous models for the Gulf Coast Aquifer System (Wood and Gabrysch, 1965; Meyer and Carr, 1979; Carr and others, 1985; Jorgensen, 1975; Dutton and Richter, 1990; Williamson and Grubb, 2001; Chowdhury and Mace, 2004; Hay, 1999; Groschen, 1985; Harden and Associates, 2002; Young

and others, 2012a; Hutchison and others, 2010; Chowdhury and others, 2004; Kasmarek and Robinson, 2004; Kasmarek and Strom, 2002) indicates that most of these models have address spatial heterogeneity in the subsurface by:

- representing the Chicot, Evangeline, and Jasper Aquifers as single layers and with average hydraulic conductivities between 0.5 and 50 ft/day;
- representing the Burkeville Confining Unit as a single layer with a relatively low permeability (about 100 times less permeable than the Evangeline and Jasper Aquifers) or as a no flow boundary beneath the Evangeline;
- representing the Catahoula typically as a no-flow boundary beneath the Jasper Aquifer; and
- not representing regional fault systems nor salt domes in the model (see Figure 2-6).

The majority of the numerical models reviewed presume that after water recharges, the resulting groundwater is primarily gravity driven by regional topography. Most of the numerical models have such large layer thicknesses (one layer per aquifer with little regard to the depth of rivers and streams) and large grid sizes (one mile or greater dimensions), that the local flow system is poorly represented given the lack of resolution to accurately represent local topography differences and placement of streams. As a result, the models have been built to represent what is sometimes referred to as “deep recharge,” which is the recharge that Toth (1963) associates with regional flow that occurs downdip.

As shown in Figure 2-9, the topography gradient is not uniform. Across the Coastal Plains, which extend approximately 60 miles inland from the shore along the entire Texas Coast, the topographic gradient is relatively flat. Across these 60 miles, the drop in topographic elevation is about 100 feet. Up dip of the Coastal Plains, the topographic relief is much greater. In GMAs 14 and 15, the Catahoula outcrops at elevations typically between 300 and 400 feet, whereas in GMA 16, the Catahoula outcrops at elevations typically between 700 and 900 feet. Based simply on geometry considerations, the Coastal Plains would act as a potential discharge area for recharge occurring at the higher elevations updip. Most, if not all, of the rivers and streams in the Coastal Plain area should be gaining groundwater along their flow routes and a

considerable amount of groundwater from the up-dip regions of the Texas Gulf Coast Aquifer System would discharge in the Coastal Plains before reaching the ocean.

By analog of the regional modeling by Toth (1963), two potentially important components of the conceptual groundwater model can be deduced from the Texas Gulf Coast topography shown in Figure 2-9. One of these components is that at the localized low topographic areas in the Coastal Plains, where significant groundwater discharge occurs to springs or major rivers, mixing of groundwater from shallow, intermediate, and deep flow systems will likely occur. The other component is that in the up-dip regions of the Gulf Coast Aquifer System, where river alluvium is at significantly lower elevations than the surrounding aquifer outcrops (for example, the location of the Brazos River Alluvium), a substantial amount of the recharge that enters at aquifer outcrops at the higher topography will flow toward the alluvium via a local flow system and be discharged to the Brazos River (or one of its tributaries) before it becomes a part of the regional flow system. Thus, up dip of the Coastal Plains, the primary source of the groundwater at springs and major rivers will be the local flow system.

Important components of a conceptual flow system are precipitation and recharge rates.

Figure 3-3 shows that the annual precipitation rates range from about 62 inches/year in the northeast to about 21 inches/year in the southwest area of the Gulf Coast Aquifer System. This large difference in recharge is expected to affect both the water quality and quantity. By using both a chloride mass balance approach and hydrograph separation using Base-Flow Index (BFI), Scanlon and others (2012) developed the spatial distribution of annual recharge values shown in Figure 3-4. Recharge rates range from <0.1 in/yr in the south to 10 in/yr in the north, correlated the variation in precipitation. The recharge values are consistent and very similar to the values used in the LCRB model (Young and others, 2006, 2009).

Table 3-1 provides average recharge rates for GMA 14, 15, and 16 as a function of distance from the up-dip extent of the Catahoula outcrop. The table shows a factor of seven difference in the recharge rates among the GMAs as well as a factor of difference three within the different down dip zones for each GMA. The large range of values shown in Table 3-1 and in Figure 3-4 suggest that the recharge dynamics vary significantly across the Gulf Coast.

As stated previously, a conceptual groundwater model should include a water budget. Based on the wide range of meteorological, geological and hydrological conditions in the Gulf Coast, a

representative water budget cannot be developed for the entire Gulf Coast Aquifer System region. Furthermore, most of the conceptual models for the Gulf Coast Aquifer System do not include a quantitative water budget. For this discussion, the conceptual water budget developed for the construction of the LCRB model (Young, 2009) is provided in Figure 3-5. Although qualitatively simple, developing a mass balance for a regional aquifer from historical data is difficult because most of the flow components, such as evapotranspiration or recharge, that comprise the mass balance cannot be directly measured. Among the flow components involving groundwater that are shown in Figure 3-5, only surface water-groundwater interaction can be reasonably estimated from historical data. The rest of the information needs to be carefully developed based on lines of evidence that include a comprehensive analysis of geohydrological data, including aquifer hydraulic properties, water levels, and water quality data.

Table 3-1 Spatial Distribution of Average Annual Recharge Values for GMA 14, 15, and 16.

Down Dip Section (miles)	GMA 14		GMA 15		GMA 16	
	Area (mi ²)	Recharge (in/yr)	Area (mi ²)	Recharge (in/yr)	Area (mi ²)	Recharge (in/yr)
0 - 25	4732	1.36	3150	0.33	4367	0.09
25-50	4402	2.16	3206	0.49	4202	0.14
50-75	3838	1.30	3122	0.47	3890	0.23
75-100	3388	0.60	2787	0.94	3527	0.41
Total Area	16,360		12,265		15,985	
Avg. Recharge(in/yr)	1.41		0.55		0.21	

The conceptualization of the down-dip boundary differs among the models created for the Gulf Coast Aquifer System. All of the models represent the ocean with general head boundaries, but they differ in the location and type of boundary used at the down-dip end of the model layers. Figure 3-6 shows a two-dimensional cross-section of the active grid cells for each of the four models along a transect. Figures 3-7 and 3-8 show a three-dimensional view of the cross sections through the four models for several transects. As shown in Figure 3-7 and 3-8, all of the models but the Central Gulf Coast Aquifer System GAM have their top model layer extend underneath the ocean for about 10 miles. This overlap with the ocean provides the opportunity for groundwater to flow out beyond the coastline and to discharge at the ocean bottom. The top layer for the Central Gulf Coast Aquifer System GAM stops at the coastline so that groundwater can flow into the ocean only by discharging to general head boundaries along the coastline.

The Northern Gulf Coast Aquifer System GAM (Figures 3-6 and 3-7) down dip boundary conditions represent the limit of freshwater in each model layer. Kasmarek and Robinson (2004) define the freshwater limit by high values of TDS, which can be as much as 10,000 ppm. For model layers 2, 3, and 4, the down dip boundary is a no-flow boundary. Kasmarek and Robinson (2004) state that the no-flow boundary at a specified location reflects an assumption of a stable downdip freshwater/saline interface. For model layer 1, general head boundaries are used to represent the interaction between the groundwater system and the ocean for an area that extends about 10 miles offshore.

In the Central Gulf Coast Aquifer System GAM (Figures 3-6 and 3-7), the down-dip boundary for the top model layer (which is the Chicot Aquifer) is represented by a general head boundary condition along the coast. The general head boundary cells do not extend beyond the coastline to include the base of the ocean or bays. The down dip boundaries for model layers 2, 3, and 4 are no-flow conditions. According to Waterstone (2003), the no-flow boundaries were set to represent the location of the 10,000 TDS contour lines by Pettijohn and others (1988).

In the LCRB Model (Figures 3-6 and 3-8), the top model layer (which represents the shallow flow zone) extends past the coast line about 10 miles. Past the coastline, the top model layer includes general head boundary conditions to allow interactions with the ocean. Model layer 2, which represents the upper Chicot Aquifer, has the same coverage as model layer 1, extending into the ocean. This boundary allows submarine groundwater discharge to occur approximately 10 miles beyond the coastline. The down-dip boundaries for models layers 3 through 6 are no flow conditions, representing the transition zone between fresh and brackish water (Young and others, 2009). This transition zone corresponds to a TDS of about 3,000 ppm which was identified by examining geophysical logs.

Documentation for the GMA 16 AGM (Figures 3-6 and 3-8) does not provide rationale or a description of the model down-dip boundary conditions. Inspection of the model files shows that model layers 4 through 6 (layer 4 is the Jasper Aquifer) represent the down-dip boundary as a no flow boundary condition. Model layers 2 and 3 (layer 2 is the Evangeline Aquifer and layer 3 is the Burkeville) represent the down-dip boundary as a general head boundary at the last grid cell. These layers extend approximately 10 miles offshore and thereby allow groundwater to flow into model layer 1. Model layer 1 (the Chicot Aquifer) extends approximately 10 miles past the

coastline. Where the ocean is present, layer 1 contains general head boundary conditions to represent interaction between the groundwater flow system and the ocean.

3.2 Simulated Groundwater Fluxes For Predevelopment Conditions

In order to help evaluate the site conceptual groundwater model, groundwater fluxes were generated for predevelopment conditions by running the Northern Gulf Coast Aquifer System GAM, the Central Gulf Coast Aquifer System GAM, the GMA 16 AGM, and the LCRB model. Predevelopment represents a quasi-steady state condition prior to the onset of pumping groundwater. The purpose of performing these simulations is to generate the groundwater flow fields necessary to develop a set of quantitative results regarding the age of groundwater and the amount of cross-flow between aquifers that can be compared with results from the analysis of the geochemical data.

A groundwater model solves for a water balance for every active grid cell. Implicit in the water balance calculation is that groundwater fluxes are calculated for all six faces of the grid cells and for any sinks and sources assigned to the grid cell. Figure 3-9 is a schematic of a single grid cell and the fluxes associated with each of its six faces. The fluxes can be used to simulate the movement of groundwater through the grid cell as shown in Figure 3-10. By tracking the movement of particles from one grid cell to another, a continuous flow path for groundwater can be developed between an active grid cell and a discharge location in the model. To generate model results useful for comparing with the geochemical data, water budgets and particle tracking results were generated for transects 1, 3, 34, 45, 5, 6, 78, and 8. The particle tracking results were generated using the starting locations shown in Figure 3-11. The water budgets were generated for the areas contained within the polygons shown in Figure 3-12.

3.2.1 Estimated Groundwater Age

A groundwater model can be used to predict the age of groundwater by tracking particles backwards to reveal the flow path taken by the particle to reach the grid cell. Reverse particle tracking was performed for eight transects using the code MODPATH (Pollack, 1994). MODPATH is a particle tracking post-processing program designed to work with the groundwater fluxes predicted by the MODFLOW (McDonald and Harbaugh, 1988) groundwater code. An effective porosity of 0.2 was used in MODPATH to estimate groundwater velocity

from groundwater flows. In addition to computing particle paths, MODPATH keeps track of the time of travel for particles moving through the system. At each of the particle seed locations shown in Figure 3-11, particles were placed in the aquifer at 100-foot depth increments and then tracked in a reverse direction (e.g., upgradient) to the source of water where the flow path originated. The particle seed locations are on lines that are five miles apart and are perpendicular to the transect line. For each of the 25 lines there are 13 particles spaced one mile apart. Thus, the number of particles associated with each of the transect layers is 325 particles. The 325 particles represent a layer of particles. For each transect, layers of particles were placed regularly at 100 foot depths. Because the models have different active domains at each transect, the number of blocks that have groundwater ages will be different for different models applied to the same transect. For instance, since the LCRB Model does not include the Jasper Aquifer, it has the least number of groundwater ages for the most up-dip grid locations.

The top plot in Figures 3-13 through 3-27 shows the age of groundwater calculated from reverse particle tracking as a color coded block, plotted on a vertical cross-section along a transect. To help locate the groundwater relative to the different aquifers, the bottoms of the model layers are shown for reference. The groundwater age assigned to each block is the average groundwater age for the 13 particles from the 13 mile-long line running perpendicular to the transect (Figure 3-11).

A general trend present in Figures 3-13 through 3-27 is that groundwater age increases with depth and with down dip distance. When each plot is viewed separately, understandable trends can be deduced. However, plot comparisons reveal large differences in the groundwater ages for the same block (for instance at 100 feet depth and 80 miles downgradient) among the same models for different transects and among the same transect for different models. This wide range of ages is not consistent with the range of recharge ranges or hydraulic properties associated with specific aquifers such as the Chicot Aquifer. The greatest variations seem to occur at the shallowest depths. For instance, the block at 80 miles down dip and a depth of 100 feet has a groundwater age that ranges from less than 200 years (for the LCRB model) to more than 150,000 years (for the Northern Gulf Coast Aquifer System GAM). Moreover, the range of groundwater ages for an aquifer in a transect can vary significantly among the models. For instance, in the Chicot aquifer in Transect 34, the variations in the groundwater age are about a

factor of 10 and 1000 for the Northern Gulf Coast Aquifer System GAM and the LCRB model, respectively. Such large differences suggest that groundwater ages estimated from groundwater models (which were primarily calibrated based on hydraulic head) may have significant uncertainty, requiring additional constraints, such as ages estimated from isotopes, to produce reasonable results.

To help compare the groundwater ages associated with the particle tracking results, groundwater ages in Figures 3-13 through 3-27 were used to develop an average age of groundwater at five different depth zones for three down-dip distance intervals in Figure 3-28. The three distance intervals represent intervals down dip that span from 20 to 35 miles, from 55 to 65 miles, and from 85 to 100 miles, respectively. The five depth categories in Figure 3-28 are 100 ft, 200 to 400 ft, 500 to 800 ft, 1000 to 1200 feet, and 1400 to 1600 feet. Several of the notable observations in Figure 3-28 are:

- for Transect 34, all of the Northern Gulf Coast Aquifer System GAM groundwater ages are greater than 100,000 years;
- all of the Northern Gulf Coast Aquifer System GAM groundwater ages for 100 ft depth are greater than 8,000 years and most of the ages are greater than 100,000 years;
- for Transects 1, 3, and 34, the Northern Gulf Coast Aquifer System GAM groundwater ages for the down dip section (85 to 100 miles) for all depths are between 100,000 and 1,000,000 years;
- for Transects 34, 45, and 5, the LCRB Model groundwater ages for 100 ft depth are about 200 years;
- for Transects 34 and 45, the LCRB Model groundwater ages increase as a function of both depth and down dip distance;
- for Transects 45, 5, 6, 78, and 8, the Central Gulf Coast Aquifer System GAM groundwater ages generally increase as a function of both depth and down dip distance;
- for the transects in GMA 15, the Central Gulf Coast Aquifer System GAM groundwater ages for 100 ft depth average about 1,000 years;

- for Transects 6, 78, and 8 the GMA 16 AGM's groundwater age averages more than 10,000 years for the 100 ft depth;
- for Transect 78 the GMA 16 AGM's groundwater age averages about 80,000 years for the 100 ft, 200-400 ft, and 500-800 ft depth intervals, and for Transect 8, the GMA 16 AGM's groundwater age averages about 12,000 years for the 100 ft, 200-400 ft, and 500-800 ft depth intervals;
- the greatest variations (in terms of relative percentage) in the groundwater ages among the models is for the 100 ft depth for the up-dip sections (20 to 35 miles), the least variation (in terms of relative percentage), in the groundwater age for the 1,400 to 1,600 depth for the mid-dip sections (55 to 65 miles); and
- in general, the largest groundwater ages are associated with the down-dip section (85 to 100 miles).

3.2.2 Components of Groundwater Flow

Computer programs that simulate groundwater flow typically produce water budgets for the modeled region, but often it is useful to have a water budget for a particular subregion of the modeled region. ZONEBUDGET (Harbaugh, 1990) calculates water budgets by tabulating the budget data that MODFLOW produces for each grid cell.

ZONEBUDGET is designed to calculate a water budget for a block of grid cells defined by a range of layers, rows, and columns. For example, a block might be defined by layers 3-4, rows 7-20, and columns 2-26. A single zone value is assigned to all the cells in a block.

ZONEBUDGET calculates the total fluxes through the outside surface area of the block of cells and tabulates the change in total groundwater flow that is caused by sinks and sources of groundwater contained within that block (or zone) of grid cells.

For eight transects shown in Figure 3-12, ZONEBUDGET was used to calculate the water budgets for four blocks per model layer. Each of these blocks are 25 miles long and 12 miles wide. The first block begins at the up-dip extent of the Catahoula Formation. The groundwater fluxes produced by ZONEBUDGET were divided by the surface area associated with the grid cells that produce the fluxes. The division of a volumetric flux (ft³/day) by an area produces a

groundwater flux with the units of ft/day. All of the fluxes calculated by ZONEBUDGET were divided by an assumed porosity of 0.2 to produce a groundwater velocity. For example, if the volumetric flux through the down-dip boundary is 10 ft³/day and the down dip area is 5 ft² then the groundwater flux is 10 ft/day (10 divided by 5 divided by 0.2).

The tables at the bottom of Figures 3-13 through 3-27 are the groundwater fluxes calculated for the respective transect shown in the figure. Negative fluxes represent losses by the block of cells and positive fluxes represent gains by the block of cells. Thus, if water is flowing in the direction toward the ocean, the flux entering the up dip portion of block of cells should be positive and the flux leaving the down dip portion of the block of cells should be negative. All of the tables of groundwater fluxes consist of the same columns, which are explained below:

- Section – identifies which of the four block of cells that is being analyzed;
- Zone – a two digit code that identifies the Section (first number) and the model layer (the second number) that is being analyzed. To help visualize the vertical extent of the zone, the zone code is printed on the cross-section shown above the table;
- Unit – the aquifer or geological unit represented by the model layer;
- Area – the area represented by the active portion of the unit in the model section. If the active area is less than 50 square miles, the record is blackened. Also, if the layer primarily represents a pinch out layer (see Young and others, 2012a), then the record is blackened;
- Updip - the groundwater flux at the updip face of the block of cells. The updip flux will usually represent the groundwater flux that is entering the block. For the block of cells in the first section, the groundwater flux will typically be zero because there is no active Gulf Coast Aquifer System up dip of the Catahoula;
- Downdip- the groundwater flux at the downdip face of the block of cells. The downdip flux will usually represent the groundwater flux that is leaving the block;
- Above – the groundwater flux at the top face of the block cells. The above flux will usually represent the cross-flow with the unit above the model layer;

- Below – the groundwater flux at the bottom face of the block of cells. The bottom flux will usually represent the cross-flow with the unit below the model layer;
- Lateral – the combined groundwater flux at the northern and southern sides of the block of cells. The lateral flow will usually represent the lateral cross-flow caused by groundwater moving toward a topographic low, a local discharge point such as a river, or a regional discharge point such the ocean;
- GHB – the groundwater flux associated with the general head boundaries. For the Northern Gulf Coast Aquifer System GAM, the GHB typically represents the recharge that is entering the flow system from land surface;
- Recharge- the groundwater flux associated with the recharge cells in MODFLOW;
- SW_Int – The groundwater flux associated with surface water-groundwater interaction associated with river cells, drain cells, and/or stream cells in MODFLOW; and
- Cross-Flow Ratio – the ratio between the groundwater flux moving along dip through the model layer and the groundwater flux entering/leaving the model layer from either above or below. A ratio of 0.1 indicates that the vertical groundwater flux is about 10% of the horizontal flux. A ratio of 2 means the vertical groundwater flux is 200% of the horizontal flux.

In the groundwater flux tables, the fluxes with magnitudes less than 1E-10 ft/day were set to zero and the negative fluxes are highlighted in yellow. Several of the notable observations in the groundwater flux tables are presented below.

Cross-Fluxes

- For Transects 34, 45, and 5, the average cross-flow ratio for the Chicot and the Evangeline Aquifer for the LCRB Model is about 0.005.
- For Transects 8, 78, 7, 5, and 45, the average cross-flow ratio for the Chicot, Evangeline, and Jasper model layers is about 0.012 for the Central Gulf Coast Aquifer System GAM. For the Burkeville, the average cross-flow is about 0.169.

Final – Hydrogeochemical Evaluation of the Texas Gulf Coast Aquifer System and
Implications for Developing Groundwater Availability Models

- For Transects 1, 3, 45, and 5, the average cross-flow ratio for the Chicot, Evangeline, and Jasper model layers is about 0.008 for the Northern Gulf Coast Aquifer System GAM. For the Burkeville, the average cross-flow is about 0.13.
- For Transects 8, 78, and 6, the average cross-flow ratio for the Chicot, Evangeline, and Jasper model layers is about 0.06 for the GMA 16 AGM. For the Burkeville, the average cross-flow is about 0.01.

Down-dip Fluxes

- For Transects 34, 45, and 5, the average geometric down-dip flux in the Chicot and the Evangeline Aquifer for the LCRB Model for the first 75 miles is about 0.005 ft/day.
- For Transects 8, 78, 7, 5, and 45, the geometric down-dip flux in the Chicot, Evangeline, and Jasper model layers for the first 75 miles is about 0.002 ft/day for the Central Gulf Coast Aquifer System GAM. For the Burkeville, the geometric down-dip flux is 0.00001 ft/day.
- For Transects 1, 3, 45, and 5, the geometric down-dip flux in the Chicot, Evangeline, and Jasper model layers for the first 75 miles is about 0.0004 ft/day for the Northern Gulf Coast Aquifer System GAM. For the Burkeville, the geometric down-dip flux is 0.0002 ft/day.
- For Transects 8, 78, and 6, the geometric down-dip flux in the Chicot, Evangeline, and Jasper model layers for the first 75 miles is about 0.0005 ft/day for the GMA 16 AGM. For the Burkeville, the average downflow flux is 0.0001 ft/day.

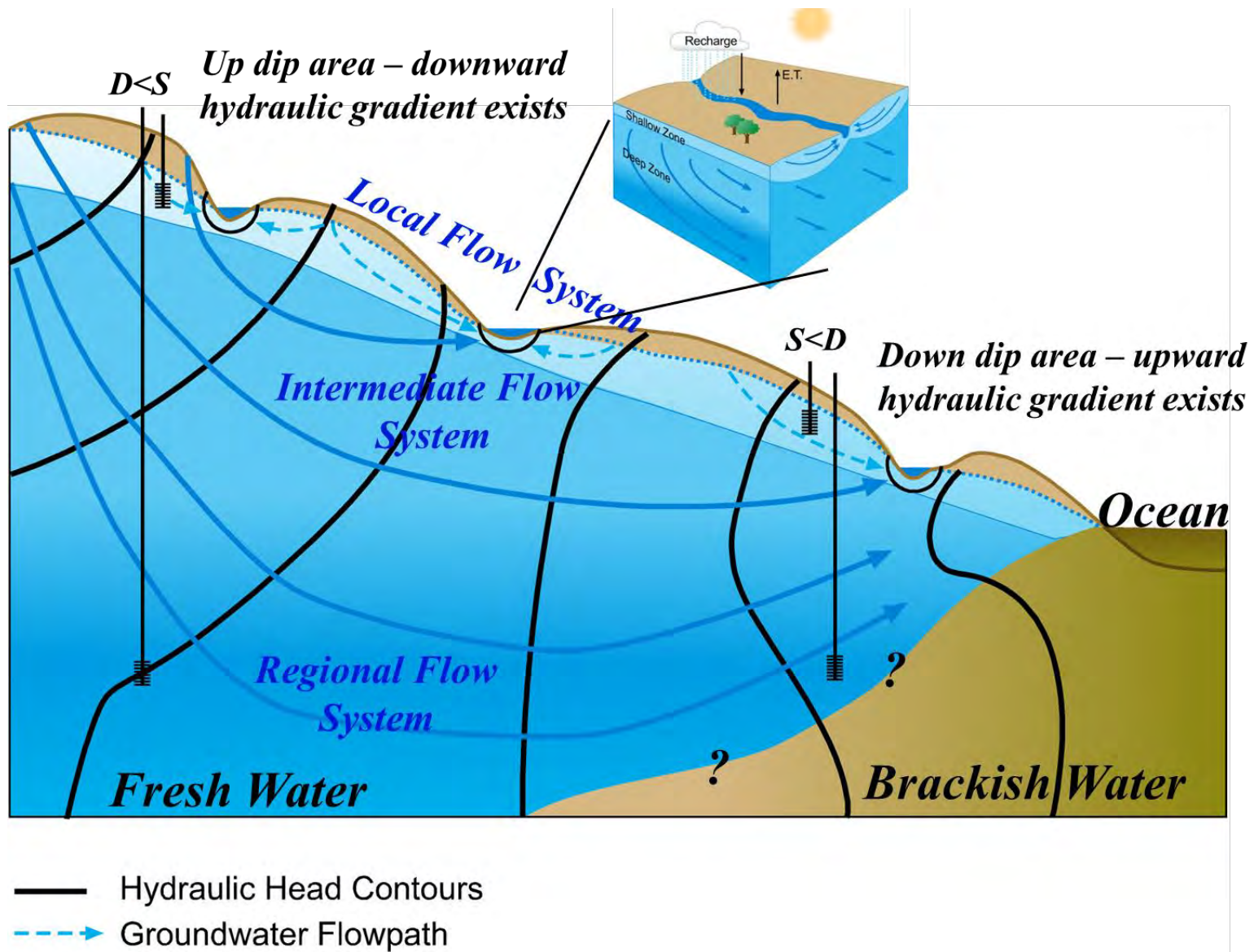


Figure 3-1 Conceptual flow model of gravity driven groundwater flow in the Texas Gulf Coast Aquifer System based on the local, intermediate, and regional flow systems.

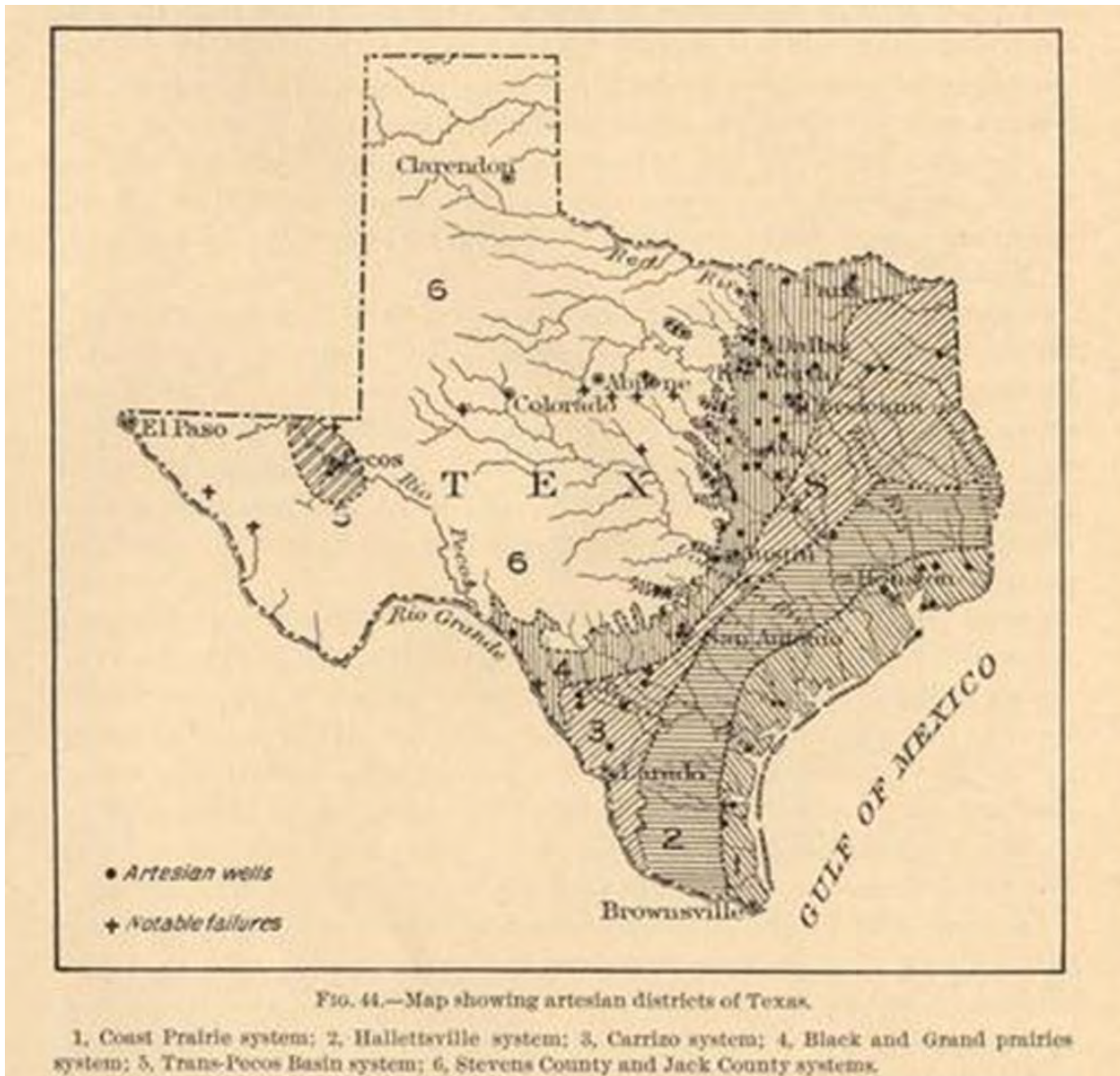


Figure 3-2 Texas Gulf Coast Area underlain by aquifers with artesian pressures (above land surface) in the early 1900's (from Hill, 1901).

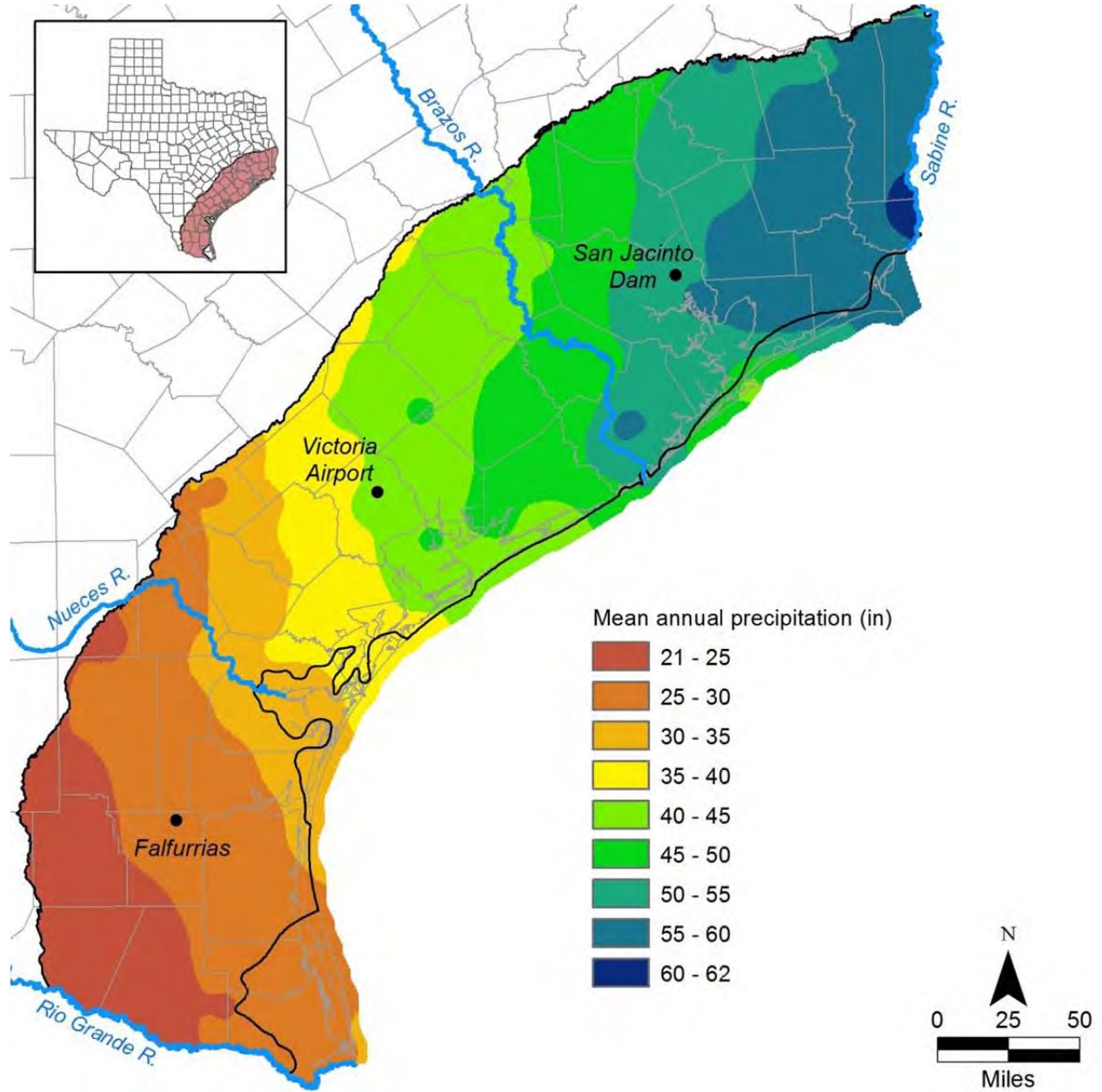


Figure 3-3 Mean annual precipitation in the Texas Gulf Coast region (1971 – 2000; PRISM www.prism.oregonstate.edu). Points represent locations of weather stations used in the study by Scanlon and others (2012). Black lines represent extent of the Gulf Coast Aquifer System study area regions bounded by the Rio Grande and Nueces Rivers, the Nueces and Brazos Rivers and the Brazos and Sabine Rivers (from Scanlon and others, 2012).

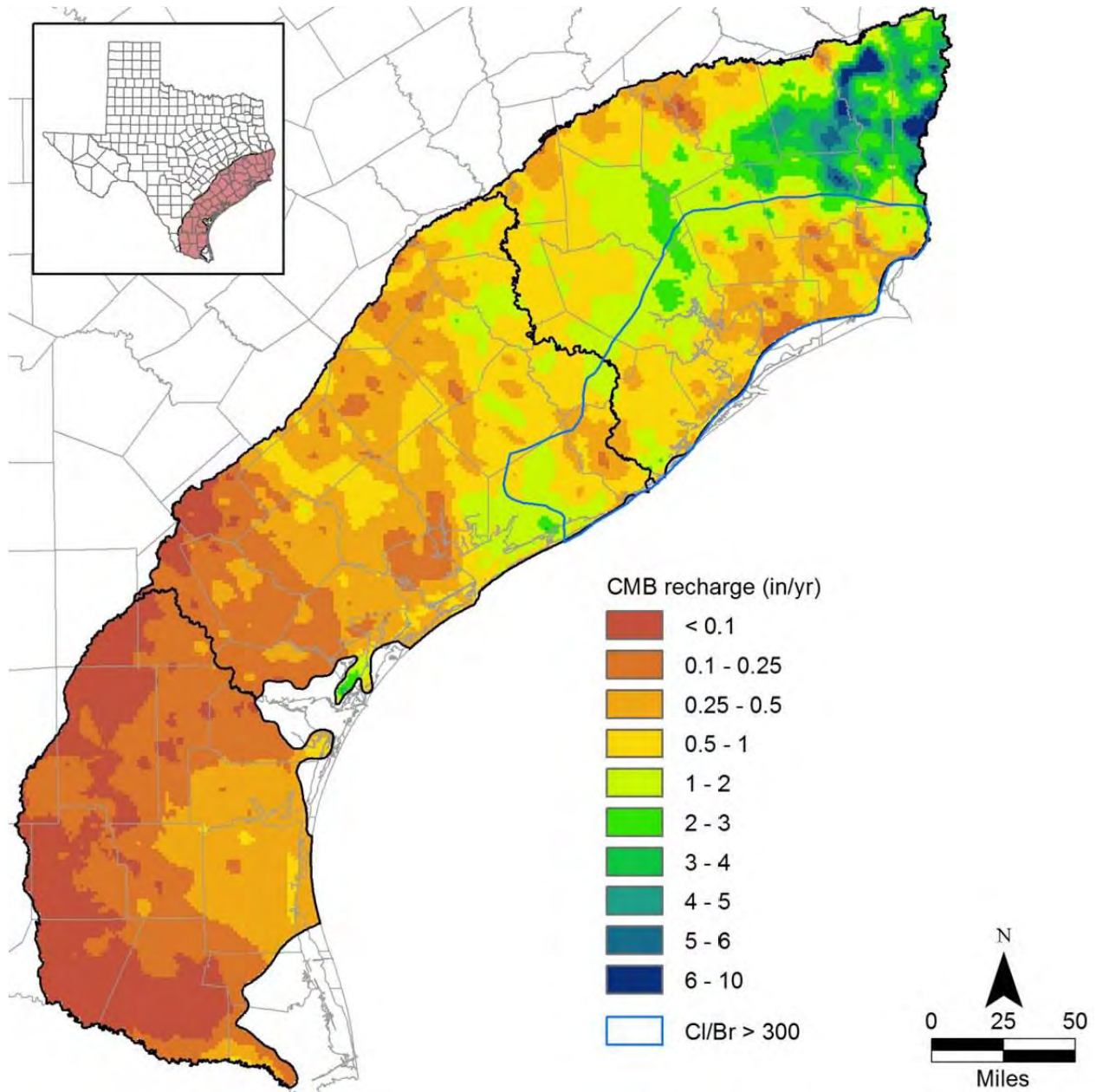


Figure 3-4 Distribution of groundwater chloride mass balance (CMB) recharge rates based on groundwater chloride concentrations and chloride concentration in bulk precipitation in the Gulf Coast Aquifer System. Blue line delineates northern region where Cl/Br > 300. Black lines represent extent of the Gulf Coast Aquifer System study area subdivided into southern, central, and northern regions (from Scanlon and others, 2012).

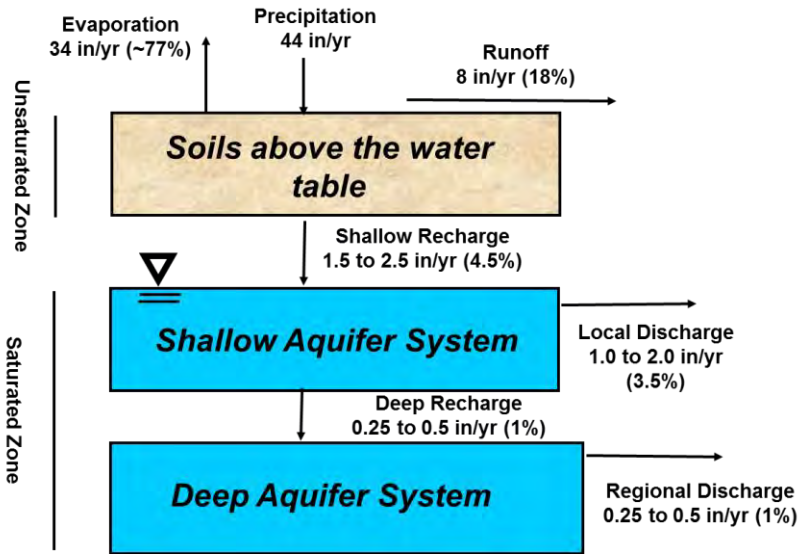


Figure 3-5 Conceptual water budget for the Lower Colorado River Basin Model (Young and others, 2006). Note that the shallow recharge includes enhanced recharge induced by the large amount of flooding that occurs with rice production in the Lower Colorado River Basin.

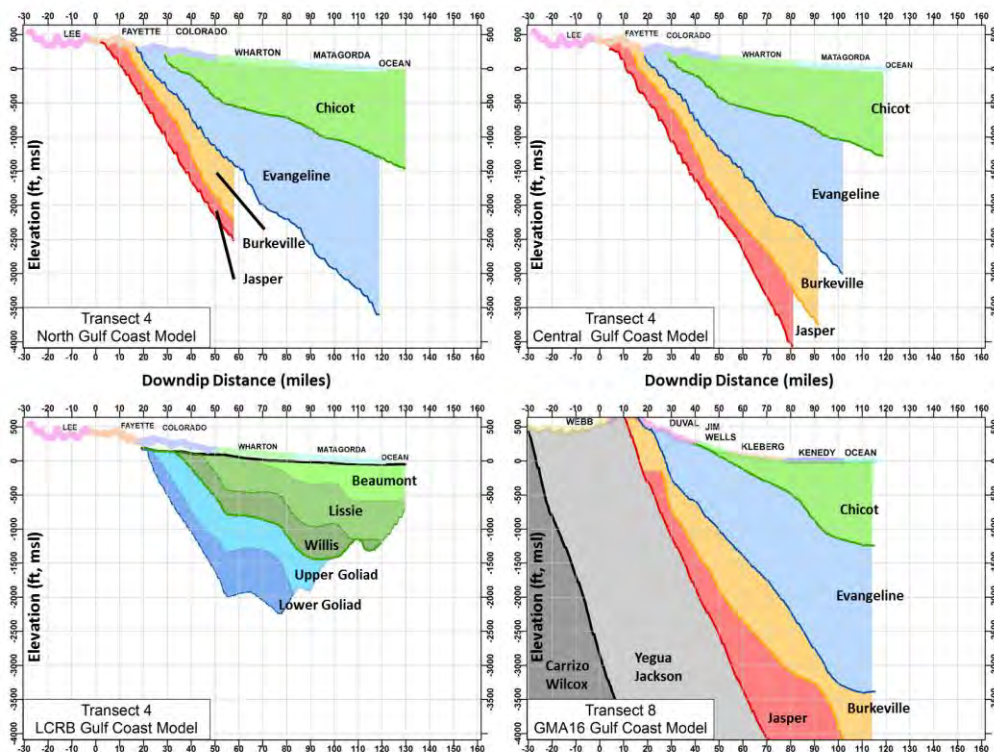


Figure 3-6 Comparison of the location of the down-dip boundary condition at Transect 4 for the Northern Gulf Coast Aquifer System GAM, Central Gulf Coast Aquifer System GAM, and the LCRB Model, and at Transect 8 for the GMA 16 AGM.

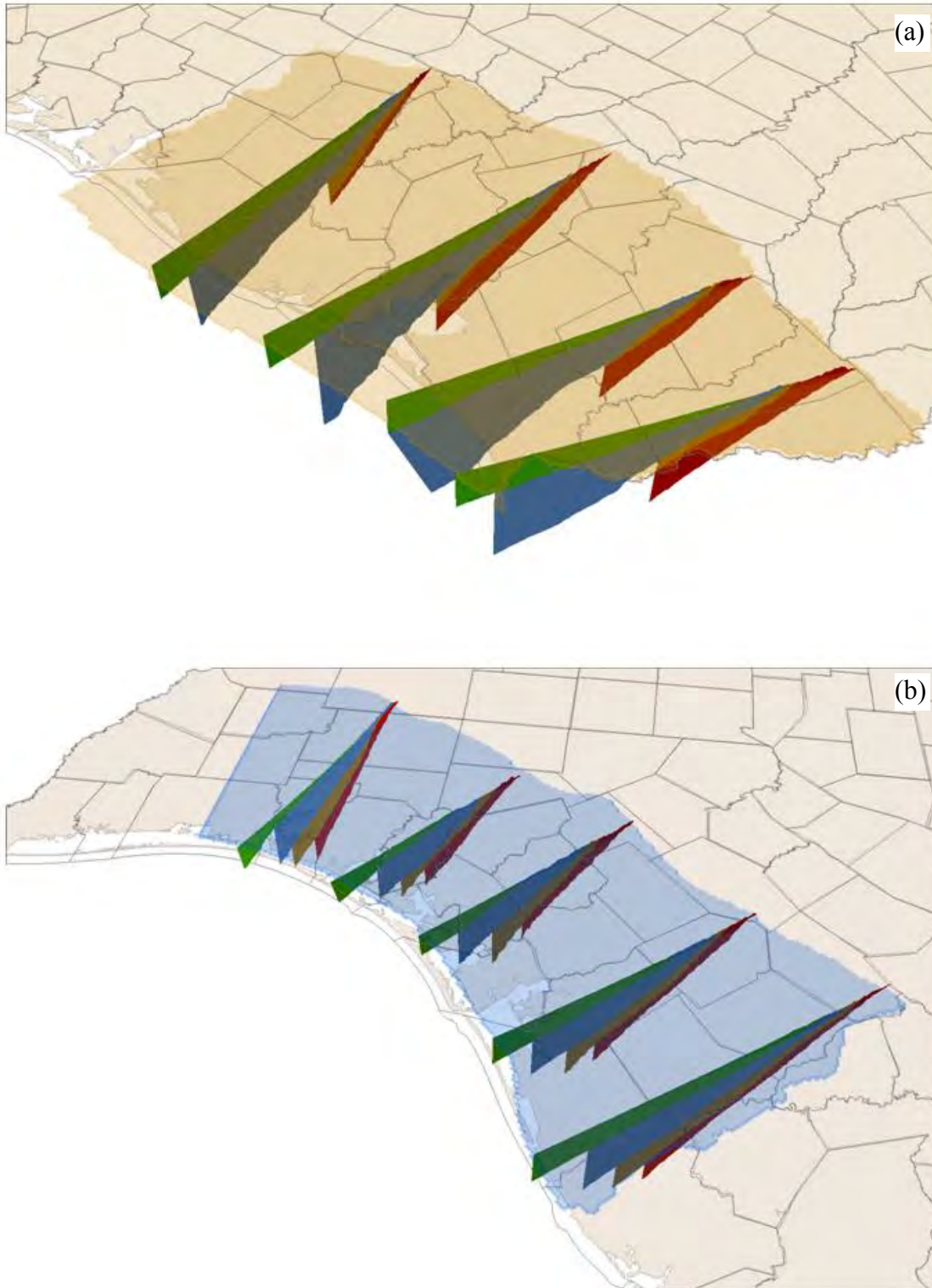


Figure 3-7 Three dimensional view of: (a) Transects 1, 2, 3, and 4 for the Northern Gulf Coast Aquifer System GAM; and (b) Transects 4, 5, 6, 7 and 8 for the Central Gulf Coast Aquifer System GAM. The shaded areas in each model represent domain of the groundwater model. The model domain is represented by the shaded area.

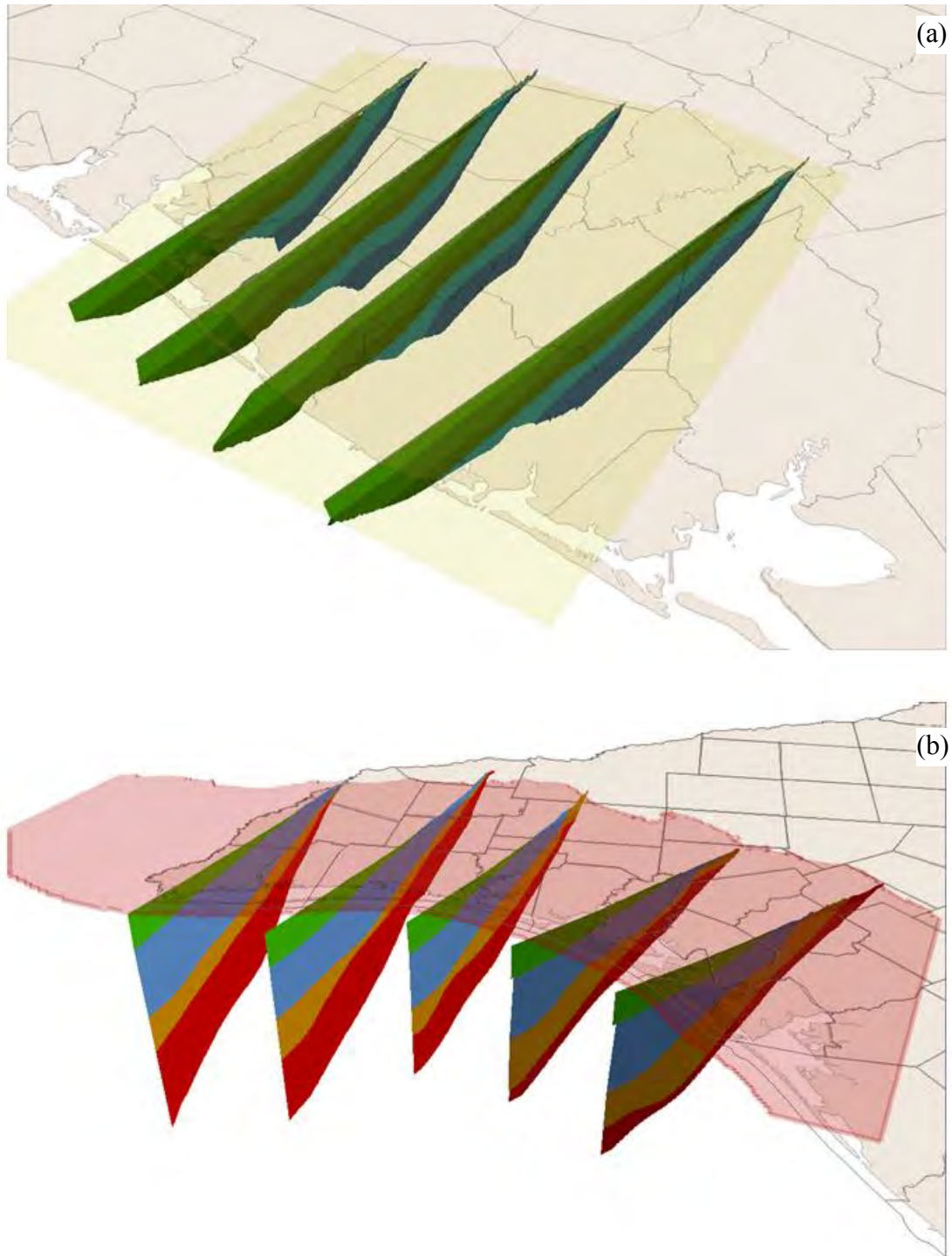


Figure 3-8 Three dimensional view of: (a) Transects 34, 4, 45, and 5 for the LCRB Model; and (b) Transects 6, 7, 8, and 9 for the GMA 16 AGM. The shaded areas in each model represent domain of the groundwater model. The model domain is represented by the shaded area.

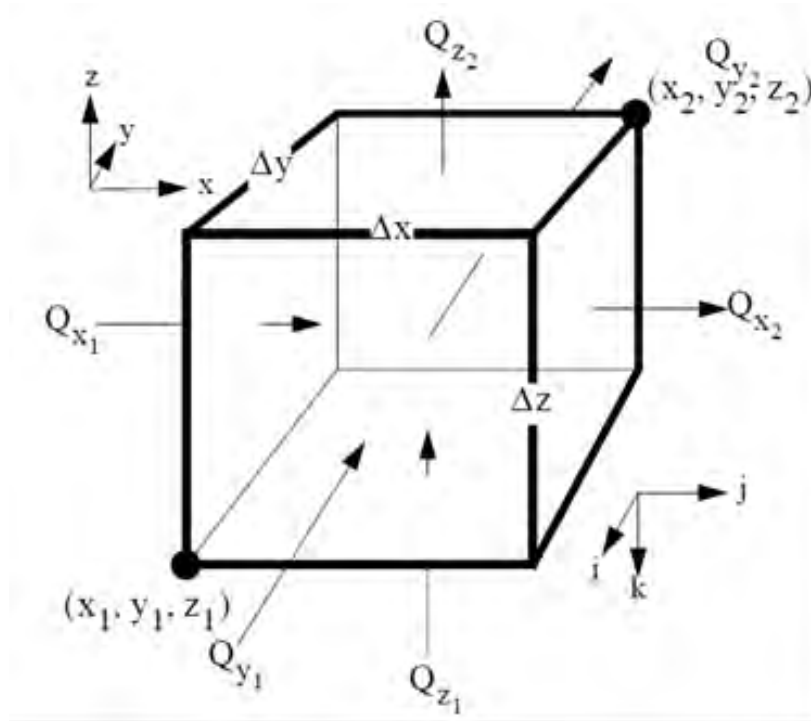


Figure 3-9 Schematic showing the groundwater fluxes through the six faces of a grid cell (from Pollock, 1994).

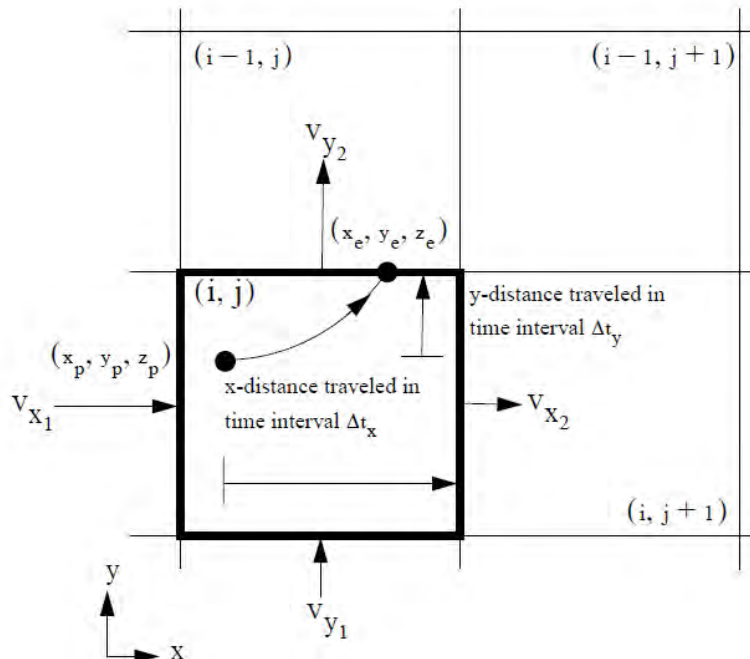


Figure 3-10 Schematic showing the computation of exit point and travel time for the case of a two-dimensional flow in the x-y plane (from Pollock, 1994).

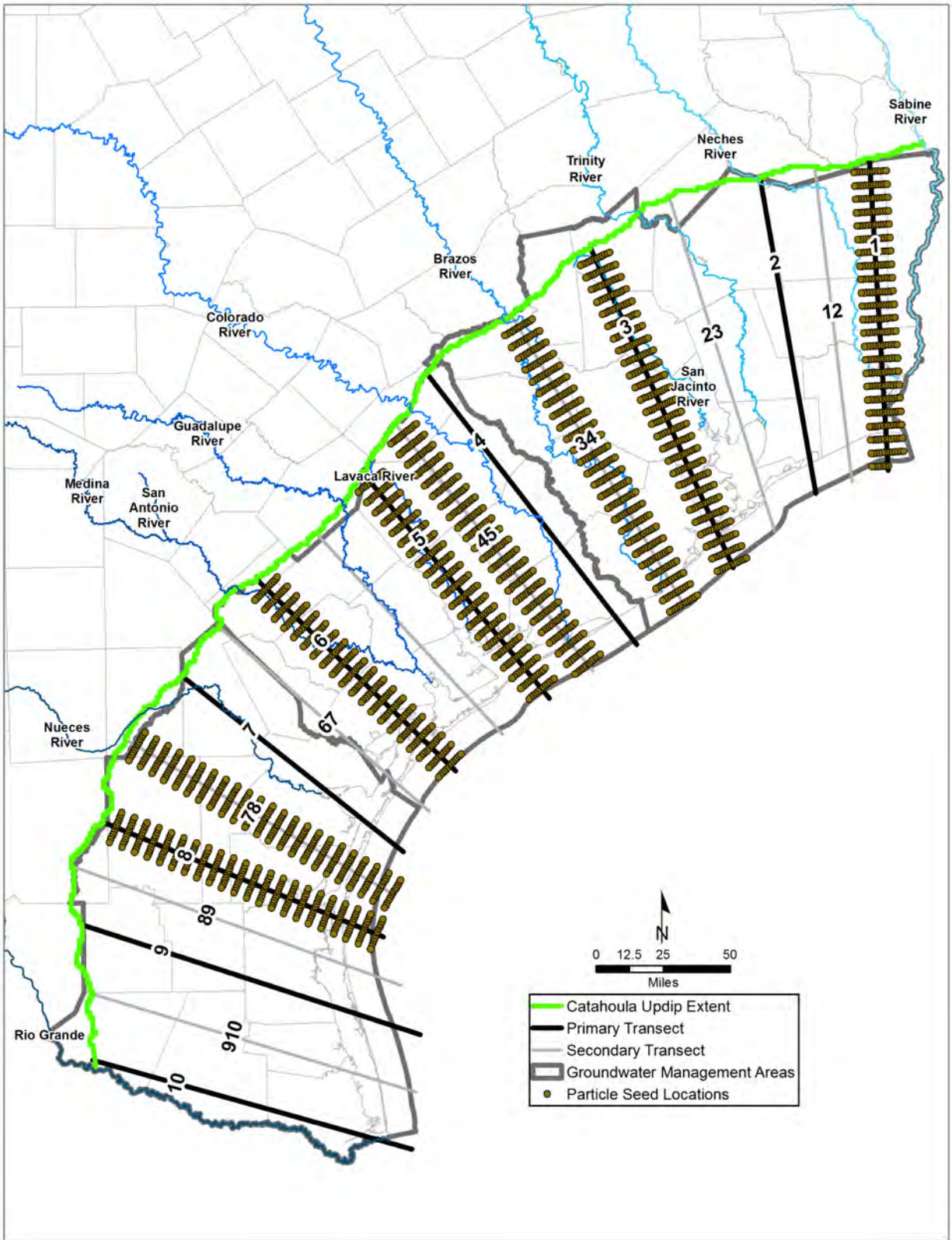


Figure 3-11 Starting locations of the particle seeds used for reverse particle tracking with MODPATH to estimate groundwater age.

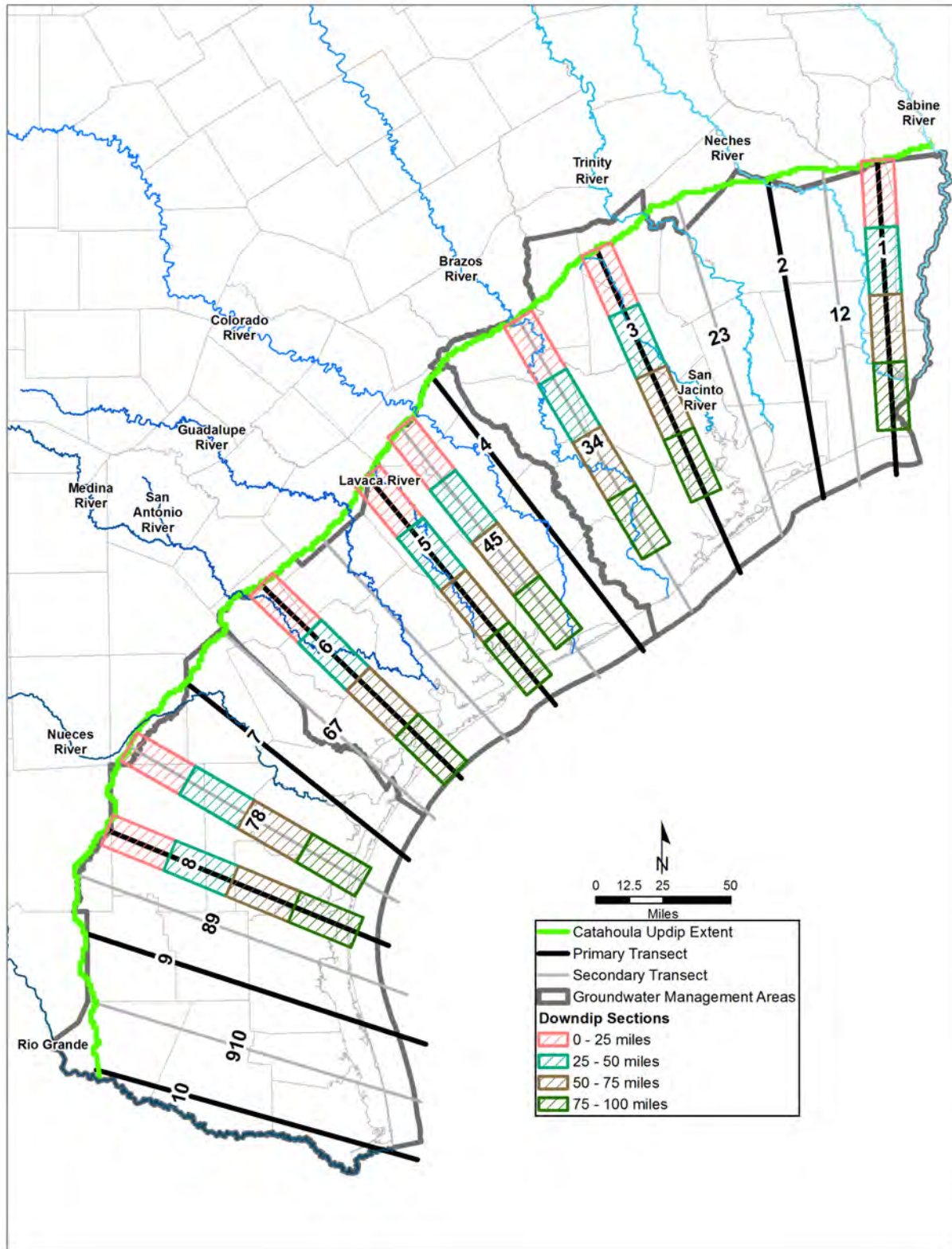
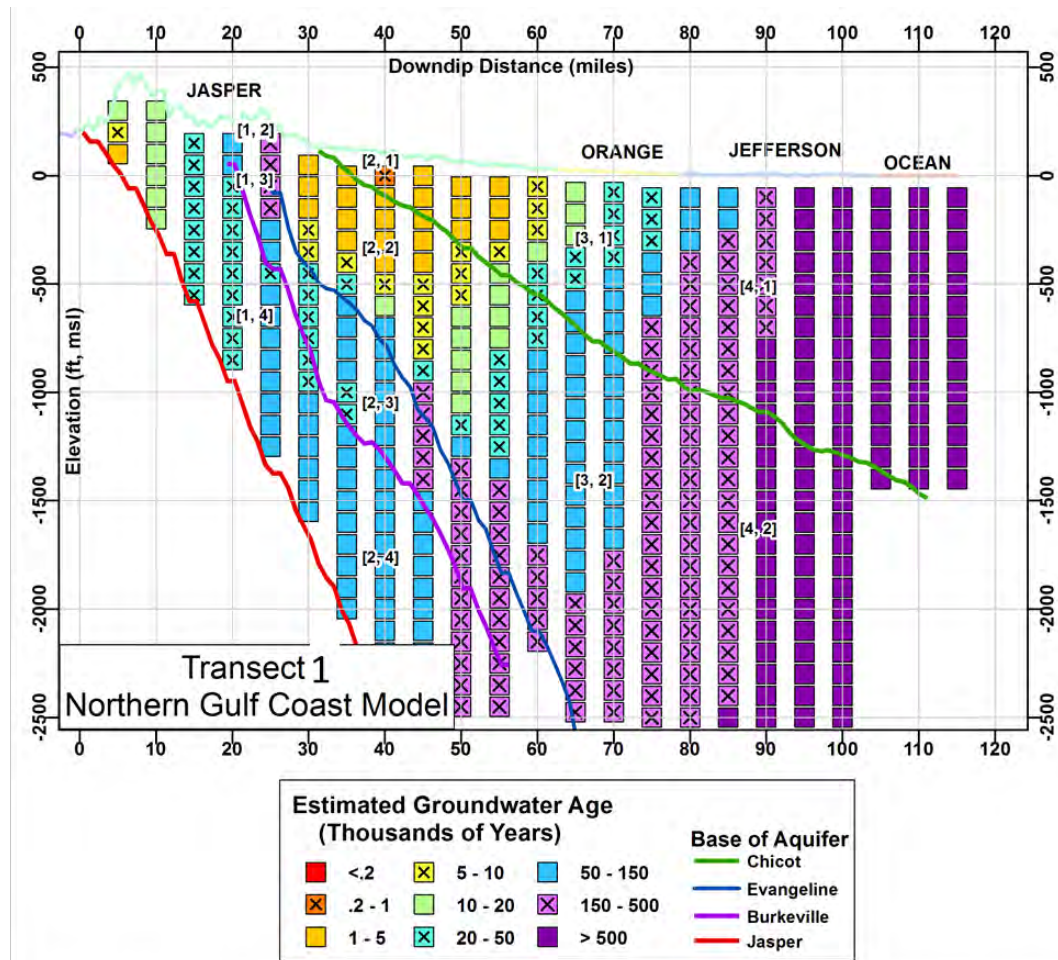


Figure 3-12 Locations of the polygons used to define the blocks of cells used to calculate the water balances of different sections of the Gulf Coast Aquifer System along the transects.

Final – Hydrogeochemical Evaluation of the Texas Gulf Coast Aquifer System and Implications for Developing Groundwater Availability Models



Section	Zone	Unit	Area (mi ²)	Average Unit Groundwater Flux (ft/day)							Cross-Flow Ratio	
				Updip	Downdip	Above	Below	Lateral	GHB	Recharge		SW Int
0 to 25 miles	[1,1]	Chicot										
	[1,2]	Evangeline										
	[1,3]	Burkeville	62	0.0E+0	-3.1E-5	3.7E-5	-8.7E-6	-2.5E-5	8.9E-7	0.0E+0	0.0E+0	1.1977
	[1,4]	Jasper	325	0.0E+0	-1.7E-3	8.7E-6	0.0E+0	-8.1E-4	1.0E-4	0.0E+0	0.0E+0	0.0052
15 to 50 miles	[2,1]	Chicot	267	0.0E+0	-1.2E-2	0.0E+0	-2.5E-5	-1.7E-2	1.1E-4	0.0E+0	0.0E+0	0.0021
	[2,2]	Evangeline	334	6.5E-3	-2.3E-3	2.5E-5	5.8E-6	-1.9E-3	1.6E-5	0.0E+0	0.0E+0	0.0038
	[2,3]	Burkeville	336	3.1E-5	-1.3E-6	-5.8E-6	5.8E-6	-1.2E-5	0.0E+0	0.0E+0	0.0E+0	0.1865
	[2,4]	Jasper	262	1.7E-3	-1.3E-4	-5.8E-6	0.0E+0	-1.1E-4	0.0E+0	0.0E+0	0.0E+0	0.0034
50 to 75 miles	[3,1]	Chicot	325	1.2E-2	-1.6E-3	0.0E+0	1.3E-5	-5.1E-4	-2.2E-5	0.0E+0	0.0E+0	0.0011
	[3,2]	Evangeline	335	2.3E-3	-3.8E-4	-1.3E-5	7.4E-6	4.2E-5	0.0E+0	0.0E+0	0.0E+0	0.0056
	[3,3]	Burkeville	87	1.3E-6	0.0E+0	-7.4E-6	7.4E-6	2.7E-7	0.0E+0	0.0E+0	0.0E+0	5.8743
	[3,4]	Jasper										
75 to 100 miles	[4,1]	Chicot	326	1.6E-3	-1.9E-5	0.0E+0	1.9E-5	5.6E-4	-4.1E-5	0.0E+0	0.0E+0	0.0123
	[4,2]	Evangeline	292	3.8E-4	-8.2E-6	-1.9E-5	0.0E+0	2.0E-4	0.0E+0	0.0E+0	0.0E+0	0.0503
	[4,3]	Burkeville										
	[4,4]	Jasper										

Figure 3-13 Transect 1 groundwater ages and groundwater fluxes calculated using the Northern Gulf Coast Aquifer System GAM. (negative values indicate flow in the opposite directions and are highlighted in yellow).

Final – Hydrogeochemical Evaluation of the Texas Gulf Coast Aquifer System and Implications for Developing Groundwater Availability Models

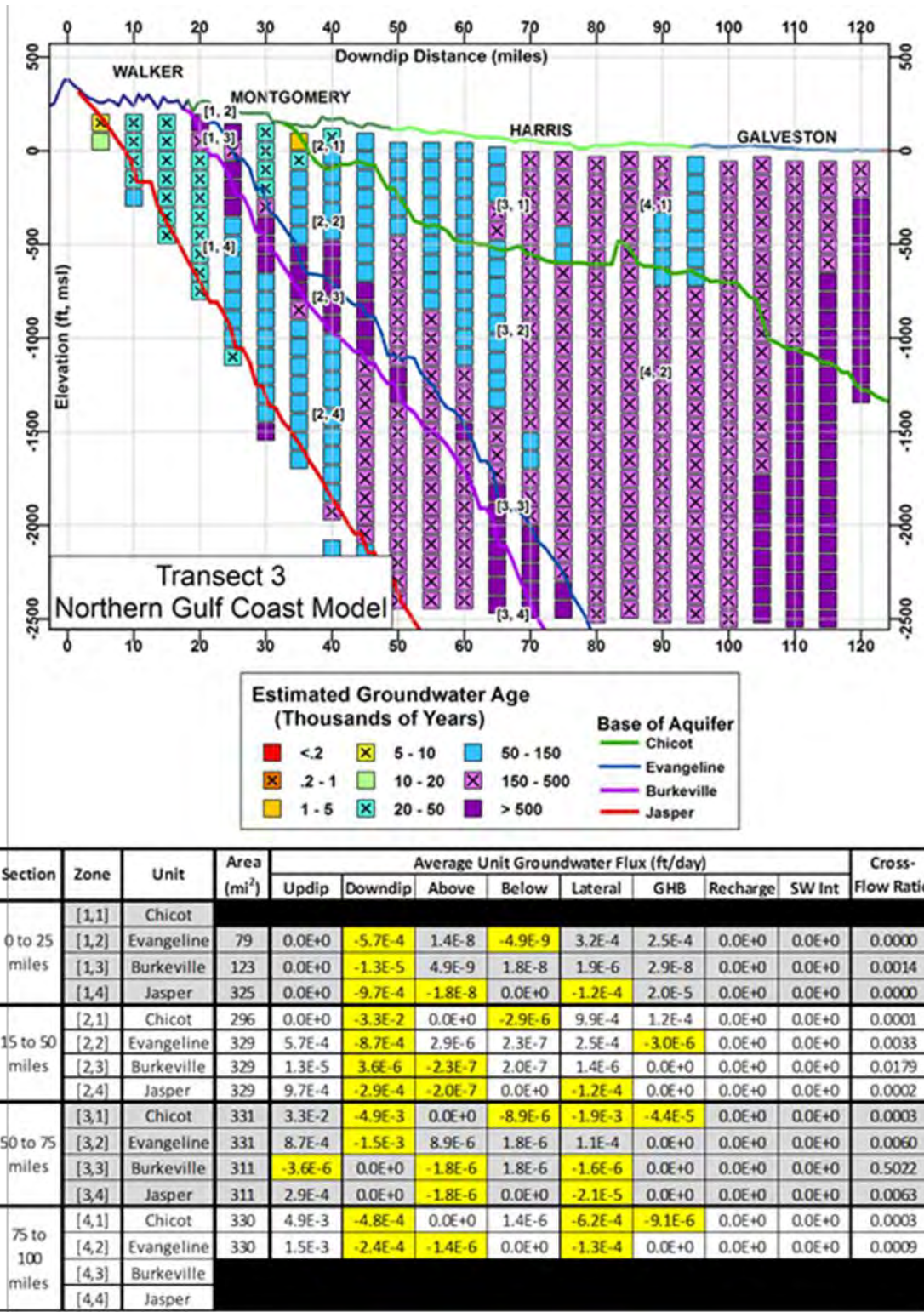
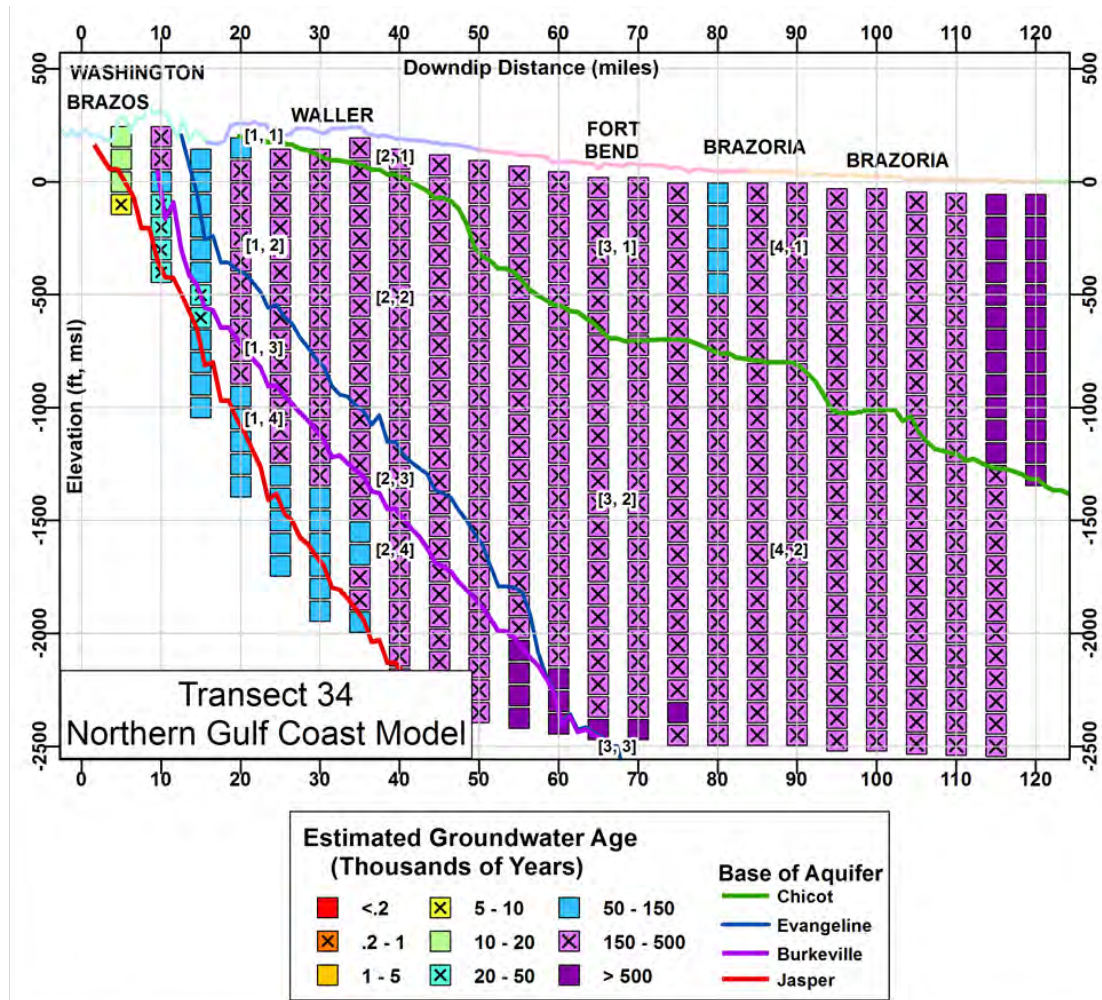


Figure 3-14 Transect 3 groundwater ages and groundwater fluxes calculated using the Northern Gulf Coast Aquifer System GAM (negative values indicate flow in the opposite directions and are highlighted in yellow).

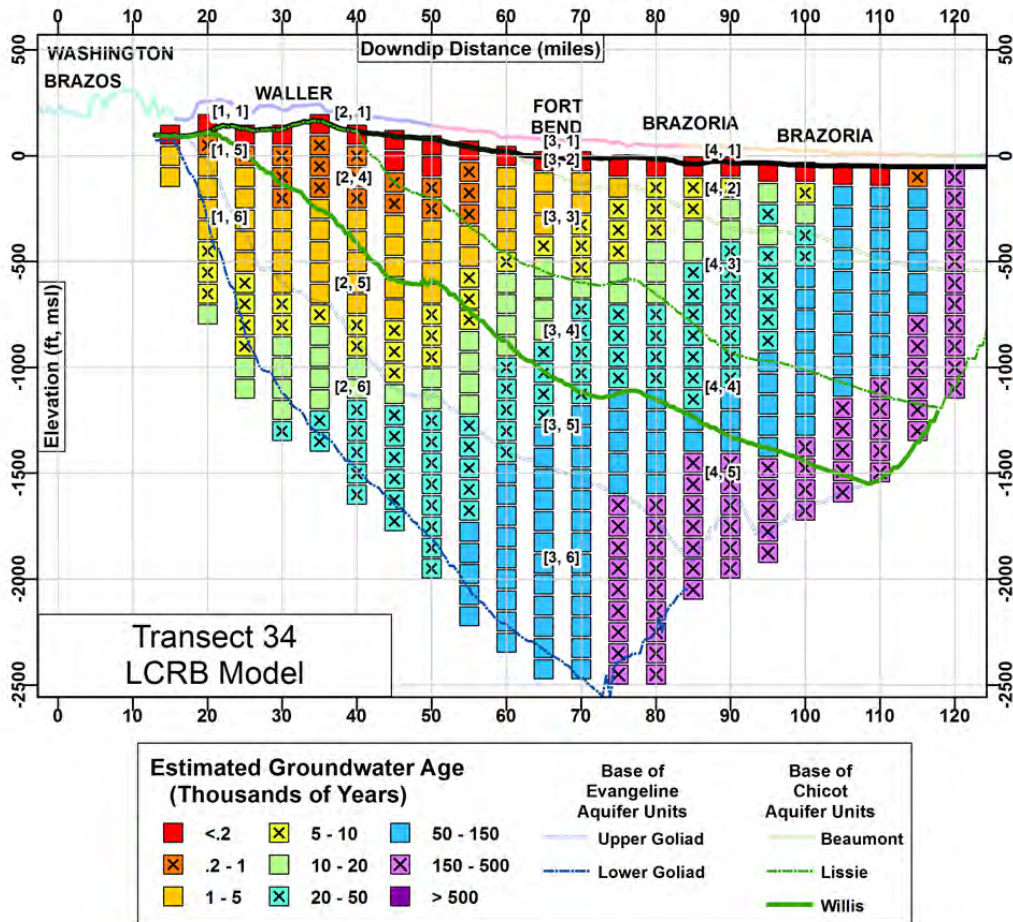
Final – Hydrogeochemical Evaluation of the Texas Gulf Coast Aquifer System and Implications for Developing Groundwater Availability Models



Section	Zone	Unit	Area (mi ²)	Average Unit Groundwater Flux (ft/day)								Cross-Flow Ratio
				Updip	Downdip	Above	Below	Lateral	GHB	Recharge	SW Int	
0 to 25 miles	[1,1]	Chicot	86	0.0E+0	-3.3E-3	0.0E+0	-1.0E-4	1.8E-4	1.1E-4	0.0E+0	0.0E+0	0.0307
	[1,2]	Evangeline	195	0.0E+0	-1.7E-3	1.0E-4	1.5E-5	2.9E-3	-1.9E-4	0.0E+0	0.0E+0	0.0583
	[1,3]	Burkeville	231	0.0E+0	-1.0E-5	-1.5E-5	1.3E-5	2.2E-5	0.0E+0	0.0E+0	0.0E+0	1.4583
	[1,4]	Jasper	336	0.0E+0	-2.8E-4	-1.3E-5	0.0E+0	8.5E-4	4.4E-7	0.0E+0	0.0E+0	0.0453
15 to 50 miles	[2,1]	Chicot	309	3.3E-3	-1.7E-2	0.0E+0	-2.2E-5	-2.5E-3	1.1E-4	0.0E+0	0.0E+0	0.0013
	[2,2]	Evangeline	327	1.7E-3	-1.5E-3	2.2E-5	3.4E-6	-2.4E-4	-1.3E-5	0.0E+0	0.0E+0	0.0129
	[2,3]	Burkeville	327	1.0E-5	-2.0E-6	-3.4E-6	3.3E-6	-8.4E-7	0.0E+0	0.0E+0	0.0E+0	0.3214
	[2,4]	Jasper	327	2.8E-4	-6.5E-5	-3.3E-6	0.0E+0	1.3E-4	0.0E+0	0.0E+0	0.0E+0	0.0119
50 to 75 miles	[3,1]	Chicot	326	1.7E-2	-3.9E-3	0.0E+0	1.9E-5	3.2E-3	-1.3E-4	0.0E+0	0.0E+0	0.0011
	[3,2]	Evangeline	326	1.5E-3	-8.5E-4	-1.9E-5	1.3E-6	3.1E-4	0.0E+0	0.0E+0	0.0E+0	0.0123
	[3,3]	Burkeville	196	2.0E-6	0.0E+0	-1.3E-6	1.3E-6	-6.1E-7	0.0E+0	0.0E+0	0.0E+0	0.6329
	[3,4]	Jasper	195	6.5E-5	0.0E+0	-1.3E-6	0.0E+0	2.3E-5	0.0E+0	0.0E+0	0.0E+0	0.0194
75 to 100 miles	[4,1]	Chicot	329	3.9E-3	-6.2E-4	0.0E+0	1.2E-5	6.6E-4	-4.5E-5	0.0E+0	0.0E+0	0.0030
	[4,2]	Evangeline	329	8.5E-4	-3.3E-4	-1.2E-5	0.0E+0	1.4E-4	0.0E+0	0.0E+0	0.0E+0	0.0138
	[4,3]	Burkeville										
	[4,4]	Jasper										

Figure 3-15 Transect 34 groundwater ages and groundwater fluxes calculated using the Northern Gulf Coast Aquifer System GAM (negative values indicate flow in the opposite directions and are highlighted in yellow).

Final – Hydrogeochemical Evaluation of the Texas Gulf Coast Aquifer System and Implications for Developing Groundwater Availability Models



Section	Zone	Unit	Area (mi ²)	Average Unit Groundwater Flux (ft/day)								Cross-Flow Ratio
				Updip	Downdip	Above	Below	Lateral	GHB	Recharge	SW Int	
0 to 25 miles	[1,3]	Shallow	176	0.0E+0	-6.0E-3	0.0E+0	6.4E-6	3.5E-2	0.0E+0	6.9E-3	-8.2E-3	0.0011
	[1,2]	Chicot - BB										
	[1,3]	Chicot - LI										
	[1,4]	Chicot-WI										
	[1,5]	Evangeline-UG	176	0.0E+0	-3.0E-3	-1.3E-5	1.4E-5	3.0E-3	0.0E+0	0.0E+0	0.0E+0	0.0047
25 to 50 miles	[1,6]	Evangeline-LG	0	0.0E+0	-1.6E-3	-1.4E-5	0.0E+0	2.8E-3	0.0E+0	0.0E+0	0.0E+0	0.0089
	[2,2]	Shallow	326	6.0E-3	-3.0E-2	0.0E+0	-2.1E-4	-3.1E-2	0.0E+0	1.1E-2	-5.5E-3	0.0070
	[2,2]	Chicot - BB										
	[2,3]	Chicot - LI	326	3.2E-7	-3.6E-2	2.1E-4	-8.1E-5	-2.4E-2	0.0E+0	0.0E+0	0.0E+0	0.0058
	[2,4]	Chicot-WI	326	8.4E-3	-1.1E-2	8.1E-5	-1.3E-5	-3.7E-3	0.0E+0	0.0E+0	0.0E+0	0.0073
50 to 75 miles	[2,5]	Evangeline-UG	326	3.0E-3	-4.6E-3	1.3E-5	9.3E-8	-3.3E-4	0.0E+0	0.0E+0	0.0E+0	0.0027
	[2,6]	Evangeline-LG	0	1.6E-3	-1.6E-3	-9.3E-8	0.0E+0	1.7E-4	0.0E+0	0.0E+0	0.0E+0	0.0001
	[3,3]	Shallow	324	3.0E-2	-5.3E-2	0.0E+0	9.3E-5	7.7E-3	0.0E+0	7.5E-4	-8.4E-4	0.0018
	[3,2]	Chicot - BB	324	1.0E-6	-7.7E-3	-9.3E-5	8.9E-5	6.6E-3	0.0E+0	0.0E+0	0.0E+0	0.0121
	[3,3]	Chicot - LI	324	3.6E-2	-8.7E-3	-8.9E-5	3.5E-5	-8.3E-5	0.0E+0	0.0E+0	0.0E+0	0.0024
75 to 100 miles	[3,4]	Chicot-WI	324	1.1E-2	-5.6E-3	-3.5E-5	2.2E-5	-8.7E-5	0.0E+0	0.0E+0	0.0E+0	0.0032
	[3,5]	Evangeline-UG	324	4.6E-3	-1.3E-3	-2.2E-5	6.6E-6	9.4E-5	0.0E+0	0.0E+0	0.0E+0	0.0048
	[3,6]	Evangeline-LG	0	1.6E-3	-1.6E-4	-6.6E-6	0.0E+0	-4.0E-5	0.0E+0	0.0E+0	0.0E+0	0.0042
	[4,4]	Shallow	317	5.3E-2	-1.5E-2	0.0E+0	6.1E-5	8.1E-3	0.0E+0	1.7E-3	-1.8E-3	0.0012
	[4,2]	Chicot - BB	317	7.7E-3	-1.8E-3	-6.1E-5	4.8E-5	1.4E-3	0.0E+0	0.0E+0	0.0E+0	0.0079
100 to 120 miles	[4,3]	Chicot - LI	317	8.7E-3	-1.7E-3	-4.8E-5	2.4E-5	4.8E-4	0.0E+0	0.0E+0	0.0E+0	0.0055
	[4,4]	Chicot-WI	315	5.6E-3	-1.1E-3	-2.4E-5	4.6E-6	2.2E-4	0.0E+0	0.0E+0	0.0E+0	0.0042
	[4,5]	Evangeline-UG	96	1.3E-3	-2.2E-4	-4.6E-6	2.5E-6	-1.8E-5	0.0E+0	0.0E+0	0.0E+0	0.0035
	[4,6]	Evangeline-LG										

Figure 3-16 Transect 34 groundwater ages and groundwater fluxes calculated using the LCRB Model (negative values indicate flow in the opposite directions and are highlighted in yellow).

Final – Hydrogeochemical Evaluation of the Texas Gulf Coast Aquifer System and Implications for Developing Groundwater Availability Models

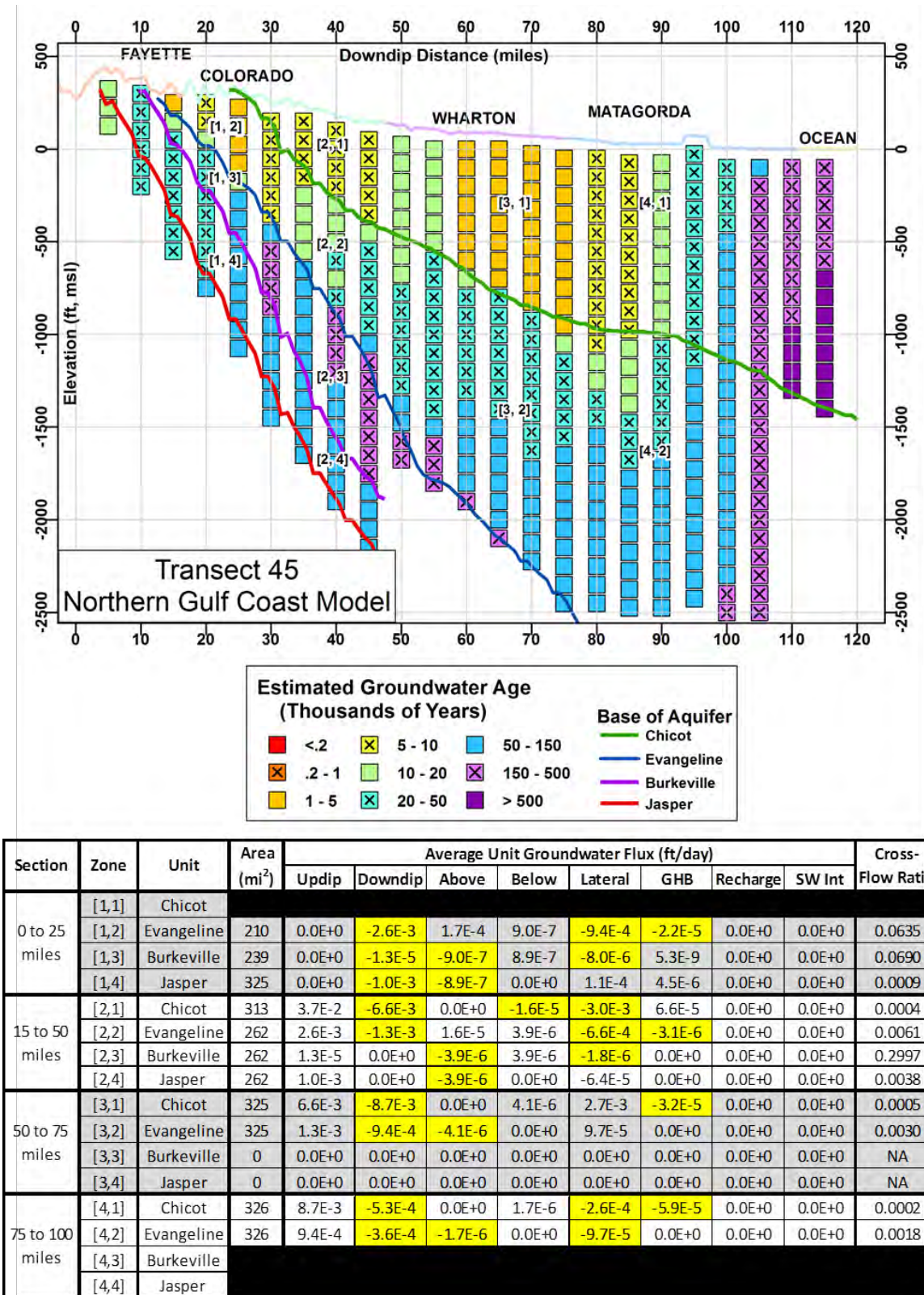
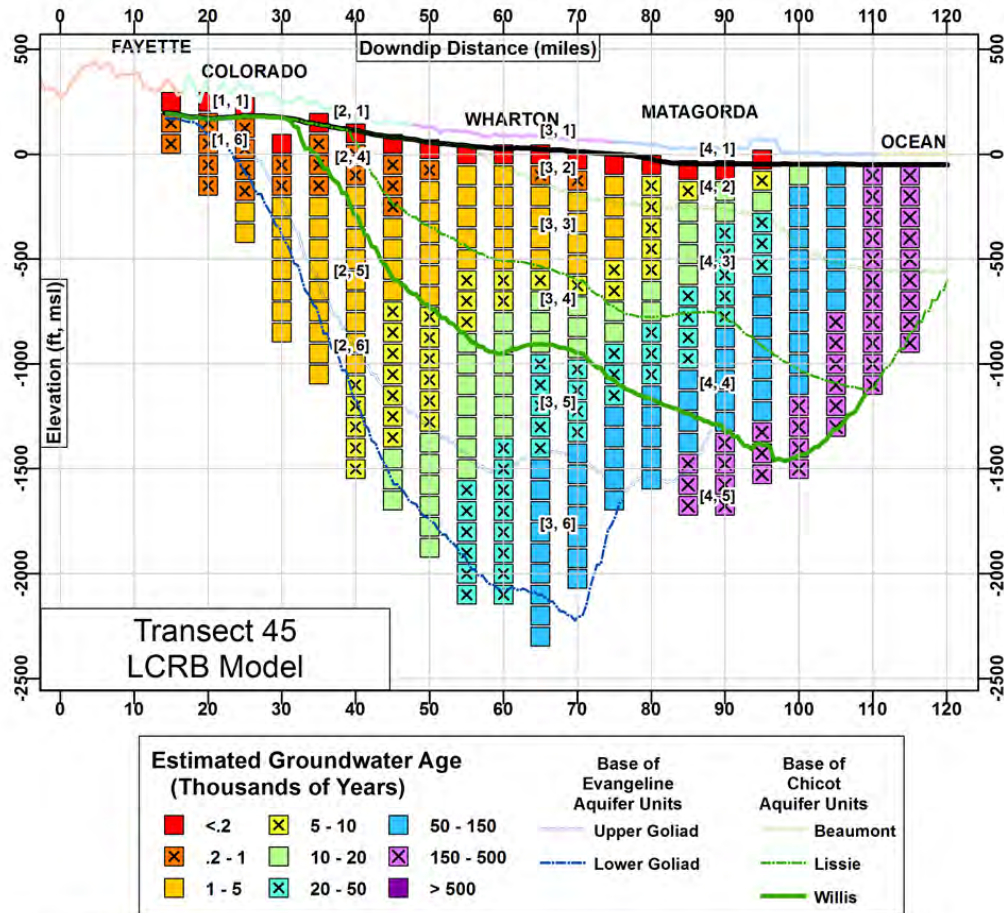


Figure 3-17 Transect 45 groundwater ages and groundwater fluxes calculated using the Northern Gulf Coast Aquifer System GAM (negative values indicate flow in the opposite directions and are highlighted in yellow).

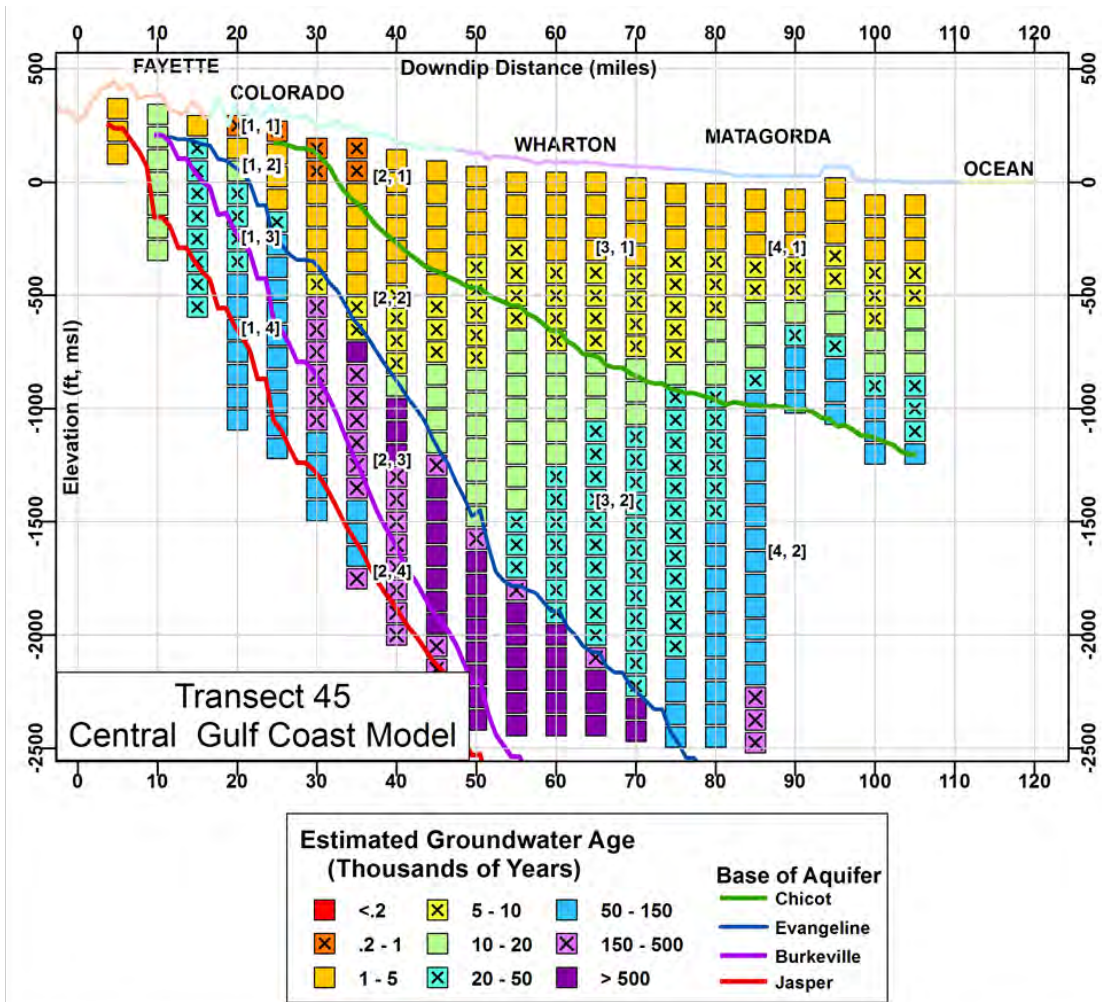
Final – Hydrogeochemical Evaluation of the Texas Gulf Coast Aquifer System and Implications for Developing Groundwater Availability Models



Section	Zone	Unit	Area (mi ²)	Average Unit Groundwater Flux (ft/day)								Cross-Flow Ratio
				Updip	Downdip	Above	Below	Lateral	GHB	Recharge	SW Int	
0 to 25 miles	[1,3]	Shallow	155	0.0E+0	-5.5E-3	0.0E+0	-9.3E-5	-1.1E-3	0.0E+0	4.4E-4	-3.4E-4	0.0170
	[1,2]	Chicot - BB										
	[1,3]	Chicot - LI										
	[1,4]	Chicot - WI										
25 to 50 miles	[1,5]	Evangeline-UG	155	0.0E+0	-1.2E-2	9.3E-5	-4.2E-5	-1.0E-2	0.0E+0	0.0E+0	0.0E+0	0.0080
	[1,6]	Evangeline-LG	0	0.0E+0	-1.1E-2	4.2E-5	0.0E+0	-5.9E-3	0.0E+0	0.0E+0	0.0E+0	0.0037
	[2,2]	Shallow	307	5.5E-3	-2.1E-2	0.0E+0	-1.5E-4	-5.6E-3	0.0E+0	5.7E-4	-4.0E-4	0.0075
	[2,2]	Chicot - BB										
50 to 75 miles	[2,3]	Chicot - LI	307	2.1E-7	-2.0E-2	1.5E-4	-9.2E-5	2.3E-4	0.0E+0	0.0E+0	0.0E+0	0.0078
	[2,4]	Chicot - WI	307	2.1E-7	-9.6E-3	9.2E-5	-4.3E-5	-3.0E-3	0.0E+0	0.0E+0	0.0E+0	0.0096
	[2,5]	Evangeline-UG	307	1.2E-2	-4.0E-3	4.3E-5	-3.1E-6	-2.4E-3	0.0E+0	0.0E+0	0.0E+0	0.0037
	[2,6]	Evangeline-LG	0	1.1E-2	-2.3E-3	3.1E-6	0.0E+0	-9.4E-4	0.0E+0	0.0E+0	0.0E+0	0.0003
75 to 100 miles	[3,3]	Shallow	307	2.1E-2	-9.0E-3	0.0E+0	2.7E-5	1.5E-3	0.0E+0	6.1E-4	-6.5E-4	0.0013
	[3,2]	Chicot - BB	307	6.8E-7	-4.4E-3	-2.7E-5	3.3E-5	5.5E-4	0.0E+0	0.0E+0	0.0E+0	0.0075
	[3,3]	Chicot - LI	307	2.0E-2	-6.7E-3	-3.3E-5	2.6E-5	-2.2E-3	0.0E+0	0.0E+0	0.0E+0	0.0017
	[3,4]	Chicot - WI	307	9.6E-3	-3.2E-3	-2.6E-5	1.4E-5	-6.5E-4	0.0E+0	0.0E+0	0.0E+0	0.0027
100 to 120 miles	[3,5]	Evangeline-UG	285	4.0E-3	-1.5E-3	-1.4E-5	6.8E-6	-3.5E-4	0.0E+0	0.0E+0	0.0E+0	0.0034
	[3,6]	Evangeline-LG	0	2.3E-3	0.0E+0	-6.8E-6	0.0E+0	-1.2E-4	0.0E+0	0.0E+0	0.0E+0	0.0030
	[4,4]	Shallow	307	9.0E-3	-6.1E-3	0.0E+0	4.1E-5	1.4E-2	-2.6E-8	5.7E-4	-6.3E-4	0.0045
	[4,2]	Chicot - BB	307	4.4E-3	-6.7E-4	-4.1E-5	3.1E-5	5.0E-4	0.0E+0	0.0E+0	0.0E+0	0.0092
120 to 140 miles	[4,3]	Chicot - LI	307	6.7E-3	-6.5E-4	-3.1E-5	9.7E-6	-1.1E-4	0.0E+0	0.0E+0	0.0E+0	0.0047
	[4,4]	Chicot - WI	186	3.2E-3	-3.6E-4	-9.7E-6	6.4E-6	-1.3E-4	0.0E+0	0.0E+0	0.0E+0	0.0030
	[4,5]	Evangeline-UG	0	1.5E-3	0.0E+0	-6.4E-6	0.0E+0	-7.9E-5	0.0E+0	0.0E+0	0.0E+0	0.0043
	[4,6]	Evangeline-LG										

Figure 3-18 Transect 45 groundwater ages and groundwater fluxes calculated using the LCRB Model (negative values indicate flow in the opposite directions and are highlighted in yellow).

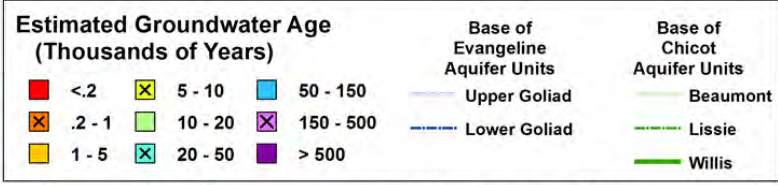
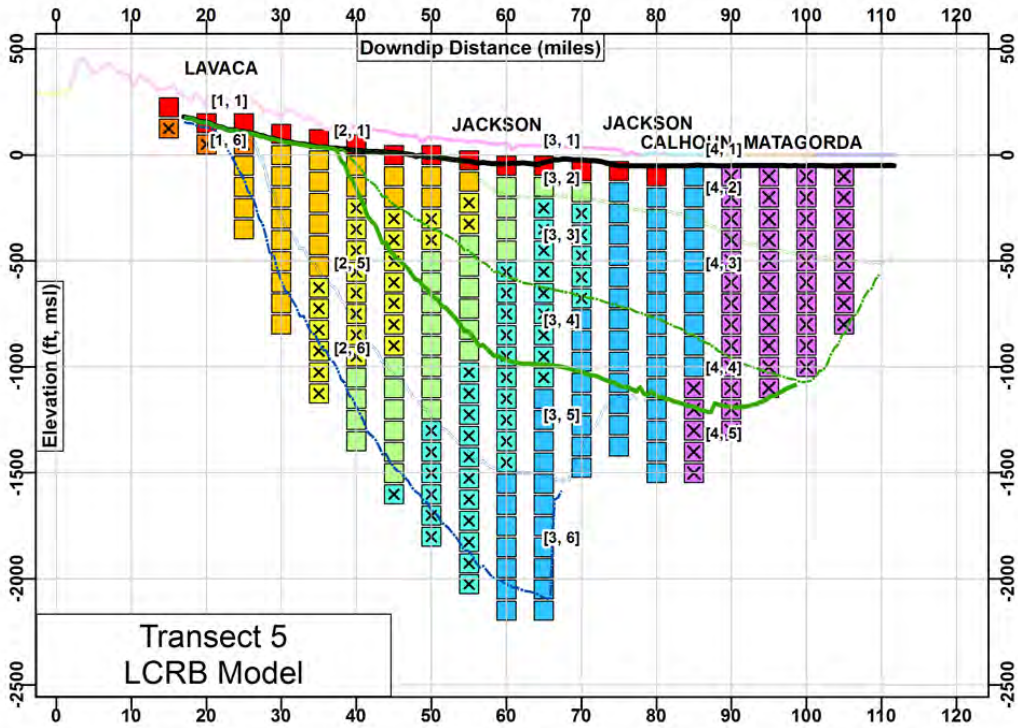
Final – Hydrogeochemical Evaluation of the Texas Gulf Coast Aquifer System and Implications for Developing Groundwater Availability Models



Section	Zone	Unit	Area (mi ²)	Average Unit Groundwater Flux (ft/day)								Cross-Flow Ratio
				Updip	Downdip	Above	Below	Lateral	GHB	Recharge	SW Int	
0 to 25 miles	[1,1]	Chicot										
	[1,2]	Evangeline	224	0.0E+0	-6.6E-3	8.0E-5	3.6E-6	-8.9E-4	0.0E+0	1.8E-4	-6.5E-5	0.0120
	[1,3]	Burkeville	253	0.0E+0	-3.3E-5	-3.6E-6	9.3E-7	-3.3E-6	0.0E+0	5.4E-6	-2.7E-6	0.1086
	[1,4]	Jasper	334	0.0E+0	-5.1E-4	-9.3E-7	0.0E+0	7.4E-5	0.0E+0	1.3E-5	-1.1E-5	0.0018
15 to 50 miles	[2,1]	Chicot	321	1.8E-2	-9.9E-3	0.0E+0	-2.8E-5	-4.1E-3	0.0E+0	4.1E-5	7.3E-5	0.0016
	[2,2]	Evangeline	326	6.6E-3	-3.0E-3	2.8E-5	6.7E-7	-1.3E-3	0.0E+0	6.6E-7	0.0E+0	0.0042
	[2,3]	Burkeville	326	3.3E-5	-1.4E-5	-6.7E-7	7.0E-7	-3.2E-6	0.0E+0	0.0E+0	0.0E+0	0.0214
	[2,4]	Jasper	326	5.1E-4	-2.5E-4	-7.0E-7	0.0E+0	-4.0E-5	0.0E+0	0.0E+0	0.0E+0	0.0014
50 to 75 miles	[3,1]	Chicot	328	9.9E-3	-1.3E-2	0.0E+0	-2.8E-6	-2.5E-3	0.0E+0	4.2E-5	7.1E-5	0.0002
	[3,2]	Evangeline	328	3.0E-3	-1.4E-3	2.8E-6	5.3E-7	-3.3E-4	0.0E+0	0.0E+0	0.0E+0	0.0009
	[3,3]	Burkeville	328	1.4E-5	-3.6E-6	-5.3E-7	7.4E-7	-6.9E-7	0.0E+0	0.0E+0	0.0E+0	0.0526
	[3,4]	Jasper	213	2.5E-4	0.0E+0	-7.4E-7	0.0E+0	-1.2E-5	0.0E+0	0.0E+0	0.0E+0	0.0029
75 to 100 miles	[4,1]	Chicot	327	1.3E-2	-9.9E-4	0.0E+0	2.8E-5	-1.6E-4	-3.1E-5	8.8E-5	-1.1E-4	0.0021
	[4,2]	Evangeline	164	1.4E-3	0.0E+0	-2.8E-5	4.2E-7	-1.3E-4	0.0E+0	0.0E+0	0.0E+0	0.0201
	[4,3]	Burkeville										
	[4,4]	Jasper										

Figure 3-19 Transect 45 groundwater ages and groundwater fluxes calculated using the Central Gulf Coast Aquifer System GAM (negative values indicate flow in the opposite directions and are highlighted in yellow).

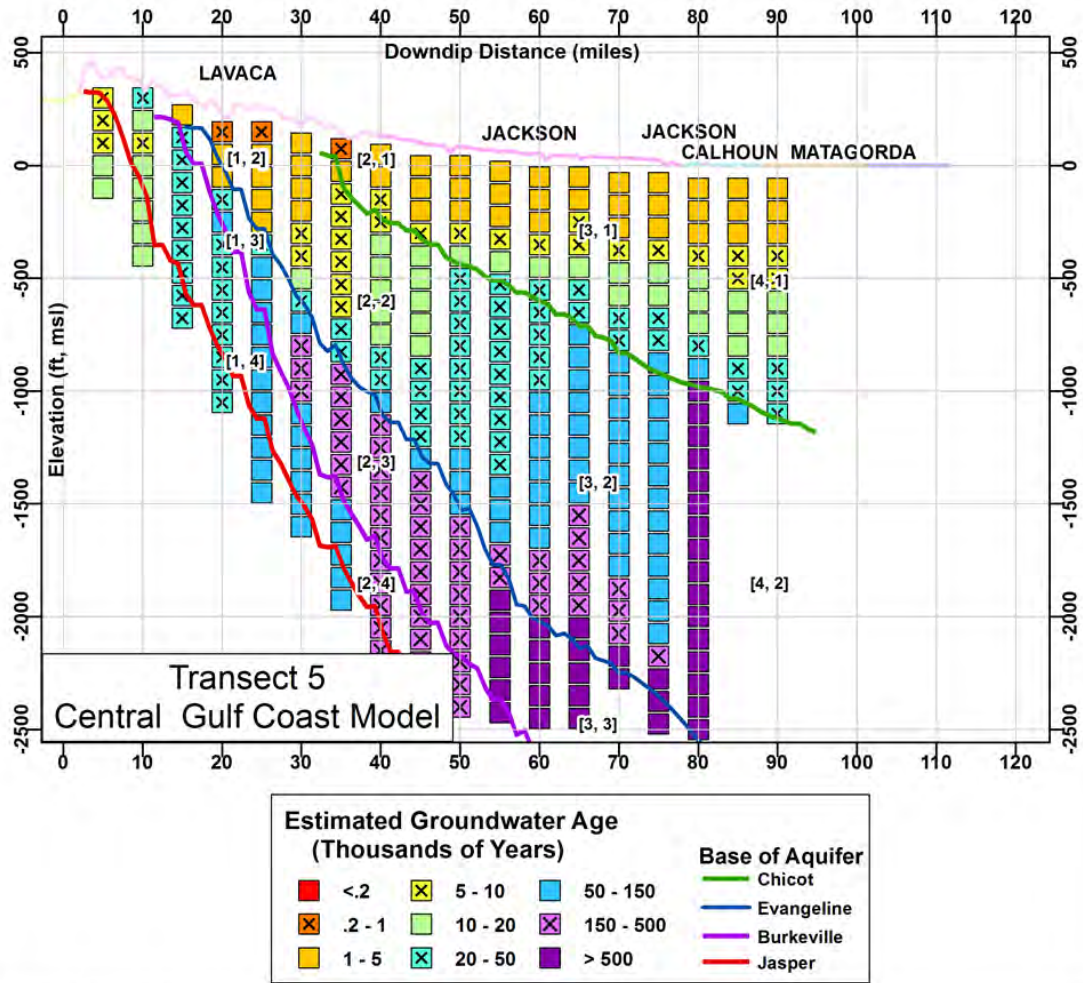
Final – Hydrogeochemical Evaluation of the Texas Gulf Coast Aquifer System and Implications for Developing Groundwater Availability Models



Section	Zone	Unit	Area (mi ²)	Average Unit Groundwater Flux (ft/day)							Cross-Flow Ratio	
				Updip	Downdip	Above	Below	Lateral	GHB	Recharge		SW Int
0 to 25 miles	[1,3]	Shallow	176	0.0E+0	-6.0E-3	0.0E+0	6.4E-6	3.5E-2	0.0E+0	6.9E-3	-8.2E-3	0.0011
	[1,2]	Chicot - BB										
	[1,3]	Chicot - U										
	[1,4]	Chicot - WI										
	[1,5]	Evangeline - UG	176	0.0E+0	-3.0E-3	-1.3E-5	1.4E-5	3.0E-3	0.0E+0	0.0E+0	0.0E+0	0.0047
	[1,6]	Evangeline - LG	176	0.0E+0	-1.6E-3	-1.4E-5	0.0E+0	2.8E-3	0.0E+0	0.0E+0	0.0E+0	0.0089
25 to 50 miles	[2,2]	Shallow	326	6.0E-3	-3.0E-2	0.0E+0	-2.1E-4	-3.1E-2	0.0E+0	1.1E-2	-5.5E-3	0.0070
	[2,2]	Chicot - BB										
	[2,3]	Chicot - U	326	3.2E-7	-3.6E-2	2.1E-4	-8.1E-5	-2.4E-2	0.0E+0	0.0E+0	0.0E+0	0.0058
	[2,4]	Chicot - WI	326	8.4E-3	-1.1E-2	8.1E-5	-1.3E-5	-3.7E-3	0.0E+0	0.0E+0	0.0E+0	0.0073
	[2,5]	Evangeline - UG	326	3.0E-3	-4.6E-3	1.3E-5	9.3E-8	-3.3E-4	0.0E+0	0.0E+0	0.0E+0	0.0027
	[2,6]	Evangeline - LG	0	1.6E-3	-1.6E-3	-9.3E-8	0.0E+0	1.7E-4	0.0E+0	0.0E+0	0.0E+0	0.0001
50 to 75 miles	[3,3]	Shallow	324	3.0E-2	-5.3E-2	0.0E+0	9.3E-5	7.7E-3	0.0E+0	7.5E-4	-8.4E-4	0.0018
	[3,2]	Chicot - BB	324	1.0E-6	-7.7E-3	-9.3E-5	8.9E-5	6.6E-3	0.0E+0	0.0E+0	0.0E+0	0.0121
	[3,3]	Chicot - U	324	3.6E-2	-8.7E-3	-8.9E-5	3.5E-5	-8.3E-5	0.0E+0	0.0E+0	0.0E+0	0.0024
	[3,4]	Chicot - WI	324	1.1E-2	-5.6E-3	-3.5E-5	2.2E-5	-8.7E-5	0.0E+0	0.0E+0	0.0E+0	0.0032
	[3,5]	Evangeline - UG	324	4.6E-3	-1.3E-3	-2.2E-5	6.6E-6	9.4E-5	0.0E+0	0.0E+0	0.0E+0	0.0048
	[3,6]	Evangeline - LG	0	1.6E-3	-1.6E-4	-6.6E-6	0.0E+0	-4.0E-5	0.0E+0	0.0E+0	0.0E+0	0.0042
75 to 100 miles	[4,4]	Shallow	317	5.3E-2	-1.5E-2	0.0E+0	6.1E-5	8.1E-3	0.0E+0	1.7E-3	-1.8E-3	0.0012
	[4,2]	Chicot - BB	317	7.7E-3	-1.8E-3	-6.1E-5	4.8E-5	1.4E-3	0.0E+0	0.0E+0	0.0E+0	0.0079
	[4,3]	Chicot - U	317	8.7E-3	-1.7E-3	-4.8E-5	2.4E-5	4.8E-4	0.0E+0	0.0E+0	0.0E+0	0.0055
	[4,4]	Chicot - WI	315	5.6E-3	-1.1E-3	-2.4E-5	4.6E-6	2.2E-4	0.0E+0	0.0E+0	0.0E+0	0.0042
	[4,5]	Evangeline - UG	96	1.3E-3	-2.2E-4	-4.6E-6	2.5E-6	-1.8E-5	0.0E+0	0.0E+0	0.0E+0	0.0035
	[4,6]	Evangeline - LG										

Figure 3-20 Transect 5 groundwater ages and groundwater fluxes calculated using the LCRB Model (negative values indicate flow in the opposite directions and are highlighted in yellow).

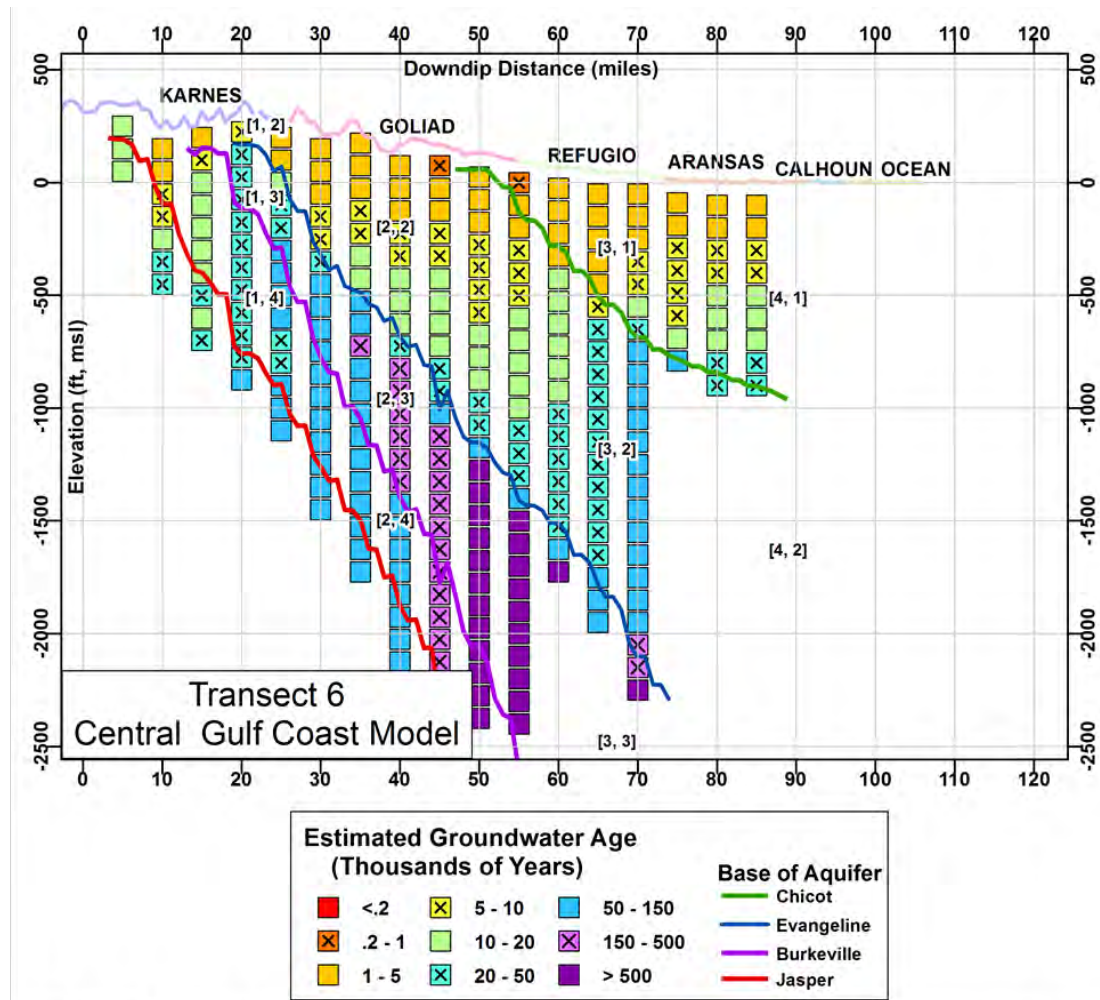
Final – Hydrogeochemical Evaluation of the Texas Gulf Coast Aquifer System and Implications for Developing Groundwater Availability Models



Section	Zone	Unit	Area (mi ²)	Average Unit Groundwater Flux (ft/day)							Cross-Flow Ratio	
				Updip	Downdip	Above	Below	Lateral	GHB	Recharge		SW Int
0 to 25 miles	[1,1]	Chicot										
	[1,2]	Evangeline	180	0.0E+0	-6.4E-3	-4.0E-5	1.3E-5	2.4E-3	0.0E+0	1.4E-3	-6.4E-4	0.0062
	[1,3]	Burkeville	227	0.0E+0	-3.0E-5	-1.3E-5	7.6E-6	1.2E-5	0.0E+0	1.1E-5	-7.6E-6	0.4251
	[1,4]	Jasper	334	0.0E+0	-5.2E-4	-7.6E-6	0.0E+0	-4.6E-4	0.0E+0	1.9E-5	0.0E+0	0.0147
15 to 50 miles	[2,1]	Chicot	296	1.8E-2	-1.5E-2	0.0E+0	4.2E-5	8.5E-3	0.0E+0	4.1E-5	-1.1E-4	0.0023
	[2,2]	Evangeline	330	6.4E-3	-2.8E-3	-4.2E-5	2.1E-6	1.4E-3	0.0E+0	4.6E-6	-1.5E-5	0.0066
	[2,3]	Burkeville	330	3.0E-5	-5.9E-6	-2.1E-6	1.9E-6	5.7E-6	0.0E+0	0.0E+0	0.0E+0	0.0692
	[2,4]	Jasper	330	5.2E-4	-9.6E-5	-1.9E-6	0.0E+0	6.6E-5	0.0E+0	0.0E+0	0.0E+0	0.0036
50 to 75 miles	[3,1]	Chicot	325	1.5E-2	-4.9E-3	0.0E+0	4.1E-5	5.5E-3	-2.1E-5	4.2E-5	-2.2E-4	0.0027
	[3,2]	Evangeline	325	2.8E-3	-3.3E-4	-4.1E-5	1.1E-6	4.8E-4	0.0E+0	0.0E+0	0.0E+0	0.0146
	[3,3]	Burkeville	224	5.9E-6	0.0E+0	-1.1E-6	3.3E-6	2.1E-6	0.0E+0	0.0E+0	0.0E+0	0.5560
	[3,4]	Jasper	72	9.6E-5	0.0E+0	-3.3E-6	0.0E+0	4.0E-5	0.0E+0	0.0E+0	0.0E+0	0.0343
75 to 100 miles	[4,1]	Chicot	224	4.9E-3	0.0E+0	0.0E+0	4.0E-5	3.3E-4	-1.1E-4	2.0E-4	-3.4E-6	0.0082
	[4,2]	Evangeline	50	3.3E-4	0.0E+0	-4.0E-5	0.0E+0	3.4E-4	0.0E+0	0.0E+0	0.0E+0	0.1205
	[4,3]	Burkeville										
	[4,4]	Jasper										

Figure 3-21 Transect 5 groundwater ages and groundwater fluxes calculated using the Central Gulf Coast Aquifer System GAM (negative values indicate flow in the opposite directions and are highlighted in yellow).

Final – Hydrogeochemical Evaluation of the Texas Gulf Coast Aquifer System and Implications for Developing Groundwater Availability Models



Section	Zone	Unit	Area (mi ²)	Average Unit Groundwater Flux (ft/day)								Cross-Flow Ratio
				Updip	Downdip	Above	Below	Lateral	GHB	Recharge	SW Int	
0 to 25 miles	[1,1]	Chicot										
	[1,2]	Evangeline	164	0.0E+0	-3.6E-3	0.0E+0	-6.9E-6	3.6E-3	0.0E+0	3.6E-5	-2.1E-5	0.0019
	[1,3]	Burkeville	223	0.0E+0	-1.2E-4	6.9E-6	-1.3E-5	-9.1E-7	0.0E+0	1.3E-5	-1.4E-6	0.1058
	[1,4]	Jasper	318	0.0E+0	-7.2E-4	1.3E-5	0.0E+0	-3.1E-4	0.0E+0	1.6E-5	-1.8E-5	0.0180
15 to 50 miles	[2,1]	Chicot	204	0.0E+0	-2.3E-2	0.0E+0	-9.8E-6	-2.9E-3	0.0E+0	4.8E-5	8.8E-5	0.0004
	[2,2]	Evangeline	326	3.6E-3	-2.9E-3	9.8E-6	1.9E-6	-2.5E-4	0.0E+0	2.1E-5	-5.2E-6	0.0027
	[2,3]	Burkeville	283	1.2E-4	-2.7E-5	-1.9E-6	2.1E-6	-3.2E-6	0.0E+0	0.0E+0	0.0E+0	0.0169
	[2,4]	Jasper	154	7.2E-4	0.0E+0	-2.1E-6	0.0E+0	-9.6E-5	0.0E+0	0.0E+0	0.0E+0	0.0029
50 to 75 miles	[3,1]	Chicot	256	2.3E-2	-8.9E-4	0.0E+0	3.6E-5	7.9E-4	-1.8E-5	4.2E-5	-1.4E-4	0.0016
	[3,2]	Evangeline	256	2.9E-3	0.0E+0	-3.6E-5	4.6E-7	7.1E-5	0.0E+0	0.0E+0	0.0E+0	0.0123
	[3,3]	Burkeville	113	2.7E-5	0.0E+0	-4.6E-7	0.0E+0	-2.9E-7	0.0E+0	0.0E+0	0.0E+0	0.0169
	[3,4]	Jasper										
75 to 100 miles	[4,1]	Chicot										
	[4,2]	Evangeline										
	[4,3]	Burkeville										
	[4,4]	Jasper										

Figure 3-22 Transect 6 groundwater ages and groundwater fluxes calculated using the Central Gulf Coast Aquifer System GAM (negative values indicate flow in the opposite directions and are highlighted in yellow).

Final – Hydrogeochemical Evaluation of the Texas Gulf Coast Aquifer System and Implications for Developing Groundwater Availability Models

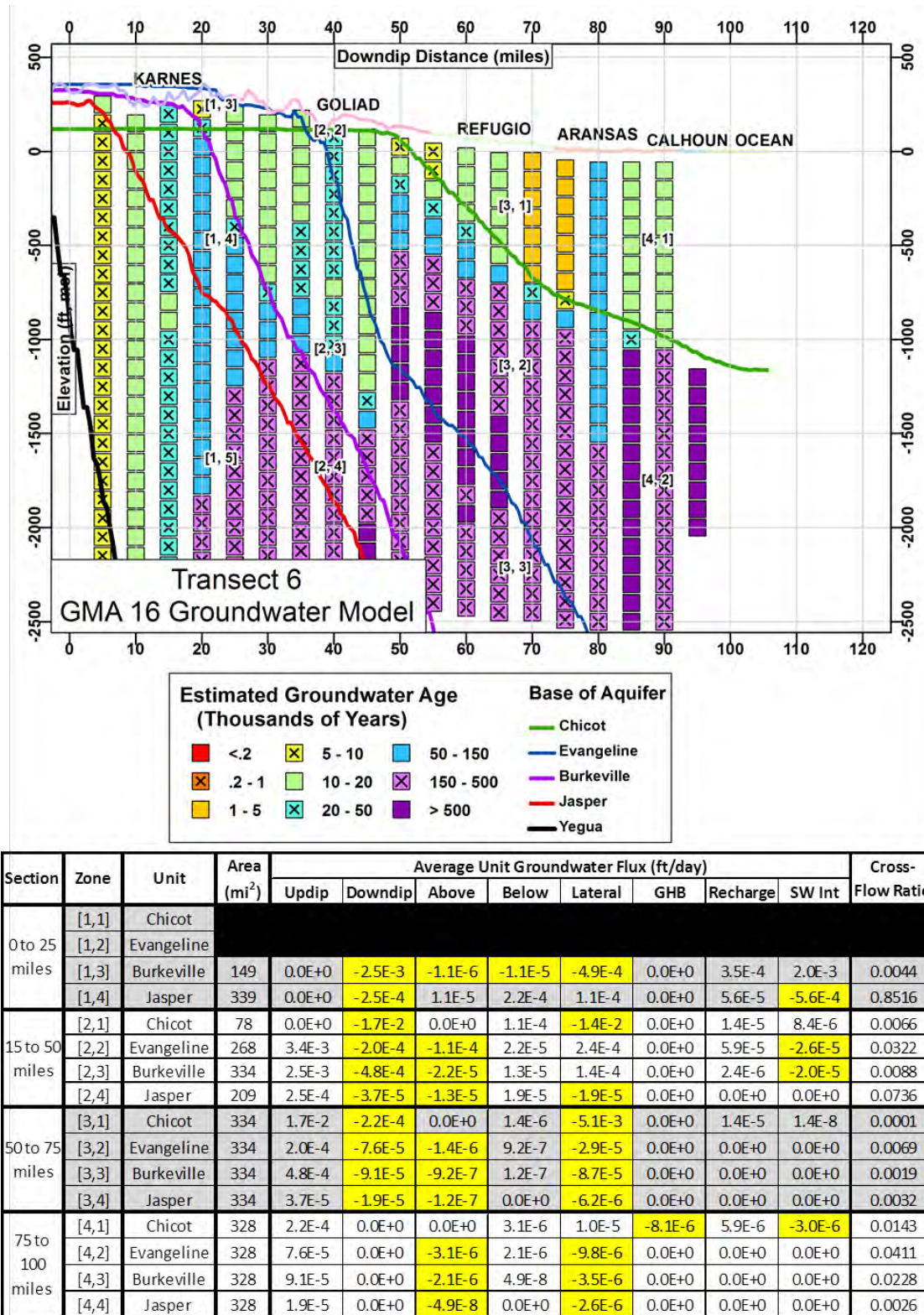
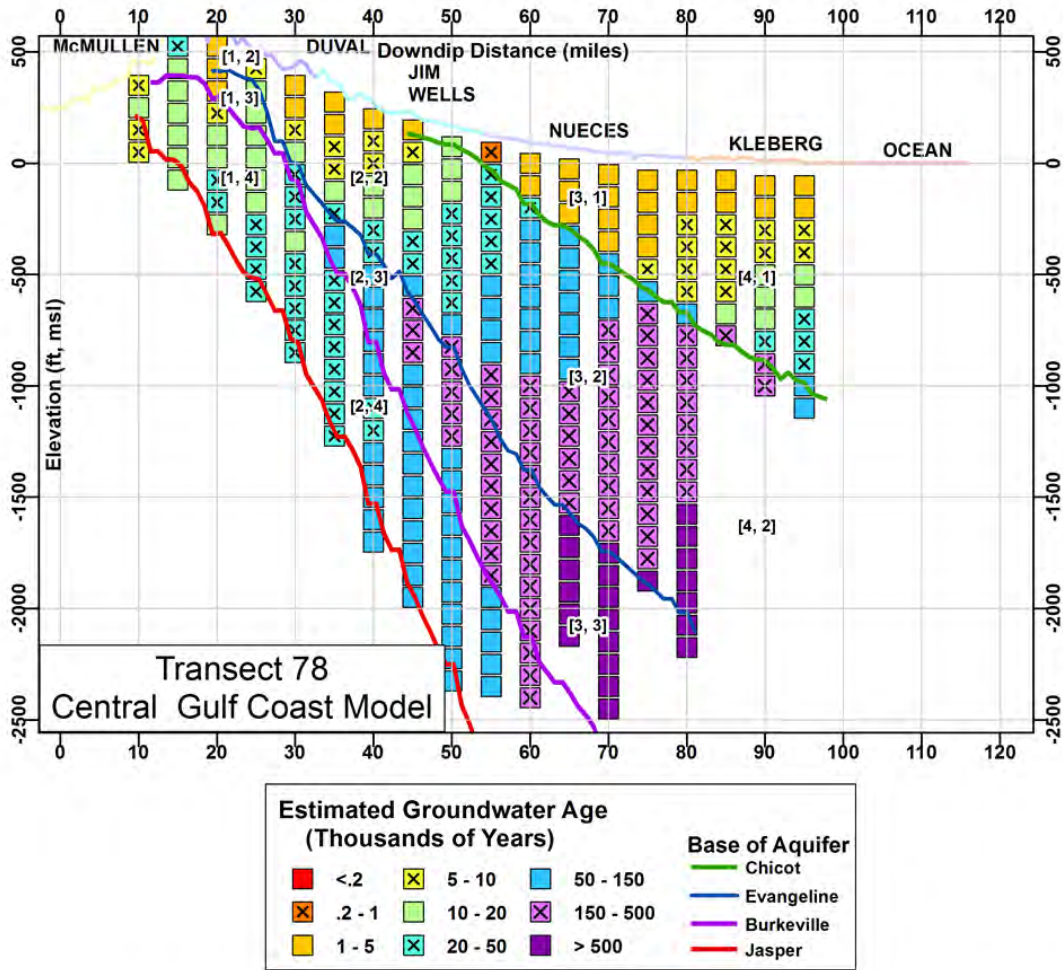


Figure 3-23 Transect 6 groundwater ages and groundwater fluxes calculated using the GMA 16 AGM (negative values indicate flow in the opposite directions and are highlighted in yellow).

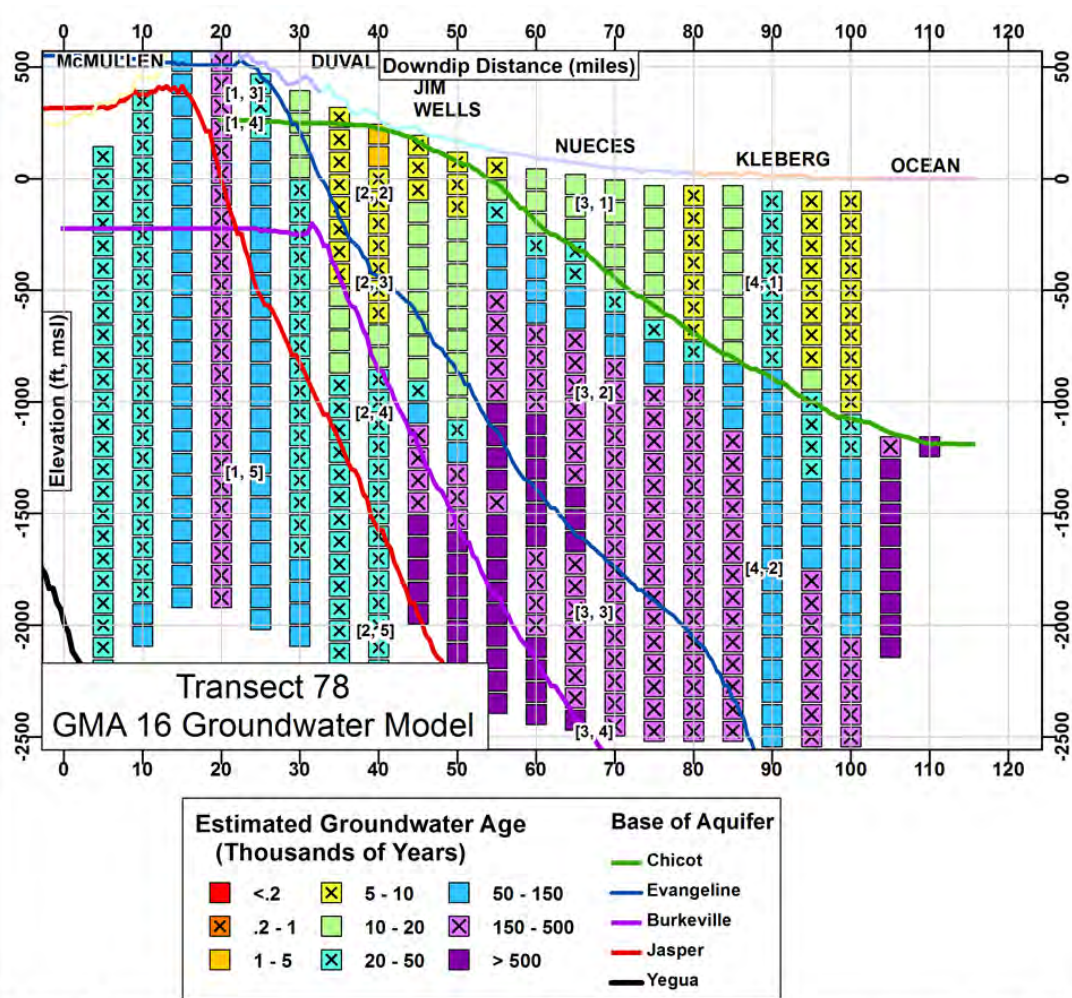
Final – Hydrogeochemical Evaluation of the Texas Gulf Coast Aquifer System and Implications for Developing Groundwater Availability Models



Unit	Area (mi ²)	Average Unit Groundwater Flux (ft/day)								Cross-Flow Ratio
		Updip	Downdip	Above	Below	Lateral	GHB	Recharge	SW Int	
Chicot										
Evangeline										
Burkeville	197	0.0E+0	-7.0E-5	1.5E-5	-3.3E-6	1.4E-4	0.0E+0	0.0E+0	0.0E+0	0.2116
Jasper	241	0.0E+0	-1.2E-3	3.3E-6	0.0E+0	-1.4E-4	0.0E+0	0.0E+0	0.0E+0	0.0028
Chicot	169	0.0E+0	-1.8E-2	0.0E+0	1.6E-5	-1.1E-4	0.0E+0	1.9E-5	-4.2E-5	0.0009
Evangeline	326	3.3E-3	-1.2E-3	-1.6E-5	7.6E-6	-5.6E-4	0.0E+0	3.9E-5	-4.1E-5	0.0048
Burkeville	331	7.0E-5	-3.1E-6	-7.6E-6	7.3E-6	-3.7E-5	0.0E+0	0.0E+0	0.0E+0	0.1087
Jasper	331	1.2E-3	-7.1E-4	-7.3E-6	0.0E+0	-2.1E-4	0.0E+0	0.0E+0	0.0E+0	0.0061
Chicot	329	1.8E-2	-3.8E-3	0.0E+0	2.6E-5	-7.0E-3	0.0E+0	2.9E-5	-4.9E-5	0.0015
Evangeline	329	1.2E-3	-4.1E-4	-2.6E-5	7.0E-6	-2.3E-5	0.0E+0	0.0E+0	0.0E+0	0.0227
Burkeville	294	3.1E-6	0.0E+0	-7.0E-6	1.4E-5	-1.8E-7	0.0E+0	0.0E+0	0.0E+0	4.6518
Jasper	143	7.1E-4	0.0E+0	-1.4E-5	0.0E+0	-3.0E-5	0.0E+0	0.0E+0	0.0E+0	0.0201
Chicot	288	3.8E-3	0.0E+0	0.0E+0	2.9E-5	-1.6E-3	-2.0E-5	2.4E-5	0.0E+0	0.0075
Evangeline	71	4.1E-4	0.0E+0	-2.9E-5	0.0E+0	-1.8E-5	0.0E+0	0.0E+0	0.0E+0	0.0700
Burkeville										
Jasper										

Figure 3-24 Transect 78 groundwater ages and groundwater fluxes calculated using the Central Gulf Coast Aquifer System GAM (negative values indicate flow in the opposite directions and are highlighted in yellow).

Final – Hydrogeochemical Evaluation of the Texas Gulf Coast Aquifer System and Implications for Developing Groundwater Availability Models



Section	Zone	Unit	Area (mi ²)	Average Unit Groundwater Flux (ft/day)								Cross-Flow Ratio	
				Updip	Downdip	Above	Below	Lateral	GHB	Recharge	SW Int		
0 to 25 miles	[1,1]	Chicot											
	[1,2]	Evangeline											
	[1,3]	Burkeville											
	[1,4]	Jasper	236	0.0E+0	-5.1E-4	0.0E+0	-5.0E-5	-6.8E-4	0.0E+0	0.0E+0	0.0E+0	0.0E+0	0.0990
15 to 50 miles	[2,1]	Chicot	128	0.0E+0	-4.9E-2	0.0E+0	1.1E-4	-7.6E-3	0.0E+0	1.1E-5	7.1E-6	0.0021	
	[2,2]	Evangeline	251	2.8E-3	-3.4E-4	-1.1E-4	3.4E-5	1.5E-3	0.0E+0	2.7E-5	1.1E-6	0.0385	
	[2,3]	Burkeville	251	0.0E+0	-1.4E-3	-3.4E-5	4.3E-5	9.0E-4	0.0E+0	0.0E+0	0.0E+0	0.0312	
	[2,4]	Jasper	211	5.1E-4	-1.2E-4	-4.3E-5	3.1E-5	1.3E-4	0.0E+0	8.1E-7	9.8E-6	0.0846	
50 to 75 miles	[3,1]	Chicot	331	4.9E-2	-4.3E-3	0.0E+0	9.6E-6	-1.7E-2	0.0E+0	1.1E-5	9.1E-6	0.0002	
	[3,2]	Evangeline	331	3.4E-4	-1.3E-4	-9.6E-6	7.8E-6	9.1E-6	0.0E+0	0.0E+0	0.0E+0	0.0281	
	[3,3]	Burkeville	331	1.4E-3	-2.6E-4	-7.8E-6	7.9E-7	1.2E-5	0.0E+0	0.0E+0	0.0E+0	0.0057	
	[3,4]	Jasper	331	1.2E-4	-2.4E-5	-7.9E-7	0.0E+0	6.9E-6	0.0E+0	0.0E+0	0.0E+0	0.0064	
75 to 100 miles	[4,1]	Chicot	332	4.3E-3	-2.1E-5	0.0E+0	4.2E-6	-1.7E-4	-7.4E-6	9.9E-6	-2.8E-5	0.0010	
	[4,2]	Evangeline	332	1.3E-4	-6.4E-6	-4.2E-6	2.6E-6	5.5E-6	0.0E+0	0.0E+0	0.0E+0	0.0317	
	[4,3]	Burkeville	332	2.6E-4	-5.5E-6	-2.6E-6	3.1E-7	-4.3E-6	0.0E+0	0.0E+0	0.0E+0	0.0099	
	[4,4]	Jasper	332	2.4E-5	-9.9E-7	-3.1E-7	0.0E+0	5.3E-6	0.0E+0	0.0E+0	0.0E+0	0.0130	

Figure 3-25 Transect 78 groundwater ages and groundwater fluxes calculated using the GMA 16 AGM (negative values indicate flow in the opposite directions and are highlighted in yellow).

Final – Hydrogeochemical Evaluation of the Texas Gulf Coast Aquifer System and Implications for Developing Groundwater Availability Models

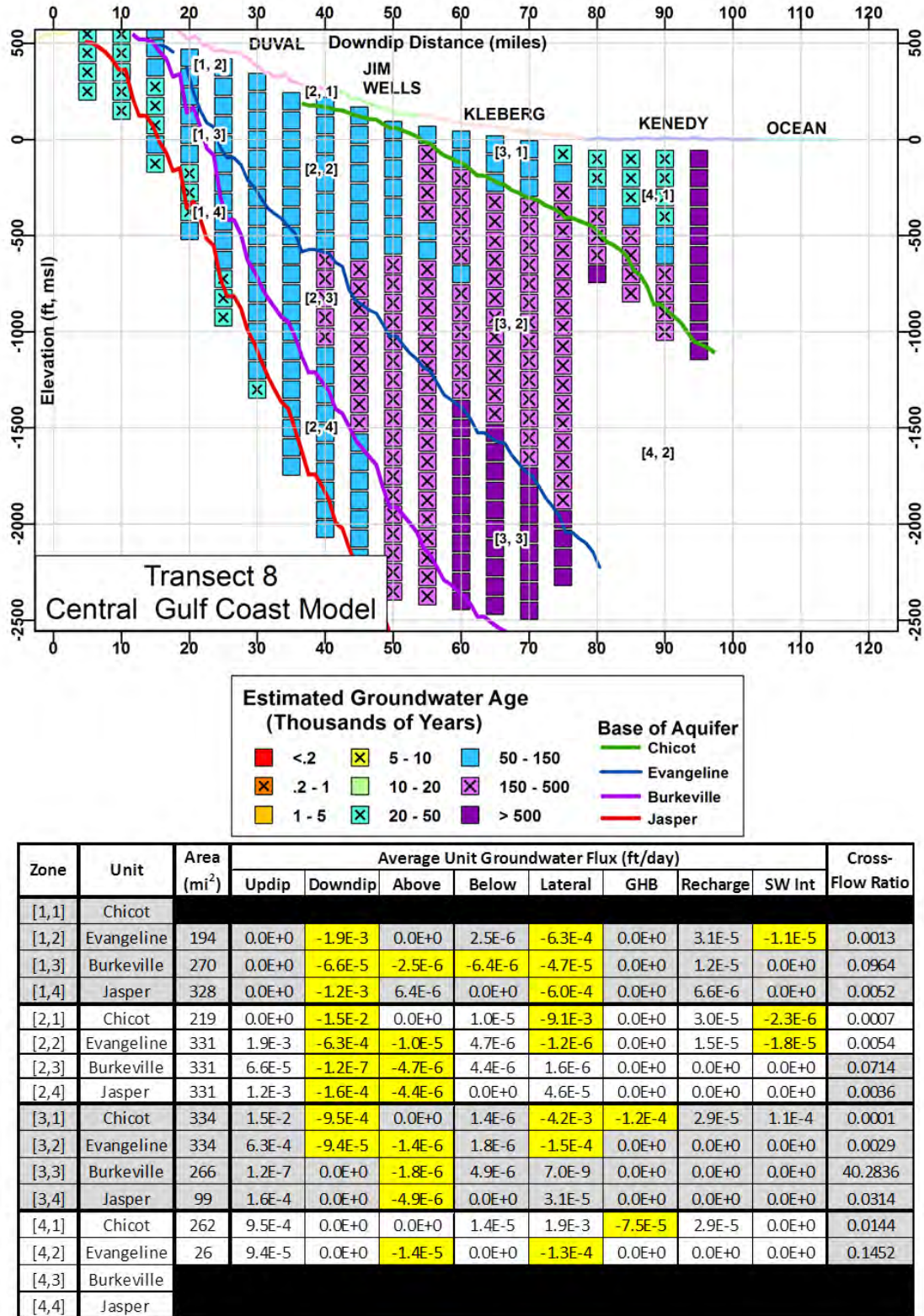
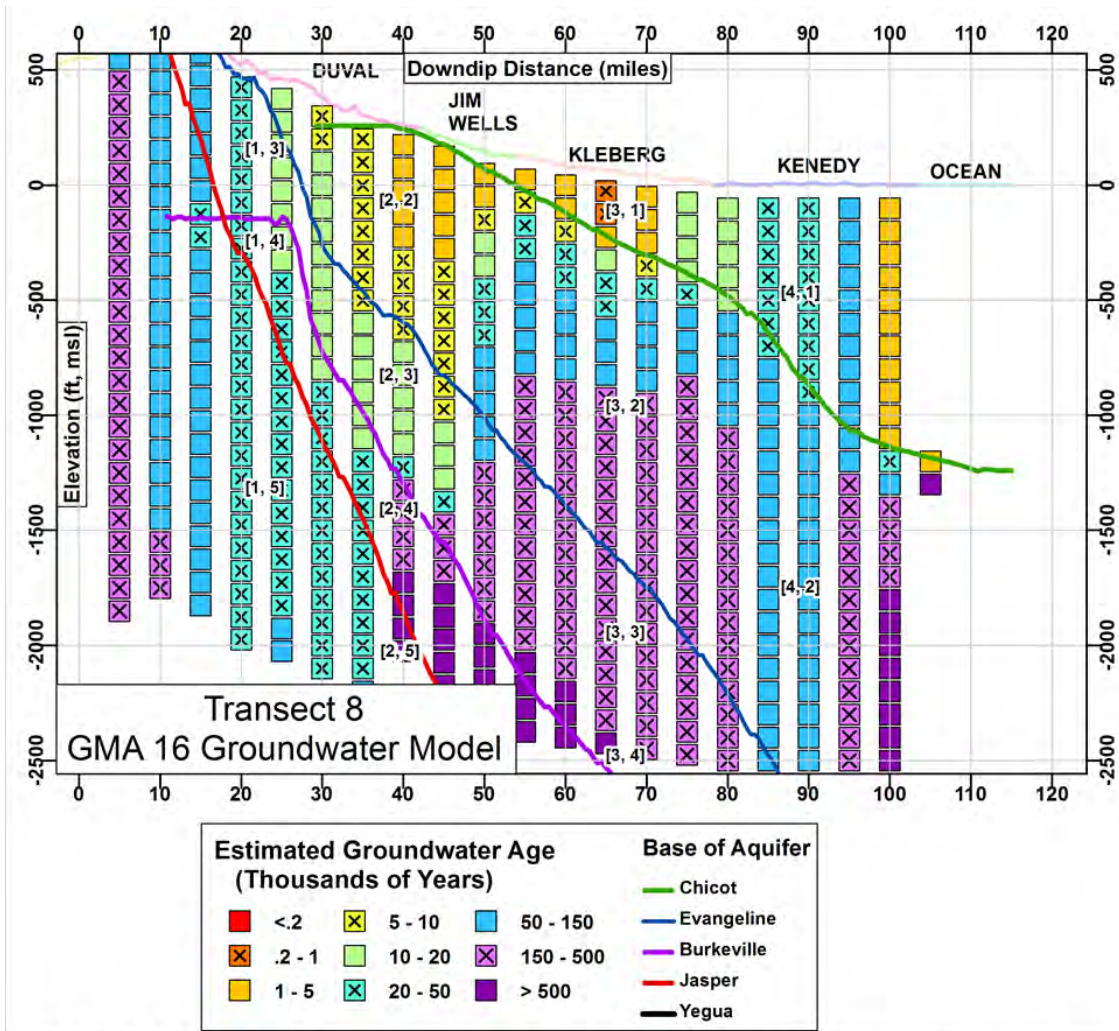


Figure 3-26 Transect 8 groundwater ages and groundwater fluxes calculated using the Central Gulf Coast Aquifer System GAM (negative values indicate flow in the opposite directions and are highlighted in yellow).

Final – Hydrogeochemical Evaluation of the Texas Gulf Coast Aquifer System and Implications for Developing Groundwater Availability Models



Section	Zone	Unit	Area (mi ²)	Average Unit Groundwater Flux (ft/day)							Cross-Flow Ratio	
				Updip	Downdip	Above	Below	Lateral	GHB	Recharge		SW Int
0 to 25 miles	[1,1]	Chicot										
	[1,2]	Evangeline	40	0.0E+0	-2.1E-3	0.0E+0	-2.5E-6	2.8E-3	0.0E+0	7.0E-5	7.3E-7	0.0012
	[1,3]	Burkeville	40	0.0E+0	-4.2E-3	2.5E-6	1.2E-4	1.7E-4	0.0E+0	0.0E+0	0.0E+0	0.0272
	[1,4]	Jasper	267	0.0E+0	-5.6E-4	-1.2E-4	-1.3E-5	-5.4E-5	0.0E+0	8.5E-5	1.4E-4	0.2066
15 to 50 miles	[2,1]	Chicot	145	0.0E+0	-5.6E-2	0.0E+0	1.4E-4	-1.3E-1	0.0E+0	1.0E-5	7.6E-6	0.0025
	[2,2]	Evangeline	329	2.1E-3	-3.8E-4	-1.4E-4	3.6E-5	2.9E-3	0.0E+0	2.0E-5	1.5E-6	0.0660
	[2,3]	Burkeville	329	4.2E-3	-7.8E-4	-3.6E-5	2.5E-5	8.8E-4	0.0E+0	0.0E+0	0.0E+0	0.0086
	[2,4]	Jasper	149	5.6E-4	-5.7E-5	-2.5E-5	5.1E-5	4.6E-5	0.0E+0	0.0E+0	0.0E+0	0.0922
50 to 75 miles	[3,1]	Chicot	329	5.6E-2	-3.6E-4	0.0E+0	5.3E-6	2.3E-2	-1.5E-8	1.0E-5	-1.0E-4	0.0001
	[3,2]	Evangeline	329	3.8E-4	-1.6E-4	-5.3E-6	3.5E-6	3.4E-5	0.0E+0	0.0E+0	0.0E+0	0.0139
	[3,3]	Burkeville	329	7.8E-4	-3.1E-4	-3.5E-6	-1.4E-7	-7.6E-5	0.0E+0	0.0E+0	0.0E+0	0.0045
	[3,4]	Jasper	329	5.7E-5	-3.9E-5	1.4E-7	0.0E+0	-2.1E-5	0.0E+0	0.0E+0	0.0E+0	0.0025
75 to 100 miles	[4,1]	Chicot	329	3.6E-4	-2.7E-6	0.0E+0	6.7E-6	4.4E-4	-1.9E-5	7.0E-6	-1.9E-6	0.0188
	[4,2]	Evangeline	329	1.6E-4	-2.3E-6	-6.7E-6	3.1E-6	5.7E-5	0.0E+0	0.0E+0	0.0E+0	0.0413
	[4,3]	Burkeville	329	3.1E-4	-2.1E-6	-3.1E-6	7.4E-7	2.0E-5	0.0E+0	0.0E+0	0.0E+0	0.0100
	[4,4]	Jasper	329	3.9E-5	-4.7E-7	-7.4E-7	0.0E+0	1.7E-5	0.0E+0	0.0E+0	0.0E+0	0.0193

Figure 3-27 Transect 8 groundwater ages and groundwater fluxes calculated using the GMA 16 Groundwater AGM (negative values indicate flow in the opposite directions and are highlighted in yellow).

Final – Hydrogeochemical Evaluation of the Texas Gulf Coast Aquifer System and Implications for Developing Groundwater Availability Models

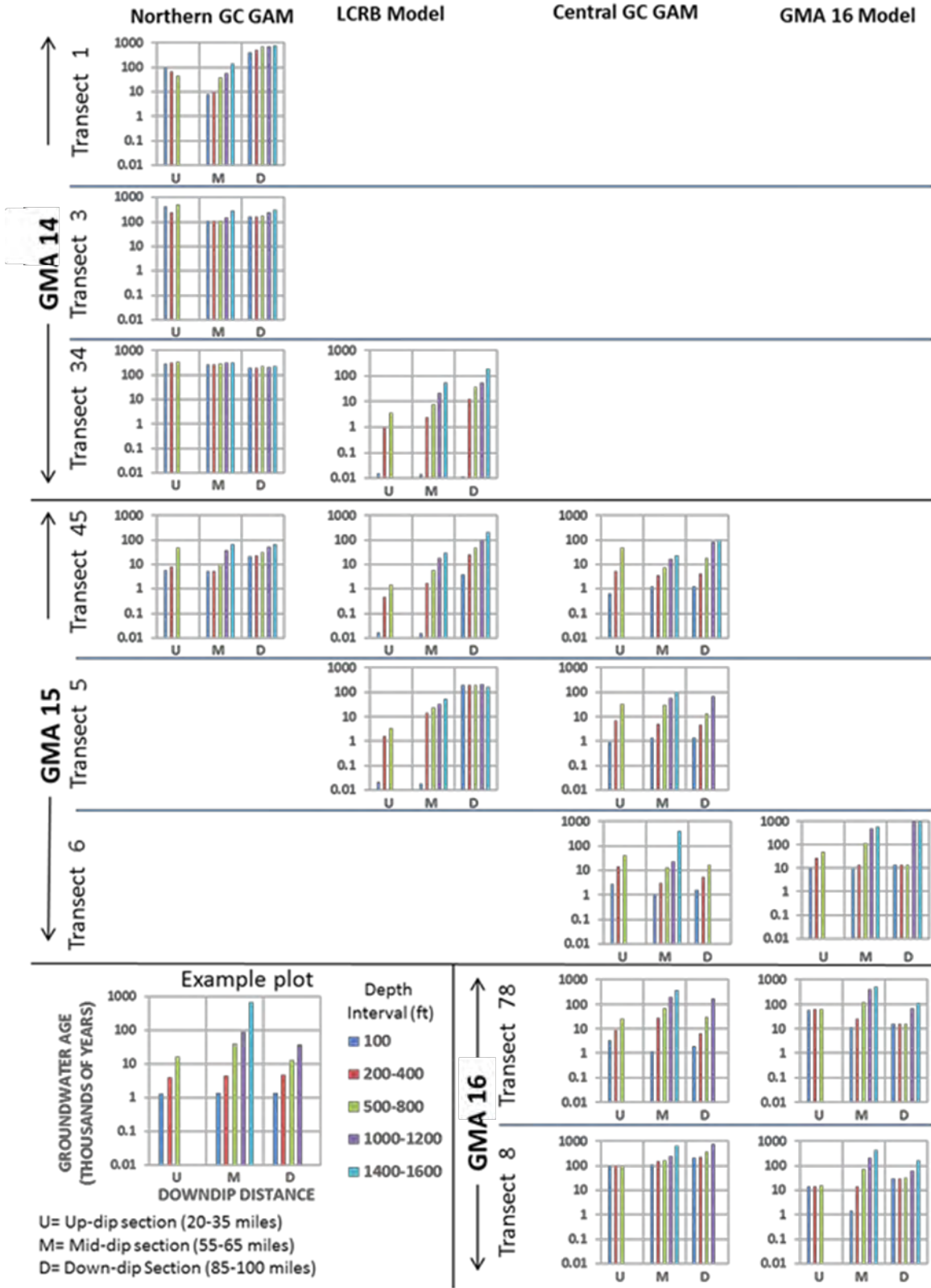


Figure 3-28 Composite averages for groundwater ages for the four groundwater models and the eight transects.

This page intentionally left blank.

4.0 Geochemical Data

This section describes the geochemical data used for the project. The project developed a comprehensive database that consists primarily of information assembled from TWDB and USGS websites and publications. Our well sampling included measuring for carbon-14(¹⁴C), stable isotopes, gases, and major anions and cations at eighteen wells along Transect 3 in GMA 14, at ten wells along Transect 5 in GMA 15, and at ten wells along Transect 8 in GMA 16.

4.1 Database

Our primary source of geochemical data was the TWDB groundwater database. We queried the TWDB database for wells located in the Gulf Coast Aquifer System footprint or within 25 miles of the updip extent of the Catahoula Formation (see Figures 1-1 and 1-3). Our query identified approximately 13,000 wells with water quality data from at least one sampling event.

In order to increase the number of wells in our database with stable isotopes and ¹⁴C, we searched university theses, state agency reports, and the USGS publications and websites. Both stable isotope and ¹⁴C data were obtained from USGS publications (Oden and others, 2010; Oden and others, 2011; Oden, 2011; and Oden and Truini, 2013) and from USGS websites. We obtained isotope data from the two USGS websites listed below. The second site URL was used by the USGS to upload information as it became available from a study of the Catahoula Formation being funded by the Lone Star GCD. :

- USGS Water Data for the Nation at <http://nwis.waterdata.usgs.gov/nwis>,
- USGS Water Quality Samples for Texas Web Site at http://nwis.waterdata.usgs.gov/tx/nwis/qwdata?aqfr_cd=122CTHL&format=station_list&sort_key=site_no&group_key=NONE&inventory_output=0&rdb_inventory_output=file&begin_date=2010-12-01&TZoutput=0&pm_cd_compare=Greater%20than&radio_parm_cds=all_parm_cds&qw_attributes=0&qw_sample_wide=wide&rdb_qw_attributes=0&date_format=YYYY-MM-DD&rdb_compression=file&list_of_search_criteria=aqfr_cd_by_name.

In addition to the USGS data, we obtained isotope information from the San Jacinto River Authority (SJRA) and from theses (Bourgeois, 1997; Chakraborty, 2007). SJRA provided us with test results from their Well 39 Catahoula Pilot Test Well. Bourgeois (1997) and Chakraborty (2007) provided stable isotope information near Brazoria County. Finally, our database also included measurements from the 38 wells sampled along Transects 3, 5, and 8 as part of this project.

The primary well specifications included in our database are latitude, longitude, land surface elevation, top of screen (TOS) and bottom of screen (BOS). The TOS and BOS refer to the highest and the lowest elevations associated with a well screen at the well. To help manage our investigations along transects, we marked the 7,000 wells that are located within six miles of one of the nineteen transects shown in Figure 1-3. For each of these 7,000 wells we calculated three spatial indices. One index is the perpendicular distance that the well is from the closest transect. This distance is always equal to or less than six miles. Another index is the distance the well is from the up-dip extent of the Catahoula outcrop. This distance ranges from 25 miles, which occurs for a few wells that intersect the Yegua-Jackson Aquifer, to about 130 miles, which occurs near the shoreline. The last index is the distance from the shoreline. This distance ranges from 0 to about 155 miles.

Less than 25% of the wells in our database of approximately 13,000 wells included screen information. For most of the analyses that we performed, wells were assigned to geologic units based on well depth. The surfaces used for geologic units above the Catahoula Formation are from Young and others (2010, 2012a) and geologic units below the Catahoula Formation are from Knox and others (2007). Table 4-1 shows the spatial distribution of the wells among the GMAs and geologic units. Figures 4-1, 4-2, and 4-3 show the spatial distribution of wells by geologic unit for GMAs 14, 15, and 16, respectively.

As shown in Table 4-1, GMA 14 has twice as many wells as either GMA 15 or 16, and about 75% of the wells have terminated in either the Chicot or Evangeline Aquifers. One most commonly sample chemical parameter is TDS. Approximately 85 percent of the wells have at least one measured TDS. Wells with a hydrochemical facies requires that their average concentrations have less than a 5% charge balance error between their major anions (SO_4 , Cl , HCO_3) and cations (Na , Ca , Mg , K). Approximately 60 percent of the wells met this

requirement. Approximately 2 percent of the wells have ^{14}C measurements and stable isotope measurements of $\delta^2\text{H}$ and $\delta^{18}\text{O}$.

Table 4-1 Spatial Distribution of Wells Among GMAs 14, 15, and 16.

	Unit	Number of wells	Wells with Screens Data	Number of Wells		
				TDS	Facies ⁽¹⁾	^{14}C
GMA 14	Chicot	2,921	299	2,273	1,885	18
	Evangeline	1,451	345	1,191	944	45
	Middle Lagarto	378	78	328	241	9
	Jasper	672	103	576	448	9
	Catahoula	189	53	169	107	5
	Yegua-Jackson	175	26	161	69	3
	Total	5,786	904	4,698	3,694	89
GMA 15	Chicot	1,037	320	956	918	23
	Evangeline	703	265	627	591	10
	Middle Lagarto	121	41	105	93	2
	Jasper	428	69	389	299	9
	Catahoula	146	23	139	76	1
	Yegua-Jackson	122	57	119	93	2
	Total	2,557	775	2,335	2,070	47
GMA 16	Chicot	829	310	726	167	5
	Evangeline	1,129	307	945	502	20
	Middle Lagarto	127	29	105	69	1
	Jasper	299	74	256	141	7
	Catahoula	117	30	105	61	1
	Yegua-Jackson	30	5	28	11	0
	Total	2,531	755	2,165	951	34
Total	Chicot	4,787	929	3,955	2,970	46
	Evangeline	3,283	917	2,763	2,037	75
	Middle Lagarto	626	148	538	403	12
	Jasper	1,399	246	1,221	888	25
	Catahoula	452	106	413	244	7
	Yegua-Jackson	327	88	308	173	5
	Total	10,874	2,434	9,198	6,715	170

(1) Hydrochemical facies were calculate for wells where the charge balance difference between the anions and cation is less than 5%.

4.2 Well Data for Transects 3, 5, and 8

In addition to geochemical data collected in our literature review, we also sampled 18 wells along Transect 3, 10 wells along Transect 5, and 10 wells along Transect 8 for the analytes listed in Table 4-2. Figures 4-4 and 4-5 show an aerial view and a cross-section view of wells associated with Transect 3. Figures 4-6 and 4-7 show an aerial view and a cross-section view of wells associated with Transect 5. Figures 4-8 and 4-9 show an aerial view and a cross-section view of wells associated with Transect 8. These maps also include the location of salt domes in the area. Appendices A through D provide the laboratory results. At a few wells, iodide samples were collected and sent to Ana-Lab Corporation for analysis. Appendix E provides the results for the iodide measurements.

Groundwater samples were collected from September 2012 to February 2013. Baer Engineering in Austin, Texas, performed the sampling events. At the end of each day of well sampling, Baer Engineering shipped the groundwater samples for analysis via overnight priority. A chain of custody was maintained for all samples. The sampling event of Transect 3 required three visits and approximately nine days to collect the samples. The sampling of Transects 5 and 8 were each completed over a five-day period. Appendix F provides the sampling and analysis plan.

Considerable effort was required to identify prospective wells and secure permission to sample the wells. Where appropriate, we coordinated with and sought assistance from groundwater conservation districts in order to identify potential wells for sampling. In GMA 14, Ms. Kathy Jones from the Lone Star GCD, Mr. Tom Michel from the Houston-Galveston Subsidence District, and Mr. Zach Holland from the Bluebonnet GCD helped with our efforts. In addition, the LSGCD provided financial assistance with sampling and analyzing samples from Catahoula and Jasper wells. In GMA 15, Mr. Tim Andruss from the Texana GCD helped with our efforts. In GMA 16, Mr. Felix Saenz from Brush County GCD, Mr. Andy Garza from Kenedy County GCD, and Mr. Alberto Garcia from Duval County GCD helped with our efforts. In addition to assistance from GCDs, we also received assistance from Mr. Mike Turco from the U.S. Geological Survey in Houston, TX; Mr. Robert Schmidt from the U.S. Department of Agriculture in Kleberg, TX; and Janie Hopkins from the TWDB in Austin, TX.

Tables 4-3, 4-4, and 4-5 provide the measured geochemical parameters from our sampling event and data assembled from our review of geochemical data for Transects 3, 5, and 8. In these three tables, measurements that have INTERA or the USGS as the “source” are for the groundwater samples collected for the “sample date” provided in the table. In these three tables, the measurements that have TWDB as the “source” represent averages for all of the measurements or that well in the TWDB database except for the isotopes. The isotope measurements including the ^{14}C measurements are for the date listed in the “sample date.” This mixture was used for the TWDB wells because for some of the TWDB wells, only a partial list of ions were sampled and analyzed at the time the isotopes samples were collected. Table 4-6 provides the chain-of-custody ID used for the wells that we sampled. This ID can be used to associate the laboratory measurements in Appendices A through F with the appropriate well. For each well, Table 4-6 also provides, when available, the TWDB state well ID, the TCEQ identification number for the public water supply well, and the USGS well identification number.

Table 4-2 Analytes collected by INTERA at Gulf Coast Aquifer System Wells.

Sample No.	Analyte	Field Methods	Lab
1	Dissolved Metals (Ca, Mg, Na, K, Fe)	250 mL plastic preserved with HNO ₃ (if filtered in the field). If not filtered in field then 250 mL unpreserved.	San Antonio Testing
2	TDS	1 L Nalgene, unpreserved	
	Alkalinity	500 mL Nalgene, unpreserved	
	pH		
	Specific Conductance		
	Br, Cl, F, SO ₄ (dissolved)		
3	Nitrate + Nitrite	250 mL Nalgene, preserved with H ₂ SO ₄	
4	H ₂ S	250 mL Nalgene, preserved with ZnC ₂ H ₃ O ₂	
	HS		
5	TOC Dissolved	500 mL Nalgene, unpreserved	Zymax
6	Fixed and hydrocarbon gas composition	1-liter glass bottles with gas extraction cap. Ship on ice.	
7	δC13 of C1, C2		
8	δD of C1, C2		
9	δO18 of H2O		
10	δD of H2O		
11	RSK 175 for C1, C2, C3		
12	Gas extraction fee		
13	Total Gas for methane, ethane, propane, butane, and pentane (for purpose of identifying thermo versus biogenic carbon sources)		
14	δS34 of SO ₄	Filtered in the field, not preserved. If SO ₄ is < 100 ppm, 100 mL Nalgene. If SO ₄ is > 100 ppm, 1 L Nalgene. Some head space is desirable. [SO ₄] unknown, just use 1 L. Samples need to get to lab within 7 – 10 days for them to precipitate out the SO ₄ into a stable form for later analysis (only a few times a year)	University of Arizona Environmental Lab
15	δO18 of SO ₄		
16	δC13 of DIC	1 l Nalgene pre-cleaned with 10% muriatic acid and DI water preserved with 4-5 mL of NaOH 50/50% w/w.	Beta Analytic
	C-14		

Final – Hydrogeochemical Evaluation of the Texas Gulf Coast Aquifer System and
Implications for Developing Groundwater Availability Models

Table 4-3 Geochemistry Measurements for Transect 3.

	Group #	3-1	3-2	3-3	3-3	3-4	3-4	3-5	3-6	3-7
Well Data	Source	TWDB	INTERA	INTERA	TWDB	INTERA	USGS	TWDB	USGS	USGS
	Sample Date	8/16/2005	9/5/2012	9/5/2012	8/16/2005	9/5/2012	9/5/2012	8/17/2005	5/9/2011	5/10/2011
	Unit	JCK	CAT	CAT	CAT	CAT	CAT	JP	ML	ML
	Land Surface Elevation (ft amsl)	280	400	408	405	417	417	210	315	240
	Screen Interval	368 - 438	380 - 440	723 - 761	723 - 761	682 - 1252	682 - 1252	153 - 193	171 - 181	98 - 118
	Major Ions									
	Total Alkalinity	64	256	108	111	260	236	194	203	239
	Bromide	0.095	<0.500	<0.500	0.337	<0.500	0.241	0.213	0	
	Fluoride	0.110	0.271	0.269	0.313	0.280	0.230	0.170	0.1	0.1
	Chloride	24	75	106	113	51	67	63	28.7	65
	Nitrite as N		<0.50	<0.50		<0.50	<0.001			
	Nitrate as N	0.030	<0.50	<0.50	0.148	<0.50	<0.01	0.183	0	
	TOC		1.8	<1.00		1.7	0.4		0	
	Sulfate	15	25	192	177	31	29	28	13.6	8.4
	Spec Cond.	1380	777	1000	945	751	758	611		
	TDS	194	483	653	629	473	470	391	281	368
	pH	6.08	7.26	7.54	7.56	7.36	7.70	7.16	7.6	7.3
	Calcium	10	75	30	32	36	37	91	67.8	98.4
	Iron		0.13	<0.050	0.15	0.12	140.00	0.15	345	
	Magnesium	1.06	2.36	<0.500	0.65	0.61	0.62	3.60	3.6	2.4
	Potassium	7.10	18.50	23.80	17.50	18.30	14.10	5.22	3.4	5.1
	Sodium	33	80	169	161	125	126	35	27.9	32.1
	Bicarbonate	78	312	131	135	316	286	236	232	278.5
Fixed Gas										
	O ₂ + Ar		16.8	12.7		10.3				
	N ₂		78.9	86.4		86.8				
	CH ₄		<0.1	<0.1		<0.1				
	CO		<0.1	<0.1		<0.1				
	CO ₂		4.4	0.9		2.9				
Gas in Headspace										
	C1		41.1	99		214				
	C2		29.3	22.8		51.9				
	C3		4.9	3.3		6.5				
	I-C4		<1.0	<1.0		<1.0				
	n-C4		2.7	1.8		4.1				
	I-C5		<1.0	<1.0		<1.0				
	n-C5		1	1.2		2.2				
Gas in Water										
	C1		2.3	5		11.6				
	C2		<1.0	<1.0		<1.0				
	C3		<1.0	<1.0		<1.0				
Isotope Analysis										
	δ ¹³ C _{C1}		ND	ND		ND				
	δ ¹³ C _{CO2}		-16.1	-21.7		-17.2				
	δ ¹³ C _{C2}		ND	ND		ND				
	δD _{C1}		ND	ND		ND				
	δD _{C2}		ND	ND		ND				
	δ ¹⁸ O		-4.5	-4.7		-4.6	-4.5			
	δD _{H2O}		-23.7	-25.2		-25.5	-21.8			
Carbon 14 Age Dating										
	Apparent C14 Age	4000	18180	13120	16480	25880	25880	14700		
	Apparent C14 Age Error		70	60		130	130			
	C13/C12 Ratio (‰)	-20.2	-18.0	-12.3	-15.8	-12.0	-11.42	-10.8	-14.87	-15.87
	pMC C14	14.75%	10.40%	19.53%	12.85%	3.99%	3.09%	8.78%	11.67%	59.75%
	pMC C14 Error		0.09%	0.14%		0.06%	0.10%		0.09%	0.20%
δS34 Analysis										
	δ34S ‰		-2.21	5.82		6.84				
	δ18O (sulfate) ‰		13.81	8.22	8.22	14.91	14.91		0.00	0.00

Final – Hydrogeochemical Evaluation of the Texas Gulf Coast Aquifer System and Implications for Developing Groundwater Availability Models

Table 4-3, continued

	Group #	3-8	3-8.5	3-9	3-10	3-11	3-11	3-12	3-13	3-14
Well Data	Source	USGS	USGS	USGS	TWDB	INTERA	USGS	TWDB	INTERA	USGS
	Sample Date	4/15/2011	11/29/2012	4/28/2011	8/24/2006	9/6/2012	9/6/2012	8/24/2006	11/15/2012	4/26/2011
	Unit	ML	CAT	JP	ML	CAT	CAT	JP	EV	CH
	Land Surface Elevation (ft amsl)	205	270	238	235	300	300	285	161	263
	Screen Interval	339 - 465	1822 - 2453	470 - 490	450 - 725	2290 - 2587	2290 - 2587	910 - 1144	320 - 335	118 - 128
Major Ions	Total Alkalinity	203	187	232	216	360	236	270	264	14
	Bromide				0.500	0.86	0.83	0.310	<0.500	
	Fluoride	0.160	1.000	0.150	0.200	2.19		0.670	0.219	0.040
	Chloride	31	84	22	18	198	233	46	20	19
	Nitrate as N				0.720	<0.5	<.01	0.310	<0.50	
	TOC					3.1	0		19.4	
	Sulfate	18	42	25	23	3	3	26	15	2
	Spec Cond.	511	766	529	515	1340	1360	756	636	96
	TDS	330	484	332	323	835	818	496	318	69
	pH	7.60	8.00	7.70	7.33	7.87	7.9	7.35	7.40	5.70
	Calcium	67	1	61	56	3	3.1	38	57	5
	Iron	0.05	20.20	0.07		<0.0	0.06		0.11	<.0032
	Magnesium	4.55	0.00	8.66	5.35	<0.5	0.12	5.85	15.70	1.46
	Potassium	5.45	3.60	5.80	6.10	9.62	6.14	8.38	4.97	1.30
Sodium	39	159	44	51	290	300	181	66	11	
Bicarbonate	247	224	261	263	436	435	329	321	16	
Fixed Gas	O ₂ + Ar					11.4			18.4	
	N ₂					60.9			78.8	
	CH ₄					25.8			<0.1	
	CO					<0.1			<0.1	
	CO ₂					1.9			2.8	
Gas in Headspace	C1					See Fixed			110.8	
	C2					107.8			<1.0	
	C3					27.9			<1.0	
	I-C4					<1.0			<1.0	
	n-C4					5.1			<1.0	
	I-C5					<1.0			<1.0	
Gas in Water	n-C5					1.4			<1.0	
	C1					7202.5			13	
	C2					0.9			<1.0	
Isotope Analysis	C3					<1.0			<1.0	
	δ ¹³ C _{C1}					-58.3			ND	
	δ ¹³ C _{CO2}					-26.4			-11.4	
	δ ¹³ C _{C2}					-45.4			ND	
	δD _{C1}					-294			ND	
	δD _{C2}					ND			ND	
	δ ¹⁸ O		-4.78		-5	-4.6		-5.5	-4.6	
δD _{H2O}		-23.9		-23.3	-25.8		-23.4	-24		
Carbon 14 Age Dating	Apparent C14 Age				20520	36580		23120	26580	
	Apparent C14 Age Error					330			150	
	C13/C12 Ratio (‰)	-12.04	-19.7	-11.8	-12.1	-17.8		-12.2	-11	-22.89
	pMC C14	6.06%	1.62%	1.02%	7.77%	1.05%		5.62%	3.66%	101.50%
	pMC C14 Error	0.06%	0.15%	0.03%	0.06%	0.04%		0.06%	0.07%	0.31%
δS34 Analysis	δ34S ‰				1.10	56.70		1.50	-4.90	
	δ18O (sulfate) ‰	0.00				14.30			14.40	0.00

Final – Hydrogeochemical Evaluation of the Texas Gulf Coast Aquifer System and
Implications for Developing Groundwater Availability Models

Table 4-3, continued

	Group #	3-15	3-16	3-17	3-18	3-19	3-20	3-21	3-22	3-23
Well Data	Source	USGS	TWDB	INTERA	INTERA	USGS	USGS	USGS	USGS	TWDB
	Sample Date	4/15/2011	8/24/2006	11/13/2012	11/13/2012	4/26/2011	3/13/2012	3/15/2012	5/4/2011	8/23/2006
	Unit	CH	JP	CH	JCK	EV	CAT	JP	EV	EV
	Land Surface Elevation (ft amsl)	195	145	205	205	132	173	173	129	136
	Screen Interval	148 - 168	1020 - 1236	260 - 290	717 - 768	647 - 710	3555 - 3595	2270 - 2300	777 - 807	736 - 1074
Major Ions	Total Alkalinity	42	222	84	240	273	150	840	243	254
	Bromide		0.273	<0.500	<0.500		62.000	0.105		0.297
	Fluoride	0.060	0.210	0.184	0.308	0.240	0.590	0.660	0.480	0.430
	Chloride	19	38	23	64	18	24400	1020	34	23
	Nitrate as N		0.183	<0.50	<0.50		<0.017	<0.01		0.265
	TOC			4.2	2.0		<0.23	1.3		
	Sulfate	2	25	4	25	17	>9.00	<0.45	1	12
	Spec Cond.	149	1245	274	804	560	61800	4630	539	575
	TDS	95	364	156	401	339	41500	2650	311	344
	pH	6.20	7.45	6.79	7.55	7.80	6.80	7.50	8.10	7.70
	Calcium	12	34	25	35	48	1370	42	21	20
	Iron	<.0032		<0.050	<0.050	0.46	17.10	1.34	0.23	
	Magnesium	3.04	5.79	4.12	9.28	12.70	85.00	2.68	6.22	5.21
	Potassium	1.83	6.94	3.17	4.42	4.58	126.00	18.40	5.08	3.00
Sodium	13	89	17	144	61	11500	943	93	105	
Bicarbonate	52	270	102	292	310	183	1022	293	308	
Fixed Gas	O ₂ + Ar			18.9	10.4		2.92	2.12		
	N ₂			74.3	87.8		12.68	15.9		
	CH ₄			<0.1	<0.1		82.5	75.3		
	CO			<0.1	<0.1					
	CO ₂			6.8	1.8					
Gas in Headspace	C1			16.1	79.9					
	C2			<1.0	5.3					
	C3			2.9	8.1					
	I-C4			<1.0	<1.0					
	n-C4			2.1	5.7					
	I-C5			<1.0	<1.0					
Gas in Water	n-C5			<1.0	2.8					
	C1			0.3	2					
	C2			<1.0	<1.0					
Isotope Analysis	C3			<1.0	<1.0					
	δ ¹³ C _{C1}			ND	ND					
	δ ¹³ C _{CO2}			-15.7	-14					
	δ ¹³ C _{C2}			ND	ND					
	δD _{C1}			ND	ND					
	δD _{C2}			ND	ND					
	δ ¹⁸ O		-5.3	-4.4	-4.6		0.37	-3.16		-4.6
δD _{H2O}		-22.4	-22.8	-23.5		-12.7	-19		-21.7	
Carbon 14 Age Dating	Apparent C14 Age		21760	4680	28080					21130
	Apparent C14 Age Error			40	170					
	C13/C12 Ratio (‰)	-21.11	-12.7	-17.6	-15.4	-9.88			-21.41	-11.3
	pMC C14	82.80%	6.66%	55.84%	3.03%	2.54%			86.90%	7.20%
	pMC C14 Error	0.28%	0.07%	0.27%	0.06%	0.07%			0.29%	0.11%
δS34 Analysis	δ34S ‰		6.10	12.30	10.20					1.90
	δ18O (sulfate) ‰	0.00		14.70	16.20	0.00				

Final – Hydrogeochemical Evaluation of the Texas Gulf Coast Aquifer System and Implications for Developing Groundwater Availability Models

Table 4-3, continued

Group #	3-24	3-25	3-26	3-27	3-28	3-29	3-30	3-31	3-32	
Well Data	Source	INTERA	INTERA	TWDB	INTERA	INTERA	INTERA	TWDB	INTERA	TWDB
	Sample Date	11/14/2012	11/15/2012	8/23/2006	11/13/2012	11/12/2012	11/13/2012	7/14/2005	11/12/2012	8/23/2006
	Unit	CH	ML	EV	CH	ML	CH	EV	JCK	CH
	Land Surface Elevation (ft amsl)	125	138	125	110	121	109	105	109	91
	Screen Interval	240 - 260	1150 - 1695	620 - 1012	236 - 256	314 - 344	260 - 280	670 - 1155	1580 - 1686	485 - 550
	Major Ions									
Total Alkalinity	160	100	254	144	132	140	210	392	153	
Bromide	<0.500	<0.500	0.500	<0.500	<0.500	<0.500	0.212	<0.500	0.315	
Fluoride	0.213	1.060	0.600	0.186	<0.100	<0.100	0.687	1.680	0.160	
Chloride	26	122	28	41	35	36	54	58	37	
Nitrate as N	<0.50	<0.50	0.440	<0.50	<0.50	<0.50	0.055	<0.50	0.530	
TOC	20.8	20.4		5.5	4.0	4.5		11.4		
Sulfate	2	1	13	6	4	3	10	<0.50	3	
Spec Cond.	442	1410	605	484	463	471	574	1070	412	
TDS	229	818	356	260	306	273	339	674	246	
pH	7.89	8.07	7.95	7.69	7.44	7.59	7.63	8.19	7.46	
Calcium	53	7	11	55	51	58	21	4	49	
Iron	<0.050	0.05		<0.050	<0.050	<0.050		<0.050		
Magnesium	4.25	1.10	2.60	4.76	3.32	4.50	4.70	0.53	5.55	
Potassium	3.09	3.40	2.10	2.88	2.40	2.72	2.24	2.26	2.37	
Sodium	28	382	130	25	30	23	102	276	31	
Bicarbonate	194	121	307	175	161	170	256	471	186	
Fixed Gas										
O ₂ + Ar	21.7	5.7		21.1	18.8	17.8		12.8		
N ₂	77.5	27.8		77.9	80.2	80.9		68.2		
CH ₄	<0.1	65.7		<0.1	<0.1	<0.1		18.5		
CO	<0.1	<0.1		<0.1	<0.1	<0.1		<0.1		
CO ₂	0.9	0.8		1.1	1	1.3		0.4		
Gas in Headspace										
C1	32.5	See Fixed		132	50.7	45		See Fixed		
C2	<1.0	57.9		1.7	1.8	3.3		211.9		
C3	5.9	<1.0		3.6	4	5.8		51.5		
I-C4	<1.0	<1.0		<1.0	<1.0	<1.0		<1.0		
n-C4	3	<1.0		2.5	2.2	3.7		12.5		
I-C5	<1.0	<1.0		<1.0	<1.0	<1.0		<1.0		
n-C5	2.6	<1.0		1.4	2.8	1.6		1.6		
Gas in Water										
C1	0.5	2041627.9		3.2	1	0.8		8125.4		
C2	<1.0	119.2		<1.0	<1.0	<1.0		<1.0		
C3	<1.0	<1.0		<1.0	<1.0	<1.0		<1.0		
Isotope Analysis										
δ ¹³ C _{C1}	ND	-48.3		-57.7	ND	ND		-51.1		
δ ¹³ C _{CO2}	-16.4	-10.3		-13.6	-12.7	-12		-16.2		
δ ¹³ C _{C2}	ND	ND		ND	ND	ND		ND		
δD _{C1}	ND	-192		ND	ND	ND		-196		
δD _{C2}	ND	ND		ND	ND	ND		ND		
δ ¹⁸ O	-4.3	-4.5	-5.6	-4.2	-4.3	-4.1		-4.6	-4.7	
δD _{H2O}	-22.7	-23.4	-21.3	-22.3	-22.4	-20.6		-26.1	-19.2	
Carbon 14 Age Dating										
Apparent C14 Age	7180	> 43500	24760	14000	16320	13820	24490	34100	14730	
Apparent C14 Age Error	40			60	70	60		300		
C13/C12 Ratio (‰)	-17.5	-8.9	-12.5	-16.5	-16.4	-14.3	-9	-10.1	-12.3	
pMC C14	40.91%		4.58%	17.50%	13.11%	17.90%	4.74%	1.43%	15.98%	
pMC C14 Error	0.20%		0.10%	0.13%	0.11%	0.13%		0.05%	0.16%	
δS34 Analysis										
δ34S ‰	n/a	n/a	6.7	10.2	10.1	12.3		n/a	9	
δ18O (sulfate) ‰	10.5	n/a		12.5	11.8	10.9		10.4		

Final – Hydrogeochemical Evaluation of the Texas Gulf Coast Aquifer System and
Implications for Developing Groundwater Availability Models

Table 4-3, continued

	Group #	3-33	3-34	3-35	3-36	3-37	3-38	3-39	3-40	3-41
Well Data	Source	TWDB	TWDB	TWDB	USGS	INTERA	USGS	USGS	USGS	USGS
	Sample Date	8/22/2006	8/22/2006	7/26/2005	8/13/2008	11/14/2012	9/22/1998	8/22/2008	8/8/2003	8/13/2008
	Unit	EV	EV	EV	EV	CH	EV	CH	EV	EV
	Land Surface Elevation (ft amsl)	117	104	79	93	74	92	92	92	90
	Screen Interval		554 - 1045	800 - 1680	652 - 1769	205 - 225	1174 - 1648	322 - 600	1072 - 1610	644 - 1284
Major Ions	Total Alkalinity	192	267	160	193	156	324	187	313	172
	Bromide	0.291	0.335	0.132		<0.5	0.25	0.11	0.27	0.15
	Fluoride	0.587	0.933	0.223	0.500	0.25	0	1.32	1.22	0.21
	Chloride	55	64	35	60	38	83.1	47.2	85.4	48.1
	Nitrate as N	0.207	0.188	0.095		<0.5				
	TOC					20.3				
	Sulfate	6	2	5	10	8	0.17	4.82	0.81	11.6
	Spec Cond.	555	724	428	586	517	830	519	856	515
	TDS	318	407	246	298	275	496	311	486	289
	pH	7.60	7.96	7.50	7.63	7.91				
	Calcium	27	14	36	41	52	8.5	66.4	8.23	47.4
	Iron			0.15		<0.0	76.6	-888	112	-888
	Magnesium	6.64	2.41	6.62	7.00	7.73	2.09	6.57	1.99	8.84
	Potassium	2.28	1.64	1.68	2.40	2.41	1.91	1.47	1.81	2.05
Sodium	83	150	45	87	54	178	24	182	46	
Bicarbonate	233	323	195	235	189	394	228	382	210	
Fixed Gas	O ₂ + Ar					23.4				
	N ₂					75.7				
	CH ₄					<0.1				
	CO					<0.1				
	CO ₂					0.8				
Gas in Headspace	C1					33.2				
	C2					7.4				
	C3					5.2				
	I-C4					<1.0				
	n-C4					1.7				
	I-C5					<1.0				
Gas in Water	n-C5					0.5				
	C1					0.3				
	C2					<1.0				
Isotope Analysis	C3					<1.0				
	$\delta^{13}\text{C}_{\text{C1}}$					ND				
	$\delta^{13}\text{C}_{\text{CO2}}$					-12.3				
	$\delta^{13}\text{C}_{\text{C2}}$					ND				
	$\delta\text{D}_{\text{C1}}$					ND				
	$\delta\text{D}_{\text{C2}}$					ND				
	$\delta^{18}\text{O}$	-4.6	-5.6			-4.6				
$\delta\text{D}_{\text{H2O}}$	-22.2	-23			-24.9					
Carbon 14 Age Dating	Apparent C14 Age	22330	24230	19540		23580				
	Apparent C14 Age Error					120				
	C13/C12 Ratio (‰)	-10.1	-12.5	-12.3		-14.4	-11.64	-9.2	-11.57	-11.16
	pMC C14	6.20%	4.90%	5.18%	3.89%	5.31%	0.33%	30.37%	0.37%	4.59%
	pMC C14 Error	0.11%	0.11%		0.12%	0.08%		0.23%		0.12%
δS34 Analysis	δS34S ‰	13.80	37.80			8.60				
	δ18O (sulfate) ‰					11.80				

Final – Hydrogeochemical Evaluation of the Texas Gulf Coast Aquifer System and Implications for Developing Groundwater Availability Models

Table 4-3, continued

	Group #	3-42	3-43	3-44	3-45	3-46	3-47	3-48	3-49
Well Data	Source	INTERA	INTERA	INTERA	INTERA	TWDB	TWDB	TWDB	TWDB
	Sample Date	11/15/2012	11/15/2012	11/14/2012	11/14/2012	8/8/2006	8/9/2006	8/9/2006	8/9/2006
	Unit	CH	CH	CH	CH	CH	CH	CH	CH
	Land Surface Elevation (ft amsl)	51	29	56	49	20	22	24	18
	Screen Interval	310 - 330	900 - 1186	990 - 1010	540 - 830	500 - 716	650 - 730		
Major Ions	Total Alkalinity	560	176	224	224	274	279	273	273
	Bromide	<0.500	<0.500	<0.500	<0.500	0.521	1.800	4.700	0.855
	Fluoride	3.150	0.242	0.603	0.572	0.877	0.875	0.550	0.668
	Chloride	128	39	89	35	137	238	646	287
	Nitrate as N	<0.50	<0.50	<0.50	<0.50	0.230	0.185	0.935	0.690
	TOC	21.1	13.5	21.1	19.7				
	Sulfate	<0.50	1	14	2	3	0	1	1
	Spec Cond.	1480	498	826	600	919	1255	2471	1427
	TDS	786	278	314	318	534	665	1334	652
	pH	8.11	7.75	8.05	8.10	7.94	7.92	7.80	8.06
	Calcium	5	40	31	31	20	20	46	15
	Iron	<0.050	0.27	0.01	0.11	0.13			
	Magnesium	1.04	6.59	6.74	6.01	4.77	4.73	14.65	4.43
	Potassium	3.18	2.60	2.46	1.97	1.63	1.90	2.80	1.67
Sodium	377	66	190	128	185	237	450	231	
Bicarbonate	674	213	270	270	332	337	331	330	
Fixed Gas	O ₂ + Ar	5.1	13	14.9	11.6				
	N ₂	26.5	73.5	84	85.1				
	CH ₄	67.7	11.4	<0.1	2.3				
	CO	<0.1	1	<0.1	<0.1				
	CO ₂	0.8	1.1	1.1	1				
Gas in Headspace	C1	See Fixed	See Fixed	49.5	See Fixed				
	C2	28.1	1360	9.9	31.8				
	C3	<1.0	163.3	7.2	11.4				
	I-C4	<1.0	54.9	<1.0	<1.0				
	n-C4	<1.0	9.2	2.3	4.8				
	I-C5	<1.0	14.5	<1.0	<1.0				
Gas in Water	n-C5	<1.0	<1.0	1.3	1.4				
	C1	2249125	296444.8	1.7	8278.8				
	C2	14.3	1028.2	<1.0	<1.0				
Isotope Analysis	C3	<1.0	107.3	<1.0	<1.0				
	δ ¹³ C _{C1}	-48.3	-46.9	ND	-60.8				
	δ ¹³ C _{CO2}	-11.6	-12.8	-13.1	-8.2				
	δ ¹³ C _{C2}	ND	-29.4	ND	ND				
	δD _{C1}	-191	-172	ND	-232				
	δD _{C2}	ND	ND	ND	ND				
Carbon 14 Age Dating	δ ¹⁸ O	-4.4	-4.3	-4.5	-4.6	-4.6	-4.6	-4.8	-4.3
	δD _{H2O}	-24.1	-22	-26	-23.9	-21	-20	-21	-17
	Apparent C14 Age	37470	15760	34590	32790	31520	30910	31220	31080
	Apparent C14 Age Error	430	70	450	270				
	C13/C12 Ratio (‰)	-9.6	-13.8	-13.2	-13.1	-12	-13.3	-12.8	-13.2
δS34 Analysis	pMC C14	0.94%	14.06%	1.35%	1.69%	1.98%	2.13%	2.05%	2.09%
	pMC C14 Error	0.05%	0.12%	0.07%	0.06%	0.08%	0.11%	0.08%	0.08%
δS34 Analysis	δ34S ‰	n/a	n/a	n/a	n/a				
	δ18O (sulfate) ‰	13.3	13	n/a	n/a				

Final – Hydrogeochemical Evaluation of the Texas Gulf Coast Aquifer System and
Implications for Developing Groundwater Availability Models

Table 4-4 Geochemistry Measurements for Transect 5.

	Group #	5-1	5-2	5-3	5-4	5-5	5-6	5-7	5-8	5-9
Well Data	Source	TWDB	INTERA	TWDB	INTERA	INTERA	TWDB	INTERA	INTERA	INTERA
	Sample Date	8/11/2009	12/11/2012	8/13/2009	12/11/2012	12/11/2012	8/11/2009	12/11/2012	12/11/2012	12/12/2012
	Unit	JCK	JCK	ML	JCK	JCK	JP	JP	JP	CAT
	Land Surface Elevation (ft amsl)	401	328	390	330	330	355	259	259	303
	Screen Interval		560 - 660		753 - 949	770 - 988	155 - 285	493 - 978	300 - 636	894 - 1030
	Major Ions									
Major Ions	Total Alkalinity	248	340	311	540	540	243	312	500	380
	Bromide	0.665	<0.500	0.659	< 0.5	<0.500	0.080	<0.500	<0.500	<0.500
	Fluoride	0.570	0.303	0.710	0.98	1.020	0.280	0.412	0.748	0.299
	Chloride	196	105	185	106	107	16	242	283	104
	Nitrate as N	0.094	<0.50	2.107	< 0.5	<0.50	0.020	<0.50	<0.50	<0.50
	TOC		19.3		3.72885	16.1		9.4	11.4	10.8
	Sulfate	58	31	49	< 0.5	<0.50	21	88	15	15
	Spec Cond.	1214	1130	1271	1340	1400	566	1600	1950	1070
	TDS	720	628	729	812	824	337	912	1190	620
	pH	6.96	7.44	6.92		7.92	6.91	7.86	8.07	8.08
	Calcium	99	32	119	6.13	8	96	22	10	5
	Iron	0.15	<0.050		< 50	<0.050		0.21	0.06	<0.050
	Magnesium	4.42	1.36	12.27	< 0.5	<0.500	2.86	5.59	1.54	<0.500
	Potassium	12.86	17.90	7.04	14.4	14.90	1.61	5.80	7.88	4.90
Sodium	141	198	124	370	386	22	380	525	308	
Bicarbonate	302	414	379	650	653	296	378	603	458	
Fixed Gas										
Fixed Gas	O ₂ + Ar		6.6		9.1	7.3		11	14.9	4.8
	N ₂		88.5		50.4	43.2		83.1	59.9	94.5
	CH ₄		2.1		39.5	48.5		3.8	24.1	0.2
	CO		0.8		<0.1	<0.1		1.2	<0.1	<0.1
	CO ₂		2		1	1		1	1	0.5
Gas in Headspace										
Gas in Headspace	C1		9362.6		See Fixed	See Fixed		15338.5	See Fixed	1096.3
	C2		14.3		73.2	15.3		67.8	96.5	4.2
	C3		5.6		5.9	<1.0		13.6	18.8	2.2
	I-C4		<1.0		<1.0	<1.0		<1.0	<1.0	<1.0
	n-C4		2		3.8	<1.0		4.2	4.5	2.4
	I-C5		<1.0		<1.0	<1.0		<1.0	<1.0	<1.0
Gas in Water										
Gas in Water	C1		692.7		14929.5	19695.9		908.9	9101.4	68
	C2		0.8		<0.1	<0.1		2.8	<0.1	<0.1
	C3		<0.1		<0.1	<0.1		0.2	<0.1	<0.1
Isotope Analysis										
Isotope Analysis	δ ¹³ C _{C1}		-46.2		-59.9	-56.6		-42.4	-41.8	-41.5
	δ ¹³ C _{CO2}		-18.5		-18.6	-17.4		-16.8	-17.9	-18.6
	δ ¹³ C _{C2}		ND		ND	ND		a -36.8	ND	ND
	δD _{C1}		-182		-226	-220		-185	-202	-195
	δD _{C2}		ND		ND	ND		ND	ND	ND
	δ ¹⁸ O	-4.23	-4.3	-4.23	-4.4	-4.5	-3.97	-4.2	-4.3	-4.5
δD _{H2O}	-25.2	-24	-24	-24.8	-24.9	-22.5	-23.3	-25.7	-26.6	
Carbon 14 Age Dating										
Carbon 14 Age Dating	Apparent C14 Age	8940	24670	12280	39010	> 43500	2570	38280	42120	17510
	Apparent C14 Age Error		120		450			490	720	80
	C13/C12 Ratio (‰)	-9.3	-12.4	-7.3	-10.5	-10.1	-7.5	-10.9	-12.3	-12.1
	pMC C14	32.85%	4.60%	21.67%	0.80%		72.59%	0.90%	0.50%	11.30%
	pMC C14 Error	0.20%	0.10%	0.19%	0.10%		0.36%	0.10%	0.10%	0.10%
δS34 Analysis										
δS34 Analysis	δ34S ‰	4.1	5.2	10.9	6	n/a	-30.6	15.2	24.4	7.5
	δ18O (sulfate) ‰		8.1		n/a	n/a		16.9	18.8	10.9

Final – Hydrogeochemical Evaluation of the Texas Gulf Coast Aquifer System and
Implications for Developing Groundwater Availability Models

Table 4-4, continued

	Group #	5-10	5-11	5-12	5-13	5-14	5-15	5-15	5-16	5-17
Well Data	Source	TWDB	TWDB	TWDB	TWDB	TWDB	INTERA	TWDB	INTERA	TWDB
	Sample Date	8/13/2009	8/11/2009	8/13/2009	8/17/2009	8/17/2009	12/10/2012	8/19/2009	12/10/2012	8/19/2009
	Unit	EV	CH	CH	CH	EV	CH	CH	EV	CH
	Land Surface Elevation (ft amsl)	219	190	165	106	64	44	44	14	
	Screen Interval				79 - 109	955 - 1308	270 - 300	270 - 300	1078 - 1223	
Major Ions	Total Alkalinity	319	334	244	320	302	268	258	336	273
	Bromide	0.840	0.639	0.363	1.469	0.738	<0.500	0.850	<0.500	0.734
	Fluoride	0.462	0.545	0.510	0.250	0.884	0.535	0.600	1.380	0.634
	Chloride	157	124	116	30	199	279	306	282	221
	Nitrate as N	1.948	0.098	0.880	0.193	0.310	<0.50	0.230	<0.50	0.267
	TOC						8.7		9.8	
	Sulfate	30	36	19	30	3	<0.50	4	<0.50	86
	Spec Cond.	1214	1095	886	751	1268	1750	1500	1910	1396
	TDS	647	626	510	447	658	1090	780	1180	761
	pH	7.10	6.97	7.09	7.10	7.86	7.70	7.46	8.01	7.03
	Calcium	133	99	91	68	6	26	27	9	83
	Iron	0.18	0.15		0.15		0.06		0.07	0.21
	Magnesium	15.81	14.55	10.57	12.27	2.20	9.84	10.18	3.51	32.44
	Potassium	1.94	2.04	0.62	2.61	1.33	2.83	2.02	3.11	3.74
Sodium	85	111	73	83	253	314	263	404	149	
Bicarbonate	388	407	297	389	366	325	313	406	332	
Fixed Gas	O ₂ + Ar						12.1		8.1	
	N ₂						70.7		40.5	
	CH ₄						16		50.9	
	CO						0.2		<0.1	
	CO ₂						0.9		0.5	
Gas in Headspace	C1						See Fixed		See Fixed	
	C2						142.9		817.1	
	C3						31.8		159.8	
	I-C4						<1.0		45.9	
	n-C4						7.4		29.6	
	I-C5						<1.0		9.5	
	n-C5						<1.0		<1.0	
Gas in Water	C1						6755.6		23628.1	
	C2						<0.1		81.7	
	C3						<0.1		12.9	
Isotope Analysis	δ ¹³ C _{C1}						-65.2		-58.3	
	δ ¹³ C _{CO2}						a 3.3		a -7.7	
	δ ¹³ C _{C2}						ND		ND	
	δD _{C1}						-207		-214	
	δD _{C2}						ND		ND	
	δ ¹⁸ O	-4.28	-4.55	-4.53	-4.28	-4.49	-4.4	-4.37	-4.2	-4.15
δD _{H2O}	-24.9	-26	-25.4	-25.2	-25.7	-25.8	-24.9	-24.7	-23.4	
Carbon 14 Age Dating	Apparent C14 Age	6260	3330	6730	9340	21180	37340	20280	37870	3770
	Apparent C14 Age Error						370		390	
	C13/C12 Ratio (‰)	-10	-10.7	-13.1	-12.9	-13.5	-13	-15.3	-7.8	-9.1
	pMC C14	45.85%	66.04%	43.25%	31.25%	7.16%	1.00%	8.01%	0.90%	62.52%
	pMC C14 Error	0.29%	0.33%	0.27%	0.19%	0.11%	0.10%	0.14%	0.10%	0.39%
δS34 Analysis	δ34S ‰	-1	10.6	-1	8.3	-1	10	-1	20.1	5.4
	δ18O (sulfate) ‰						6.6		(n/a)	

Final – Hydrogeochemical Evaluation of the Texas Gulf Coast Aquifer System and
Implications for Developing Groundwater Availability Models

Table 4-4, continued

	Group #	5-18	5-19	5-19	5-20
Well Data	Source	TWDB	INTERA	TWDB	INTERA
	Sample Date	8/19/2009	12/10/2012	8/17/2009	12/10/2012
	Unit	CH	CH	CH	CH
	Land Surface Elevation (ft amsl)		16	16	2
	Screen Interval		390 - 600	390 - 600	190 - 200
	Major Ions				
Major Ions	Total Alkalinity	298	304	317	368
	Bromide	0.100	<0.500	0.050	<0.500
	Fluoride	0.480	1.090		1.770
	Chloride	80	206	249	202
	Nitrate as N	0.020	<0.50	0.180	<0.50
	TOC		9.8		11.9
	Sulfate	12	9	20	9
	Spec Cond.	879	1520	1414	1660
	TDS	487	956	800	1040
	pH	7.20	8.14	8.01	7.95
	Calcium	59	5	6	10
	Iron		0.06	0.15	<0.050
	Magnesium	23.00	2.49	3.70	4.90
	Potassium	4.10	2.43	2.70	4.08
Sodium	94	319	312	324	
Bicarbonate	363	366	383	445	
Fixed Gas					
Fixed Gas	O ₂ + Ar		16		13.4
	N ₂		83.3		85.6
	CH ₄		<0.1		<0.1
	CO		0.3		0.3
	CO ₂		0.4		0.7
Gas in Headspace					
Gas in Headspace	C1		205.4		196.3
	C2		8.3		7.4
	C3		5.1		3.3
	I-C4		<1.0		<1.0
	n-C4		2.4		2.4
	I-C5		<1.0		<1.0
	n-C5		<1.0		<1.0
Gas in Water					
Gas in Water	C1		10.4		10.5
	C2		<0.1		<0.1
	C3		<0.1		<0.1
Isotope Analysis					
Isotope Analysis	δ ¹³ C _{C1}		ND		ND
	δ ¹³ C _{CO2}		-20.3		-20.3
	δ ¹³ C _{C2}		ND		ND
	δD _{C1}		ND		ND
	δD _{C2}		ND		ND
	δ ¹⁸ O	-4.11	-4.1	-4	-3.8
	δD _{H2O}	-22.3	-22.4	-22.5	-21.1
Carbon 14 Age Dating					
Carbon 14 Age Dating	Apparent C14 Age	7220	38800	21220	38930
	Apparent C14 Age Error		440		450
	C13/C12 Ratio (‰)	-10	-11.9	-13.3	-11.4
	pMC C14	40.69%	0.80%	7.12%	0.80%
	pMC C14 Error	0.25%	0.10%	0.11%	0.10%
δS34 Analysis					
δS34 Analysis	δ34S ‰		26.9		38.1
	δ18O (sulfate) ‰		19.6		19.7

Final – Hydrogeochemical Evaluation of the Texas Gulf Coast Aquifer System and
Implications for Developing Groundwater Availability Models

Table 4-5 Geochemistry Measurements for Transect 8.

Group #	8-1	8-2	8-3	8-4	8-5	8-6	8-7	8-8	8-9	
Well Data	Source	INTERA	INTERA	INTERA	TWDB	INTERA	INTERA	TWDB	TWDB	INTERA
	Sample Date	1/24/2013	1/24/2013	1/24/2013	8/21/2006	1/22/2013	1/22/2013	8/22/2006	5/21/2005	1/23/2013
	Unit	CAT	JP	JP	CAT	EV	EV	EV	ML	EV
	Land Surface Elevation (ft amsl)	848	773	775	595	442	376	371	374	379
	Screen Interval	440 - 460	236 - 345	230 - 315	540 - 560	732 - 780	308 - 328	248 - 482	1500 - 1600	82 - 102
Major Ions	Total Alkalinity	288	320	312	415	224	296	262.5	225.8	304
	Bromide	1.080	0.599	0.611	2.7	0.834	1.370	0.8	0.9	0.607
	Fluoride	0.889	0.670	0.641	3.9	0.656	1.170	1.3	0.6	0.543
	Chloride	293	152	161	2935	226	473	349.5	173.4	204
	Nitrate as N	3.400	<0.5	0.910	5.6	4.600	6.790	28.4	0.2	7.610
	TOC	9.5	9.4	10.2		7.9	6.8		9.3	11.1
	Sulfate	111	106	102	238	75	19	204.5	157	51
	Spec Cond.	1910	1450	1420		1480	2660			1520
	TDS	1220	956	964	5720	948	1750	1197	780	1020
	pH	8.21	7.94	8.03		7.28	7.22			6.74
	Calcium	6	7	7	69.1	59	92	35.9	6.1	127
	Iron	<0.050	<0.050	<0.050		<0.050	<0.050			<0.050
	Magnesium	4.14	2.06	2.15	16.9	19.90	32.50	15	0.3	20.50
	Potassium	10.50	6.60	6.54	67.9	13.40	19.80	11.5	2.6	7.06
	Sodium	490	414	395	2060	214	441	360	281	122
Bicarbonate	346	387	377	506.4	273	361	320.3	267.9	371	
Fixed Gas	O ₂ + Ar	13.7	13.7	13.8		16.2	18.9			17.3
	N ₂	76.4	76.4	85.7		83.2	78.5			72.1
	CH ₄	9.3	9.3	<0.1		<0.1	<0.1			<0.1
	CO	0.3	0.3	0.3		<0.1	<0.1			<0.1
	CO ₂	0.4	0.4	0.2		0.6	2.6			10.6
Gas in Headspace	C1	65.3	See Fixed	1232.5		19.3	22			9.8
	C2	6.2	78.8	7.7		2.5	1.4			0.6
	C3	4.6	25.6	3.1		2.1	2			0.4
	I-C4	<1	<1	<1		<0.1	<0.1			<0.1
	n-C4	<1	<1	<1		2.3	1.9			<0.1
	I-C5	<1	<1	<1		<0.1	<0.1			<0.1
	n-C5	<1	<1	<1		<0.1	<0.1			<0.1
Gas in Water	C1	2.5	5059.5	103.2		0.1	0.8			0.1
	C2	<0.1	1.7	<0.1		<0.1	<0.1			<0.1
	C3	<0.1	<0.1	<0.1		<0.1	<0.1			<0.1
Isotope Analysis	δ ¹³ C _{C1}	ND	-43	-42.2		ND	ND			ND
	δ ¹³ C _{CO2}	-14	-14.5	-13		-14.4	-14.4			-17.4
	δ ¹³ C _{C2}	-25.4	-54.7	-55.9		ND	ND			ND
	δD _{C1}	ND	-175	-171		ND	ND			ND
	δD _{C2}	ND	ND	ND		ND	ND			ND
	δ ¹⁸ O	-4.8	-4.8	-4.6	-4.4	-4.8	-4.4	-4.5		-4.3
	δD _{H2O}	-28.1	-25.9	-30	-21.9	-29.5	-28.8	22.2		-28.7
Carbon 14 Age Dating	Apparent C14 Age	32660	33840	36990	20440	34940	5610	18490		101.4
	Apparent C14 Age Error	230	260	360		290	30			0.4
	C13/C12 Ratio (‰)	-10.1	-10.3	-10.3		-12.3	-13	-8.2		-16.9
	pMC C14	1.71%	1.48%	1.00%	7.85%	1.29%	49.74%	10.00%		101.38%
	pMC C14 Error	0.05%	0.05%	0.04%	0.09%	0.05%	0.18%	0.10%		0.37%
δS34 Analysis	δ34S ‰	12.3	11.2	11.2		10.5	14.1			14.4
	δ18O (sulfate) ‰	6.6	14.4	7.2		9.3	8.7			7.3

Final – Hydrogeochemical Evaluation of the Texas Gulf Coast Aquifer System and Implications for Developing Groundwater Availability Models

Table 4-5, continued

	Group #	8-10	8-11	8-12	8-13	8-14	8-15	8-16	8-17	8-18
Well Data	Source	INTERA	INTERA	TWDB	INTERA	TWDB	INTERA	TWDB	TWDB	TWDB
	Sample Date	1/23/2013	1/22/2013	8/22/2006	1/22/2013	8/24/2006	1/23/2013	8/24/2006	8/23/2006	8/23/2006
	Unit	EV	CH	EV	EV	EV	EV	EV	CH	EV
	Land Surface Elevation (ft amsl)	383	301	290	150	110	73	50	29	30
	Screen Interval	492 - 542	314 - 614	285 - 385	410 - 712	400 - 500	555 - 615	540 - 640	740 - 780	996 - 1042
	Major Ions									
Total Alkalinity	248	188	196.3	176	225.2	232	180	202	183	
Bromide	1.100	1.33	2	0.78	0.7	0.58	0.500	0.500	0.500	
Fluoride	0.738	0.61	0.9	0.44	0.6	0.55	0.400	0.500	0.600	
Chloride	336	397	845.7	201	174.4	163	277	249	318	
Nitrate as N	2.030	7.47	21	1.62	13.8	2.34	1.770	0.440	0.440	
TOC	9.0	7.8		2.4		5.7				
Sulfate	452	105	297	209	150.6	200	363	286	242	
Spec Cond.	2500	2030		1570	1310	1550	1982	1760	1965	
TDS	1680	1320	2040	1040	775.	1060	1205	1076	1109	
pH	7.42	7.16		7.65		7.37				
Calcium	66	125	192.3	38	49.3	36	34	25	18	
Iron	<0.050	<0.0		<0.0		<0.0				
Magnesium	28.30	31.7	77.1	6.15	17.8	8.79	9.60	6.80	4.30	
Potassium	16.10	14.7	20.2	11.1	9.7	10.2	9.00	7.30	4.90	
Sodium	433	216	413.3	262	196.4	260	382	361	394	
Bicarbonate	302	229	239.6	214	274.8	282	220	247	223	
Fixed Gas										
O ₂ + Ar	12.1	20.6		20.6		17.1				
N ₂	85.9	77.5		77.7		81.1				
CH ₄	<0.1	<0.1		<0.1		<0.1				
CO	0.6	<0.1		<0.1		<0.1				
CO ₂	1.4	1.9		1.7		1.8				
Gas in Headspace										
C1	58.1	9.8		20.5		29.4				
C2	8.4	0.8		1.3		3.7				
C3	5.8	1.7		3.2		4.2				
I-C4	<0.1	<0.1		<0.1		<0.1				
n-C4	3.3	2		2		1.4				
I-C5	<0.1	<0.1		<0.1		<0.1				
n-C5	<0.1	<0.1		<0.1		<0.1				
Gas in Water										
C1	0.4	<0.1		0.1		0.2				
C2	<0.1	<0.1		<0.1		<0.1				
C3	<0.1	<0.1		<0.1		<0.1				
Isotope Analysis										
δ ¹³ C _{C1}	ND	ND		ND		ND				
δ ¹³ C _{CO2}	-13.9	-14.5		-13.2		-12.7				
δ ¹³ C _{C2}	ND	ND		ND		ND				
δD _{C1}	ND	ND		ND		ND				
δD _{C2}	ND	ND		ND		ND				
δ ¹⁸ O	-4.4	-4.4	-4.3	-4	-4.1	-4.1	-4.2	-4.2	-4.3	
δD _{H2O}	-26.9	-28.6	-22.1	-27	-21.6	-25.7	-22.4	-20.9	-22.5	
Carbon 14 Age Dating										
Apparent C14 Age	18920	16220	12380	19920	18240	35810	20750	20190	20200	
Apparent C14 Age Error	70	60		80		310				
C13/C12 Ratio (‰)	-13.4	-17	-9.7	-10.4	-7.6	-9.2	-7	-8.6	-8.3	
pMC C14	9.49%	13.28%	21.40%	8.38%	10.32%	1.16%	7.55%	8.10%	8.09%	
pMC C14 Error	0.08%	0.10%	0.16%	0.08%	0.10%	0.04%	0.08%	0.09%	0.09%	
δS34 Analysis										
δ34S ‰	12.6	13.3		12.9		14.8				
δ18O (sulfate) ‰	21.5	8.7		8.2		12.1				

Final – Hydrogeochemical Evaluation of the Texas Gulf Coast Aquifer System and Implications for Developing Groundwater Availability Models

Table 4-5, continued

	Group #	8-19
Well Data	Source	TWDB
	Sample Date	8/23/2006
	Unit	CH
	Land Surface Elevation (ft amsl)	15
	Screen Interval	919 - 1019
Major Ions	Total Alkalinity	159
	Bromide	0.500
	Fluoride	1.000
	Chloride	401
	Nitrate as N	0.440
	TOC	
	Sulfate	275
	Spec Cond.	2230
	TDS	1266
	pH	
	Calcium	16
	Iron	
	Magnesium	3.30
Potassium	4.20	
Sodium	452	
Bicarbonate	184	
Fixed Gas	O ₂ + Ar	
	N ₂	
	CH ₄	
	CO	
	CO ₂	
Gas in Headspace	C1	
	C2	
	C3	
	I-C4	
	n-C4	
	I-C5	
Gas in Water	n-C5	
	C1	
	C2	
Isotope Analysis	C3	
	$\delta^{13}\text{C}_{\text{C1}}$	
	$\delta^{13}\text{C}_{\text{CO2}}$	
	$\delta^{13}\text{C}_{\text{C2}}$	
	$\delta\text{D}_{\text{C1}}$	
	$\delta\text{D}_{\text{C2}}$	
	$\delta^{18}\text{O}$	-4.2
$\delta\text{D}_{\text{H2O}}$	-22.9	
Carbon 14 Age Dating	Apparent C14 Age	21150
	Apparent C14 Age Error	
	C13/C12 Ratio (‰)	-8.4
	pMC C14	7.18%
	pMC C14 Error	0.09%
δS34 Analysis	δS34S ‰	
	δ18O (sulfate) ‰	

Final – Hydrogeochemical Evaluation of the Texas Gulf Coast Aquifer System and Implications for Developing Groundwater Availability Models

Table 4-6 State Well Numbers and Secondary Well IDs for the Wells in Transects 3, 5, and 8.

Group #	Source	Chain of Custody ID	TWDB Well Number	TCEQ PWS ID	Group #	Source	Chain of Custody ID	TWDB Well Number	TCEQ PWS ID
3-1	TWDB	NA	6011904		5-1	TWDB	NA	6731602	
3-2	INTERA	G2360052A0	6019601	G2360052A	5-2	INTERA	NFR Energy		
3-3	INTERA	G2360074A	6020401	G2360074A	5-3	TWDB	NA	6732704	
3-3	TWDB	NA	6020401	G2360074A	5-4	INTERA	G1430003A	6739505	G1430003A
3-4	INTERA	Huntsville Well, #9	6020503	G2360001G	5-5	INTERA	G1430003D	6739604	G1430003D
3-4	USGS	NA	6020503	G2360001G	5-6	TWDB	NA	6740504	
3-5	TWDB	NA	6027602		5-7	INTERA	G1430001C	6633403	G1430001C
3-6	USGS	NA	6028802		5-8	INTERA	G1430001E		G1430001E
3-7	USGS	NA	6035503		5-9	INTERA	City of Yoakum	6747608	G0620003P
3-8	USGS	NA	6036410		5-10	TWDB	NA	6641202	
3-8.5	USGS	NA			5-11	TWDB	NA	6641904	
3-9	USGS	NA	6035907		5-12	TWDB	NA	6650207	
3-10	TWDB	NA	6036809		5-13	TWDB	NA	6651704	
3-11	INTERA	MUD#3,Well#3		G1700116C	5-14	TWDB	NA	8003303	
3-11	USGS	NA		G1700116C	5-15	INTERA	1200032A/LNRA	8004710	G1200032A
3-12	TWDB	NA	6044318		5-15	TWDB	NA	8004710	G1200032A
3-13	INTERA	Kuntry Katfish	6044317	G1700456A	5-16	INTERA	1200004AJCWA	8012402	G1200004A
3-14	USGS	NA	6045114		5-17	TWDB	NA	8012202	
3-15	USGS	NA	6045513		5-18	TWDB	NA	8013815	
3-16	TWDB	NA	6045712		5-19	INTERA	G1200022D Cape Caranchua WSC	8021217	G1200022D
3-17	INTERA	G1700555A	6052107	G1700555A	5-19	TWDB	NA	8021217	
3-18	INTERA	G1700555B		G1700555B	5-20	INTERA	G0290027A Port Alto Hoa District 1	8021901	G0290027A
3-19	USGS	NA	6045716						
3-20	USGS	NA			Group #	Source	Chain of Custody ID	TWDB Well Number	TCEQ PWS ID
3-21	USGS	NA							
3-22	USGS	NA	6053516		8-1	INTERA	G2400006	8433203	G2400006D
3-23	TWDB	NA	6053417		8-2	INTERA	Bruni HS	8434405	G2400009A
3-24	INTERA	IRE Fawn Trail		G1700808A	8-3	INTERA	CBW	8434404	G2400003D
3-25	INTERA	SWJA Well 2-C-17001978	6053713	G1700197B	8-4	TWDB	NA	8419303	
3-26	TWDB	NA	6053821		8-5	INTERA	G0660014B	8436605	G0660014B
3-27	INTERA	LLMHP		G1700344B	8-6	INTERA	Benavides 328	8429201	G0660001A
3-28	INTERA	Spring Baptist Church		G1013201B	8-7	TWDB	NA	8429311	G0660001F
3-29	INTERA	Candlelight WP	6061522	G1010532B	8-8	TWDB	NA	8437202	
3-30	TWDB	NA	6061525		8-9	INTERA	M102	8437205	
3-31	INTERA	Cypress Klein Utility, Plant #3		G1010431C	8-10	INTERA	M542	8429907	
3-32	TWDB	NA	6061905		8-11	INTERA	G0660015B		G0660015B
3-33	TWDB	NA	6061722		8-12	TWDB	NA	8430606	
3-34	TWDB	NA	6505213		8-13	INTERA	G0660015B	8448117	G0660015B
3-35	TWDB	NA	6506528		8-14	TWDB	NA	8448301	
3-36	USGS	NA	6505814		8-15	INTERA	Dawson	8333602	
3-37	INTERA	Bergville-Regan Street		G1010099A	8-16	TWDB	NA	8350203	
3-38	USGS	NA	6513222		8-17	TWDB	NA	8350307	
3-39	USGS	NA	6513221		8-18	TWDB	NA	8351902	
3-40	USGS	NA	6513224		8-19	TWDB	NA	8352702	
3-41	USGS	NA	6513214						
3-42	INTERA	Well 8420	6514512	G1010013GA					
3-43	INTERA	Well 10003	6523127	G1011570B					
3-44	INTERA	Well J - Pearland	6529604	G0200008J					
3-45	INTERA	Well F - Pearland	6530604	G0200008F					
3-46	TWDB	NA	6539310						
3-47	TWDB	NA	6540412						
3-48	TWDB	NA	6548202						
3-49	TWDB	NA	6548502						

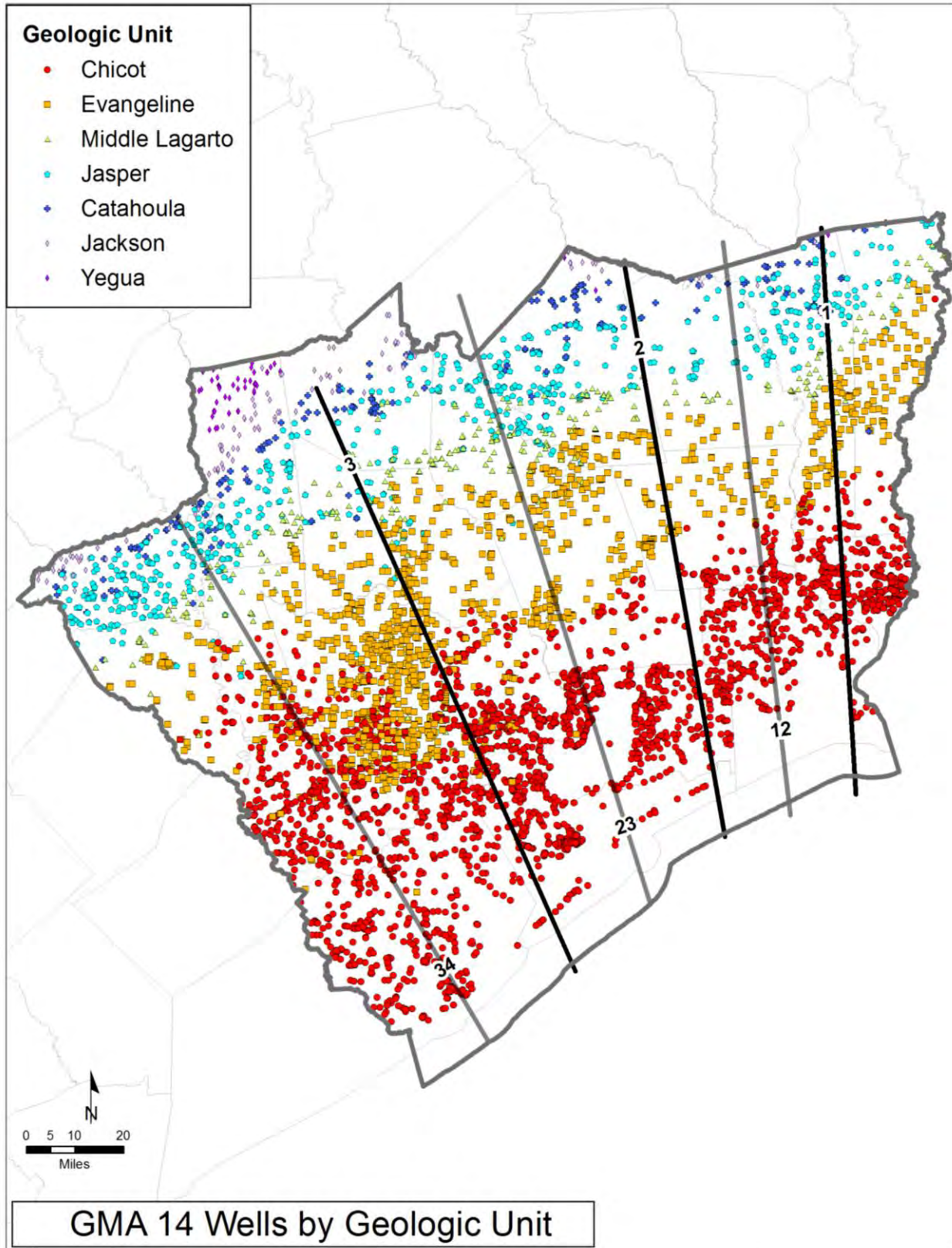


Figure 4-1 Wells with water quality measurements in GMA 14.

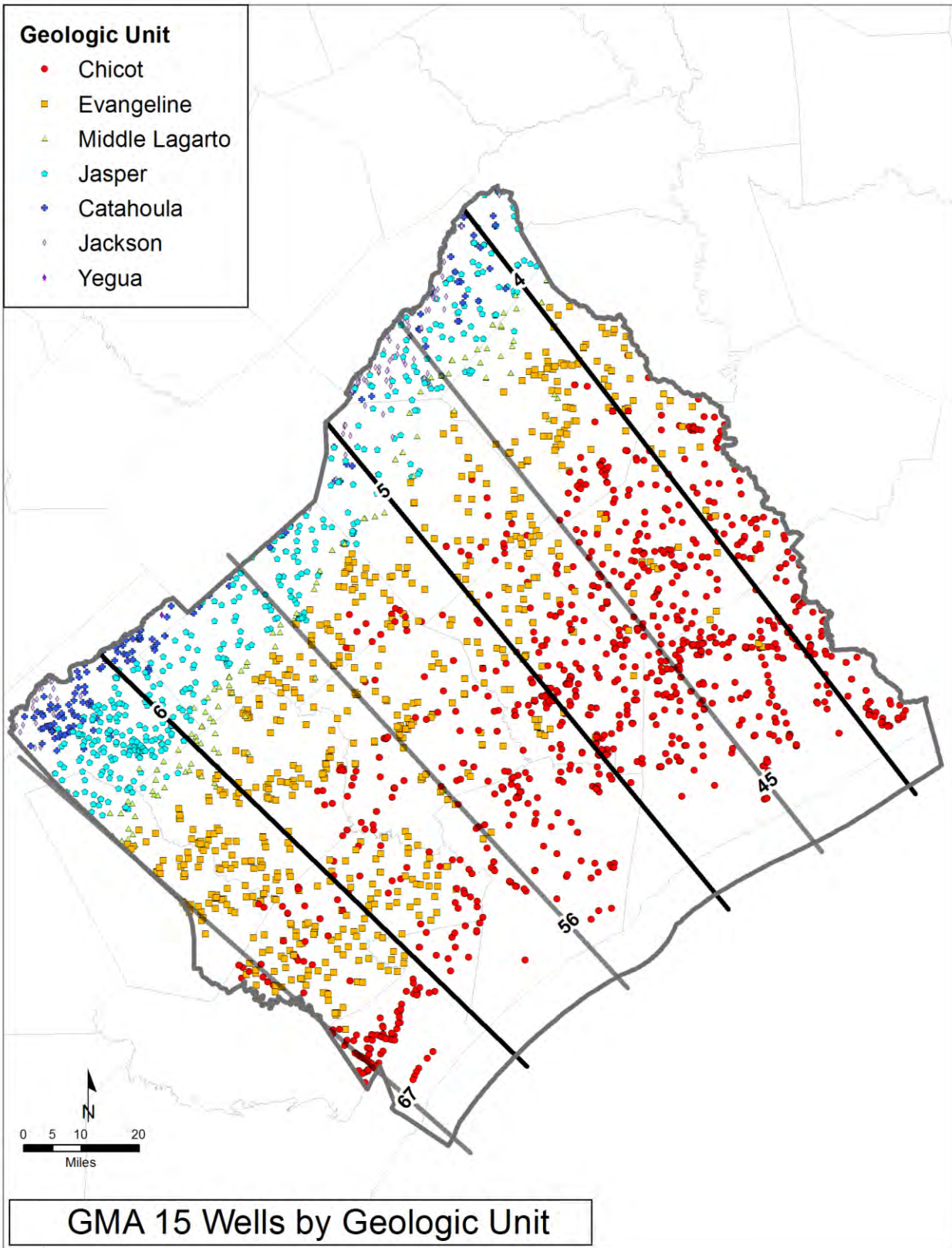


Figure 4-2 Wells with water quality measurements in GMA 15.

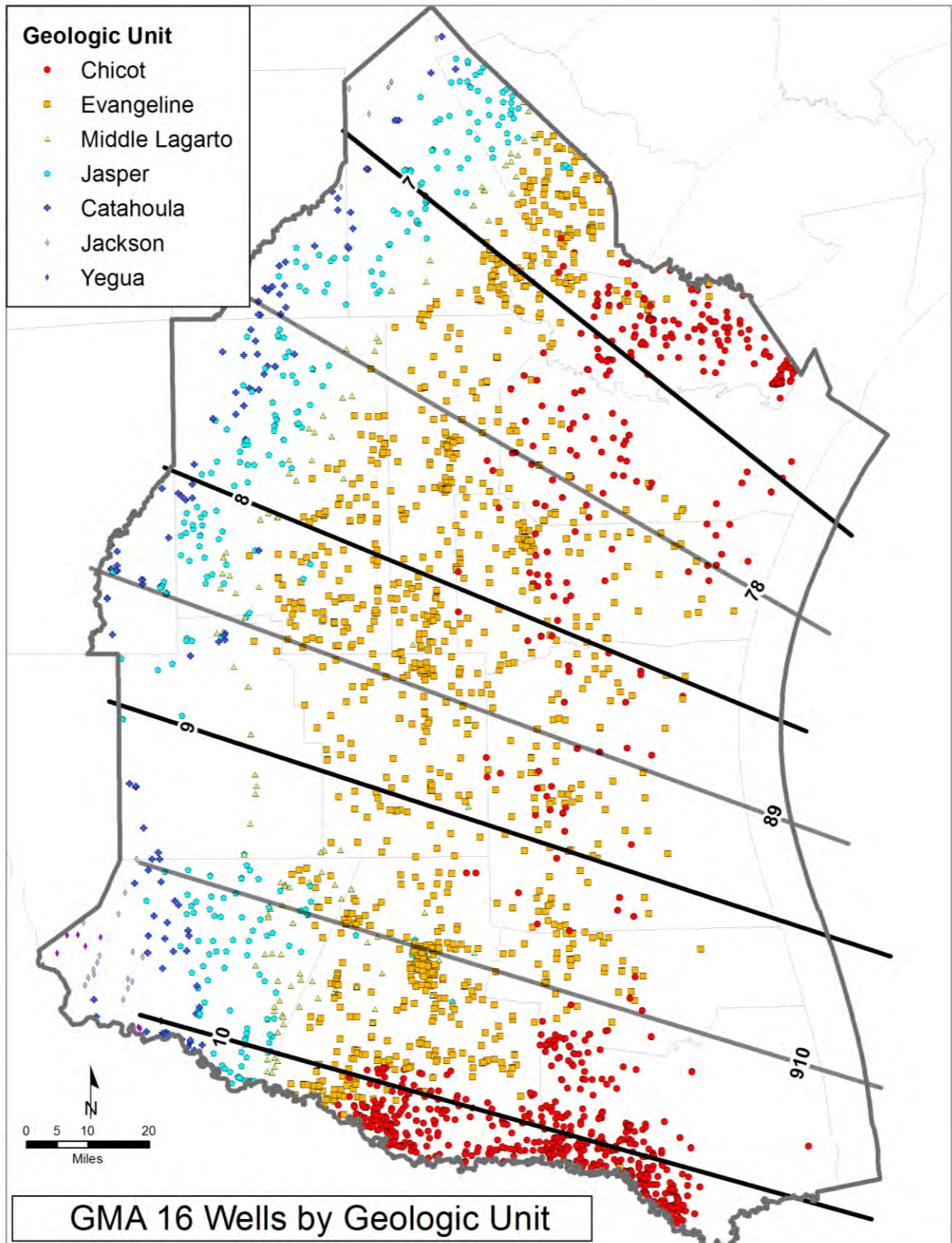


Figure 4-3 Wells with water quality measurements in GMA 16.

Final – Hydrogeochemical Evaluation of the Texas Gulf Coast Aquifer System and Implications for Developing Groundwater Availability Models

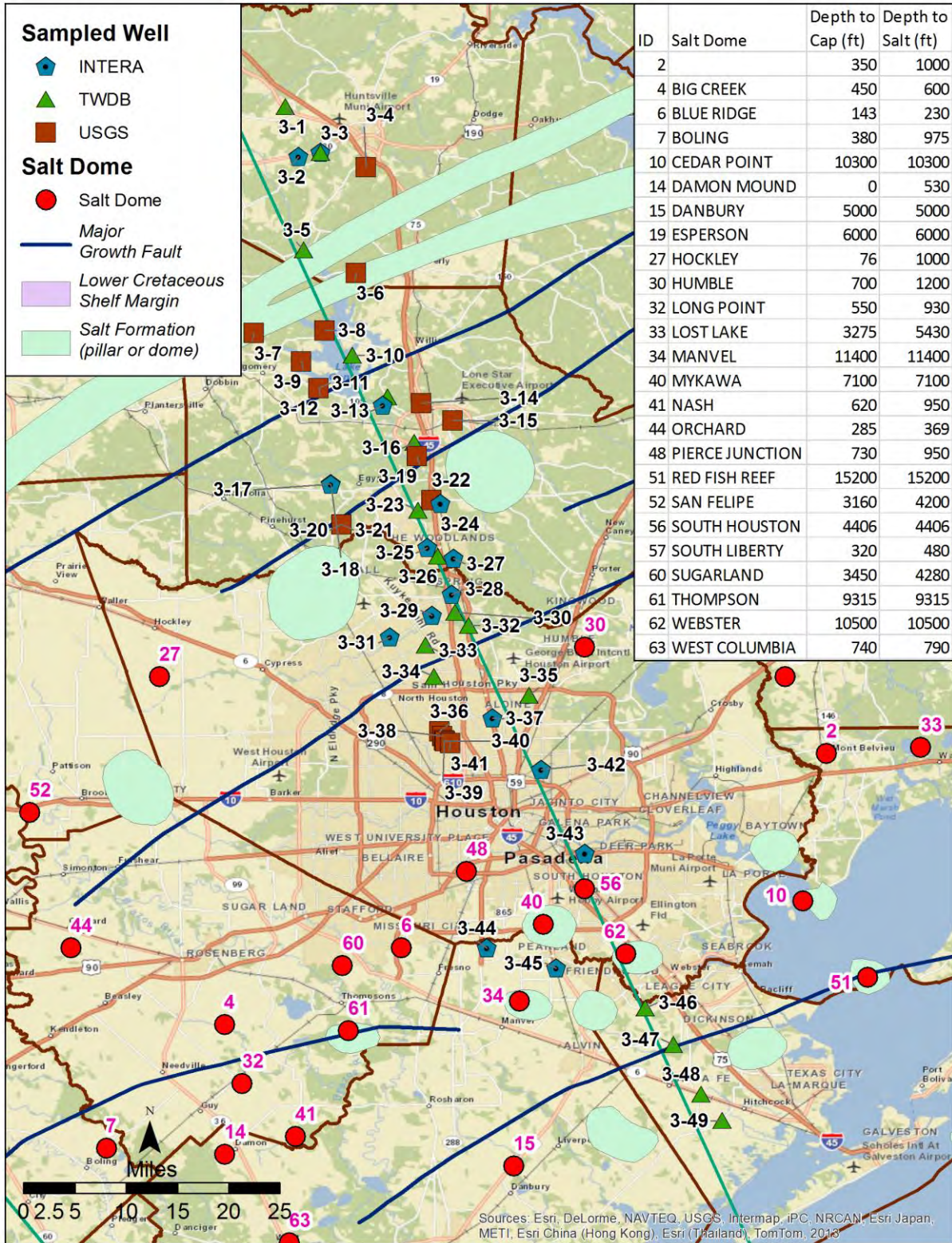


Figure 4-4 Aerial view of the wells with isotope data that are associated with Transect 3. Wells that were sampled as part of this project are labeled as INTERA wells.

Final – Hydrogeochemical Evaluation of the Texas Gulf Coast Aquifer System and Implications for Developing Groundwater Availability Models

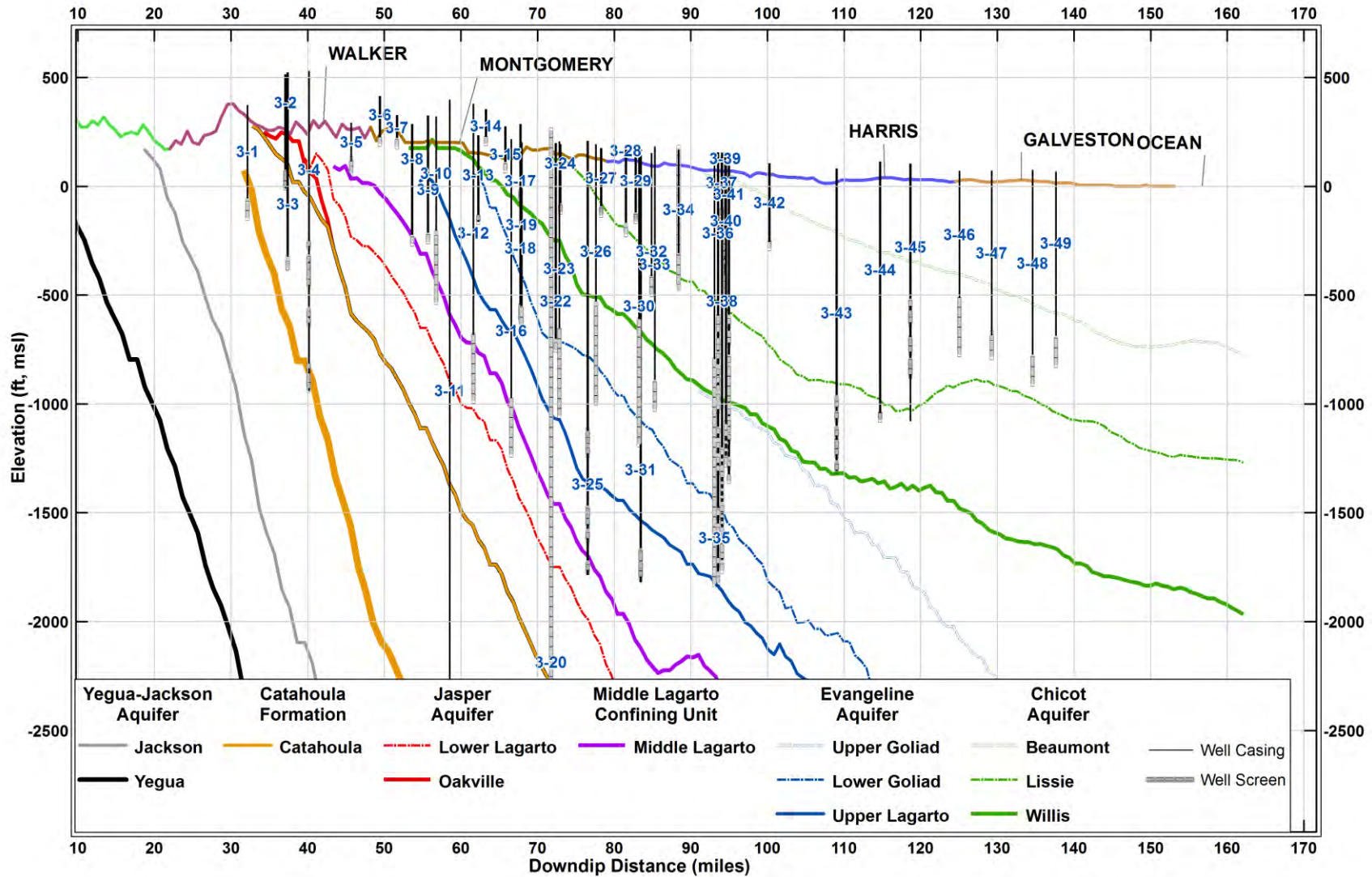


Figure 4-5 Cross-sectional view of the wells with isotope data associated with Transect 3. (Note: surfaces represent the bottom of each geological formation).

Final – Hydrogeochemical Evaluation of the Texas Gulf Coast Aquifer System and Implications for Developing Groundwater Availability Models

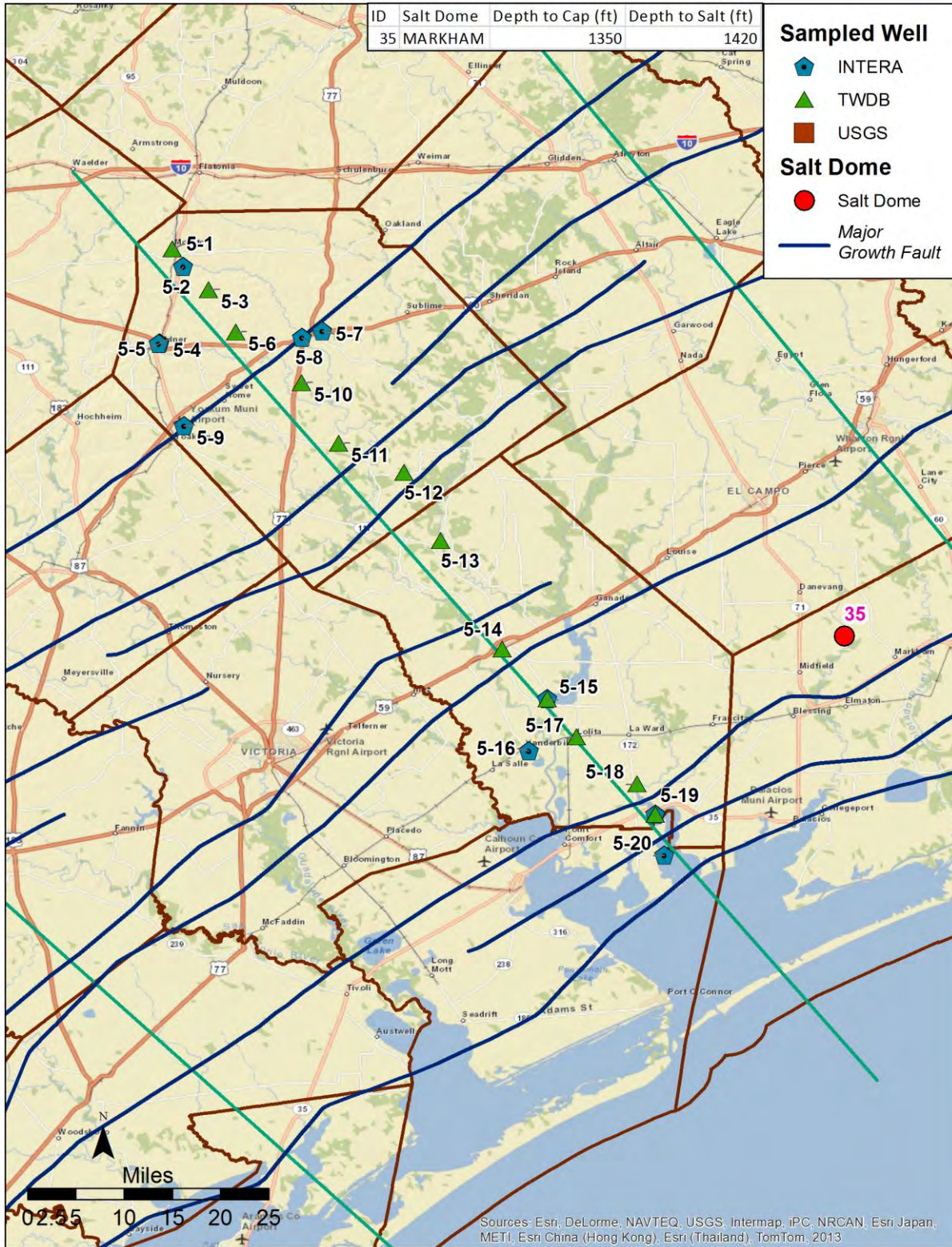


Figure 4-6 Aerial view of the wells with isotope data that are associated with Transect 5. Wells that were sampled as part of this project are labeled as INTERA wells.

Final – Hydrogeochemical Evaluation of the Texas Gulf Coast Aquifer System and Implications for Developing Groundwater Availability Models

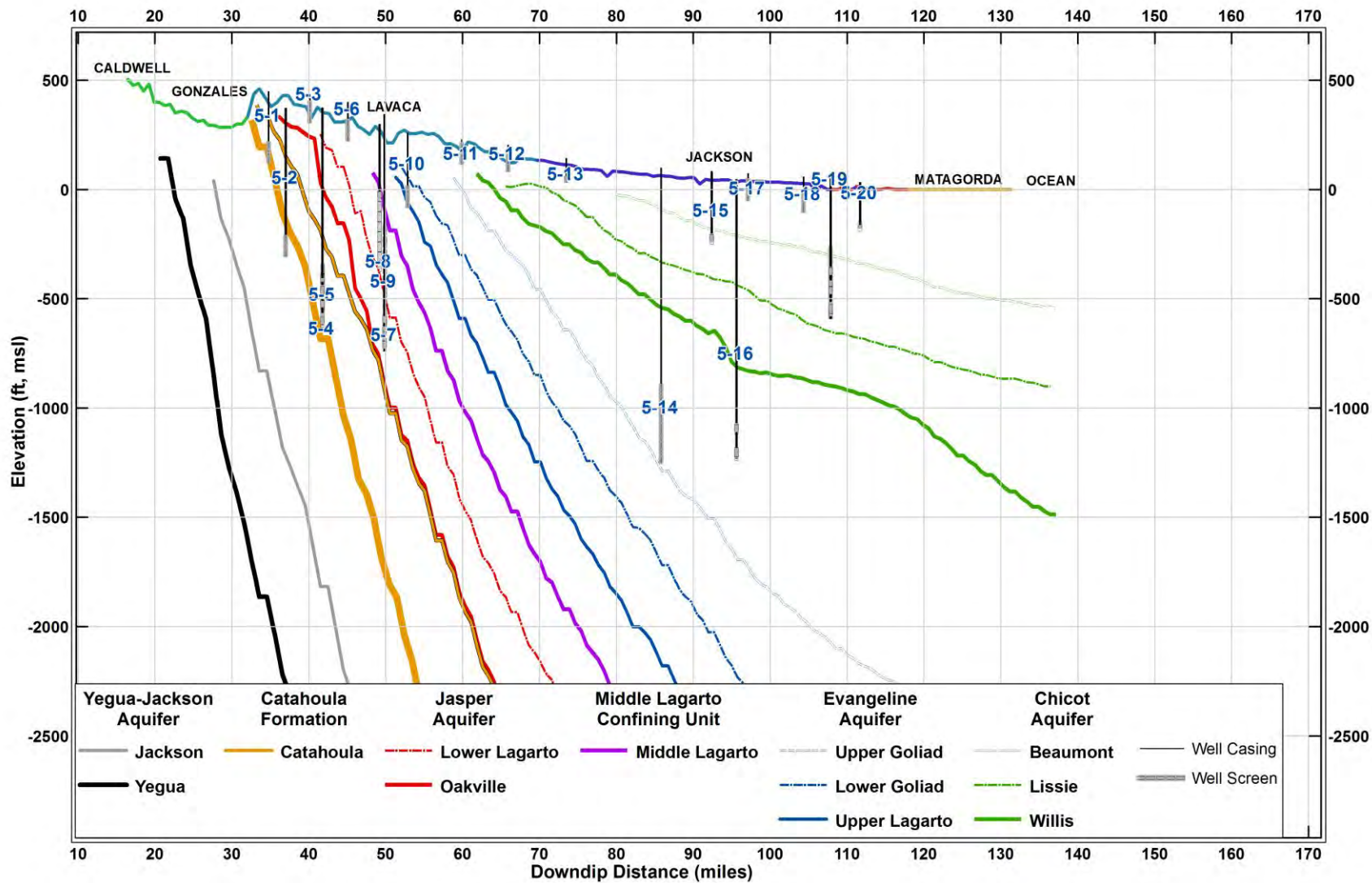


Figure 4-7 Cross-sectional view of the wells with isotope data associated with Transect 5. (Note: surfaces represent the bottom of each geological formation).

Final – Hydrogeochemical Evaluation of the Texas Gulf Coast Aquifer System and Implications for Developing Groundwater Availability Models

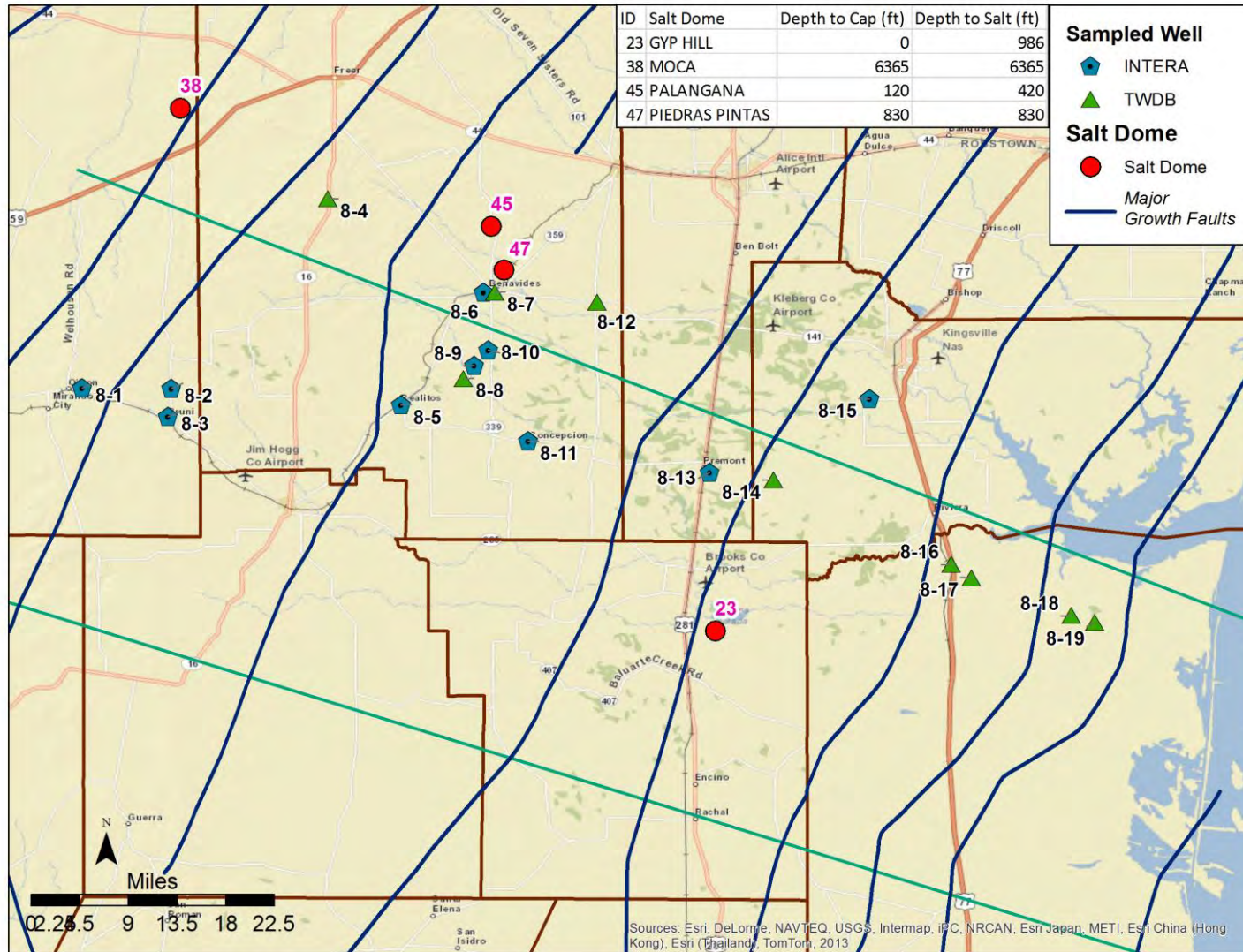


Figure 4-8 Aerial view of the wells with isotope data that are associated with Transect 8. Wells that were sampled as part of this project are labeled as INTERA wells.

Final – Hydrogeochemical Evaluation of the Texas Gulf Coast Aquifer System and Implications for Developing Groundwater Availability Models

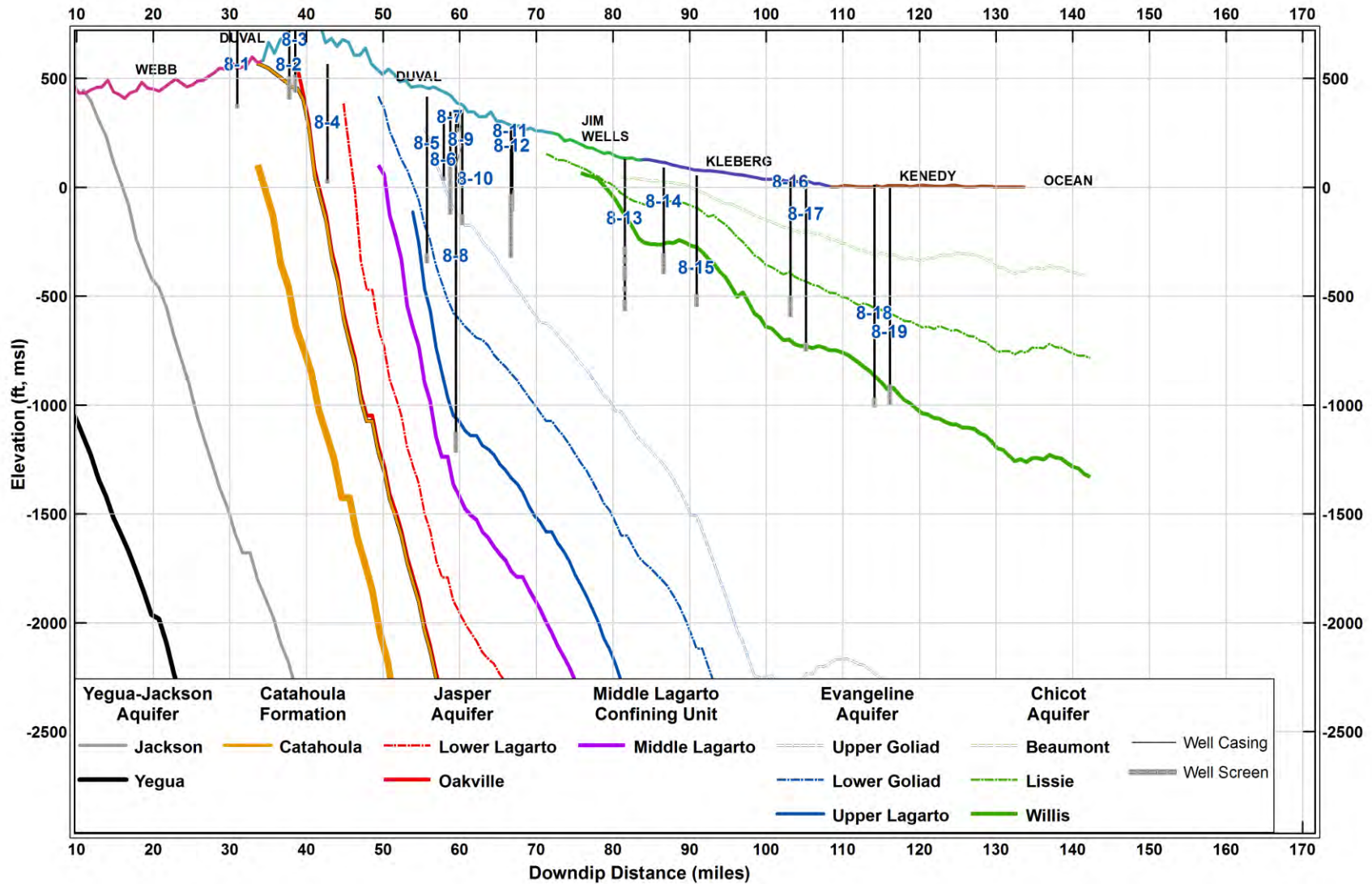


Figure 4-9 Cross-sectional view of the wells with isotope data associated with Transect 8. (Note: surfaces represent the bottom of each geological formation).

5.0 Potential Sources of Groundwater Salinity

This section discusses sources of salinity that may have contributed to the increased Total Dissolved Solids (TDS) concentrations that occurs near the coastline of the Texas Gulf Coast. One of the key conceptual issues associated with modeling the Gulf Coast Aquifer System is the boundary conditions downdip of the regional models that are used to represent the transition from fresh water to brackish water and/or the transition from slightly saline water to moderately saline water. A prerequisite for proper assignment of the downdip boundary condition is a proper understanding of the factors that can change the TDS of groundwater near the coast.

5.1 Groundwater Salinity

Groundwater salinity is usually expressed as TDS, and less commonly as chloride content (mg/L) or electrical conductivity (EC, in $\mu\text{S}/\text{cm}$). Dissolved solids in groundwater may contain various salt constituents (e.g., halite, anhydrite, carbonates, gypsum, fluoride-salts, and sulfate-salts) at different concentration levels. Groundwater often is classified into a number of discrete salinity classes. Groundwater salinity can be classified based on TDS concentrations: fresh (0-1,000 mg/L), brackish (1,000-10,000 mg/L), saline (10,000-30,000 mg/L), and brine (>100,000 mg/L) (Freeze and Cherry, 1979). Alternatively, salinity can be classified into fresh (0-1,000 mg/L), slightly saline (1,000-3,000 mg/L), saline (3,000-10,000 mg/L), very saline (10,000-35,000 mg/L) and briny (>35,000 mg/L) (Robinove and others, 1958).

In general, low-TDS groundwater is relatively young, occurs in the shallower subsurface, and tends to be actively recharged. In contrast, a large part of all saline groundwater occurs in more or less stagnant conditions at greater depths and may have been there for many thousands of years. Continuous dissolution of aquifer minerals over geologic times may have enriched the mineral content in the groundwater (Weert and others, 2009).

Natural and anthropogenic processes may give rise to groundwater salinity. While natural processes may affect an aquifer over a large areal extent, anthropogenic processes generally have a limited local effect. Natural processes include sea salt sprays in coastal aquifers, seawater intrusion, diffusion and pumping of connate water, expulsion of mineralized compaction water upwelling of formation brine, dissolution of bedded evaporite in sediment sequences, and dissolution of halite from salt domes.(Williams, 1999; Barlow, 2003; Weert and others, 2009).

Anthropogenic processes include infiltration of saline irrigated water, leakage of saltwater pits, pumping induced salt water intrusion, and use/agricultural practices, and oil and gas wells. (Hudak and Wachal, 2001a, 2001b; Richter and Kreitler, 1993; Barlow and Reicard, 2010).

5.2 Sea Salt Spray

Sea salt spray includes marine aerosols along with chlorinated gases and halocarbons that are carried into coastal areas by winds (Yvon-Lewis and Butler, 2002; Solomon and others, 2005; Butler and others, 2007). Atmospheric Cl and Br availability decreases along the wind path with increasing distance from the ocean, resulting in higher Cl and Br deposition rates near the coast than inland (Eriksson, 1960; Davis and others, 1998; Edmunds and others, 2002; Alcala and Custodio, 2008). Deposition of and subsequent dissolution of sea salt spray is a common source to groundwater salinity in coastal aquifers (Alcala and Custodio, 2008). For example, the source of practically all chloride in New York City's Long Island's groundwater under pre-development condition was sea salt spray introduced through infiltration of precipitation (Frank and McClymonds, 1972). In coastal areas in Holland, windblown salt from the sea spray deposits considerable amounts of sodium and chloride on the conifer plants, which washes down during rainfall altering the quality of groundwater (Arjen, 2006).

5.3 Saltwater Intrusion

Saltwater intrusion is widespread in many coastal aquifers worldwide (Barlow and Reicard, 2010). Saltwater contamination can occur by lateral intrusion from the ocean; upward intrusion from deeper, more saline zones of a groundwater system; and downward intrusion from coastal waters are the main mechanisms that dictate the scale of saltwater contamination. Therefore, saltwater intrusion may be limited to small parts of an aquifer or may be of regional extent causing closure of many groundwater supply wells. The extent of saltwater intrusion is controlled by the hydrogeologic setting, the history of groundwater withdrawals and recharge rates, the three-dimensional distribution of saline water, and freshwater drainage.

The seaward limit of freshwater in the coastal aquifers is controlled by a number of factors, including the amount of freshwater flowing through each aquifer, the thickness and hydraulic properties of each aquifer and adjacent confining units, the current geographic distribution of saline surface water, and the geologic history of global sea-level fluctuations. For instance, in

some of the confined aquifers along the Atlantic Coast, relatively fresh groundwater has been found tens of kilometers offshore. Its presence has been attributed to freshwater recharge that occurred over at least the past 900,000 years during periods when sea levels were lower than at present (Meisler 1989). In other areas, such as southern Florida, confining conditions and sluggish groundwater flow are thought to have contributed to the presence of large inland areas of residual seawater that entered the aquifers during the Pleistocene, when sea level was higher than its current level (Sprinkle, 1989). Inland areas of saline water also can be found near estuaries, where saltwater is carried up river channels by high tides and infiltrated into the adjoining freshwater aquifers.

Notable areas in the North American where saltwater intrusion has occurred includes southeastern Florida, the northern shores of San Francisco Bay and Monterey Bay in California (Edwards and Evans, 2002), and south along Baja California (Jimenez and Marin, 2004; Conagua, 2007a; Conagua, 2007b). In Europe, saltwater intrusion is a major concern in the coastal aquifers of Belgium and Netherlands where several rivers with low hydraulic gradients bring seawater intrusion risks to locations inland (SWIM, 2008). In Asia, saltwater intrusion is a major problem in the Bengal delta where intensive groundwater development for irrigation purposes as well as reduced freshwater flow in the tidal inlets has enhanced lateral seawater intrusion (Khan and others, 2008).

The increased risk of saltwater intrusion from global warming and a rise in sea level is observed across the globe (Weert and others, 2009). Sea level rise induced by long-term climate change and groundwater development in coastal regions can cause migration of saltwater from the coast. Tide gauge records from Rockport, Port Mansfield, and South Padre Island in South Texas indicate that the sea level has risen at a rate of about 0.25 mm/yr to 2.8 mm/yr between 1948 and 2003 (Venkatamaran and Uddameri, 2011). The Intergovernmental Panel for Climate Change (Metz and others, 2007) Global Climate Change Models (GCMs) have projected a sea level rise between 20 cm and 87 cm by the year 2100 across South Texas.

The area where freshwater flowing seaward and saltwater mixes is called the mixing or transition zone. The transition zone ranges from less than 30 m thick in relatively thin aquifers to as much as 670 m thick and 60 km wide in thick, confined aquifers along the Northern Atlantic Coastal Plain, where global sea-level fluctuations caused repeated advance and retreat of the landward

position of the freshwater-saltwater interface. The front of the mixing zone is characterized by ion exchanges where the Ca attached to the clay surfaces in the aquifer matrix will be replaced by dissolved Na. Mg and K may also exchange for Na; however, Na-Ca exchanges are most common. Since Cl is chemically conservative and does not participate in any chemical reaction, that makes Na/Cl ratio an important tracer for seawater intrusion. The Na/Cl ratio value of seawater (~0.85M) is in contrast to halite dissolution brines (~ 0.65 M) and oil-field/deep basin brines (<0.5 M). The mixing of the waters will result in an increase in both Ca and HCO₃ through carbonate dissolution. Sulfate reduction can further dissolve additional carbonates. Additional bromide from the seawater as well as trace concentrations of iodide, strontium, and fluoride may be swiped from the ocean or estuary bottoms during advancement of the seawater front (Richter and Kreitler, 1993; Custodio, 1987).

5.4 Connate Water and the Effects of Pumping

Connate water commonly occurs in marine sediments where the seawater was deposited with the rock matrix and is still retained in the interstices of the sediments. Connate water may also result from later marine transgressions, direct flooding by seawater, or seawater intrusion (Weert and others, 2009). Connate water trapped in the sediment matrix may not flush out after the sea has retreated. The displacement or mixing of the connate water generally occurs on a regional scale over long periods of geologic time when: (1) the permeable unit is uplifted so that its outcrop occupies a position that permits recharge by meteoric water, and (2) the downdip portions of the unit have outlets through which the original formation water can be displaced (Domenico and Robbins, 1985). In some cases, definite outlets are not readily available, and the formation both receives and discharges fluid progressively downdip like a leaky conduit into lower permeability rocks. These connate waters can migrate into fresh water parts of the aquifer due to excessive pumping. If pumping rates in freshwater sections are high enough, saline water can readily move from nearby mixing zones into the well's capture zone, resulting in groundwater salinization. Under natural conditions, migration of connate saline groundwater tends to be extremely slow because connate water may remain at steady state with meteoric water for displacement of their contained fluids. The steady state condition may vary from a scenario with near meteoric water uniformly distributed in the whole formation to a scenario in which a spatial variation in TDS concentration ranging from meteoric water in the recharge areas to highly

concentrated water at the discharge ends of the system. Dissolved concentration patterns of connate water may further depend on contrasts in hydraulic conductivity, as seen in the Milk River sandstone in southern Alberta. In this case, zones of dilute water within narrow, high-conductivity pathways are interspersed with marked increases in chloride concentration in adjacent, lower-permeability rock (Domenico and Robbins, 1985).

Residual connate waters trapped during sedimentation in the clayey portions of the Texas Gulf Coast Aquifer System may contribute to salinity. Numerous clay or shale beds that compartmentalize water-bearing sands may still locally help retain connate waters. This retention would explain the trace to very low percentages of modern carbon composition found at shallow depths, even in outcrop areas where the modern carbon would be expected to be high. These low concentrations suggest that some of these fossil waters could well have formed from older recharge (Chowdhury and others, 2006; Chowdhury and Mace, 2004).

The depth of connate water can vary from location to location. Jorgensen (1977) suggested that freshwater has flushed the original saltwater out of the aquifer to a depth of 2,200 feet in the Houston area, but only to a depth of 150 feet in Galveston. He indicated that flushing may have been more effective in the past, during lower stands of sea level (Frazier, 1974). Bachman (1979) reported that the average depth of the base of the freshwater occurs at depths of about 2,000 feet below land surface. In contrast, artesian conditions of saline aquifers underlying Duval County make the base of the saline water appear near land surface (Wood and others, 1963).

5.5 Formation Brine Upwelling from Geopressured Zone

A substantial body of data collected in recent years documents the importance of fault zones as conduits of vertical fluid migration into ancient sediments (Losh and others, 1999; Mozley and Goodwin, 1995; Anderson and others, 1994; Billeaud and others, 1994; Echols and others, 1994; Zimmerman, 1994; McManus and Hanor, 1993; Esch and Hanor, 1995; Galloway and others, 1986). Evidence indicates that subsurface fluids can migrate vertically into modern sediments via growth faults (Kuecher and Roberts, 2000; Kuecher, 1995a, 1995b; Mitchell-Tapping, 1995; Verberne, 1992; Morgan, 1961). Galloway and others (1986) states that growth-fault zones function as major conduits for large-scale circulation of both ground waters and hydrocarbon fluids within the sedimentary prism. The available data suggest that deep-seat fault-bound

compartments, episodically release large quantities of water, gas, and oil vertically into shallower aquifers via fault planes (Losh and others, 1999; Alexander and Handschy, 1998; Cartwright and others, 1998; Lin and Nunn, 1997; Waples, 1991). The model presented in Figure 5-1 summarizes the current conceptualization of this system. Evidence for fluid movement out of the geopressured zone includes (a) the updip-directed lateral gradient in hydraulic head and (b) salinity greater than seawater occurring updip of the limit of growth faults (Dutton and others, 2006). Furthermore, in the convergence zone where brackish-to-saline waters (3–30 g/L) exist, the salinity more likely indicates mixing of meteoric water with modified seawater or saline water from the geopressured zone than the presence of connate estuarine fluids.

As part of their work in demonstrating that linear distributions of saline-water plumes in shallow aquifer sands are associated with active faults in Louisiana, Kuecher and others (2001) developed a working model for how regional growth faults respond to the basinal buildup of fluid and gas volumes. This model consists of the following mechanisms:

- (a) geopressured fluid and gas from deep shale masses exceeds the strength of the fault's sealing gouge,
- (b) fluids enter the fault zone and migrate vertically until reservoirs adjacent to the fault or the surface or both are encountered,
- (c) volume decreases at depth in the geopressured shale mass in response to the volume of expelled fluids and hydrocarbons,
- (d) excess pore pressures are attenuated in the deep shale mass,
- (e) the down-thrown block subsides, and
- (f) the fault gouge reseals.

Bourgeois (1997) investigated the source of the brackish water wells in the shallow Chicot Aquifer in Brazoria County around fault zones that lacked chloride trends from the coast or from known salt dome locations. Bourgeois (1997) suggested that up to 3 to 5% of the geopressured brine migration vertically along faults would be sufficient to account for the salinity observed in the coastal brackish water wells in the Chicot Aquifer. Lindsay (2009) also suggested that the brackish waters in Fort Bend, Brazoria and Galveston counties are derived from migration of

geopressured brine. Similarly, when Kazmann (1970) investigated differences in chloride concentration between aquifers north and south of the Baton Rouge Fault, the investigation indicated that faults do in fact transport basinal saline fluids vertically from deep aquifers into shallow aquifers.

5.6 Bedded Halite and Evaporites

Groundwater may become saline by dissolving salts from evaporates or carbonate layers during its flow through or along such subsurface bodies. Groundwater flowing through aquifers may become brackish to saline as it moves in a downward direction, given adequate time and other conditions to favor dissolution of salts. Inland groundwater salinization is particularly common in arid and semiarid sedimentary groundwater basins. This can be attributed to mineral concentration during evapotranspiration of shallow groundwater, subsurface dissolution of evaporite minerals, and filtration through clay or shale beds. These processes may result in formation waters that are much more saline than the preceding connate waters, as well as highly variable spatial salinity distributions (Hanor, 1994). Different components of salinity can originate from different source areas. For example, in the Hueco Bolson, chloride concentrations were strongly correlated with lithologic formations and both Cl/Br and ^{36}Cl ratios suggested the primary chloride source is halite dissolution within a specific lithologic unit. In contrast, sulfur isotopes indicated that most sulfate originates from the dissolution of the Tularosa basin Permian gypsum sources (Durhan and others, 2007).

5.7 Salt Domes

Hydrochemical patterns in groundwater near salt domes provide information about flow of dome-related fluids into surrounding freshwater aquifers. Because most salt domes have been densely drilled in the quest for petroleum, the most commonly available data for measuring groundwater salinities in the near-dome environment are geophysical logs from oil and gas wells. These can be used to establish empirical relationship between groundwater salinity and electrical conductivity (Jones and Buford, 1951).

The evidence for dissolution of salt dome minerals in shallow groundwater is conclusive. Geophysical logs have been used to identify high-salinity plumes within otherwise fresh water sands near several Gulf Coast Aquifer System salt domes and to map actual sand/dome contacts

(Wesselman 1971 and 1972; Hamlin and others, 1988). Indeed, dissolution of salt domes by groundwater has been documented, and the amount of salt removed has been quantified (Seni and Jackson, 1984; Bruno and Hanor, 2003). Wesselman (1971 and 1972) identifies high salinities in shallow sands near salt domes in Chambers, Fort Bend, and Jefferson counties. At Barbers Hill salt dome, Hamlin and others (1988) used closely spaced well logs to map individual sand bodies and groundwater salinities near the dome, revealing a complicated pattern of vertical and lateral salinity variation. In one lower Chicot aquifer sand, a plume of high-salinity groundwater extends away from the salt dome in the direction of regional groundwater flow (Figure 5-2). Similar saline plumes extending away from salt domes in the direction of groundwater flow have been documented in the Carrizo-Wilcox aquifer in East Texas (Fogg and others, 1983) and in Germany (Klinge and others, 2002).

Chemical and isotopic analyses of groundwater are less abundantly available than geophysical logs but can be used to reveal both fluid sources and flow patterns. Banga and others (2002) used multi-element chemistry and isotopic tracers to document vertical flow patterns in deep sandstones (below freshwater) around South Liberty salt dome in Liberty County. They show that oil field brines near the salt dome are a mixture of shallow meteoric waters and deep formation waters. The presence of a meteoric component in deep brines indicates downward flow along the flanks of the salt dome. The implication of the South Liberty salt dome study is that shallow fresh groundwater flows across the top of the salt dome, dissolves salt, becomes increasingly dense, and then flows downward along the dome flanks driven by a density gradient.

Based on above information, shallow salt domes have the potential to increase groundwater salinities in the Gulf Coast Aquifer System in two ways: first by direct dissolution and transport of soluble dome minerals and second by providing pathways for groundwater mixing between shallow freshwater and deep saline-water aquifers. One of the potential ways to detect the impact of salt domes is through the ratio of different chemicals. Most salt domes contain no iodide or bromide and therefore, halite dissolution provides low Br/Cl and I/Cl ratios. Halite dissolution brines have Br/Cl weight ratios of 9×10^{-5} to 5×10^{-4} and I/Cl ratios in the range of 1×10^{-6} to 1×10^{-5} . In oilfield brines, Br/Cl ratios are much greater than 1×10^{-3} and I/Cl ratios greater than 2×10^{-5} (Whittemore, 1988; Richter and Kreitler, 1993). The geopressured brine in

the Gulf Coast Aquifer System have Br/Cl values that ranges from 9×10^{-4} to 2.6×10^{-3} (Bourgeois, 1997).

In addition to halite dissolution, anthropogenic sources of aquifer contamination are not uncommon around salt domes. Anthropogenic contamination includes cap-rock brine disposal and storage facility failure. High-volume brine disposal elevates cap rock fluid pressures in shallow intervals laterally adjacent to freshwater sands, reversing pre-development hydraulic gradients and creating the potential for aquifer contamination (Hamlin and others, 1988). Petroleum storage cavern facilities have failed and leaked product into surrounding freshwater sands (Seni and others, 1984, Seni and Jackson, 1984, and Seni and others, 1985). Barbers Hill salt dome has the greatest concentration of underground storage caverns in the world and historically has been the site of high-volume cap-rock brine disposal (Figures 2-15, 2-16). Gas storage and transportation facilities are concentrated at Barbers Hill, which is located 20 miles east of Houston, and numerous accidents have occurred, the most recent being in early 2011 (Fowler, 2011).

5.8 Agriculture and Irrigation

Like precipitation, irrigation provides water necessary for optimal crop growth. However, irrigation adds a considerable amount of salts to soils relative to precipitation in non-irrigated areas. Salinity buildup depends on irrigation water quality, evapotranspiration rates, root-zone depth, soils, and climate. Because root-water uptake excludes most salts, soil water salinity levels may build up when water drainage or percolation through the root zone is insufficient (Scanlon and others, 2010). This salt left behind may adsorb to the soil matrix, drain to the surface water system or percolate below the root zone (Weert and others, 2009). It may reach an aquifer and contribute to a progressive increase in groundwater salinity. Large-scale irrigation may raise shallow groundwater tables leading to water-logging and direct evaporation from the exposed or near surface water table. High chloride concentrations may correspond to irrigation efficiencies with respect to drainage and are caused by deficit irrigation with minimal flushing. Perchlorate (ClO_4) can accumulate under irrigated agro-ecosystems. Groundwater salinization resulting from irrigation is more commonly restricted to the shallow zone below the groundwater table.

Agriculture-induced nitrate loadings have drawn considerable interest as a result of increasing nitrate leaching rates from soils receiving large amounts of fertilizer. Although nitrate gradients could be present in the subsurface, it is not clearly understood whether the concentration gradient was caused by the transient nature of input or subsequent reactions such as denitrification. Earlier researchers indicated that nitrate loading in groundwater is transient based on high tritium concentrations in these waters (Libra and others, 1987) and more recently researchers suggest that the vertical distribution of nitrate in groundwater is a function of long term changes including active denitrification (Postma and others, 1991). In arid/semiarid soils, nitrate may also accumulate naturally by microbially assisted mineralization of soil litter and nitrification of NH_4^+ (Sprenst, 1987). Baseline concentrations of nitrate in groundwater beneath grassland in temperate regions are typically below 2 mg/L $\text{NO}_3\text{-N}$ and concentrations significantly above this are generally considered indications of anthropogenic pollution.

Most $\text{NO}_3\text{-N}$ accumulation occurs below the root zone. In addition, any pesticides applied during irrigation may provide additional evidence of migration of irrigation return flow into the aquifer. Limited ^{15}N data from the southern part of the Gulf Coast Aquifer System suggests that nitrate observed in a few selected wells are not derived from fertilizer but manure applications (Chowdhury and Mace, 2004).

5.9 Oil and Gas Activities

Although most saltwater contamination problems result from the movement of saltwater within aquifers, oil and gas activities can provide pathways for vertical migration across interconnected aquifers due to open boreholes, abandoned wells, improperly constructed or corroded wells, and dredged channels (Metz and Brendle 1996, Dutton and others, 2000; Weert and others, 2009). In addition, past practices of disposing oil field brine into surface pits have increase groundwater salinity. In 1969, the Texas Railroad Commission (TRC) prohibited using unauthorized pits to dispose of oilfield brine (RCT, 1993). However, pits are still being used for drilling fluid and emergency saltwater storage. Typical saltwater contamination from oil field brine is associated with high bromide, iodide (if marine), low sulfate, and relatively high concentrations of trace metals including barium, arsenic, and strontium.

Based on a statistical analysis of water quality parameters from a “near” and an “away” group of wells in the Gulf Coast Aquifer System, Hudak and Wachal (2001b) conclude that chloride,

bromide, and TDS concentration, and bromide-chloride ratios are significantly higher in water wells near oil/gas wells. Hudak and Wachal (2001b) define a well as either “near” or “away” on whether or not an oil/gas well was within 750 meters of the water well. Their significantly higher threshold is 5% based on the Kruskal-Wallis one-way analysis of variance by rank test (Kruskal and Wallis, 1952), a non-parametric method for testing whether samples originate from the same distribution. Observed bromide-chloride ratios were significantly higher in the “near” than the “away” water wells – medians were 0.0053 and 0.0036, respectively. Hudak and Wachal (2001b) suggest that mixing between fresh groundwater and brine could account for the higher bromide-chloride ratios observed in water wells.

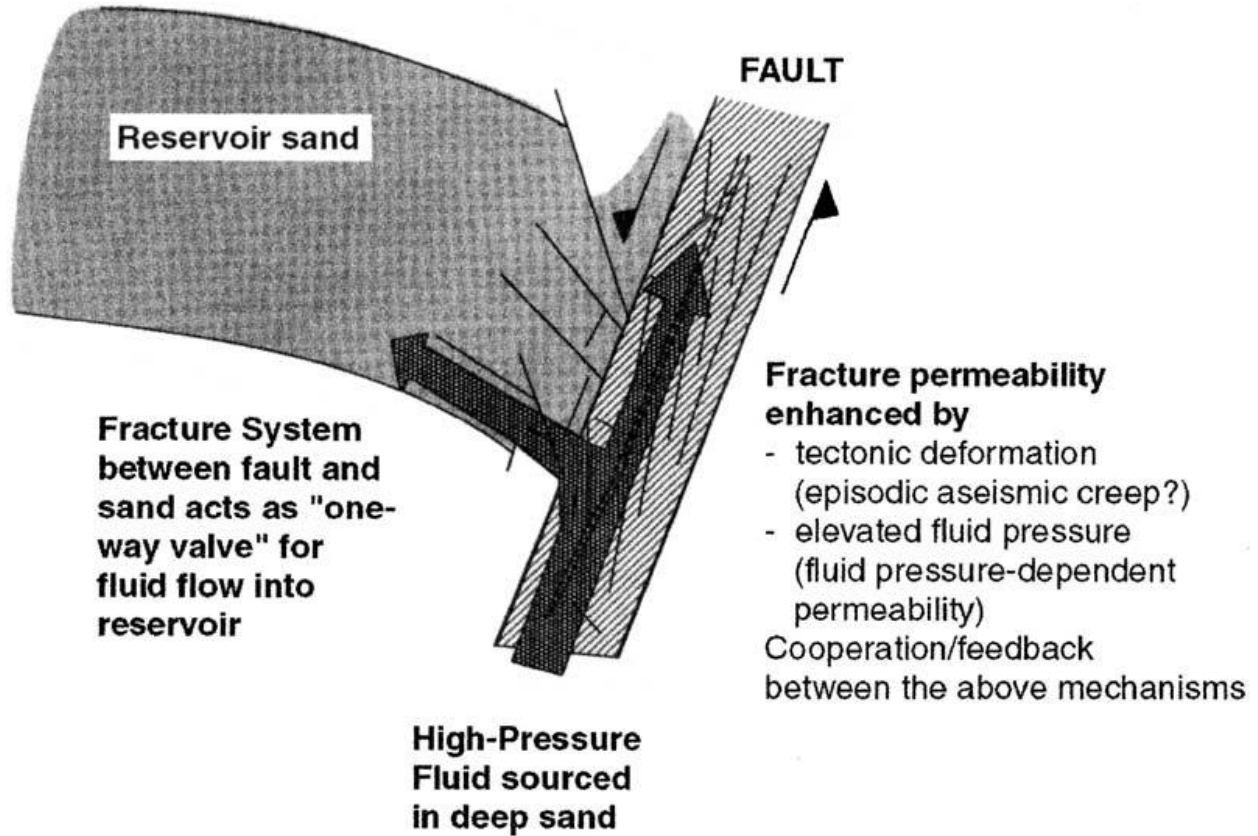


Figure 5-1 Model proposed by Losh and others (1999) of vertical transport of fluids into reservoirs along the trace of a fault (from Kuecher and others, 2001).

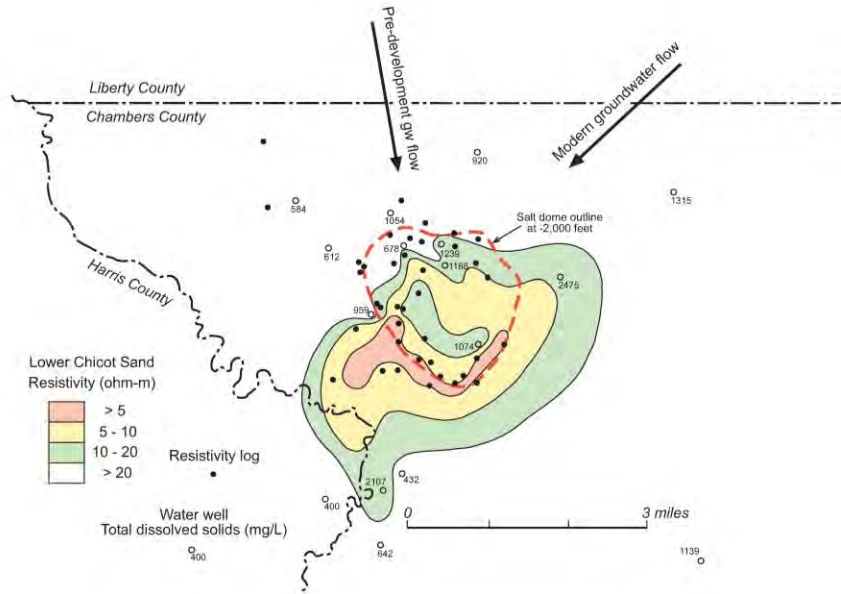


Figure 5-2 Resistivity map of the lower Chicot aquifer at Barbers Hill salt dome (modified from Hamlin and others, 1988). Water wells completed in this lower Chicot sand are also shown along with total dissolved solids measurements. Low resistivities around the southern and southwestern dome flanks delineate a high-salinity plume extending away from the salt dome in the down-flow direction.

This page intentionally left blank.

6.0 Cations and Anions

6.1 Overview of Geochemical Reactions

Groundwater is subject to multiple geochemical processes as soon as rainwater infiltrates the land surface and moves from the recharge areas along a flowpath to a well. Chemical composition of groundwater collected at a well is a summation of all these processes acquired along the flowpath that imparts to the water its unique chemical signatures. Geochemical reaction processes along groundwater flow paths thus can lead to regional variations in water composition that evolve in the direction of flow (Glynn and Plummer, 2005). These processes and impacts are dependent on a number of factors including chemical composition of the recharge water; evapotranspiration; interactions with gases in the unsaturated zone located between the water table and the land surface; chemical reactions between water and aquifer minerals; and mixing with other groundwater of different compositions, surface water, or water altered by human activity.

Precipitation that serves as the source of most groundwater contains small concentration of atmospheric constituents, dissolved gases, sodium chloride and other salts derived from marine aerosols. Perhaps the most important contribution of precipitation is not the mineral constituents but the presence and action of carbon dioxide, CO₂. Precipitation in chemical equilibrium with atmospheric CO₂ is slightly acidic (pH ~ 5.5), which can contribute to the dissolution of aquifer minerals and formation of precipitates and thus increase chemical constituents of groundwater. Percolating groundwater reacts with CO₂ derived from plant respiration and decay of organic matter, which can lower the pH depending on whether the flow system is open to the atmosphere, thus replenishing the CO₂ pool, or the flow system is isolated resulting in a limited flux of CO₂.

Flow patterns in regional aquifers, deduced from mapping hydrochemical facies and zones, can indicate flow directions that occurred over time scales considerably greater than the time scale over which present-day, or even pre-development water levels were established. Differences between regional flow directions deduced from hydrochemical patterns and those indicated by a modern (pre-development) potentiometric surface can indicate changes in hydraulic conditions (e.g., recharge rate) on a shorter, more recent time scale than those responsible for

hydrochemical observations (Plummer and others, 2004a, 2004b, 2004c; Sanford and others, 2004a, 2004b).

6.1.1 Redox Reactions

Oxidation and reduction (Redox) processes play an important role in geochemical reactions and affect the chemical quality of groundwater in all aquifer systems. Redox reactions are defined as reactions in which electrons are transferred. The species receiving electrons is reduced, the one donating electrons is oxidized. Redox reactions determine the mobility of many inorganic compounds as well as biologically important materials such as nitrogen and sulfur. In addition, redox conditions govern the biological degradation of complex hydrocarbon contaminants (McMahon and others, 2011; Drever, 1997; Vance, 1996). Redox levels in groundwater are determined essentially by the relative rates of introduction of oxygen and consumption of oxygen by bacterially mediated decomposition of organic matter (occasionally utilizing sulfides, ferrous silicates, or carbonates). For example, reactions that consume oxygen include sulfide oxidation ($2\text{O}_2 + \text{HS}^- = \text{SO}_4^{2-} + \text{H}^+$), iron oxidation ($\text{O}_2 + 4\text{Fe}^{+2} + 4\text{H}^+ = 4\text{Fe}^{3+} + 2\text{H}_2\text{O}$), nitrification ($2\text{O}_2 + \text{NH}_4^+ = \text{NO}_3^- + 2\text{H}^+ + \text{H}_2\text{O}$), manganese (II) oxidation ($\text{O}_2 + 2\text{Mn}^{2+} + 2\text{H}_2\text{O} = 2\text{MnO}_2 + 4\text{H}^+$), and iron sulfide oxidation ($15\text{O}_2 + 4\text{FeS}_2 + 14\text{H}_2\text{O} = 4\text{Fe}(\text{OH})_3 + 8\text{SO}_4^{2-} + 16\text{H}^+$). Reduction reactions that consume organic matter in groundwater include aerobic degradation ($\text{CH}_2\text{O} + \text{O}_2 = \text{CO}_2 + \text{H}_2\text{O}$), denitrification ($5\text{CH}_2\text{O} + 4\text{NO}_3^- = 2\text{N}_2 + 4\text{HCO}_3^- + \text{CO}_2 + 3\text{H}_2\text{O}$), manganese (IV) reduction ($\text{CH}_2\text{O} + 2\text{MnO}_2 + 3\text{H}^+ = 2\text{Mn}^{2+} + \text{HCO}_3^- + 2\text{H}_2\text{O}$), ferric iron reduction ($\text{CH}_2\text{O} + 4\text{Fe}(\text{OH})_3 + 7\text{H}^+ = 4\text{Fe}^{2+} + \text{HCO}_3^- + 10\text{H}_2\text{O}$), sulfate reduction ($\text{CH}_4 + \text{SO}_4^{2-} = \text{HS}^- + \text{HCO}_3^- + \text{H}_2\text{O}$), and methane fermentation ($2\text{CH}_2\text{O} + \text{H}_2\text{O} = \text{CH}_4 + \text{HCO}_3^- + \text{H}^+$). All of the above redox reactions can potentially determine chemical constituents that will remain in solution.

Evolution of redox processes is dependent on several factors including the source and distribution of electron donors and acceptors, relative rates of redox reaction and groundwater flow, aquifer confinement, position in the flow system, and degree of groundwater mixing (McMahon and others, 2011). Oxygen-rich recharge water could percolate through fractures in bare rock, or through organic-rich sediments. In the first case, the water will be oxidizing and have significant redox buffer capacity, while in the second case, the water may be anaerobic and retain little redox buffer capacity. Redox conditions will also be controlled by the distribution and reactivity of organic matter. Much of the organic matter is refractory having been converted under higher temperatures and pressures to compounds that cannot be utilized by bacteria. For

instance, coal should reduce any sulfate in groundwater in a coal seam but high sulfate could be present in groundwater containing coal seams because sulfate reducing bacteria cannot utilize the compounds present in coal. Many of the redox buffers (MnO_2 , $\text{Fe}(\text{OH})_3$, and Fe_2O_3) occur in large quantities in groundwater, which slows down the reactions that can lower the redox potential (or pE) of the water (Drever, 1997). Residence time of the groundwater as well as flow velocities control redox conditions. Long residence time and low flow velocity generally develops lower pE.

In groundwater flow system studies, it is important to note that redox gradients are largely vertical in the recharge areas of unconfined aquifers whereas longitudinal redox gradients predominate in confined aquifers. Electron-donor limitations can result in the preservation of reducing conditions occurring in groundwater over flow distances of many kilometers and groundwater residence times of several thousand years in some aquifers. Where electron donors are abundant, redox conditions can evolve from oxygen reducing to methanogenic over substantially shorter flow distances and residence times (McMahon and others, 2011).

6.1.2 Dissolution-Precipitation Reactions

All groundwater in aquifers are either saturated, oversaturated, or undersaturated with respect to a specific mineral phase. Groundwater tends to dissolve a mineral when groundwater is undersaturated with respect to that mineral. Minerals precipitate when groundwater is oversaturated with respect to that mineral. Mineral saturation also relates to ion activity product (IAP). When IAP for a mineral is less than the equilibrium constant (K_{sp}) then the solution is undersaturated. When $\text{IAP} > K_{sp}$, the solution is saturated with respect to that mineral.

Saturation index (SI) is defined as: $\text{SI} = \log_{10}(\text{IAP}/K_{\text{mineral}})$. Because of uncertainties inherent in the calculation of SI, ranges of $\text{SI} = 0 \pm 0.5$ to $0 \pm (5\%)(\log K_{\text{mineral}})$ are often considered (Deutsch, 1997).

Equilibration of groundwater with a mineral is the primary criterion for deciding whether or not a mineral is reactive in the aquifer environment. The equilibration could largely be controlled by dissolution-precipitation reactions. Groundwater pH, temperature, and ionic strength of the solution mainly control dissolution-precipitation reactions. A single dissolution-precipitation reaction can involve many chemical constituents and multiple dissolution reactions may involve a single constituent. For example, undersaturated fresh water moving through the aquifer containing gypsum will dissolve the mineral and release Ca and SO_4 . The dissolution reaction

will increase Ca and SO₄ concentrations in the groundwater. If the groundwater now becomes saturated with CaCO₃ then both HCO₃ and Ca will precipitate out from the groundwater depleting their concentrations. Multiple reaction processes can therefore recycle the same ions in solution depending on groundwater geochemical conditions.

6.1.3 Ion Exchange Reactions

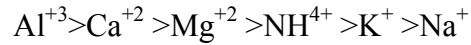
Most minerals under normal aquifer conditions have a net negative electrical charge on their surfaces. Negatively charged surfaces tend to attract and hold positively charged ions. Solid phases with large specific surface area reside in the clay fraction and therefore clay minerals are the most effective exchangers. Adsorption suggests that the chemical is taken up into the solid, and exchange involves replacement of one element for another on the solid surface.

Adsorption capacity depends on the clay fraction present, clay content, organic matter, and oxide or hydroxide content.

Ions with a greater electrical charge have a greater tendency to become absorbed than ions with a smaller charge. For example, divalent ions such as calcium (Ca⁺⁺) or magnesium (Mg⁺⁺) more readily adsorbed than monovalent ions such as sodium (Na⁺) or potassium (K⁺). When a group of chemical elements have the same electrical charge, smaller hydrated ions sorb more readily than the larger hydrated ions. Clay minerals with their layer lattice type structure act as more effective ion exchangers. Cation exchange capacity (CEC) is often measured in soils to determine ion exchange behavior by an uptake or release of ammonium ions. CEC is often measured using the following equation: $CEC \text{ (meq/kg)} = 7 \times (\% \text{clay}) + 35 \times (\% \text{C})$ (Breeuwsma and others, 1986). Typical CEC values for clays are as follows: smectites = 80-150 meq/kg, vermiculites = 120-200 meq/kg, illites = 10-40 meq/kg, kaolinite = 1-10 meq/kg, and chlorite <10 meq/kg (Drever, 2002).

Under steady-state chemical conditions, the composition of a cation exchanger will be in equilibrium with the resident groundwater. When the water composition changes as a result of pollution or acidification or due to moving salt/fresh water interface, the cation exchanger readjusts its composition to the new groundwater concentrations. The exchanger thus acts as a temporary buffer that may completely alter the concentrations in the water (Appello and Postma, 2006).

Chemical constituents in groundwater have varying affinity for sorption reactions:



Calcium and sodium ions are often involved in ion exchange. When groundwater flows through an aquifer the exchange causes a decrease in calcium and a corresponding rise in sodium governed by the following equation: $[Ca_{clay}]/[Na_{clay}]^2 = K([Ca^{2+}]/[Na^{+}])$ where $[Ca_{clay}]$ and $[Na_{clay}]$ refers to activity of calcium and sodium on exchange sites and $[Ca]$ and $[Na]$ are activities of calcium and sodium in the groundwater and K is the equilibrium constant.

Because cation exchanges are reversible, they can be driven forward or backward by manipulating the relative concentration of reactants and products (1). Ions can also be replaced by forming precipitates (2) forming a gas (3), valence dilution (4), or complimentary cations (5).

(1) $Ca-X + 2Na^{+}$ (high conc.) \leftrightarrow $(Na)_2 -X + Ca^{2+}$ (low conc.) where X is the exchange site.

(2) $Ca-X + Na_2CO_3 \leftrightarrow (Na)_2 -X + CaCO_3$ (precipitate). This reaction will be driven completely to the right because $CaCO_3$ as a product is precipitated out of solution.

(3) $NH_4 -X + NaOH \leftrightarrow Na-X + NH_4OH \leftrightarrow Na -X + H_2O + NH_3$ (g) NH_3 is lost as a gas, therefore the reaction is shifted completely to the right and all exchangeable NH_4^{+} are replaced by Na^{+} .

(4) Dilution of the equilibrium solution favors the retention of higher valence cations.

(5) Exchange one cation for another in the presence of a third (or complimentary) cation becomes easier as the retention strength of the third cation increases.

Coastal groundwater is often dominated by Ca^{2+} and HCO_3^{-} ions derived from dissolution of carbonate minerals and therefore the exchangers are also dominated by adsorbed Ca^{2+} . In contrast, Na^{+} and Cl^{-} are the dominant ions and sediment in contact with seawater will have Na on the exchanger. When seawater intrudes fresh water, an exchange of cations occurs: $Na^{+} + 1/2 Ca-X \rightarrow Na-X + 1/2 Ca^{2+}$ where X indicates the exchanger. In the above reaction, Na is taken up by the exchanger and Ca is released. Since Cl remains the same due to their conservative chemical behavior, water quality changes from a $NaCl$ to $CaCl_2$ -type water. During freshening of the aquifer, when fresh water intrudes a saline water aquifer, the reaction is reversed: $Na-X + 1/2 Ca^{2+} \rightarrow Na^{+} + 1/2 Ca-X$. The sediment now absorbs Ca while Na is released, which produces $NaHCO_3$ -type water. Sequential redox changes may also be used to characterize groundwater at different positions along flowpaths and provide additional information on residence times

(Edmunds and others, 1984). At the outcrop most groundwater is aerobic, but with progressive downgradient flow the dissolved oxygen is consumed by inorganic or microbially mediated processes, leading to anaerobic conditions marked by sharp changes in the redox potential.

6.1.4 Chemical Evolution of Groundwater

Groundwater is subject to multiple geochemical processes (see Figure 6-1) as soon as rainwater infiltrates the land surface and begins moving from a recharge to a discharge location. As groundwater passes through the subsurface, its chemical signatures are modified by these processes. The solutes that are present in groundwater are derived from two main sources: 1) inputs from atmospheric precipitation, which have their origin from both marine salts and continental dust and 2) acquisition during weathering and water-rock interactions (Cook and Herczeg, 2000). Table 6-1 lists the range of constituent concentrations for precipitation. Along the Texas Gulf Coast, the composition of rainfall is similar to ocean water, dilute and slightly acidic. Figure 6-2 shows the estimated chloride distribution in bulk precipitation across the Gulf Coast. The chloride concentration varies from 14 mg/L along the coastline to about 1 mg/L near the up-dip extent of the Catahoula. Similar trends are expected for the other major ions present in seawater.

Table 6-1 Reported constituent concentration ranges for precipitation (from Hem, 1985).

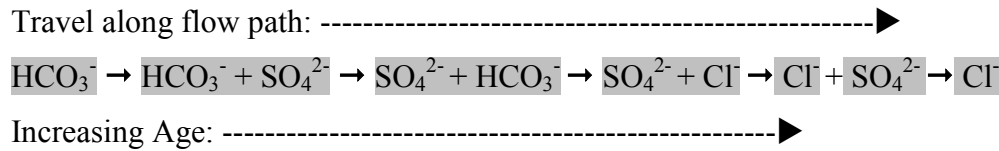
Constituent	Concentration Range in Precipitation(mg/L)
Calcium	0.0 to 1.41
Sodium	0.0 to 9.4
Sulfate	0.7 to 7.6
Chloride	0.2 to 17.0
Nitrate-Nitrogen	0.0 to 0.14

Once rainfall enters the soil, its constituents' concentrations increase as a result of evaporation and its carbon dioxide concentration increases as a result of plant respiration and microbiological degradation of soil organic matter. The CO₂ partial pressure in the soil unsaturated zone is normally much higher than that of the earth's atmosphere. In the soil, CO₂ partial pressure in the range of 10⁻³ to 10⁻² bars is typical (Freeze and Cherry, 1979). In groundwater, the carbon dioxide acts as a weak acid that modifies the groundwater chemistry by the weathering of

minerals. Two common reactions are the dissolution of calcite (CaCO₃) and the weathering of silicate minerals to form clays:

- Dissolution of calcite: $\text{CO}_2 + \text{CaCO}_3 + \text{H}_2\text{O} \leftrightarrow 2\text{HCO}_3^- + \text{Ca}^{2+}$
- Weathering of silicate minerals to clays: $2\text{CO}_2 + 2\text{NaAlSi}_3\text{O}_8 + 11\text{H}_2\text{O} \leftrightarrow \text{Al}_2\text{Si}_2\text{O}_5(\text{OH})_4 + 2\text{Na}^+ + 2\text{HCO}_3^- + 4\text{H}_4\text{SiO}_4$

As a result of being modified by geochemical processes, the groundwater chemical signature evolves along a groundwater flow path. Changes in the chemical signature are often similar to those observed by Chebotarev (1955). Chebotarev (1955) reviewed more than 10,000 chemical measurements from water wells in Australia and concluded that groundwater tends to evolve chemically toward the composition of seawater and that this evolution typically includes the following regional changes in dominant anion species:



Domenico (1972) states that the evolutionary development of the bicarbonate-sulfate-chloride sequence identified by Chebotarev (1955) above can be compared with the process of mineral formation by evaporation of surface-water bodies:

“With evaporation, concentration of the soluble salts occurs, and when super saturation with any salt is achieved, that salt is precipitated. The least soluble salts are precipitated first, and the most soluble last, with the order being calcite (bicarbonate), gypsum (sulfate), and halite (chloride). Halite remains in solution until its normal marine salinity of 35,000 ppm has increased to 337,000 ppm. Whereas evaporation is the mechanism of concentration in surface-water bodies, the relative solubility of the rocks in a dynamic flow system is the responsibility factor in groundwater basins. With evaporation, a vertical zonation of evaporate deposits is anticipated; with groundwater flow it is the chemical constituents in solution that reflect zonation.”

For a large sedimentary basin, the anion-evolution sequence described by Chebotarev (1955) can be described by three main zones, which correlate in a general way with depth (Domenico, 1972; Freeze and Cherry, 1979).

1. The upper zone – characterized by active groundwater flushing through the relatively well-leached rocks. Water in this zone has HCO_3^- as the dominant anion and is low in total dissolved solids.
2. The intermediate zone – with less active groundwater circulating and higher total dissolved solids. Sulfate is normally the dominant anion in this zone.
3. The lower zone – with very sluggish groundwater flow. Highly soluble minerals are commonly present in this zone because very little groundwater flushing has occurred. High chloride concentrations and high total dissolved solids are characteristic of this zone.

For large aquifer systems, Chebotarev (1955) suggests that salinity should generally increase: with depth; with distance from the recharge area; with proximity to the sea (where applicable); and with duration of contact with aquifer minerals, which can also be referred to as residence time as measured from time of recharge. Ophori and Toth (1989) and Back (1966) are among the notable studies that document the anion-evolution sequence of Chebotarev (1955). Ophori and Toth (1989) show that the spatial distribution of ions in the Ross Creek Basin in Alberta, Canada shows good correlation with basin flow regimes. In that study, low dissolved solids, high $\text{Ca}^{2+}/\text{Mg}^{2+}$ ratios, low SO_4^{2-} , and high HCO_3^- coincide and occur in recharge areas. Whereas high TDS, low $\text{Ca}^{2+}/\text{Mg}^{2+}$ ratios, high SO_4^{2-} , and low HCO_3^- mark the discharge areas. Similarly, Back (1966) identified highest concentrations of calcium and magnesium in the recharge areas underlain by calcareous clays and highest sodium concentrations in discharge areas, the latter a result of ion exchange and salt-water intrusion. As a result of his findings, Back (1966) proposed the concept of hydrochemical facies as a means for detection of regional relations between the chemical character of groundwater, lithology, and regional flow patterns. Freeze and Cherry (1979) define hydrogeochemical facies as distinct zones that have cation and anion concentrations describable within defined composition categories. As a general rule, the name of a hydrogeochemical facies includes the name of the major cations and/or the name of the major anions. Examples of hydrogeochemical facies names are a sodium-chloride (Na-Cl)

facies, a calcium-bicarbonate-chloride (Ca-HCO₃-Cl) facies, and a calcium-magnesium (Ca-Mg) facies. Figure 6-3 shows the general relationship between hydrochemical facies and geochemical processes in a coastal aquifer.

6.2 Geochemistry Characterization

6.2.1 Ocean Water

Because water is a powerful solvent, a great number of materials found in seawater are dissolved, and thus exist in their ionic forms. Salinity is the term used to describe the concentration of inorganic, dissolved salts in seawater. The average salinity of the ocean is 35,000 ppm (by weight). The primary chemicals comprising ocean water are chloride (55.03%) and sodium (30.59%), which make up 85.62% of the dissolved constituents. Table 6-2 provides a detailed breakdown the chemicals that comprise more than 99% of the ocean water’s dissolved constituents. Table 6-3 lists the ion ratios for several of the ion pairs that may be useful for determining whether ocean water is mixing with groundwater near the coast.

Table 6-2 Composition of Ocean Water with a Salinity of 35,000 ppm (Anthoni, 2006).

Chemical Ion (symbol)	Valence	Concentration ppm, mg/kg	Percentage of salinity %	Molecular Weight	mmol/kg
Chloride (Cl)	-1	19345	55.03	35.453	546
Sodium (Na)	+1	10752	30.59	22.99	468
Sulfate (SO ₄)	-2	2701	7.68	96.062	28.1
Magnesium (Mg)	+2	1295	3.68	24.305	53.3
Calcium (Ca)	+2	416	1.18	40.078	10.4
Potassium (K)	+1	390	1.11	39.098	9.97
Bicarbonate (HCO ₃)	-1	145	0.41	61.016	2.34
Bromide (Br)	-1	66	0.19	79.904	0.83
Borate (BO ₃)	-3	27	0.08	58.808	0.46
Strontium (Sr)	+2	13	0.04	87.62	0.091
Fluoride (F)	-1	1	0.003	18.998	0.068
Iodine (I)	-1	0.06	0.0002	166.9	0.0004

Note: valence is the charge of the ion

Note: mmol/kg represents millimoles per kilogram

Table 6-3 Ion Ratios for Ocean Water (Anthoni, 2006).

Ion Ratio	Value	Ion Ratio	Value
Cl/Br	657.8	Br/Cl	0.0015
Cl/SO ₄	19.4	SO ₄ /Cl	0.0515
Cl/Ca	52.5	Ca/Cl	0.0190
Cl/Na	1.2	Na/Cl	0.8571
Na/Ca	45.0	Ca/Na	0.0222

By careful analysis of water samples collected during the Challenger expedition of the late 1800's it was discovered that all of the major constituents occur everywhere in the same relative proportions even though the amount of water in the mixture varies (Anthoni, 2006). These major solutes are called conservative because their concentrations are stable over time in the oceans. This means that the ratios of these ions to one another are constant throughout most of the ocean because the oceans are very well mixed.

Salinity is somewhat higher in the Atlantic Ocean (36,900 mg/L) than in the Pacific ocean (33,600 ppm) and salinity can be significantly lower in bays and near shore areas where fresh water mixes with ocean water. The influence of fresh-water inflow on water quality is illustrated by samples taken at increasing distance from the shore along the Texas Gulf Coast. Chloride concentrations increase from 3,200 mg/L at the mouth of the Houston Ship Channel at Galveston Bay to 13,000 to 14,000 mg/L three miles offshore and to 18,000 mg/L twenty-five miles offshore (Jorgensen, 1977).

Water samples from various sea-water intrusion sites suggest that cation exchange can alter the composition of intruding ocean water (Richter and Kreitler, 1991). On bivariate plots of Ca versus Cl, K versus Cl, and Na versus Cl, cation exchange is suggested by some of the samples, as calcium content is greater and sodium and potassium contents are smaller than in the well-defined mixing trends indicated by other samples. For chloride concentrations less than 1,000 mg/L the mixing trends are less well defined because the local fresh-water variations dominated over the relatively uniform sea-water composition (Richter and Kreitler, 1991).

6.2.2 Formation Water (Brines)

The Catahoula Formation represents the bottom of the Gulf Coast Aquifer System. At depths below 3,000 feet, most of the groundwater in the Catahoula Formation is not meteoric water and is formation water. Kreitler and others (1988) assembled nearly 850 hydrochemical analyses of

groundwater from the Catahoula Formation and performed additional sampling and hydrochemical analysis to fill data gaps. The chemical analysis were primarily between the depths of 4,000 and 12,000 feet.

Figure 6-4 shows plots of TDS versus depth for groundwater samples from the Catahoula taken within GMA 14, 15, and 16. The data shows a wide range of brine concentration for all depths. The majority of the TDS concentrations fall between 10,000 mg/L and 100,000 mg/L TDS with the highest concentrations occurring in GMA 14. In GMA 14, the about 20% of the samples have TDS values greater than 10,000 mg/L.

Figure 6-4 includes a plot of Br versus Cl concentration for the Catahoula water. The plot contains data that can be categorized into two groups. One group is characterized by Br concentrations increasing with increases in Cl concentration (the high trend) and the other group is characterized with a Br concentration that is nearly constant with increasing Cl (the low trend). Plotting Cl/Br versus Cl, and Na/Cl versus Cl similarly shows separation of two populations (Kreitler and others, 1988). The “low end trend” data are primarily from GMA 14. These data are consistent with the majority of the Na and Cl in solution coming from halite dissolution from salt dome area. The “high trend “ data are primarily from GMA 15 and GMA 16. These data are consistent with the majority of the Na and Cl in solution s originating from upward leakage from the undercompacted geopressured section.

Table 6-4 provides the averages and medians for the concentrations of TDS and of the major constituents of the Catahoula Formation water in GMA 14, 15, and 16. Table 6-5 provides the averages and medians for the ion ratios Cl/Br, Cl/SO₄, Cl/Ca, Cl/Na, and Na/Ca for the Catahoula Formation water in GMA 14, 15, and 16. The results show that the composition of the formation water is very similar in GMA 15 and 16 and the difference observed in GMA 14 can be explained by the addition of Na-Cl solution caused by the dissolution of the salt domes.

Table 6-4 Ion Concentrations for Formation Water in the Deep Catahoula.

GMA	Statistic	Constituent (mg/L)							
		TDS	Cl	Na	Ca	Mg	SO ₄	K	Alkalinity
14	average	81,209	43,318	26,420	2,071	404	79	222	593
	median	66,900	38,851	23,994	1,568	199	34	180	450
15	average	52,978	32,369	18,993	1,239	195	101	186	670
	median	59,691	36,314	21,545	1,052	179	33	130	321
16	average	59,401	35,693	20,032	2,523	271	90	107	615
	median	66,038	39,850	21,994	1,175	181	42	69	413

Table 6-5 Ion Ratios for Formation Water in the Deep Catahoula.

Statistic	Ion Ratio	GMA			Ion Ratio	GMA		
		14	15	16		14	15	16
Average	Cl/Br	1568.1	919.9	684.3	Br/Cl	0.0006	0.0011	0.0015
Median		1428.7	688.8	593.0		0.0007	0.0015	0.0017
Average	Cl/SO4	5132.5	3473.7	3615.3	Cl/SO4	0.0002	0.0003	0.0003
Median		1177.6	1149.6	874.6		0.0008	0.0009	0.0011
Average	Cl/Ca	50.0	46.2	32.8	Ca/Cl	0.0200	0.0217	0.0305
Median		18.1	19.3	19.2		0.0551	0.0518	0.0522
Average	Cl/Na	1.1	1.1	1.1	Na/Cl	0.9459	0.9332	0.9035
Median		1.1	1.1	1.1		0.9427	0.9316	0.9290
Average	Na/Ca	40.9	46.8	34.0	Ca/Na	0.0245	0.0214	0.0294
Median		16.8	18.1	17.4		0.0594	0.0553	0.0573

6.2.3 Groundwater Characterization

Since the pioneering work of Back (1966), a common approach to characterize groundwater is by their hydrogeochemical facies. Typically, the name of a hydrogeochemical facies includes the name of the major cations and/or the name of the major anions. Examples of hydrogeochemical facies names are a sodium-chloride (Na-Cl) facies, a calcium-bicarbonate-chloride (Ca-HCO₃-Cl) facies, and a calcium-magnesium (Ca-Mg) facies.

In order to determine the hydrochemical facies for an aquifer, it is necessary to convert the mass concentrations of the major ions into terms of chemical concentration. The conversion from mass concentration to chemical concentration is performed by dividing the chemical's mass concentration by its equivalent weight. For instance, calcium has an atomic weight of 40.08 meq/mg, and a valence of 2⁺, so it has an equivalent weight of 20.04 mg/meq. Thus, a calcium concentration of 100 mg/L is equivalent to about 5 meq/L.

A common method for illustrating the hydrochemical facies distribution for an aquifer is with a Piper diagram (Piper, 1944). A Piper diagram shows the relative concentrations of six to seven ions that make up 95 to 100% of ions in a groundwater sample using two triangular diagrams and a central quadrilateral. Figure 6-5 shows a Piper diagram that has been partitioned into chemical facies used by Back (1966) to characterize the groundwater in an Atlantic coastal aquifer. As shown in Figure 6-5, one of the triangular diagrams (on the lower right) is for anions and the other triangular diagram (on the lower left) is for cations. The quadrilateral is used to assign the hydrochemical facies to the groundwater sample. Readers interested in knowing more about Piper diagrams and how to construct Piper diagrams are referred to Freeze and Cherry (1979).

Figures 6-6 through 6-8 show Piper diagrams for groundwater samples collected from wells associated with the 19 transects in the GMA 14, 15, and 16. For each GMA, a Piper diagram was

constructed for the major hydrostratigraphic units in the Gulf Coast Aquifer System and the Yegua-Jackson Aquifer.

For GMA 14, Figure 6-6 shows that the distribution of hydrochemical facies for the Evangeline Aquifer, Jasper Aquifer, and Middle Lagarto are very similar. For most of the geological units, the predominant anion in the groundwater sample is HCO_3 . The predominant cation is either Na or Ca. Thus, these three geological units are characterized by Ca-HCO_3 , Na-HCO_3 , and Ca-Na-HCO_3 facies. The Chicot has a wider coverage of facies that includes five major facies, which include the three previous facies plus the Na-Cl-HCO_3 and Na-Cl facies. The latter two facies represent facies including the Cl anion, which is typically associated with a longer residence time than the HCO_3 anion. A review of the well locations in GMA 14 (see Figure 4-1) and salt dome locations (see Figure 2-6) suggests that the higher occurrence of Cl could be a result from sampling bias because the Chicot sampling locations are in closer proximity to two chloride sources for the Gulf Coast Aquifer System. These two sources are halite dissolution from salt domes and the intrusion of seawater caused by pumping or the atmospheric transport of seawater.

For GMA 16, Figure 6-8 shows that the distribution of hydrochemical facies for the Chicot and Evangeline Aquifers are very similar. Figure 4-3 shows the sampling distribution in the Chicot and Evangeline Aquifer in GMA 16. Unlike GMA 14, the facies with the Chicot and Evangeline aquifers are primarily associated with Cl and not HCO_3 . Because of the significantly less salt domes in GMA 16, the most likely cause for the higher percent of Cl in GMA 16 is that the GMA 16 groundwater has a significantly longer residence times than does groundwater in GMA 14. In GMA 16, the Middle Lagarto, Jasper Aquifer, and the Catahoula Formation have facies distributions that generally mimic the distribution for the Chicot and the Evangeline Aquifers.

For GMA 15, Figure 6-7 shows facies for the geologic units have hydrogeochemical facies distribution generally lie between the endpoint distributions observed in GMA 14 and GMA 16. In addition, the Na-HCO_3 facies is less prevalent than the Ca-HCO_3 facies in GMA 15.

6.3 Regional Groundwater Flow and Geochemistry

Approximately 95% of the TDS in the Gulf Coast Aquifer System groundwaters is comprised of the major ions calcium, sodium, potassium, magnesium, bicarbonate, chloride, and sulfate.

Figures 6-9 through 6-13 shows ion concentrations for depth intervals of 0 to 200 feet, 200 to 500 feet, and 500 to 1,000 feet for the Gulf Coast Aquifer System. Figures 6-14 through 6-16 shows the ratios(based on charge concentration) between two ions for depth intervals of 0 to 200 feet, 200 to 500 feet, and 500 to 1,000 feet. These figures were created using the following three-step process: 1) calculate the average concentration at each of the 13,000 well locations shown in Figures 4-1 through 4-3; 2) assign each well to a depth interval based on the depth of the well; and 3) contour the average concentration measurements in each depth interval using the kriging tools in ArcMap. To help the reader interpret the interpolated concentration values, each plot shows the locations of the measured concentration values, the locations of salt domes, and the up-dip extent of the Catahoula.

Tables 6-6 through 6-8 provide the average and median concentrations for the measured concentrations of TDS and major ions and calculated ratios for selected ion pairs for GMA 14, 15, and 16 for the four depths shown in the Figures 6-9 through 6-17 after the measurements have been grouped by down-dip distances. The down-dip distances are measured relative to the up-dip extent of the Catahoula Formation, which is the western most portion of the Catahoula outcrop. Along this up-dip extent, a datum of 0 miles is assigned and down dip direction is measured eastward toward the ocean at 25 mile intervals. In the tables, the down dip interval of “-25 to 0 miles” refers to distances west of the Catahoula and includes wells that do not intersect the Gulf Coast Aquifer System but the Yegua-Jackson Formation. For most of the Gulf Coast Aquifer System the shoreline occurs at a down-dip distance between 100 and 125 miles. If less than 20 concentrations were available for calculating a bin (designated by depth and down-dip distance), neither an average nor median concentration was calculated and a “X” was placed in the box.

A review of the concentration data shows that the southern part of the Gulf Coast Aquifer System contains significantly higher concentration of chloride, sulfate, and sodium than does the northern part of the Gulf Coast Aquifer System. One way to quantify this difference is to calculate average and median concentrations for the three GMA areas and compare the values.

Final – Hydrogeochemical Evaluation of the Texas Gulf Coast Aquifer System and Implications for Developing Groundwater Availability Models

Table 6-6 Average and Median Values for Chemical Concentrations and Ion Ratios for GMA 14. (note the ion ratios are dimensionless)

ID	Depth (ft)	GMA 14 Average Concentration (mg/L)						GMA 14 Median Concentration (mg/L)					
		Down Dip Distance (miles)						Down Dip Distance (miles)					
		-25-0	0-25	25-50	50-75	75-100	100-125	-25-0	0-25	25-50	50-75	75-100	100-125
TDS	0 - 200	660	375	136	452	829	1,033	922	333	142	383	684	1,048
	200 - 500	736	649	224	423	841	1,237	806	677	345	479	615	1,332
	500 - 1000	704	562	305	332	766	1,197	530	616	476	418	484	1,385
	1000 - 2000	688	556	354	434	1,033	0	473	632	356	539	453	0
CL	0 - 200	136	79	32	114	295	546	52	48	27	60	257	248
	200 - 500	118	190	36	115	280	707	100	101	47	53	126	398
	500 - 1000	159	134	40	82	300	500	68	52	38	41	100	474
	1000 - 2000	107	0	44	74	369	0	30	0	63	78	62	0
SO ₄	0 - 200	85	22	5	23	44	23	55	10	3	8	17	10
	200 - 500	126	37	6	7	19	14	63	10	5	5	3	3
	500 - 1000	60	20	12	9	9	5	49	8	10	12	3	2
	1000 - 2000	55	0	25	10	19	0	39	0	24	14	11	0
HCO ₃	0 - 200	295	229	66	248	382	441	274	223	47	371	399	480
	200 - 500	392	330	178	246	379	533	303	318	188	240	547	530
	500 - 1000	424	335	236	229	329	397	521	343	358	337	312	528
	1000 - 2000	508	0	267	277	386	0	573	0	276	394	363	0
Ca	0 - 200	74	66	17	56	76	58	53	53	12	45	108	54
	200 - 500	13	44	36	46	26	38	4	37	29	63	25	30
	500 - 1000	8	29	42	41	21	27	3	22	65	64	23	32
	1000 - 2000	3	0	29	23	23	0	2	0	46	29	12	0
Na	0 - 200	143	61	25	98	220	315	94	52	18	63	171	309
	200 - 500	266	194	39	106	297	426	173	103	26	55	225	467
	500 - 1000	262	179	63	80	263	424	199	189	77	49	255	316
	1000 - 2000	273	0	100	143	371	0	181	0	91	180	170	0
Mg	0 - 200	22	7	4	14	19	21	13	5	4	13	13	18
	200 - 500	3	4	4	8	8	21	2	3	3	5	8	16
	500 - 1000	2	3	6	6	7	11	2	1	9	9	4	12
	1000 - 2000	1	0	4	5	9	0	1	0	6	6	3	0
K	0 - 200	4	5	3	2	2	6	4	6	2	1	3	4
	200 - 500	5	8	3	2	2	4	7	6	3	3	1	4
	500 - 1000	4	6	3	2	2	2	2	6	3	3	2	2
	1000 - 2000	2	0	3	3	6	0	2	0	4	2	1	0
CL/SO ₄	0 - 200	12	12	14	56	99	229	3	5	7	9	20	10
	200 - 500	11	146	15	54	173	356	1	4	12	13	71	150
	500 - 1000	41	119	9	23	217	336	2	12	5	8	94	169
	1000 - 2000	21	0	7	22	164	0	1	0	3	12	14	0
Cl/Br	0 - 200	0	518	303	693	0	0	0	518	251	857	0	0
	200 - 500	0	628	472	1,092	1,784	1,211	0	791	593	1,539	2,310	825
	500 - 1000	0	523	434	718	1,005	0	0	516	376	473	796	0
	1000 - 2000	0		471	703	0	0	0		471	599	0	0
Na/Ca	0 - 200	10	4	3	5	8	8	1	1	3	2	3	4
	200 - 500	69	9	2	8	19	12	58	3	1	1	22	9
	500 - 1000	115	13	3	6	19	16	88	7	1	2	20	19
	1000 - 2000	147	0	12	11	25	0	121	0	2	8	33	0
Na/Cl	0 - 200	3.2	2.0	1.5	1.8	1.7	1.5	2.3	2.1	1.3	1.5	1.4	1.9
	200 - 500	6.6	2.7	2.1	2.1	2.7	2.0	5.1	2.0	1.5	1.5	2.1	3.0
	500 - 1000	7.5	3.9	3.3	2.6	2.9	1.6	5.5	5.6	2.8	1.8	4.4	1.4
	1000 - 2000	9.4	0	6	3	4	0.0	7.6	0.0	5.5	4.5	4.2	0.0

Final – Hydrogeochemical Evaluation of the Texas Gulf Coast Aquifer System and Implications for Developing Groundwater Availability Models

Table 6-7 Average and Median Values for Chemical Concentrations and Ion Ratios for GMA 15. (note the ion ratios are dimensionless)

ID	Depth (ft)	GMA 15 Average Concentration (mg/L)					GMA 15 Median Concentration (mg/L)				
		Down Dip Distance (miles)					Down Dip Distance (miles)				
		-25-0	0-25	25-50	50-75	75-100	-25-0	0-25	25-50	50-75	75-100
TDS	0 - 200	1,316	905	750	1,339	3,752	1,303	688	908	1,136	1,003
	200 - 500	968	936	572	893	1,017	947	1,011	761	904	638
	500 - 1000	883	791	530	1,021	579	789	1,015	514	865	661
	1000 - 2000	848	X	794	1,068	X	696	X	505	838	X
CL	0 - 200	334	279	236	560	1,960	165	247	150	333	301
	200 - 500	236	299	147	350	392	159	252	105	191	153
	500 - 1000	222	204	127	383	158	104	133	152	285	85
	1000 - 2000	254	195	237	408	X	44	201	108	272	X
SO ₄	0 - 200	397	84	47	71	244	184	43	28	48	35
	200 - 500	266	92	33	33	37	129	62	32	17	16
	500 - 1000	151	40	28	44	17	70	46	16	27	24
	1000 - 2000	82	X	X	31	X	37	X	X	19	X
HCO ₃	0 - 200	227	315	329	360	353	341	325	506	373	501
	200 - 500	233	324	298	337	371	355	328	317	518	338
	500 - 1000	360	423	310	343	330	406	388	338	513	309
	1000 - 2000	425	X	408	387	X	288	X	362	378	X
Ca	0 - 200	130	137	115	127	178	87	109	146	78	70
	200 - 500	84	95	72	72	44	53	136	104	69	33
	500 - 1000	32	40	52	40	37	29	40	45	25	52
	1000 - 2000	25	X	28	26	X	23	X	26	11	X
Na	0 - 200	224	157	127	321	1,090	107	116	166	155	231
	200 - 500	215	212	114	220	326	112	135	166	150	181
	500 - 1000	284	254	131	343	169	206	224	181	293	179
	1000 - 2000	295	X	X	381	X	214	X	X	312	X
Mg	0 - 200	31	18	23	43	138	18	14	21	24	22
	200 - 500	23	12	17	19	18	17	12	21	20	16
	500 - 1000	9	8	12	12	13	8	4	10	9	20
	1000 - 2000	5	X	6	10	X	7	X	7	5	X
K	0 - 200	13	10	3	4	6	15	6	2	3	7
	200 - 500	8	10	3	3	4	7	10	3	2	3
	500 - 1000	7	8	4	3	2	10	11	2	3	2
	1000 - 2000	6	X	3	3	X	9	X	4	4	X
CL/SO ₄	0 - 200	8	7	8	70	29	1	5	6	11	18
	200 - 500	5	24	10	62	99	1	7	10	9	13
	500 - 1000	11	28	12	114	37	2	7	7	7	10
	1000 - 2000	26	X	X	308	X	1	X	X	34	X
Cl/Br	0 - 200	X	556	607	597	831	X	756	904	541	822
	200 - 500	X	781	465	508	658	X	906	448	737	615
	500 - 1000	X	589	753	X	549	X	513	511	X	729
	1000 - 2000	X	631	453	X	X	X	631	441	X	X
Na/Ca	0 - 200	3	1	1	4	6	1	1	1	1	3
	200 - 500	9	3	2	10	13	2	1	2	1	6
	500 - 1000	36	14	4	31	11	6	11	2	9	4
	1000 - 2000	48	57	19	27	X	27	43	6	27	3
Na/Cl	0 - 200	1.6	1.2	1.2	1.3	1.3	1.3	1.0	1.6	1.2	1.7
	200 - 500	2.1	1.5	1.3	1.3	1.9	1.5	1.2	1.9	1.2	1.5
	500 - 1000	3.4	2.7	1.7	1.4	2.2	4.0	2.4	2.4	1.4	2.9
	1000 - 2000	4.3	3	2	2	X	5.2	2.9	3.2	1.7	2.0

Final – Hydrogeochemical Evaluation of the Texas Gulf Coast Aquifer System and Implications for Developing Groundwater Availability Models

Table 6-8 Average and Median Values for Chemical Concentrations and Ion Ratios for GMA 16. (note the ion ratios are dimensionless)

ID	Depth (ft)	GMA 16 Average Concentration (mg/L)					GMA 16 Median Concentration (mg/L)				
		Down Dip Distance (miles)					Down Dip Distance (miles)				
		-25-0	0-25	25-50	50-75	75-100	-25-0	0-25	25-50	50-75	75-100
TDS	0 - 200	2,390	1,456	1,976	2,217	2,126	3,068	1,713	1,517	1,688	2,468
	200 - 500	2,586	1,834	1,508	1,606	2,423	528	1,652	1,249	1,432	2,064
	500 - 1000	2,340	1,335	1,120	1,162	1,362	956	1,321	1,061	955	1,252
	1000 - 2000	1,471	0	1,509	2,574	0	859	0	1,087	2,315	0
CL	0 - 200	684	555	739	688	644	481	380	845	264	339
	200 - 500	1,189	757	539	524	709	119	623	616	552	522
	500 - 1000	1,020	472	359	358	472	96	226	338	408	545
	1000 - 2000	0	0	0	0	0	0	0	0	0	0
SO ₄	0 - 200	805	269	394	468	504	662	114	415	360	607
	200 - 500	472	277	237	304	711	36	113	224	260	921
	500 - 1000	111	380	162	200	333	40	99	107	130	412
	1000 - 2000	0	0	0	0	0	0	0	0	0	0
HCO ₃	0 - 200	275	326	346	359	416	288	497	337	374	630
	200 - 500	251	315	314	351	428	236	332	315	512	428
	500 - 1000	569	360	332	299	252	741	353	327	439	371
	1000 - 2000	0	0	0	0	0	0	0	0	0	0
Ca	0 - 200	99	163	185	164	112	146	136	229	162	92
	200 - 500	81	96	101	78	94	35	68	121	57	82
	500 - 1000	16	43	55	36	21	14	58	61	31	15
	1000 - 2000	12	0	0	0	68	9	0	0	0	40
Na	0 - 200	693	381	439	539	561	536	267	429	357	589
	200 - 500	832	571	384	455	698	156	479	313	406	612
	500 - 1000	886	433	330	372	477	352	417	313	304	408
	1000 - 2000	548	0	0	0	0	329	0	0	0	0
Mg	0 - 200	25	38	65	70	61	20	31	69	57	60
	200 - 500	16	25	40	35	55	6	15	29	23	46
	500 - 1000	6	12	20	15	6	8	15	26	13	4
	1000 - 2000	0	0	0	0	0	0	0	0	0	0
K	0 - 200	17	12	15	9	10	21	10	9	11	12
	200 - 500	7	14	11	8	7	6	10	10	7	8
	500 - 1000	6	17	10	8	6	7	16	10	13	5
	1000 - 2000	0	0	0	0	0	0	0	0	0	0
CL/SO ₄	0 - 200	2	8	4	4	3	1	4	3	1	2
	200 - 500	140	26	5	103	2	3	4	6	2	1
	500 - 1000	33	6	8	3	2	5	3	3	3	3
	1000 - 2000	14	2	2	7	3	2	3	2	7	2
Cl/Br	0 - 200	0	584	548	684	0	0	551	528	706	0
	200 - 500	525	1,536	633	689	967	501	548	894	601	1,389
	500 - 1000	0	0	1,384	509	532	0	0	882	778	732
	1000 - 2000	0	0	0	0	0	0	0	0	0	0
Na/Ca	0 - 200	18	3	2	3	5	3	1	3	3	3
	200 - 500	21	19	5	9	9	2	9	4	5	7
	500 - 1000	51	27	8	14	27	52	8	11	9	20
	1000 - 2000	147	0	0	0	0	53	0	0	0	0
Na/Cl	0 - 200	1.7	1.2	1.1	1.5	1.8	2.3	1.1	1.5	1.4	2.5
	200 - 500	1.7	1.6	1.3	1.7	1.9	2.0	1.9	1.2	1.6	1.9
	500 - 1000	3.9	1.9	1.7	1.7	1.9	4.7	2.9	1.6	1.7	1.8
	1000 - 2000	4.8	0	0	0	1.6	4.9	0.0	0.0	0.0	2.5

Table 6-9 Comparison of Major Ion and TDS Concentrations among GMA 14, GMA 15, and GMA 16.

Chemical ID	GMA 16 Concentration (mg/L)		Ratios			
			GMA16/GMA14		GMA16/GMA15	
	average	median	average	median	average	median
TDS	1,693	1,533	4.9	4.1	2.1	1.8
CL	647	616	7.7	11.1	2.7	3.3
SO ₄	294	216	16.5	31.4	4.6	5.3
HCO ₃	325	370	1.6	1.9	1.0	1.0
Ca	136	139	3.4	4.3	1.3	1.1
Na	444	372	5.6	7.5	2.9	2.6
Mg	42	36	8.8	9.4	2.4	2.1
K	13	10	2.9	2.4	2.0	1.8

The results of this comparison are provided in Table 6-9 for TDS and the seven major ions for a shallow aquifer zone defined by a maximum depth of 500 feet and down-dip distances between 0 and 50 miles. For all constituents, the highest concentrations occur in GMA 16. To quantify the differences among the GMA concentrations, the ratios were calculated for each constituent to compare differences in concentrations between GMA 16 and GMA 14 and in concentrations between GMA 16 and GMA 15. The most noticeable differences among the GMAs occur for sulfate and chloride and the least differences occur for bicarbonate and calcium. Sulfate and chloride concentration values are between 7 and 31 times greater than the concentration values in GMA 14 and are between 2 and 5 times greater than the concentration values in GMA 15, respectively. The bicarbonate and calcium concentration values are between 1.5 and 4.5 times greater than the concentration values in GMA 14 and are between 1.0 and 1.5 times greater than the concentration values in GMA 15, respectively. In semi-qualitative terms, the concentrations values in GMA 16 are about double the values in GMA 15 and the values in GMA 15 are about double the values in GMA 14. This relationship suggests that difference in latitude is a rough indicator of relative differences in concentration values. Because latitude is an indicator of precipitation, recharge, and evaporation potential along the Gulf Coast, the observed concentration trends are consistent to the findings of Chowdhury and others (2006) and Back (1966).

Based on their study of the evolution of geochemistry in coastal aquifers, Back (1966) and Chowdhury and others (2006) identify among the key factors that affect groundwater concentrations are rainfall levels, matrix mineralogy, evaporation rates, and the flow path/residence time of the water. As shown in Figure 3-3, the precipitation varies from about 60 inch/year in the northeast to about 21 inches in the southwest. Across the Texas Gulf Coast, pan evaporation rates vary from about 70 inches/year in the southwest to about 45 inches/year in the northeast (Larkin and Bomar, 1983). As a result of the relatively low precipitation and high evapotranspiration potential, the southern Gulf Coast Aquifer System should have a much lower recharge rate than the northern Gulf Coast. Figure 3-4 shows that recharge (as estimated by chloride mass balance) varies from less than 0.1 inches/year in the southern Gulf Coast Aquifer System to greater than 6 inches/year in the northern Gulf Coast. As a result of these conditions, the recharge in the south (GMA 16) will concentrate salts at the surface and should have a greater residence time than in the north (GMA 14).

The significantly higher ion concentrations in the south are consistent with the lower recharge rates in the south and possibly less permeable deposits in the south. According to Back (1966), the finer-grained deposits and hence lower permeability deposits will lead to an increase in concentrations from two different effects: (1) the smaller grains of any soluble material will go into solution more readily than coarse grain of the same material, and (2) the smaller grain size causes a decrease in permeability that requires a longer residence time to traverse the same flow distance. Therefore, in an area of fine-grained material containing abundant soluble minerals, we would expect the water to have higher dissolved-solids content closer to the recharge area than it would have in an area of coarser sediments containing less soluble material.

Visual inspection of the percent sand maps for the Chicot and the Evangeline Aquifer prepared by Young and others (2010, 2012a) show large differences of sand and clay percentages along the Gulf Coast Aquifer System but the importance of the differences is difficult to judge. One of the reasons for the difficulty is that whereas the Chicot is the sandier aquifer in the north, the Evangeline is the sandier aquifer in the south. Whether it is from primarily as a result of lower recharge rates or lower permeability deposits, the gradual increase in ion concentrations with movement toward the south is a strong indication that GMA 16 has lower average groundwater flow rates and longer residence times than does GMA 14.

Figure 6-18 was created to help illustrate the changes in the average concentration with down-dip distance and depth. The information plotted in Figure 6-18 is from Tables 6-6 through 6-8. Two relationships that are readily apparent is that the concentration trends do not appreciably change with depth for many of the constituents and that the most significant changes in concentration occur near the start or the end of the plotted line segments. The large concentration changes near the start of the line segments are attributed to the transition zone between the Yegua-Jackson Aquifer and the Catahoula Formation. The large concentration changes near the end of the line segments are attributed to the transition into areas influenced by salts from the dissolution of salt domes and brines upwelling in the vicinity of growth faults and salt domes.

6.3.1 Evidence for Salt Domes Contributing to Evaluated TDS Concentrations

Figures 6-9 and 6-10 shows the clustering of high concentration chloride and TDS near several of the salt domes in northern Gulf Coast Aquifer System. This association is depth dependent as TDS and chloride concentrations increase with depth. At the depth interval between 1,000 to 2,000 feet, there are concentration changes of about 1,500 ppm that occur over a few tens of miles. Numerous hydrogeologists (Lindsay(2009), Chowdhury and Turco (2006), Richter and Kreitler (1991), Hamlin (2006); Kreitler and others (1988) have identified the salt domes and salt formations as major source of chloride in the Houston Embayment area (Brazoria, Harris, and Liberty counties). A primary diagnostic for tracing the elevated chloride levels to the salt domes is the chloride-bromide ratios.

Although compounds of chloride are soluble, compounds of bromide are even more soluble. As a result, as water is evaporated, halite will precipitate first, leaving a residual brine enriched in Br. Because Br has large ionic radii, bromide is virtually excluded in the halite lattice. In the specific case of evaporation of sea water, the residual brine after halite precipitation ceases will have a Cl/ Br ratio of about 500, and the first halite to precipitate will have a Cl/Br ratio of about 9000 (McCaffrey and others, 1987). Therefore, halite dissolution provides rapid increases in Cl/Br ratios with increasing Cl concentrations. Moreover, both Cl and Br are conservative elements and do not chemically react with the aquifer materials, such as in ion exchanges or adsorption, retaining the original chemical signatures acquired at recharge. Cl/Br ratios of fresh water in the inland coastal areas are generally less than 500, marine waters have values of about 650, and halite dissolution in excess of 650 reaching up to 40,000 (Davis and others, 1998). For

identifying dissolution of halite as a key source for chloride concentration Davis and others (1998) state that Cl/Br ratio between 1,000 and 10,000 is diagnostic.

Figure 6-14 shows plots of interpolated Cl/Br ratios. Despite the general scarcity of measured values, the plot clearly shows that values of Cl/Br greater than 500 occur in the vicinity of salt domes and that these correlations are greatest at the two lower depths. The increase of high Cl/Br ratios with increasing depth is attributed the fact that many of the salt domes do not extent sufficiently upward to penetrate the Chicot and Evangeline aquifers. Among the interesting aspects of Figure 6-14 is that Cl/Br ratios greater than 500 occur near several salt domes in the up dip areas of GMA 16. Because of a lack of measurement locations with depth, the relationship between salt dome location and high Cl/Br ratios is not well established as a function of depth. The general lack of data has caused the plots of Cl/Br ratio in Figure 6-18 to show somewhat inconsistent results at different depths.

6.3.2 Evidence for Geopressure Zones Contributing to Elevated TDS Concentrations

The initial assumption about any high TDS concentration in these coastal samples is often either intrusion of seawater from the Gulf of Mexico (e.g., Dutton and Richter, 1990) or from inadequate flushing of connate/formation water by meteoric water. However, it is unlikely that present day locations of high TDS values are a result of either sea water intrusion or residual connate water. One of the primary reasons is that the sea level is currently relatively high compared to its location during the last 75,000 years. Except for about the last 12,000 years, the sea level has been about 60 meters (about 200 feet) lower than its current location. Figure 2-8 shows that the sea level has remained relatively stable during the last 7,000 years. But prior to 12,000 years ago, the sea level was about 60 meters (200 feet) lower and prior to 20,000 years ago, sea level was about 120 meters (400 feet) lower. Gerber and others (2010) provide sea level information prior to 20,000 years ago. They show that from 75,000 years ago to about 28,000 years ago, the sea level remained at approximately 50 meters (160 feet) below its current levels, and that during the last 75,000 years the sea level reached its nadir at about 130 meters (420 feet) below current sea levels about 22,000 years ago.

These low ocean level prior to 12,000 years ago and especially 22,000 years ago would have transformed the entire current day Texas Gulf Coast as a recharge zone and would have promoted deep meteoric groundwater flow into areas that are currently under the ocean. As a result, flushing of any connate water and deepening of the meteoric zone would have been much

greater than it is now. This observation has been previously made by Jorgensen (1977). Moreover, both Bourgeois (1997) and Lindsay (2009) conclude that upwelling of geopressured brines is the primary source of the high TDS values along the northern Texas Gulf Coast based on analysis of ion ratios among chloride, bromide, and iodide in brine and seawater.

As previous discussed in this report, the source for the brines located in the geopressure zone (see Figure 6-4) and the primary mechanism for vertical transport of the brines is along salt formations and growth faults that connect the geopressure zone to meteoric zone (see Section 5.7). By performing simple mass balance calculations, Bourgeois (1997) and Lindsay (2009) show that only about 2 to 4% of the brine is needed to mix with the meteoric water to produce the elevated TDS levels observed along the coastline in Brazoria and Matagorda counties.

Although no work similar to Bourgeois (1997) and Lindsay (2009) has been performed in south Texas in the upper Gulf Coast Aquifer System, Kreitler and others (1988) performed similar work in the lower Gulf Coast Aquifer System. Kreitler and others (1988) conclude that deeper Catahoula groundwater predominantly represents original depositional waters that have subsequently dissolved salt domes or been mixed with a high-Br Na-Cl brine. They conclude that vertical migration and leakage from the undercompacted geopressured section has occurred in south and central Texas. They suggest that the pathways through which compactional waters from the geopressure system can reach land surface or the fresh-water section and bypass the brine hydrostatic section is up structural discontinuities such as faults and flanks of salt domes.

Figure 6-18 shows that in north Texas where the salt domes near the coastline are most numerous, significant increases in TDS and chloride concentrations occur near the coastline at all depths, whereas in central and south Texas where the salt domes near the coast are fewest, the increase in TDS and chloride concentration toward the coast is variable with depth. Among the reasons for the lack of evidence in GMA 16 and the lower region of GMA 15 is the TDS of groundwater flowing toward the coast is significantly higher. As a result, an addition of TDS contributed by an up swell of 1% to 4% of brine into the groundwater flow would not be as significant.

6.3.3 Evidence for Significant Difference in Recharge Rates between the Outcrops for the Jackson and the Catahoula Outcrops

In Figure 6-9 there are abrupt changes or discontinuities in the TDS concentration values in GMA 14 and 15 at the line designating the up dip extend of the Catahoula Formation. West of this line, the TDS concentrations at the shallowest depths are typically above 750 mg/L but within a few miles east of the line, the TDS concentrations drop below 250 mg/L. This type of discontinuity in TDS concentrations also occurs at depths between 200 and 500 feet but begins to dissipate at depths greater than 1000 feet.

Based on a review of Figures 6-9, 6-11, and 6-13, the significant reduction in TDS is primarily caused by reduction in SO_4 and Na concentrations. In GMA 14 and 15, the SO_4 concentrations in the upper zone of the Yegua-Jackson Aquifer are typically above 200 mg/L whereas within a few miles into the Catahoula Formation, the SO_4 concentrations drop to values below 50 mg/L and typically less than 25 mg/L. Similarly, the Na concentrations drop from about 200 mg/L to less than 100 mg/L across the transition zone.

The abrupt reduction of TDS, SO_4 , and Na is attributed to a dilution caused by a significant increase in the recharge rate. An additional factor for the reduction of SO_4 may be the precipitation of gypsum (CaSO_4) that is caused by change in chemical conditions that include increases in the availability of Ca caused by the CO_2 saturated infiltrating water mixing with the groundwater. Much of the outcrop of the Catahoula is comprised of deposits with more than 50% sands near the contact with the Jackson Formation (Galloway and others, 1982; LGB Guyton and Intera, 2012). But much of the Jackson outcrop is typically comprised of deposits with less than 20% sands near the contact with the Catahoula (Knox and others, 2007). As a result of these differences, significantly less recharge should occur in the Jackson Formation than in the Catahoula Formation in the northern Gulf Coast Aquifer System where soil where humid and wet conditions often exist. In south Texas where dry and arid conditions are common and recharge is approaching 0.1 inch/yr as a result of climatic conditions, the recharge rates in the Jackson and Catahoula formations are presumed to be similar. Hence, the differences in the TDS, and SO_4 and Na are between the two formations are not visually evident.

In the northern Gulf Coast, where higher recharge occurs in the Catahoula Formation, the presumption is made that the higher recharge rate will raise the redox potential (as measured by the pE) of the groundwater to create enhanced conditions for the precipitation of gypsum. Thus,

as groundwater flows from the Jackson Formation into the Catahoula, the sulfate is reduced by precipitation of gypsum and by dilution caused by recharge fluxes in the Catahoula that are at least comparable to the inflow flux from the Jackson Formation.

6.3.4 Evidence for Recharge Occurring Across most of the Gulf Coast

The concentration of calcium in groundwater is often largely controlled by solution- and gas-phase equilibria that involve carbon dioxide species. In the presence of a gas phase containing CO₂, computations of calcite solubility can be made in terms of the partial pressure of carbon dioxide (p_{CO_2}) and pH. The CO₂ content of normal air is 0.03 percent (by volume), or 0.0003 atmosphere. At 25°C the solubility of Ca is about 20 mg/L. However, the partial pressures of carbon dioxide (p_{CO_2}) in soil air commonly 10-100 times the levels reached in the atmosphere (Bolt and Bruggenwert, 1978). The carbon dioxide content of soil air for the most part results from plant respiration and from decay of dead plant material. Because CO₂ gas is exchanged with groundwater in the soil the soil zone is considered an open system.

Observations and calculations of p_{CO_2} , for in soils commonly give values between $10^{-1.0}$ for and $10^{-2.5}$ for p_{CO_2} (Bolt and Bruggenwert, 1978), in the gas phase, which provide a Ca solubility of between 180 mg/L and 50 mg/L. As discussed in Section 6.1.3, as calcium-rich waters leave the open system in the soil zone and enter the closed system (isolated from air exchange), calcium concentrations decrease for two reasons: the dissolved carbon dioxide concentrations decrease, lowering the solubility of Ca, and on the clay surfaces Ca is exchanged for Na, which causes a corresponding rise in Na.

Because of the reactions between dissolved CO₂ and carbonates, Ca concentrations above 50 mg/L can be used as an indicator for recharge. The value of 50 mg/L is selected, because it is two and an half times the Ca concentration (e.g., 20 mg/L) that would be produced with carbonate rich groundwater in equilibrium with p_{CO_2} concentration in the air. However, Ca concentrations below 50 mg/L do not necessarily indicate that recharge is not occurring because other conditions may limit Ca concentrations. These conditions could occur where, the soil zone is shallow and/ or the soil zone is sufficient saturated that there is limited contact between gas and groundwater, or where recharge is so great that there insufficient opportunity for all of the infiltrating groundwater to equilibrate with the p_{CO_2} in the soil gas.

Figure 6-12 shows that for depths between 0 and 200 feet, the majority of Ca concentrations in GMA 15 and 16 are above 50 mg/L. However in GMA 14, about half of the area, which is

primarily located in the northeast portion of GMA 16, has concentration less than 30 mg/L. The reason for these low concentrations is attributed to high recharge rates and high water tables. Based on a map of depths to water levels in the Gulf Coast Aquifer System (Scanlon and others, 2005) the range for these depths are about 10 to 20 feet for GMA 14, about 20 to 30 feet for GMA 15, and about 30 to 40 feet for GMA 16. As shown in Figure 3-4, the area where the estimated rate of recharge is greater than 2 inches/year correlated extremely well with the area in Figure 6-12 where Ca concentrations are less than 30 mg/L. The high recharge rates and the short unsaturated zone in GMA 16 combine to prevent groundwater from being saturated with sufficient CO₂ generate Ca concentrations above 30 mg/L.

6.4 Hydrochemical Facies and Concentration Contours Along Transects

Numerous hydrogeologists (Chebotarev, 1955; Glynn and Plummer, 2005; Back, 1966; Domenico, 1972; Ophoir and Toth, 1989; Clark and Fritz, 1997) demonstrate that salinity and ion distributions change with distance from the recharge area; with proximity to the sea; and with duration of contact with aquifer minerals or residence time. Another way to view these findings is that potential groundwater flow paths and mixing zones can be identified by changes in groundwater chemistry.

To assist in guiding our interpretation of the chemistry data, we have restricted our evaluation to the chemical data collected on the nineteen transects shown in Figure 1-3. A major presumption in our analysis is that groundwater flow is toward the ocean and parallels the axis of the transect. The purpose of the evaluations is to assess the flow conditions between and within the major units of the Gulf Coast Aquifer System, namely the Chicot Aquifer, the Evangeline Aquifer, the Middle Lagarto, the Jasper Aquifer, and the Catahoula Formation. Among the flow issues of concern are preferential flows, sources of recharge and discharge, zones of mixing, and alignment of flow direction with stratigraphic boundaries.

6.4.1 Factors Affecting the Interpretation of Transect Data

Among the concerns with analyzing chemical data are limitations associated with sampling a small portion of an aquifer system that encompasses a wide range of conditions. In this section, several of the concerns with spatial variability, temporal variability, and sampling bias are identified.

6.4.1.1 Spatial Variability

Based on the information presented in this and previous sections, Table 6-10 was created to summarize the major factors that need to be considered when interpreting our dataset to extract information useful for evaluating the site conceptual groundwater models for the Gulf Coast Aquifer System. Most of these factors have been identified and discussed in this and previous sections of the report.

Table 6-10 Factors that increase spatial variability in an aquifer’s concentration distribution.

Source	Factor	Description	Consequence
Aquifer Condition	Aquifer Hydraulic Heterogeneity	Mixture of sands and clay zones of various length and thicknesses with different hydraulic properties	Lack of a predictable regional migration with flow being controlled by localized flow paths
	Aquifer Mineralogic Heterogeneity	Mixture of sands and clay zones of various lengths and thicknesses with different mineralogies	Different cation capacities and soluble compounds will affect the nature and extent of the evolution of the groundwater chemistry
	Faults	Offsets in the sand deposits partially block horizontal flow	Flow path is convoluted and does not mimic the slope in the hydraulic gradient
	Salt Formations	Salt domes and pillars that penetrate near or into Gulf Coast Aquifer System	Abrupt changes in Na and Cl concentrations and possible enhanced vertical flow
	Geopressure Zones	Depths greater than 4,000 feet where pressure heads are above land	Nonmeteoric water is transported upward to meteoric waters near grow faults & salt domes, or other
	Formation Water	Waters with TDS typically greater than 50,000 ppm	Provides source of high TDS water and older waters that could mix with meteoric water
	Rivers and Lakes	Surface water bodies losing water to the groundwater system	Location where changes in the source term chemistry can change abruptly
	Sea Salt Spray	Marine aerosols carried across coastal areas	Introduces unknown chemical components into precipitation
Anthropogenic Condition	Agriculture and Irrigation	Large scale application of chemicals and/or enhanced recharge	Introduces contaminants to shallow zones different from the ambient condition
	Oil & Gas Surface Pits	Storage of brines in surface pits	Introduces contaminants to shallow zones different from the ambient condition
	Leaking Oil & Gas Wells	Abandoned or older wells provide cross-flow over large vertical distances	Introduces contaminants to deep zones different from the ambient condition
	Pumping	Pumping causes significant vertical or lateral movement of chemicals	Causes mixing of chemicals among flowpaths that would not otherwise mix under pre-development conditions

6.4.1.2 Temporal Variability

The flow patterns deduced from analysis of the chemical data is a result of hydrological conditions that occurred over time scales considerably greater than the time scale over which present-day, or even pre-development water levels were established. For instance, several of the

¹⁴C analyses in Tables 4-3, 4-4, and 4-5 indicate that considerable groundwater in the Gulf Coast Aquifer System is between 20,000 to over 40,000 years old. Yet, as discussed in Sections 2.3 and 6.3.2, the present day shoreline and sea level have existed for less than 7,000 years, and for most of the last 40,000 years, the sea level has been significantly lower than its current level. At about 22,000 years ago the sea level was about 130 meters (420 feet) below current sea level and the shoreline was approximately 80 miles from its present position. Low sea levels prior to 12,000 years ago and especially 22,000 years ago would have transformed the entire current day Texas Gulf Coast into a recharge zone and would have promoted deep meteoric groundwater flow into areas that are currently under the ocean. Besides sea level, another aquifer condition where long-term temporal variability is relevant is climatic conditions. During the last 40,000 years major shifts in the amount and distribution of precipitation and evaporation have occurred (Gerber and others, 2010). These shifts would have likely increased recharge rates by orders of magnitudes in southern Gulf Coast.

6.4.1.3 Sampling Bias

The ability to extract credible and accurate information about three-dimensional flow paths and mixing zones from chemistry data requires accurate and comprehensive three-dimensional concentration data. Accurate data that is sparse does not provide the level of detail required to properly characterize concentration gradients or changes in chemistry that are necessary to delineate flow directions or mixing zones. In addition, if wells are not aligned along the same flow paths, problems in interpretation might occur because of differences in the source terms and ages of the waters. Table 6-11 lists the major sources of sampling bias that are of concern to this project. The purpose of this table is to remind the reader that despite our best efforts with obtaining groundwater samples, sampling bias cannot be avoided and will always introduce variability and uncertainty in our analyses.

6.4.2 Transect Data

In this section, the chemical data from selected transects will be reviewed for evidence of flow paths, sources of recharge, and mixing zones. The analysis will be based on concepts similar to those used to analyze natural gradient tracer tests using environmental tracers. These concepts incorporate the hydrochemical processes summarized by Figure 6-1 that affect the transport of major ions as well as the relationship illustrated in Figure 6-3 among flow regimes, hydrochemical facies, and geochemical processes.

Table 6-11 Sources of Sampling Bias.

Source	Description	Consequence
Non-downgradient alignment	Wells are offset too far vertically or laterally	The sampled wells are a part of different flow paths with different evolutionary chemistry
Large distance between wells	Interwell distances are too large	Important or vital information about the geochemical evolution is not captured
Long Well Screens	Long well screen samples from many different flow paths	Causes artificial mixing in the vertical
Leaky Well Annulus	Wells intercepts groundwater above the screen interval via a leaky annulus	Causes artificial mixing in the vertical
Collection or Analytical Error	Sampling and analysis error	Introduces error and biases into the measured concentrations
Unrepresentative Location	Sample location does not sample water characteristic of regional flow system	Measured concentrations have a bias caused by natural variability that is an outlier from regional trend

For each GMA, the chemical concentrations and the hydrochemical facies will be plotted and analyzed for two transects. For GMA 14, the two transects are 3 and 34. For GMA 15, the two transects are 5 and 56. For GMA 16, the two transects are 8 and 89. Figure 1-3 shows the location of these six transects. The three ion concentrations that will be analyzed include Cl, Ca, and Na. These ions were selected because: 1) they are key participants in the chemical evolution of groundwater described by Chebotarev (1955) and Domenico (1972); 2) they are used to define hydrochemical facies (Back, 1966); 3) they typically occur in groundwater across a wide concentration range; and, 4) the geochemical reactions that control their transport in groundwater systems are well known. Listed below are some important attributes and properties associated with Cl, Na, and Ca.

Chloride (Cl) - Chloride is considered one of the most ideal tracers because of its relatively inertness. For instance, Kaufman and Orlob (1956) found that chloride ions moved with the water through most soils tested with less retardation or loss than any of the other tracers tested, including tritium that had actually been incorporated into the water molecules. Chloride is the least common major ion present in the earth's crust. Chloride concentrations in sandstones, shales, and carbonates is about 15 ppm, 170 ppm, and 305 ppm, respectively (Hem, 1985). Despite its relatively low abundance, Cl is often present in groundwater systems because Cl does not form salts of low solubility, is not significantly adsorbed on mineral surfaces, and participates in only a few vital biochemical roles. Near the Texas coast, rain water can contain appreciable chlorides, but these amounts typically decreases rapidly in a landward direction. Except for about a

5-mile buffer around the coastline, the chloride concentration in precipitation is expected to average between 3 mg/L and 0.5 mg/L across the Gulf Coast Aquifer System (see Figure 6-2). Based on information in Section 6.2, Cl is the most prevalent ion in seawater (~19,000 mg/L) and in formation water in the Catahoula (~40,000 mg/L).

Calcium (Ca) - The most common forms of calcium in sedimentary rock are carbonates. The two crystalline forms, calcite and aragonite, both have the formula CaCO_3 , and the mineral dolomite can be represented as $\text{CaMg}(\text{CO}_3)_2$. Limestone consists mostly of calcite with mixtures of magnesium carbonate and other impurities. Besides carbonates, calcium also complexes with sulfate to form gypsum. Gypsum is a common mineral, with thick and extensive evaporite beds in association with sedimentary rocks. In sandstone and other detrital rocks, calcium carbonate commonly is present as a cement between particles or a partial filling of interstices. As discussed in Section 6.3.4, Ca concentrations above 50 mg/L can be used as an indicator for recharge except for the northeast area of GMA 16. In the northeast area of GMA 16, high recharge rates and high water tables prevent Ca from reaching concentrations above 50 mg/L in the soil zone and/or shallow saturated zone. As the calcium rich waters level the soil zone which is an open system and exposed or high levels of gaseous CO_2 and enters into the saturated groundwater system, which is isolated from gas exchange, calcium concentrations usually decrease for two reasons: the dissolved carbon dioxide concentrations decrease lowering the solubility of Ca, and on the clay surfaces, Ca is exchanged for Na, which causes a corresponding rise in Na.

Sodium (Na) - In sandstones, sodium may be present in unaltered mineral grains, as an impurity in the cementing material, or as crystals of readily soluble sodium salts. In sandstones, Na is typically present as adsorbed ions on mineral surfaces, especially by minerals having high cation-exchange capacities such as clays. However, Na has a much weaker interaction with clays than do divalent ions such as Ca. As such, in freshwater systems Ca often replaces sodium on clays, which leads to gradual increases in Na concentration in groundwater along the chemical evolution of a flow path. After sodium has been brought into solution, it tends to remain in solution because there are no precipitation reactions that can maintain low Na concentrations in water, in the way that carbonate precipitation controls calcium concentrations. As discussed in Section 6.2, Na is the most prevalent cation in seawater (~10,800 mg/L) and in formation water in the

Catahoula (~20,000 mg/L). In both seawater and formation water (or brines), the molar ratio for Na/Cl is about 1.0.

The important points regarding using Cl, Ca, Na, and hydrochemical facies with regard to evaluating the chemical data for evidence of flow paths, mixing zones, and ages are:

1. Cl is a conservative tracer that has minimal interaction with the soil. Abrupt increases in Cl concentrations over short distances indicate a localized source of Cl such as salt domes, upswelling of formation water from the geopressure zone, contamination from former surface pits, or salt water intrusion.
2. Calcium will be used as a non-conservative tracer by inferring that the direction of groundwater movement is aligned with decreasing calcium concentrations. Ca concentrations of about 50 mg/L near the groundwater surface or more will be used to designate recharge zones except for the northeast portion of the Gulf Coast Aquifer System where recharge rates are greater than 2 inches/yr based on Figure 3-4.
3. Na will be used as a non-conservative tracer by inferring that the direction of groundwater flow is aligned with increasing sodium concentration as a result of continued ion exchange reactions with Ca. Abrupt increases in Na concentrations over short distances indicate a localized source of Cl such as salt domes, upswelling of formation water from the geopressure zone, contamination from former surface pits, or salt water intrusion.

The concentration data for a transect will be shown on a vertical cross-section that shows the geologic formations. The placement of the measurement from a well will be located using the down-dip location of the well as the x-axis and the depth of the well as the y-axis. The concentration measurement will be plotted as a line with a vertical length of 10 feet and a color code that determines its concentration.

6.4.2.1 GMA 14

Figures 6-19 through 6-26 show Cl, Ca, and Na concentration maps and hydrochemical facies maps for Transects 3 and Transect 34. Figure 6-27 shows the hydrochemical facies map for Transect 23. Within the footprint of the Gulf Coast Aquifer System, the transition sequence between the hydrochemical facies is consistent with the findings of Chebotarev (1955), the facies progression shown in Figure 6-3, and observations by Back (1966). Across the outcrop of the

Gulf Coast Aquifer System near Walker County, the Ca-HCO₃ facies in Figure 6-22 occurs near ground surface. With increases in distance down dip and with depth, the Ca-HCO₃ facies transitions into Ca-Na-HCO₃ facies, which transitions into Na-HCO₃ facies, which transitions into Na-Cl facies. These transition sequences indicate that groundwater flow paths are beginning in Walker and Montgomery counties and traveling toward coast along the directions shown by the arrows in Figure 6-22. The hydrochemical facies sequences and locations in Transect 34 (Figure 6-26) and Transect 23 (Figure 6-27) are consistent and generally agree with the hydrochemical facies shown for Transect 3 with several exceptions. These exceptions are primarily the occurrence of a chloride dominant hydrogeochemical facies that is out of sequence. For Transect 23 shown in Figure 6-27, the two areas where Na-Cl facies are abundance are near Polk and Chambers counties. The occurrence of Na-Cl is primarily attributed to the dissolution of halite from salt domes.

As should be expected, the concentration maps indicate groundwater flow paths similar to those inferred from the hydrochemical facies map. Figures 6-20 and 6-24 show that the Ca concentrations near the surface are greater than 50 mg/L which indicates that recharge is occurring along most of Transects 3 and 34. For Transect 3, a large portion of the transect has Ca concentrations greater than 50 mg/L near the surface. A notable area where Ca concentrations are below 20 mg/L is at distances 30 to 40 miles down dip. This area is near the toe of Lake Conroe. Near Lake Conroe recharge rates should be higher than the surrounding area. Given that recharge is high near and beneath Lake Conroe because the lake is a constant recharge source, the low Ca concentrations are attributed to the lack of a well-developed soil zone in the vicinity of Lake Conroe. The lack of an aerated soil zone prevents the groundwater from being saturated with sufficient concentrations of CO₂ to generate Ca concentrations above 30 mg/L.

In Transect 34, the Ca concentration (Figure 6-24) shows three zones where fingering and significant offsets occur in the “50 to 200 mg/L” category. Groundwater flow may be occurring within these zones at slightly different rates or that vertical mixing is minimal between the zones. The most pronounced offset occurs for about 30 miles along the base of Willis and Upper Goliad formations. A similar offset occurs in Transect 3 in the Ca “50 to 200 mg/L” concentration category for a about 15 miles along the base of the Willis. The offset in Ca contours between the Willis and Upper Goliad in Transect 3 is better defined by the Na contours, which show an offset

of about 30 miles. In fact, the Na concentrations indicate that groundwater is moving at a faster rate in the Willis and Lissie than in the Upper Goliad below and the Beaumont above. Along Transect 3, additional fingering of a Na front (see Figure 6-21) also appears evident in the Lower Lagarto (Upper Jasper) compared to the Middle Lagarto. This possible zone of higher groundwater flow rate is also mapped by the chloride concentration.

The inferred flow arrows for Transects 3 and 34 generally support down-dip flow at angles similar to the dip of the geologic formations to depths greater than 1,000 feet. Inference of flow directions at depths greater than 1,000 feet is hindered by a lack of data. Based on the limited data within 10 to 20 miles of the coast, the groundwater flow appears to be slightly downward or horizontal. There is no compelling evidence to indicate that the bulk groundwater flow is upward toward the ocean. However, a potential issue of some importance associated with the hydrochemical facies and the concentration Cl contours is the source of chloride near the coast. Near the coast, as well as locations near salt domes, the elevated concentrations of Cl are correlated with high Na concentrations. Previous discussion has demonstrated that a source of chloride and sodium along the coastal counties are an upward migration of brines along growth faults and salt domes and dissolution of salt domes.

Figure 6-28 shows that with the ratios of Na/Cl for Transects 3 & 34 are dependent on the chloride concentration. For chloride values less than 400 ppm, the Na/Cl ratio averages 3.0. For chloride values greater than 400 ppm, the Na/Cl ratio averages 1.2. The change in the Na/Cl ratios at high chloride concentrations suggests that a chloride source may be contributing to the higher Cl values. In the vicinity of Transect 3 & 34, seawater, salt domes, and deep formation water (brines) could be the Cl source. For pure salt, seawater (Table 6-3), and brine (Table 6-4), the Na/Cl ratios are 0.65, 0.86, and 0.95, respectively. Thus, all three of these sources are potential candidates based on the Na/Cl ratios.

If seawater were the primary source of for the increase in Cl concentrations, about 3% mixing ratio of meteoric water and sea water would be needed to increase Cl concentration from about 500 to over 1,000 ppm. This 3% mixture would raise the SO₄ concentration (per values in Table 6-2) by 81 ppm. As shown in Figure 6-24, SO₄ concentration does not increase with increases in Cl concentration above 1,000 ppm for Transects 3 and 34 and about 95% of the samples with Cl concentrations above 1,000 ppm that have SO₄ concentrations below 80 ppm. A similar calculation for brines shows that the amount of mixing would be about 1.25% and the

increase in SO_4 concentrations would be less than 1 ppm. After consideration of the measured SO_4 concentrations, the primary source of high Cl and Na concentrations near the coast is not sea water but is the dissolution from salt domes and/or upward migration of brines along growth faults and salt domes and dissolution of salt domes.

6.4.2.2 GMA 15

Figures 6-29 through 6-37 show Cl, Ca, and Na concentration maps and hydrochemical facies maps for Transects 5 and Transect 56. Figure 6-29 shows the hydrochemical facies map for Transect 4. Within the footprint of the Gulf Coast Aquifer System, the transition sequence between the hydrochemical facies is generally consistent with the findings of Chebotarev (1955), the facies progression shown in Figure 6-3, and observations by Back (1966). For Transect 5 (see Figure 6-32) the Chebotarev progression occurs for the Evangeline and the Chicot Aquifers. Across the outcrop of the Evangeline aquifer in Lavaca County, the Ca-HCO_3 facies occurs near ground surface at the outcrop of Gulf Coast Aquifer System. With increases in down-dip distance or in depth from the outcrop, the Ca-HCO_3 facies transitions into Ca-Na-HCO_3 facies. The hydrochemical facies sequences associated with Transects 56 and 4 are consistent with the Transect 5 sequences with two differences. One difference is that both Transects 56 and 4 have a large area where Na-Cl facies dominate near the coast. Another difference is the absence of Ca-HCO_3 facies in Transect 56 (see Figure 6-36), which is more of a result of a relatively high sodium concentration than of relatively low calcium concentrations.

The absence of a Ca-HCO_3 in Transect 56 in the outcrop also occurs for all of the Transects in GMA 16. Thus, the Ca-HCO_3 is prevalent in GMA 14, is absent in GMA 16, is sometimes present in the northern regions of GMA 15. This set of results is attributed to the decrease in the recharge rates from the northeast to the southwest. In the area of high recharge rates, the recharge provides sufficient flushing to prevent the build of high sodium concentrations near the water level – thus, allowing the Ca ions from the dissolution of carbonates to dominate. In the areas of low recharge rates, the Na concentrations build up as a result of the high evaporation rates. South of Transect 56, the Na concentrations are high enough to prevent the occurrence of Ca facies.

As expected, the concentration maps indicate groundwater flow paths similar to those inferred from the hydrochemical facies map. Figure 6-30 shows Ca concentrations greater than 50 mg/L occur across most of the Gulf Coast Aquifer System outcrop in Transect 5. A region in the

middle of Jackson County where Ca concentrations are less than 50 mg/L may be caused by high water levels near Lake Texana (see discussion above concerning high water levels near Lake Conroe). These high Ca concentrations suggest that recharge is prevalent and occurring along most of Transect 5.

The inferred groundwater flow directions from Transects 5, 56, and 4 suggest horizontal flow toward the coast with some preferential fingering along geological formations. For Transect 56, the Ca concentration (see Figure 6-34) suggests preferential flow near the base of the Lissie and the Upper Goliad – an observation that is supported by the pattern in the Na concentration maps (see Figure 6-35). In Transect 5, the Ca and Na data (see Figures 6-30 and 6-31) suggest that there has been deeper penetration of high Ca and Na concentrations in the Evangeline Aquifer than in the Jasper Aquifer. This deeper penetration may be an indicator of the vertical rate of groundwater migration. However, this speculation is difficult to further substantiate because of the scarcity of data for the deeper regions of the Middle Lagato and Jasper Aquifer and the large spatial variability in the concentration measurements.

One of the most difficult portions of the transects to evaluate is near the coast where the spatial variability among the concentration measurements is the greatest. Near the coast, there are instances where Cl concentrations less than 50 mg/L are within a few miles of values greater than 500 mg/L in Transect 56 and where Cl concentration values greater than 1,000 mg/L are within a few miles of values less than 100 mg/L. Similar examples of large concentrations are evident in the Na concentration maps. As was the case in GMA 14, the high values of chloride and sodium appear to be correlated.

Figure 6-28 shows that the ratios of Na/Cl for Transects 5 & 56 are dependent on the chloride concentration. For chloride values less than 1000 ppm, the Na/Cl ratio averages 1.9. For chloride values greater than 1000 ppm, the Na/Cl ratio averages 0.94. The change in the Na/Cl at high chloride concentrations suggests that the source for the high chloride concentrations is contributing a solution that has a Na/Cl ratio that is less than 1.9. In the vicinity of Transects 5 and 56, seawater and deep formation water (brines) could be the Cl source. For seawater (Table 6-3) and brine (Table 6-4), the Na/Cl ratios are 0.86, and 0.93. Thus, both of these sources are potential candidates based on the Na/Cl ratios.

If seawater were the primary for the increase in Cl concentrations, about a 3% mixing ratio of meteoric water and sea water would be needed to increase Cl concentration from about 500 ppm

to over 1,000 ppm. This 3% mixture would be expected to raise the SO₄ concentration (per values in Table 6-2) by 81 ppm. As shown in Figure 6-28, SO₄ concentrations do not increase with the increase in Cl concentrations above 1,000 ppm and approximately 50% of the groundwater samples with Cl concentrations above 1,000 ppm that have SO₄ concentrations below 80 ppm. A similar calculation for brines shows that the amount of mixing would be about 1.25% and the increase in SO₄ concentrations would be about 1 ppm. After consideration of the measured SO₄ concentrations, the primary source of high Cl and Na concentrations, with the source of high chloride values in Transect 5 and 56, is the dissolution from salt domes and/or upward migration of brines along growth faults and salt domes and dissolution of salt domes.

6.4.2.3 GMA 16

Figures 6-38 through 6-45 show Cl, Ca, and Na concentration maps and hydrochemical facies maps for Transects 8 and Transect 910. Figure 6-46 shows the hydrochemical facies map for Transect 89. The facies maps consist primarily of Na-Cl and Na-Cl-HCO₃ facies. The low recharge rates and the high evaporation rates have contributed to a buildup of Na and Cl concentrations near the surface which prevents the Ca facies from occurring. The lack of an evolving series of facies hinders the ability to infer flow directions.

For Transect 8, the high Ca concentrations (see Figure 6-39) in Duval and Jim Wells suggest recharge is occurring across these counties. The majority of the concentrations are in the Upper Goliad and within a few hundred feet of the Chicot Aquifer. The pattern in the well placement suggest that drillers are detecting a significant improvement in either water quality or production after they drill through the Chicot Aquifer and then intersect the Evangeline Aquifer. This apparent flow zone is supported by the trend in Na (see Figure 6-40) and Ca concentration data. The Ca concentration profile includes an updip zone of 50 to 200 mg/L, a mid-dip zone of 20 to 50 mg/L, and a down-dip zone of <20 mg/L. The Cl concentration profile includes updip and down-dip zones of 200 to 1,000 mg/L with a lower mid-dip zone of 50 to 200 mg/L. The anomalous result for the Cl profile is attributed to a shallow salt dome (see Figure 4-8, 6-10, and 6-14) near the updip zone. This impact of the salt dome on water quality is not readily apparent in Figures 6-10 and 6-14. The lack of a “bump” of higher concentrations of Cl and Na near the salt dome is attributed to the relatively high background values for these ions in south Texas and the averaging process associated with the kriging interpolation routine has smoothed out the few high measurements of Na and Cl that do exist near the salt dome.

Figure 6-28 shows that with the ratio of Na/Cl for Transects 8 and 910 are correlated to chloride concentration. For chloride values less than 1,000 ppm, the Na/Cl ratio averages 1.8. For chloride values greater than 1,000 ppm, the Na/Cl ratio averages 0.90. The change in the Na/Cl at high chloride concentrations suggests that a chloride source may be contributing to the higher Cl values. In the vicinity of Transects 8 and 910, salt domes, seawater and deep formation water (brines) could be the Cl source. For salt, seawater (Table 6-3) and brine (Table 6-4), the Na/Cl ratios are 0.65, 0.86, and 0.93. Thus, these three sources are potential candidates based on the Na/Cl ratios.

If seawater were the primary source for the increase in Cl concentrations, about 3% mixing ratio of meteoric water and sea water would be needed to increase Cl concentration from about 500 ppm to over 1,000 ppm. This 3% mixture would be expected to raise the SO₄ concentration (per values in Table 6-2) by 81 ppm. As shown in Figure 6-28 there are no discernable trends in SO₄ concentrations above chloride concentrations of about 400 ppm. A similar calculation for brines shows that the amount of mixing would be about 1.25% and the increase in SO₄ concentrations would be about 1 ppm. After consideration of the measured SO₄ concentrations, the primary source of high Cl and Na concentrations, with the source of high chloride values in Transect 8 and 910, is the dissolution from salt domes and/or upward migration of brines along growth faults and salt domes and dissolution of salt domes.

6.4.3 Implication of the Transect Data to Mixing, Flow Paths, and Age from the Transect Data

Maps showing hydrochemical facies and Ca, Na, and Cl concentrations exhibit significant spatial variability. The primary reason attributed to the variability is natural variability in the aquifer system, anthropogenic impacts, and sampling bias. Nearly order-of-magnitude oscillations and fluctuations in concentration are not uncommon over the scale of five to 10 miles. Sometimes the source for the variability could be attributed to a nearby salt dome or to infiltrating surface waters, but most often, the cause of the variation was not identified. Despite the variability in the data, large-scale trends and patterns in the concentration data could be identified by drawing zones of concentration whose values were based on the most dominant data in the zone. By simultaneously analyzing the concentration and the hydrochemical facies maps, information on a groundwater flow system can be inferred.

The maps of the Ca concentrations data suggest that recharge is occurring over most of the Gulf Coast Aquifer System. Recharge locations were mapped based on Ca concentrations over 50 mg/L. Primarily because of a lack of measurements in shallow wells, recharge could not be confirmed within about 10 miles of the coastline in most of the transect data.

For all transects, groundwater flow paths were inferred from transition sequences in hydrochemical facies, by decreases in Ca concentrations, and by increases in Na and/or Cl concentrations. All of the transects suggest groundwater flow paths were toward the coast with a vertical component that approximates the dip angle of the geologic formations. Within an aquifer such as the Chicot or Evangeline, vertical variation in facies and/or concentrations are identifiable at lengths much shorter than the thickness of the aquifer. Sometimes the interval of similar concentrations could be associated with one or more geological formations. Several of the transects clearly provided evidence of preferential flow within a geologic formation. In GMA 14, the Na and Ca concentration data from Transect 3 shows preferential groundwater movement in the Lissie and Willis formations compared to the overlying Beaumont Formation and the underlying Upper Lagarto Formation. In GMA 15, Na and Ca concentration data from Transect 56 suggests preferential groundwater movement in the Lissie and the Upper Goliad. In GMA 16, the bicarbonate facies and the Ca concentration data suggests preferential flow in the Upper Goliad.

For GMA 14, 15, and 16 the transect data illustrated both single and groups of measurements where significant increases in Cl and Na occurred over short distances. Using relationships involving Cl/Br ratios, Na/Cl ratios versus Cl concentrations, and SO₄ concentrations versus Cl concentrations, the transects show that dissolution of salt domes and upwelling of brines is responsible for most of the Cl concentrations above 1,000 mg/L.

Although not discussed as part of the GMA transect data, the concentration and hydrofacies data for the Yegua-Jackson Aquifer is often very different from the data for the Catahoula Aquifer in GMA 15 and 16. For instance, although there are Na-SO₄ facies in the Jackson outcrop, these facies do not extend into the Catahoula Formation but instead are replaced by Ca-HCO₃ facies. This abrupt transition has been noted in Section 6.3.3 and is interpreted as an indicator of significantly higher recharge in the Catahoula than in the Yegua-Jackson.

6.5 Brazos River Alluvium

Within GMA 14, the Brazos River Alluvium contains the Brazos River in Washington, Grimes, Austin, Waller and Fort Bend counties (see Figure 1-1). Wells were considered to sample groundwater from the Brazos River Alluvium if the bottom of the well was above the base of the alluvium as defined by Shah and others (2007). Wells were considered to sample groundwater from the aquifer below the Brazos River Alluvium if the bottom of the well was more than 20 feet below the base of the Brazos River Alluvium as defined by Shah and others (2007).

After the wells were assigned as either in the Brazos Alluvium or surrounding the Brazos Alluvium, the major ion concentrations and ratios of major ions were reviewed. The Ca and Mg ions (see Figure 6-47) have the greatest concentration differences between the Brazos River Alluvium and the Gulf Coast Aquifer System deposits. The spatial distribution of the ratios of these two ions and each ion's concentrations is shown in Figures 6-47 to 6-49. Figure 6-48 shows that groundwater in the Brazos River Alluvium is consistently higher in calcium than is groundwater in the adjacent aquifers. Whereas the Ca concentrations in the Brazos River Alluvium is consistently between 100 and 200 mg/L, the Ca concentrations in the adjacent aquifers is consistently lower and typically between 50 and 100 mg/L. This type of water difference and a slight enrichment in the $\delta^2\text{H}$ and $\delta^{18}\text{O}$ are the reasons that Chowdhury and others (2010) conclude:

“Groundwater from the Queen City, Sparta, and Evangeline aquifers near the lakes has more depleted isotopes and a sodium-bicarbonate composition that differentiates it from the more enriched isotope and calcium-sodium-bicarbonate composition of groundwater from the Brazos River Alluvium Aquifer. These differences in chemical and isotopic compositions suggest that there may not be any significant upward discharges from the Queen City, Sparta, and Evangeline aquifers into the Brazos River Alluvium Aquifer and the Brazos River. (pg. 1)”

Based on our interpretation of the data, neither the chemical nor the isotopic composition of the groundwater indicates whether or not significant upward, downward, or lateral discharges from the Gulf Coast Aquifer System occurs into the Brazos River Alluvium. Our analysis also suggests that the geochemical data does not provide sufficient lines of evidence to estimate the relative magnitude of inflows into the Brazos River Alluvium Aquifer from adjacent aquifers. Our analyses is inconclusive because the primary reason for the difference in water quality

characteristics of the Brazos River Alluvium appears to be because of differences in soil and microbial conditions cause the CO₂ partial pressures to be slightly higher in the alluvium than CO₂ partial pressures in the adjacent aquifers. As discussed previously, higher CO₂ partial pressures will produce higher Ca concentrations in the infiltrating water that are responsible for the shifts from the predominant Na-HCO₃ facies in the aquifers to the Ca-Na-HCO₃ facies in the alluvium.

Chowdhury and others (2010) provide results of isotopic analysis for eight wells in the Brazos River Alluvium and they report that the “Brazos River Alluvium Aquifer has more depleted isotopic values than the river and lake water, with δ²H and δ¹⁸O values that range from -34 to -29‰ and -5.2 to -4.5‰, respectively,” (pg. 46). Four of the wells in the Brazos River Alluvium are located in GMA 14 and their isotopic values are shown in Table 6-12. In addition, Table 6-12 presents the isotopic values for the two Gulf Coast Aquifer System wells that are presented by Chowdhury and others (2010). The set of values for the Brazos River Alluvium and the Evangeline Aquifer are similar and cannot be shown to be from different populations using conventional statistical tests. Thus, for the Gulf Coast Aquifer System section of the Brazos River Alluvium the isotopic data does not suggest whether significant upward discharge occurs from the Queen City, Sparta, and Evangeline aquifers into the Brazos River Alluvium Aquifer and the Brazos River.

Table 6-12 Stable Isotope concentration for the wells in the Brazos River Alluvium and the Evangeline Aquifer (from Chowdhury and others, 2012).

Sample Type	State Well Number	County	δ ² H‰	δ ¹⁸ O‰
Brazos River Alluvium	66-08-702	Waller	-30	-4.6
	66-08-703	Waller	-32	-4.8
	66-08-111	Waller	-31	-4.8
	59-63-802	Austin	-30	-4.6
	<i>Average</i>	-	<i>-30.75</i>	<i>-4.7</i>
Evangeline Aquifer	66-08-103	Waller	-31	-4.8
	59-64-701	Austin	-30	-4.9
	<i>Average</i>	-	<i>-30.5</i>	<i>-4.85</i>

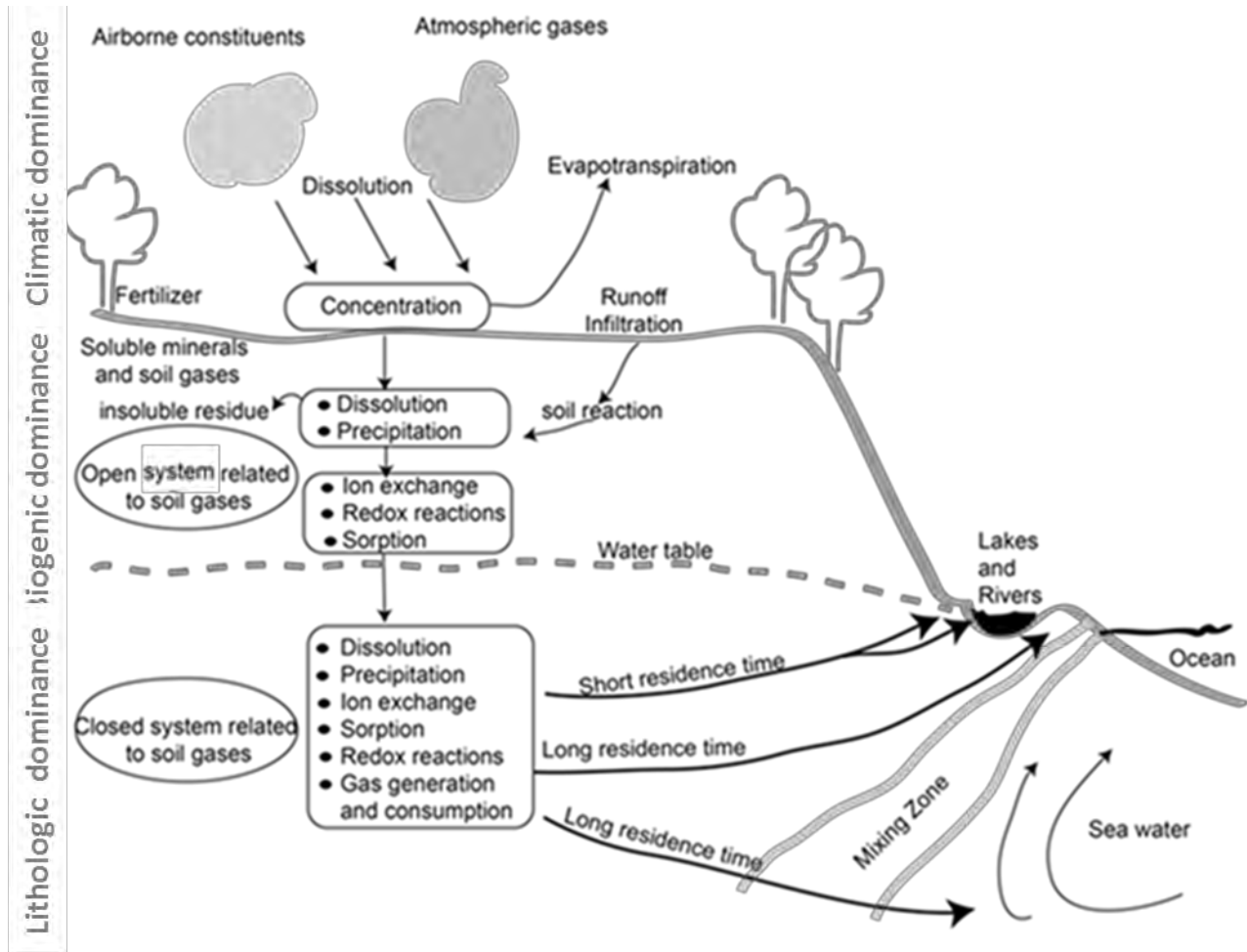


Figure 6-1 Conceptualized groundwater flow system incorporating hydrochemical processes that affect reactions and transport involving major ions (modified after Back and others, 1983; Herczeg and Edmunds, 2000). The distinction between an open and closed system is based on whether the aquifer is connected to atmospheric gases such as CO₂ and O₂.

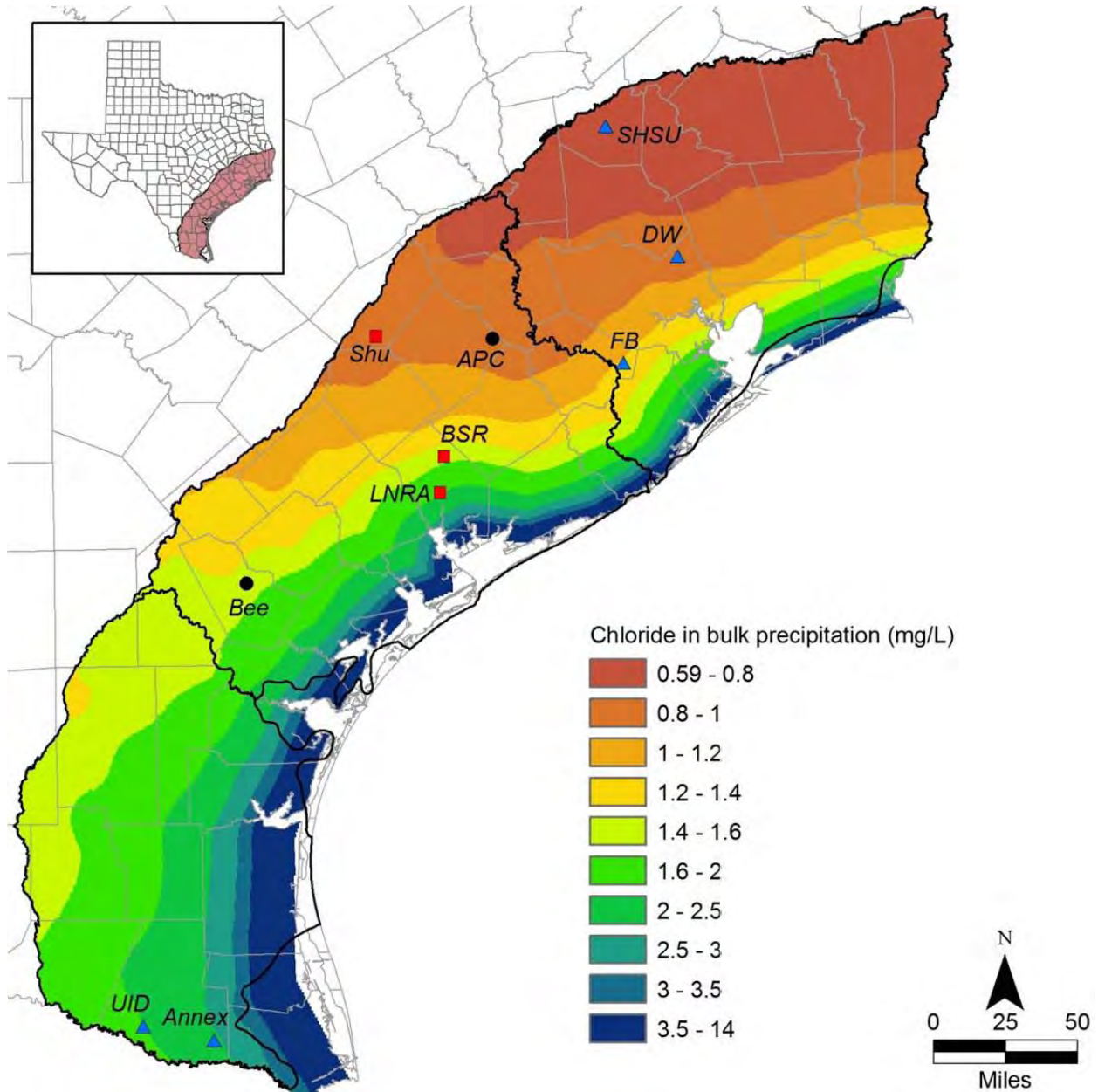


Figure 6-2 Estimated distribution of mean annual chloride concentrations in bulk precipitation in the study area based on mass deposition and the distribution of mean annual precipitation. Wet chloride deposition from NADP was multiplied by two to account for dry deposition. Points represent locations of open (bulk) precipitation collectors at the NADP sites (circles), and at sites hosted by the Lavaca-Navidad River Authority (LNRA, squares) and by the TexasET Network (Texas A&M University, triangles) (from Scanlon and others, 2012).

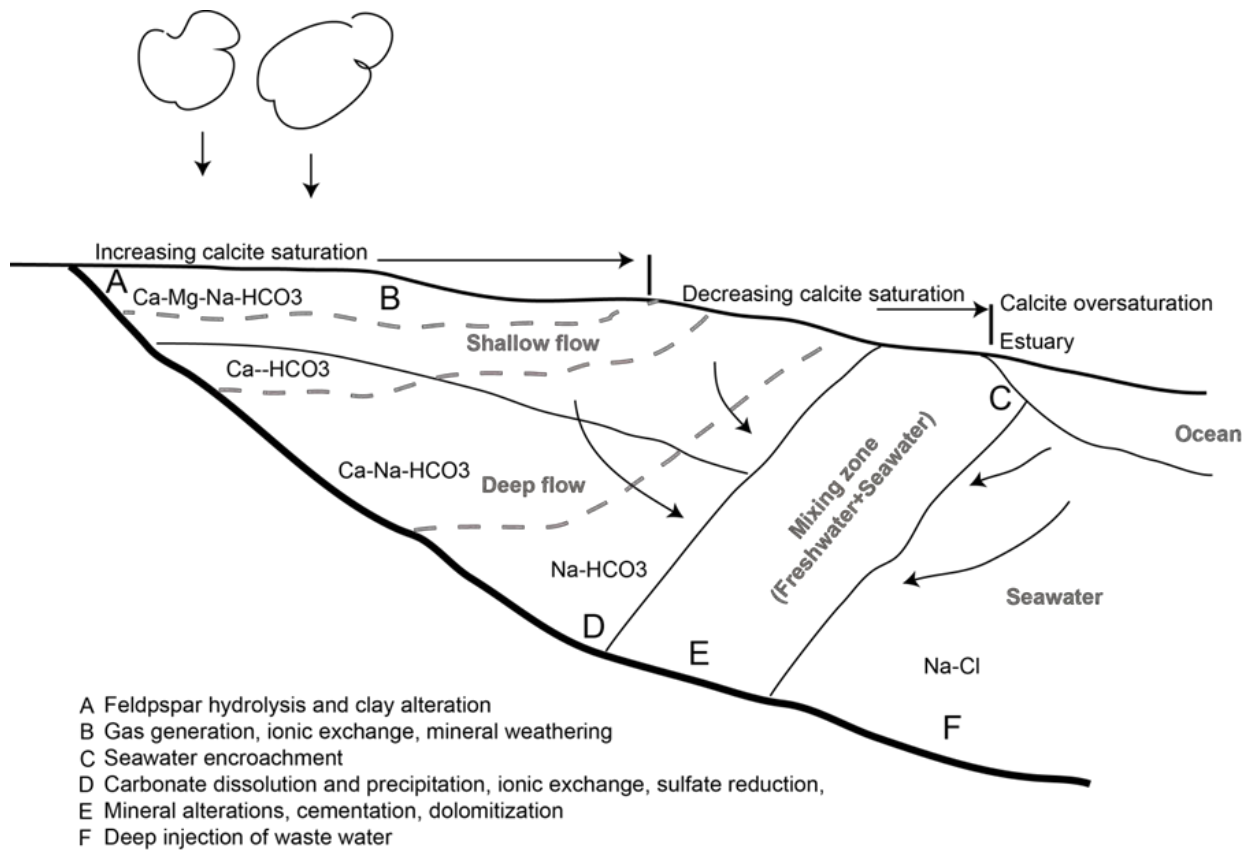


Figure 6-3 Relationship between flow regimes, hydrochemical facies, and geochemical processes in a coastal aquifer (modified after Back, 1966 and Custodio, 1987)

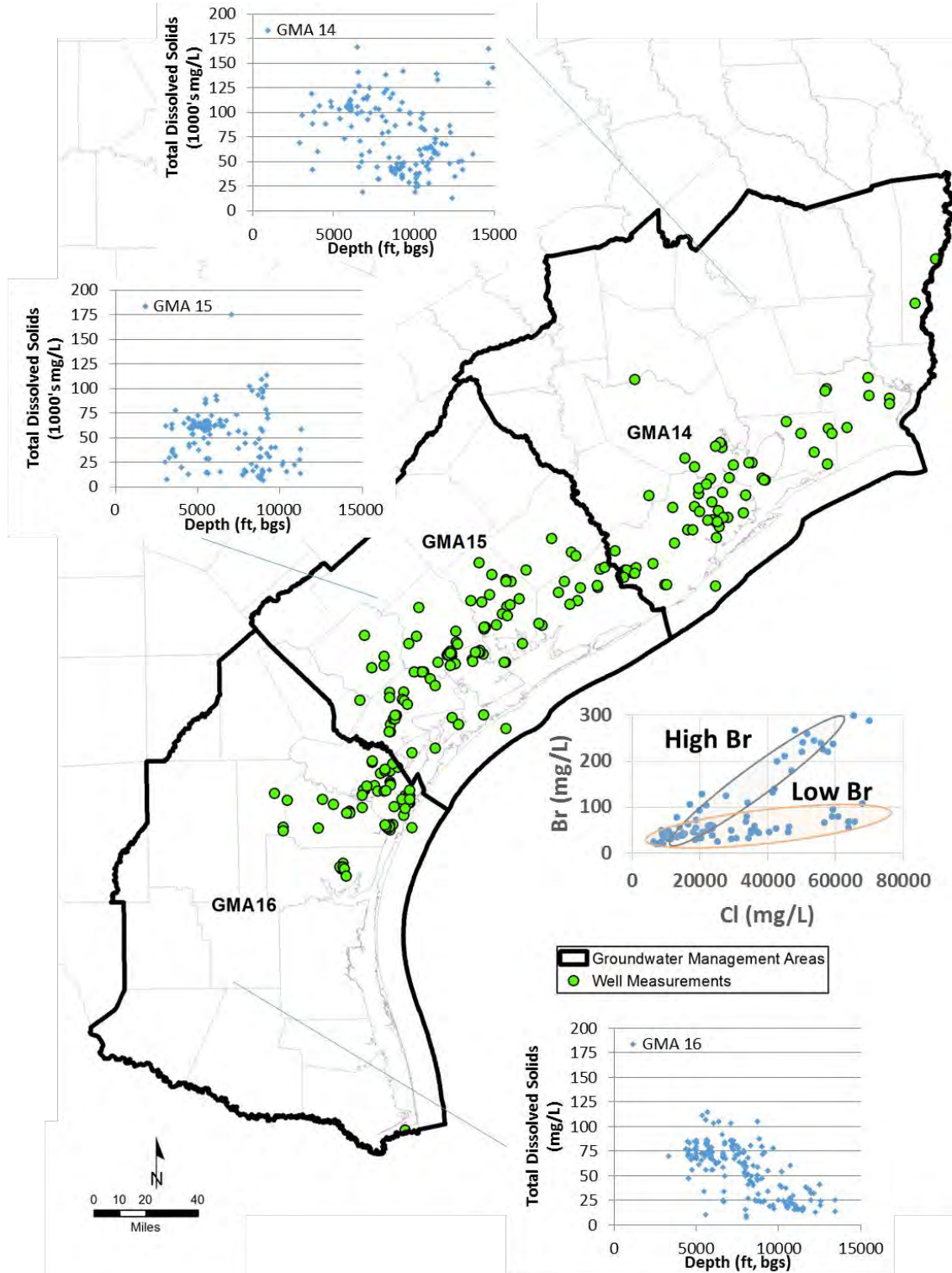


Figure 6-4 Measured Total Dissolved Solids concentration in the Catahoula Formation for GMA 14, GMA 15, and GMA 16 and a bivariate plot of bromide concentrations versus chloride concentrations for groundwater samples from the Catahoula Formation. (Note that bgs stands for below ground surface).

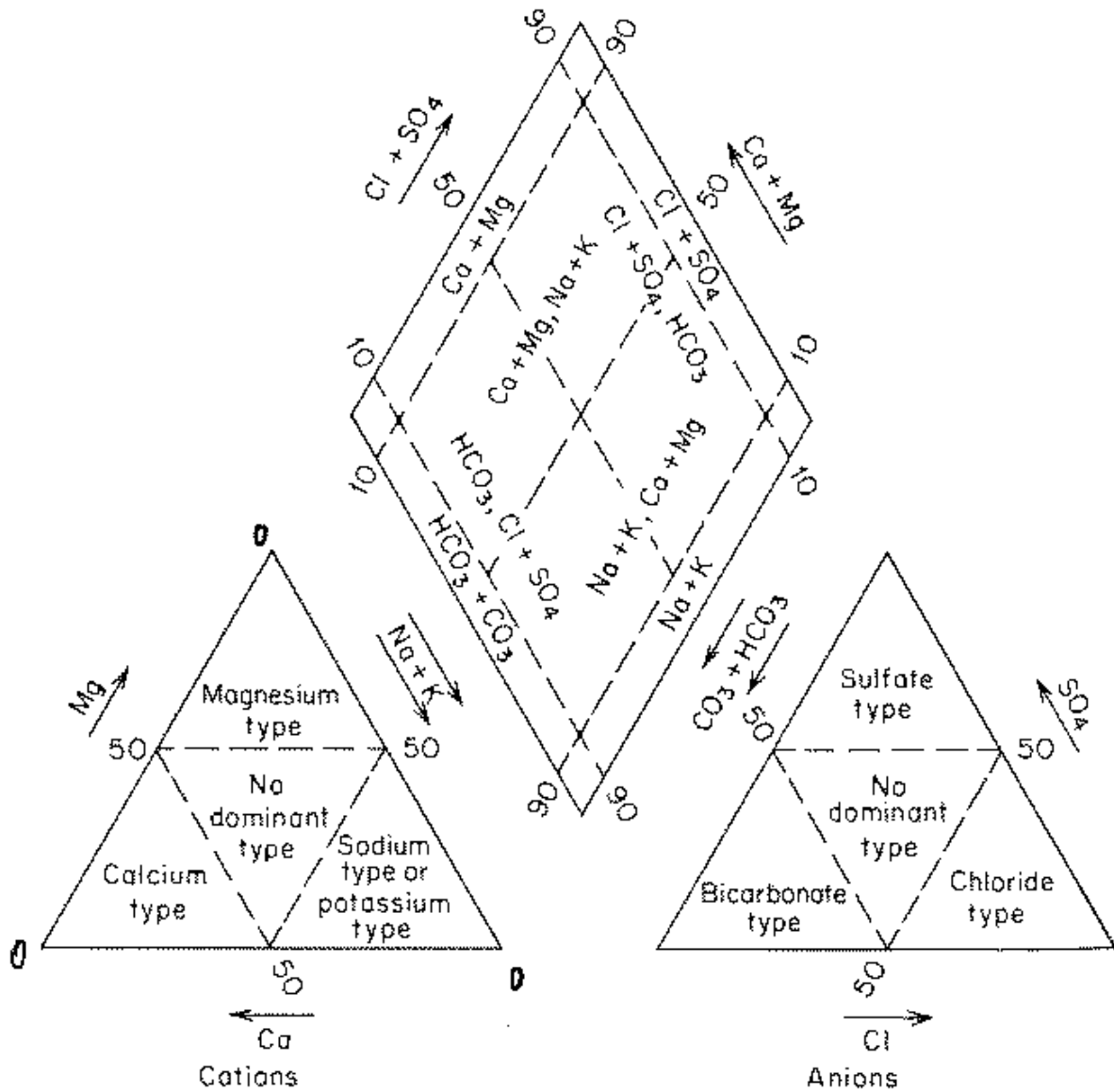


Figure 6-5 Classification diagram for anion and cation facies in terms of major-ion percentages. Water types are designated according to the domain in which they occur on the diagram segments (after Morgan and Winner, 1962; Back, 1966) (from Freeze and Cherry, 1979).

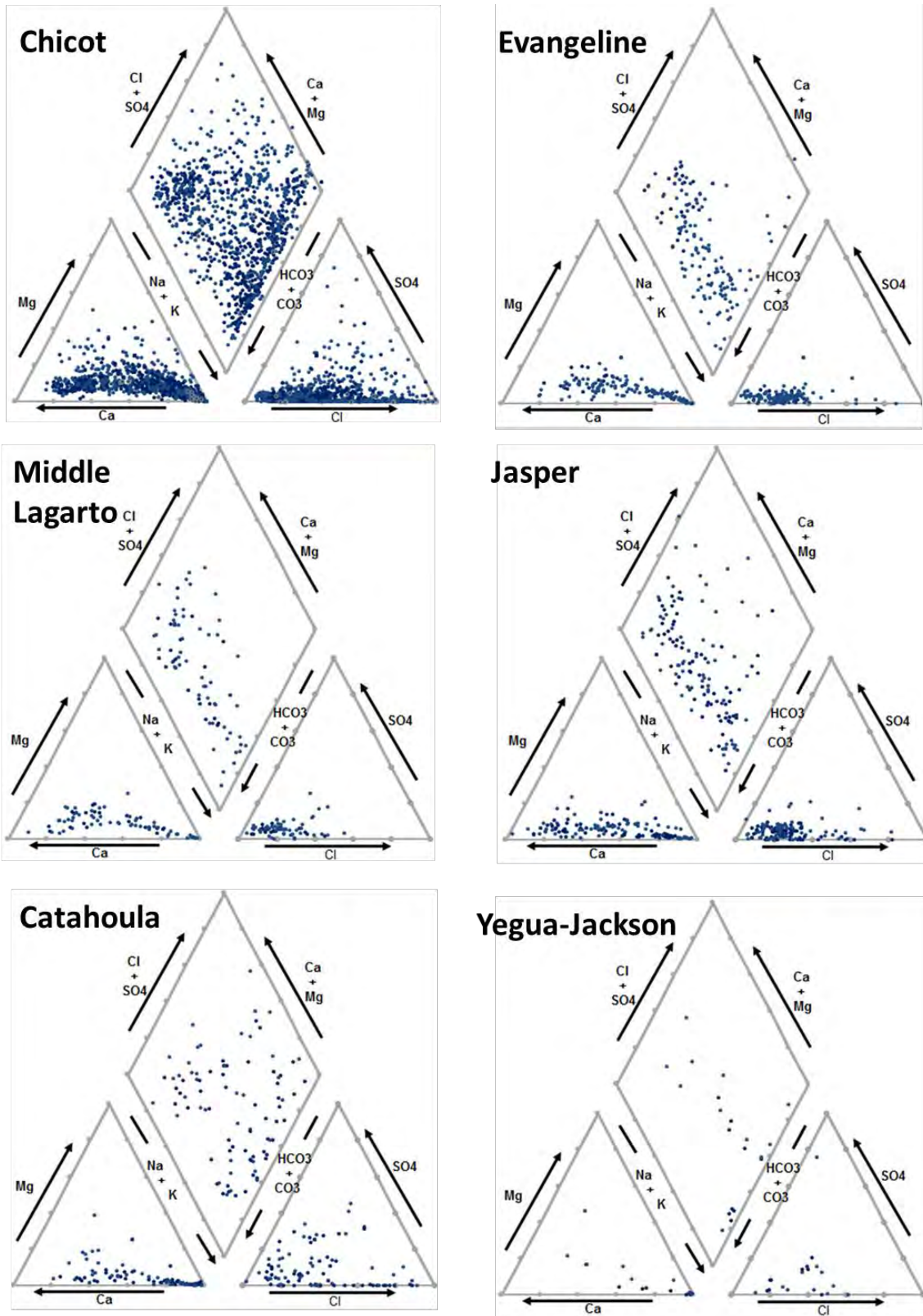


Figure 6-6 Piper Diagram for the Chicot, Evangeline, Middle Lagarto, Jasper, Catahoula, and Yegua-Jackson Units in GMA 14.

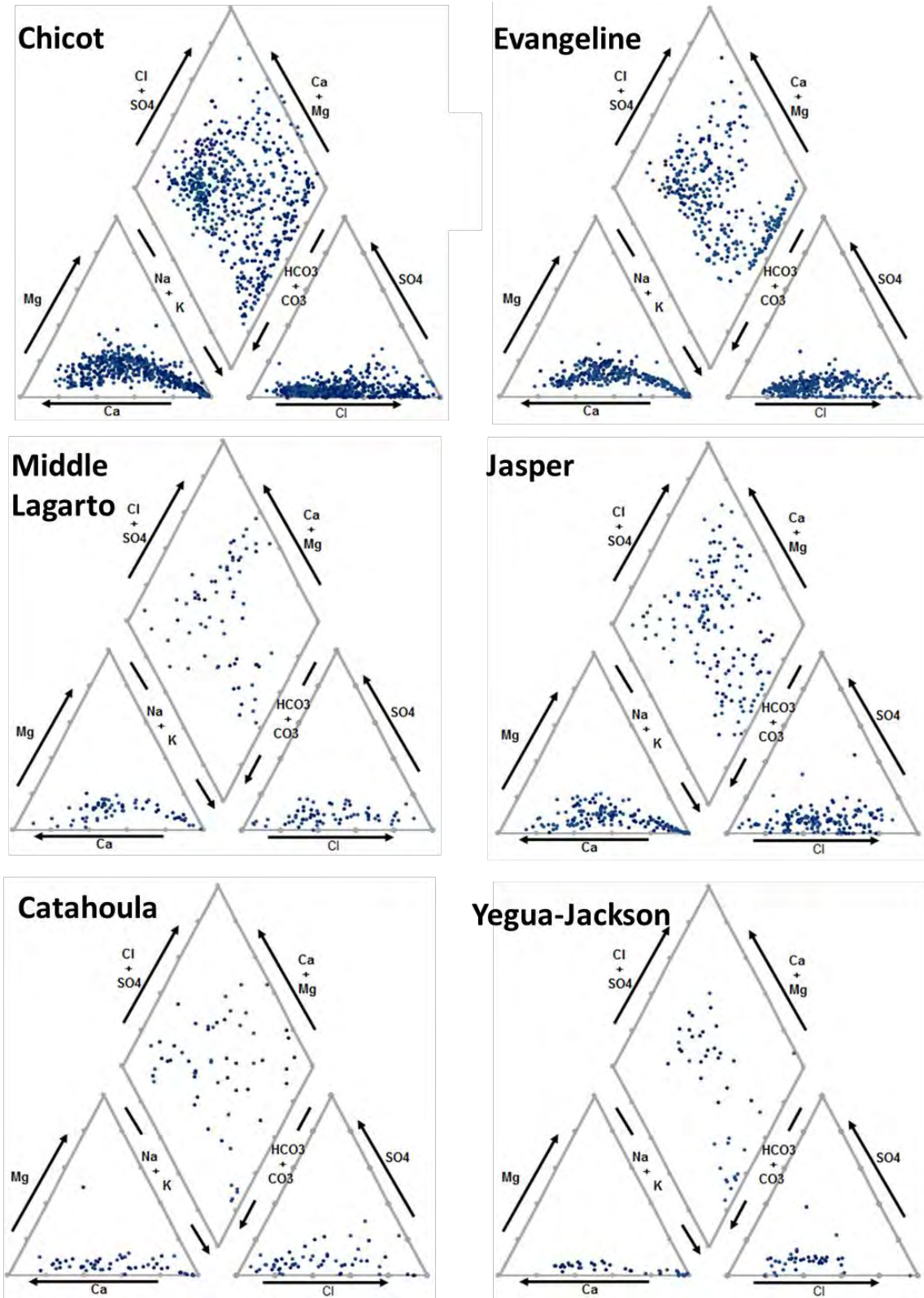


Figure 6-7 Piper Diagram for the Chicot, Evangeline, Middle Lagarto, Jasper, Catahoula, and Yegua-Jackson Units in GMA 15.

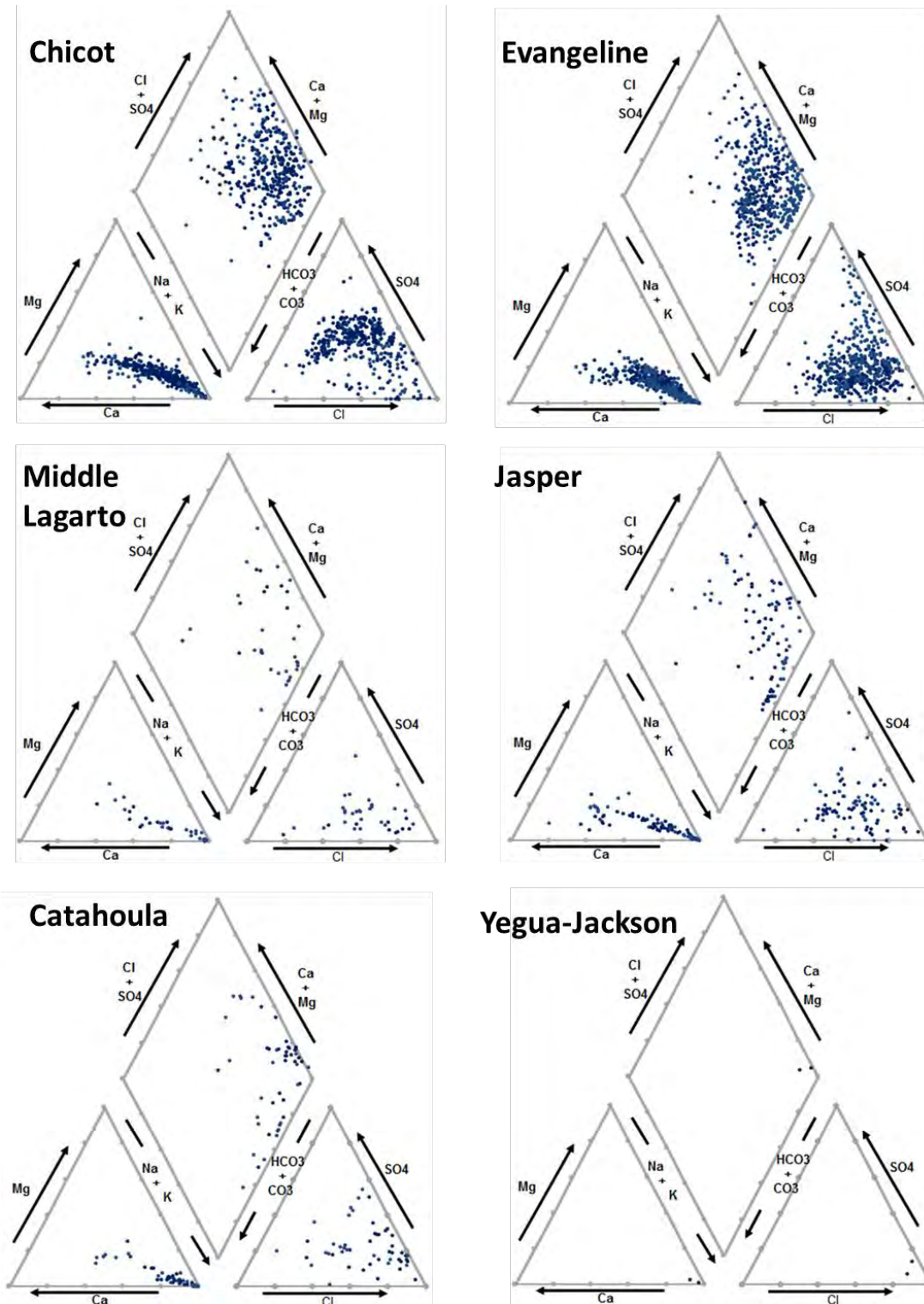


Figure 6-8 Piper Diagram for the Chicot, Evangeline, Middle Lagarto, Jasper, Catahoula, and Yegua-Jackson Units in GMA 16.

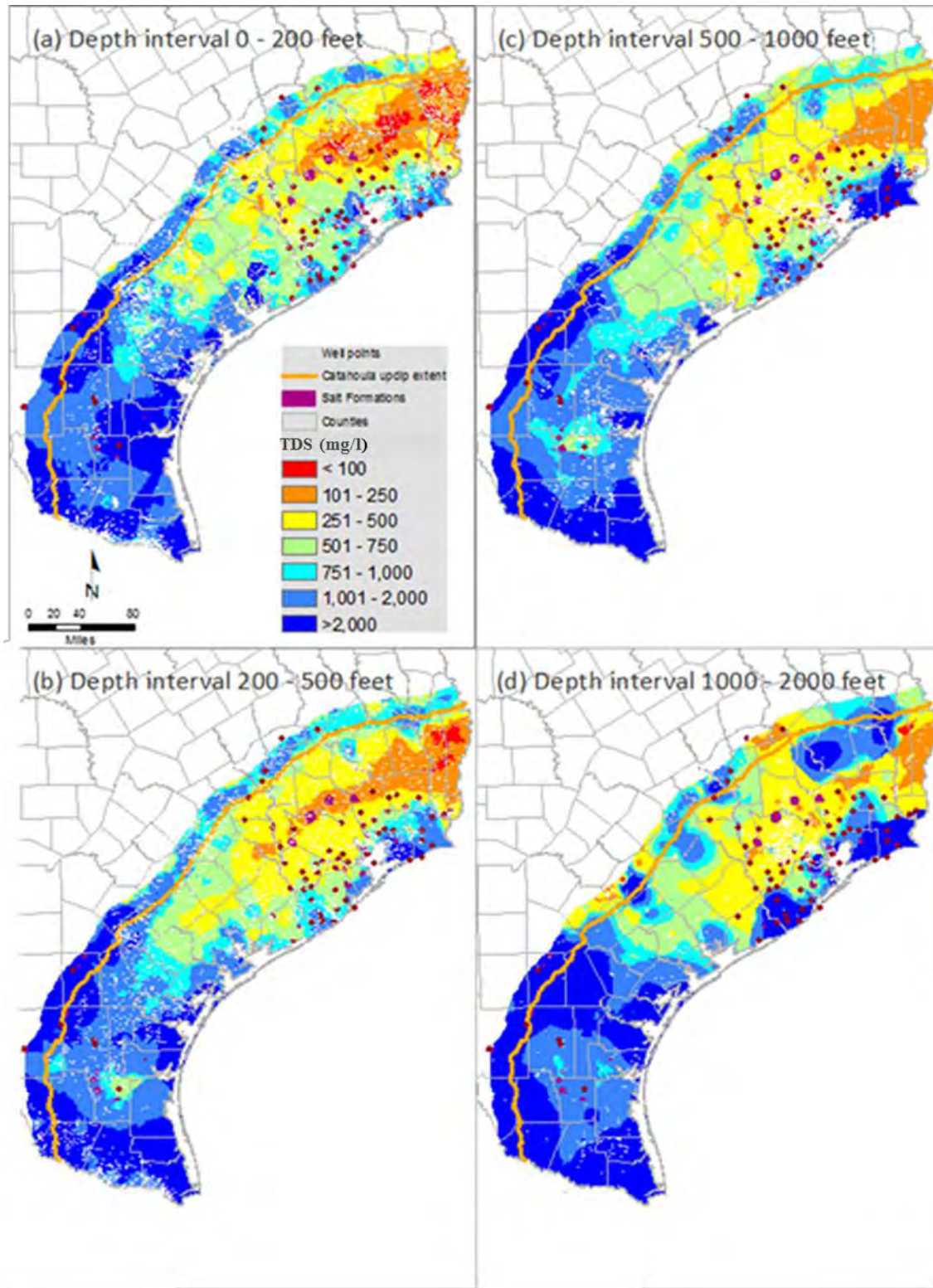


Figure 6-9 Total Dissolved Solids concentrations as a function of depth estimated by kriging point measurements from the TWDB groundwater database.

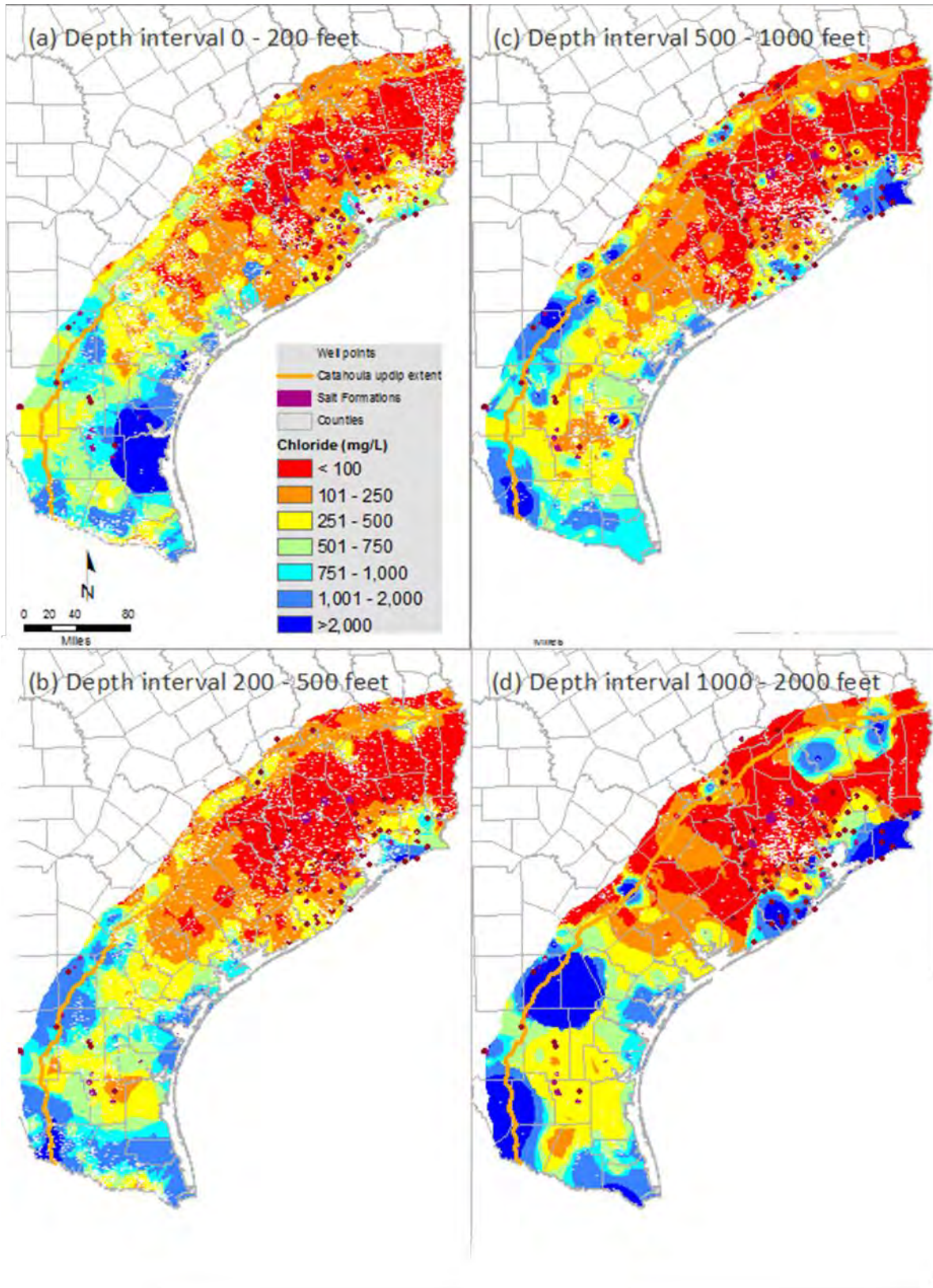


Figure 6-10 Chloride concentrations as a function of depth estimated by kriging point measurements from the TWDB groundwater database.

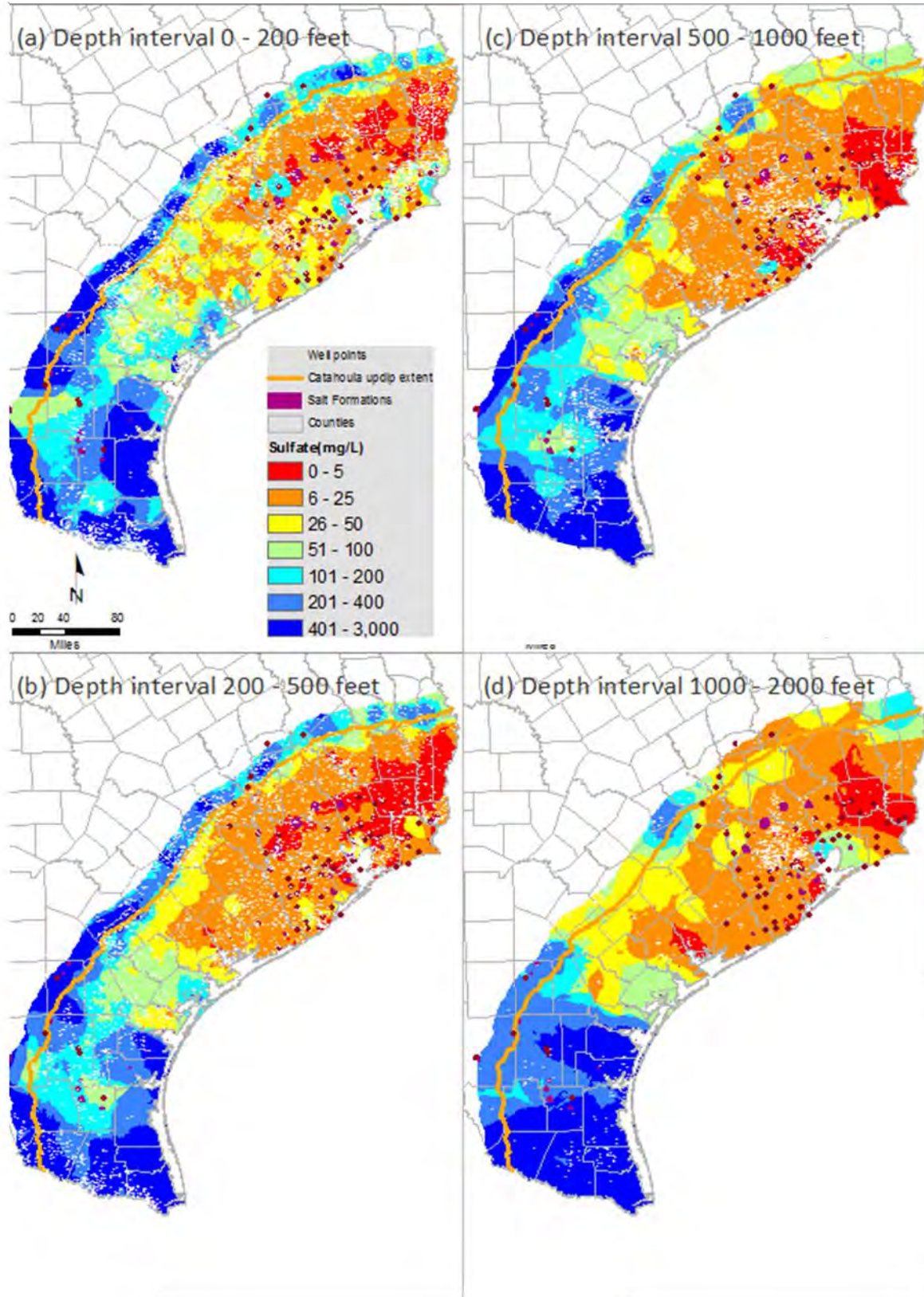


Figure 6-11 Sulfate concentrations as a function of depth estimated by kriging point measurements from the TWDB groundwater database.

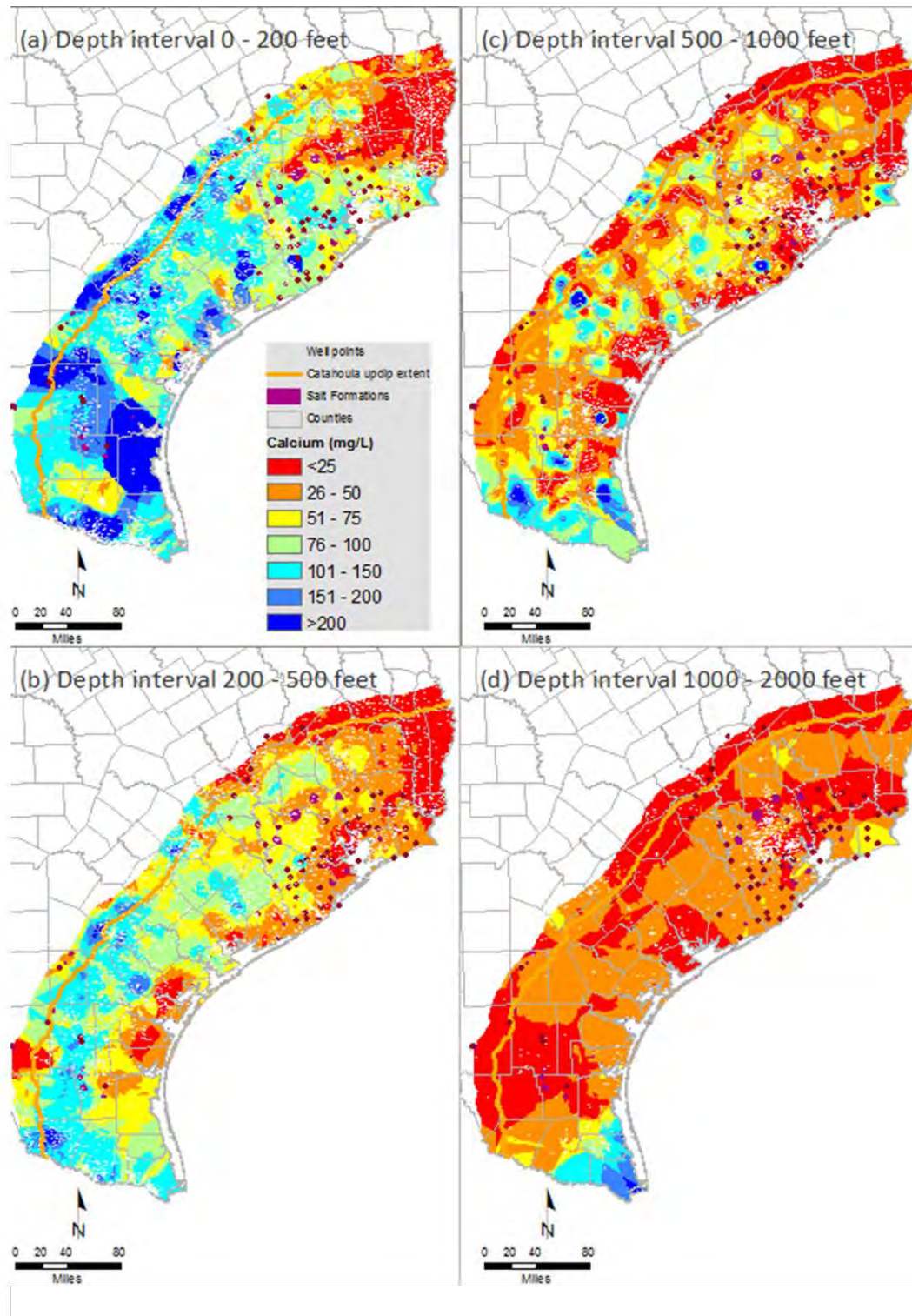


Figure 6-12 Calcium concentrations as a function of depth estimated by kriging point measurements from the TWDB groundwater database.

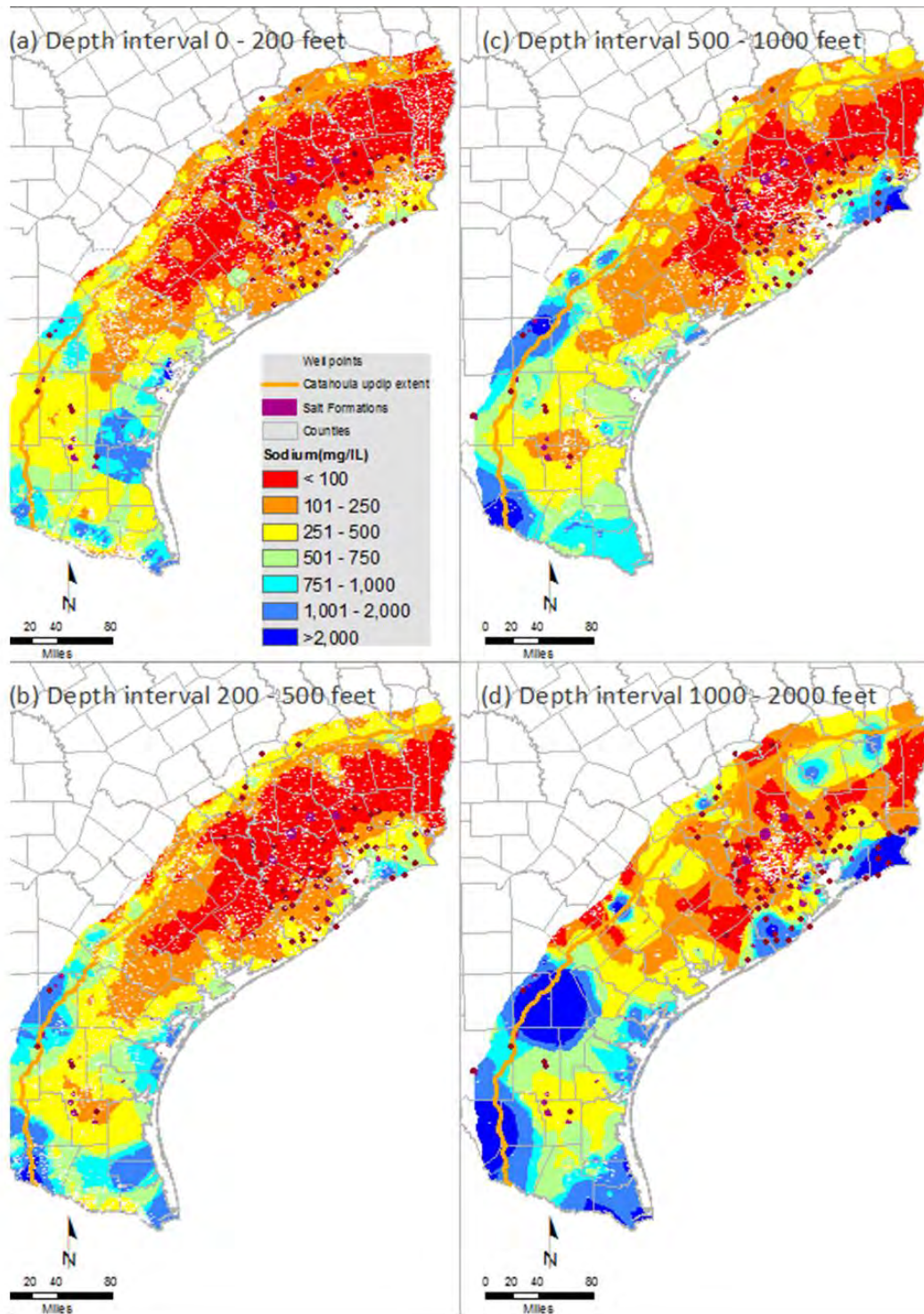


Figure 6-13 Sodium concentrations as a function of depth estimated by kriging point measurements from the TWDB groundwater database.

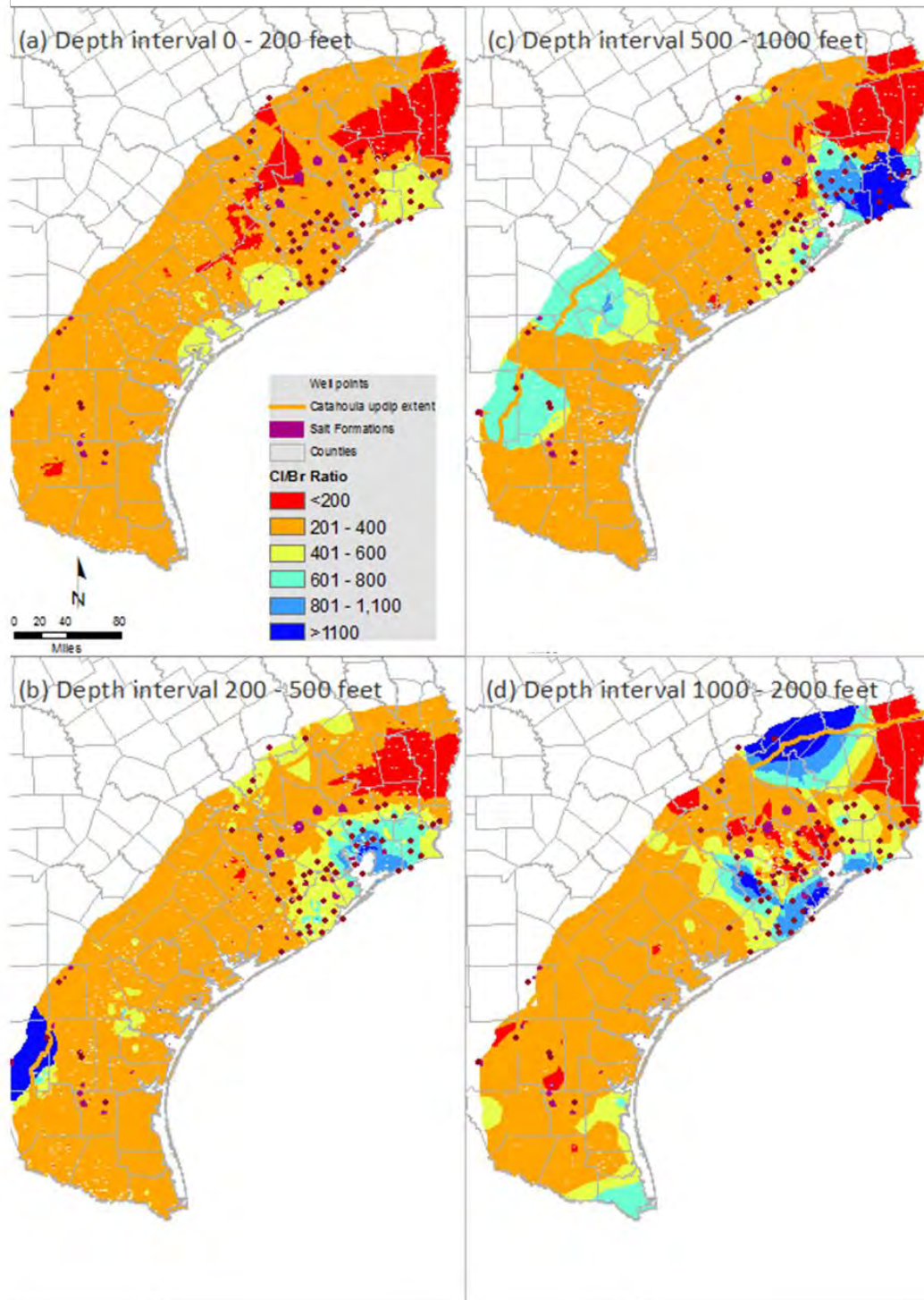


Figure 6-14 Ratio of chloride to bromide milliequivalents as a function of depth estimated by kriging point measurements from the TWDB groundwater database.

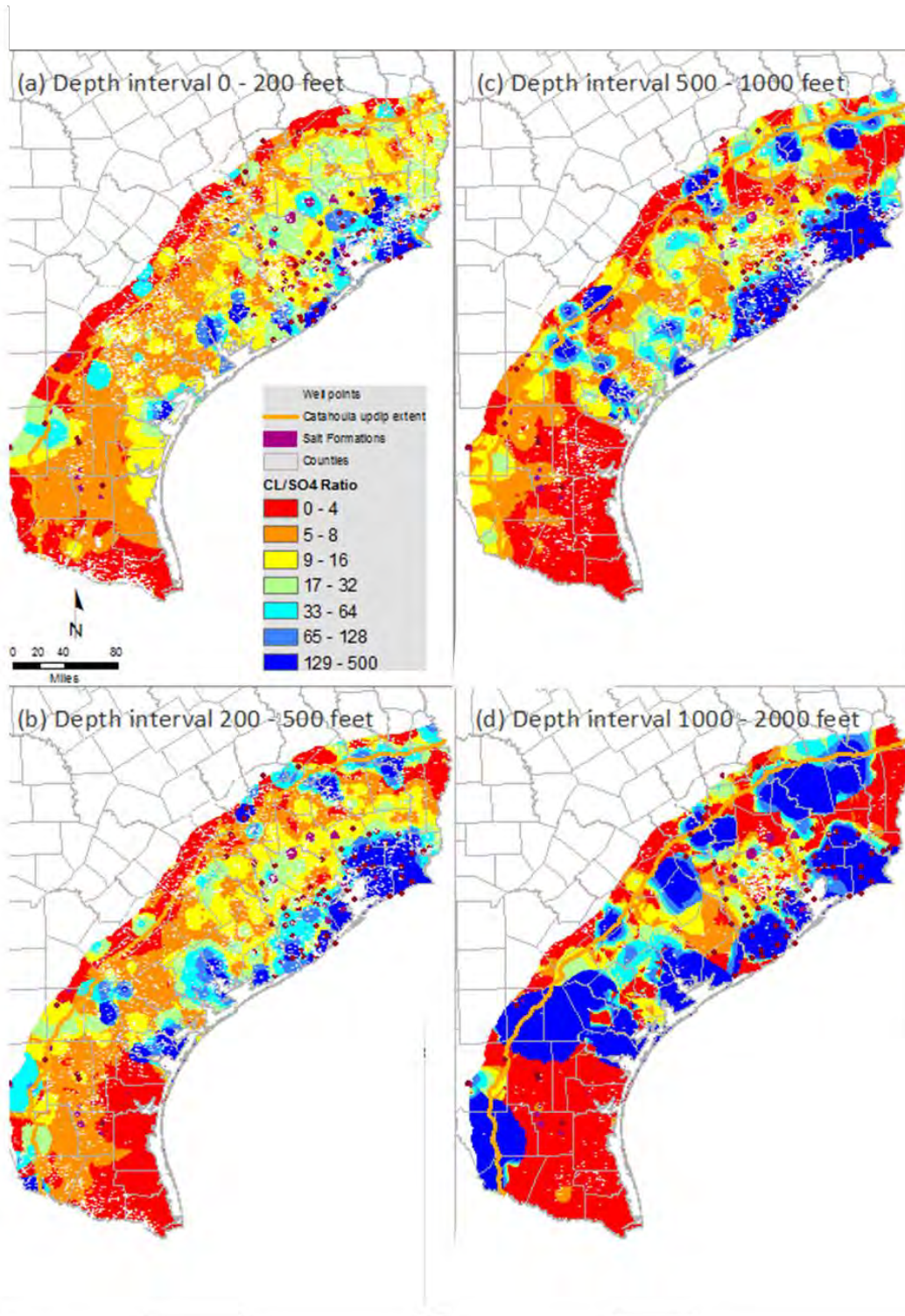


Figure 6-15 Ratio of chloride to sulfate milliequivalents as a function of depth estimated by kriging point measurements from the TWDB groundwater database.

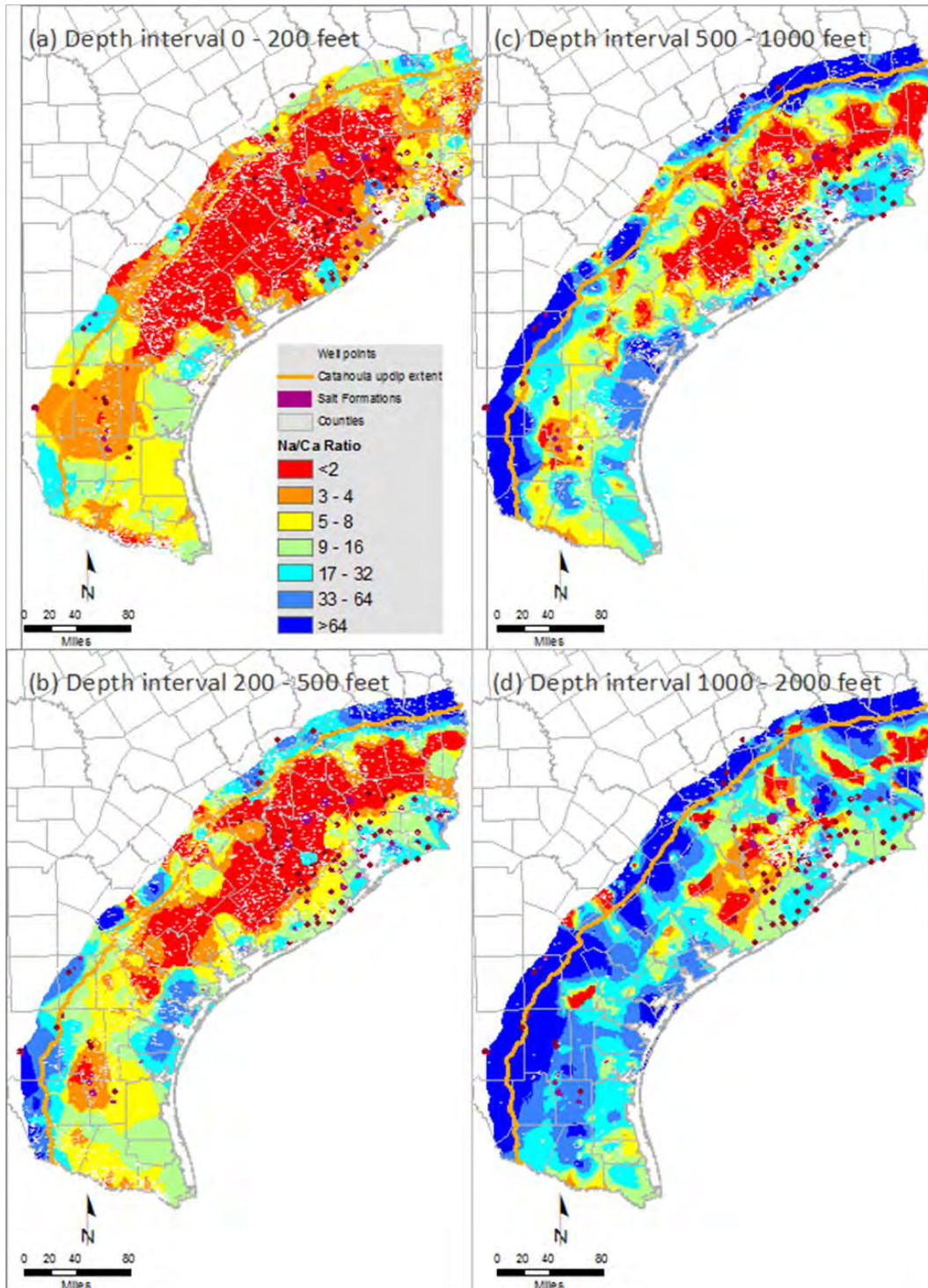


Figure 6-16 Ratio of sodium to calcium milliequivalents as a function of depth estimated by kriging point measurements from the TWDB groundwater database.

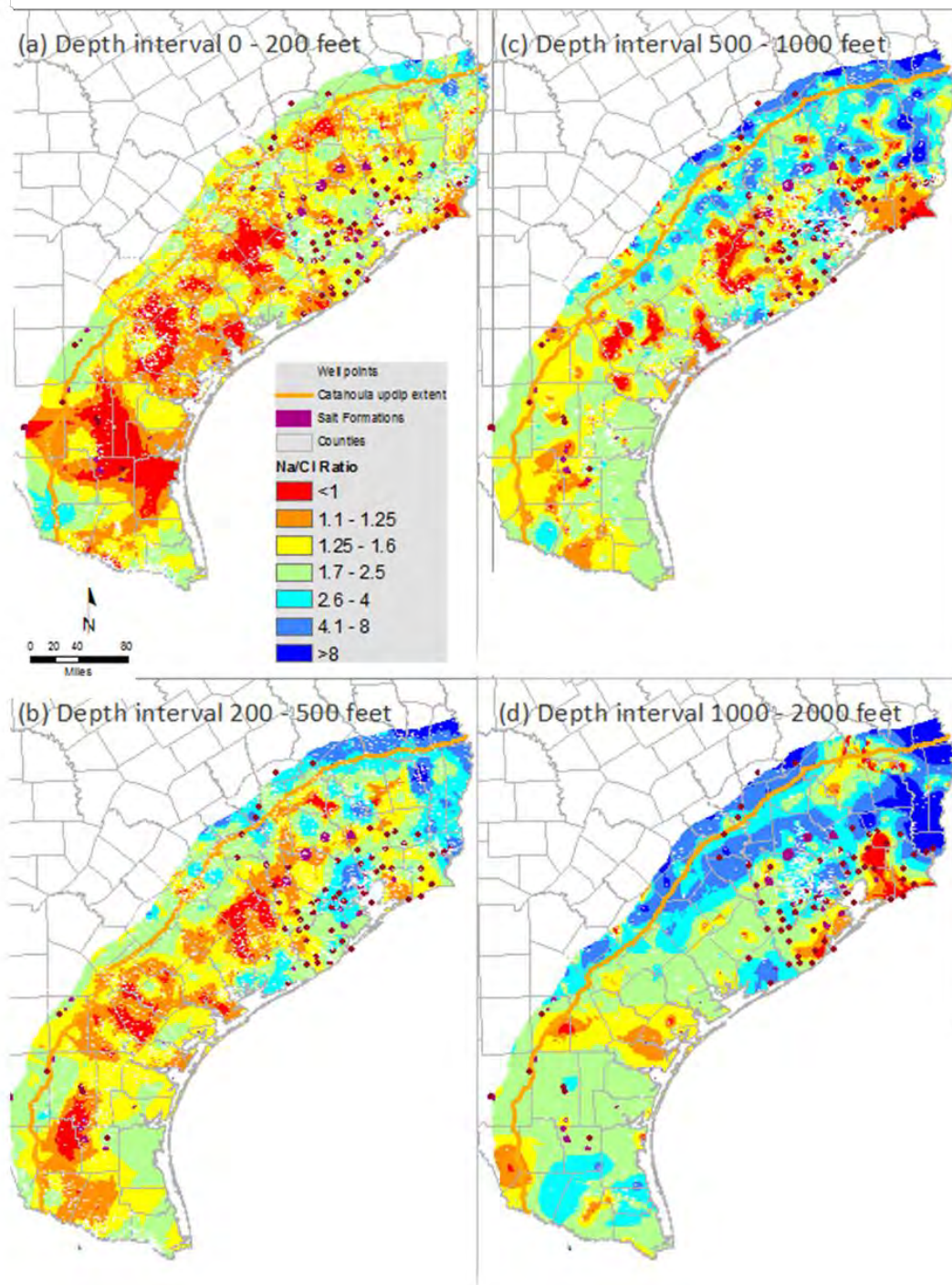


Figure 6-17 Ratio of sodium to chloride milliequivalents as a function of depth estimated by kriging point measurements from the TWDB groundwater database.

Final – Hydrogeochemical Evaluation of the Texas Gulf Coast Aquifer System and Implications for Developing Groundwater Availability Models

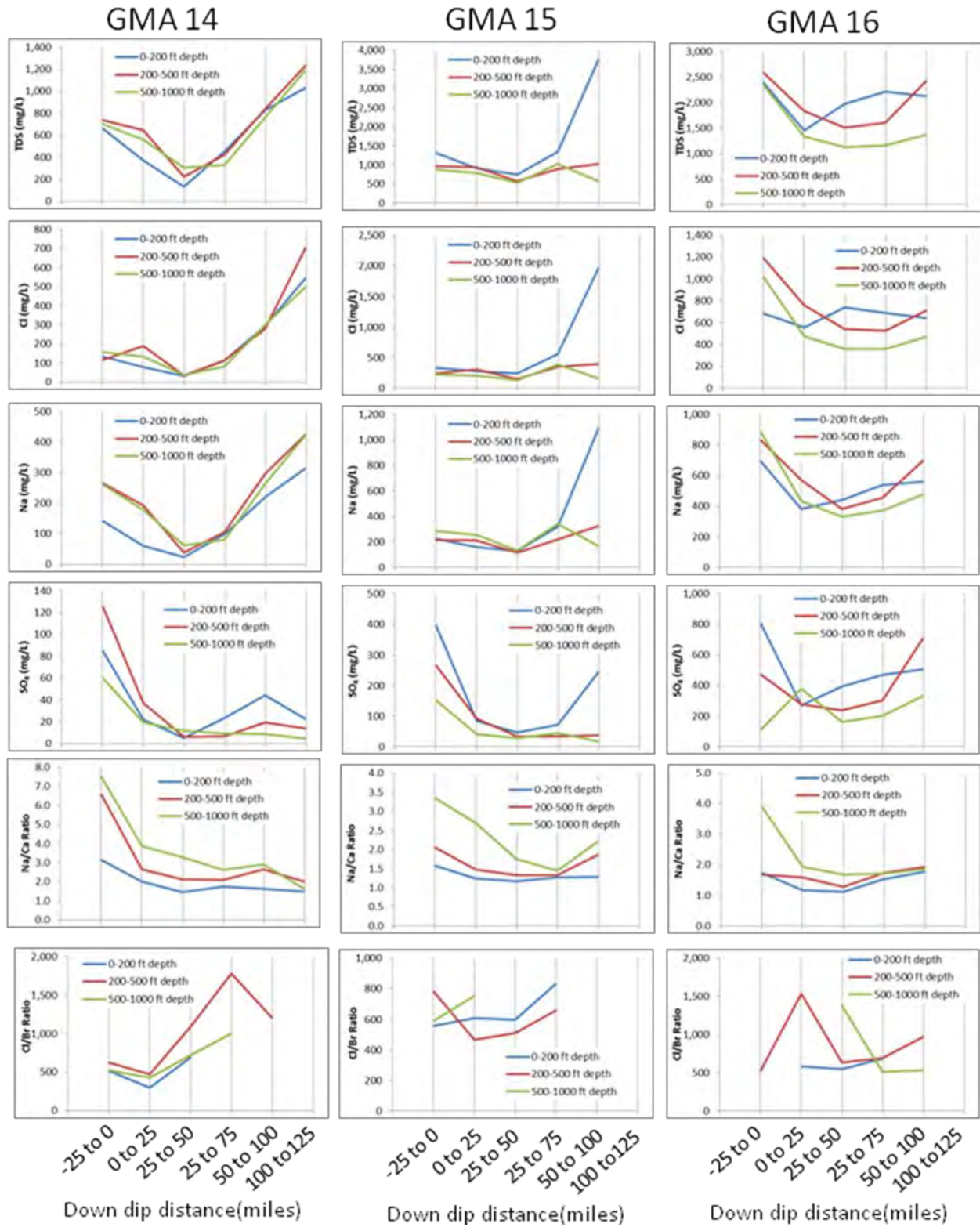


Figure 6-18 Selected Ion Concentrations and Ion Ratios as a function of depth and down dip distance for GMA 14, GMA 15, and GMA 16.

Final – Hydrogeochemical Evaluation of the Texas Gulf Coast Aquifer System and Implications for Developing Groundwater Availability Models

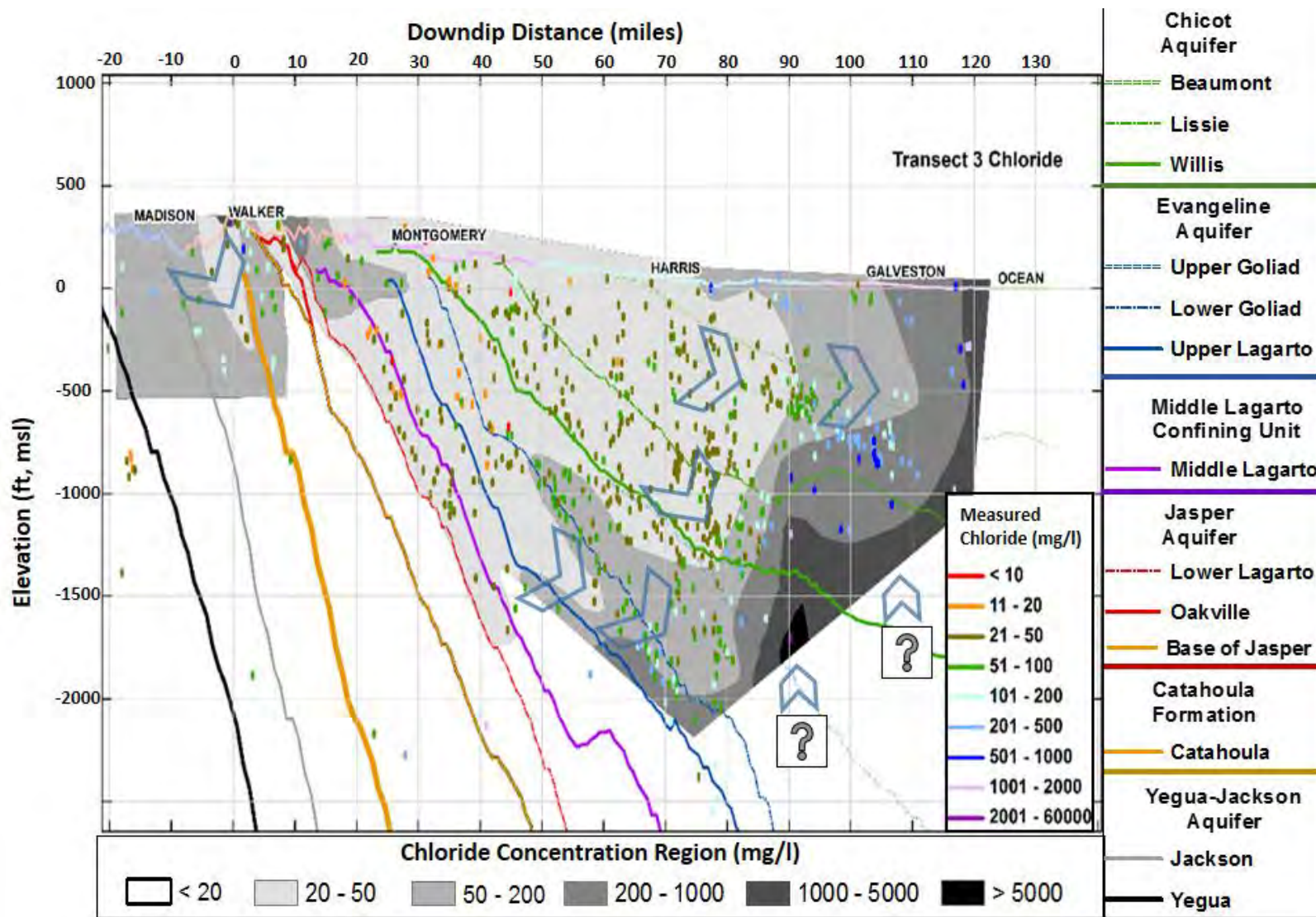


Figure 6-19 Concentration Maps for Cl for Transect 3 in GMA 14. (Note Lake Conroe is located at approximately downdip distances of 24 miles to 32 miles). (Note: surfaces represent the bottom of each geological formation).

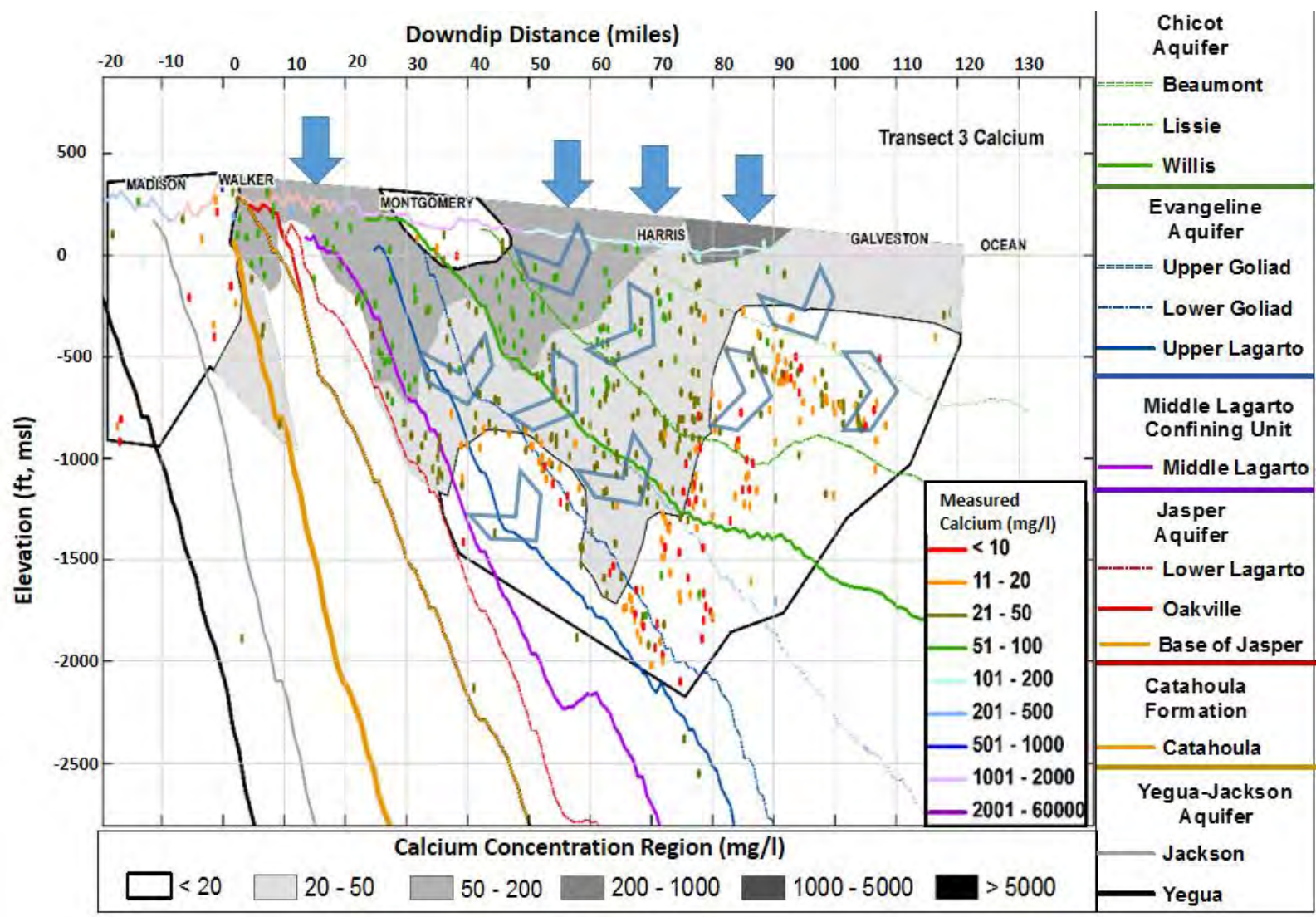


Figure 6-20 Concentration Maps for Ca for Transect 3 in GMA 14. (Note Lake Conroe is located at approximately down-dip distances of 24 miles to 32 miles). (Note: surfaces represent the bottom of each geological formation).

Final – Hydrogeochemical Evaluation of the Texas Gulf Coast Aquifer System and Implications for Developing Groundwater Availability Models

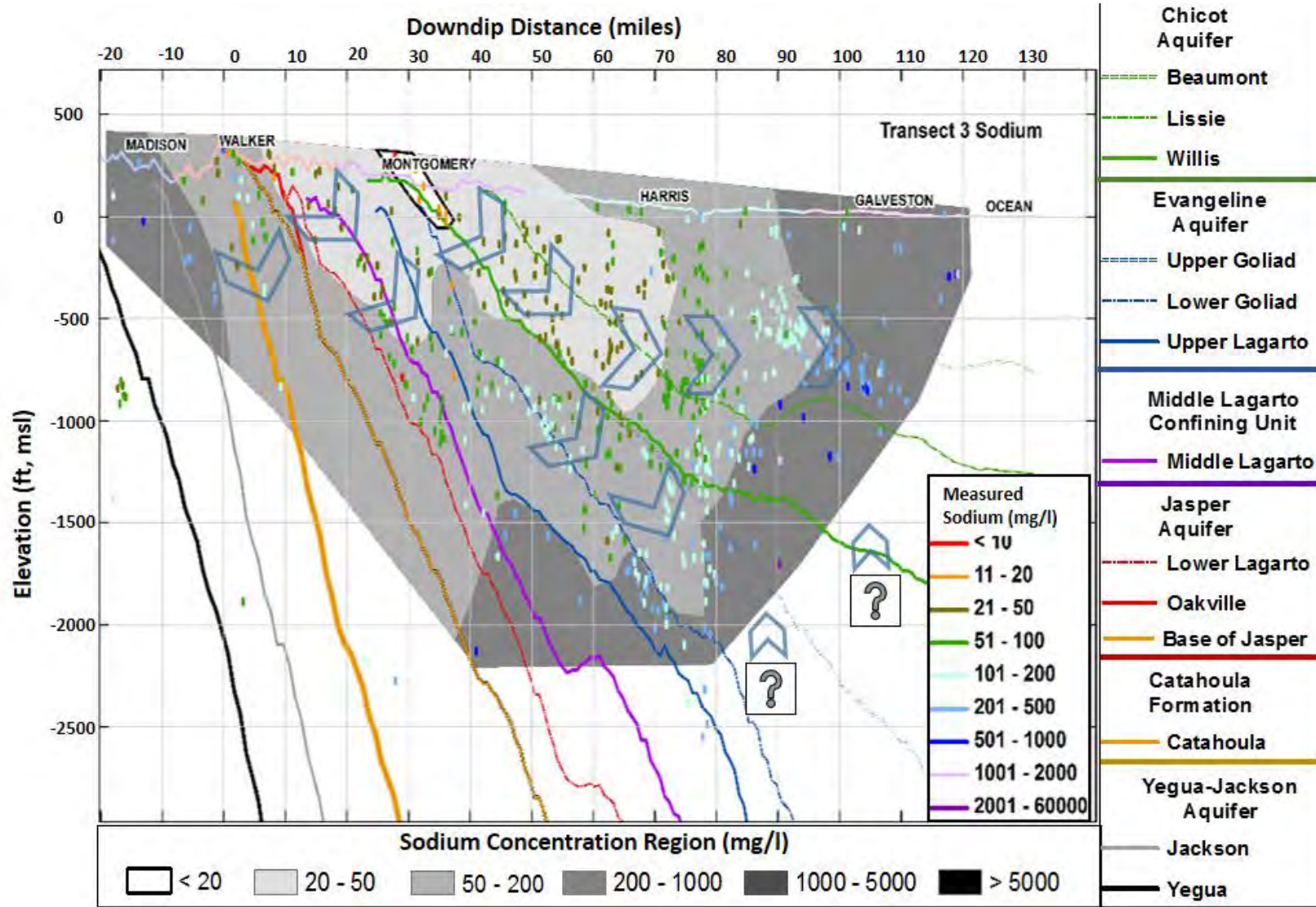


Figure 6-21 Concentration Maps for Na for Transect 3 in GMA 14. (Note Lake Conroe is located at approximately downdip distances of 24 miles to 32 miles). (Note: surfaces represent the bottom of each geological formation).

Final – Hydrogeochemical Evaluation of the Texas Gulf Coast Aquifer System and Implications for Developing Groundwater Availability Models

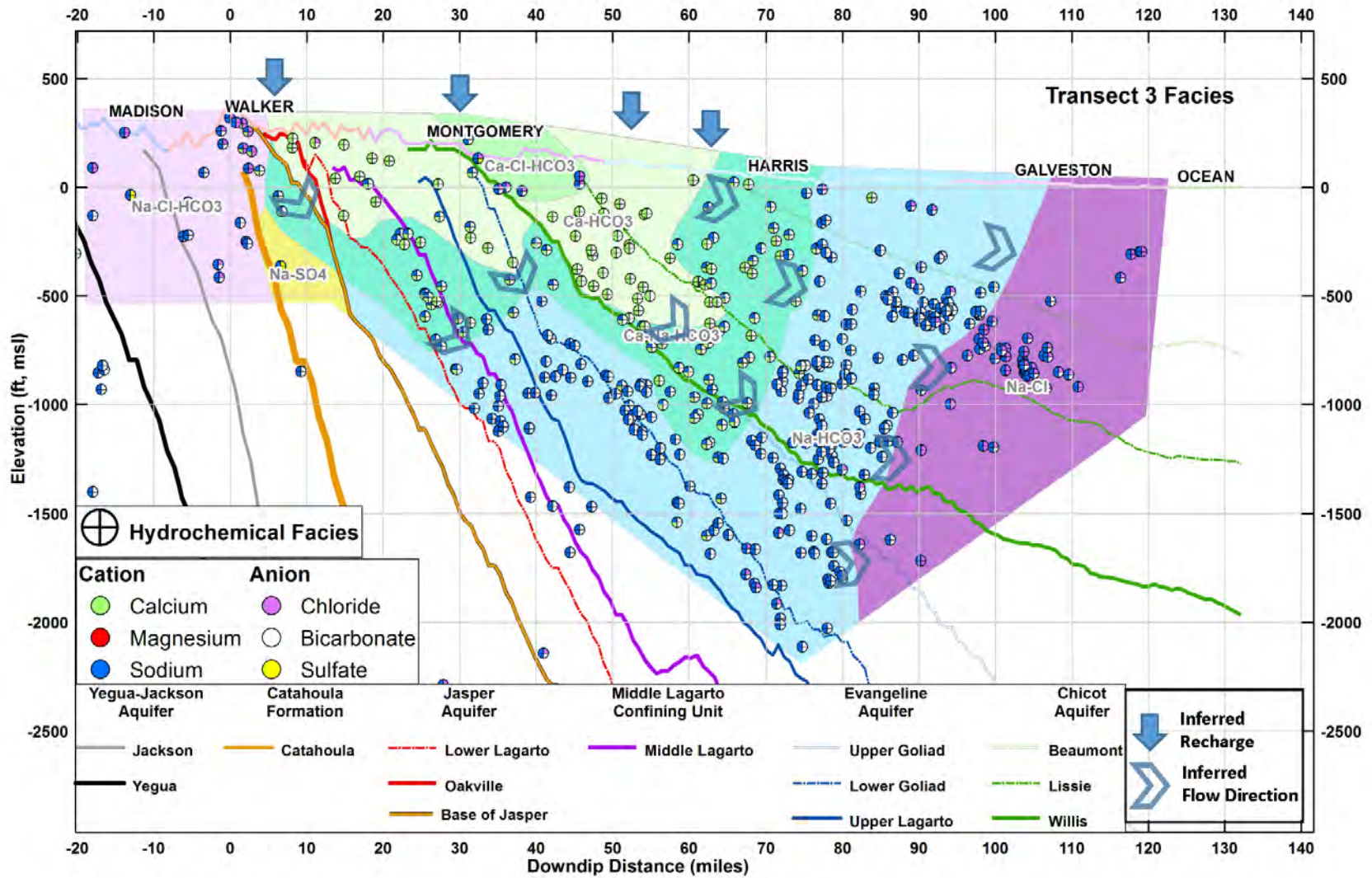


Figure 6-22 Hydrochemical facies for Transect 3 in GMA 14. (Note Lake Conroe is located at approximately downdip distances of 24 miles to 32 miles). (Note: surfaces represent the bottom of each geological formation).

Final – Hydrogeochemical Evaluation of the Texas Gulf Coast Aquifer System and Implications for Developing Groundwater Availability Models

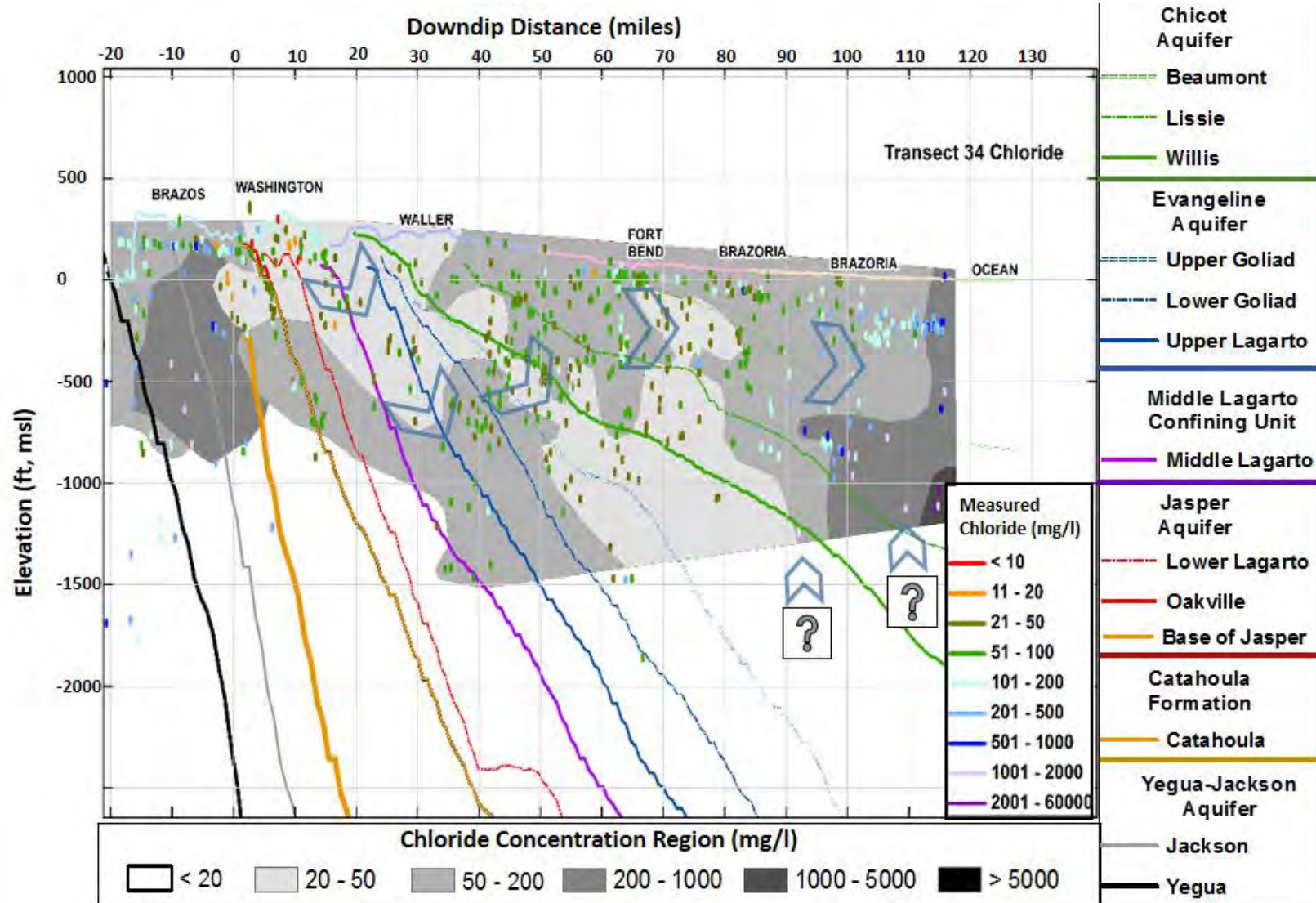


Figure 6-23 Concentration Maps for Cl for Transect 34 in GMA 14. (Note: surfaces represent the bottom of each geological formation).

Final – Hydrogeochemical Evaluation of the Texas Gulf Coast Aquifer System and Implications for Developing Groundwater Availability Models

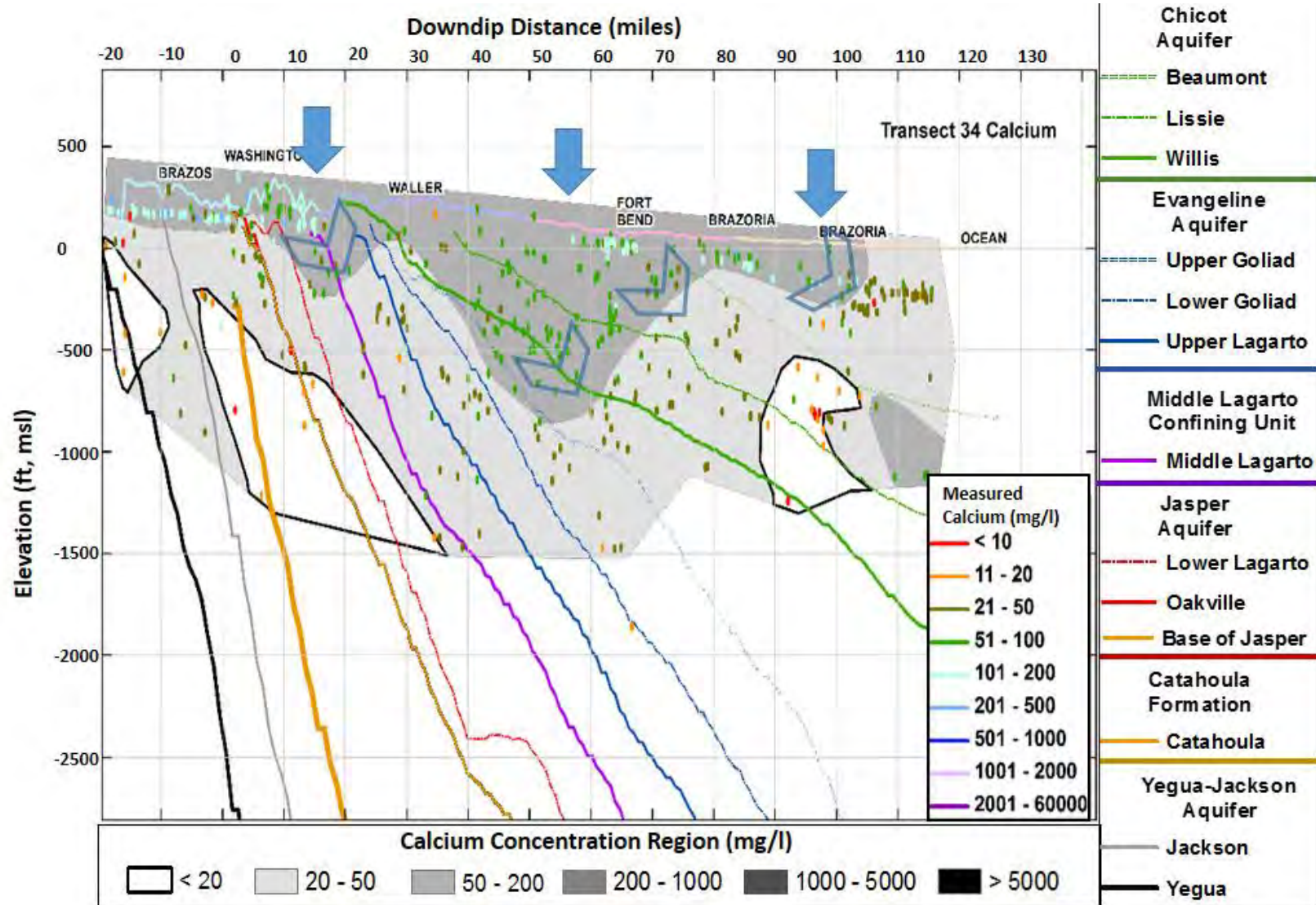


Figure 6-24 Concentration Maps for Ca for Transect 34 in GMA 14. (Note: surfaces represent the bottom of each geological formation).

Final – Hydrogeochemical Evaluation of the Texas Gulf Coast Aquifer System and Implications for Developing Groundwater Availability Models

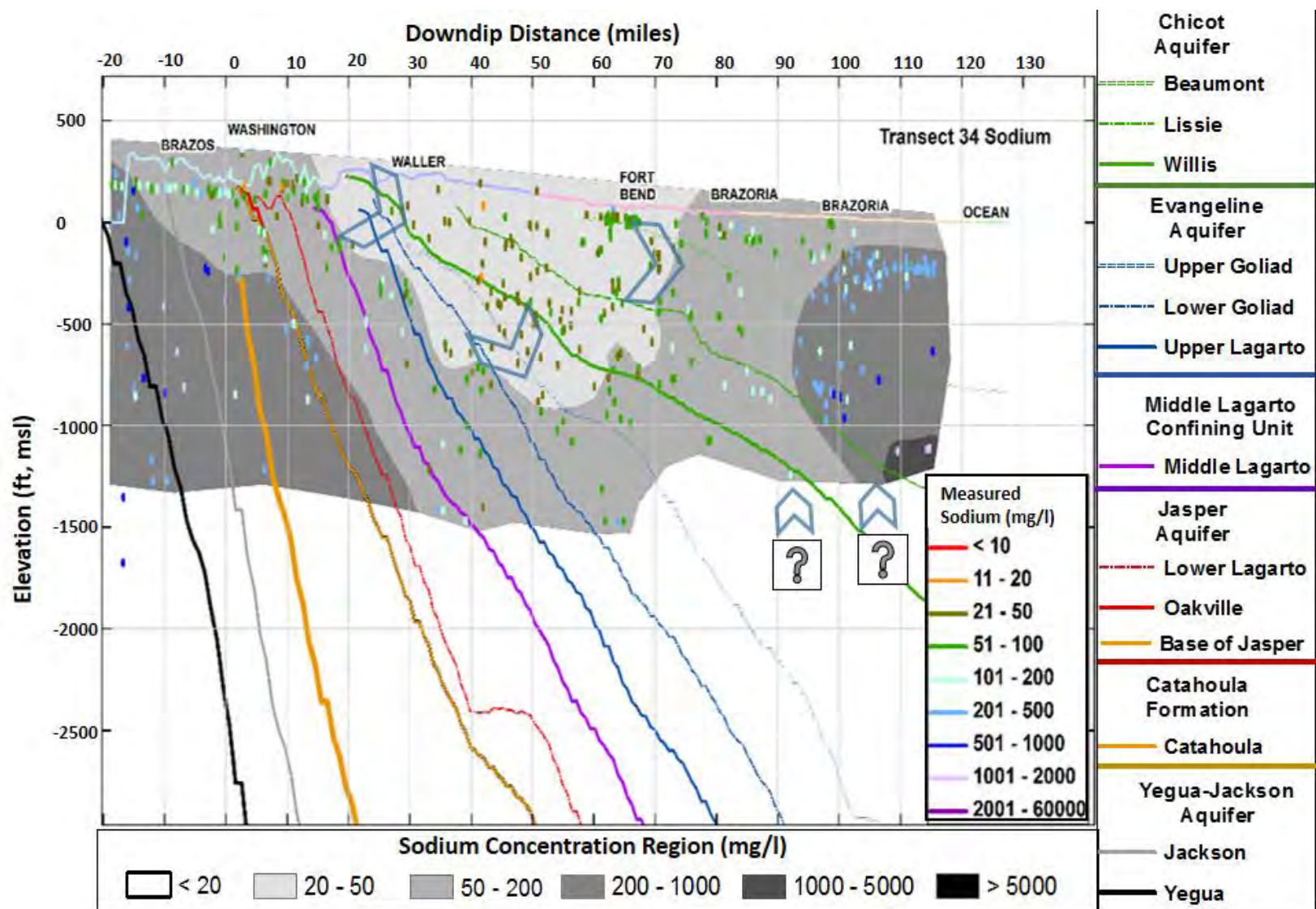


Figure 6-25 Concentration Maps for Na for Transect 34 in GMA 14. (Note: surfaces represent the bottom of each geological formation).

Final – Hydrogeochemical Evaluation of the Texas Gulf Coast Aquifer System and Implications for Developing Groundwater Availability Models

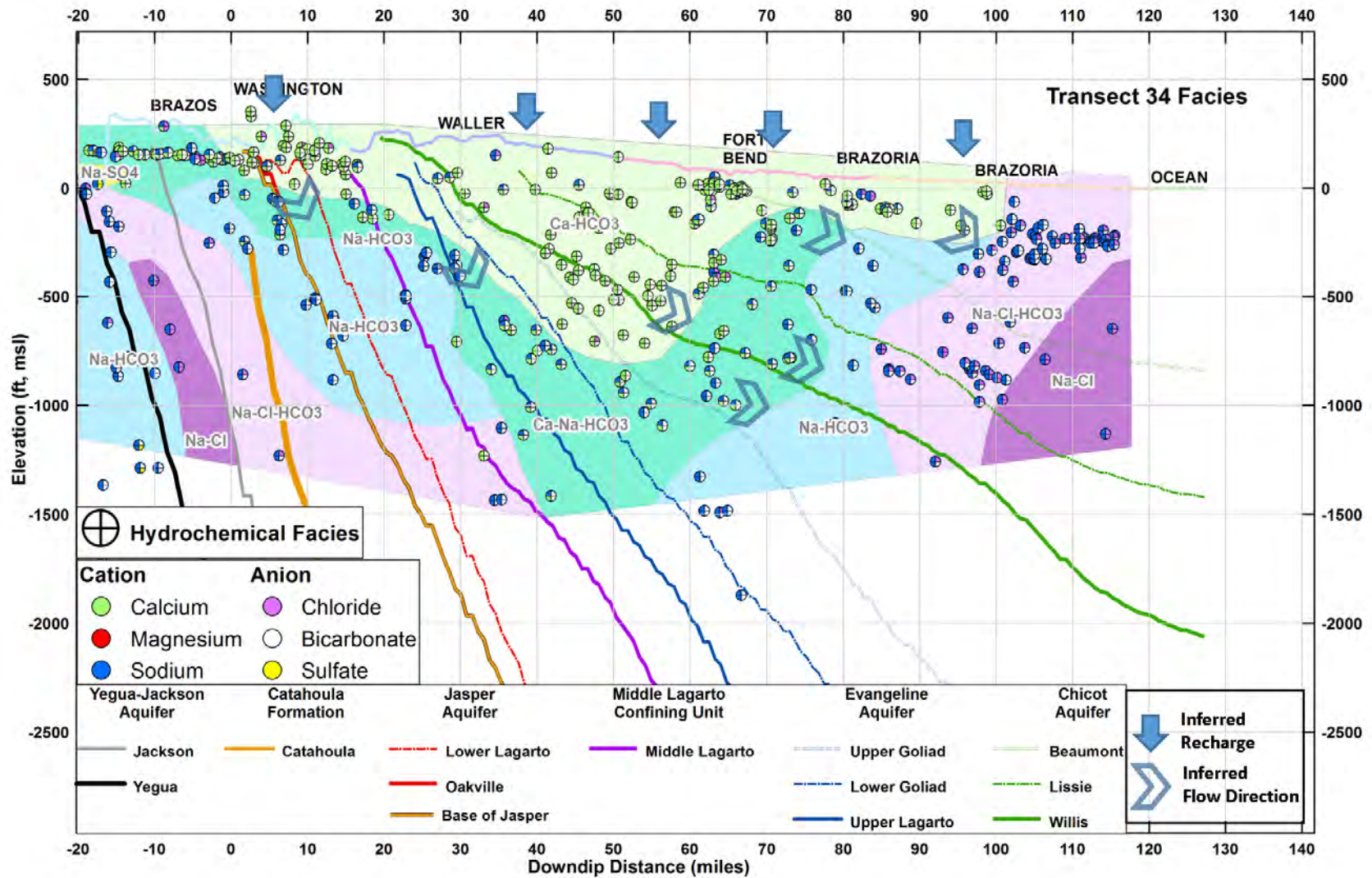


Figure 6-26 Hydrochemical facies for Transect 34 in GMA 14. (Note: surfaces represent the bottom of each geological formation).

Final – Hydrogeochemical Evaluation of the Texas Gulf Coast Aquifer System and Implications for Developing Groundwater Availability Models

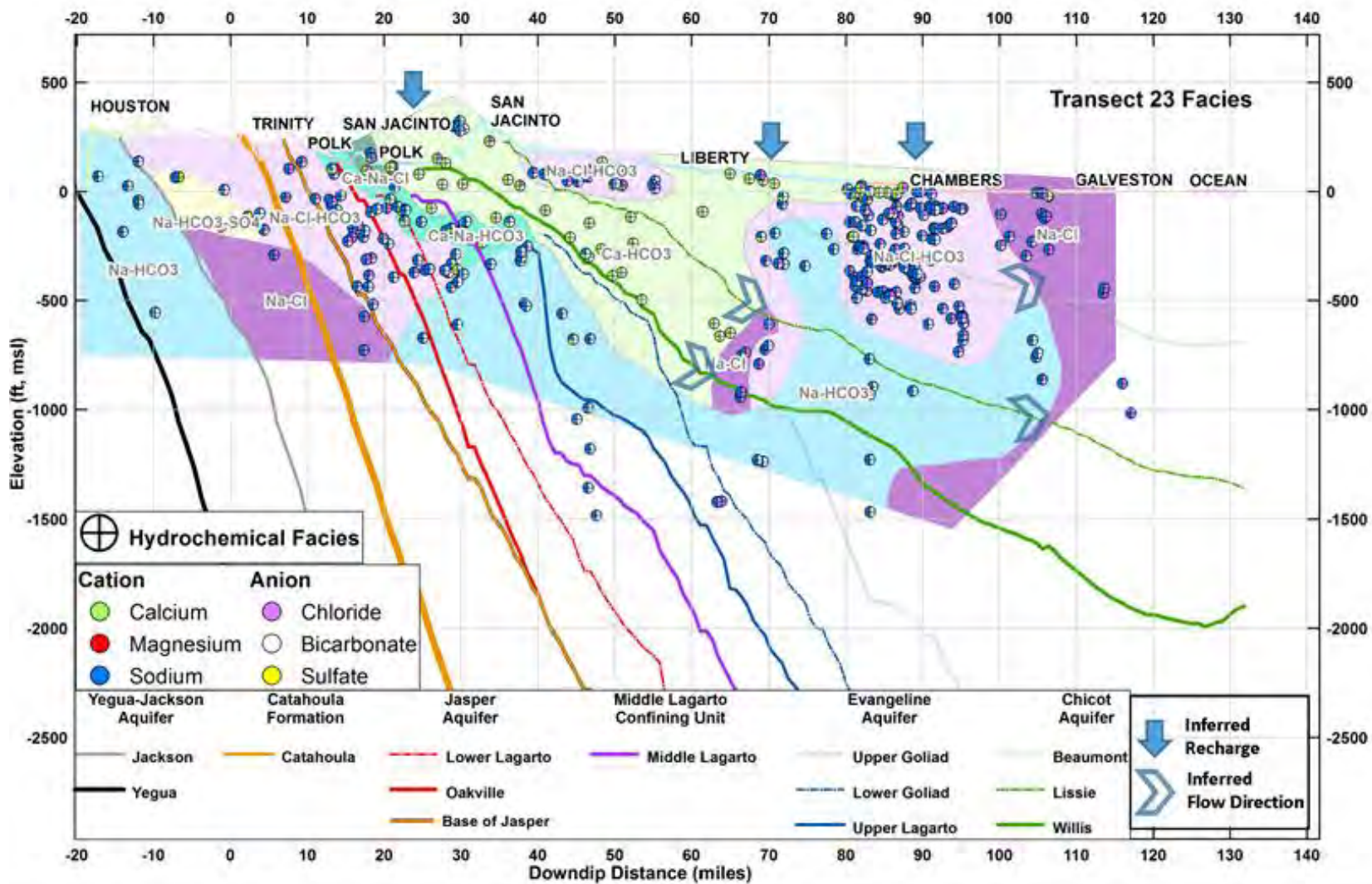


Figure 6-27 Hydrochemical facies for Transect 23 in GMA 14. (Note: surfaces represent the bottom of each geological formation).

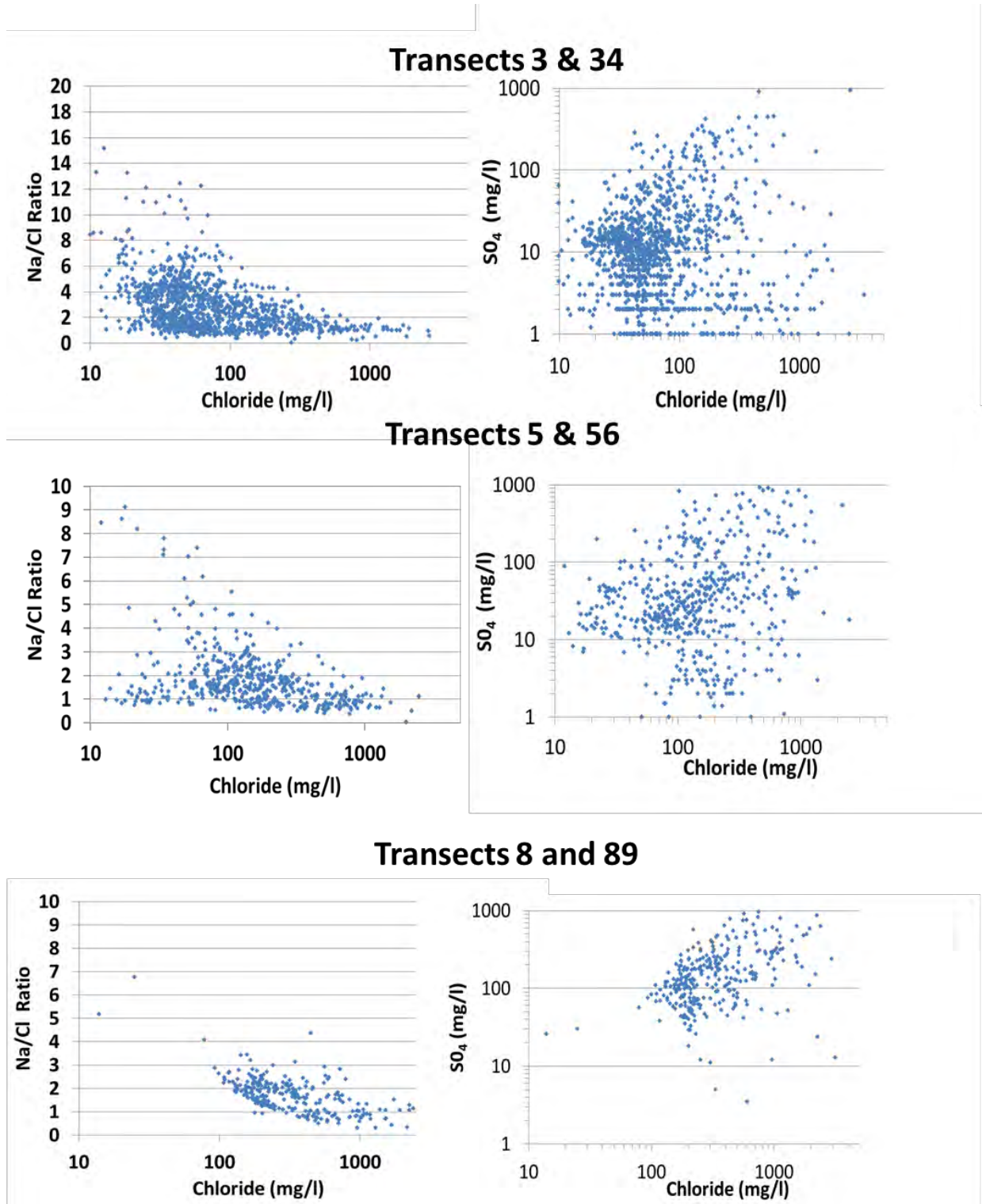


Figure 6-28 Bivariate plots of Na/Cl ratio versus chloride and SO₄ versus chloride for transects in GMA 14, 15, & 16.

Final – Hydrogeochemical Evaluation of the Texas Gulf Coast Aquifer System and Implications for Developing Groundwater Availability Models

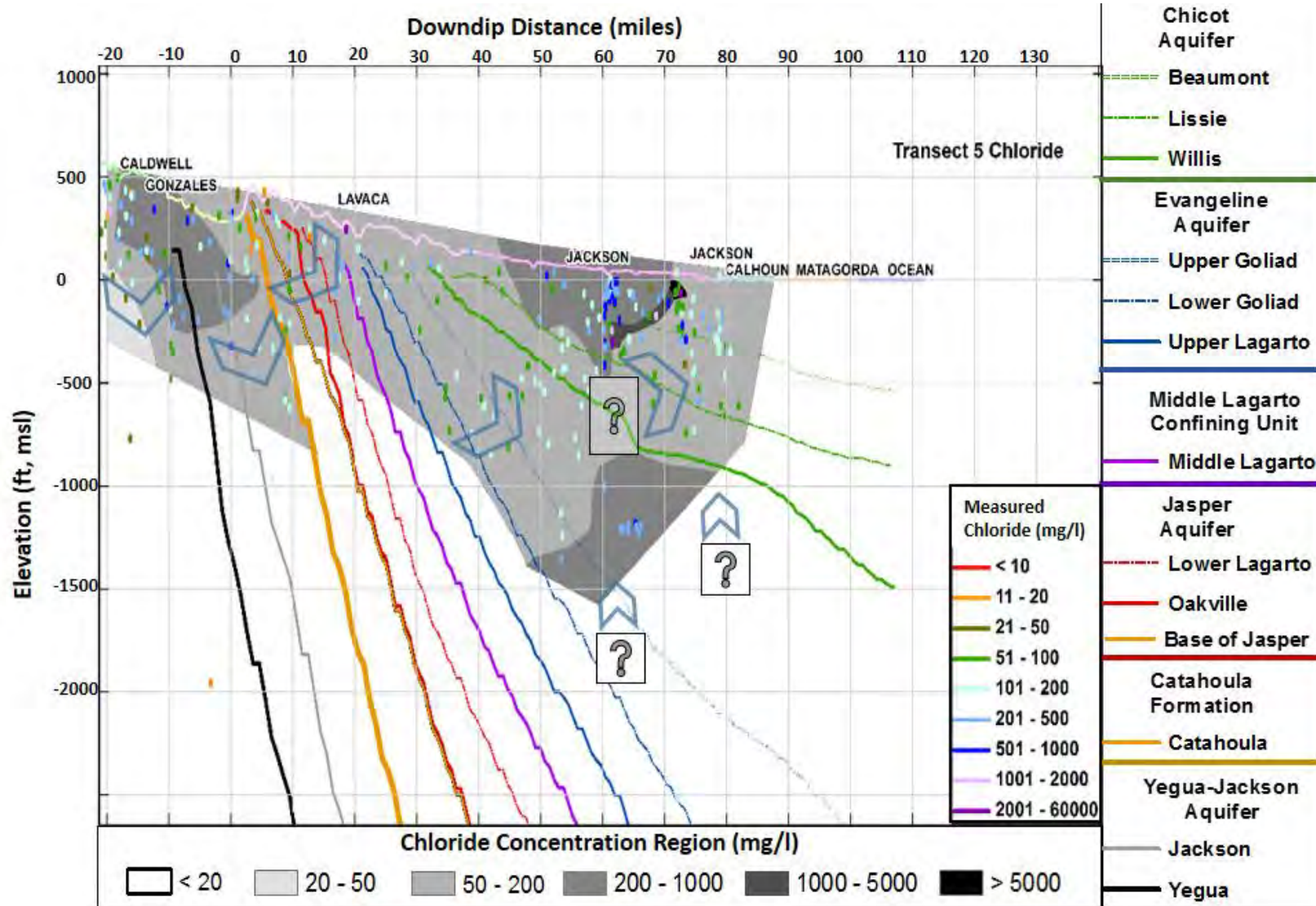


Figure 6-29 Concentration Maps for Cl for Transect 5 in GMA 15. (Note: surfaces represent the bottom of each geological formation).

Final – Hydrogeochemical Evaluation of the Texas Gulf Coast Aquifer System and Implications for Developing Groundwater Availability Models

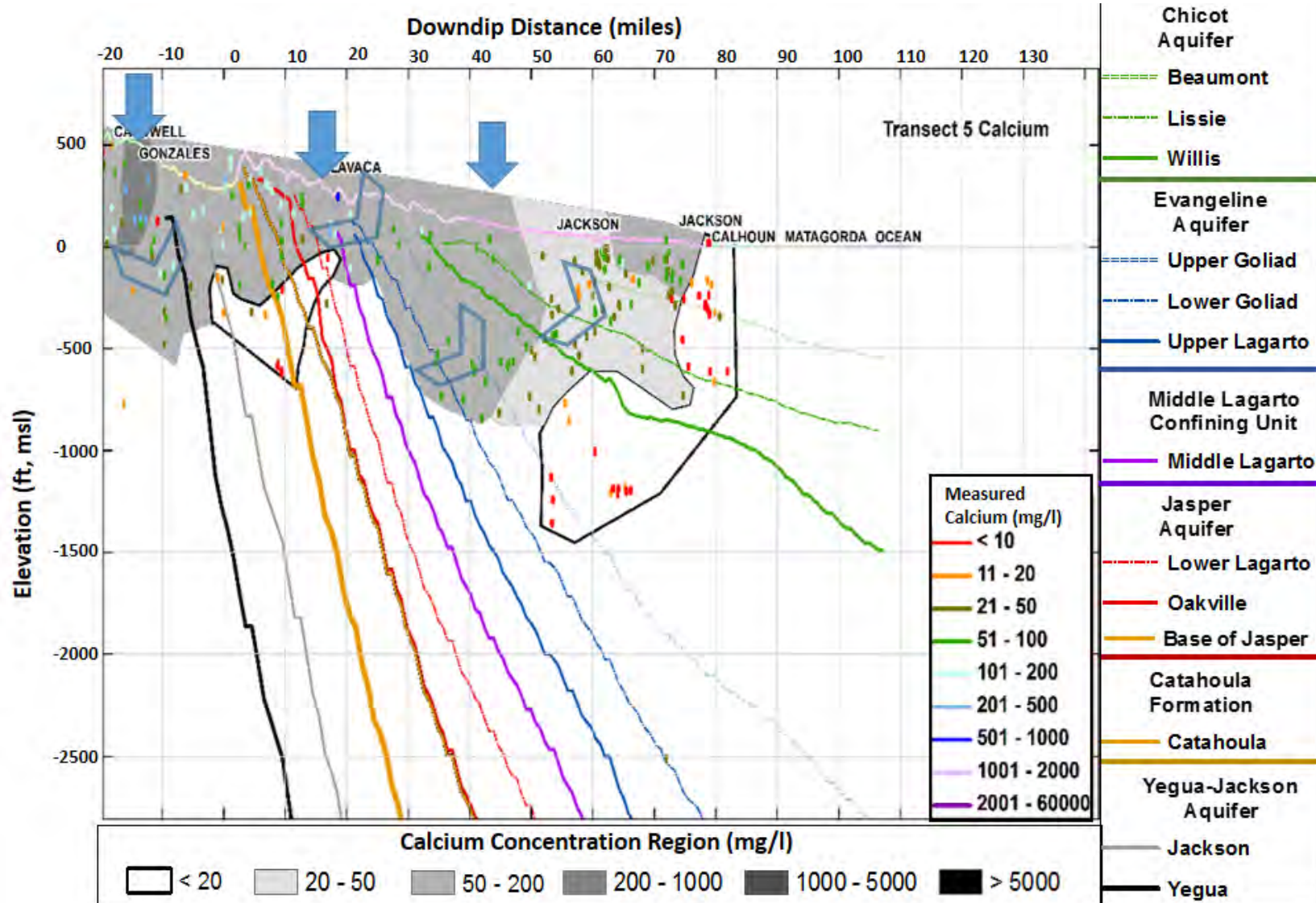


Figure 6-30 Concentration Maps for Ca for Transect 5 in GMA 15. (Note: surfaces represent the bottom of each geological formation).

Final – Hydrogeochemical Evaluation of the Texas Gulf Coast Aquifer System and Implications for Developing Groundwater Availability Models

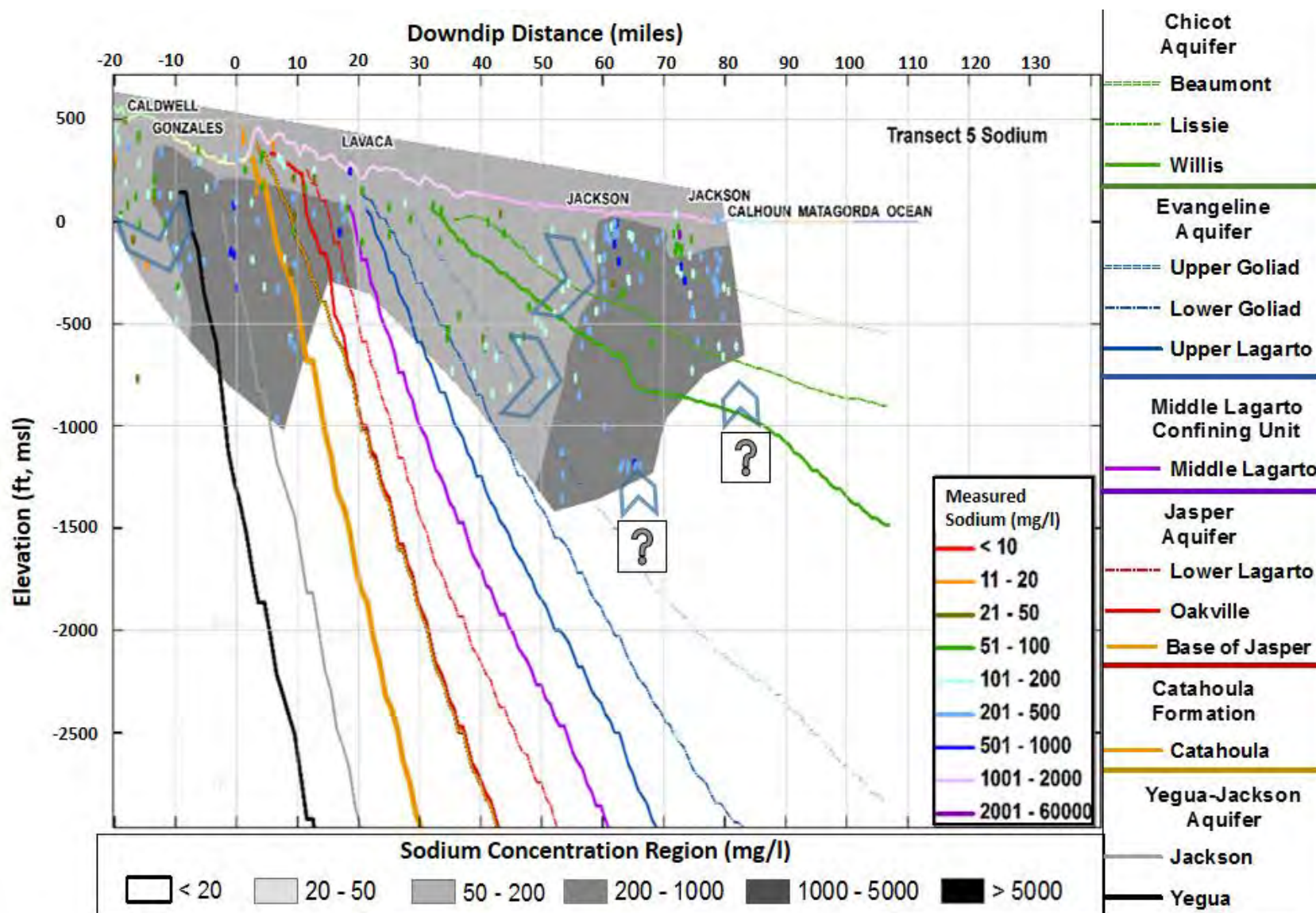


Figure 6-31 Concentration Maps for Na for Transect 5 in GMA 15. (Note: surfaces represent the bottom of each geological formation).

Final – Hydrogeochemical Evaluation of the Texas Gulf Coast Aquifer System and Implications for Developing Groundwater Availability Models

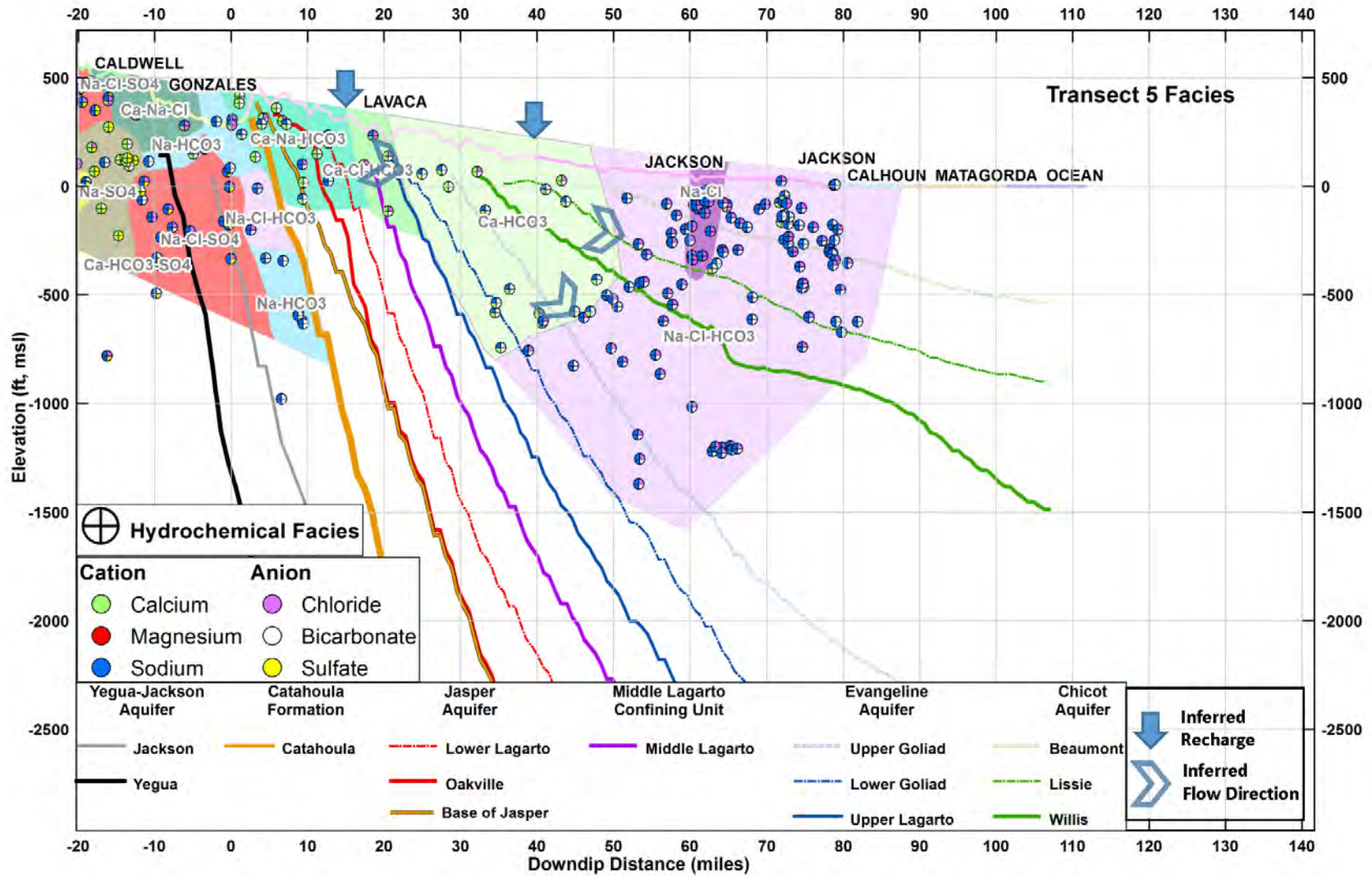


Figure 6-32 Hydrochemical facies for Transect 5 in GMA 15. (Note: surfaces represent the bottom of each geological formation).

Final – Hydrogeochemical Evaluation of the Texas Gulf Coast Aquifer System and Implications for Developing Groundwater Availability Models

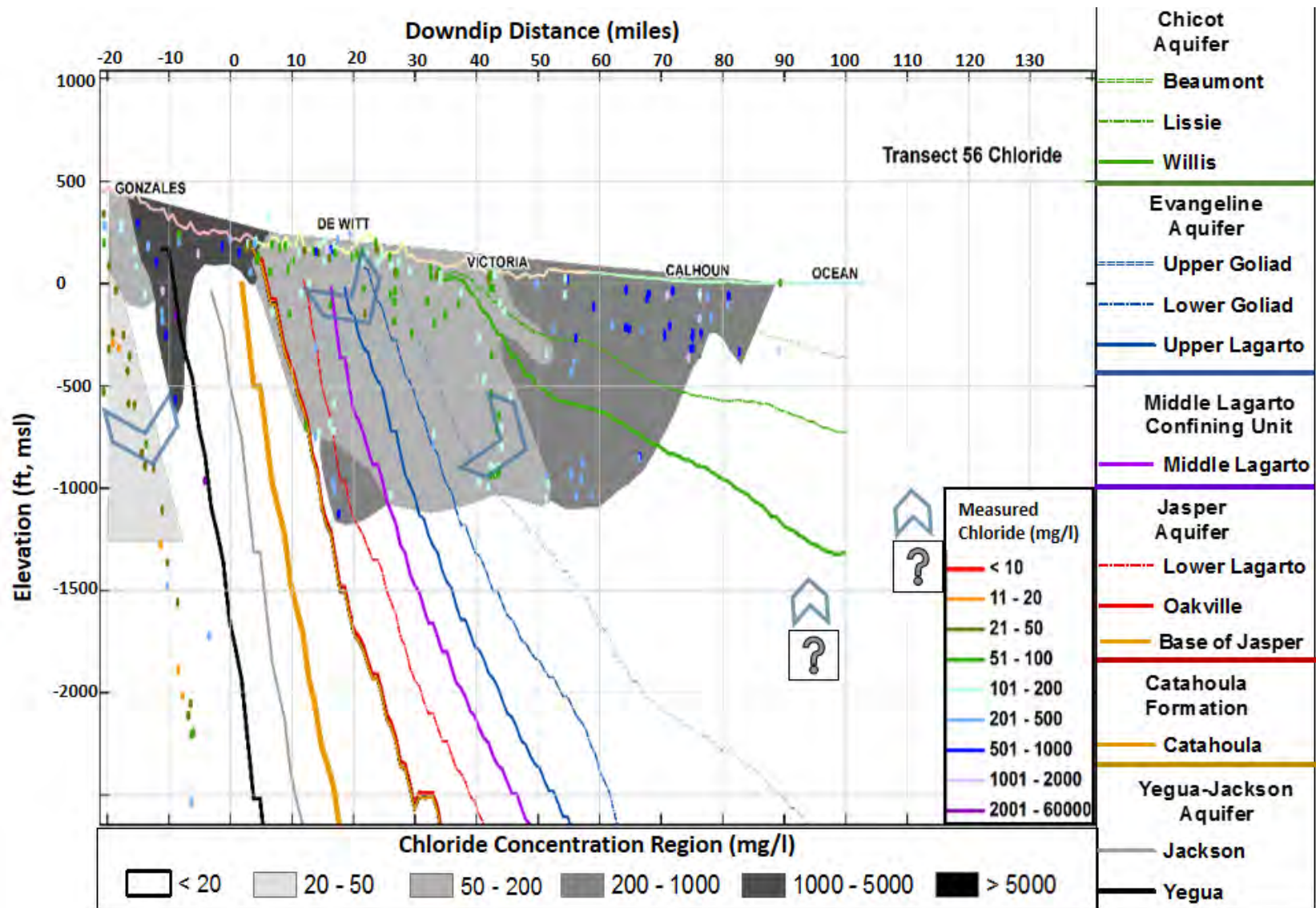


Figure 6-33 Concentration Maps for Cl for Transect 56 in GMA 15. (Note: surfaces represent the bottom of each geological formation).

Final – Hydrogeochemical Evaluation of the Texas Gulf Coast Aquifer System and Implications for Developing Groundwater Availability Models

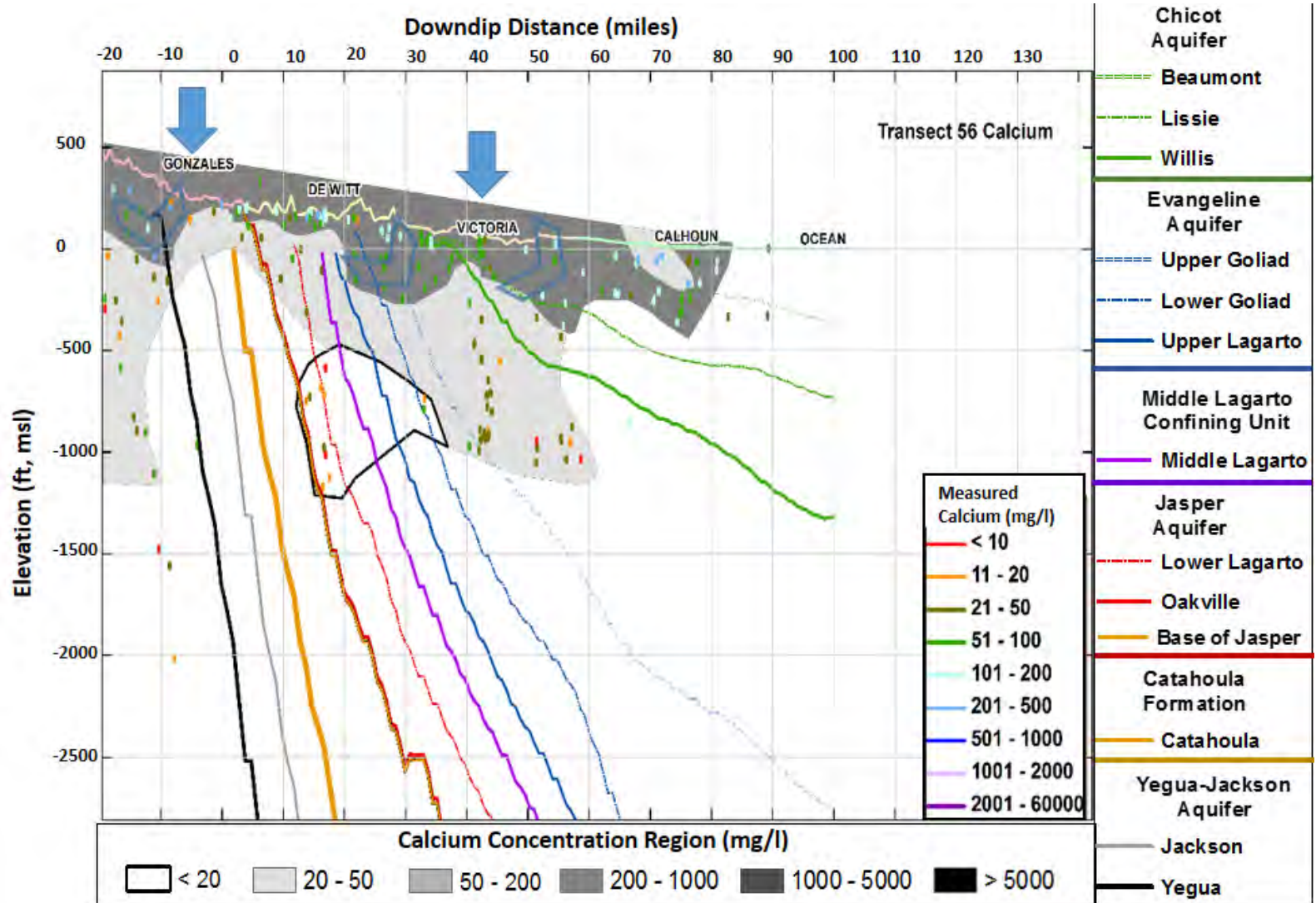


Figure 6-34 Concentration Maps for Ca for Transect 56 in GMA 15. (Note: surfaces represent the bottom of each geological formation).

Final – Hydrogeochemical Evaluation of the Texas Gulf Coast Aquifer System and Implications for Developing Groundwater Availability Models

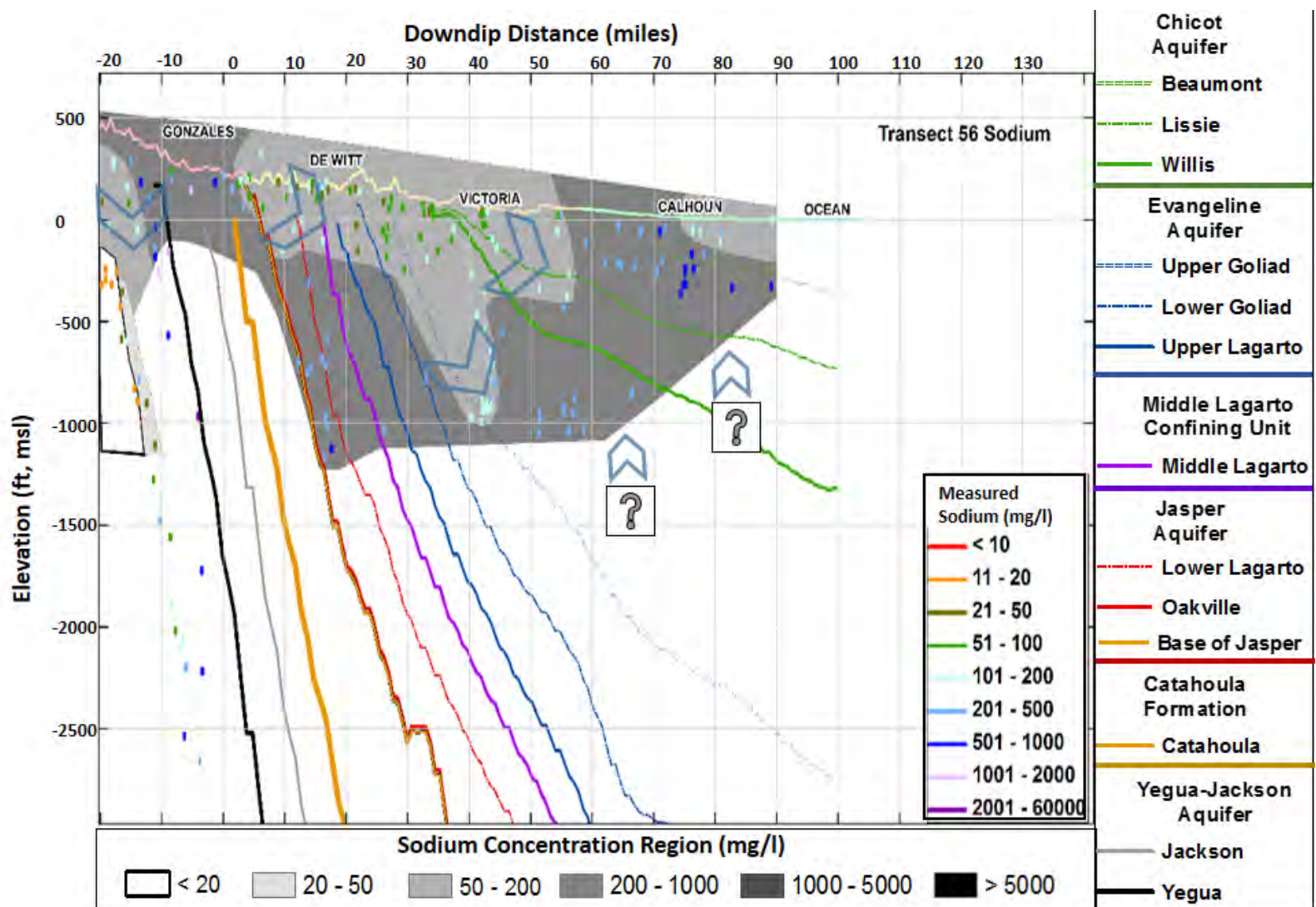


Figure 6-35 Concentration Maps for Na for Transect 56 in GMA 15. (Note: surfaces represent the bottom of each geological formation).

Final – Hydrogeochemical Evaluation of the Texas Gulf Coast Aquifer System and Implications for Developing Groundwater Availability Models

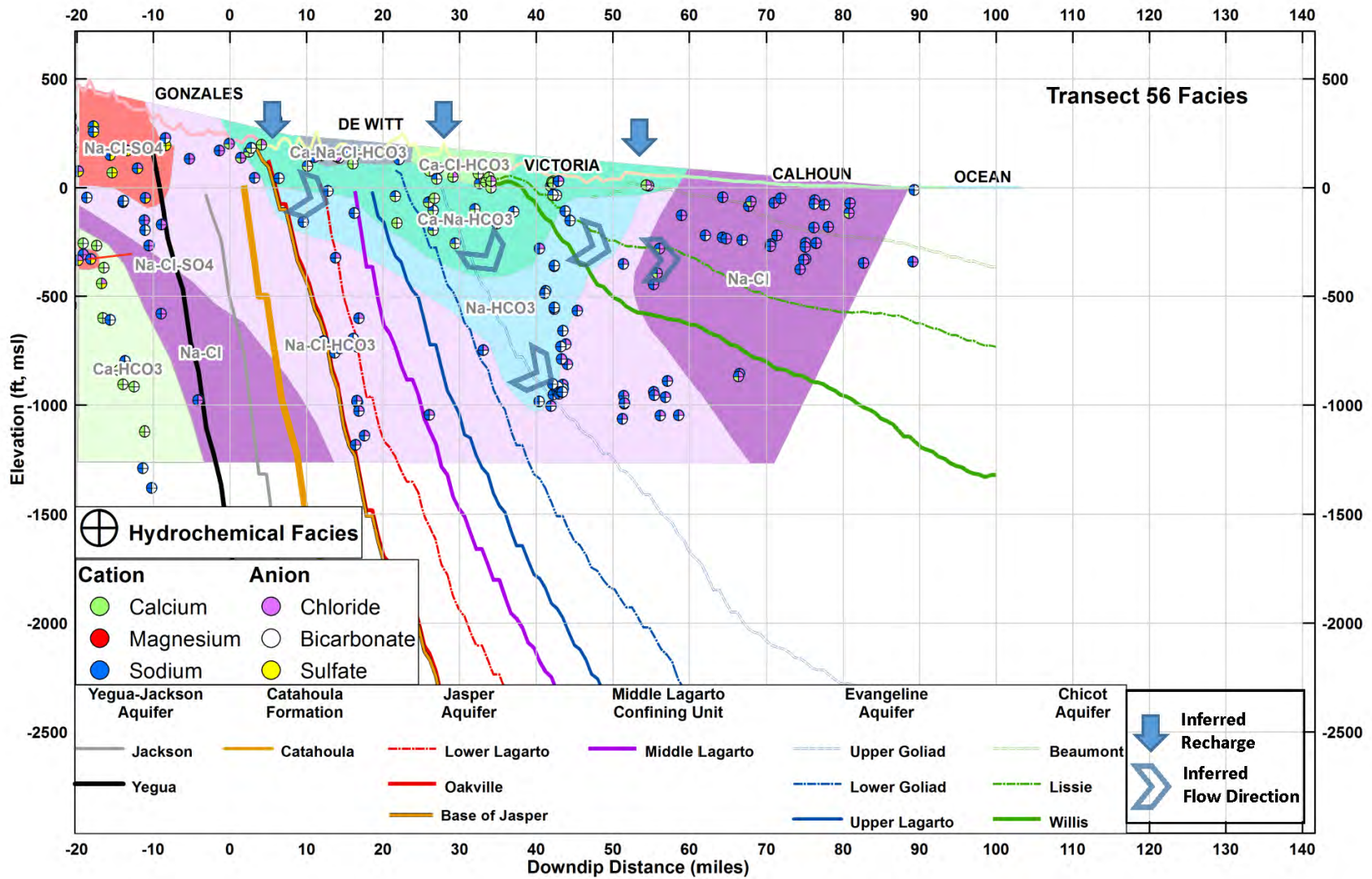


Figure 6-36 Hydrochemical facies for Transect 56 in GMA 15. (Note: surfaces represent the bottom of each geological formation).

Final – Hydrogeochemical Evaluation of the Texas Gulf Coast Aquifer System and Implications for Developing Groundwater Availability Models

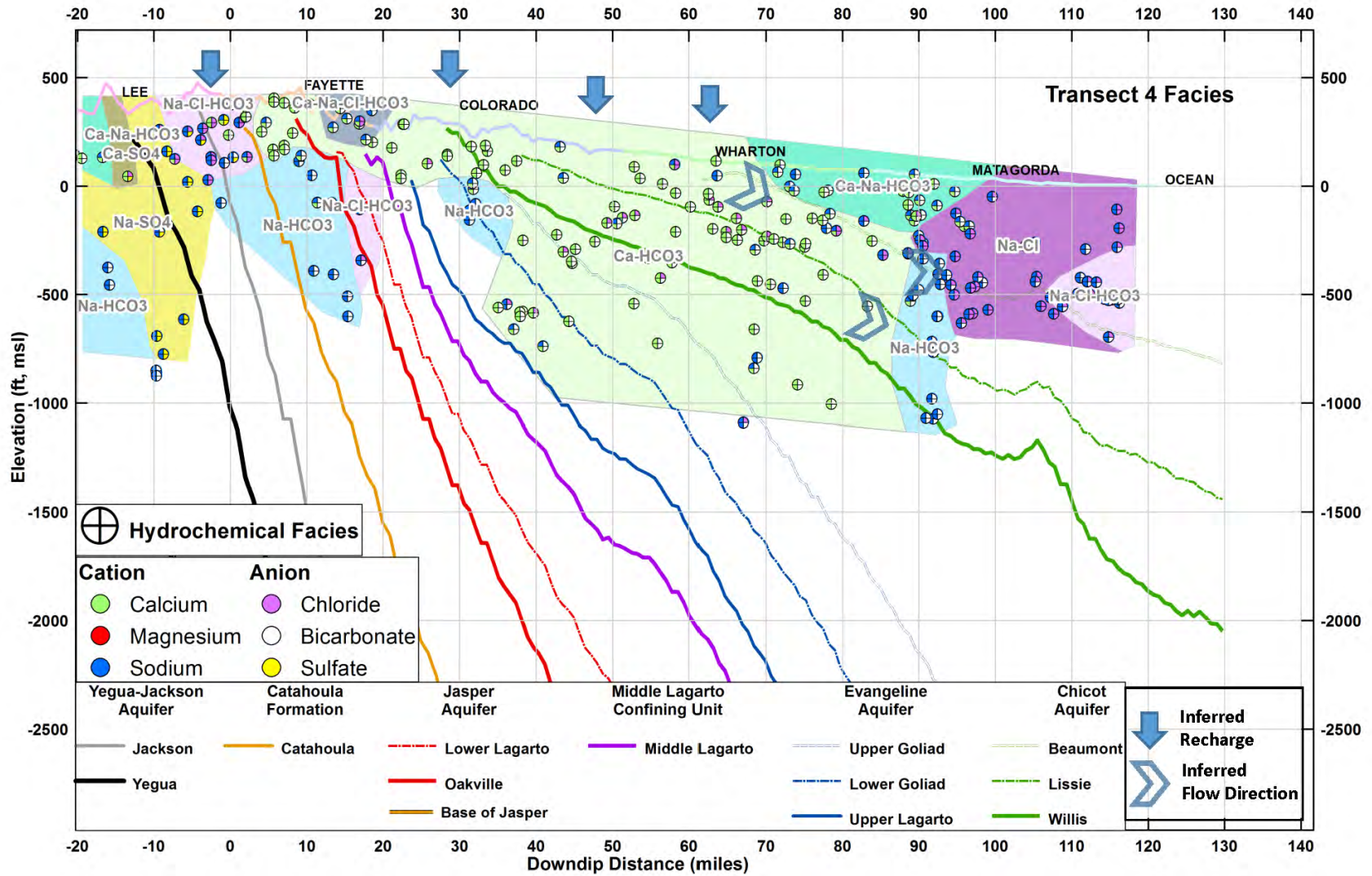


Figure 6-37 Hydrochemical facies for Transect 4 in GMA 15. (Note: surfaces represent the bottom of each geological formation).

Final – Hydrogeochemical Evaluation of the Texas Gulf Coast Aquifer System and Implications for Developing Groundwater Availability Models

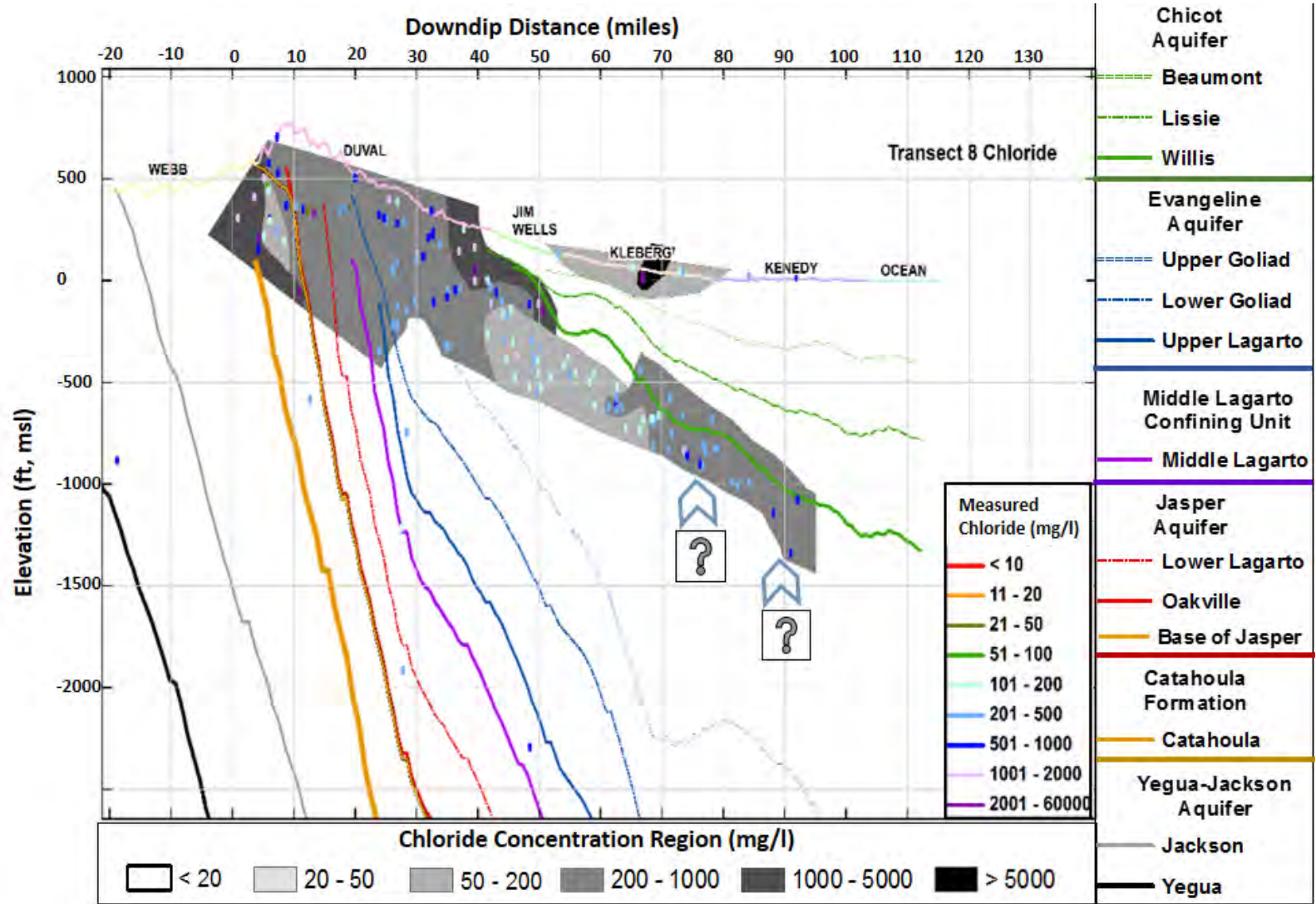


Figure 6-38 Concentration Maps for Cl for Transect 8 in GMA 16. (Note: surfaces represent the bottom of each geological formation).

Final – Hydrogeochemical Evaluation of the Texas Gulf Coast Aquifer System and Implications for Developing Groundwater Availability Models

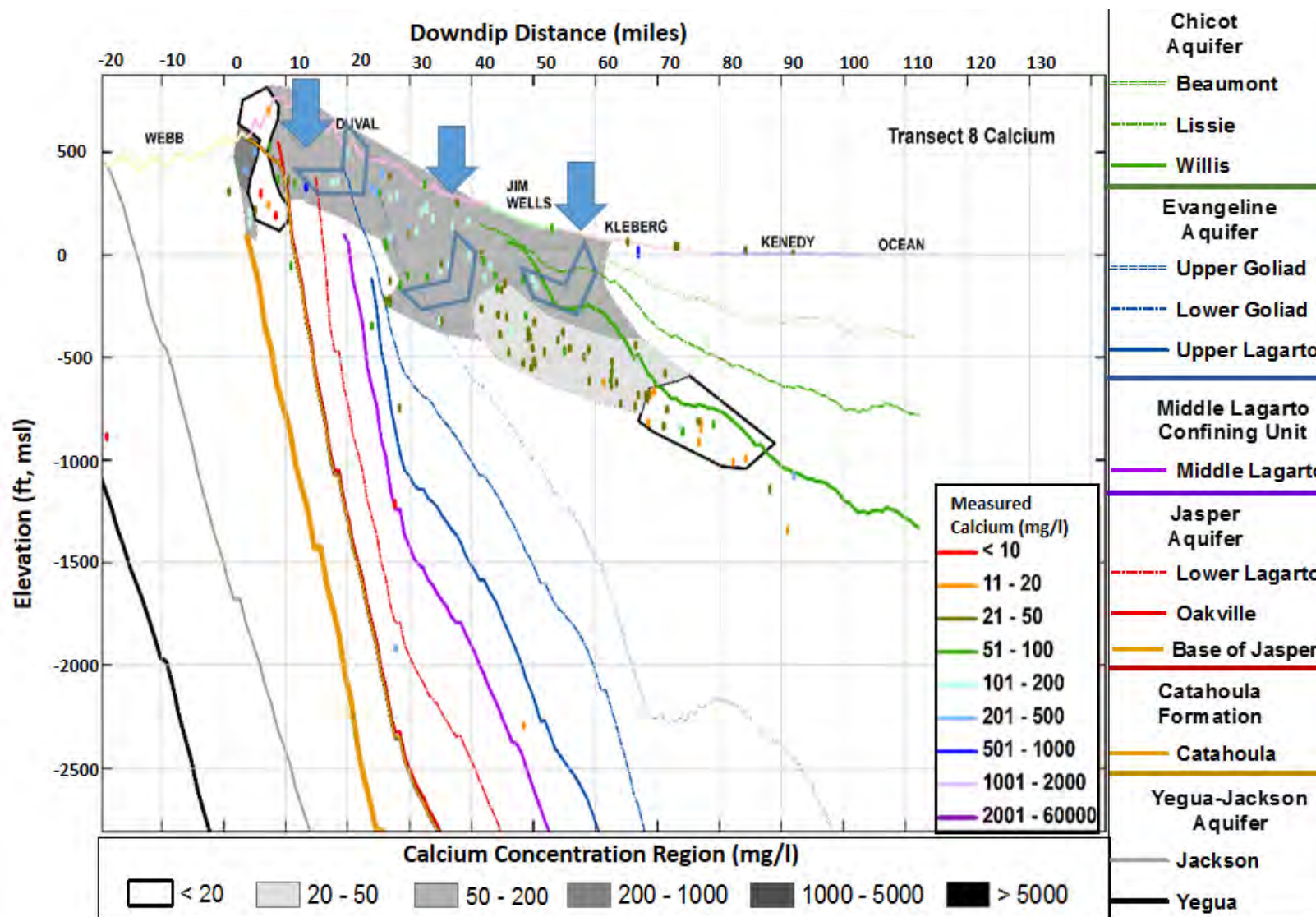


Figure 6-39 Concentration Maps for Ca for Transect 8 in GMA 16. (Note: surfaces represent the bottom of each geological formation).

Final – Hydrogeochemical Evaluation of the Texas Gulf Coast Aquifer System and Implications for Developing Groundwater Availability Models

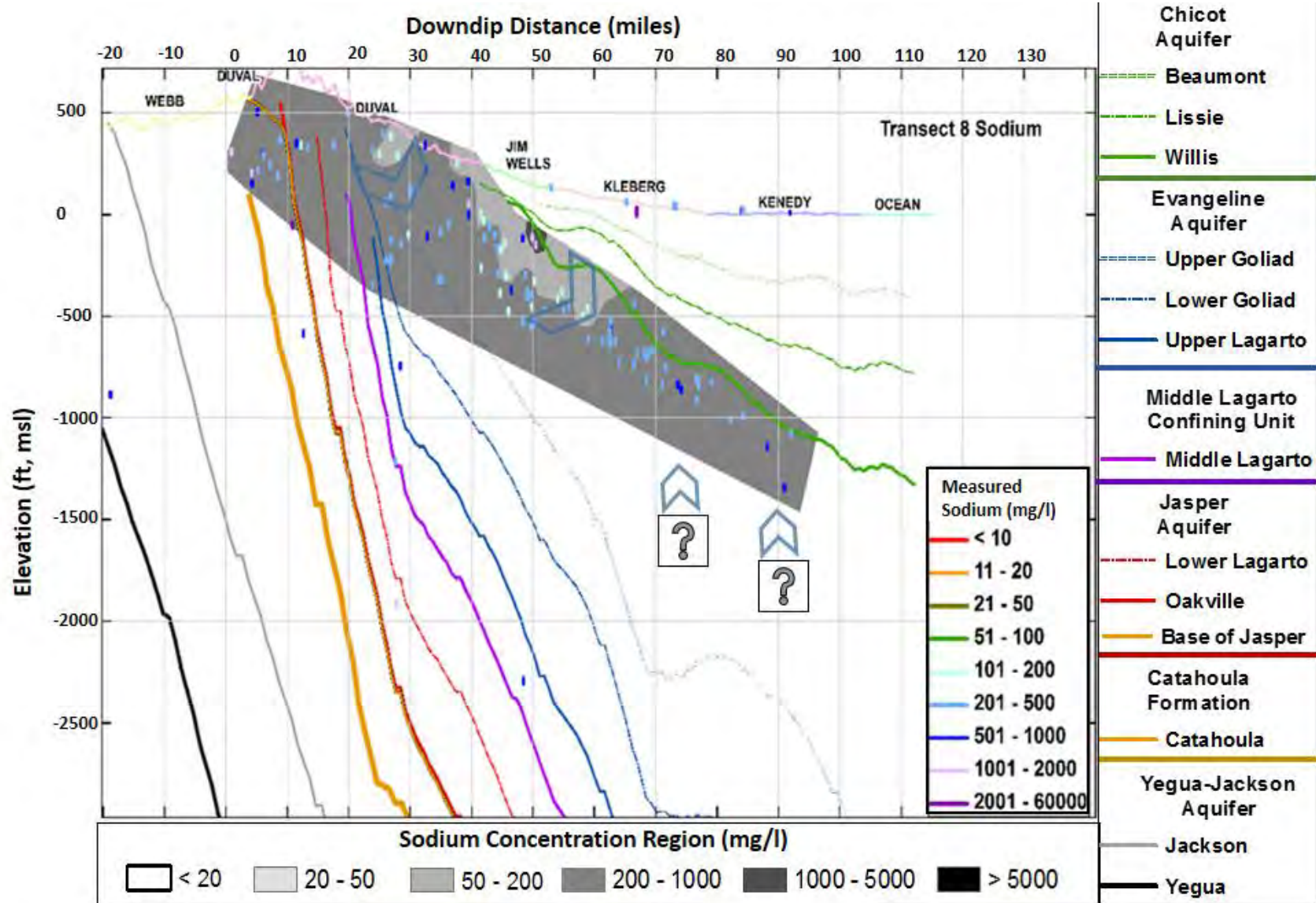


Figure 6-40 Concentration Maps for Na for Transect 8 in GMA 16. (Note: surfaces represent the bottom of each geological formation).

Final – Hydrogeochemical Evaluation of the Texas Gulf Coast Aquifer System and Implications for Developing Groundwater Availability Models

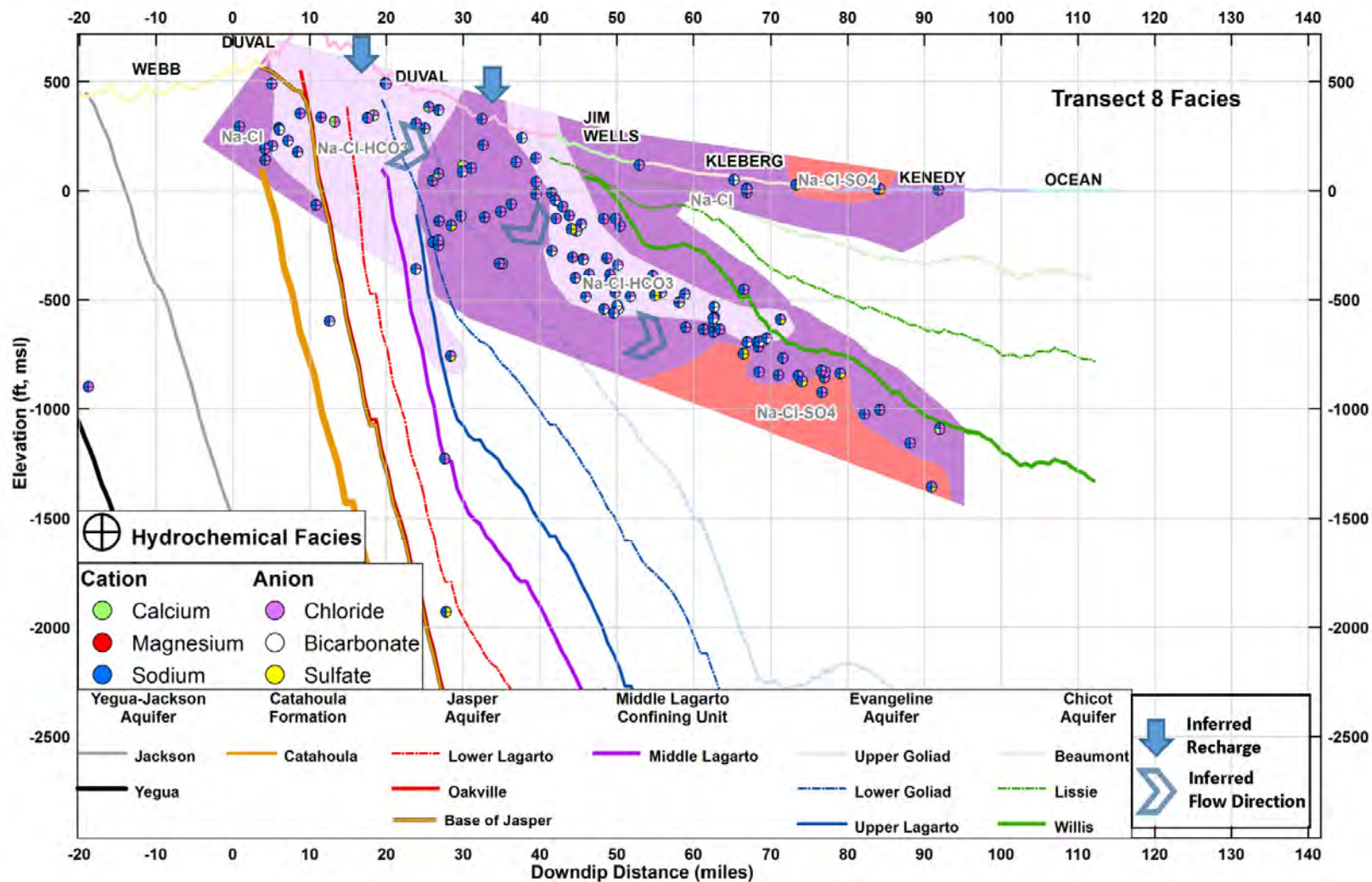


Figure 6-41 Hydrochemical facies for Transect 8 in GMA 16. (Note: surfaces represent the bottom of each geological formation).

Final – Hydrogeochemical Evaluation of the Texas Gulf Coast Aquifer System and Implications for Developing Groundwater Availability Models

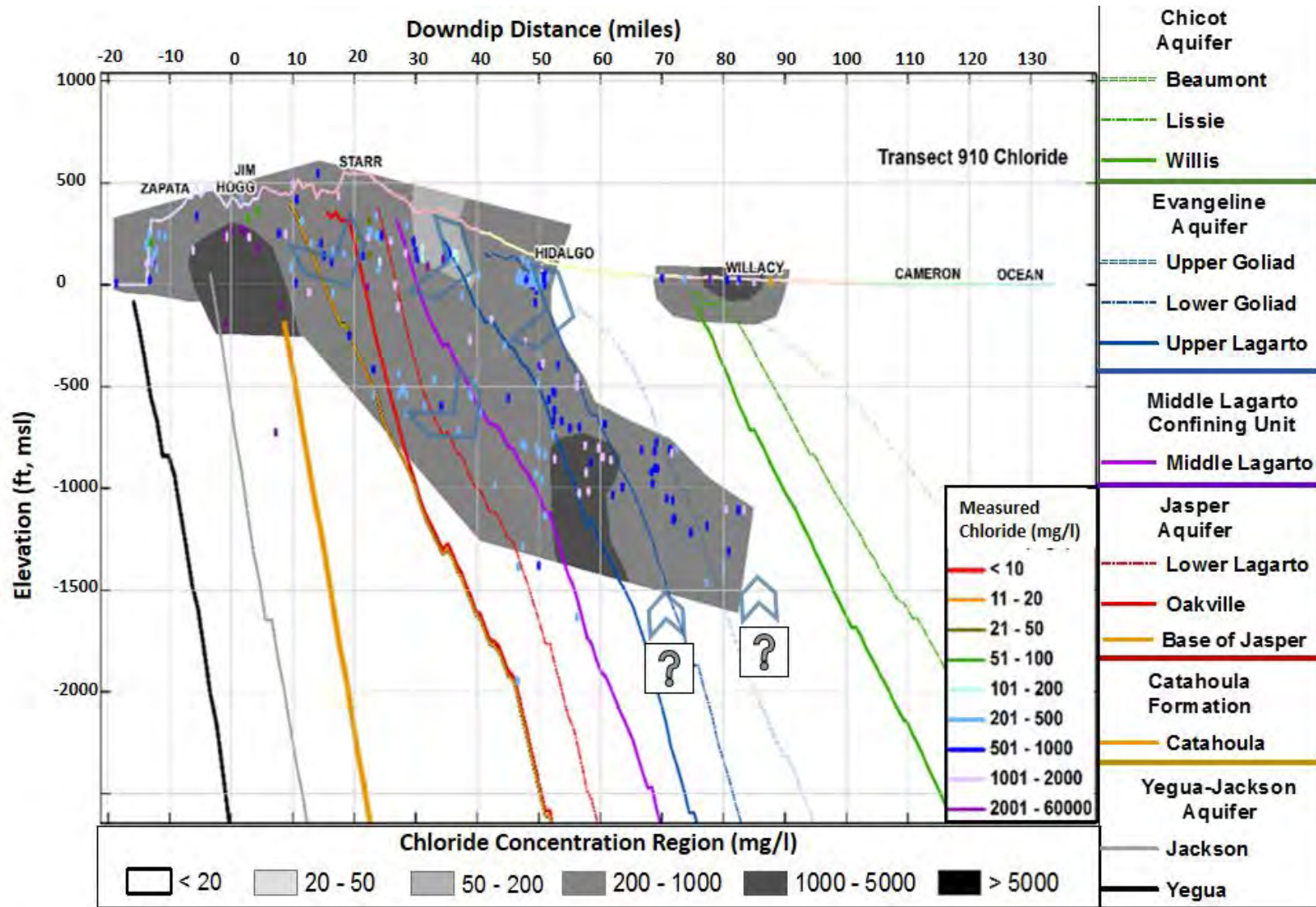


Figure 6-42 Concentration Maps for Cl for Transect 910 in GMA 16. (Note: surfaces represent the bottom of each geological formation).

Final – Hydrogeochemical Evaluation of the Texas Gulf Coast Aquifer System and Implications for Developing Groundwater Availability Models

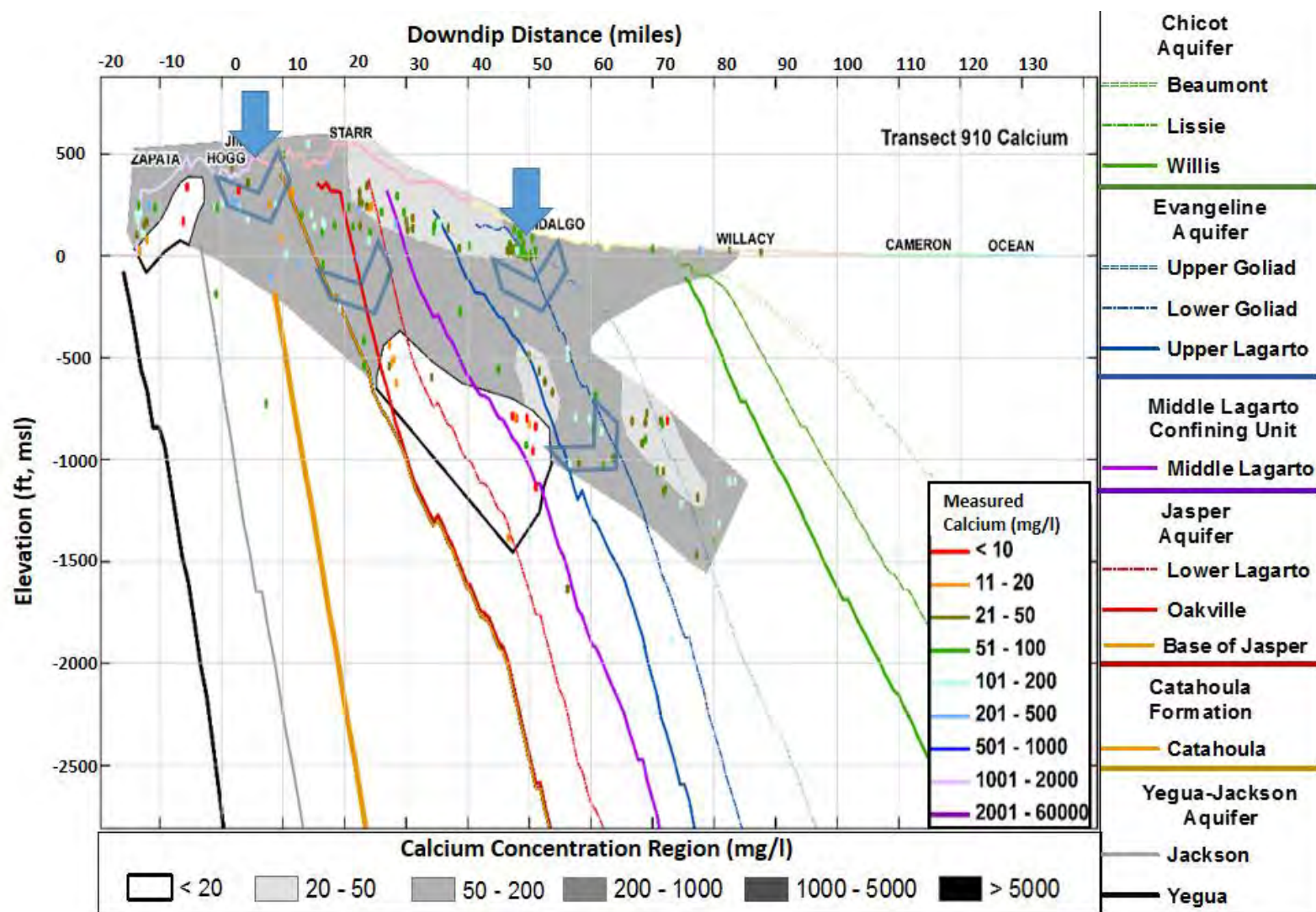


Figure 6-43 Concentration Maps for Ca for Transect 910 in GMA 16. (Note: surfaces represent the bottom of each geological formation).

Final – Hydrogeochemical Evaluation of the Texas Gulf Coast Aquifer System and Implications for Developing Groundwater Availability Models

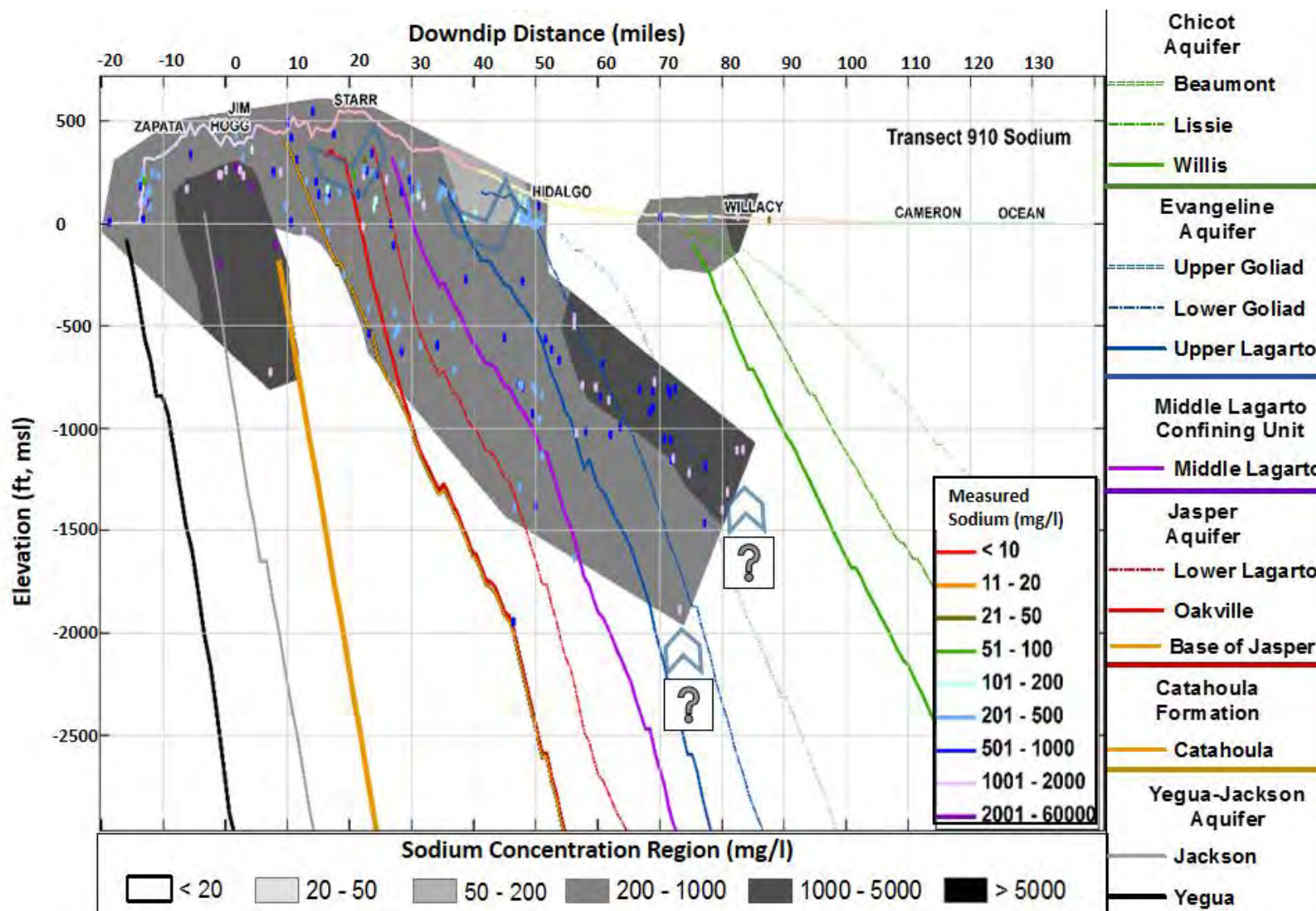


Figure 6-44 Concentration Maps for Na for Transect 910 in GMA 16. (Note: surfaces represent the bottom of each geological formation).

Final – Hydrogeochemical Evaluation of the Texas Gulf Coast Aquifer System and Implications for Developing Groundwater Availability Models

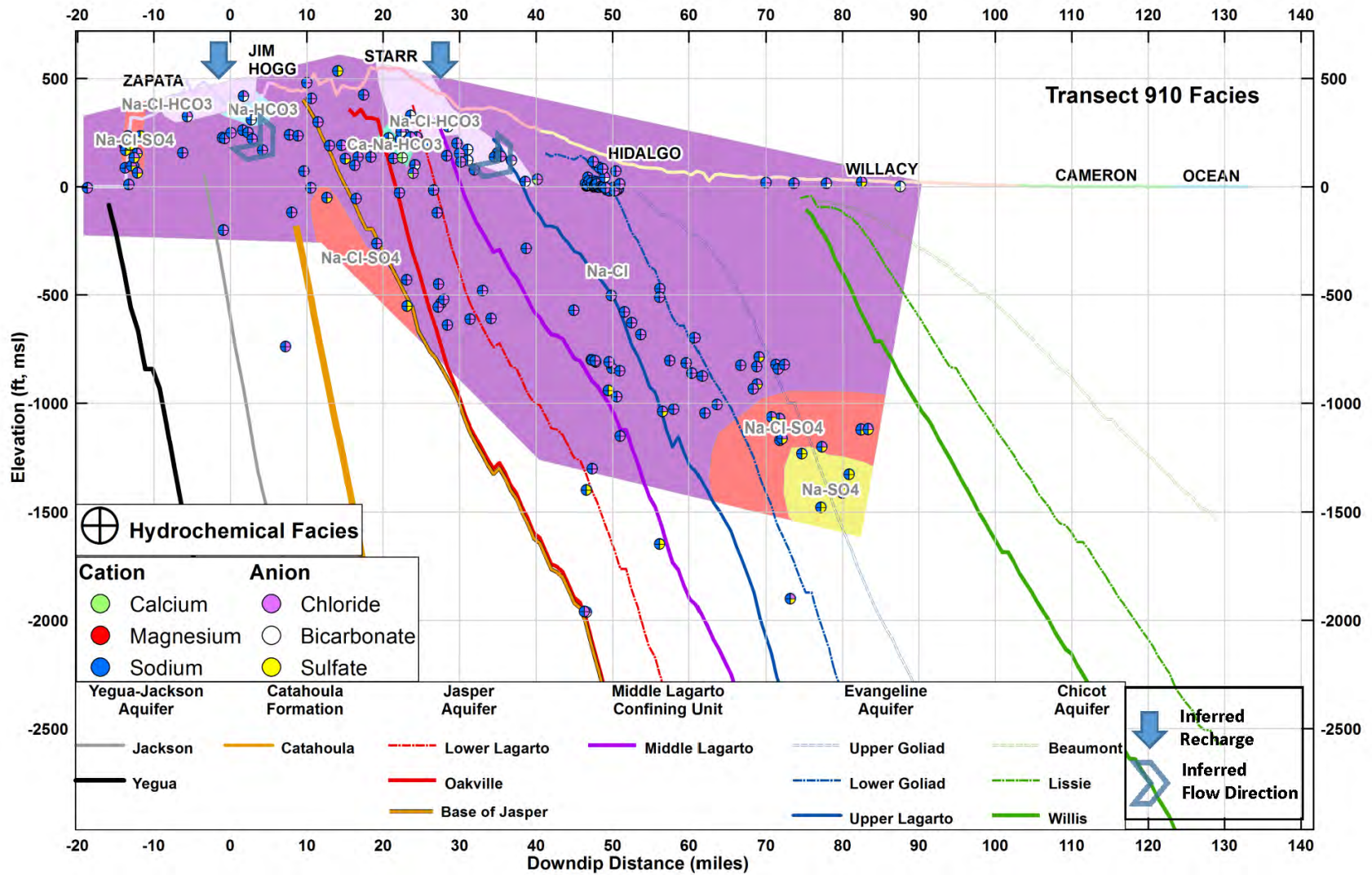


Figure 6-45 Hydrochemical facies for Transect 910 in GMA 16. (Note: surfaces represent the bottom of each geological formation).

Final – Hydrogeochemical Evaluation of the Texas Gulf Coast Aquifer System and Implications for Developing Groundwater Availability Models

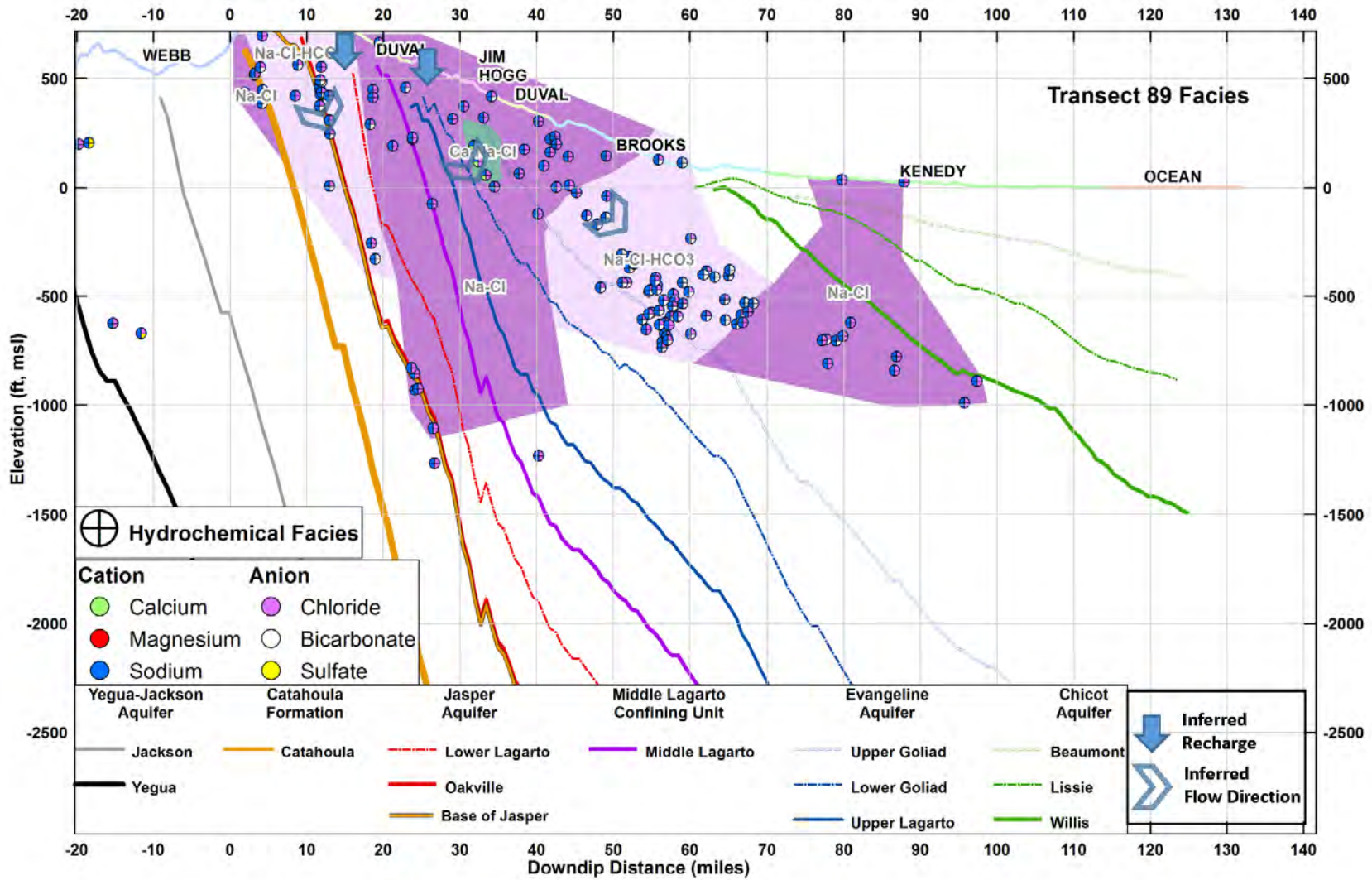


Figure 6-46 Hydrochemical facies for Transect 89 in GMA 16. (Note: surfaces represent the bottom of each geological formation).

Final – Hydrogeochemical Evaluation of the Texas Gulf Coast Aquifer System and Implications for Developing Groundwater Availability Models

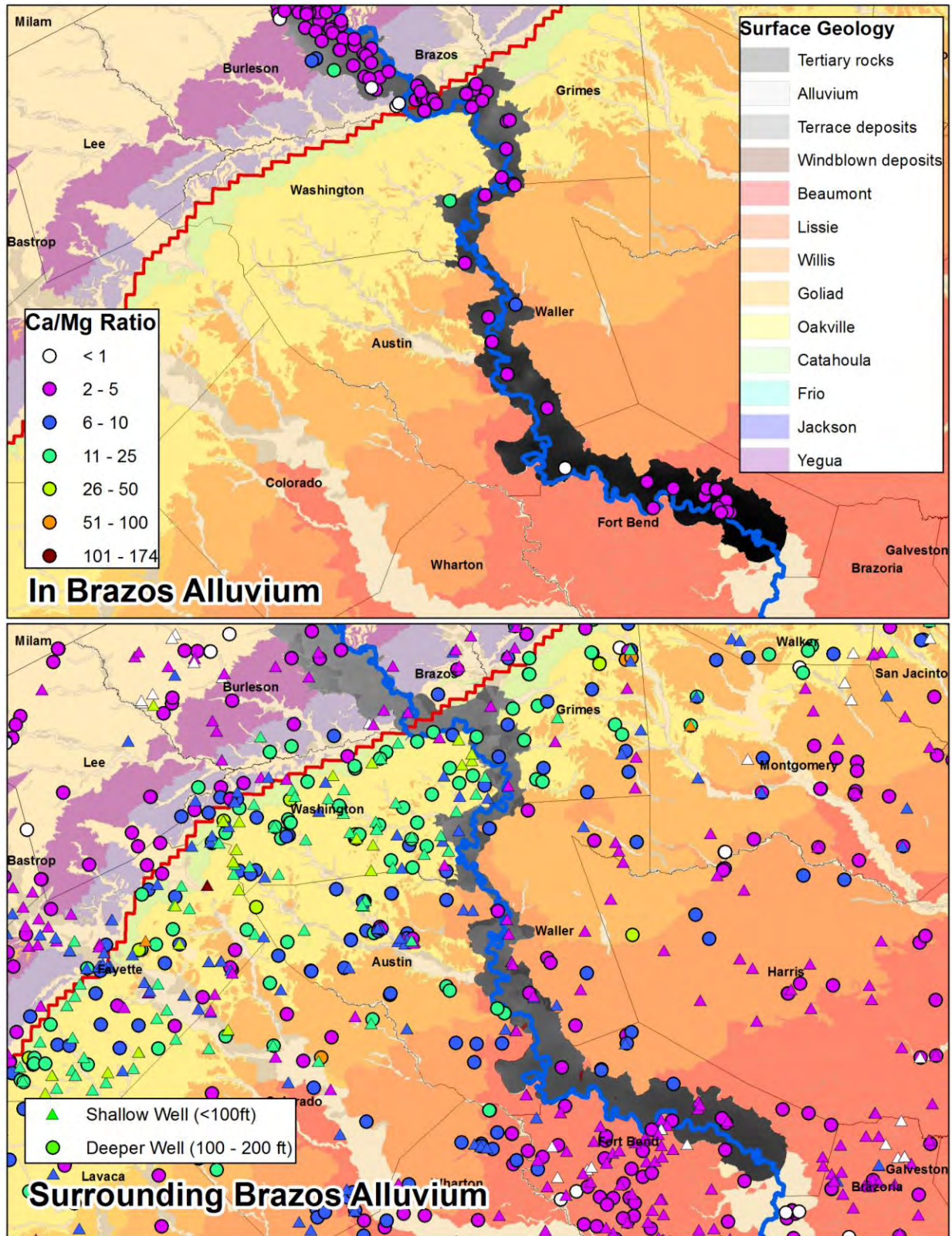


Figure 6-47 Calcium/Magnesium ratios for wells intersecting the Brazos River Alluvium and for wells that intersect deposits surrounding the Brazos River Alluvium.

Final – Hydrogeochemical Evaluation of the Texas Gulf Coast Aquifer System and Implications for Developing Groundwater Availability Models

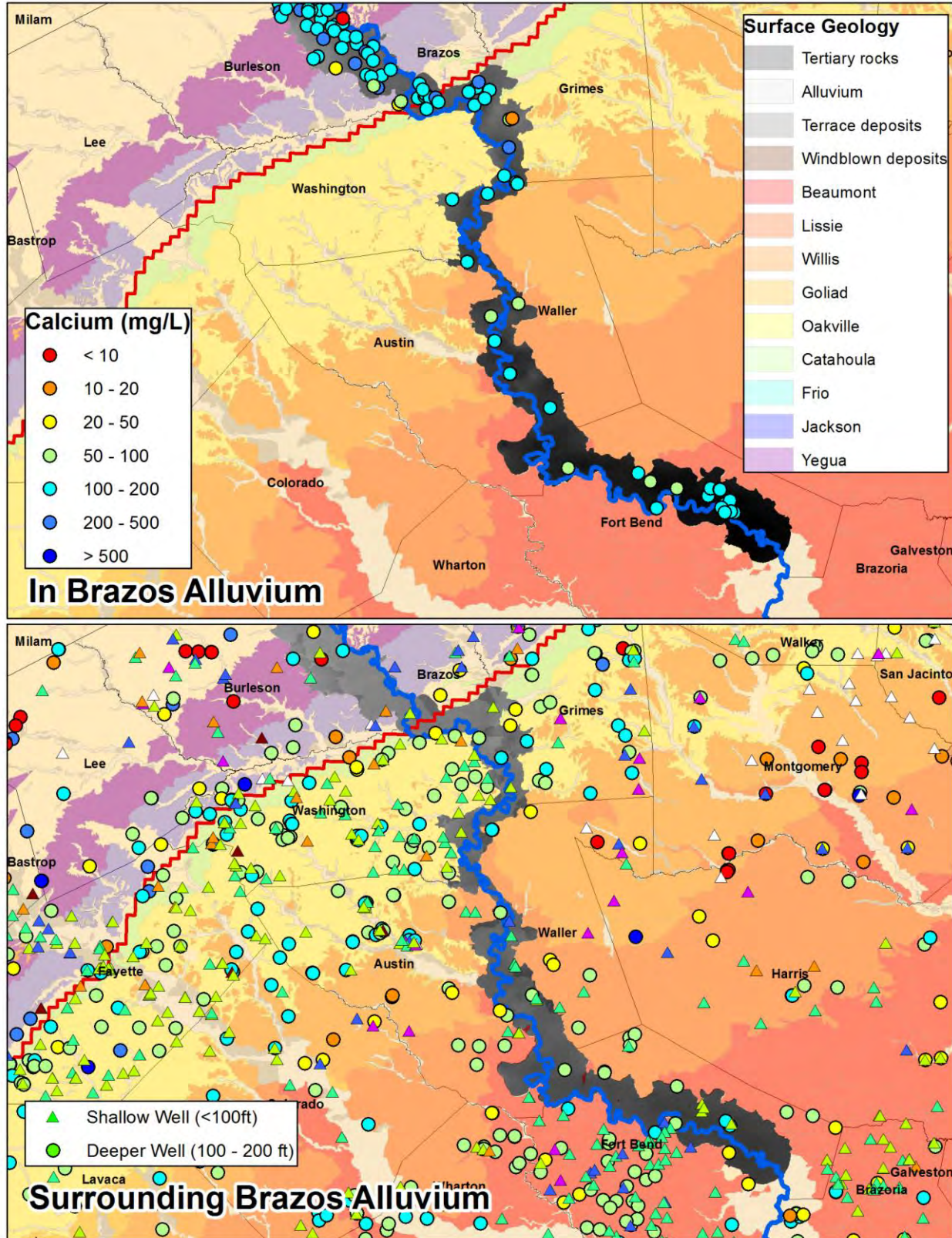


Figure 6-48 Calcium concentrations for wells intersecting the Brazos River Alluvium and for wells that intersect deposits surrounding the Brazos River Alluvium.

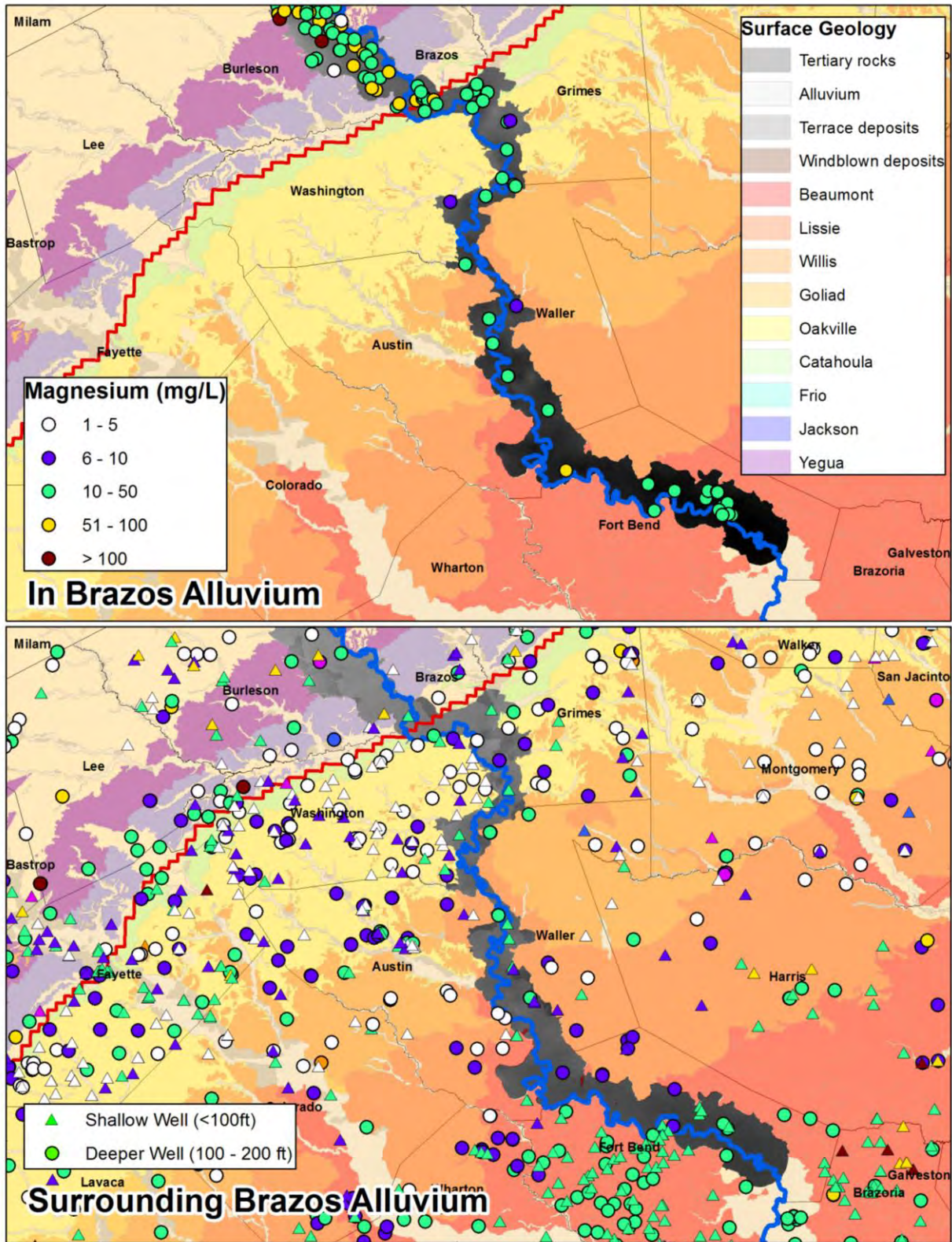


Figure 6-49 Magnesium concentrations for wells intersecting the Brazos River Alluvium and for wells that intersect deposits surrounding the Brazos River Alluvium.

7.0 Stable Isotopes

This section discusses measurements from stable isotopes. The isotopes of hydrogen and oxygen in water and the isotopes of hydrogen and carbon in method are used to develop hypothesis regarding the mixing and flow paths of groundwater.

7.1 Basic Concepts and Definitions

Isotope characteristics are determined by mass differences of the nucleus of an isotope of a specific atom. The nucleus is composed of proton and neutrons; that together gives the atomic weight of an element. For example, oxygen has 8 protons and 8 neutrons giving it an atomic weight of 16 ($^{16}_8\text{O}$). Only 0.2% of oxygen has 10 neutrons ($^{18}_8\text{O}$). Thus, the number of neutrons can vary and the range can be limited by the degree of instability caused by too few or too many neutrons. The representative isotopic compositions of the stable isotopes of hydrogen and oxygen are provided in Table 7-1.

Table 7-1 Abundance of hydrogen and oxygen isotopes (from Cook and Herczeg, 2000).

Element	Isotope	Abundance
Hydrogen	^1H	0.99985
	^2H	0.00015
Oxygen	^{16}O	0.99757
	^{17}O	0.00038
	^{18}O	0.00205

Stable isotopes do not disintegrate or decay and often record and retain isotopic composition of the parent material molecules of the same element with different masses reactive at different rates with other molecules. These differences cause partitioning or fractionation to occur during physical and chemical processes. In kinetic processes, statistical mechanics predicts the lighter (lower atomic mass) of two isotopes will be more reactive; hence, the lighter isotope is usually concentrated in reaction products and the heavier isotope becomes concentrated in the reactants (Cook and Herczeg, 2000).

Because variations in isotopes are relatively small, stable isotope ratios are reported relative to a standard as δ (called “delta”) values in units of parts per thousand (per mill and written as ‰).

The definition for δ is:

$$\delta_x = \delta_{x\text{-standard}} = \left[\frac{R_x}{R_{\text{standard}}} - 1 \right] \times 1000 \quad \text{Equation 7.1}$$

In equation 7.1, the subscript “x” refers to a measured value, the subscript “standard” refers to a chemical standard used by analytical laboratories, and the variable “R” represent a ratio being measured such as $^2\text{H}/^1\text{H}$ or $^{18}\text{O}/^{16}\text{O}$. For instance, a $\delta^{18}\text{O}$ of +30‰ indicates that the measured sample is enriched (or “heavy”) in ^{18}O by 3% relative to a laboratory standard. Similarly, a $\delta^{18}\text{O}$ of -30‰ indicates that the measured sample is depleted (or ‘light) in ^{18}O by 3% relative to a laboratory standard.

Isotopic compositions mix conservatively. In other words, the isotopic compositions of mixtures are intermediate between the compositions of the end members. Despite the awkward terminology (i.e., the notation and units of ‰) and negative signs, the compositions can be treated just like any other chemical constituent (e.g., chloride content) for making mixing calculations. The isotopic composition of substances formed by combining two or more substances is therefore determined by mass balance using $\delta_1 n_1 + \delta_2 n_2 + \delta_3 n_3 + \delta_4 n_4 + \delta_5 n_5 = \delta_f (n_1 + n_2 + n_3)$ where δ_1 is the δ value of component 1, n equals the amount of substance (atoms) in component 1 and δ_f is the δ value of the product (Coplen and others, 2000). Because of this additive property, the δ value for two mixing substances can be easily calculated if the δ value for each substance is known. For instance, the addition of 60% of water A with a $\delta^{18}\text{O}$ of -30‰ with 40% of water B with a ^{18}O of +10‰ will produce a water with a $\delta^{18}\text{O}$ of -14‰.

7.2 $\delta^2\text{H}$ and $\delta^{18}\text{O}$ in Precipitation

The $\delta^2\text{H}$ and $\delta^{18}\text{O}$ values for precipitation worldwide behave predictably, falling along the global meteoric water line (GMWL), which was originally defined by Craig (1961) but adjusted in 1993 by Rozanski and others (1993). In Figure 7-1, the GMWL is defined by Equation 7.2, which was developed by Rozanski and others (1993). In Equation 7.2, the values for $\delta^2\text{H}$ and $\delta^{18}\text{O}$ are measured against a standard called the Vienna Standard Mean Ocean Water (VSMOW). The VSMOW is a standard prepared by the International Atomic Energy Agency (IAEA) from

distilled seawater. Equations 7.3 and 7.4 define the meteoric water line for the contiguous 48 states in North America and for Texas, respectively (Kendall and Coplen, 2001).

$$\delta^2\text{H} = 8.13 \times \delta^{18}\text{O} + 10.8 \quad \text{Equation 7.2}$$

$$\delta^2\text{H} = 8.11 \times \delta^{18}\text{O} + 8.99 \quad \text{Equation 7.3}$$

$$\delta^2\text{H} = 7.5 \times \delta^{18}\text{O} + 2.3 \quad \text{Equation 7.4}$$

Variations in the ratios of $\delta^2\text{H}$ and $\delta^{18}\text{O}$ will occur over time as a result of temporal variations in temperature and storm characteristics. Winter precipitation is usually depleted in $\delta^2\text{H}$ and $\delta^{18}\text{O}$ relative to summer rains. Two precipitation studies in the southern United States close to our study area illustrate isotopic variations that can occur over time and distance. Pape and others (2010) analyzed precipitation at approximately bimonthly intervals in Austin, Texas, from 1999 to 2007. The $\delta^{18}\text{O}$ ranged from -12.6‰ to -1.1‰ and had a mean value of -4.1‰ . Pape and others (2010) developed Equation 7.5 as the Local Meteoric Water Line for Austin, Texas. Lambert and Aharon (2008) analyzed monthly precipitation samples from January 2005 to May 2008 for a site in Tuscaloosa, AL. The $\delta^{18}\text{O}$ ranged from -12.5‰ to 1.9‰ and had a mean value of -4.7‰ . Equation 7.6 is the LMWL for Tuscaloosa, AL.

$$\delta^2\text{H} = 7.1 \times \delta^{18}\text{O} + 6.7 \quad \text{Equation 7.5}$$

$$\delta^2\text{H} = 7.0 \times \delta^{18}\text{O} + 9.5 \quad \text{Equation 7.6}$$

The two main factors that control the isotopic signature of precipitation at a given location are: 1) the temperature of condensation of the precipitation, and 2) the degree of rainout of the air mass (the ratio of water vapor that has already condensed into precipitation to the initial amount of water vapor in the air mass). With increasing temperature, precipitation becomes enriched in the heavier isotopes, ^{18}O and ^2H , in a linear relationship. Temperature affects fractionation at a rate of approximately 0.5‰ for every 1°C for oxygen (Clark and Fritz, 1997). Among the factors that affect the relationships expressed by a meteoric water line are: (1) altitude, (2) latitude, (3) continental effects, (4) seasonal variation, (5) amount effect, and (6) apparent temperature relationship. Altitude effect is caused by topography and local climate with typical gradients of -0.15 to -0.5‰ ^{18}O , and -1.5 to -4‰ per 100m for ^2H (Clark and Fritz, 1997). Altitude effect is most commonly seen on mountains interior to a continent. $\delta^2\text{H}$ and $\delta^{18}\text{O}$ contents decrease with increasing latitude. The $\delta^2\text{H}$ and $\delta^{18}\text{O}$ isotopes decrease inland from a

coast due to removal of moisture from air masses as they are orographically uplifted. Evaporation increases the $\delta^2\text{H}$ and $\delta^{18}\text{O}$ content of precipitation of small rainfall events than large rainfall events (Coplen and others, 2000). Based on these factors, precipitation in cooler regions and in lower altitudes tend to be depleted in ^{18}O , whereas precipitation in warmer regions and in higher altitudes tend to be enriched in ^{18}O .

7.3 $\delta^2\text{H}$ and $\delta^{18}\text{O}$ in Groundwater

$\delta^2\text{H}$ and $\delta^{18}\text{O}$ values in groundwater are representative of values in precipitation that recharge the groundwater, unless some process after the water reaches the earth's surface as precipitation causes isotopic fractionation, and consequently, deviation from meteoric water lines. Some processes that cause fractionation are evaporation, exchange with the aquifer matrix, or recharge that occurred at a different temperature or under a different climate. Local meteoric water lines also may deviate from the GMWL. Shifts in $\delta^{18}\text{O}$ values may be affected by interaction with the aquifer matrix. Calcite interactions in carbonate aquifers or more complex exchanges with the rock matrix in geothermal systems are commonly observed causes of shifts in the $\delta^{18}\text{O}$ values. In general, there are fewer shifts in the $\delta^2\text{H}$ in aquifer systems because fifty percent or more of the total oxygen in the system is usually resident in the rocks, but almost all of the hydrogen in the system is in the water (Drever, 1997).

Stable isotopes are often used to track water molecules derived from specific recharge source areas during groundwater movement from the outcrop to the saturated zone. Solute concentrations and isotopes acquired from rainfall, and modified during recharge, provide information on the history of a water parcel. Changes that occur in the subsurface due to evapotranspiration, dissolution-precipitation reactions, and isotopic exchanges can provide information on the origin, rates of movement, and evolution of water, and thus help in characterization of the groundwater flow system.

Because the ultimate origin of groundwater is from precipitation, stable isotopes of oxygen and deuterium (^2H) are often interpreted using the $\delta^2\text{H}$ and $\delta^{18}\text{O}$ plot with GMWL as a reference line. Several processes cause water to deviate from the GMWL. The impact of these processes on the ratio between $\delta^2\text{H}$ and $\delta^{18}\text{O}$ and the value of $\delta^{18}\text{O}$ are shown in Figure 7-2 and are discussed below.

Evaporation: Evapotranspiration from arid or semi-arid land can cause the soil moisture and hence groundwater to be enriched in $\delta^2\text{H}$ and $\delta^{18}\text{O}$. The effects of evaporation will be a function of vegetation, soil type, the residence time for the unsaturated water, and depth to the water table.

High Temperature Exchange with Rocks: The exchange of isotopes between the subsurface material and groundwater will occur because meteoric water is often highly depleted in ^{18}O compared to the minerals in the groundwater. In circulating groundwater systems, isotope exchange will not occur at rates that can cause quantitative significant changes in the groundwater until the system is at least above 100°C .

Exchange with Hydrogen Sulfide (H_2S): Among the gases that are produced and often emitted by oil & gas reservoirs in the Texas Gulf Coast are methane and hydrogen sulfide, H_2S . Where high concentrations of sulfate produce sufficient H_2S , groundwater can become enriched in $\delta^2\text{H}$ in groundwater to the point where H_2S is depleted by over 500%.

Hydration of Silicates: Hydration of silicates occurs at temperatures below 300°C but where there are very low water-rock ratios and the contact period is over long geologic times. Reactions such as the alteration of feldspar (anorthite) to clay (kaolinite) results in a significant uptake of water, which causes fractionation of ^{18}O between the groundwater and the silicate structure.

The Na-Cl salinity isotopic composition found in many sedimentary basins such as the Gulf Coast Aquifer System indicate that the brines originated as seawater that experienced salinity increases through evaporation or evaporite dissolution (Clark and Fritz, 1997). Clayton and others (1966) summary of brine compositions show a trend of ^{18}O enrichment with minor ^2H enrichment.

From about 4,000 to 10,000 feet deep, brine occurs in the Catahoula Formation in the Texas Gulf Coast (Kreitler and others, 1988). At the shallower depths not under geopressure, Kreitler and others (1988) report a transition zone characterized by mixing of meteoric water with in situ formation water. Salinities vary laterally and vertically, typically ranging from 10,000 ppm to 50,000 ppm TDS. In the lower parts of the brine section that are not under geopressure, waters are assumed to be original formation waters and several million years old, with salinities varying from 80,000 to 150,000 ppm TDS.

7.3.1 Measured Values of $\delta^2\text{H}$ and $\delta^{18}\text{O}$ in the Texas Gulf Coast

Figure 7-3 presents the results of $\delta^2\text{H}$ and $\delta^{18}\text{O}$ measurements assembled as part of this study as well as results for the deep and very deep Catahoula assembled by Kreitler and others (1988). The well depths associated with the measurements from this study are less than 1,800 ft except for the Transect 3 well number 20, which has a depth of about 4,000 feet. With the exception of few of the samples, the ratio of $\delta^2\text{H}$ to $\delta^{18}\text{O}$ plot along the GWML within ± 2 ‰ $\delta^{18}\text{O}$ and within ± 10 ‰ $\delta^2\text{H}$. Most of the data points from the three transects plot along and slightly to the left of the GMWL, indicating their derivation from modern recharge events under similar humid climatic conditions that exist today. The exception is Well 3-20, which plots significantly enriched with $\delta^{18}\text{O}$ relative to the GWML and has similar characteristics with the signatures for the deep Catahoula samples from Kreitler and others (1988). The significant enrichment of the deep Catahoula samples is attributed to the high temperature exchange with rocks (see Figure 7-2).

To help minimize problems with mixing of groundwater at various depths across long well screens and problems with wells being screened across two different depth categories, all wells from this study with known well screens greater than 250 feet were omitted from Figure 7-3. Out of approximately 180 wells with stable isotope measurements, 85 wells had screen information, and 15 wells had wells screens longer than 250 feet.

The proximity of the stable isotopes signatures from this study to the GWML in Figure 7-3 indicates that the sample groundwater is meteoric water. To investigate whether there is evidence of a hydrogeologic process that could help explain some of the scatter, the data was partitioned into groups based on amount that the $\delta^{18}\text{O}$ has been enriched or $\delta^2\text{H}$ depleted relative to the GWML. Figure 7-4 shows that the isotopic values in Group 3 (enriched $\delta^{18}\text{O}$ and/or depleted $\delta^2\text{H}$) tend to plot in GMA 16, whereas the values in Group 1 (depleted $\delta^{18}\text{O}$ and/or enriched $\delta^2\text{H}$) tend to plot in or near GMA 14. The Group 3 data plots primarily in GMA 16, which is the warmest and driest GMA and therefore the GMA with the greater evaporation potential. Because evaporation (see Figure 7-2) of soil moisture and groundwater leads to enriched $\delta^{18}\text{O}$ and depleted $\delta^2\text{H}$ values, evaporation is considered as the primary reason for the spread of data points below the GWML in Figure 7-3. As a result of evaporation, the concentration or buildup of rainfall constituents in the soil moisture is expected to be the greatest in GMA 16.

To help investigate the geochemical processes responsible for the scatter of points above the GWML (see Zone 1 in Figures 7-3 and 7-4), the stable isotope data was plotted as a function of depth and GMA. Because several isotope samples are in GMA 12 and 13, these samples were included in the analysis despite being from the Yegua-Jackson aquifer. For GMA 12, 13, 14, 15, and 16, the mean and median were calculated for wells with depths greater and less than 500 ft. The range of these means and medians are shown in Table 7-2 for GMA 12 and 13 and for GMA 14, 15, and 16. Table 7-2 shows that the means and medians are similar among the GMAs 14, 15, and 16 for the analysis of $\delta^{18}\text{O}$ and $\delta^2\text{H}$ measurements. This result indicates that the hydrogeologic process(es) contributing to the shift in isotopic ratios above the GWML line is not caused by a process that is depth-dependent, and hence time dependent, signature and is not localized geographically. Although some of the processes in Figure 7-2 may account for shift above the GWML, we have been able through our analysis to identified whether any of these processes or just localized spatial variability in rainfall is the primarily reason for the groundwater samples with isotopic signatures above the GWML.

One of the observations in Table 7-2 is that there are the large differences between the isotopic signatures for GMA 12 and 13 and those for GMA 14, 15, and 16. These differences suggest that isotopic measurements may be used to identify whether groundwater is from the Gulf Coast Aquifer System or the Yegua-Jackson Aquifer. However, in the authors opinion there is insufficient data to more thoroughly investigate this relationship. Additional work and data should be collected to determine whether there is a statistical significance between in the isotopic composition of groundwater between at the transition between the Yegua Jackson and the Gulf Coast Aquifer System.

Table 7-2 Comparison of the Means and Medians for $\delta^{18}\text{O}$ and $\delta^2\text{H}$ value for isotope measurements in GMAs shown in Figure 7-4.

Isotope	Statistic	Wells in Each GMA Group			
		12 and 13		14, 15, 16	
		< 500 ft depth	>500 ft depth	< 500 ft depth	>500 ft depth
$\delta^{18}\text{O}$	Range of Means	-5.2 to -5.0	-5.3 to -4.9	-4.4 to -4.2	-4.6 to -4.2
	Range of Medians	-5.1 to -5.0	-5.3 to -5.0	-4.4 to -4.1	-4.6 to -4.3
$\delta^2\text{H}$	Range of Means	-29 to -30	-29 to -30	-27 to -22	-26 to -22
	Range of Medians	-30 to -30	-30 to -30	-26 to -22	-26 to -22

7.3.2 Evidence for Mixing, Flow Paths, and/or Age

All of the $\delta^{18}\text{O}$ and $\delta^2\text{H}$ measurements of groundwater samples taken from the Groundwater Aquifer System from well with depths less than 1,800 feet bgs have isotopic signatures that closely match the GWML. Groundwater from wells with depths greater than 4,000 feet bgs from the Catahoula Formation have isotopic signature that are not close to the GWML and have TDS concentration that qualify as a brine. The up dip regions of the Catahoula are meteoric while the downdip regions of the Catahoula are suspected of containing large amounts of formation water that has not been flushed by meteoric water. The isotopic signatures of groundwater is consistent with the Gulf Coast Aquifer System consisting primarily of meteoric water and with a base that consists of brine in the deeper and downdip regions of the Catahoula and possibly the Jasper Aquifer.

Based on water level measurement in the deep Catahoula from Kreitler and others (1988) and from Well 3-20 (LBG Guyton and INTERA, 2012), it appears that the vertical hydraulic gradient is upward from the brine in the Catahoula Formation to the meteoric water. Near the coastline, the groundwater samples do not exhibit and observable enrichment of $\delta^{18}\text{O}$ and $\delta^2\text{H}$. Enrichment of $\delta^{18}\text{O}$ and $\delta^2\text{H}$ would occur if salt water intrusion from the ocean had mixed with the groundwater.

7.4 $\delta^2\text{H}$ and $\delta^{13}\text{C}$ in Methane

Methane (chemical symbol CH_4) is a ubiquitous gas, found in natural environments ranging from deep crustal settings and sedimentary basins to soils, surface waters, and the atmosphere. As a component of carbonate evolution in groundwaters, it participates in the carbon cycle and contributes to greenhouse gases. Methane is a highly reduced form of carbon that can play an important role in many geochemical reactions in the subsurface. In shallow sediment, methane is produced and consumed by bacterial processes. In the deeper sections of the Earth's crust, methane is produced by the conversion of organic matter under the influence of elevated temperatures or thermogenic processes (Aravena and others, 1995; Schoell, 1980).

The bacterial formation of methane in the shallow subsurface follows two principle pathways, i.e., via CO_2 reduction and fermentation. The reactions for these pathways are shown below. The reaction pathway (i.e., acetate fermentation or CO_2 reduction) will affect differently the isotopic composition of the methane and the evolution of the dissolved inorganic carbon. In

acetate fermentation, (reaction 1) the surrounding water produces only one of four hydrogen molecules to the product methane while in CO₂ reduction (reaction 2) all the methane hydrogen is related to the deuterium of the surrounding water (Schoell, 1980, Martini and others, 2008). Therefore, reaction (2) should show more of a positive correlation between δ²H-H₂O and δ²H-CH₄ (Osborn and McIntosh, 2010) than would reaction 1.



When evaluating the effects of fermentation and CO₂ reduction on the production of methane, not only it is important to recognize the different effect each has on the isotopic make up of methane but also the aging aspect associated with the sequence of methane formation. Schoell (1980) states that in very general terms, fermentation usually precedes CO₂ reduction. In a situation where formation is the predominant process in very young, recently deposited sediments, there is the likelihood that methane would be lost to the atmosphere before it could become trapped and buried (Jenden and Kaplan, 1988; Coleman and others, 1988). This aging aspect is consistent with the observation that all bacterial gases in oil/gas reservoirs and older marine sediments are similar and have the isotopic character for methane derived by CO₂ reduction (Claypool and Kaplan, 1974; Schoell, 1980).

Thermogenic gases are typically associated with coal bed and oil & gas formation and are formed at deeper depths by: (1) thermal cracking of sedimentary organic matter into hydrocarbon liquids and gas (this gas is co-genetic with oil, and is called "primary" thermogenic gas), and (2) thermal cracking of oil at high temperatures into gas ("secondary" thermogenic gas) and pyrobitumen. Bacterial generated gas is very dry (i.e., it consists almost entirely of methane) and typically contains above 1,000 times more methane than ethane. In contrast, thermogenic gas can be dry, or can contain significant concentrations of "wet gas" components (ethane, propane, butanes) and condensate (C₅₊ hydrocarbons).

Based on a review of the isotopic composition of methane from areas that encompass bacterial and thermogenic methanes, Schoell (1980) identified the areas on a plot of δ²H_{CH₄} versus δ¹³C_{CH₄} that are diagnostic to the source of methane. Figure 7-5 maps these areas along with the isotopic signatures for the groundwater samples that contained sufficient methane gas to have the isotopic composition of their hydrogen and carbon atoms determined. As shown in Figure 7-5, nearly all

measured data points fall in the thermogenic field designated for methane formed during thermal cracking of kerogen or hydrocarbons (Aravena and others, 1995; Clark and Fritz, 1997; Schoell, 1980). Because ethane and propane are generally not coproduced during microbial methanogenesis, the presence of higher-chain hydrocarbons is often used as another indicator of deeper thermogenic gas (Aravena and others, 1995; Osborn and others, 2011). In the groundwater samples with higher concentrations of methane, the presence of C₂ and C₃₊ compounds are present, which supports a possible thermogenic origin of the gas.

A positive correlation of $\delta^2\text{H}_{\text{H}_2\text{O}}$ and $\delta^2\text{H}_{\text{CH}_4}$ is often considered a strong indicator of microbial methane (Osborn and McIntosh, 2010). In the Gulf Coast Aquifer System, $\delta^2\text{H}_{\text{CH}_4}$ and $\delta^2\text{H}_{\text{H}_2\text{O}}$ fails to show any such relationship(in Figure 7-6) for the entire data set. The lack of a positive correlation between the two sources of hydrogen supports a non-methanogenic origin of most of the methane.

7.4.1 Transect 3 (GMA 14)

There are 18 measurements of fixed gas composition in the collected sample (Table 4-3), and of those, six samples had measureable methane, and in all six cases, there are substantial quantities of other heavier hydrocarbon gas fractions which confirms this to be fugitive thermogenic gas, probably from lower stratigraphic intervals. The measurements of the $\delta^{13}\text{C}$ of methane range from $\delta^{13}\text{C}_{\text{C}_1}$ of -46.9‰ to -60.8‰ and the $\delta^2\text{H}_{\text{C}_1}$ of methane range from -294‰ to -172‰.

These fall in the range expected for thermogenic gas (Figure 7-5). The dissolved hydrocarbon gases are in all cases, believed to be predominantly from thermogenic origin, probably diffusing from depth, and the gas fraction and isotopic signature supports the fugitive origin rather than any *in situ* organic oxidation/reduction reactions indicative of a process that would impact the age calculations. Similarly the $\delta^{13}\text{C}$ of carbon dioxide ranges from -8.2‰ to -21.7‰ and does not infer oxidation of organic material along the flow path which would be more depleted or an origin in significant amounts from deep hydrocarbon reservoirs which would provide a strongly enriched isotopic signature.

7.4.2 Transect 5 (GMA 15)

The dissolved hydrocarbon gases are in some samples a significant mole percent of the fixed gas composition, whereas in most other transects the methane fixed gas content is below detection limit. Of the 10 samples analyzed for fixed gas content in Transect 5, all but two (5-19 and 5-20) have measureable methane ranging from 0.2 to 50.9 percent of the dissolved gas by volume

(Table 4-4). Many of these samples are from deep wells, the deepest being 1,235 feet below land surface (bls), while three are relatively shallow (200, 300, and 324 ft. bls). The presence of wetter gas or higher carbon fractions, e.g., C₂-C₄ in virtually all samples is a thermogenic signature. This is accompanied by $\delta^{13}\text{C}_{\text{C}_1}$ in the range of -41.5‰ to -59.9‰ which is a commonly observed range for thermogenic gas; however, with the exception of the value at Well 5-15 at -65‰, which is suspected of being mixed sources of thermogenic and biogenic gas (see Figure 7-5). The $\delta^2\text{H}_{\text{C}_1}$ are in the range of -182‰ to -226‰, which eliminates fermentation as a process but does allow for some coal-bed methane generated by carbon dioxide reduction locally. The mixed source interpretation for samples $\delta^{13}\text{C}_{\text{C}_1}$ near -60.0‰ is also supported by the disproportionately high percent of methane to ethane in some samples. The biogenic gas component may have been derived from sources such as lignite in the lithologic section, but methanogenesis in which methane is formed from carbon dioxide reduction is not significant enough to impact the general groundwater carbonate chemistry, because the residual carbon dioxide $\delta^{13}\text{C}$ is not noticeably enriched. Rather the $\delta^{13}\text{C}_{\text{CO}_2}$ is as depleted as typical soil carbon dioxide in the -20‰ to -17‰ range.

7.4.3 *Transect 8 (GMA 16)*

The dissolved hydrocarbon gases in all cases were at low concentrations and from thermogenic origin, probably diffusing from depth, and the gas fraction and isotopic signature supports the fugitive origin rather than any *in situ* organic oxidation reaction indicative of a process that would impact the age calculations. Only two samples produced sufficient methane for analysis of isotopic composition. These two samples had a $^{13}\text{C}_{\text{C}_1}$ of about -43‰ and a $\delta^2\text{H}_{\text{C}_1}$ of about -171‰. As shown in Figure 7-5, these values produce a ratio that indicates gases of thermogenic origin. Similarly the $\delta^{13}\text{C}$ of carbon dioxide is almost invariant in the -14‰ range and does not infer oxidation of organic material along the flow path or an origin in significant amounts from deep hydrocarbon reservoirs.

7.4.4 *Evidence for Mixing, Flow Paths, and Age*

Morton (1980) discussed in detail methane entrapment in the geopressed aquifers of the Texas Gulf Coast, where substantial quantities of methane are contained within Tertiary sediments that exhibit abnormally high temperature and pressure gradients. Some of the methane occurs as dispersed free gas and some is dissolved in the hot overpressured brines (Morton, 1980). The methane gas can readily escape through faults or other hydraulic conduits from the geopressed

sections due to buoyancy, migration in the form of bubbles or through cross-formational flow upgradient into the shallower parts of the aquifer. Multiple lines of evidence suggest that the gas in the sampled groundwater is thermogenic in origin formed in the deeper parts of the Gulf Coast Aquifer System. The presence of thermogenic methane at all transects confirms that there are pathways for vertical migration to occur from depths measured in the thousands of feet to the zone of meteoric water. However, exact pathways for methane migration and brine migration cannot be definitively determined and quantified in absence of detailed characterization of the subsurface.

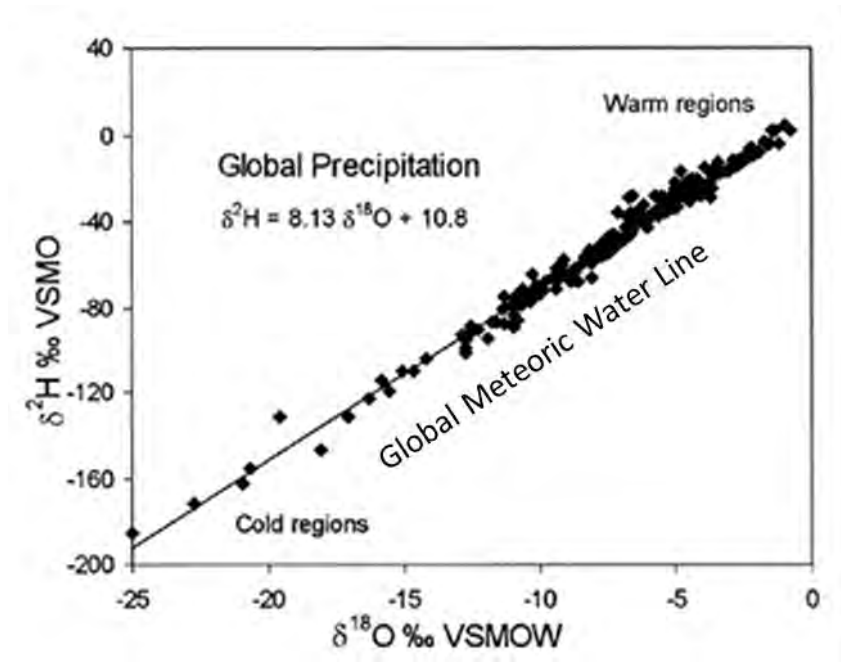


Figure 7-1 The meteoric relationship between $\delta^{18}\text{O}$ and $\delta^2\text{H}$ in precipitation. Data are weighted average annual values for precipitation monitored at stations in the International Atomic Energy Agency global network as compiled by Rozanski and others (1993) (modified from Figure 2-1 from Clark and Fritz (1997)).

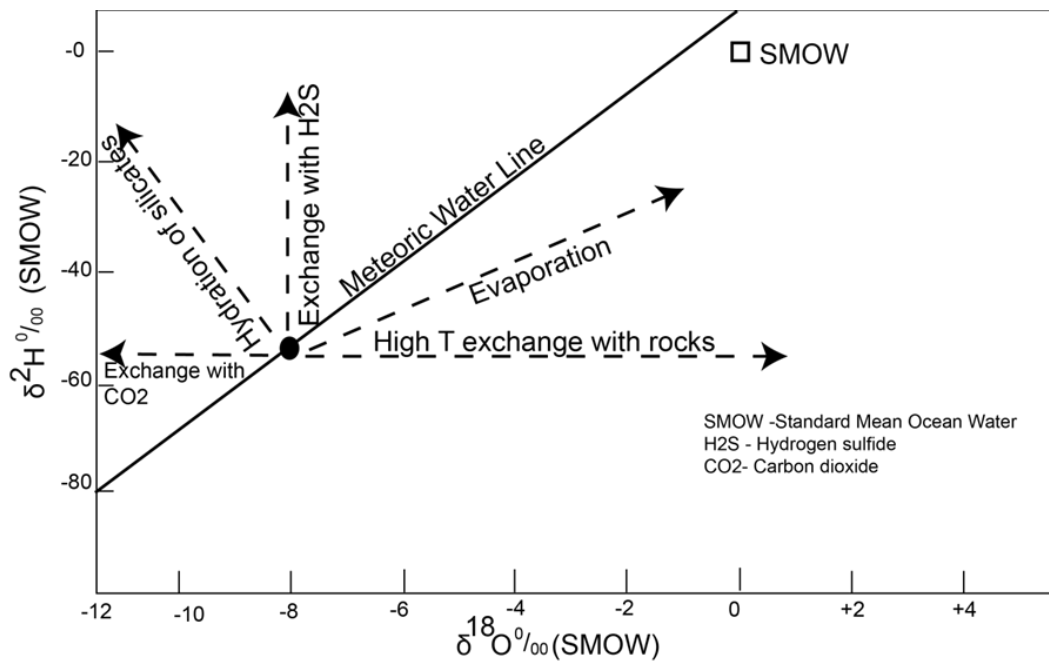


Figure 7-2 Isotope exchange processes that can modify the isotopic composition of meteoric water (after Clark and Fritz, 1997).

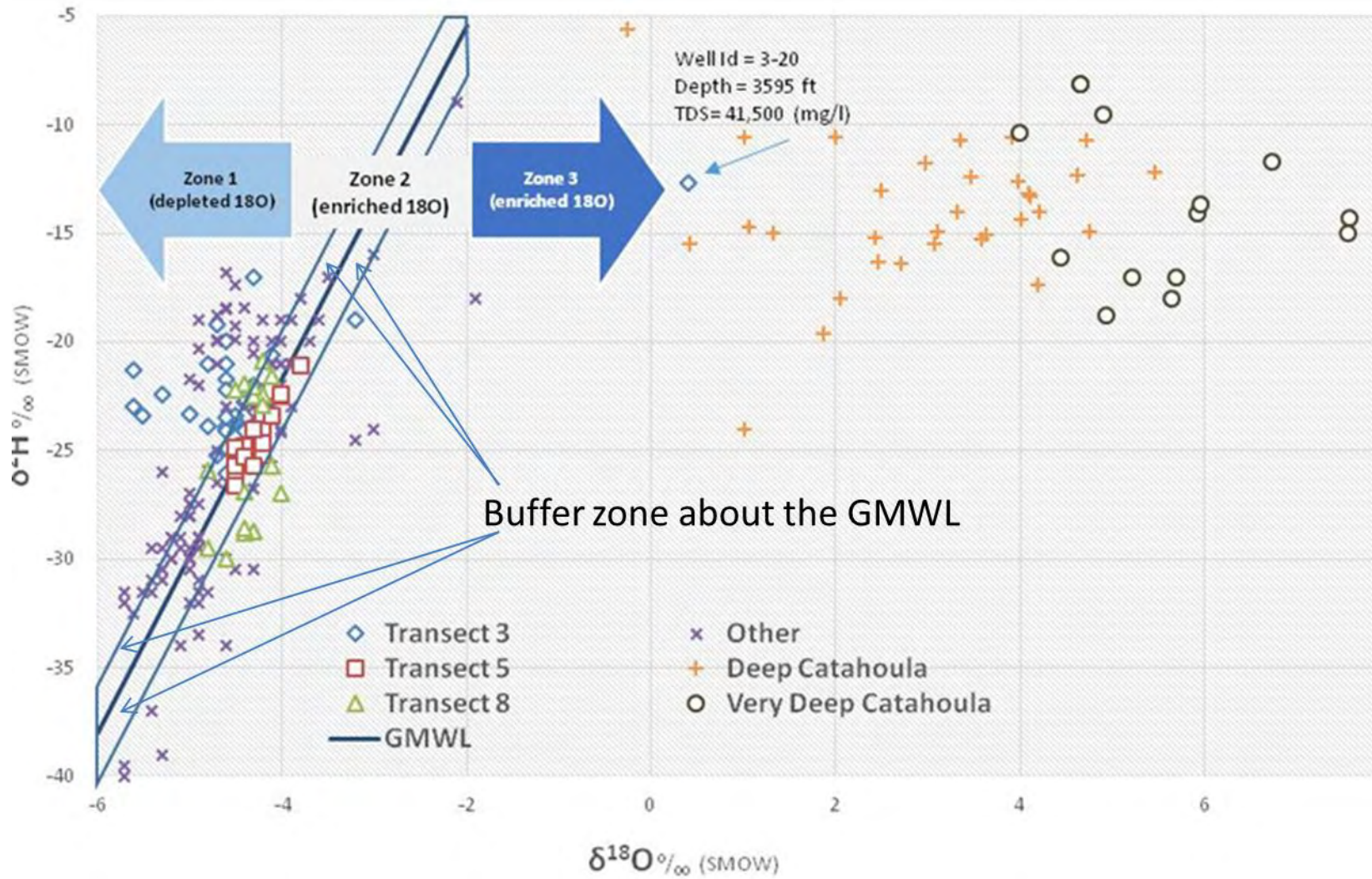


Figure 7-3 Comparison of the relationship between $\delta^{18}\text{O}$ and $\delta^2\text{H}$ for groundwater samples compiled as part of this study, from the deep Catahoula study by Kreitler and others (1988), and from a very deep Catahoula study by the EPA.

Final – Hydrogeochemical Evaluation of the Texas Gulf Coast Aquifer System and Implications for Developing Groundwater Availability Models

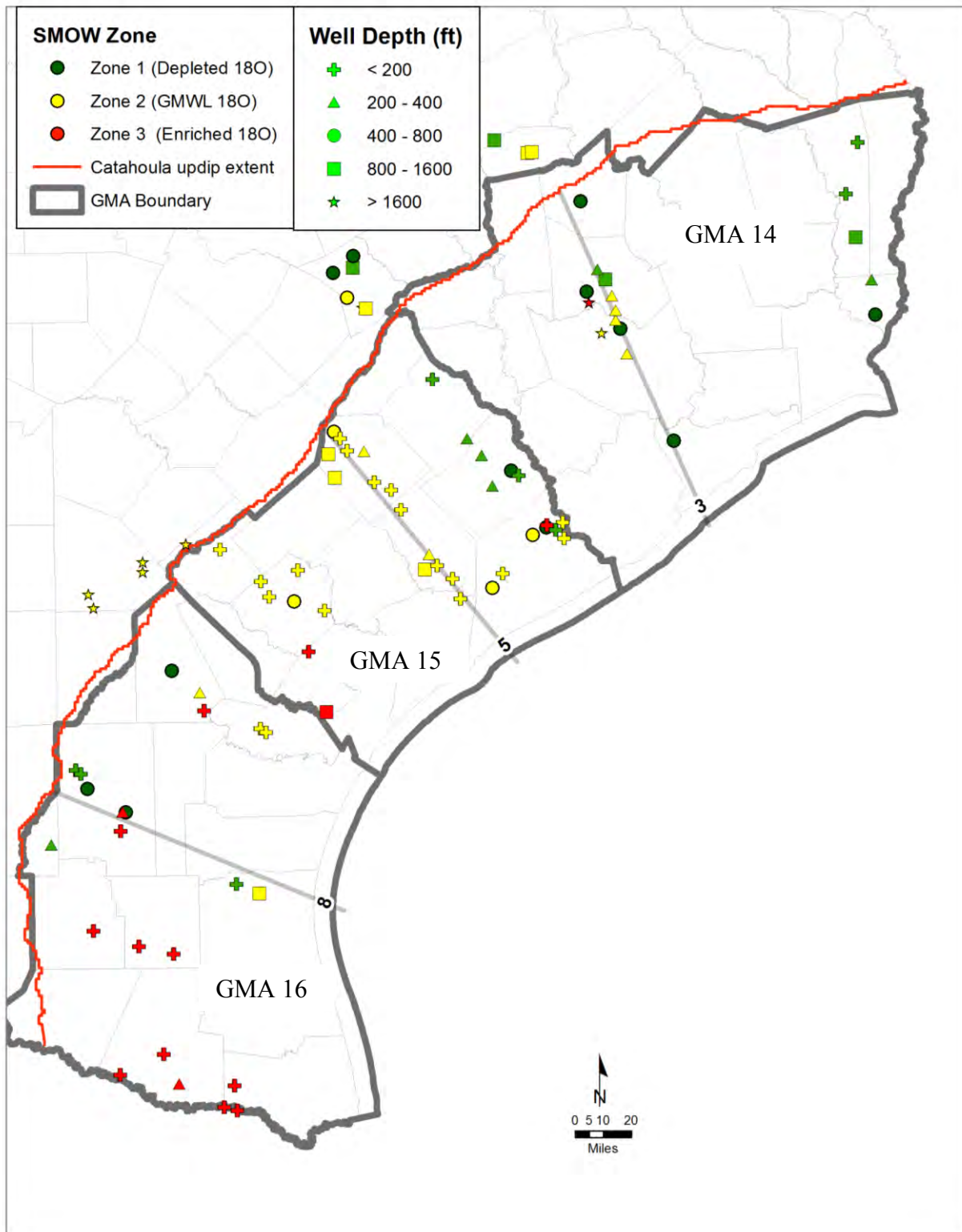


Figure 7-4 Location of the groundwater samples with $\delta^{18}\text{O}$ and $\delta^2\text{H}$ relationships that plot above ($\delta^{18}\text{O}$ depleted), very close to, and below ($\delta^{18}\text{O}$ enriched) the meteoric line.

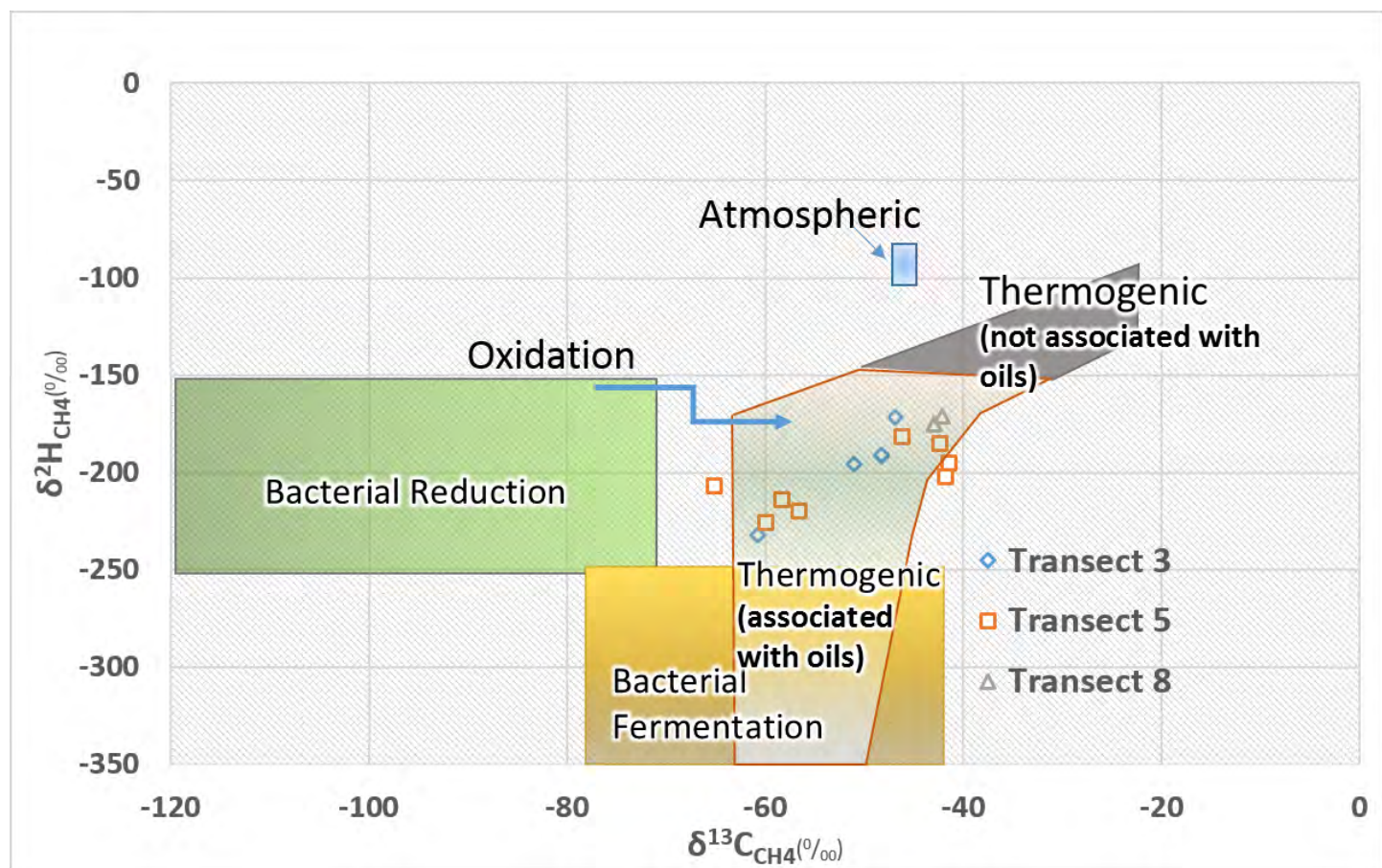


Figure 7-5 $\delta^2\text{H}_{\text{CH}_4}$ and $\delta^{13}\text{C}_{\text{CH}_4}$ compositions of methane gas of multiple origins. Note that thermogenic methane is more enriched in $\delta^{13}\text{C}_{\text{CH}_4}$ than methane of bacterial origin. Most of the methane gas from the Gulf Coast Aquifer System falls within the thermogenic field. The grey shaded area within the thermogenic field is for methane associated with oil and the dark-shaded area is non-associated. Methane of bacterial origin could form either by reduction or fermentation (see text). Note small overlap areas between bacterial fermentation and thermogenic fields. Dashed areas outline fields of methane by their origin (Schoell, 1988). Arrow shows possible oxidation of bacterial methane that can transform its isotopic compositions similar to thermogenic methane.

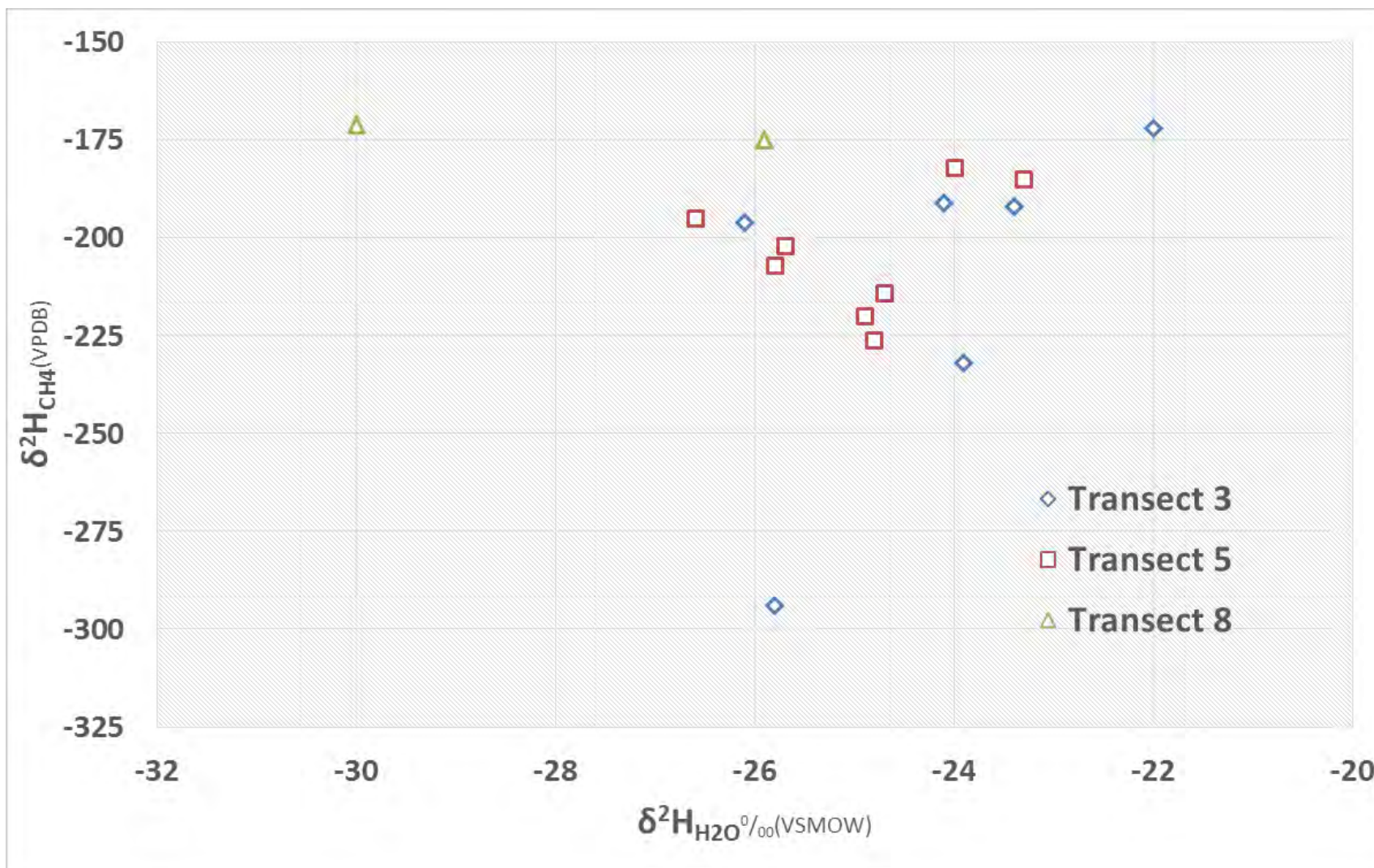


Figure 7-6 A cross-plot of $\delta^2\text{H}_{\text{CH}_4}$ and $\delta^2\text{H}_{\text{H}_2\text{O}}$ of groundwater samples from wells sampled along transects 3 and 5. Note random scatter in the data and an absence of any preferential trend.

Final – Hydrogeochemical Evaluation of the Texas Gulf Coast Aquifer System and
Implications for Developing Groundwater Availability Models

This page intentionally left blank.

8.0 Carbon 14

This section presents and applies method for estimating groundwater age based on measurements of radioactive carbon. These methods use either uncorrected or corrected ^{14}C measurements to calculate groundwater age based on the international accepted half-life for ^{14}C .

8.1 Estimating Groundwater Age from ^{14}C

There are three naturally occurring isotopes of carbon, ^{12}C , ^{13}C , and ^{14}C ; ^{12}C and ^{13}C are stable, and ^{14}C is radioactive. Table 8-1 lists the abundance of these isotopes. All of the carbon isotopes have 6 protons; they differ in the number of neutrons each atom has. ^{12}C , ^{13}C , and ^{14}C have 6, 7, and 8 neutrons, respectively. ^{14}C is produced in the upper layers of the troposphere and the stratosphere by the absorption of thermal neutrons by nitrogen atoms. Natural production of ^{14}C in the upper atmosphere is balanced by decay and burial to maintain a steady-state atmospheric $^{14}\text{CO}_2$ activity that was about one ^{14}C atom per 10^{12} stable atoms prior to the testing of nuclear devices. Above-ground nuclear tests that occurred in several countries between 1955 and 1980 dramatically increased the amount of ^{14}C in the atmosphere and subsequently in the biosphere. By 1965, the ^{14}C concentration in the atmosphere was approximately double the concentration prior to testing. Since the late 1960s the concentration levels have steadily decreased.

Table 8-1 Abundance of carbon isotopes (from Clark and Fritz, 1997).

Element	Isotope	Abundance
Carbon	^{12}C	0.989
	^{13}C	0.011
	^{14}C	<0.000000000001

8.1.1 Half-life Calculation Approach Using Uncorrected ^{14}C

American physical chemist Willard Libby led a team of scientists in the post-World War II era to develop a method to measure ^{14}C activity. Mr. Libby and his team of scientists were the first to measure ^{14}C 's rate of decay and they established 5,568 years \pm 30 years as the half-life for ^{14}C (Cook and Herzceg, 2000).

The age established by Mr. Libby is still used as the international convention and is used by Beta Analytic Inc (www.radiocarbon.com). Beta Analytic Inc, performed all ^{14}C measurements for this project. The basic ^{14}C age determination calculation used by Beta Analytic Inc is as follows:

$$t = - 8033 \ln (\delta^{14}\text{C}_{\text{measured}} / \delta^{14}\text{C}_{\text{standard}}) \quad \text{Equation 8-1}$$

where:

t = the ^{14}C apparent age of the sample that is uncorrected and uncalibrated

8033= the decay constant of ^{14}C , i.e., the half-life divided by $\ln 2$. A half-life of 5,568 years for carbon 14 is used, as per international convention

\ln = the natural logarithm

$\delta^{14}\text{C}_{\text{measured}}$ = the measured net ^{14}C content of the sample

$\delta^{14}\text{C}_{\text{standard}}$ = the ^{14}C content of the modern standard

Measured ^{14}C is usually expressed in terms of percent modern carbon (pMC). Rewriting Equation 8-1 using pMC becomes Equation 8-2. Thus, a pMC of 0.5 has a ^{14}C age of 5,568 years.

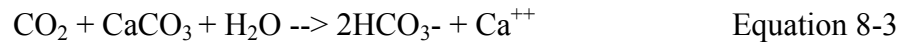
$$t = - 8033 \ln (\text{pMC}/100\%) \quad \text{Equation 8-2}$$

8.1.1.1 Consideration for “Dead” Carbon

A major complication in determining a best estimate of time since recharge, or the “age” of the groundwater, occurs as a result of other sources and losses of carbon to the groundwater during transit. These carbon transfers are primarily the nuclides of ^{13}C and ^{12}C , but also have a ^{14}C content associated with the carbon source. This amount of ^{14}C associated with a carbon transfer reaction can vary between a maximum equal to the atmospheric values and zero. A carbon transfer of zero would occur, for example, in limestone formed long in the past which has since lost the ^{14}C to the completed radioactive decay process. Fossil or dead carbon refers to the carbon that has a pMC equal to 0 because the carbon atom has been isolated from the atmosphere or other sources of ^{14}C for approximately 50,000 years.

Common carbon transfers in groundwater include reactions with carbonate minerals, organic material, carbon dioxide, other hydrocarbon gasses, etc., many of which no longer contain ^{14}C , but the reaction with these phases can affect the mass of dissolved inorganic carbon (DIC) in

groundwater. These alterations to carbon content change the apparent or observed age, because the age is based on the measurement of ^{14}C in the DIC, and thus a measured ^{14}C content, or estimated age, must be corrected to account for other carbon sources and losses. For the Gulf Coast Aquifer System, the most common reactions that would cause a dilution of the ^{14}C would be the reaction with calcite in Equation 8-3. As seen in Equation 8-3, the fossil carbon (pMC=0) in the calcite in the aquifer would contribute half of the bicarbonate ions after the calcite has dissolved into solution.



Several methods for quantifying the dilution effect on the ^{14}C in the DIC are based on calculating the dilution effect of ^{13}C in the DIC. The dilution of ^{13}C can be calculated because it is a stable isotope that does not decay over time. By convention and experience it has been the case that the most efficient way to measure ^{13}C is by the ratio of ^{13}C and ^{12}C . This ratio is commonly written $\delta^{13}\text{C} \text{ ‰}$ and is defined as:

$$\delta^{13}\text{C} \text{ ‰} = \left(\frac{^{13}\text{C}/^{12}\text{C}_{\text{sample}}}{^{13}\text{C}/^{12}\text{C}_{\text{standard}}} - 1 \right) \times 1000 \quad \text{Equation 8-4}$$

The primary reason for tracking the ^{13}C in a groundwater system is to have a “marker” that can be used to model the exchange of carbon in the groundwater with others sources of carbon that interact with the groundwater and change the DIC of the groundwater. Sources of carbon in the soil zone include carbon dioxide and sources of carbon in the aquifer include carbonates such as calcite. Modeling the exchange of carbon between sources such as carbon dioxide and calcite requires that the chemical reactions are known and the percentage of ^{13}C and ^{14}C is known for each carbon source. By knowing all of the major carbon sources and how the sources interact with the groundwater, then the amount of remaining “soil derived” ^{14}C still in the groundwater DIC can be estimated for any point along the flow path, from the recharge location to that down gradient location. This computed or adjusted ^{14}C value is compared to the initial ^{14}C value, yielding the best estimate of the amount of soil zone ^{14}C lost by decay based on the ^{14}C half-life of 5568 years; thus the age since recharge is determined.

Once the groundwater enters the saturated groundwater zone, the reaction of the groundwater with carbon sources shifts the concentration ^{13}C and ^{14}C from its original concentration at its point of origin. This shift typically caused “dead” carbon to be added into the groundwater. “Dead” carbon is carbon without any measureable ^{14}C . For instance, calcite that is over millions

of years old would have long ago lost any ^{14}C that may have existed in the minerals when they were formed. There are two commonly used methods to account for the impact of “dead” carbon on the dilution of ^{14}C concentrations by adjusting the measurement of pMC based on the $\delta^{13}\text{C}$ value for the groundwater sample. The first approach is a simple correction that assumes that ^{14}C and $\delta^{13}\text{C}$ are only diluted by reactions with carbonates along the flowpath (Pearson, 1965; Pearson and White, 1967), and the second is an inverse method using a numerical model to account for all reasonable carbon sources and any contributing chemical reactions (Plummer and others, 1994). These two methods will be called the Pearson method and the NETPATH method and they will be discussed later in this section.

8.1.1.2 Consideration for Mixing

The effect on ^{14}C apparent age by mixing between hypothetical waters of diverse ages can be quantitatively examined. In this examination the concept of mass-age is important to understand. Each water molecule enters the aquifer system and has a definite residence time. The mass-weighted average of all such inputs is the apparent, or mass-age of the water (Bethke and Johnson, 2008). The ^{14}C activity that each water molecule contributes to the mixture is not in linear proportion to the mass-age, however, owing to the non-linear relationship between elapsed time and ^{14}C activity as given by Equations 8-1 and 8-2 and owing to the fact that “old” water has a pMC of 0.

A groundwater sample consisting of 50% water with a pMC of 100% and an age of <1 year and 50% water with a pMC of 0% that is over 45,000 years old will produce a solution with a pMC of 50%. Using Equation 8-2, the estimated groundwater age of water with a pMC of 50% is 5,568. However, the average of the actual groundwater ages is more than 22,500 years before present (ybp). Just a 5% solution of 500 year old water (pMC = 94%) with “fossil water” would produce a water with a pMC of 4.7% and an estimated age of 24,561 ybp based on Equation 8-2. Table 8-2 provides additional calculations using measurements of ^{14}C from two groundwater samples from our database that have a pMC of 93% and 1.5%. The table shows that significantly different ages are calculated by averaging the age and by averaging the pMCs.

Among the conditions that will lead to mixing of groundwater samples are sampling from long well screens and significant changes in groundwater flow directions over time. Both of these conditions have caused an unknown, but potentially important, amount of mixing in the sampled

groundwater in the Gulf Coast Aquifer System. Many of the wells sampled as part of this project have well screens longer than 100 feet and these wells typically have multiple sampling zones. At the very least groundwater mixing will occur across the length of the screen. Depending on the well construction, the age of the pumping well, and the pumping rate, the zone of mixing could be several times greater than the well screen because of the large vertical hydraulic gradients that can occur near a pumping well. In situations where the well screen is not properly sealed, the mixing at the well screen may provide an avenue for the downward migration of very young water to mix with older water. Based on the significant climatic and sea level changes that have occurred along the Texas Gulf Coast during its paleohistory (Section 2.6), groundwater flow paths are expected to have been significantly different now than what they were about 20,000 years ago when sea level was approximately 400 feet lower, the coast line was about 100 miles offset to the east, and a much cooler climate prevailed. Moreover, with flow paths that may cover about 100 miles, require over 20,000 years of travel time, and transect several geologic units from outcrop recharge to discharge at the ocean, the hydrodynamic dispersion (Domenico and Schwartz, 1990) of these water particles is expected to be miles in both the lateral and longitudinal directions.

Table 8-2 Calculated Ages for Mixtures of Groundwater with Different pMCs.

Mixing Group	Well ID*	Mixture	Groundwater Age (ybp) based on:		Age 1 - Age 2 <u>(Age1-Age2)</u> (Age1)
			1	2	
			Weighted Average of Groundwater Ages	Weighted Average of Groundwater pMCs	
1	1	0.5	18,592	6,061	12,531 (0.67)
	2	0.5			
2	1	0.1	4,184	1,419	2,765 (0.66)
	2	0.9			
3	1	0.9	32,999	18,302	14,697 (0.45)
	2	0.1			

* well ID=1, ¹⁴CpMC = 1.05%, ¹⁴C age =36,601ybp, δ13C=-17.4

* well ID=2, ¹⁴CpMC = 93%, ¹⁴C age =553 ybp, δ13C=-17.2

8.1.2 NETPATH Mass Balance Approach

NETPATH (Plummer and others, 1994) is code that simulates geochemical mass-balance reactions between initial and final waters along a hydrologic flow path. A mass-balance model is

defined as the masses (per kilogram H₂O) of a set of plausible minerals and gases that must enter or leave the initial solution in order to define exactly a set of selected elemental, electron transfer, and isotopic constraints observed in a final (evolutionary) water. NETPATH uses chemical and isotopic data for waters from a hydrochemical system. The processes of dissolution, precipitation, ion exchange, oxidation/reduction, degradation of organic compounds, incongruent reaction, gas exchange, mixing, evaporation, dilution, isotope fractionation, and isotope exchange can be considered. Geochemical mass-balance reaction models are examined between selected evolutionary waters for every possible combination of the plausible phases that account for the composition of a selected set of chemical and isotopic constraints in the system.

The NETPATH code implements the calculations necessary to perform age corrections for ¹⁴C. The NETPATH code includes a database program for storing and editing chemical and isotopic data for use in NETPATH. The NETPATH approach considers dissolution of calcite, ion exchange reactions involving calcium, magnesium, and sodium, as well as the oxidation of lignite or incorporation and loss of carbon dioxide along the flowpath.

The calculation performed in NETPATH is constrained by two important procedures. First, the change in groundwater composition between wells must be accounted for by reaction with minerals, gasses, or ion exchange. If this difference cannot be balanced with stoichiometric reactions, then the pathway is not considered correct, either because of incorrect reaction formulation or possibly the effect of mixing with water sources not yet identified. Secondly, the thermodynamic reaction state of minerals must be monitored such that the model does not allow precipitation of a phase which is actually undersaturated. This calculation of thermodynamic reaction state is done as part of the NETPATH approach by using the geochemical equilibrium model WATEQF (Plummer and others, 1976).

Example Application

The recharge area for the Chicot aquifer along Transect 3 can serve as an example of the NETPATH modeling process using three wells (Wells 3-14, 3-15, 3-17). Table 4-3 lists their measured geochemistry and Figures 4-4 and 4-5 shows their locations. The chemical composition at the well locations is consistent with an evolving composition from recharge to downgradient groundwater locations. Well depths are 128 feet, 168 feet, and 290 feet below land surface and, as is discussed later in this section, the groundwater flow in this segment of the transect is from recharge in the immediate vicinity through the locations of these wells to depths

of more than 1,000 feet along lithologically influenced permeability pathways. The question is whether the evolving water chemical composition and computed ^{14}C age supports this flowpath. The initial well, Well 3-14, is problematic because the measured ^{14}C activity is greater than 100 pMC (Table 4-3). This measurement means that the ^{14}C exceeds that expected from normal cosmogenic activity as defined by the internationally recognized standard. The source of this excess ^{14}C is likely recent recharge that incorporates the ^{14}C generated as the result of nuclear weapons testing beginning in the 1950s. Water of such a recent age is not compositionally consistent with the water in downgradient samples, so Well 3-14 cannot be included in the age determination process.

NETPATH can simulate the change in chemical and isotopic composition between any two wells. In this case we are interested in the first well and second well in a flow path, and we need to adjust the change in ^{14}C for carbon contributions from other sources along the flowpath using the $\delta^{13}\text{C}$, and a rigorous match for the chemical compositional mass transfer. For the ^{14}C adjustment to be correct at Well 2; however, this calculation relies on a correct ^{14}C age at Well 1, and only the measured ^{14}C value, not the corrected ^{14}C value, is available for Well 1. There are numerous assumptions that can be made about the conditions of the soil zone which allow for the estimate of a corrected ^{14}C value at Well 1, and these are discussed in Plummer and others (1994). The most common approach is to assume that the soil zone carbon dioxide has a $\delta^{13}\text{C}$ value derived from land plants of -25‰, that the ^{14}C content in the soil CO_2 is 100 pMC, and that any carbonate phases such as calcite, dolomite, siderite, or magnesium rich calcite all have a $\delta^{13}\text{C}$ of 0 ‰, and a ^{14}C of 0 pMC. Using these assumptions, the “mass balance” approach reacts the soil CO_2 with a list of common phases such as gypsum, pyrite, dolomite, carbon dioxide, and ion exchange to compute the $^{14}\text{C}_{\text{corrected}}$ value at Well 1.

The user then must specify the measured initial chemical and isotopic compositions of Wells 1 and 2, and all the minerals and gases and their intrinsic chemical and isotopic compositions. NETPATH requires a rigorously defined mathematical solution to account for the change in composition. Based on the water compositions of any initial and final well, and a specified number of phases and constraints (elements, or stable isotopes), the model must exactly account for all mass transfers between the wells. If the calculation fails, it means that some elements cannot be accounted for with this selected set of phases, and either the phases are wrong, or there

may be extenuating circumstances such as mixing with other groundwater sources of different composition which are not accounted for in the model.

Experience has shown that the most common circumstance is that NETPATH computes an excessive number of models, and there are many mineral compositions and combinations that are possible, and therefore many reaction pathways or “models” must be examined. There are additional checks and considerations that assist in defining the best reaction pathway, which will provide the best estimate of corrected age.

Table 8-3 lists six NETPATH simulations model out of many times that number that are generated if some reasonable geochemical intuition is not applied. The values in the columns represent millimoles of mineral or gas phase that either precipitate or evolve as a gas (negative) or dissolve (positive). Column 1 lists the phases that were considered in all possible combinations, and these are the phases expected to be present at some concentration in the soil and aquifer matrix. The remaining columns provide the mass transferred in order to achieve a solution, and values are only given for the minerals involved in a specific model.

Many more phases are likely present in trace concentrations throughout the aquifer, but are eliminated from consideration because they are unlikely to affect the general groundwater composition to any significant extent. The following elements and stable isotopes are the "constraints," meaning these elements must be accounted for in the change in composition between Well 1 and Well 2: C, Ca, Cl, Fe, K, Mg, Na, S, $\delta^{13}\text{C}$, and $\delta^{34}\text{S}$. The objective of NETPATH modeling is not to completely define the groundwater composition for all elements analyzed, but to determine the corrected age at the point of sample collection in the well. The six models depict different combinations of phases that will yield the same net change in the 8 elements and two stable isotopes.

In the case of this example process all six models yield the same corrected ^{14}C age of 1,934 ybp, rather than the measured age of 4,680 at Well 3-17. In this case, all models yield the same result for ^{14}C but the reaction pathway for each is different. This set of reaction pathways is a special case because the $\delta^{13}\text{C}$ was used as a constraint. In many cases there is not solution if this constraint is required because the model requires an exact mathematical solution. In the case of no exact fit, then the best model selected is the one with the computed $\delta^{13}\text{C}$ that is closest to the

Table 8-3 Results of modeling groundwater evolution from recharge location through 3-15 and 3-17 in the Chicot aquifer, Transect 3.

Model No.	From Recharge through Well 1 (3-15) to Well 2 (3-17)					
	1	2	3	4	5	6
$^{14}\text{C}_{\text{MEAS}}$ (ybp)	4680	4680	4680	4680	4680	4680
$^{14}\text{C}_{\text{COR}}$ (ybp)	1934	1934	1934	1934	1934	1934
$\delta^{13}\text{C}_{\text{MEAS}} = -17.6\text{‰}$	-17.6	-17.6	-17.6	-17.6	-17.6	-17.6
Calcite	0.44	0.44	0.44	0.04	0.44	0.44
Gypsum	0.02	0.02	0.02	0.02	0.02	
Goethite	-0.0008	-0.05	-0.0008	-0.005	-0.0008-	-
Pyrite	0.002	0.002	0.002	0.002	0.002	-
Lignite	-	-	-	-	-	-
NaCl	0.11	0.11	0.11	0.11	0.11	-
$\text{CO}_2(\text{gas})$	-0.14	-0.14	-0.14	-0.14	-0.14	-0.14
Fluorite	-0.05	-0.12	-0.07	-0.11	-0.20	-
Ca/Na Ex	0.08	-0.01	0.06	0.02	-	0.12
Mg/Na Ex	-0.04	0.007	-0.04	-	-0.04	-0.04
K/Na Ex	0.03	-	-	-	-0.03	-0.03
Plagioclase	-	-	-	-	0.24	-
K-Spar	-	-	0.03	0.005	-	-
Biotite	-	0.03	-	0.03	-	-

1. Initial soil ^{14}C is 100 pMC; $\delta^{13}\text{C}_{\text{soil}} = -25\text{‰}$; calcite $^{14}\text{C} = 0$ pMC, and $\delta^{13}\text{C} = 0\text{‰}$.
2. Silicates are constrained only by Ca, Na, or K.
3. All models were constrained by $\delta^{13}\text{C}$, all but model 6 were constrained by $\delta^{34}\text{S}$ value of 12.3.
4. All six models yield the same corrected ^{14}C age.
5. NETPATH calculation using Mass Balance for adjusting ^{14}C at Well 1.

measured value. Furthermore, this set of models also indicates that many of the selected minerals are useful in explaining the chemical changes between wells, but are not essential to the accounting of the carbon sources affecting this segment of the aquifer. The simplest solution of calcite, CO_2 , and ion exchange actually provides the needed correction. In this case there are no additional carbon sources needed to explain the change in chemistry or the change in $\delta^{13}\text{C}$; in other portions of the aquifer it will be shown that lignite, *in situ* carbon dioxide, and methane will need to be considered.

It is instructive to note that some models can be eliminated based on other factors. For example the mineral fluorite (CaF_2) is in the list, but the element fluoride is not, and the model indicates that this is a potential method for lowering the calcium concentration by precipitating fluorite. The thermodynamic assessment however indicates that fluorite is undersaturated so no model

requiring precipitation of fluorite is valid. Fluorite could be eliminated since the actual mass of calcium transferred is small.

Similarly although the feldspars (plagioclase, and orthoclase or K-spar) are included, the model is not given the entire mineral composition as a set of constraints, it only considers the Ca, K, or Na content since other components such as Al and Si are not included. Neither Si and Al were measured, so the model assumes that they are conserved, meaning the concentration in the endmember wells is zero, and the minerals can dissolve or precipitate, but the contributed concentrations of Al and Si are not considered. In all models the feldspar contribution is small and because other constituents in the feldspar minerals are not considered, and do not appear to make any difference in the age calculation, the feldspars are probably not important. Similar reasoning applies to biotite.

Finally, the isotopic composition of sulfur is important in other groundwater locations but not here. It is reassuring to note that the computed $\delta^{34}\text{S}$ matches the measured value in the second well, indicating the sulfur mass transfer is probably described correctly, but it also does not affect the age calculation. Thus, the simplest model uses a minimal number of phases and still provides a plausible age correction from 4,680 ybp to 1,934 ybp.

8.1.3 Pearson Correction Approach

The Pearson correction is based on the assumptions and equations used by Pearson and White (1967) to estimated groundwater age from ^{14}C measurements based on $\delta^{13}\text{C}$ for an Eocene Carrizo Sand in Atascosa and adjacent counties. Their conclusions were that the ^{14}C ages of DIC were generally reflecting the age of the groundwater and that because of mineral dissolution, the carbon content was being modified along the flow path, resulting in an apparent age that is slightly older than the probable actual age. They proposed equations to account for both the reactions in soil zone of the recharge area and reactions along the flow path in which carbonate minerals were dissolving and adding mass without changing the ^{14}C concentration in the water. Pearson and White (1967) presume that the $\delta^{13}\text{C}$ of soil gas carbon dioxide and calcite for the Carrizo aquifer in south Texas are -25‰ and 0‰ respectively, and that most reactions with carbon dioxide occurred in the shallow groundwater which was open to the atmosphere and thus the ^{14}C content was 100 percent modern carbon (pMC) of the expected content. Reactions with calcite can occur in the soil zone or in the aquifer downgradient from recharge, but the extent of reaction is based on the assumption that contribution of carbon to the groundwater DIC is

evidenced by a modified $\delta^{13}\text{C}$ of groundwater by the $\delta^{13}\text{C}$ of calcite which adds carbon but not ^{14}C . Calcite was given a $\delta^{13}\text{C}$ of 0. ‰ based on the assumption that it was a marine carbonate.

For simple groundwater systems consisting of clean predominantly sandy aquifers, well constrained between aquitards, and with defined flow systems with little mixing from cross-formational flow, the Pearson-White correction appears reasonable. The Pearson-White correction works best if the aquifer is a clean sand with no sources of carbon other than calcite, and no significant incorporation of carbon dioxide beyond the recharge area. As the groundwater moves downgradient, however, it becomes confined and closed to atmospheric or soil carbon dioxide. Reactions with carbon dioxide and organic material must account for the different isotopic content and absence of new ^{14}C entering the groundwater. This detailed accounting for mass and isotope transfer is done in NETPATH.

Example Application

The Pearson-White correction factor involves the application of relatively few equations (Clark and Fritz, 1997) and thus can be easily explained. The $\delta^{13}\text{C}$ mixing model-correction factor is calculated using the following equation:

$$q = (\delta^{13}\text{C}_{\text{DIC}} - \delta^{13}\text{C}_{\text{carb}}) / (\delta^{13}\text{C}_{\text{rech}} - \delta^{13}\text{C}_{\text{carb}}) \quad \text{Equation 8-5}$$

where:

q = the dilution factor

$\delta^{13}\text{C}_{\text{DIC}}$ = the measured $\delta^{13}\text{C}$ of groundwater

$\delta^{13}\text{C}_{\text{carb}}$ = the measured $\delta^{13}\text{C}$ of calcite being dissolved

$\delta^{13}\text{C}_{\text{rech}}$ = the measured $\delta^{13}\text{C}$ of the recharge

There are several approaches estimating for $\delta^{13}\text{C}_{\text{carb}}$ and $\delta^{13}\text{C}_{\text{rech}}$. These methods are discussed in textbooks by Clark and Fritz (1997) and Cook and Herczeg (2000). For our study we have used fixed values of -25‰ and -0‰ for $\delta^{13}\text{C}_{\text{rech}}$ and $\delta^{13}\text{C}_{\text{carb}}$, respectively. Thus, for a sample with a pMC of 21.67% and a $\delta^{13}\text{C}_{\text{DIC}}$ of -7.3‰, the dilution factor is 0.292. Using Equation 8-4, the uncorrected pMC provides a groundwater age of 12,284 ybp and the corrected pMC of 74.21% provides a groundwater age of 2,395 ybp.

8.2 ¹⁴C Ages Based on NETPATH Mass Balance Approach

As is the case for all transects examined in this section, NETPATH can be used to adjust ages from ¹⁴C using a concise approach with a small set of dissolved ion and gas concentrations. The essential components are major ions involved in solubility of carbonate minerals, limited ion exchange reactions, carbon dioxide, methane, and byproducts of oxidized organic material. Greater confidence in the age corrections is gained as other reactions are included in the modeling that: 1) describe plausible evolution between wells defined by the water composition change; and 2) most importantly, yield in the resultant calculations a final carbon stable isotopic value that matches the measured value. Other dissolved constituents are frequently quantified that are not part of the calculation of corrected ¹⁴C age, but support the interpretation, and add information about the environment of the aquifer.

An implicit assumption in the NETPATH Mass Balance approach is that the sequence of wells are aligned along a flow path and that the same water molecules are moving via piston flow from one well screen to another. Based on our evaluation of the data, this assumption is unlikely to be met in any well combination available for analysis. In many possible flow scenarios between wells, the chemistry between wells is highly variable and cannot be explained without invoking some type of mixing involving a third source of constituents. The measured ¹⁴C_{MEAS} ages and chemical composition in the wells along the transect are variable. The variability in measured age with depth, with distance along the transect, and with respect to geologic formation is only partially understood at present, and is the consequence of many factors, including: 1) pumping impacts that promote mixing within the aquifer; 2) different screen lengths (varying between 25 feet to over 300 feet) that promote mixing in the well screen; 3) infiltration from agricultural, activity surface impoundments, and/or anthropogenic activities; 4) dissolution from salt domes; 5) vertical flow along growth faults; 6) partial blockage of down-dip flow at faults; and 7) preferential flow paths at both the local and regional scales.

8.2.1 *Transect 3 in GMA 14*

There are 49 wells in Transect 3; 46 wells which have a measured ¹⁴C_{MEAS} value, of which two are modern values. The sampled wells are a combination of data in the Texas Water Development Board database, wells recently sampled by the USGS, and samples collected by this study (see Table 4-3). Well depths range from 118 to 2,587 ft. bls; with screened intervals identified for all wells. All wells are located within a band along the transect that is

approximately 120 miles long and 12 miles wide (see Figure 4-4). The Transect 3 wells and lithology are plotted in Figure 8-1. For the Oakville and younger formation, the lithology includes average sand percentage and the intervals of sand identified in geophysical logs near Transect 3 from Young and others (2012a). A visual review of the lithologic data suggests all of the formations are comprised of appreciable sands and that the Chicot Aquifer has greatest amount, with sand fractions greater than 70% sand and with sand beds greater than 100 feet.

The geochemical facies map for Transect 3 (Figure 6-20) supports a simple flow system where Ca-HCO₃ water is recharging the groundwater system for about 60 miles and then is flowing toward the ocean as it evolves into a Ca-Na-HCO₃, then a Na-HCO₃, and then a Na-Cl waters as result of its interaction with the aquifer. The general trend in the uncorrected ¹⁴C ages in Figure 8-2 supports a regional flow path that is consistent with the flow directions that can be inferred in Figure 6-20 based on the evolution of groundwater as described by the relationships shown in Figure 6-3. As shown in Figures 6-19 and 6-20, the chemical evolution is consistent with the carbonate system, with high calcium concentrations (above 100 ppm) in the recharge areas and gradually lower calcium concentrations occurring down dip. Despite the regional trends in the chemistry, there is considerable variability in concentrations at some well clusters. Whereas some sampled wells clustered in close proximity to one another have similar chemical and isotopic compositions, other adjacent wells within a few miles of each other with similar screened intervals are chemically quite different. As a result, the well concentration values as a whole do not reveal a continuous regional flow path along which a series of NETPATH simulations can be performed for well pairs that begin at the up-dip extent of Transect 3 and end near the ocean. The variable chemistry among close wells suggests that groundwater flow is largely controlled by sand rich sections that finger through lower permeability deposits.

Table 8-4 provides notes on each of the Transect 3 wells with regard to the NETPATH simulations. The farthest down dip wells are Wells 3-44 through 3-49. These wells are in the Chicot lower permeability zone, generally deeper than 700 or 800 feet, and all are old groundwater with measured ¹⁴C_{MEAS} greater than 30,000 ybp and no defined upgradient flow system or younger wells in a defined flow path. The final set of NETPATH runs are associated with one of the following two well groups:

- Chicot Aquifer Segment (Wells 3-14, 3-15, 3-17, 3-24, 3-27, 3-28, 3-29, 3-32, and 3-43);
and

Final – Hydrogeochemical Evaluation of the Texas Gulf Coast Aquifer System and Implications for Developing Groundwater Availability Models

- Jasper/Lagarto flow segment (3-1, 3-6,3-8, 3-10, 3-12, 3-16, and 3-23).

Table 8-4 Comments Regarding the Evaluation of Wells in Transect 3 for NETPATH Simulations.

Well	Note Regarding Evaluation for NETPATH Simulation
3-1	Used in the Jasper/Lagarto Model
3-2	Too deep/low permeability in the Catahoula to model along an identified transect
3-3	Too deep/low permeability in the Catahoula to model along an identified transect
3-4	Too deep/low permeability in the Catahoula to model along an identified transect
3-5	Elevated concentrations, appears contaminated and not representative
3-6	Used in the Jasper/Lagarto Model
3-7	Shallow, too far down dip, old age indicates low permeability, not used with modeled zones
3-8	Used in the Jasper/Lagarto Model
3-8.5	Too deep
3-9	Shallow, too far down dip, old age indicates low permeability, not used with modeled zones
3-10	Used in the Jasper/Lagarto Model
3-11	Too deep
3-12	Used in the Jasper/Lagarto Model
3-13	Not defined as a flow zone
3-14	¹⁴ C measurement indicates modern carbon
3-15	Used in the Chicot Model
3-16	Used in the Jasper/Lagarto Model
3-17	Used in the Chicot Model
3-18	Not defined as a flow zone
3-19	Not defined as a flow zone
3-20	Not defined as a flow zone (no ¹⁴ C data)
3-21	Not defined as a flow zone (no ¹⁴ C data)
3-22	Not defined as a flow zone
3-23	Used in the Jasper/Lagarto Model
3-24	Used in the Chicot Model
3-27	Used in the Chicot Model
3-28	Used in the Chicot Model
3-29	Used in the Chicot Model
3-32	Used in the Chicot Model
3-43	Used in the Chicot Model
3-44	Deeper Chicot deposits, age estimated greater than 30,000 ybp, no defined flow path
3-45	Deeper Chicot deposits, age estimated greater than 30,000 ybp, no defined flow path
3-46	Deeper Chicot deposits, age estimated greater than 30,000 ybp, no defined flow path
3-47	Deeper Chicot deposits, age estimated greater than 30,000 ybp, no defined flow path
3-48	Deeper Chicot deposits, age estimated greater than 30,000 ybp, no defined flow path
3-49	Deeper Chicot deposits, age estimated greater than 30,000 ybp, no defined flow path

8.2.1.1 Chicot Aquifer Segment

Wells sampled in the freshwater flow system for the Chicot aquifer in Montgomery County range in depth from 128 to 1192 ft. bls (Figure 8-1). The linear surface distance from the Catahoula outcrop to the deepest and most distant downgradient well is approximately 80 miles. This freshwater flow zone is characterized as a calcium bicarbonate rich zone wedged between lower permeability and more sodium rich lithologies as depicted in a groundwater chemistry facies cross section (Figure 6-20).

The initial Well 3-14 is screened from 118 ft. to total well depth of 128ft. bls, and has a measured $^{14}\text{C}_{\text{MEAS}}$ of 101.5% pMC, meaning the value is greater than modern carbon. This indicates that at least a portion of the groundwater has arrived at that well location since the 1950s, after atmospheric nuclear weapons testing, and is not representative of the shallow water that was present when deeper groundwater was recharged. This well was not considered in the NETPATH modeling. .

General chemical composition of samples along the Chicot transect can be used to build a conceptual understanding of the flow system (Figures 8-3 through 8-5). The $^{14}\text{C}_{\text{MEAS}}$ indicates two populations of data: 1) the initial wells of 3-14, 3-15, 3-17, and 3-24 which increase steadily in uncorrected age; and 2) the balance of the wells which have essentially the same uncorrected age of from 14,000 to 16,000 ybp. The overall inorganic chemical composition can be illustrated by a few principal constituents such as total alkalinity, TDS, sodium, chloride, calcium and magnesium; these constituents cluster in the general distribution, with an initial increase through the first four wells, followed by similar composition for the balance of the wells.

NETPATH models for this zone yield consistent results for the first 4 wells (omitting Well 14) with the general age corrections defined by a minimum set of reactions: calcite dissolution, ion exchange, and a chloride source assumed from the marine clays represented by sodium chloride dissolution. The simulations assume an open system to soil carbon dioxide with a $\delta^{13}\text{C}$ of -25‰ and ^{14}C of 100% pMC only for the initial mass balance reaction from soil zone to Well 3-17. Subsequent to Well 3-17, well to well models use the measured $\delta^{13}\text{C}_{\text{CO}_2}$ for each well (Table 8-3) and a ^{14}C of 0% pMC for any reactive carbon dioxide.

Well 3-24 is the point at which the groundwater has attained equilibrium with respect to calcite, and as can be seen in Table 8-5, subsequent to Well 3-24, the NETPATH models have a small

amount of either precipitation or dissolution of calcite. This is suggested because at Well 3-24 the dissolved calcium and bicarbonate concentrations cease the steady increase attributed to calcite dissolution. From Well 3-24 to 3-43 the calcium and bicarbonate concentrations are essentially the same with small well to well variations, which can be simulated by a small amount calculated mass transfer with respect to calcite. There is a relatively larger dissolution mass for Well 3-43, probably the result of fugitive carbon dioxide arriving at that horizon as a result of thermogenic gas migration.

Table 8-5 Results of NETPATH modeling of groundwater evolution from recharge location through 3-15 and 3-17 to Well 43 in the Chicot Aquifer, Transect 3.

Wells	NETPATH MODEL (Initial and Final Well) ⁽¹⁻⁴⁾						
	Soil/15-17	17-24	24-27	24-28	24-29	24-32	24-43
Calcite	0.438	0.899	-0.204	-0.179	-0.116	-0.152	0.403
δ CO ₂	-0.138	-	-0.101	-0.303	-0.247	0.178	0.05
Lignite	-	0.242	-	-	-	-	-
NaCl	0.043	0.082	0.423	0.251	0.285	0.310	0.375
Ca/Mg Ex	0.116	0.218	-0.274	-0.144	-0.261	-0.060	0.723
Mg/Na Ex	-0.044	-0.005	-0.021	0.038	-0.010	-0.053	-0.096
K/Na Ex	-0.034	0.002	0.005	0.018	0.009	0.018	0.013
δ ¹³ C _{MEAS} (‰)	-17.6	-17.5	-16.5	-16.4	-14.3	-12.3	-13.8
δ ¹³ C _{CALC} (‰)	-17.5	-14.0	-17.6	-16.9	-17.0	-17.3	-15.8
¹⁴ C _{MEAS} (ybp)	4380	7186	14,000	16,320	13,820	14,730	15,760
¹⁴ C _{COR} (ybp)	1,934	3,604	12,297	14,691	12,115	12,671	13,189
CO ₂ (δ ¹³ C ‰)	-25	-16.4	-13.6	-12.7	-12.0	-12.0 ⁽⁵⁾	-12.8
CO ₂ (pMC)	100	0	0	0	0	0	0
SI (Calcite)	-1.2	0.5	0.3	-0.04	0.2	0.1	0.3

1. Initial soil ¹⁴C is 100 pMC; δ¹³C_{soil} = -25‰; calcite ¹⁴C = 0 pMC, and δ¹³C = 0‰.
2. Silicates are constrained only by Ca, Na, or K.
3. All models compared computed versus measured δ¹³C.
4. NETPATH calculation uses the mass balance method for adjusting ¹⁴C at Well 15; the user defined method is used elsewhere.
5. Estimated value

The enrichment in δ¹³C from soil zone values of -25‰ for CO₂ to intermediate values of -16 to -14‰ DIC in subsequent wells along the flow path is a straightforward evidence of calcite dissolution. Although other carbon sources are allowed in the model, they are not required to simulate the observed chemical and isotopic changes. In the segment from Well 3-17 to Well 3-24, lignite oxidation rather than carbon dioxide incorporation seemed to be a better solution, but the reaction with lignite and generation of biogenic methane was not indicated for any deeper wells. No methane was measured as a fixed gas component until Well 3-43, at which

point the methane mole percent was 11.4, and gas components C1-C5 were measured indicating this was thermogenic gas, probably migrating from deeper reservoirs. The $\delta^{13}\text{C}_{\text{CH}_4}$ was -46.9‰ supporting the assessment of thermogenic origin (see Section 7.4) .

The difference in measured ^{14}C ages for Wells 3-27, 3-28, 3-29, 3-32, and 3-43 is negligible, all having $^{14}\text{C}_{\text{MEAS}}$ between ~14,000 and 16,000 ybp, and not in sequential order with respect to flow; consequently, NETPATH models between each of these wells were not successful. The age changes and $\delta^{13}\text{C}$ have small reversals and the chemical compositions are similar, NETPATH solutions could not be obtained as well to well comparisons among these five wells. Considering the similar age and composition of Wells 3-27 through 3-43, the conceptual model could be that during the post 10,000 ybp time frame, flow in the Chicot changed. Perhaps due to Pleistocene climatic changes or more rapid sea level transgression, yielding a hydraulic pressure change, that altered a more rapid groundwater flow to a slowed or even blocked downgradient movement, causing the deeper groundwater to accumulate rather than continue down dip or across formational boundaries. This might explain the large accumulation of groundwater at depth with similar characteristics.

As a verification of similar age for this deeper groundwater, NETPATH models were generated from Well 3-24 which is the last well along the reactive portion of the flow, to each of the five similar wells, and plausible solutions are generated for each, indicating that each could be considered representative of the deeper and similar water (Table 8-3). The $^{14}\text{C}_{\text{MEAS}}$ values in all modeled segments were in need of correction as the result of addition of calcite to the DIC in groundwater. The corrected ages, $^{14}\text{C}_{\text{ADJ}}$, are provided in Table 8-5.

The nine wells listed in Table 8-5 appear to be from aquifer zones that are sufficiently connected to represent a continuous and discernible zone of groundwater flow from recharge to depth. Between Well 3-14 and Well 3-43 along Transect 3 there are 21 additional wells which were not included in the discussion above for the following reasons: one well produces from the Jasper, one from the Middle Lagarto, three are deep municipal wells (3,595 feet, 2,300 feet, 1,686 feet bls), 13 wells produce from the Evangeline, and three additional Chicot wells are discussed below.

The three Chicot wells are 3-37, 3-39, and 3-42. Two wells, 3-37 and 3-42, are shallow (225 feet and 330 feet bls) and further down Transect 3 thus completed in the lithologic section above the flow zone discussed earlier. At that point in the section, the lithology has changed and is less

permeable with more clastic components, and the uncorrected ages (23,580 and 37,470 ybp) support the conceptual model of slower migration and more isolated nature of groundwater represented by these two shallow wells; consequently these two wells were not considered consistent with the Chicot flow system discussed above. Well 39 is deeper (620 feet bls) but it has five separate screened intervals beginning 322 feet bls and continuing to total depth; thus sampled water is the result of mixing from many zones. The chemical composition is different from surrounding wells with higher sodium and chloride, lower bicarbonate, and the $\delta^{13}\text{C}$ is much more enriched (-9.2 ‰) and the $^{14}\text{C}_{\text{MEAS}}$ is much younger (9,573 ybp). This well has anomalous screened characteristics and composition relative to other adjacent wells, is not considered representative of the Chicot flow zones being investigated, and has not been included in the modeling component.

8.2.1.2 Jasper/Lagarto Flow Segment

Examination of the facies sections for Cl and $^{14}\text{C}_{\text{MEAS}}$ (Figure 6-20) indicates continuity among samples downgradient along an indicated flow path which would be bounded above and below by lower permeability Middle Lagarto and lower Jasper. Six of the samples collected for this study align with this flow zone (Wells 3-6, 3-8, 3-10, 3-12, 3-16, and 3-23). Although the Jasper/Middle Lagarto aquifer has a relatively well-defined continuous low TDS region that can be identified on all facies sections, this zone does not have a sampled well directly upgradient to this identified region which could represent a recharge well. We have elected to consider both Well 3-1, an upgradient shallow well in the Jackson, and the downgradient Well 3-6 in the Middle Lagarto as representing a range of compositions, and a mixing model using these two as the upgradient sources is employed. These two wells are modeled individually for age correction, then combined for the downgradient NETPATH simulations.

Table 8-6 provides the NETPATH results for the simulations, as with all NETPATH runs. The simulation is from a well to a downgradient well along an assumed flow path. Several of the well pair runs were performed using different reactions to investigate how different reactions would affect the groundwater age based on the adjusted carbon 14 age.

8.2.1.3 Sulfur and Chlorine Isotopes

Figure 8-6 shows the Jasper/Lagarto flow system and the Chicot flow zone have similar ranges for $\delta^{34}\text{S}$. There are two obvious outliers of enriched $\delta^{34}\text{S}$ that are greater than 35‰ that are

Final – Hydrogeochemical Evaluation of the Texas Gulf Coast Aquifer System and
Implications for Developing Groundwater Availability Models

Table 8-6 Results of NETPATH modeling of groundwater evolution from one well to another down-gradient well for wells in the Middle Lagarto and the Jasper Aquifer along Transect 3.

	Soil to Recharge Well to Well 3-1		Soil to Recharge Well to Well 3-6		Well 3-6 to Well 3-8			Well 3-6 to Well 3-10, or to Well 3-12, or to Well 3-16, or to Well 3-23				
	3-1	3-1	3-6	3-6	3-8	3-8	3-8	3-10	3-12	3-16	3-23	
¹⁴ C _{MEAS} ybp	4,000	4,000	17,256	17,256	22,520	22,520	22,520	22,520	23,120	21,760	21,130	
¹⁴ C _{MEAS} pMC	60.73	60.73	11.67	11.67	6.06	6.06	6.06	7.77	5.62	6.66	7.20	
¹³ C _{MEAS} DIC	-20.2	-20.2	-14.9	-14.9	-12.0	-12.0	-12.0	-12.1	-12.2	-12.7	-11.3	
<i>Mass Transfer⁽¹⁾</i>												
calcite	0.82	0.83	2.12	2.12	1.40	1.40	0.55	0.84	1.54	0.72	1.37	
dolomite	-	-	-	-	-	-	-	-	-	-	-	
CO _{2(g)}	3.48	3.47	3.11	3.11	-	-	-0.63	-0.34	0.37	-0.18	-0.23	
Ca/Na Ex	0.74	0.74	0.57	0.57	0.70	0.70	0.61	1.23	2.43	1.68	2.55	
Mg/Na Ex	-0.04	-0.04	-0.35	-0.35			0.17	0.13	0.11	0.11	0.14	
K/Na Ex	-0.18	0.06	-0.09	1.71	-1.16	-1.17	-0.05	-2.34	0.15	-2.14	-2.81	
NaCl	0.24	-	1.80	-	-	-	-1.96	-0.3	0.5	0.27	-0.16	
gypsum	0.16	0.16	0.14	0.14	0.73	0.07	0.04	0.09	0.13	0.12	-0.02	
K-spar	-	0.24	-	1.80	-							
<i>Computed Values</i>												
¹⁴ C _{COR} (ybp)	2,358	2,358	13,463	13,463	17,135	18,063	18,576	16,128	18,369	17,580	16,063	
¹⁴ C _{COR} (pMC)	80.80	80.80	59.48	59.48	8.60	53.87	57.33	54.66	51.85	55.86	50.26	
δ ¹³ C DIC calc.	-20.2	-20.2	-14.9	-14.9	-12.0	-12.0	-12.5	-12.4	-12.2	-12.8	-11.3	
¹⁴ C _{COR} (ybp) ²	2,287	2,287	13,099	13,099	16651	16651	16651	14691	17357	16319	14751	
NOTES:						(3)			(3)			

Notes: ¹ millmoles; ² Pearson Method;

associated with low sulfate concentration. These high values are consistent with sulfate reduction in the aquifer at these two locations that generated a depleted sulfide (probably H₂S) and a residual enriched sulfate. Most of the $\delta^{34}\text{S}$ values of sulfate along this transect are assumed to reflect oxidation of pyrite near the recharge area with little subsequent change along the flowpath; consequently these data are not considered influential in the age calculations.

In evaluating the sulfur isotopes, the groundwater values for $\delta^{34}\text{S}$ were judged with regard to $\delta^{34}\text{S}$ of seawater and of marine clays. The $\delta^{34}\text{S}$ of seawater dissolved sulfate is estimated to be approximately 21‰ (Thode, 1991), and pyrite in the marine shales are conventionally known to range from around 15‰ to values as depleted at -20‰ (Thode, 1991), depending on the specific original local environment of deposition and diagenetic circumstances. These aquifer sediments were exposed to oxygenated surface water during recharge and thus sulfide minerals such as pyrite would have oxidized and generated sulfate. Locally, in wet-dry cycles in the soil zone or shallow aquifer sediments could have precipitated gypsum with a $\delta^{34}\text{S}$ similar to that of the shale signature, rather than the marine sulfate value. Consequently, recharging waters that dissolve the gypsum or oxidize pyrite will yield dissolved sulfate that clusters in the shale range of $\delta^{34}\text{S}$. No marine signature is evident; nor is there a defensible suggestion of a trend of changing values with distance or depth.

Chlorine-36 is a cosmogenic isotope with a half-life of 301,000 years and is used both for dating very old groundwater and or indications of mixing with modern recharge which would contain the isotope derived from nuclear testing over the past 60 years. There are two significant complications with use of ³⁶Cl in groundwater age dating: 1) the first is that the concentration expected for a geographic location estimated based on geomagnetic latitude which affects the atmospheric generation of ³⁶Cl from cosmic ray bombardment of argon gas, and atmospheric circulation patterns; and 2) is ingrowth of ³⁶Cl from neutron bombardment of chlorine during the decay of radionuclides such as uranium and thorium. Bentley and others (1986) estimated the atmospheric ratio of ³⁶Cl to stable chlorine to be near 160×10^{-15} , which is the value we assume to represent recharge. Nuclear testing released pulses of ³⁶Cl into the atmosphere in excess of $5,000 \text{ }^{36}\text{Cl}/\text{Cl} \times 10^{-15}$ in the mid-1950s to mid-1960s.

Ten measurements of ³⁶Cl were made along Transect 3: one in the Chicot aquifer, four in the Jasper/Lagarto, and 5 miscellaneous wells were sampled. Figure 8-7 illustrates the distribution of these data along the transect. The recharge ratio of 160×10^{-15} for this region is exceeded only

twice, in samples from 3-34 (227.5×10^{-15}) and 3-46 ($1,276 \times 10^{-15}$), and these two wells are deep enough that these values are surprisingly large and indicate some contribution from modern water. Recirculation of shallow water, or contribution from modern water used in drilling the wells would be the most plausible explanations. Neither of these wells are part of well-defined flow system and are isolated at present from a hydrogeologic interpretation. The balance of the wells have similar values with no clear trend of decreasing ^{36}Cl concentration with distance; and except for Well 3-49, these wells have similar chloride concentrations ranging from 18 to 55 mg/L Cl. Other than the evidence of modern water in Well 3-34 and Well 3-46, the ^{36}Cl are too few, too similar, and probably too random to provide any contribution to the discussion of age of groundwater along this transect.

8.2.1.4 Application of the Pearson Correction for ^{14}C Age Estimates

The two defined flow zones of the Chicot and the Jasper/Lagarto are candidates for using a mass transfer model such as NETPATH to correct the $^{14}\text{C}_{\text{MEAS}}$ to more reasonable estimated ages of the groundwater. Other wells in the transect have not been placed into a defined flow system yet, and therefore cannot be modeled with this approach. It was also noted that the correction method of Pearson, which assumes simplified carbonate chemistry, with most of the defining reactions occurring early in the flow path in an open system environment, matched the NETPATH estimates well enough to infer that a simplified estimate of age based on the Pearson correction, albeit devoid of mass balance chemistry, was better than relying on the uncorrected age. Consequently, for example only, Table 8-7 is a list of wells along the transect, with the measured $^{14}\text{C}_{\text{MEAS}}$ and the Pearson estimate for comparison. A key message that can be gleaned from the table is that the Pearson correction typically reduces the uncorrected ^{14}C ages by about 4,000 to 7,000 years.

8.2.2 Transect 5 in GMA 15

There are 20 wells in Transect 5 with both chemical analyses and ^{14}C measurements; 10 wells are in the TWDB database from prior sampling (2009) and ten wells were sampled as part of this project in 2013 (see Table 4-4). Well depths range from 120 to 1,235 feet bls, with screened intervals identified for the majority but not all wells. All wells are located within a band along the transect that is approximately 100 mi long and 12 miles in width (see Figure 4-6).

Transect 5 wells and lithology are plotted in Figure 8-8. For the Oakville and younger formation, the lithology includes average sand percentage and the intervals of sand identified in

Table 8-7 Application of Pearson Correction ($^{14}\text{C}_{\text{cor}}$) to Measured ^{14}C ($^{14}\text{C}_{\text{meas}}$) along Transect 3.

Well	Transect Distance (mi)	$^{14}\text{C}_{\text{meas}}$ (ybp)	$^{14}\text{C}_{\text{cor}}$ (ybp)	$\delta^{13}\text{C}$ (‰)	Well	Transect Distance (mi)	$^{14}\text{C}_{\text{meas}}$ (ybp)	$^{14}\text{C}_{\text{cor}}$ (ybp)	$\delta^{13}\text{C}$ (‰)
1	1.3	4000	2287	-20.2	27	47.5	14000	10662	-16.5
2	6.3	18180	15541	-18	28	50.7	16320	12933	-16.4
3	6.6	13120	7422	-12.3	29	52	13820	9333	-14.3
4	9.3	25880	19984	-12	30	52.4	24490	16283	-9
5	14.9	14700	7958	-10.8	31	52.7	34100	26819	-10.1
6	18.4	17256	13083	-14.87	32	54	14730	9032	-12.3
7	20.6	4137	486	-15.87	33	54.5	22330	15049	-10.1
8	22.6	22520	16651	-12.04	34	57.6	24230	18622	-12.5
9	22.8	36834	30803	-11.8	35	62.2	19540	13842	-12.3
10	25.9	20520	14691	-12.1	37	63.2	23580	19149	-4.4
11	27.9	36580	33851	-17.8	38	63.2	45899	39758	-11.6
12	30.8	23120	17357	-12.2	39	63.7	9573	1543	-9.2
13	31.4	26580	19985	-11	40	63.8	44980	38791	-11.6
15	34.8	1516	157	-21.1	41	64.1	24752	18273	-11.2
16	35.7	21760	16319	-12.7	42	69.4	37470	29782	-9.6
17	36.9	4680	1861	-17.6	43	78.4	15760	10987	-13.8
18	36.9	28080	24188	-15.4	44	83.9	34590	29460	-13.2
19	36.9	29505	22047	-9.8	45	87.8	32790	27599	-13.1
22	41.3	1128	Modern	-21.4	46	94.2	31520	25624	-12
23	42	21130	14751	-11.3	47	98.4	30910	25840	-13.3
24	42.1	7180	4315	-17.5	48	103.8	31220	25842	-12.8
25	45.7	>43500	-	-8.9	49	106.8	31080	25950	-13.2
26	46.8	24760	19192	-12.5					

geophysical logs near Transect 3 from Young and others (2012a). A visual review of the lithologic data suggest that the Chicot and Evangeline aquifers consist of appreciable sands that appear to be more frequent and thicker up dip than down dip. Figure 8-8 shows a notable decrease in sand percentages in the Middle Lagarto and the Jasper aquifer as compared with the Chicot and Evangeline Aquifers.

The geochemical facies map for Transect 5 (Figure 6-26) supports a regional evolution of groundwater chemistry down dip of the Jasper. Near the Jasper outcrop, the shallow waters are dominated by Ca-Na-HCO₃ facies, which gradually evolves to a Ca-HCO₃ facies in the up-dip

regions of the Chicot and the Evangeline aquifers, and then evolves to Na-Cl-HCO₃ facies at the down-dip region of the Chicot and Evangeline aquifers. The uncorrected ¹⁴C ages in Figure 8-9 supports a regional flow path that is consistent with the flow directions inferred from the distribution of hydrochemical facies. As shown in Figure 6-25, the chemical evolution is consistent with the carbonate system where calcium concentrations between 50 and 100 ppm occur in the recharge areas and gradually lower calcium concentrations occur down dip. Despite the regional trends in the chemistry, there is considerable variability in concentrations at some well clusters. Whereas some sampled wells clustered in close proximity to one another have similar chemical and isotopic compositions, other adjacent wells within a few miles of each other with similar screened intervals are chemically quite different. As a result, the well concentration values as a whole do not reveal a continuous regional flow path along which a series of NETPATH simulations can be performed for well pairs that begin at the up-dip extent of Transect 5 and end near the ocean.

Table 8-8 provides notes on each of the Transect 5 wells with regard the NETPATH simulations. Each of the 20 sampled wells is classified as a distinct circumstance with characteristic age, composition, and flow regime as described below.

- Shallow wells modeled as flow from recharge to the well with no subsequent well identified along a flow path (Wells 5-1, 5-3, 5-12, 5-13, and 5-18).
- Shallow wells with no mathematical solution for flow from recharge to the well, corrected ages are post-modern, probably water from mixed sources and surface anthropogenic activity (Wells 5-6, 5-10, 5-11, 5-17).
- Groundwater that measures and corrects to old ages is present along the entire transect, and seems to represent a continuous zone with no plausible upgradient wells (Wells 5-2, 5-4, 5-5, 5-7, 5-8, 5-14, 5-15, 5-16, 5-19, 5-20).

8.2.2.1 Shallow Wells with NETPATH Solution

In other transects, an indication of flow zones can be derived from facies cross-sections using lithology and distribution of major dissolved ion compositions. Along Transect 5 there is an indication of preferential flow in the Chicot and possibly the Evangeline. Unfortunately the ¹⁴C_{MEAS} samples in these regions are not located in these zones. The consequence is that the ¹⁴C data do not contribute useful information to these zones; conversely, there are five wells that are

Table 8-8 Comments Regarding the Evaluation of Wells in Transect 5 for NETPATH Simulations.

Well	Note Regarding Evaluation for NETPATH Simulation
5-1	Shallow aquifer wells modeled as recharge directly to the sampled well.
5-2	Groundwater 25k to 45k years before present; continuous deep zone, no wells that can be modeled as upgradient wells.
5-3	Shallow aquifer wells modeled as recharge directly to the sampled well.
5-4	Groundwater 25k to 45k years before present; continuous deep zone, no wells that can be modeled as upgradient wells.
5-5	Groundwater 25k to 45k years before present; continuous deep zone, no wells that can be modeled as upgradient wells.
5-6	Shallow aquifer wells with no modeling solution directly from recharge; model dates are post-modern, probably mixed with unknown wells.
5-7	Groundwater 25k to 45k years before present; continuous deep zone, no wells that can be modeled as upgradient wells.
5-8	Groundwater 25k to 45k years before present; continuous deep zone, no wells that can be modeled as upgradient wells.
5-9	Enigmatic well, all sampled upgradient wells are old >25 to 45k ybp.
5-10	Shallow aquifer wells with no modeling solution directly from recharge; model dates are post-modern, probably mixed with unknown wells.
5-11	Shallow aquifer wells with no modeling solution directly from recharge; model dates are post-modern, probably mixed with unknown wells.
5-12	Shallow aquifer wells modeled as recharge directly to the sampled well.
5-13	Shallow aquifer wells modeled as recharge directly to the sampled well.
5-14	Groundwater 25k to 45k years before present; continuous deep zone, no wells that can be modeled as upgradient wells.
5-15	Groundwater 25k to 45k years before present; continuous deep zone, no wells that can be modeled as upgradient wells.
5-16	Groundwater 25k to 45k years before present; continuous deep zone, no wells that can be modeled as upgradient wells.
5-17	Shallow aquifer wells with no modeling solution directly from recharge; model dates are post-modern, probably mixed with unknown wells.
5-18	Shallow aquifer wells modeled as recharge directly to the sampled well.
5-19	Groundwater 25k to 45k years before present; continuous deep zone, no wells that can be modeled as upgradient wells.
5-20	Groundwater 25k to 45k years before present; continuous deep zone, no wells that can be modeled as upgradient wells.

essentially isolated with no continuity to deeper wells along a continuing indicated flow path. These wells are 5-1, 5-3, 5-12, 5-13, and 5-18 with depths of 320, 130, 120, 120, and 160 feet bls. Table 8-9 summarizes results from NETPATH simulations and the application of the Pearson Method for chemical reactions associated with reproducing the measured major ions and isotope concentrations at Wells -1, 5-3, 5-12, 5-13, and 5-18. This is plausible since the flowpath is likely a shallow system with oxygenated water and represents the zone on maximum weathering reactions.

Table 8-9 Results of NETPATH modeling of groundwater evolution from one well to another down-gradient well for wells in the Chicot for Wells 5-1 and 5-3.

	Soil to Recharge Well to Well 5-1, Well 5-3, Well 5-12, Well 5-13, or Well 5-18				
	5-1	5-3	5-12	5-13	5-18
$^{14}\text{C}_{\text{MEAS}}$ ybp	8,940	12,280	6,730	9,340	7,220
$^{14}\text{C}_{\text{MEAS}}$ pMC	32.85	21.67	43.25	31.25	40.69
$^{13}\text{C}_{\text{MEAS}}$ DIC	-9.3	-7.3	-13.3	-12.9	-10.0
$\delta^{34}\text{S}$ meas	4.1	10.9	-1.0	8.3	-
Mass Transfer⁽¹⁾					
calcite	3.77	5.46	2.70	3.59	3.81
$\text{CO}_{2(\text{g})}$	2.23	2.25	2.97	3.82	2.87
Ca/Na Ex	1.70	2.89	0.44	1.55	1.86
Mg/Na Ex	-0.18	-0.51	-0.44	-0.50	-0.95
K/Na Ex	-2.43	-4.60	-0.11	0.68	
NaCl	5.53	5.22	3.27	0.85	2.26
gypsum	0.40	0.40	0.11	0.23	0.13
pyrite	0.10	0.05	-	-	-
Computed Values					
$^{14}\text{C}_{\text{ADJ}}$ (ybp)	1,019	2,456	1,579	4,140	456
$^{14}\text{C}_{\text{ADJ}}$ (pMC)	37.16	29.17	52.36	51.57	43.00
$\delta^{13}\text{C}$ DIC calc	-9.3	-7.3	-13.1	-12.9	-10.8
$\delta^{34}\text{S}$ calc	4.1	10.9	-1.0	8.3	
$^{14}\text{C}_{\text{ADJ}}$ (ybp) ²	996	2,391	1,539	4,025	modern

NOTES:

¹ millmoles

² Pearson Method

8.2.2.2 Shallow Wells with No NETPATH Solution

Some wells along Transect 5 were of a chemical and isotopic composition for which a NETPATH model could not be constructed that would simulate the chemistry and match the measured $\delta^{13}\text{C}$ value of the well. There are four wells that fail to generate valid mathematical solutions for a corrected age (Wells 5-6, 5-10, 5-11, and 5-17); the results yield post-modern ages using both NETPATH and the Pearson correction. The wells may be mixed water with contributions from surface contamination or are recycled water from anthropogenic use. All four wells are relatively shallow, 175, 333, 114, and 123 feet bls.

Well 5-9 is an enigmatic well with multiple screened intervals, and a completed depth of 1,030 feet bls, 17.5 miles along Transect 5, with a measured $^{14}\text{C}_{\text{MEAS}}$ of 17,510 ybp, but is surrounded by wells of much older ages. The three closest and most directly upgradient wells are 5-4, 5-7 and 5-8 with $^{14}\text{C}_{\text{MEAS}}$ ages of 39,010, 38,250 and 42,120 ybp. No correction using NETPATH seems plausible and groundwater compositions are similar enough that a unique

composition is not indicated. At present this well is considered an isolated case and is not further considered.

8.2.2.3 Sulfur Isotope

Along Transect 5, the values range for $\delta^{34}\text{S}$ range from -30.6‰ to 38.1‰. The explanation for the range is similar that provided for the $\delta^{34}\text{S}$ ranges observed for Transect 3. The sulfur isotope results can be divided into three groups: 1) one value of -30.6‰, 2) a range of values from -1‰ to 15.2‰, and 3) four strongly enriched values from 20.10‰ to 38.10‰. The first value is evidence of bacterial reduction in a shallow well (~175 ft. bls) with a corrected ^{14}C age of modern, indicating contamination from surface processes and not useful or representative of typical recharge. The second group is a range typical of oxidation of sulfide minerals such as pyrite in the shallow subsurface, where recharging water is oxygenated and reactive with sulfide minerals in the abundant clastic lithology. The third group represents residual sulfate that has been lowered in concentration by sulfate reduction; and as sulfate is reduced, the generated sulfide (probably as H_2S) would be significantly depleted in $\delta^{34}\text{S}$, and the remaining sulfate would be consequently enriched in $\delta^{34}\text{S}$ in the range of values observed. Marine sulfate has a $\delta^{34}\text{S}$ of ~20‰ and the residual sulfate values observed in this latter part of Transect 5 are more enriched than that, as much as 38.1‰. The sulfate concentration in each of these four wells is low, and in Well 5-16 the sulfate concentration is actually below the detection limit. Although the process of pyrite oxidation generates minerals such as gypsum in the soil zone, the amount of gypsum subsequently dissolved during recharge is small, and although the added calcium is considered in the modeling, it has little effect on the corrections to the calculated age.

8.2.2.4 Region of Groundwater with Measured and Pearson Corrected Old ^{14}C Dates

Regional sampling along any given transect has the intent of identifying zones of flow that can be further clarified with additional sample collection; nevertheless, samples will be obtained that for many reasons do not fit anticipated flow systems. Flow systems in this region are disrupted and redirected by variations in lithology from poorly permeable clastics to high quality sands, and precise sampling is often hindered by well location, screened intervals and wells not aligned with existing flow systems. Nevertheless, along Transect 5 there are 10 wells that have a similar characteristic of having “old” groundwater ages, both measured and corrected without specific hydrogeologic evidence of continuity (Table 8-8). Table 8-10 include ^{14}C ages based on the

correction method of Pearson, which assumes simplified carbonate chemistry and again could be used to infer a simplified estimate of age. The Pearson correction, albeit devoid of mass balance chemistry, was better than relying on the uncorrected age.

The wells in Table 8-10 are in different lithologies and formations ranging from Jackson to Chicot, have a broad a range of depths, but have similar ages except for 5-2 and 5-14, which are younger but still measure greater than 20,000 ybp, similar $\delta^{13}\text{C}$ and Cl values over a narrow range. These wells seem to infer a deeper and older groundwater continuum, but not mixed with an upwelling deep source of extremely saline brine.

Table 8-10 Comparison of measured $^{14}\text{C}_{\text{MEAS}}$ to Pearson corrected ^{14}C values for “old” groundwater along Transect 5.

Well	Transect Distance (mi)	Well Depth (ft)	$^{14}\text{C}_{\text{MEAS}}$ (ybp)	$^{14}\text{C}_{\text{ADJ}}$ (ybp)	$\delta^{13}\text{C}$ (‰)	TDS (mg/L)	Cl (mg/L)	Formation
2	4.5	320	24670	19037	-12.4	628	105	-
4	9.4	962	39010	32041	-10.5	812	106	Jackson
5	9.5	529	>43500	-	-10.1	824	107	Jasper
7	16.8	540	38280	31612	-10.9	912	242	Jasper
8	16.9	324	42120	36422	-12.3	1190	283	-
14	53.5	1318	21180	16230	-13.5	658	199	Evangeline
15	60.0	300	37340	32087	-13.0	1090	279	Chicot
16	63.3	1235	37870	28514	-7.8	1180	282	Chicot
19	75.5	620	38800	32837	-11.9	956	206	Chicot
20	79.3	200	38930	32622	-11.4	1040	202	Chicot

8.2.3 Transect 8 in GMA 16

There are 18 wells in Transect 8 with both chemical analyses and ^{14}C measurements; eight are in the TWDB database from prior sampling (2006) and 10 are samples collected for this project in 2013 (see Table 4-5). Well depths range from 102 to 1,052 feet bls; with screened intervals identified for all wells. All wells are located within a band along the transect that is approximately 90 mi long and 20 miles in width (Figure 4-9). The Transect 8 wells and lithology are plotted in Figure 8-10. For the Oakville and younger formation, the lithology includes average sand percentage and the intervals of sand identified in geophysical logs near Transect 3 from Young and others (2012a).

A visual review of the data suggest that the upper two formations (e.g., the Beaumont and the Lissie) in the Chicot Aquifer and the lower two formations (e.g., the Lower Goliad and the

Upper Lagarto) are relatively sand poor. Figure 8-10 indicates that the most sandy units occur in up-dip extent of the Willis and the upper regions of the Upper Goliad. In this zone of sandy deposits is about 100 feet thick that originate and extends from the outcrop of the Upper Goliad and extends downdip about 100 miles.

Several important issues regarding this transect are the skewed location of the Wells 8-1, 8-2, and 8-3 and the proximity of salt domes to the transect. Wells 8-1, 8-2, and 8-3 are located approximately 12 miles south of Transect 8. Within a few miles of Wells 8-6 and 8-7 are two salt domes, with depths to salt about 500 feet below ground surface. The hydrogeochemical facies map for Transect 8 (Figure 6-31) supports a simple system where a Na-Cl-HCO₃ facies occur in the outcrop of Oakville and Lagarto formations and transitions to a Na-Cl facies that occupies most of the Upper Evangeline and Lower Chicot Aquifers. The values of uncorrected ¹⁴C ages in Figure 8-11 supports a regional flow path in the upper Evangeline that begins in the outcrop and continues downdip for approximately 70 miles. As shown in Figure 6-30, the chemical evolution consistent with the carbonate system is well illustrated by the high calcium concentrations (above 100 ppm) in the recharge areas that gradually reduce with distance down dip until the concentrations reach about 10 ppm.

Despite evidence of a regional flow path in the Upper Evangeline as indicated in the ¹⁴C ages, calcium concentrations, and sandy bed locations, applications of successful NETPATH simulations are prevented by large fluctuations in the chloride concentrations (Figure 6-30). Review of the chloride concentrations shows highly variable levels for well clusters that are located a few miles apart. This large variability is attributed to the complex flow and transport processes that occur around salt domes. Partly because of the high spatial variability in chlorides, the geochemical modeling for the sampled wells along this transect does not reveal any defendable continuous regional flow path whose chemistry changes between wells can be modeled using NETPATH. Whereas some sampled wells are clustered in close proximity to one another and have similar chemical and isotopic compositions, other adjacent wells within a few miles of each other with similar screened intervals are chemically quite different as discussed below. In order to try to model the geochemistry along Transect 8, each of the 18 sampled wells is classified as distinct circumstances or as part of a cluster of wells with characteristic age, composition, and flow regime as described below:

- Cluster of 3 wells in Webb County, off the transect, no upgradient wells, and old ^{14}C ages (8-1, 8-2, 8-3);
- Well 8-4 with an anomalous composition, 5 to 10 times that of all other wells;
- Wells 8-5 and 8-15 have deep screens relative to surrounding wells, ages >35,000 ybp, and no correlation in chemistry and age with surrounding wells;
- Well 8-9 is influenced by recent recharge having a modern ^{14}C age;
- Cluster of 5 wells with elevated TDS, especially Cl, above that of downgradient wells in the Evangeline Aquifer; no upgradient wells have been sampled for ^{14}C content for comparison (8-6, 8-7, 8-10, 8-11, 8-12);
- Cluster of 6 downgradient wells in the Evangeline Aquifer, all with similar composition and similar age (~ 20,000 ybp) and no upgradient wells (8-13, 8-14, 8-16, 8-17, 8-18, 8-19); and
- Well 8-15 with deep screen and old measured ^{14}C age of >35,000 ybp which does not correlate with any nearby surrounding wells.

8.2.3.1 Well Cluster in Webb County

The three wells in southeastern Webb County (Figures 4-8 and 8-10) are located in the most upgradient portion of Transect 8 and are inconsistent in depth of sample and measured age with a flow path originating at the beginning of the transect. All three wells are within 10 miles of each other, are approximately 20 miles south of the transect, and are the most removed wells from the transect. These wells are of similar depths (320 to 460 feet bls), exhibit a Na-Cl-HCO₃ water composition, have TDS values ranging from 956 to 1220 mg/L, and yielded similar measured $^{14}\text{C}_{\text{MEAS}}$ ages of 32,660, 33,840 and 36,990 ybp (Figure 8-11). These wells are at the beginning of the transect for this region, yet the measured ages are among the five oldest uncorrected ages seen along the entire transect. It appears that the wells are producing from the Catahoula or Jasper Formation in clay rich sediments, whereas most downgradient wells on the transect produce from younger and the more sandy Evangeline Aquifer. Relative to almost all other downgradient wells, the sodium, bicarbonate, and pH values of the Webb County wells are higher, and the chloride, sulfate and calcium concentrations are lower. Considering age,

composition and location, it appears that these three wells are not part of the principal, and generally shallower, flow system being analyzed as part of this transect.

In the absence of upgradient wells with chemical and isotopic data, the conventional methods for assessing or correcting the ^{14}C carbon ages are less reliable; however, estimates of a possible correction factor for the ^{14}C age can be made with the following assumptions. The NETPATH simulation is constructed such that a synthesized upgradient well in a recharge location was assumed to have a dilute dissolved solute composition, a carbon dioxide content typical of soil gas, e.g., $\delta^{13}\text{C}$ of -25‰ and a ^{14}C content of 100 pMC. Available reactive minerals would include calcite or dolomite that would have a $\delta^{13}\text{C}$ of 0 ‰ and ^{14}C of 0 pMC. In this circumstance the solute composition would be derived entirely from mineral dissolution, ion exchange and incorporation of carbon dioxide. Two results for each of the three wells are shown in Table 8-11 for the three reaction paths from directly to each well in Webb County as an example. The minerals and ion exchange are reasonable for this aquifer system or for shallow soil or alluvial sediments. The only substantive difference between the example NETPATH results is the use of dolomite as a substitute for calcite in the selected reactions.

Table 8-11 NETPATH modeling results for Transect 8 Involving Wells 8-1, 8-2, and 8-3.

	Soil to Recharge Well to Well 8-1		Soil to Recharge Well to Well 8-2		Soil to Recharge Well to Well 8-3	
	8-1	8-1	8-2	8-2	8-3	8-3
$^{14}\text{C}_{\text{MEAS}}$ ybp	32,660	32,660	33840	33840	36,990	36,990
$^{14}\text{C}_{\text{MEAS}}$ pMC	1.71	1.71	1.48	1.48	1.00	1.00
$^{13}\text{C}_{\text{MEAS}}$ DIC	-10.1	-10.1	-10.3	-10.3	-10.3	-10.3
Mass Transfer⁽¹⁾						
calcite	3.45	3.10	3.82	3.65	3.70	3.52
$\text{CO}_2(\text{g})$	2.33	2.33	2.67	2.67	2.59	2.59
Ca/Na Ex	4.45	4.28	4.75	4.66	4.59	4.50
Mg/Na Ex	-0.17		-0.08		-0.09	
K/Na Ex	4.51	4.51	4.41	4.41	3.64	3.64
NaCl	8.27	8.27	4.29	4.29	4.55	4.54
gypsum	1.16	1.16	1.1	1.1	1.06	1.06
dolomite	-	0.17	-	0.08	-	0.09
Computed Values						
$^{14}\text{C}_{\text{ADJ}}$ (ybp)	26,142	26,142	27498	27498	30,739	30,739
$^{14}\text{C}_{\text{ADJ}}$ (pMC)	40.40	40.40	41.2	41.2	41.20	41.20
$\delta^{13}\text{C}$ DIC calc	-10.1	-10.1	-10.3	-10.3	-10.3	-10.3
$^{14}\text{C}_{\text{ADJ}}$ (ybp) ²	25,379	25,379	26,717	26,717	29,867	29,867

Notes:

¹ millmoles

² Pearson Method

The results in Table 8-11 indicate that a correction from a measured ^{14}C age of 32,660 ybp to an adjusted age of 26,142 ybp will solve the required dissolved solute mass that accounts for the change in water composition from recharge to Well 8-1, and the consequent computed $\delta^{13}\text{C}$ of the DIC matches exactly the measured $\delta^{13}\text{C}$. The change in $\delta^{13}\text{C}$ from soil zone to Well 8-1 can be described as incorporation of soil carbon dioxide and dissolution of either calcite or dolomite. As an example of another simplified approach, the adjustment to the measured ^{14}C age using the Pearson correction method yields a similar result.

The same computation for Wells 8-2 and 8-3 was performed with similar degrees of age correction and also yielded a correct $\delta^{13}\text{C}$ for DIC. This computation is for a hypothetical circumstance of recharge to deep wells. Were detailed upgradient age and composition data available for these wells, it is more likely that most of the dissolution and ion exchange occurred early in the flow path when the aquifer was an open system, followed by slow continued alteration in composition along the flow path in a closed system until the composition in Well 8-1 was attained. It is likely that this evolutionary pathway is incorrect given the spatial variability observed in the measured chloride concentrations, and other common processes such as mixing and changes in flow direction that occurred over the prior 25,000 years. Nevertheless, the correction calculation was useful in that it indicates the plausibility of this degree of correction (~6,000 years) in order to account for the observed $\delta^{13}\text{C}$ of the DIC.

Wells downgradient from Webb County are younger and of different composition (See Figures 8-11 and 6-30); however Well 8-5 (TWDB 8436605) is of similar $^{14}\text{C}_{\text{MEAS}}$ age (34,940 ybp), has a screened interval at 540 to 560 feet bls, and is deep enough that it could be mixing with the same water from this Webb County source. A plot of the environmental isotopes $\delta^2\text{H}$ and $\delta^{18}\text{O}$ clearly indicate that groundwater sources of well samples collected from different segments of the transect are similar, and may represent essentially the same groundwater system (Figure 8-13). Note that the $\delta^2\text{H}$ and $\delta^{18}\text{O}$ for the three Webb County wells are similar to that of Well 8-5, but Well 8-5 may have mixed to some small extent with water from the Evangeline. As shown in Figure 8-10, Wells 8-1 through 8-4 are all located in the Jasper/Catahoula Formation. It is noted also that there exists a few per mil difference between clusters of wells and there is the suggestion that prior climate may have influenced these values; however, the population is too small to be statistically significant, differences are small, and do not correlate with age or location in the flowpath.

Several constituents such as bicarbonate, sulfate, and sodium are substantially lower in Well 8-5 than in the Webb County wells, so mixing would be required to yield the composition observed in 8-5, because removal of these constituents is not plausible by precipitation based on the thermodynamic assessment for common phases containing these constituents. Modeling of well-to-well evolution and ^{14}C correction was attempted, but for these wells it was unsuccessful; the conceptual model of flow along this transect should not include these wells as part of the shallow flow system because they are inconsistent with the downgradient wells in measured ^{14}C age, chemical, and isotopic composition.

8.2.3.2 Wells 8-4 and 8-9

Well 8-4 (TWDB 8419303) is the fourth well along the transect but is not directly down gradient from the Webb County wells (Figure 4-8). The $^{14}\text{C}_{\text{MEAS}}$ is 20,440 ybp, which is within reason for the distance from the recharge area, but the composition is not consistent with any other wells in the vicinity. The TDS is 8,062 mg/L and chloride is 4,420 mg/L, both of which are essentially an order of magnitude above all wells along the 100-mile transect. It is bracketed by wells both upgradient and downgradient with more commonly observed compositions. The well was completed between zones of sandy shale in an interval described as a streaky sand, saline, and yielded only 20 gpm (TWDB). It appears to be isolated and of poor quality and not part of the general flow system. One possible reason for the high TDS and chloride values is upswelling of salinity from the salt dome approximately 10 miles hydraulically upgradient. This hypothesis is supported by an average Cl/Br ratio greater than 800 at Well 8-4 and the interpolated values of Cl/Br ratios plotted in Figure 6-14.

The shallowest well along the transect is Well 8-9 which is in the Evangeline aquifer 102 feet bls, with a screen set from 82-102 feet bls. The TDS is 1,020 mg/L and the water type is Na-HCO₃ with elevated nitrate (7.6 mg/L). In addition, the $^{14}\text{C}_{\text{MEAS}}$ is greater than 100 pMC, indicating recent water with significant shallow surface water interactions. No tritium measurements are available to support the indication of modern water; however, this well indicates that this region is receiving modern recharge, may have significant local infiltration from surface activities, and appears to be chemically and isotopically modified by anthropogenic processes such as agriculture, and is therefore problematic for modeling compositional evolution and age corrections between wells. In the vicinity of Well 8-9 active irrigation is ongoing. The

measurement of $^{14}\text{C}_{\text{MEAS}}$ is greater than 100% is attributed to a leaky seal around the well at the surface which is allowing some irrigation leakage into the well annulus.

8.2.3.3 Region of Elevated TDS in the Evangeline Aquifer

In the middle of the transect between mile 30 and 50, Wells 8-6, 8-7, 8-10, 8-11, and 8-12 are clustered in the same area and all have significantly different composition than either upgradient or downgradient wells. Uncorrected ages range from 5,610 to 18,920 ybp and the TDS is consistently between 1,320 and 2,076 mg/L, with a mean value of 1,617mg/L. The upgradient and adjacent wells, the Webb County wells, plus Wells 8-5 and 8-9, have a mean TDS value of 1,022 mg/L, while the next five downgradient wells have a mean TDS of 1,031 mg/L. This zone of elevated TDS is in the Middle Evangeline with a depth range for the screened intervals of 328 to 634 feet bls. These five wells are unconnected to the upgradient samples and do not fit with the downgradient flow system identified for the Upper Evangeline, and are considered an isolated zone with insufficient surrounding data to define the origin of this zone of distinct but incompletely understood groundwater.

Although the ages increase from the first to the second well, the third well has a similar age and the subsequent wells decrease in $^{14}\text{C}_{\text{MEAS}}$; attempts to model the evolution between these wells is also complicated by the inconsistent chloride and sodium, which is difficult to explain except by mixing or dilution. The wells seem connected by process, which means that they may have all experienced evaporation, or mixing in similar geographical locations or under similar climatic circumstances, but the rigorous computation describing the chemical and isotopic evolution between the wells was not successful and may require considering unidentified waters that provide mixing and dilution. The most plausible explanation for the localized high levels of TDS is that the groundwater chemistry is being affected by dissolution of salt from the nearby salt domes shown in Figure 4-8.

In the absence of upgradient ^{14}C measurements or applicable data for groundwater composition, a correction to the ^{14}C age based on NETPATH simulations could not be done. A simple correction using the Pearson and White approach yields an estimated age for the first well (8-6) of 2,150 ybp (76.2 pMC) compared to the $^{14}\text{C}_{\text{MEAS}}$ of 5,610 ybp; this large correction is because of the significantly enriched $\delta^{13}\text{C}$ of -13.0‰ for such a young ^{14}C measurement. This correction is approximate but the correction to a much younger age is reasonable. Subsequent modeling

from Well 8-6 and 8-10 to 8-11 was not successful because of the missing or inconsistent groundwater composition.

8.2.3.4 Upper Evangeline Flow

The six wells at the end of the transect (8-13, 8-14, 8-16, 8-17, 8-18, and 8-19) are similar in water composition and uncorrected age (Table 4-5). The average age is near 20k ybp over a transect distance of 30 miles, and the $\delta^{13}\text{C}$ values are similar as well. These wells are screened in the sandy section of the Upper Evangeline or Lower Chicot (Figures 8-10 and 8-11). Chloride concentrations in these wells are progressively increasing with depth (277 to 401 mg/L) and with transect distance; the possibility of mixing with a deeper more saline source water is possibly suggested, however the increase in chloride is small.

Mixing of different water sources, especially if they are of widely different age or climatic history should also be reflected as a difference in the environmental isotopes hydrogen and oxygen ($\delta^2\text{H}$ and $\delta^{18}\text{O}$). A plot of these isotopic values for all wells along the transect is shown in Figure 8-13. The six deeper wells at the end of the transect cluster together, but it can also be seen that three additional wells (8-7, 8-12, and 8-14) tightly cluster with the deep wells. In cross section these wells all align in what could be interpreted as a lithologically similar downdip flow system, beginning with Well 8-7 and ending with Well 8-19 (Figure 8-10). The $\delta^2\text{H}$ and $\delta^{18}\text{O}$ support the similar origin of the water, and the tightness of the cluster of these isotopic indicators suggest little mixing or dilution with water from other sources. This zone of contiguous freshwater is also suggested in the GMA regional maps for both Cl and TDS distribution in which a region of less concentrated water was identified in the center of GMA 16 in the interval to 500 feet depth, and in cross section in the Upper Evangeline (Figures 6-9 and 6-10). The uncorrected $^{14}\text{C}_{\text{MEAS}}$ values are so similar and do not increase significantly with distance along the transect, nor does the general composition consistently evolve in a recognizable pattern. Nevertheless, the $\delta^2\text{H}$ and $\delta^{18}\text{O}$ tightly connect the wells in this flow system.

Linking these wells together chemically is difficult because of the large variability in the first few wells, especially with respect to chemically conservative constituents such as chloride, which are variable. Consequently, modeling the evolution in composition from well-to-well and correcting for ^{14}C age by adjusting for changes in the carbonate system was unsuccessful. It is suspected that the first two wells are impacted by anthropogenic activities, probably agricultural

processes, because the nitrate concentration is significantly higher in Well 8-7 and 8-12 (29.2 and 21.3 mg/L) than any other wells in the transect, especially the deepest four wells (with nitrate concentrations of 1.8 to 0.4 mg/L). Similarly, the TDS and especially sodium and chloride could be impacted by agricultural processes because they are not solubility limited whereas the presence of gypsum and calcite in the soil will limit the concentration of other common ions because of their low solubility. The $^{14}\text{C}_{\text{MEAS}}$ for Well 8-12 is also younger than either the preceding well or any subsequent well also supporting the conceptual model that this zone was impacted by surface processes. In order to obtain approximate corrections to the measured ages, the simple Pearson and White correction is applied. This approximation assumes a soil carbon dioxide $\delta^{13}\text{C}$ of -25‰, and further assumes that most of the reaction with carbonate occurs near the recharge area, and that carbon entering the system along the flow path is from calcite with a $\delta^{13}\text{C}$ of 0‰. These results are given in Table 8-12 for demonstration of generally expected range of correction only, and do not imply a simple evolution from recharge to each well.

The similarity in age of all the wells is indicative of a hydrologic process that seems to obstruct continuous flow either to deeper subsea regions or upward as cross formational flow. The water has the physical characteristics of stagnation and homogenation perhaps by diffusion to a reservoir or region with essentially the same age. Reversals in hydraulic gradients due to sea water transgression would undoubtedly be transferred to these depths however the ages, and the process is still undefined for this region.

Table 8-12 Chemistry and ^{14}C Ages for the Upper Evangeline Flow System.

Well	Transect Distance (mi)	Na (mg/L)	Cl (mg/L)	NO ₃ (mg/L)	Ca (mg/L)	HCO ₃ (mg/L)	SO ₄ (mg/L)	$^{14}\text{C}_{\text{MEAS}}$ (ybp)	$^{14}\text{C}_{\text{ADJ}}$ (ybp)	$\delta^{13}\text{C}$ ‰
8-7	35.9	367	401	29.2	38	322	210	18,490	11,328	-8.2
8-12	44	430	843	21.2	200	239	313	12,380	6,567	-9.7
8-14	63.8	214	170	14.1	49	266	139	18,240	10,467	-7.6
8-16	80.3	382	277	1.8	34	220	363	20,750	12,317	-7
8-17	82.3	361	249	0.4	25	247	286	20,190	13,410	-8.6
8-18	91.3	394	318	0.4	18	223	242	20,200	13,135	-8.3
8-19	93.3	452	401	0.4	16	174	275	21,150	14,181	-8.4

8.2.3.5 Sulfur Isotopes

The $\delta^{34}\text{S}$ values are tightly constrained ranging only from 10.5‰ to 14.4‰ (Figure 8-12) for the entire transect. When viewed in the context of values from the other transects, which range generally from -30‰ to 40‰ the values in Transect 8 are almost invariant with respect to sulfate concentration, well depth, or distance along the transect. It is noteworthy that the sulfate concentration is relatively high even from early in the transect, and ranges from 19 to 452 mg/L in the wells with $\delta^{34}\text{S}$ measurements; nevertheless the fact that the $\delta^{34}\text{S}$ does not vary with concentration indicates that sulfate reduction is not likely a contributing process.

The options for the source of sulfate are small: airborne particulates, evaporite minerals in the region such as gypsum and anhydrite, residual marine sulfate, or oxidation of pyrite in marine shales. It is unlikely that airborne particulates or evaporite minerals would have had such a uniform isotopic contribution since the Pleistocene, when some of the deeper zones were recharged. The $\delta^{34}\text{S}$ of seawater dissolved sulfate would have been near 21‰, and pyrite in the marine shales are conventionally known to range from around 15‰ to values as depleted as -20‰, depending on the specific original local environment of deposition and diagenetic circumstances (Thode, 1991). It seems plausible that the process of sulfate generation is from sulfide mineral oxidation. These aquifer sediments were exposed to oxygenated surface water during recharge and thus sulfide minerals such as pyrite would have oxidized and have generated sulfate. As discussed before, the local wet dry cycles in the soil zone or shallow aquifer sediments could have precipitated gypsum with a $\delta^{34}\text{S}$ similar to that of the shale signature, rather than the marine sulfate value. Consequently, recharging waters that dissolve the gypsum or oxidize pyrite will yield dissolved sulfate that clusters in the shale range of $\delta^{34}\text{S}$.

No marine signature is evident, nor is there defensible suggestion of a trend of changing values with distance or depth. Although sulfate concentrations are relatively high, computations with the geochemical model accompanying NETPATH confirm that none are supersaturated with respect to gypsum; thus, the potential to dissolve gypsum in the soils zone exists now and in the past. This transect is located in a more arid environment and thus the sulfate concentration would periodically become elevated in the soil and shallow unsaturated zone due to slow infiltration and low water contents. It may be possible to correlate sulfate concentrations with climatic variations assuming little mixing and only small changes along the flow path. All groundwater $\delta^{34}\text{S}$ values of sulfate along this transect are assumed to reflect oxidation of pyrite

near the recharge area with little subsequent change along the flowpath; consequently these data are not considered influential in the age calculations.

8.3 ¹⁴C Ages Based on Pearson Method

Some of the difficulty associated with developing a successful application of NETPATH between wells is attributed to spatial heterogeneity in the aquifer hydraulic and geochemical properties and large amounts of mixing of waters between wells. Given the task of investigating and quantifying relevant trends and patterns in the ¹⁴C data, NETPATH simulations are restrictive because they cannot be applied successfully to most of the measured ¹⁴C data. In the previous section, the NETPATH mass balance method and the Pearson Method typically produced corrected groundwater ages within 5%. For this reason, the Pearson Method will be applied to all the pMC measurements in order to set of corrected ¹⁴C ages that can be used to investigate and characterize the Gulf Coast Aquifer System groundwater flow system.

8.3.1 Factors affecting the Relationship between Groundwater Ages with Depth

Although one should expect that the age of groundwater should generally increase with depth, there are several factors that can complicate this relationship because this relationship is dependent on the flow history and the mixing of the water being sampled at the well. Among the primary causes for the different groundwater ages for a particular aquifer depth is the spatial variability in the hydraulic conditions and properties of the different geological media and the flow system encountered by the groundwater along its pathway to the well. To illustrate the importance this type of spatial variability, we consider two scenarios for flow to a well that is about 300 feet deep. The first scenario involves a well located beneath a sandy outcrop a top of a hill in northeast portion of the Gulf Coast Aquifer System. In this scenario, the recharge rate is high and the vertical and horizontal hydraulic gradients are high. In this first scenario there is a likelihood that relatively young water will be found at a depth of 300 feet. The second scenario involves a well located in a clayey formation that intersects groundwater flowing toward a spring in the southwest portion of the Gulf Coast Aquifer System where topography is relatively flat. In this second scenario, groundwater is moving relatively slow as a result of small hydraulic gradients, relatively low recharge rates, relatively low hydraulic permeability values in the formation. As a result there is likely old water migrating to the spring that did not originate from above the well screen but rather far away. In this second scenario there is a likelihood that much older water will be found at a depth of 300 feet than in the first scenario.

The discussion of the two scenarios above identifies some of the factors important to understanding and characterizing groundwater ages. The factors include climate (which can be represented by the GMA), the hydraulic property of the subsurface deposits (which can be represented by the geological formation), and the proximity to recharge and discharge areas (which is represented by the proximity to outcrop areas and major rivers).

Figure 8-14 shows plots of uncorrected and corrected ^{14}C age versus depth. The ^{14}C ages were corrected using the Pearson Method as described in Section 8.1.3. Despite considerable scatter in the data, Figure 8-14 shows a general trend of increasing groundwater age with well depth for both the corrected and uncorrected age. A comparison between the uncorrected and corrected groundwater ages in Figure 8-14 shows that the primary correction of the Pearson Method is to shift groundwater ages by about 3,000 to 7,000 years. For about twenty of the uncorrected ages, the application of the Pearson Method produces a negative groundwater age. Negative values are plotted with an age of 0 and are presumed to indicate that the sample contained “modern” carbon (see Section 8.1).

Besides using the field data in Figure 8-14, a relationship between depth and groundwater age and the factors that affect that relationship can be gleaned from the particle tracking simulations discussed in Section 3. An example of this type of information produced by the particle tracking simulations is shown in Figure 3-19, which shows groundwater ages for Transect 45 that were determined using the Central Gulf Coast Aquifer System GAM. For a depth of 1,000 feet bgs, the range of groundwater ages in the Gulf Coast Aquifer System predicted by the Central Gulf Coast Aquifer System GAM is from 10,000 to over 150,000 years. Similarly, the model predicts that groundwater with ages between 7,000 and 10,000 years exits at groundwater depths between 500 and 800 feet. In fact, the map of groundwater ages in Figure 3-19 could be used to compare groundwater age in a well to the age predicted by groundwater model. All one needs to know is the downdip distance and the depth of the well. For instance, using Figure 3-19 the predicted groundwater age of water sampled by a well with bottom elevation of -550 feet msl and downdip distance of 40 miles is between 5,000 and 10,000 ybp (this grid block is marked by the zone “[2,2]”).

8.3.2 Relationship between Measured and Predicted Groundwater Age and Geological Unit

Figures 8-15 through 8-17 show that the groundwater ages less than 5,000 ybp typically occur in or near outcrop and that groundwater with ages greater than 20,000 ybp typically occur near the coastline. Thus, groundwater age generally increases not only with depth but also with distance away from recharge areas. To help identify whether different age-depth relationships exist among the eleven geological formations that comprise the Gulf Coast Aquifer System, Figures 8-18 through 8-21 were created. For each of the eleven charts, we visually mapped a blue shaded region to illustrate how groundwater age varies with depth. The blue shaded region is based on our interpretation of the data and is not based on any statistical metrics. In drawing the shaded blue area, the corrected ^{14}C ages of 0 years were ignored in the analysis as were outliers. In addition, several of the older ages at depths less than 400 feet were ignored when they did not fit the trend of increasing age with depth. Out of the eleven geologic formations, only the data for the Lissie Formation did not support an easily definable trend between groundwater age and depth that could be illustrated by the blue shaded region. The Lissie data suggests two distributions exist after 15,000 years – a shallow group of points at a depth of about 300 feet (which were not encompassed by the blue shaded region) and a second group of points at a depth of about 700 feet. The two data groups are hypothesized to represent two pathways traveled by water to enter the Lissie Formation. The shallow pathway was through the low to moderately low permeability deposits in the overlying Beaumont. The deeper pathway was through the moderate to higher permeability pathways in the Lissie or in the underlying Willis. For our analysis the region was drawn to cover the deeper set of points.

Within the blue shaded region, we have identified a “best fit” linear relationship between groundwater age and well depth. For some of the geological formation, a single line is adequate to describe the data. These charts include those for the Beaumont Formation, the Lower Lagarto Formation, the Oakville Formation, and the Catahoula Formation. For each of these four formations, there are not more than two data points before 10,000 ybp. As a result, it is difficult to determine if the single line is an appropriate fit to ages less than and greater than 10,000 ybp. For the remaining charts, two lines are needed to describe the relationship between groundwater age and well depth. For these geologic formations, the linear relationship between well depth and groundwater ages appears to change between 10,000 and 15,000 ybp, which is the breakpoint where the two lines with different slopes are connected. This breakpoint indicates the depth

where a change occurs in the vertical migration rate of ground in a geological formation. Table 8-13 identifies which formations have a breakpoint connecting two linear trends and at what depth the breakpoint occurs. Table 8-13 shows that there are three geological formations for which there are sufficient data at early and later times to justify the drawing of two different lines. These geological formations are for the Lissie (GMA 14), the Willis (GMA 14 and 15), and the Upper Goliad (GMA 16).

Because the break in the slope could be significant to our interpretation and use of the groundwater age data, we explored two possible causes for the breakpoints. The first is that the dip angle of the formation changes with distance and becomes flatter with increasing depth the breakpoint depth listed in Table 8-13. For instance, that depth at which the breakpoint occurs in the Upper Goliad is approximately 1,000 feet. Inspection of the geologic cross-sections (see Figures 4-5, 4-7, and 4-9) do not indicate any notable changes in the dip angle of the Upper Goliad in the three GMAs above 1,500. Similar checks on the geologic cross-sections confirm that a physical change in the dip angle of the formation is not responsible for the change in slope. The second cause, and the one we attribute to the breakpoint, is that the current groundwater regional flow system is reflective of about the last 10,000 years, and before 10,000 years ago, the significant changes in groundwater flow conditions were gradually occurring for about 20,000 years because of changes in the shoreline location and sea level (Figures 2-8 and 2-9). The three key periods of this paleohistory for the Chicot and Upper Evangeline waters are:

- 1) 30,000 to 20,000 years ago – Groundwater was part of a larger regional flow system than it is today because of a lower ocean level and more distant shore line. Also the base of the meteoric water was deeper than it is currently. Much of the Chicot footprint currently above sea level was being actively recharged and groundwater typically has a large vertical downward flow component.
- 2) 20,000 to 10,000 years ago – As ocean levels rose 400 feet and the shoreline moved inland from about 50 miles in GMA 16 and about 100 miles in GMA 14, the base of the meteoric water rose. Beneath the Chicot footprint that is above sea level today, the downward hydraulic gradients gradually lessen and even reversed as movement in the deep Gulf Coast Aquifer System began to slow as the regional flow system shrunk in response to the transgression of the coastline caused by a rise in sea level.

- 3) 10,000 years ago to present – The ocean level reached stability about 7,000 ybp and the Gulf Coast Aquifer System regional flow system achieved the current equilibrium with the current shore line, sea level and recharge condition. Groundwater with an age greater than 10,000 years is a mixture of waters that has been a part of regional flow systems that have changed with changes in sea levels and recharge conditions.

Table 8-13 Depths where Groundwater of Age 10,000 ybp occurs for Different Geologic Formations.

Geologic Formation	Approximate Depth (ft):		GMA that contributed more than two ¹⁴ C measurements on trend line with ages less than 10,000 ybp		
	That corresponds to a groundwater age of 10,000 ybp	At which a second linear trend occurs	14	15	16
Beaumont	200	NA	-	-	-
Lissie	450	650	√	-	-
Willis	600	850	√	√	-
Upper Goliad	700	1000	-	-	√
Lower Goliad	350	400	-	-	-
Upper Lariato	550	550	-	-	-
Middle Lagarto	250	400	-	-	-
Lower Lagarto	550	NA	-	-	-
Oakville	300	NA	-	-	-
Catahoula	800	NA	-	-	-

8.4 Evidence for Groundwater Mixing, Flow Paths, and Age

Regional flow paths inferred from both corrected and uncorrected ¹⁴C ages are consistent with flowpaths inferred from the evolutionary sequence of hydrochemical facies discussed in Section 6. However, at the local scale of a few miles and tens of miles, the significant spatial variability in the chemical concentration prevents application of NETPATH because of the rigorous mass balance requirements. Most of our attempts to connect wells via a NETPATH run were unsuccessful because there are no solutions physically possible. The limited success with NETPATH simulations occurs primarily when the travel paths were restricted to within a geologic unit or aquifer. This observation suggests that the groundwater flow tends to follow the dip of the geologic units. Our consistent problems with trying to develop NETPATH runs covering numerous sequence of well pairs that could cover tens of miles because of variable chemistry suggests that groundwater flow is largely controlled by sand rich sections that finger through a lower permeability matrix. This observation was made in all GMAs and was

confirmed by the visual inspection of maps of sand bed thickness identified from numerous geophysical logs mapped to Transect 3 in GMA 14, Transect 5 in GMA 15, and Transect 8 in GMA 16.

The successful NETPATH solutions that were performed typically required only a minimum set of reactions: calcite dissolution, ion exchange, and a chloride source assumed from a marine clay represented by sodium chloride dissolution. These NETPATH runs demonstrated that carbonate reactions were the main players associated with diluting measurement of ^{14}C with “dead” carbon and causing an overestimate of groundwater age. For this reason, the Pearson Method was considered a useful tool for providing a quick method for lessening the bias associated with ^{14}C measurements that were known to be diluted based on their enriched $\delta^{13}\text{C}$ measurement. For the majority of our cases where we compared corrected ^{14}C ages by using the NETPATH mass balance approach or the Pearson Method, the Pearson Method produced results that were within 5% of the NETPATH groundwater age.

The absence of having a rigorous accounting the mass transfer associated with chemical reactions allows the Pearson Method to be used in situations where NETPATH cannot. Such use of the Pearson Methods runs the risk that errors could in estimating groundwater age if reactions other than those involving carbonates are primarily responsible for modifying carbon concentration in groundwater. However, based on the favorable comparison between the results between the Pearson Method and the NETPATH method, the assumption underlying the use of the Pearson Method across the entire Gulf Coast Aquifer System is justified.

The Pearson Method was used to correct 170 ^{14}C on groundwater ages. The correct values indicated all of these ages where reviewed using several different perspective. The most useful of these perspectives was to analyze the groundwater ages after they had been parsed out to geologic units that housed the wells that were sampled. This grouping of the data provided a useful approach for graphically developing types of relationships for each geologic unit. One relationship is the range of groundwater ages that have been measured at a specific depth. The other relationship is the range of depths where groundwater of a specific age has been measured. As discussed briefly, these values can verify a groundwater model result for a predevelopment flow system. The analysis of these graphical relationships indicates that the significant change in the regional groundwater flow system occurred between 10,000 and 15,000 years ago. This change is attributed to the paleohistory of the Gulf Coast Aquifer System which explains that

about 22,000 years ago the shore line was 100 miles toward the sea and sea level was about 400 feet lower. For this reason, the groundwater ages greater than 15,000 ybp should not be used to infer flow directions or magnitudes.

The corrected ^{14}C ages were used to calculate approximate depths in 11 geologic formations that approximated age of groundwater would be about 10,000 ybp. This calculation can be used to provide a general check on the reasonable of groundwater flow files generated by regional models for predevelopment conditions. Based on data availability, the most reliable results are for the depth calculations of 300 to 600 feet for the Lissie in GMA 14, of 400 to 800 feet for the Willis in GMA 14 and 15, and of 600 to 1,100 feet for the Upper Goliad in GMA 16. Table 8-14 compares these measured depth intervals to the intervals predicted by the regional groundwater models discussed in Section 3. The predicted depth intervals were extracted by visual analysis of Figure 3-16 for Transect 34. In this figure, the 10,000 ybp contour is represented by the contour that separates the blocks designating groundwater ages of 5,000 to 10,000 ybp (yellow boxes with an “x”) and the blocks designating groundwater ages of 10,000 to 20,000 ybp (green boxes). The comparisons show very good agreement between the set of values estimated from the corrected ^{14}C measurements and the LCRB model results for Transect 34 and 45 and the Central Gulf Coast Aquifer System GAM model for Transect 45.

Table 8-14 Comparison of Measured and Predicted Depth Intervals for Groundwater that is 10,000 years old for the Lissie, Willis, and Upper Goliad Formations.

Source of Depth Estimate			Estimated Depth Range where Groundwater has an Age of 10,000 ybp					
			Lissie		Willis		Upper Goliad	
			Upper Limit	Lower Limit	Upper Limit	Lower Limit	Upper Limit	Lower Limit
¹⁴ C Measurements Corrected			300	600	400	800	600	1100
LCRB Model	Transect 34	GMA 14	250	600	600	850	900	1100
LCRB Model	Transect 45	GMA 15	250	650	600	800	800	1400
Northern Gulf Coast Aquifer System GAM	Transect 34	GMA 14	(1)	(1)	(1)	(1)	(1)	(1)
Northern Gulf Coast Aquifer System GAM	Transect 45	GMA 15	250	650	600	800	200	300
Central Gulf Coast Aquifer System GAM	Transect 45	GMA 15	400	500	400	700	700	800
Central Gulf Coast Aquifer System GAM	Transect 8	GMA 16	(1)	(1)	(1)	(1)	(1)	(1)
GMA 16 AGM	Transect 8	GMA 16	(1)	(1)	(1)	(1)	100	600

(1) Groundwater in formation is significantly older than 10,000 ybp.

Final – Hydrogeochemical Evaluation of the Texas Gulf Coast Aquifer System and Implications for Developing Groundwater Availability Models

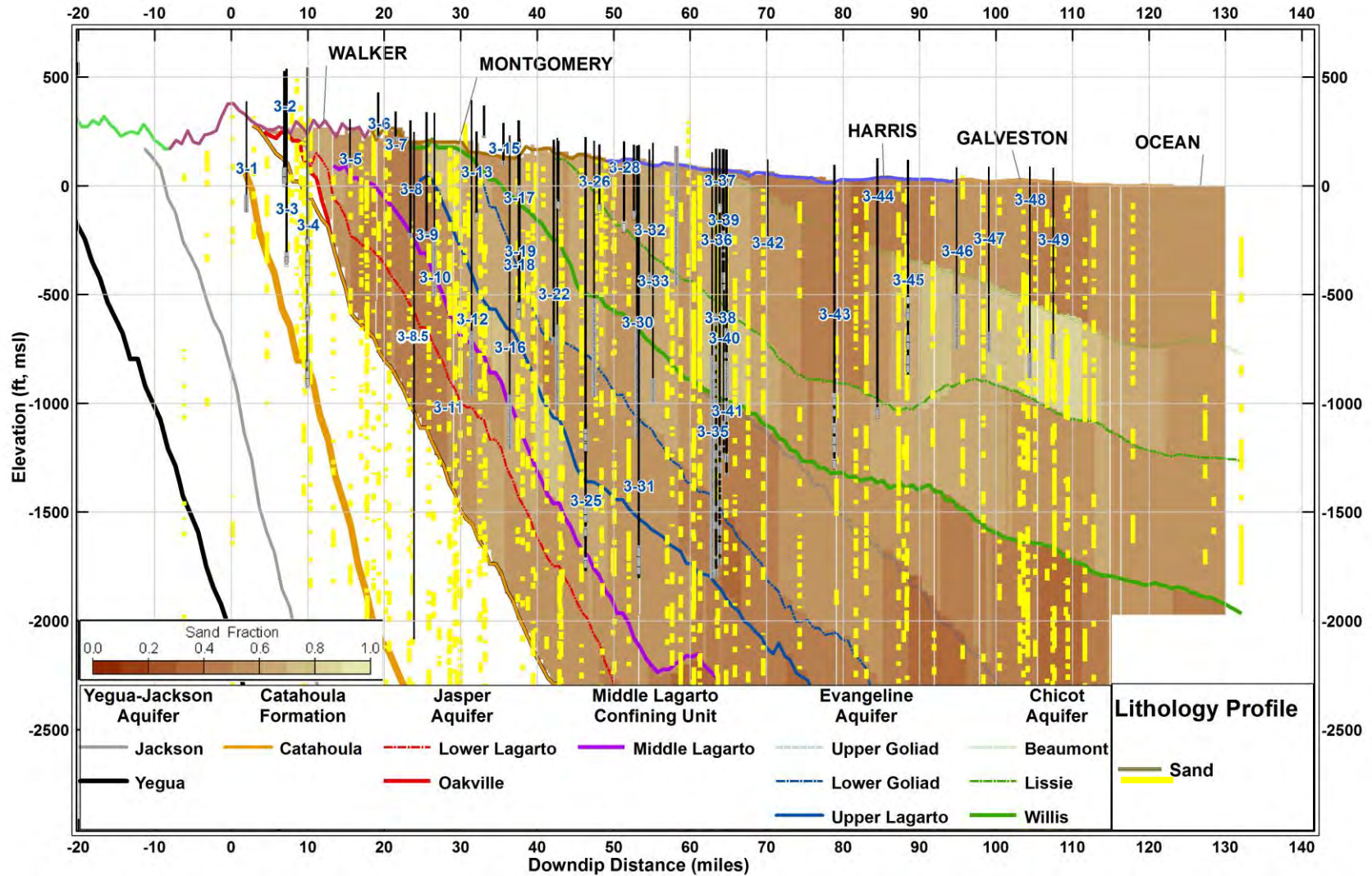


Figure 8-1 Vertical cross-section of Transect 3 showing sampled groundwater wells, geologic formations, average sand percentages, and sand beds identified from geophysical logs. (Note: surfaces represent the bottom of each geological formation).

Final – Hydrogeochemical Evaluation of the Texas Gulf Coast Aquifer System and Implications for Developing Groundwater Availability Models

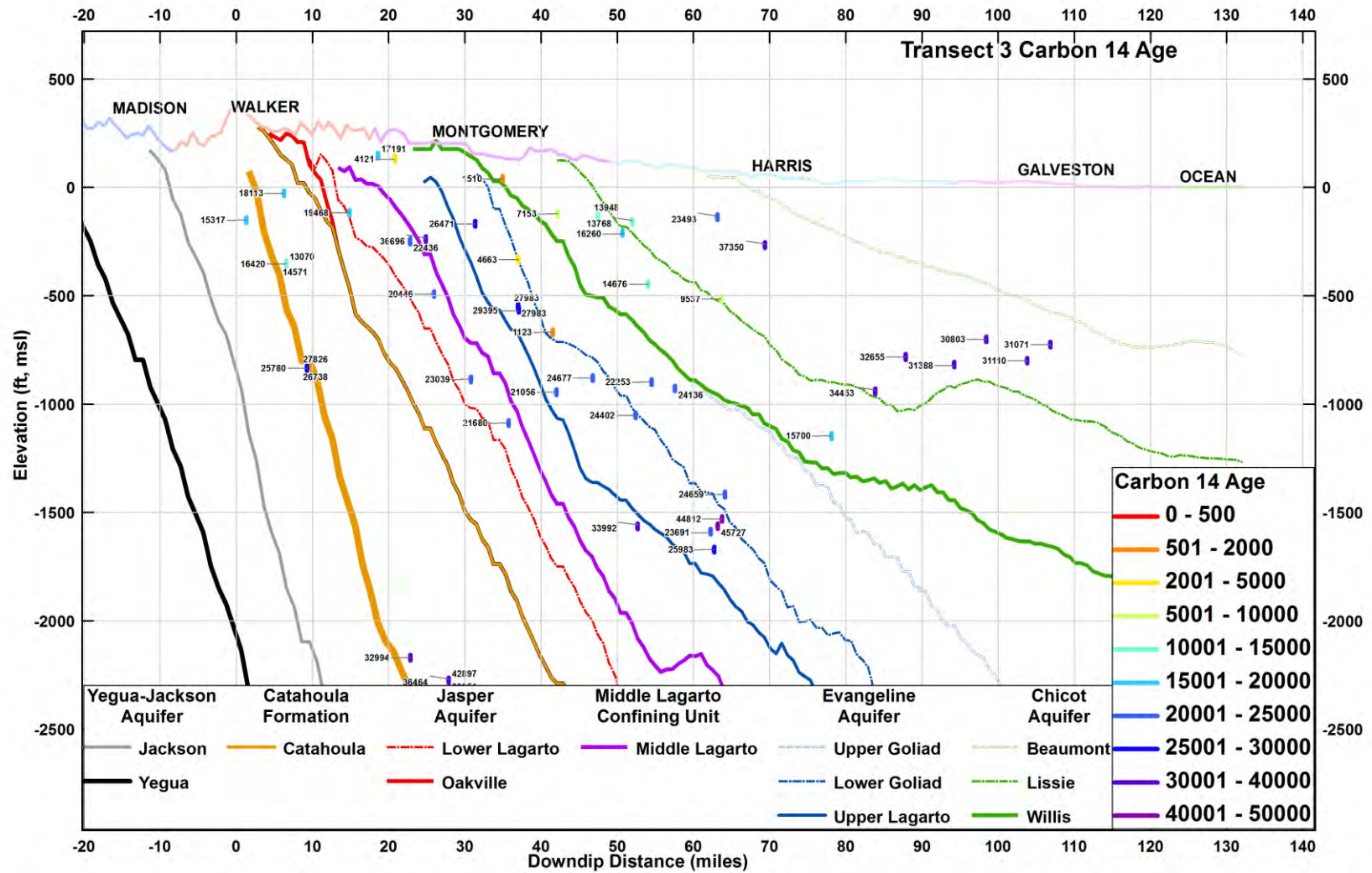


Figure 8-2 Vertical cross-section of Transect 3 showing uncorrected ¹⁴C dates for wells. (Note: surfaces represent the bottom of each geological formation).

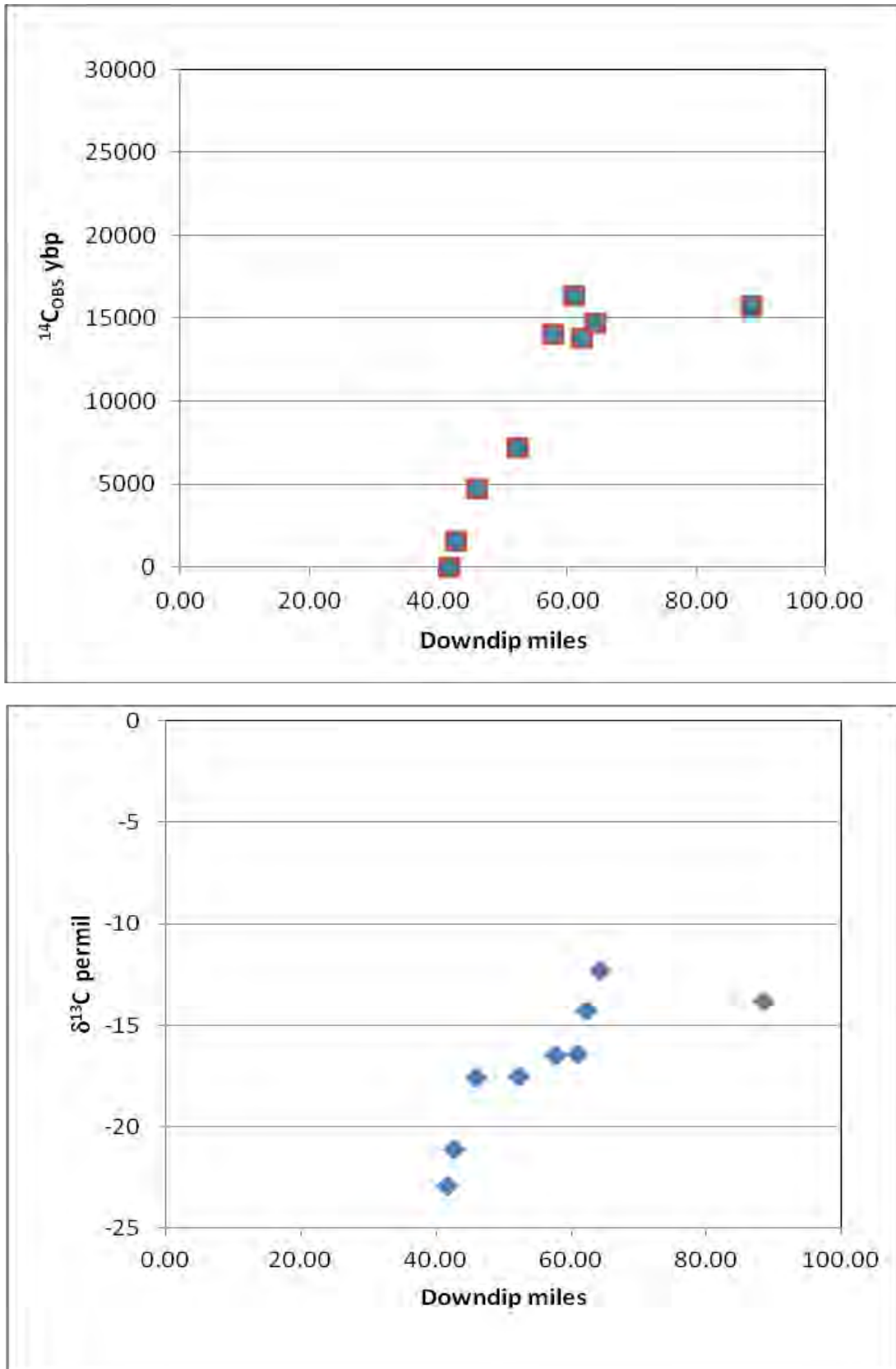


Figure 8-3 Carbon isotopic data for the Chicot Aquifer segment along Transect 3.

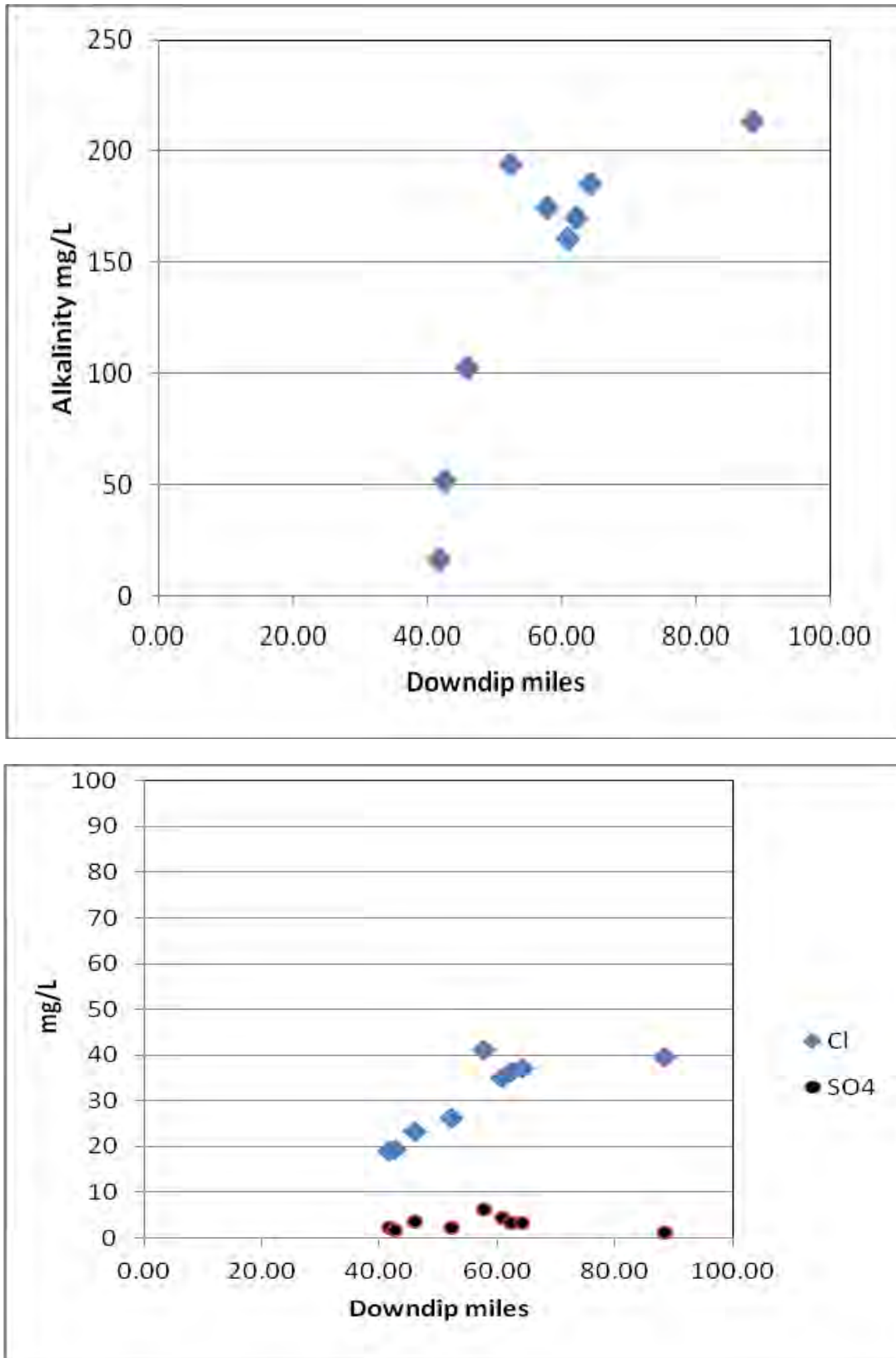


Figure 8-4 Anion composition for Chicot Aquifer segment along Transect 3.

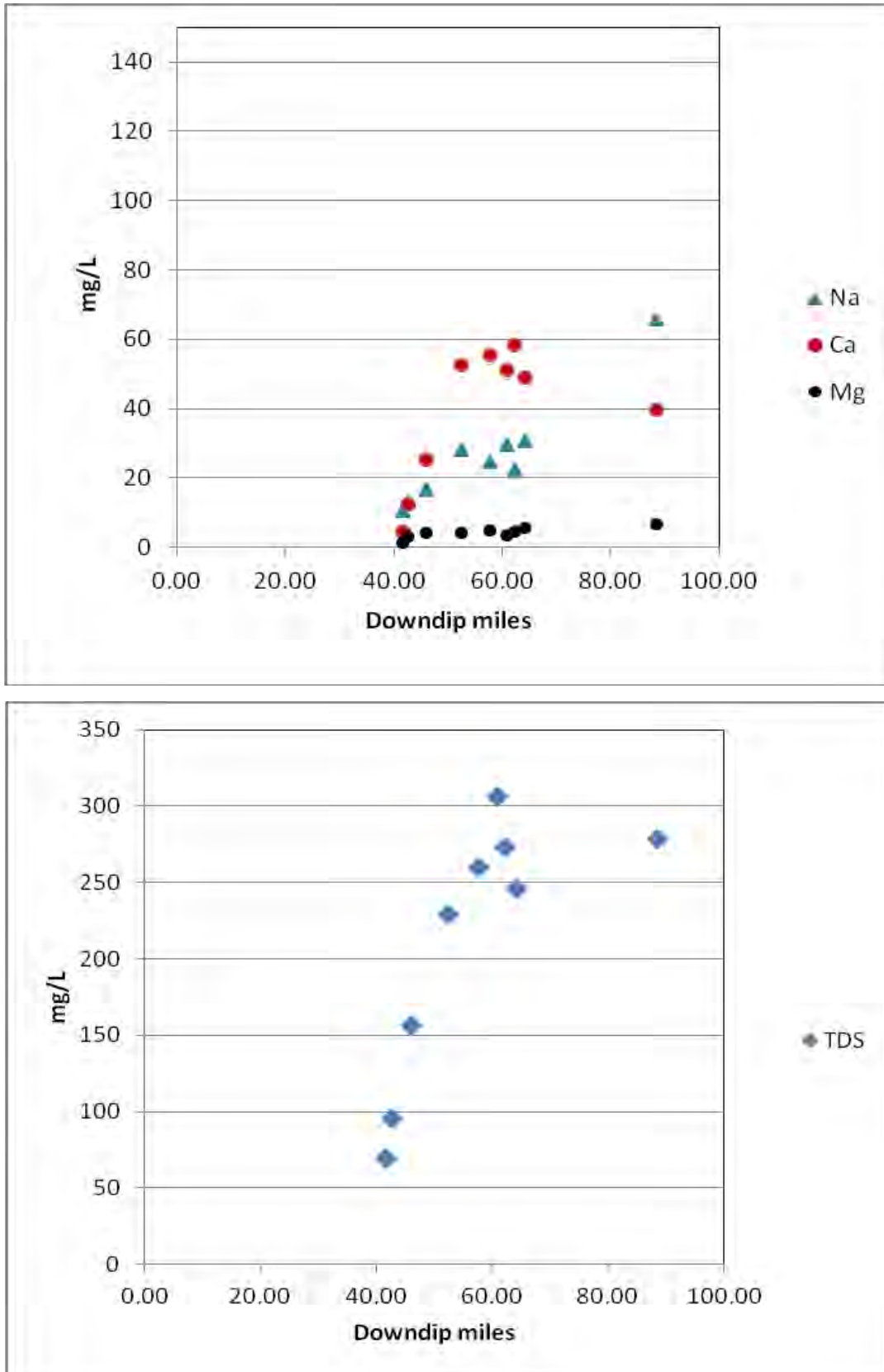


Figure 8-5 TDS composition for Chicot Aquifer segment along Transect 3.

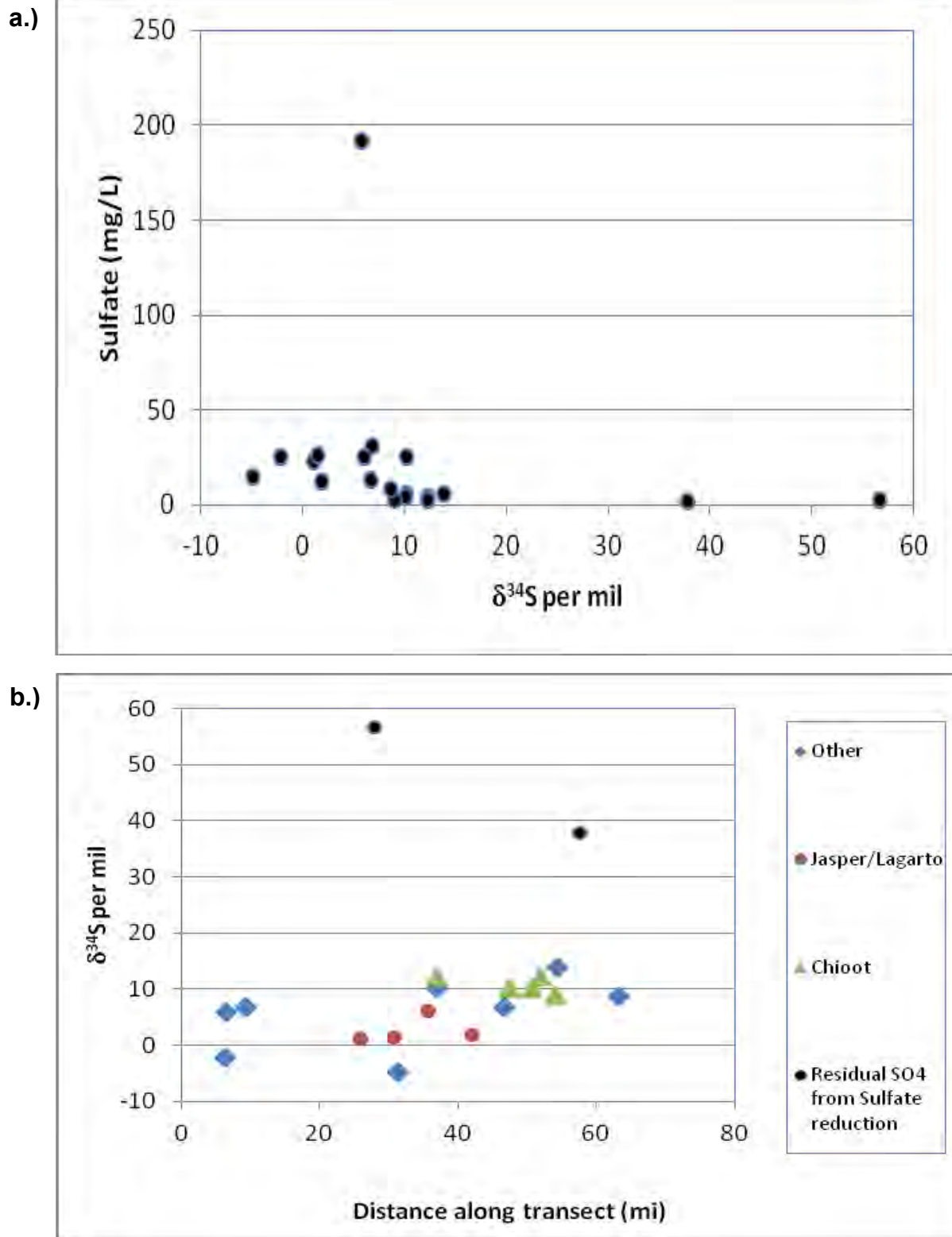


Figure 8-6 Sulfur isotopic sulfate for Transect 3 with respect to a) sulfate concentration and b) distance along Transect 3 from the Catahoula outcrop.

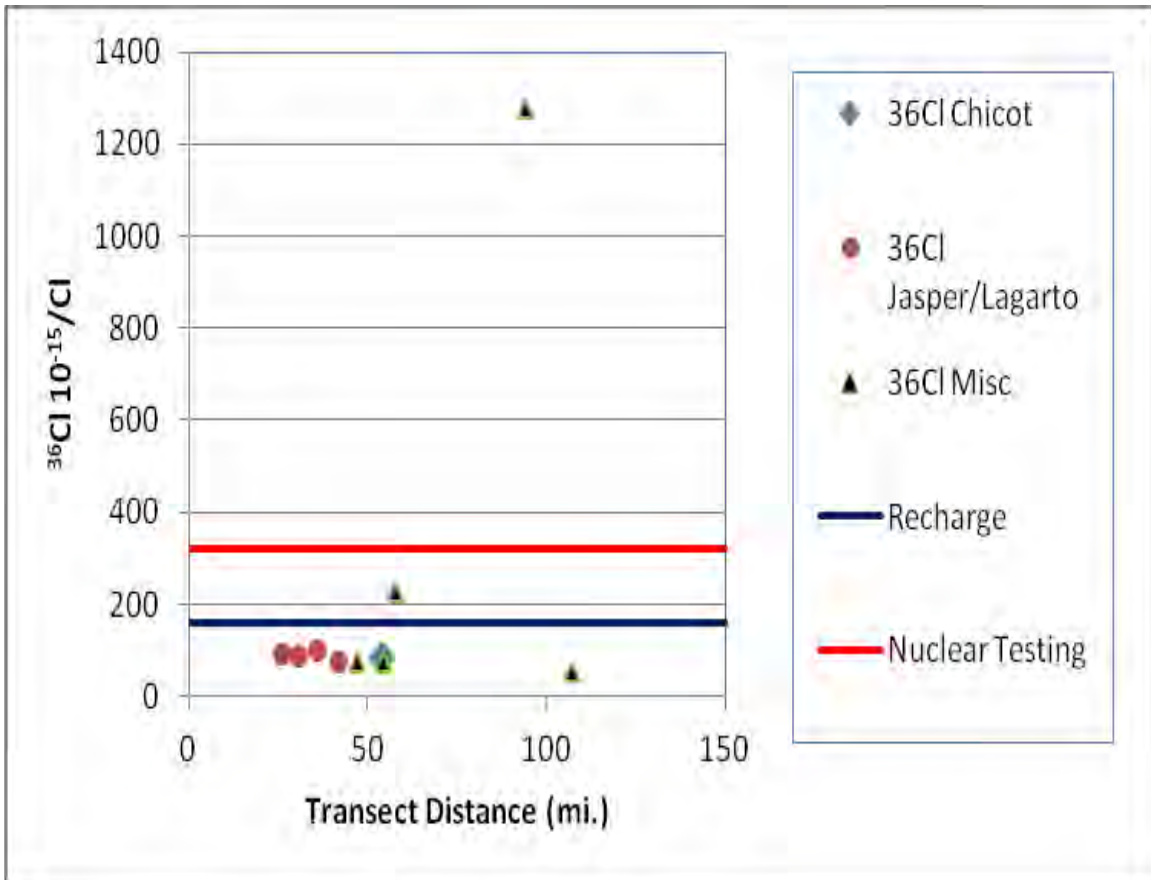


Figure 8-7 ^{36}Cl Chlorine to Chloride as function of transect distance along Transect 3.

Final – Hydrogeochemical Evaluation of the Texas Gulf Coast Aquifer System and Implications for Developing Groundwater Availability Models

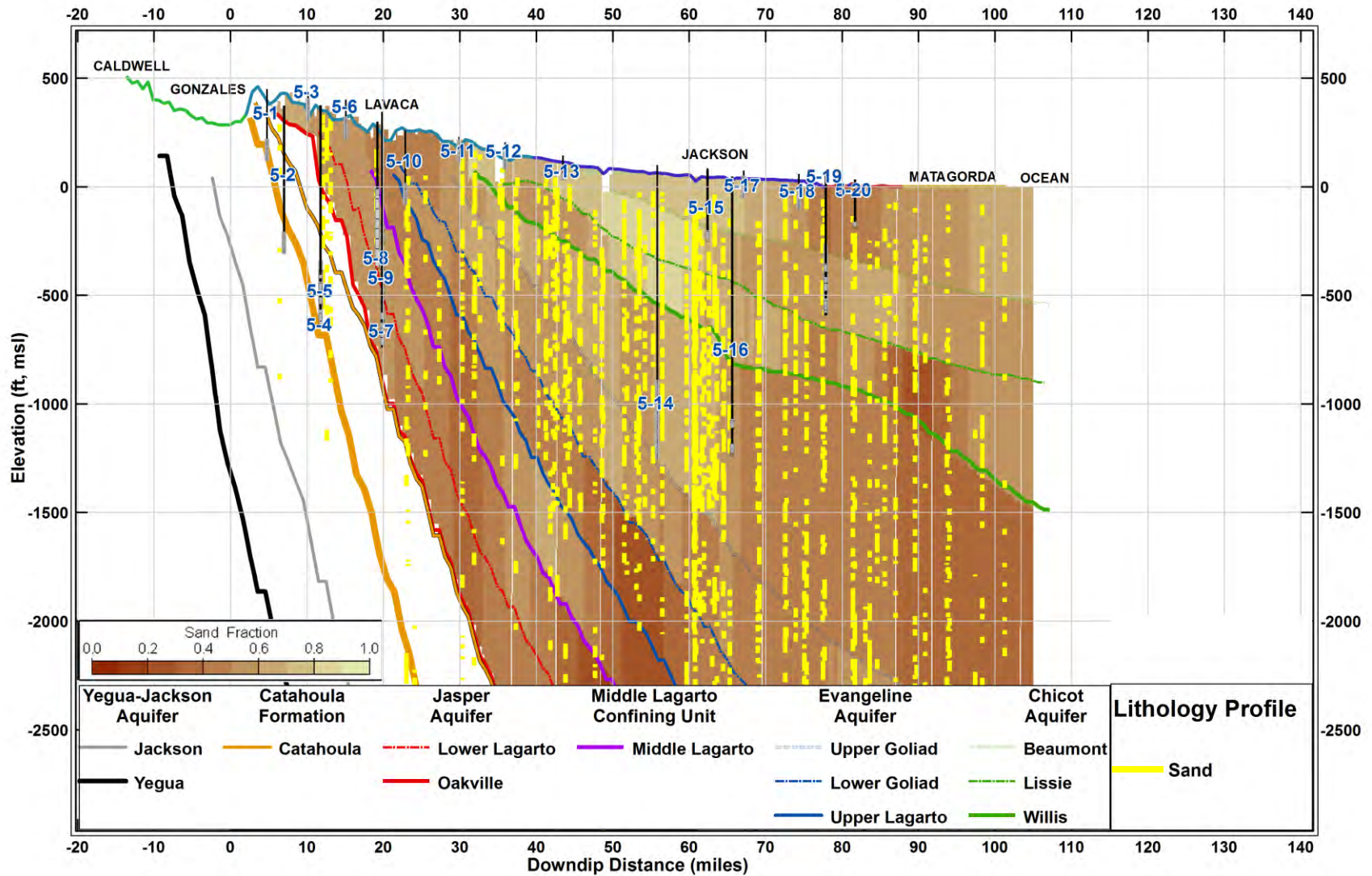


Figure 8-8 Vertical cross-section of Transect 5 showing sampled groundwater wells, geologic formations, average sand percentages, and sand beds identified from geophysical logs. (Note: surfaces represent the bottom of each geological formation).

Final – Hydrogeochemical Evaluation of the Texas Gulf Coast Aquifer System and Implications for Developing Groundwater Availability Models

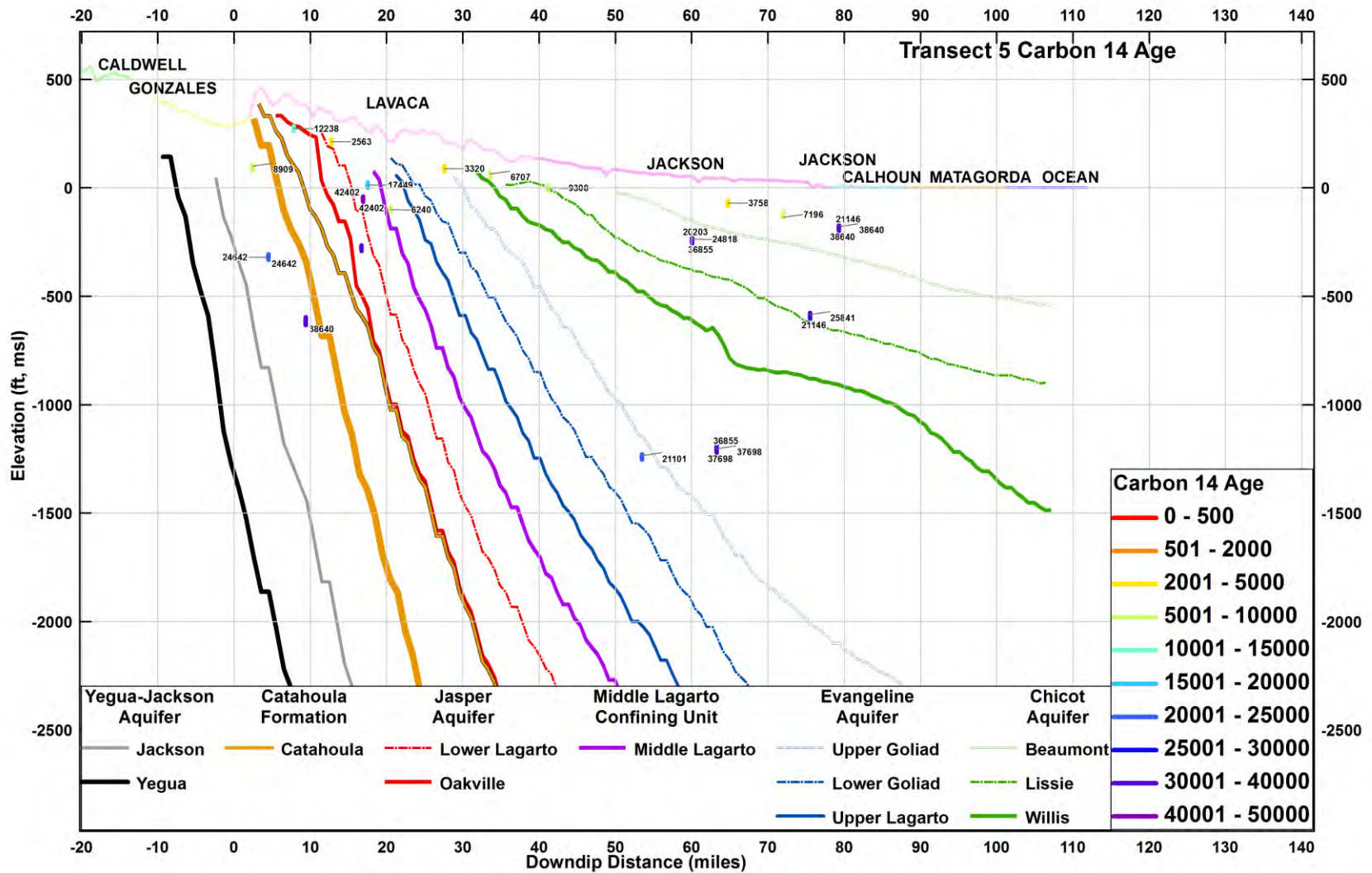


Figure 8-9 Vertical cross-section of Transect 5 showing uncorrected ¹⁴C dates for wells. (Note: surfaces represent the bottom of each geological formation).

Final – Hydrogeochemical Evaluation of the Texas Gulf Coast Aquifer System and Implications for Developing Groundwater Availability Models

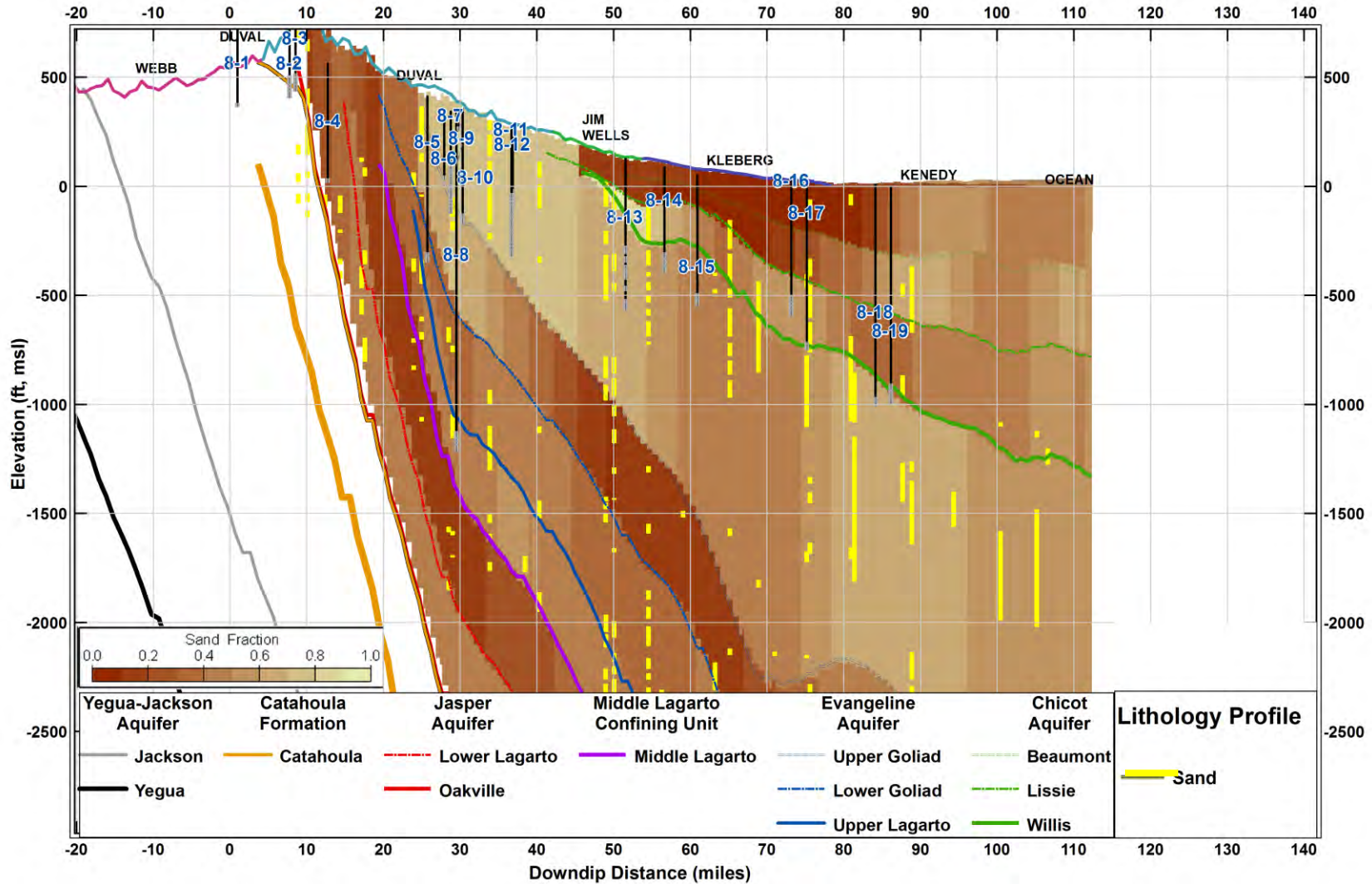


Figure 8-10 Vertical cross-section of Transect 8 showing sampled groundwater wells, geologic formations, average sand percentages, and sand beds identified from geophysical logs. (Note: surfaces represent the bottom of each geological formation).

Final – Hydrogeochemical Evaluation of the Texas Gulf Coast Aquifer System and Implications for Developing Groundwater Availability Models

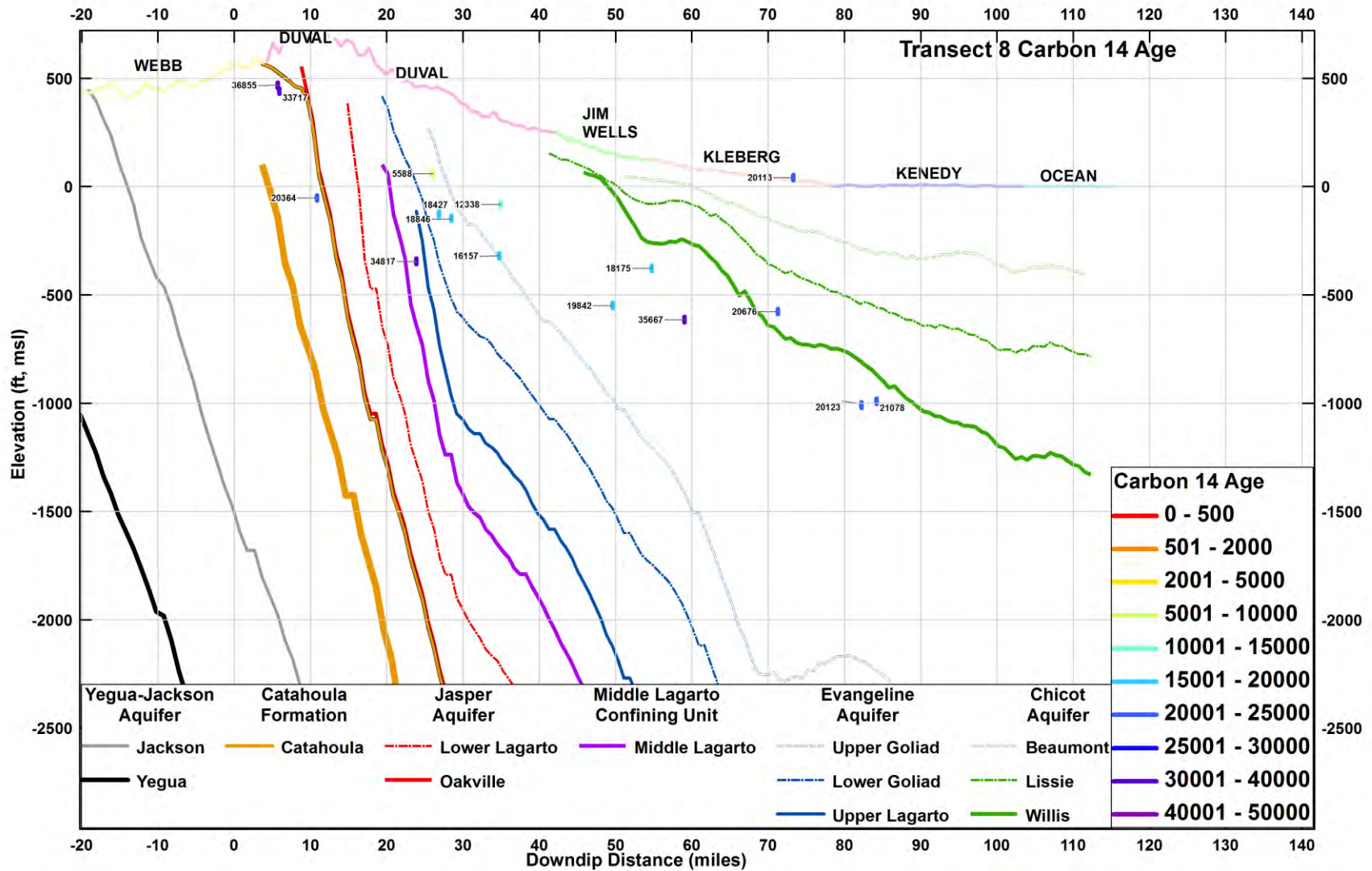


Figure 8-11 Vertical cross-section of Transect 8 showing uncorrected ¹⁴C dates for wells. (Note: surfaces represent the bottom of each geological formation).

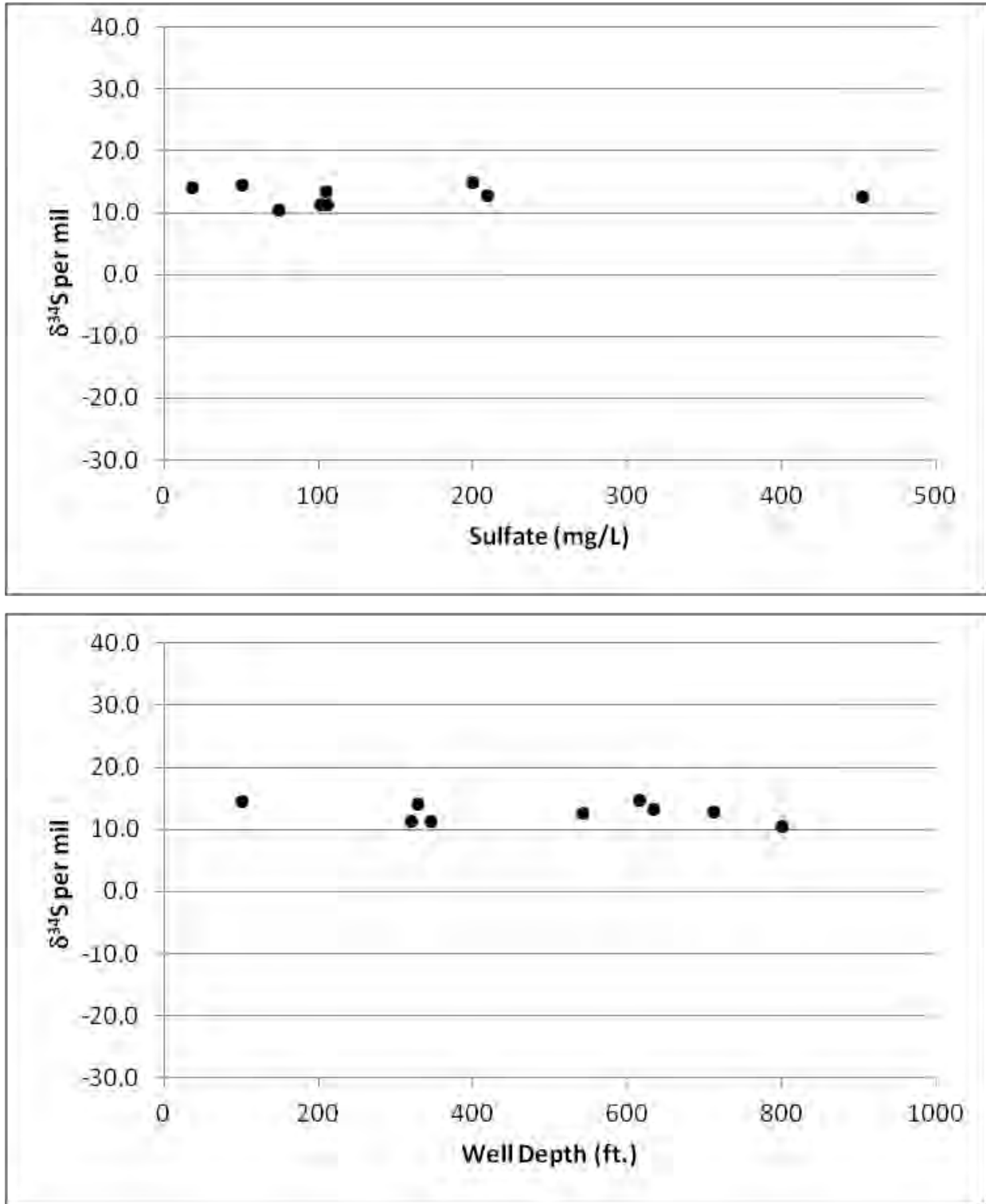


Figure 8-12 $\delta^{34}\text{S}$ plotted as a function of sulfate concentration and well depth for Transect 8.

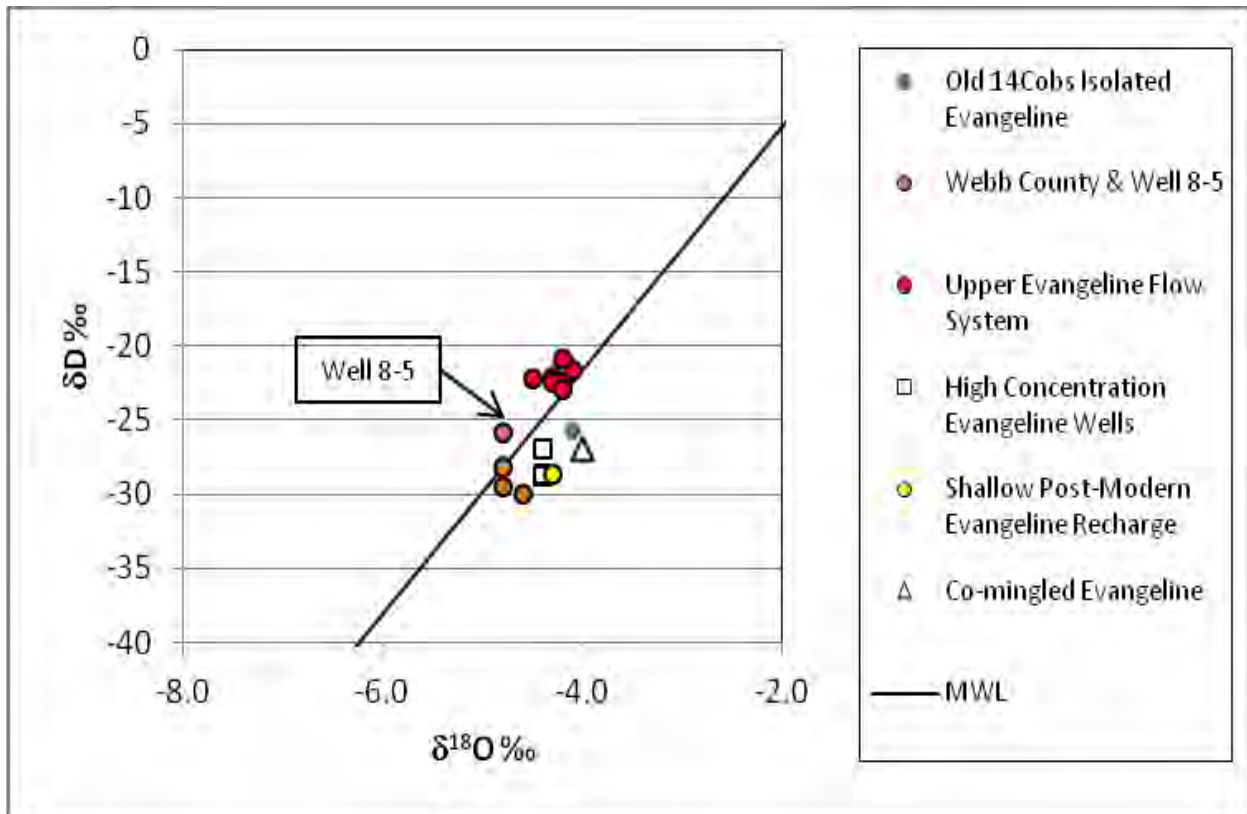


Figure 8-13 Environmental isotope data for Transect 8 wells.

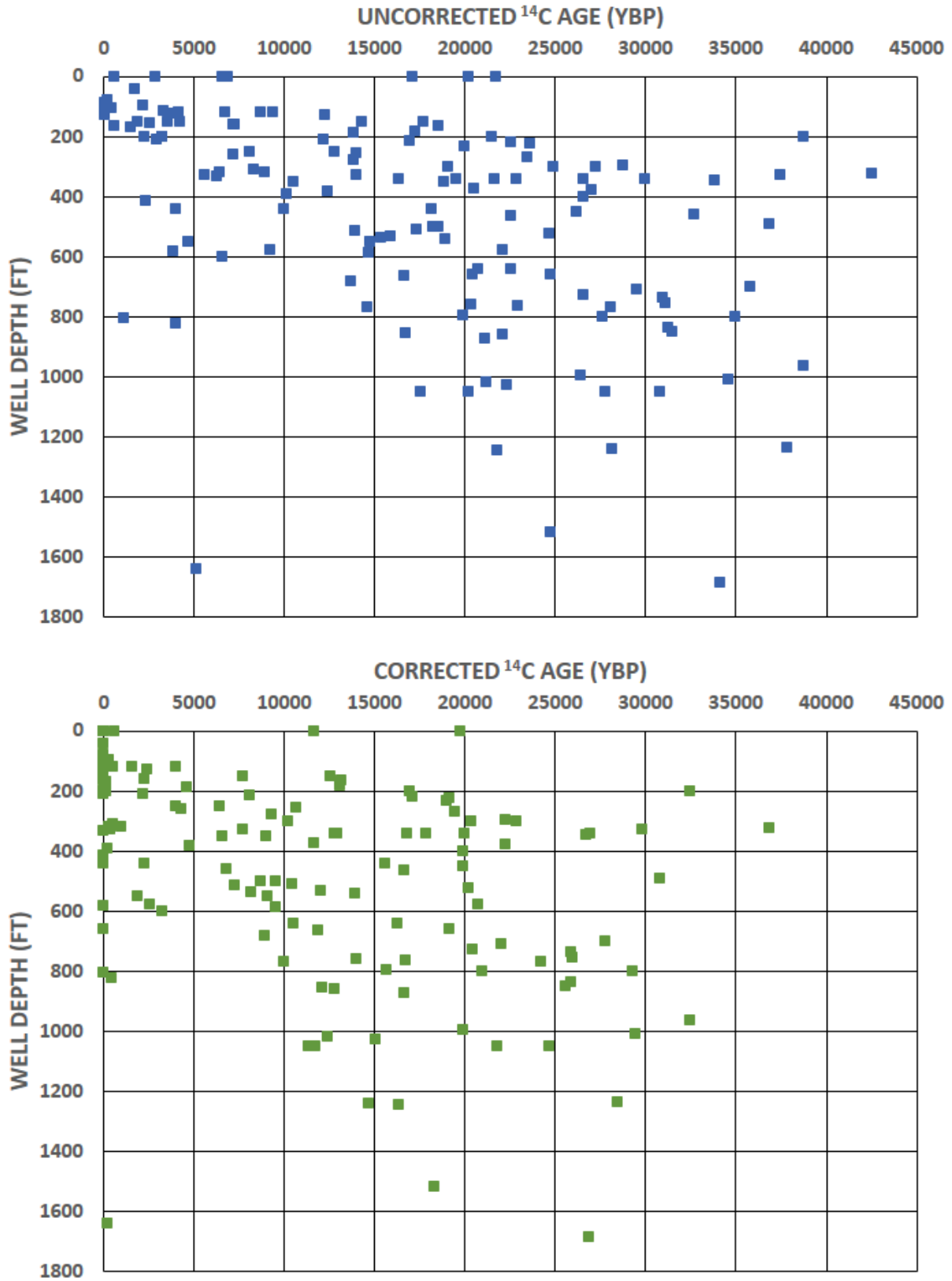


Figure 8-14 Distribution of groundwater age versus depth for ¹⁴C values that are uncorrected and for ¹⁴C values that are corrected using the Pearson method.

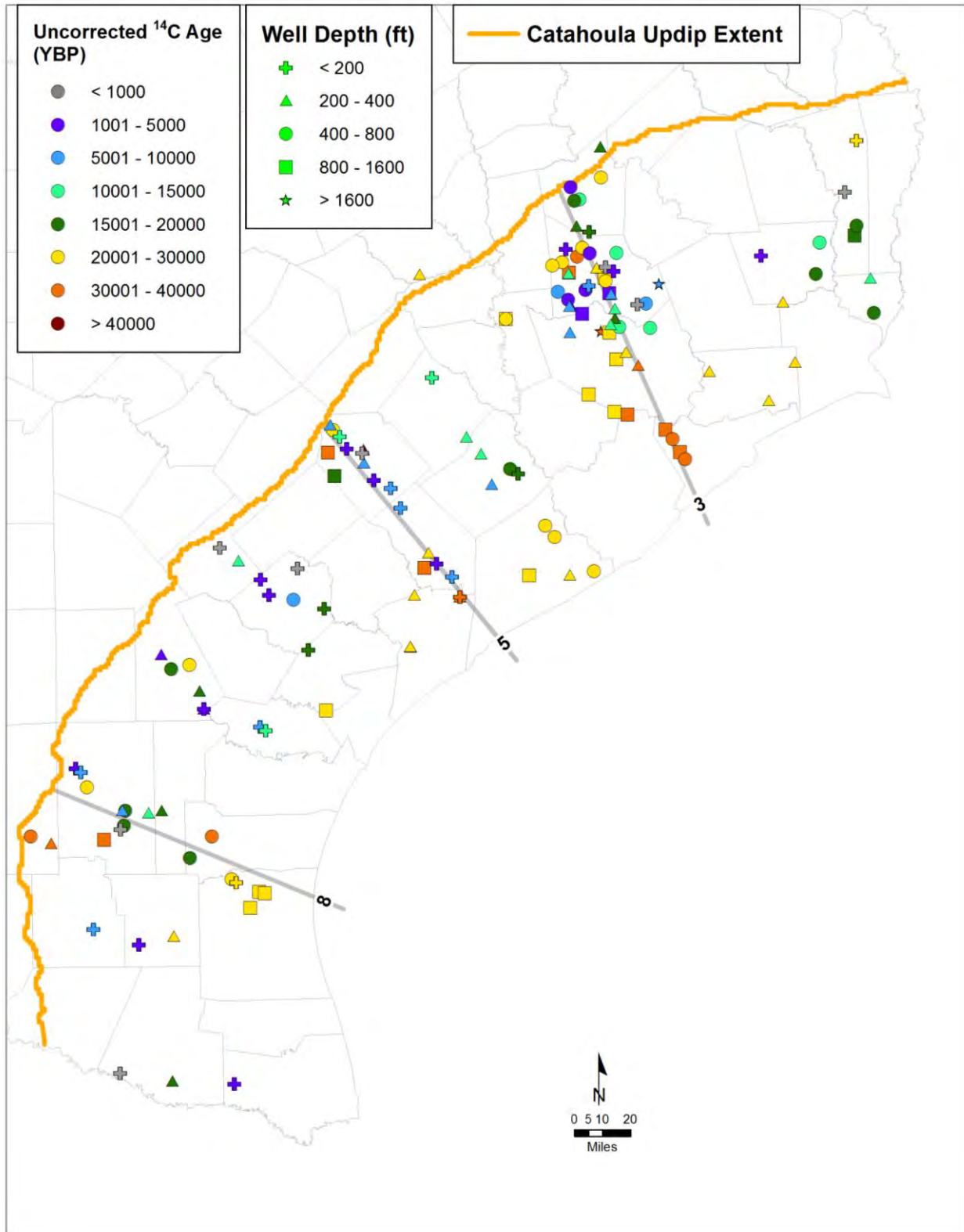


Figure 8-15 Groundwater ages based on the Pearson Method for the entire Gulf Coast Aquifer System.

Final – Hydrogeochemical Evaluation of the Texas Gulf Coast Aquifer System and Implications for Developing Groundwater Availability Models

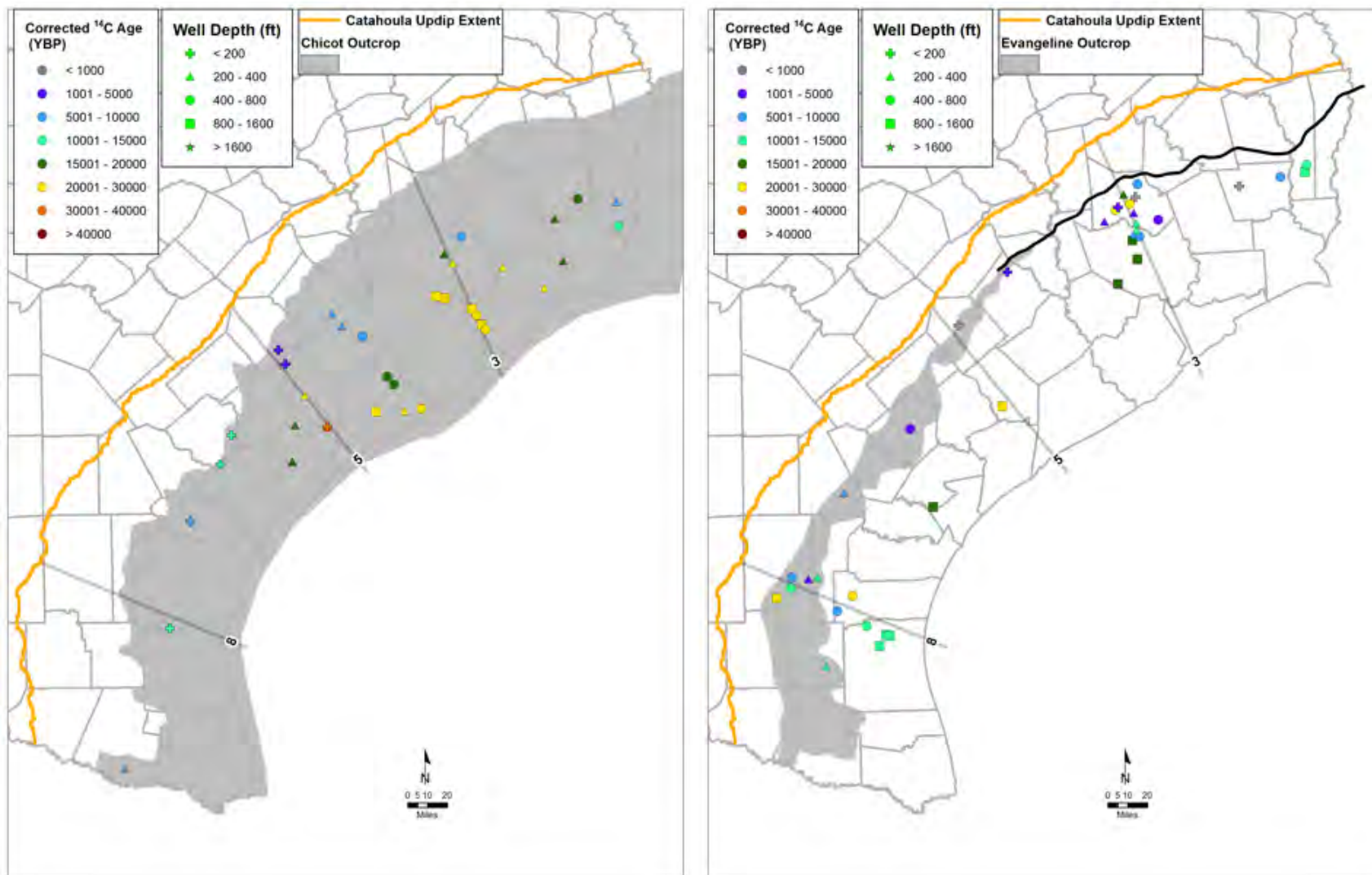


Figure 8-16 Groundwater ages based on the Pearson Method for the Chicot and the Evangeline Aquifers.

Final – Hydrogeochemical Evaluation of the Texas Gulf Coast Aquifer System and Implications for Developing Groundwater Availability Models

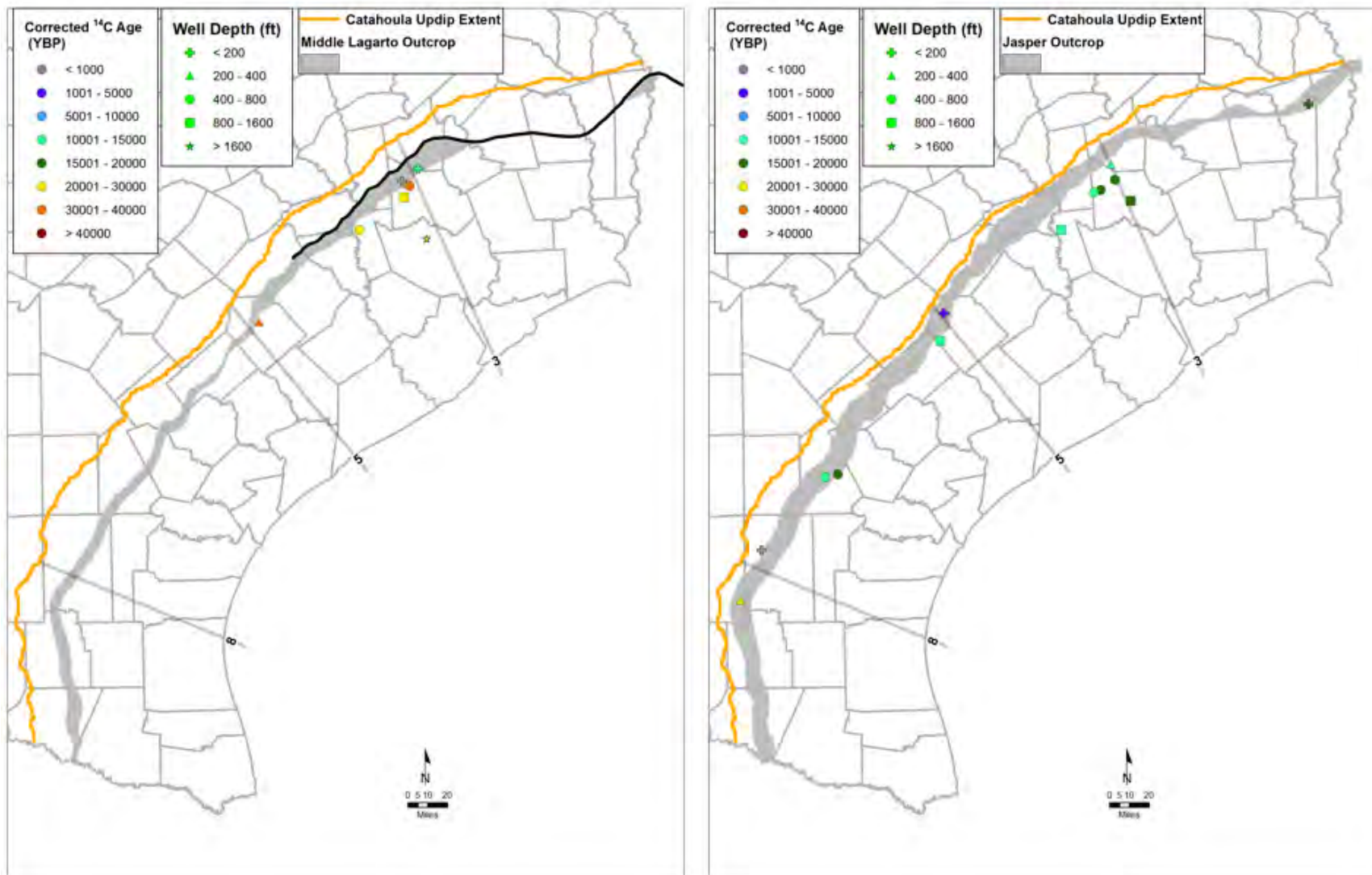


Figure 8-17 Groundwater ages based on the Pearson Method for the Middle Lagarto, Jasper Aquifer, the Catahoula, and the Jackson Formation.

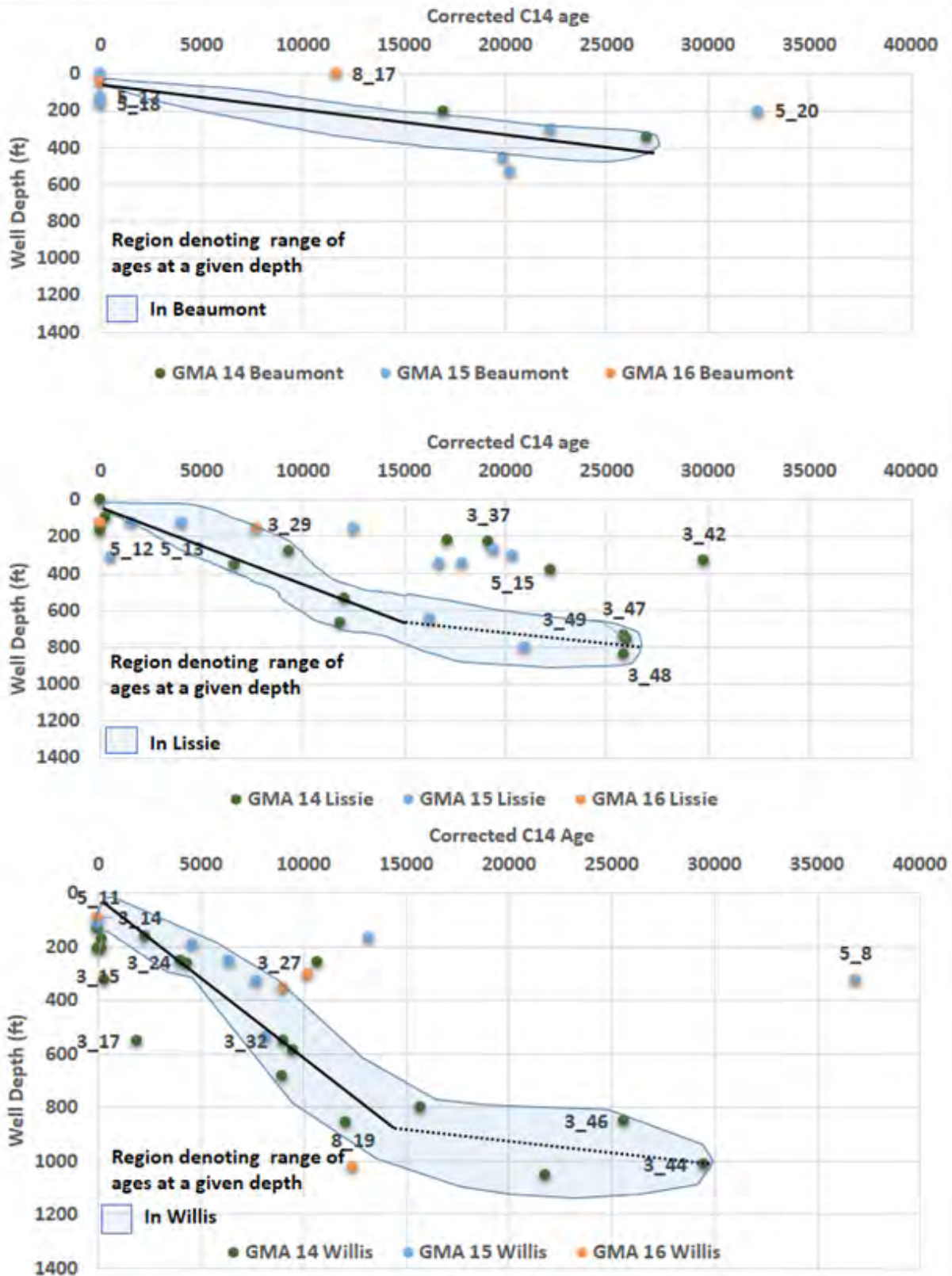


Figure 8-18 ¹⁴C ages corrected using the Pearson Method versus depth for samples from the Beaumont, Lissie, and Willis formations.

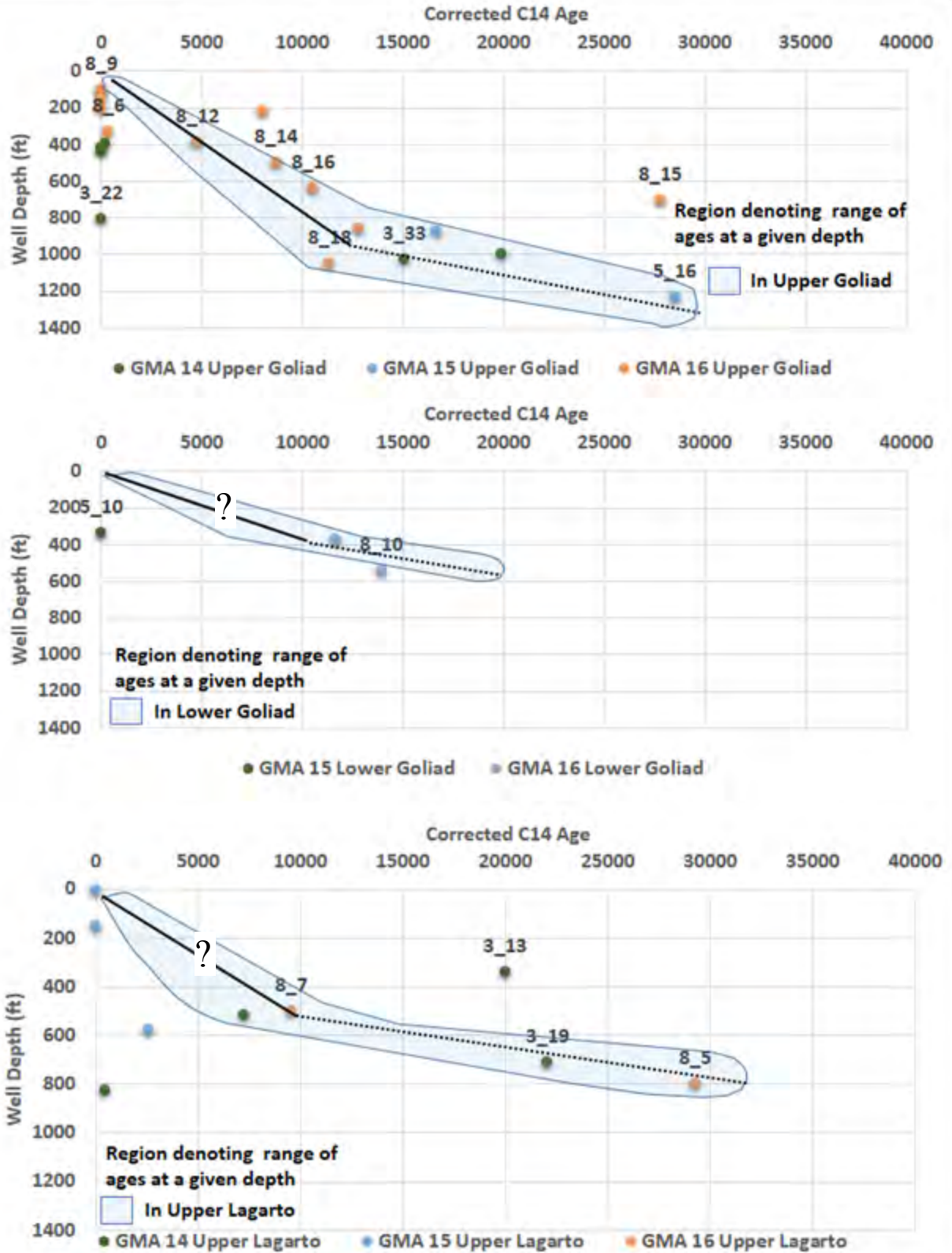


Figure 8-19 ¹⁴C ages corrected using the Pearson Method versus depth for samples from the Upper Goliad, Lower Goliad, and Upper Lagarto formations.

Final – Hydrogeochemical Evaluation of the Texas Gulf Coast Aquifer System and Implications for Developing Groundwater Availability Models

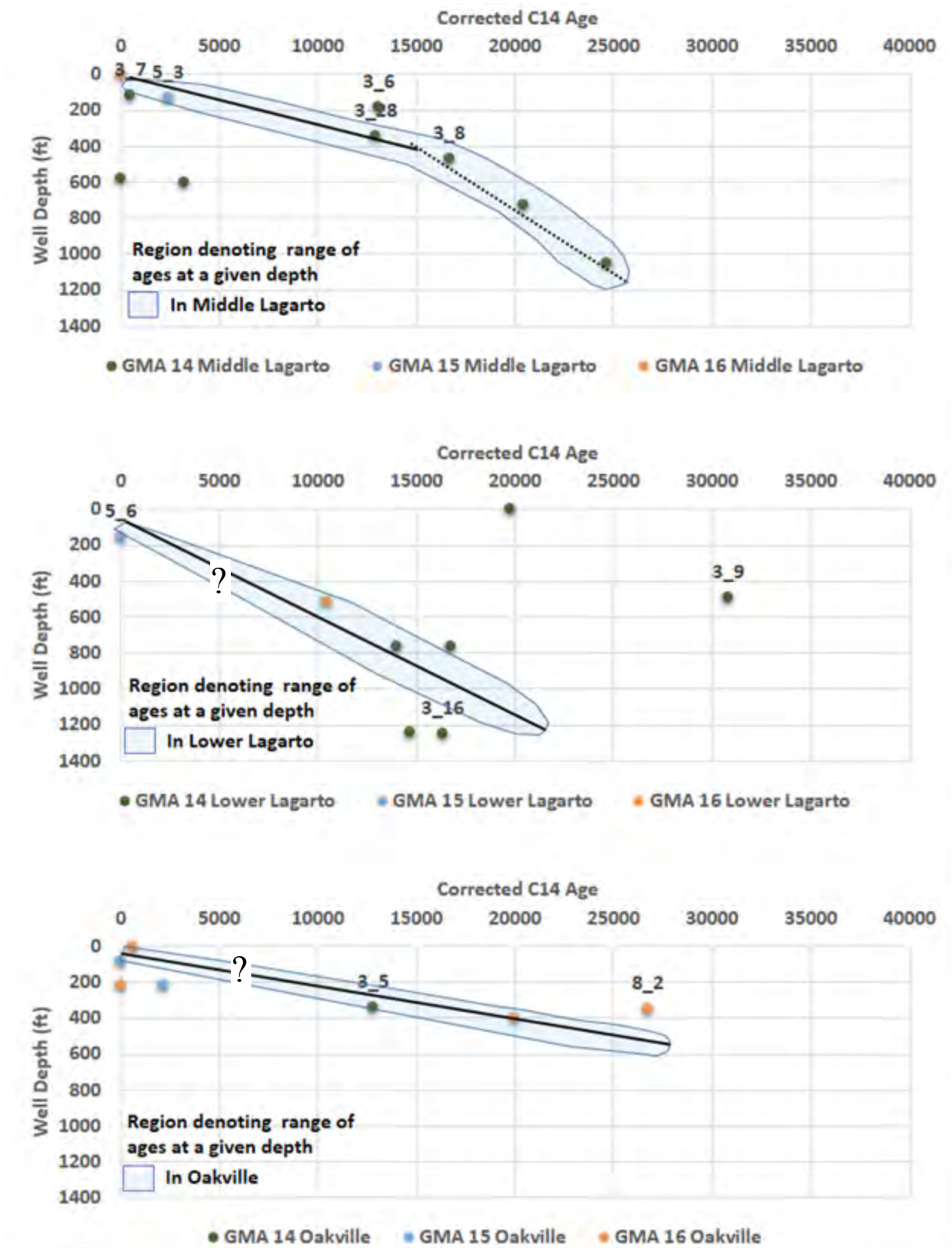


Figure 8-20 ^{14}C ages corrected using the Pearson Method versus depth for samples from the Middle Lagarto, Lower Lagarto, and Oakville formations.

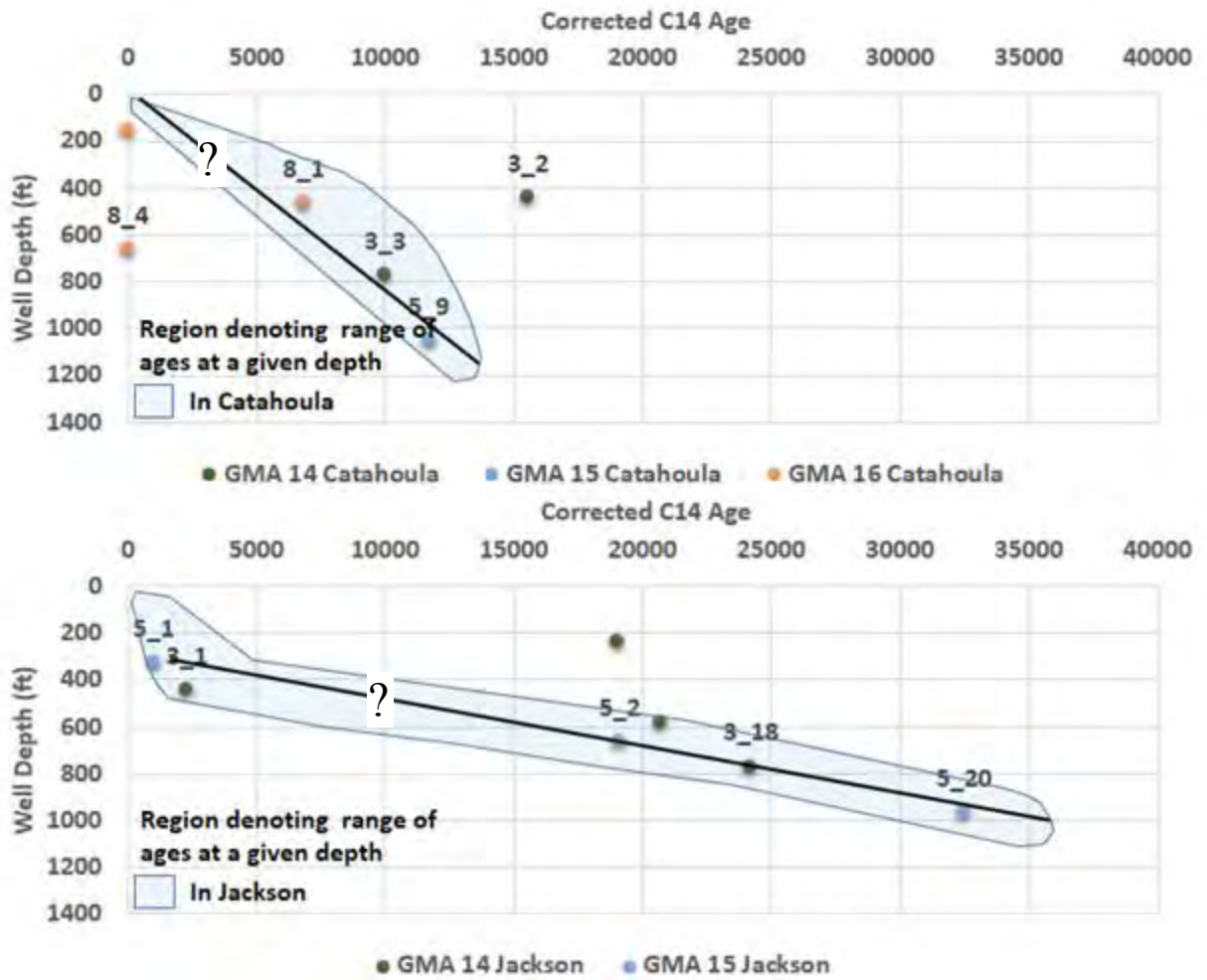


Figure 8-21 ¹⁴C ages corrected using the Pearson Method versus depth for samples from the Catahoula and Jackson formations.

This page intentionally left blank.

9.0 Summary

This section summarizes the key findings of our geochemical data analysis, discusses the implications of the data analysis for the conceptual flow model of the Gulf Coast Aquifer System, and identifies key considerations for implementing the conceptual flow model in a numerical groundwater model.

9.1 Review of the Gulf Coast Aquifer System and Key Findings

The Gulf Coast Aquifer System consists of eleven geologic formations and three aquifers. From youngest to oldest, the aquifers are the Chicot Aquifer, the Evangeline Aquifer, and the Jasper Aquifer. The Chicot Aquifer includes, from youngest to oldest, the Beaumont and Lissie formations of Pleistocene-age and the Pliocene-age Willis Formation. The Evangeline Aquifer includes the upper Goliad Formation of earliest Pliocene-age and late Miocene-age, the lower Goliad Formation of middle Miocene-age, and the upper unit of the Lagarto Formation (a member of the Fleming Group) of middle Miocene-age. The Jasper Aquifer includes the lower Lagarto unit of early Miocene-age, the early Miocene Oakville sandstone member of the Fleming Group, and the portions of the Oligocene-age Catahoula Formation. The Middle Lagarto Formation separates the Evangeline Aquifer and the Jasper Aquifer. Below the Jasper Aquifer is the Catahoula Formation. Below the Gulf Coast Aquifer System lies the Yegua-Jackson Aquifer. Above the Gulf Coast Aquifer System in GMA 14 lies the Brazos River Alluvium Aquifer.

We assembled construction specifications and geochemical measurements for approximately 13,000 wells from the Gulf Coast Aquifer System and from the Yegua-Jackson Aquifer. These data were compiled from the TWDB and USGS databases, data tables from university theses, and from sampling events we conducted from September 2012 to February 2013. Detailed mapping of geochemical data was performed to help assess the conceptual flow model for the Gulf Coast Aquifer System by evaluating lines of evidence for groundwater mixing, flow paths, and ages. These maps consist of areal plots and vertical cross-sections of ions, ion ratios, hydrogeochemical facies, stable isotopes, and groundwater ages based on ^{14}C .

One of the key findings was the limitations of geochemical modeling in our study area. Our difficulties using NETPATH to simulate changes in chemical concentrations between wells

indicates that groundwater flow between wells is more complicated than expected. Multiple potential scenarios can cause variations in measured concentrations in the Gulf Coast Aquifer System that cannot be explained by geochemical modeling alone. A review of lithologic profiles along several transects suggests that groundwater flow through the geological units is not characterized by the bulk movement of large regional slugs of water but rather is largely controlled by sand rich sections that finger through lower permeability deposits. Therefore, neighboring wells may not intersect the same groundwater flow path. There are also many probable chemical sources in the region including salt domes, growth faults, and surface contamination. If one of these sources occur between two wells, geochemical modeling will misrepresent the flow. Changes in recharge distribution (induced by climate or land use changes) and changes in discharge locations (induced by changes in sea level) have also affected our study area by changing regional flow patterns and causing mixing of groundwaters. There are also many large well screens in the study area which can introduce sampling bias and mixing. In this study, large well screens have lengths greater than 100 feet and/or are screened across multiple geological formations. Despite these limitations, however, our geochemical modeling analysis still provided valuable insights into the conceptual flow model for the Gulf Coast Aquifer System.

Because halite contains very low concentrations of Br (much less than sea water or shallow groundwater), we used high Cl/Br ratios in groundwater as evidence for dissolution of halite from salt domes. Primarily in GMA 14, but also in GMAs 15 and 16, the dissolution of halite (NaCl) from salt domes and other salt formations can account for large differences in Cl, Na, and TDS concentrations over distances of a few miles or less. In addition to salt domes, upwelling of brines (TDS concentrations between 40,000 ppm and 80,000 ppm) along growth faults that intersect the geopressure zone is a significant source of Cl and Na in groundwater. One of the indicators that was used to identify upwelling of brines as a source of elevated TDS and not sea water was low Cl/SO₄ ratios in the groundwater. Previous studies have documented the vertical migration of brines into meteoric groundwater along growth faults that intersect the geopressured zone. This study corroborates these findings. We estimate that only about 1.5% to 3% mixture of brines is sufficient to produce the TDS concentrations between 1,000 and 1,500 ppm that commonly exist within the down-gradient regions of the Chicot and Evangeline aquifers.

Thermogenic gases in groundwater also offer compelling evidence that upward migration is occurring along growth faults. Thermogenic gases are typically associated with coal bed and oil and gas formations and are formed at deeper depths by: (1) thermal cracking of sedimentary organic matter into hydrocarbon liquids and gas, and (2) thermal cracking of oil at high temperatures into gas. In GMA 14, 15, and 16, thermogenic methane was measured in groundwater samples. The methane was identified by mapping $\delta^2\text{H}_{\text{CH}_4}$ versus $\delta^{13}\text{C}_{\text{CH}_4}$ on a diagnostic plot for different types of methane. In the samples with higher concentrations of methane, ethane and propane gases were also present. The presence of ethane and propane with methane supports a thermogenic origin for the gases. The source of the thermogenic methane is the geopressed aquifers of the Texas Gulf Coast, where substantial quantities of methane are contained within Tertiary sediments that exhibit abnormally high temperature and pressure gradients.

While there is significant chemical variability at the local scale, regional groundwater flow paths could nevertheless be inferred from our geochemical analysis. Specific methods included examining the following: evolutionary development of the bicarbonate-sulfate-chloride anion sequence; the occurrence of high Ca and HCO_3 concentrations in recharge areas; the increase of Na concentrations and decrease of Ca concentrations along flow paths in a closed system environment as a result of exchange of Ca for Na on clays; and the general increase in salinity concentrations with depth and distance from the recharge source. This analysis indicated that groundwater flows are consistently toward the coast and generally down-dip. Toward the coast, the down dip angle becomes less steep and more horizontal – a result that is consistent with the general smaller dip angle of the younger formations.

The flow paths inferred from our geochemical analysis are consistent with the flow paths inferred from the distribution of ^{14}C measurements that are corrected for “dead” carbon using the Pearson method. “Dead” carbon refers to carbon that has been isolated from the atmosphere or other sources of ^{14}C for approximately 50,000 years (which is the approximate age limit that ^{14}C measurements can be used to date groundwater). The addition of dead carbon (such as by the dissolution of carbonates) will result in an older ^{14}C age because it is replacing or diluting the younger carbon. A primary source of dead carbon is marine carbonates, which are prevalent in the mineralogy of the Gulf Coast Aquifer System deposits. The Pearson method corrects the ^{14}C value using measurement of $\delta^{13}\text{C}$ and a simplified carbonate chemistry based on reactions

occurring early in the flow path in an open system environment. Despite its simplifying assumptions, the Pearson correction typically produced corrected groundwater ages within 5% of ages predicted by the more complicated NETPATH simulations. For most wells, the Pearson correction reduces the uncorrected ^{14}C ages by about 4,000 to 7,000 years.

The “Pearson corrected” ^{14}C measurements are used to identify a range of groundwater ages as a function of depth for the eleven geological formations that comprise the Gulf Coast Aquifer System. Based on an examination of these relationships, we conclude that the current groundwater regional flow system is reflective of hydrogeological conditions that have existed since 7,000 to 10,000 ybp. Between 10,000 ybp and 30,000 ybp, significant changes in groundwater flow conditions occurred in response to continual changes in shoreline locations and sea levels. During the last 30,000 years, the important aspects of the paleohistory of the Gulf Coast Aquifer System can be grouped into the following 10,000 year periods:

- 1) 30,000 to 20,000 years ago – Groundwater was part of a larger regional flow system than it is today because of a lower ocean level and more distant shore line. Also the base of the meteoric water was deeper than it is currently. Much of the Chicot footprint currently above sea level was being actively recharged and groundwater typically has a large vertical downward flow component.
- 2) 20,000 to 10,000 years ago – As ocean levels rose 400 feet and the shoreline moved inland from about 50 miles in GMA 16 and about 100 miles in GMA 14, the base of the meteoric water rose. Beneath the Chicot footprint that is above sea level today, the downward hydraulic gradients gradually lessen and even reversed as movement in the deep Gulf Coast Aquifer System began to slow as the regional flow system shrunk in response to the transgression of the coastline caused by a rise in sea level.
- 3) 10,000 years ago to present – The ocean level reached stability about 7,000 ybp and the Gulf Coast Aquifer System regional flow system achieved the current equilibrium with the current shore line, sea level and recharge condition. Groundwater with an age greater than 10,000 years is a mixture of waters that has been a part of regional flow systems that have changed with changes in sea levels and recharge conditions.

Based on the “Pearson corrected” groundwater ages, the depth above which water is younger than 10,000 years and thus a part of the current regional flow system is about 450 feet for the

Lissie Formation, 600 feet for the Willis Formation, and 700 feet for the Upper Goliad Formation. Because of a lack ^{14}C measurements in other formations, the depth above which groundwater is younger than 10,000 years is estimated with less confidence, but these depths appear to be between 250 feet to 800 feet.

9.2 Implications for the Conceptual Flow Model

The overarching concept for groundwater flow in the majority of, if not all, Gulf Coast Aquifer System groundwater numerical models for GMAs 14, 15, and 16 is that basinal flow can be subdivided into local, intermediate, and regional flow regimes. The major driver for the local, shallow flow system is the difference in topography between adjacent hills and valleys. Recharge to local flow regimes occurs in topographically high areas, and discharge occurs in nearby low areas, such as stream valleys. The shallow flow system occurs primarily in the outcrop or unconfined portion of the aquifer and is characterized by flow paths on the scale of a few miles, travel depths measured in tens of feet, and travel times that last between a month and several decades. Intermediate flow paths are longer and deeper than local flow paths and can underlie several local flow regimes. An example of an intermediate flow path would be the migration of groundwater from the perimeter of a watershed for a major river to a discharge location near the river. Regional flow regimes extend from regional recharge areas such as outcrops and discharge areas near the coastline. The regional system is composed of confined to semi-confined aquifers and is characterized by groundwater flow paths involving travel distances measured on a scale of tens of miles, travel depths in the range of 500 to 3,000 feet, and travel times that range between 50 and 40,000 years. The major topographic driver for the regional flow system is the difference between the water levels in the updip regions of the aquifer (e.g., in Colorado and Lavaca counties) and the downdip portion of the aquifer (e.g., near Matagorda and Brazoria counties). Thus, regional groundwater flow is primarily toward the coast and the groundwater movement tends to be much slower than in either the intermediate or shallow flow systems.

Near the coast where there may be little to no topographic relief, the delineation among the local, intermediate and regional flow system is expected to be less well defined and mixing among the three flow systems is expected to increase. In particular, regional flow paths that originated from up-dip areas are expected to have their flow paths affected by the location of topographic lows

associated with major rivers and perhaps even discharge into those rivers before discharging into the ocean.

Important components of a conceptual model for the Gulf Coast Aquifer System flow system are inflows from other aquifer systems, distribution of recharge rates, groundwater interaction with rivers, groundwater interaction with the ocean, relative differences in permeability among the different geologic formations, and estimates of groundwater age. Listed below are implications for the conceptual flow model for GMAs 14, 15, and 16 based on the findings of this project:

The up dip boundary for the Gulf Coast Aquifer System should be up dip extent of the Catahoula Formation outcrop: The Gulf Coast Aquifer System GAMs for GMAs 14, 15, and 16 use the outcrop of the Jasper Aquifer as mapped by the SWAP dataset (Strom and others, 2003) to define the updip boundary of the Gulf Coast Aquifer System. However, the findings of this study suggest that the updip boundary for the Gulf Coast Aquifer System should actually be moved farther west to the base of the Catahoula Formation. The change in the up dip boundary from the outcrop of the Jasper aquifer to the outcrop of the Catahoula Formation seems appropriate based on our study conclusion that a natural break in the groundwater chemistry occurs at the transition between the outcrops of the Jackson and Catahoula Formations. Across this transition, our geochemical analysis shows that a significant change in the TDS, SO₄, and Na concentrations occurs in GMA 14 and 15. In addition, the recommended change seems appropriate because considerable fresh and slightly saline water exists in the Catahoula Formation that is not a part of the Jasper Aquifer. This fact is shown in Figure 9-1 and Figure 9-2, which map the percent of Catahoula that is fresh water and slightly saline water, respectively, in the southern portion of GMA 14. The TDS contours for 1,000 ppm and 3,000 ppm extend into Montgomery County along Transect 3 approximately 7 miles and 17 miles, respectively. But the Jasper Aquifer does not include any of the Catahoula Formation in Montgomery County along Transect 3.

The downdip boundary for regional Gulf Coast Aquifer System should allow groundwater discharge across a large area of the ocean bottom: Two of three Gulf Coast Aquifer System GAMs extend the regional flow system to approximately 10 miles past the coastline. These two GAMS allow the exchange of flow between the ocean and the groundwater in the Chicot. One of the Gulf Coast Aquifer System GAMs has the down dip boundary of the regional flow system terminate at the coast line. The groundwater flow paths inferred from the geochemical data

suggest that near the coast the groundwater flow is predominantly horizontal or slightly downward. These inferred groundwater flow directions are in agreement with the general findings of Glover (1959). For the scenario of no pumping along the coastline, Glover (1959) shows that groundwater discharge should extend outward into the ocean. Glover's analysis shows that the distance that groundwater flows into the ocean is a function of flow rate in the aquifer, the permeability of the aquifer, and the density differences between the ocean water and groundwater.

The bottom boundary of regional Gulf Coast Aquifer System should be based on where the TDS concentrations is not less than 10,000 ppm and preferably greater: The depth at which the model layers are become inactive represents the bottom boundary of the model. The documentation for the Gulf Coast Aquifer System GAMs suggests that depth of the active model is based on where the TDS concentrations are about 10,000 ppm. The selection of 10,000 ppm TDS seems to be based on practical way of identifying the farthest down dip penetration of groundwater from the meteoric zone. This criterion appears reasonable as long as due consideration is given to the impact of dissolution from salt domes to increase TDS concentrations above 10,000 ppm and concerns expressed by Dutton and others (2006). For the Carrizo-Wilcox Aquifer, Dutton and others (2006) show groundwater flow continues past the base of fresh water; because the freshwater limit is determined by gradual addition of solutes by water-rock reactions, contributions by upwelling of saline solutions from the geopressed zones, and by diffusive addition of salts from adjacent low-permeability deposits. Dutton and others (2006) caution against placing a downdip no-flow boundary at or near the limit of freshwater because it could significantly impact numerical simulation results. They support placing the boundary at the location where vertical hydraulic gradients experience a reversal. This location occurs where the upward gradients from the geopressed zones converge with downward gradients in the hydropressure zone.

The conceptual model of regional groundwater flow system should be constrained by estimates of groundwater age calculated from ^{14}C measurements: Our application of reverse particle tracking demonstrates the three Gulf Coast Aquifer System GAMs and the LCRB model provide estimates of groundwaters ages that can typically differ by 20,000 years or more. As discussed in the later in this section, many of the predicted ground ages exceed 150,000 ybp and are unrealistically old. Such large differences in predicted groundwater ages

illustrates the need for some type of groundwater age constraints be included as a part of the conceptual model. Our geochemical analysis indicates that the vast majority, if not all, Gulf Coast Aquifer System groundwater samples from depths less than 1,000 feet should have ages less than 10,000 ybp. For the three geological formations that have the most extensive set of ^{14}C measurements, the depths associated with groundwater with an age of approximately 10,000 ybp can be further constrained. These depth ranges are 300 to 600 feet for the Lissie in GMA 14, 400 to 800 feet for the Willis in GMAs 14 and 15, and 600 to 1,100 feet for the Upper Goliad in GMA 16.

A conceptual water budget should be developed and guided by recharge estimates by Scanlon and others (2012) after appropriate uncertainty estimates have been developed:

Based on results from our geochemical analysis and findings from our literature review, we adopted the spatial distribution of recharge rates developed by Scanlon and others (2012) to be included as part of the data used to develop a conceptual water budget for the Gulf Coast Aquifer System. Using a chloride mass balance (CMB) approach, Scanlon and others (2012) estimated recharge rates across the entire Gulf Coast Aquifer System. These rates vary between 10 in/yr occurring in northeast of GMA 14 to <0.1 in/yr in southwest of GMA 16. The CMB-based recharge rates are close to recharge rates developed by Young and others (2006) and Scanlon and others (2012) from baseflow and they are consistent with our geochemical analysis spatial distribution of Ca concentrations above 50mg/L that recharge is occurring across most, if not all, of the Gulf Coast. Because of the many assumptions and data uncertainties associated with developing these recharge rates, the use of the CMB-based recharge values should be used as best available information with the understanding that they are subject to revision based on additional data or analyses.

Despite being the best set of recharge rates available for the Gulf Coast, we are not fully endorsing the rates provided by Scanlon and others (2012) for two reasons. One reason is that Scanlon and others (2012) do not provide a comprehensive explanation for how they developed their maps of chloride. Another reason is that Scanlon and others (2012) do not provide uncertainty estimates for the chloride values and other parameters used to recharge estimates. When using the recharge estimates from Scanlon and others (2012) we recommend that analyses should be performed to assign confidence limits to the recharge rates. In addition, there is the need to acknowledge based on the work of Young and others (2006) that annual and seasonal

changes in recharge rates can be significant and they occur as a result of changes in precipitation and evapotranspiration rates.

Proper conceptualization and representation of groundwater mixing and flow paths

requires vertical layering smaller than the thicknesses of the major aquifers: All of the GAMs represent the Chicot, Evangeline, and Jasper aquifers as single model layers. A review of the vertical cross-sections of these aquifers in GMAs 14, 15, or 16 shows that the layer thicknesses of the Chicot and Jasper aquifers are usually greater than 500 feet and that the thickness of the Evangeline Aquifer is often greater than 1,000 feet. Our geochemical analysis shows that closely spaced wells can provide very different chemistries at different depths across the aquifer that suggest significant differences in the groundwater flow or age. These difference suggest that important detail in the flow system is lost by modeling 500- to 1,000-foot thick aquifer zones using a single grid cell. As a result, the conceptualization of groundwater flow paths, velocities, and water budgets should be performed based at a scale smaller than the aquifer thickness. Based on hydrogeological considerations, the vertical layering that is recommended to use the thicknesses of the geological formations that comprise the major aquifers.

A continuous, low permeability “Burkeville” confining unit does not exist up dip at the outcrop:

As noted by Baker (1979), the Burkeville Confining Unit in the SWAP database represents the low permeability deposits that lie between the Jasper and the Evangeline aquifers. Baker (1979) states that these low permeability deposits are from several geological formations. Young and others (2010, 2012a) identify these formations as the Upper, Middle, and Lower Lagato Formations. At the down dip region of these formations, Young and others (2010, 2012a) show that the coastal deposits contain high clay fractions. Based on the analysis of these coastal deposits by hydrogeologists such as Baker (1979), the Gulf Coast Aquifer System GAMs were developed to include a “Burkeville” layer represented by a continuous, low permeability layer that is about 100 times less permeable than the deposits in the Evangeline and Jasper aquifers. If this assumption is valid, then the a low permeability of the Burkeville Confining Unit would significantly increase residence times and in turn would cause increases in the groundwater ages calculated from the ^{14}C measurements, TDS concentrations, and Cl concentrations. However, none of these changes are evident in our data for the outcrop area between the Jasper and Evangeline aquifers. In fact, the sand percentage picks made by Mr.

Baker for several Gulf Coast Aquifer System projects do not indicate that a continuous, low permeability deposits lies between the outcrops of the Evangeline and Jasper aquifers. For instance, Mr. Baker made sand picks for 23 geophysical logs in DeWitt County (Young and others, 2012b). An analysis of these picks for the Evangeline Aquifer, Burkeville Confining Unit, and the Jasper Aquifer produces average sand percentages of 53.2%, 53.6%, and 45.0%, respectively. Thus, in DeWitt County this data does not support the existence of a traditional Burkeville Confining Unit that is represented in the Gulf Coast Aquifer System GAMs. Mr. Baker has also made over picks of clays and sand percentages for on over 700 geophysical logs in the Gulf Coast Aquifer System (Young and others 2010, 2012a). Analysis of these picks for the location of the Burkeville Confining Unit also do not support the conclusion that in the up dip regions, the Burkeville model layer is significantly less permeable than either the Evangeline or Jasper deposits.

Groundwater from the Gulf Coast Aquifer System flows into the Brazos River Alluvium aquifer but the relative magnitude of the inflows are unknown: Our geochemical analysis suggests that groundwater flows from the Gulf Coast Aquifer System into the Brazos River Alluvium Aquifer. Previous researchers (Chowdhury and others, 2010) have suggested that there may not be any significant upward movement from the Evangeline Aquifer into the Brazos River Alluvium. Our data analysis indicate that despite the significant differences in chemistry between the Evangeline Aquifer and the Brazos River Alluvium, the geochemical data does not provide sufficient lines of evidence to support Chowdhury and others (2010) suggestion that there is not any significant upward movement from the Evangeline Aquifer into the Brazos River Alluvium. Moreover, the field data is sufficiently limiting that we cannot confirm whether or not downward flow from the Brazos River Alluvium is occurring to underlying units where pumping has significantly lower the pressure head in the underlying units. This latter limitation exists because of the lack of an adequate network of staged piezometers in areas of high pumping in the Gulf Coast Aquifer System near the Brazos River.

9.3 Considerations for Implementing the Conceptual Model in a Numerical Model

The two Gulf Coast Aquifer System GAMs, the GMA AGM, and the LCRB model presented and discussed in Section 3 are based on similar conceptual flow models for the Gulf Coast Aquifer System and they were calibrated using similar water level data sets. However, several of

the models produce very different results for groundwater ages and fluxes for the same transects. Some of the most extreme differences between model results occur for Transect 34. For Transect 34, the Northern Gulf Coast Aquifer System GAM produced groundwater ages for the Chicot and Evangeline aquifers that are predominantly older than 150,000 ybp even for depths less than a few hundred feet. In contrast, the LCRB model produced groundwater ages orders of magnitude lower. Such differences in model results occur because the model were constructed differently. Two areas where model construction is important to the successfully representing the conceptual model is the numerical representation of recharge and surface-groundwater interactions.

Implementation of Recharge: Figure 9-3 shows the recharge distribution of Scanlon and others (2012). Figures 9-4 through 9-7 shows simulated net flux through the land surface of the four groundwater models discussed in Section 3. The net flux is expressed as inches/year and positive fluxes represent recharge into the aquifer and negative fluxes represent discharge from the aquifer. An example of discharge from the aquifer is groundwater flow into a river. Figures 9-3 through 9-7 use the same symbology so that the net fluxes among the different models can be compared. The LCRB model, the Central Gulf Coast Aquifer System GAM, and the GMA 16 AGM use the MODFLOW's recharge package to simulate recharge and either the MODFLOW's river package or stream package to simulate groundwater/stream interactions. The Northern GC GAM uses MODFLOW's general head boundary (GHB) package to represent both recharge and groundwater /stream interactions. The spatial distribution of fluxes generated by the GHB package is very different from those generated by the combination of recharge and river/stream packages. The GHBs package generated the majority of recharge at the high elevations in the up dip regions of the model. In fact, recharge occurs on only about 35% of the model domain and spatial distribution of recharge is unrelated to previously discussed precipitation or evaporation distributions. Where recharge occurs, the average rate is about 0.6 inch/yr and the maximum rate is about 20 in/yr. Discharge occurs over 65% of the model domain and the spatial distribution of the discharge is not well correlated with the location of major rivers. Based on information presented in this study, the GHB approach used by the Northern Gulf Coast Aquifer System GAM should not be used to represent recharge in a regional groundwater model because its inability to produce reasonable magnitudes and spatial distributions of recharge and discharge. The problems associated with the GHB approach are realized in the physically unrealized groundwater ages shown for Transect 34 in Figure 3-15.

Figure 3-15 shows nearly all of the groundwater ages produced by the Northern Gulf Coast Aquifer System GAM along Transect 34 are older than 150,000 ybp. These old ages apply even to groundwater just a few hundred feet below land surface. The reason for these unrealistically old water is that Transect 34 lies where primarily discharge is occurring in the Northern Gulf Coast Aquifer System GAM. As a result, the source of the groundwater near the land surface is not the recharge from above but rather tens of miles away in the topographic highs.

Implementation of Groundwater-Surface Water Interaction: Several studies of river baseflows (Young and others, 2009; Scanlon and others, 2012) in the Gulf Coast Aquifer System demonstrate that the major rivers such as the Brazos River and the Colorado River are primarily receiving groundwater from the aquifers through most of their reach. Thus, in Figures 9-5 through 9-7, negative fluxes (aka discharges) should be mapped where the major rivers are located. For the LCRB model, negative fluxes occur along the reaches for all major rivers and their major tributaries. However, this relationship does not occur for the Central Gulf Coast Aquifer System GAM (Figure 9-6) and for the GMA 16 AGM (Figure 9-7). The net fluxes produced by the GMA 16 AGM and the Central Gulf Coast Aquifer System GAM, large reaches of major rivers lose water. For the conditions of no-pumping, a major factor affecting how MODFLOW's river and stream package simulates the exchange of between groundwater and surface water is the bottom elevation to a river bed. If this elevation is set too high, the elevation of the river could be above the water level in the aquifer, and the river will discharge into the aquifer. This situation is attributed to the numerous locations in Figures 9-6 and 9-7, where the river grid cells are losing water to the aquifer. As discussed by Young and others (2006) the 1 mile grid cell in the GAMs is sometimes too large to properly simulate groundwater-surface water interaction in the Gulf Coast. As a result of this concern, the LCRB model was constructed using 0.25 mile square cells and detailed topographic maps. Thus, an important aspect about implementing groundwater-surface water recharge in numerical model is properly sized grid cells and accurate topographic information. For pumping conditions, another concern for accurately simulation groundwater-surface water interaction is the vertical spacing of the layers. The key issue with pumping conditions, is to have sufficient resolution the vertical spacing to accurately represent the shallow flow system. Without sufficient resolution in the vertical layer, the intermediate or deep flow system will control the interaction with the river and not the shallow flow system (Young and others, 2012a).

Implementation of Model Calibration: The particle tracking results in Section 3 shown that different groundwater models, which have been accepted as adequately calibrated, can produce drastically different groundwater flow directions, groundwater flow rates, water balances, and recharge rates. Such differences are highlighted particularly well by the significant difference simulation results discussed in Section 3 from the LCRB model and from the Northern Gulf Coast GAM. For relatively shallow groundwater water along Transect 34 under predevelopment conditions, the LCRB model provides estimated groundwater age of about 200 ybp (see Figure 3-16) whereas the Northern Gulf Coast GAM provides estimated groundwater age of about 250,000 ybp (see Figure 3-15). Such large differences strongly suggest demonstrating matches to historical water levels is not sufficient criteria to ensure that the groundwater model is adequately representing the site conceptual model, which includes not only groundwater levels but also aquifer properties and recharge rates. In order to help to better constrain the development of numerical models, it appears prudent to include as part of a model calibration process an evaluation of the simulated spatial distribution and magnitudes of groundwater age to groundwater ages estimated from ^{14}C data.

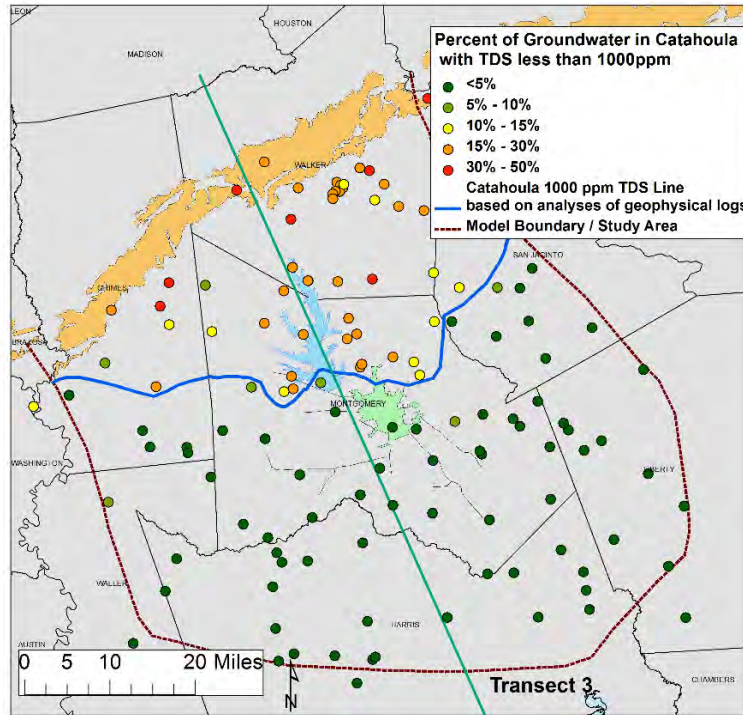


Figure 9-1 Distribution of the percent of the Catahoula Formation in the vicinity of Montgomery County with TDS concentrations below 1,000 ppm based on the analysis of geophysical logs (modified from LGB Guyton and INTERA, 2012).

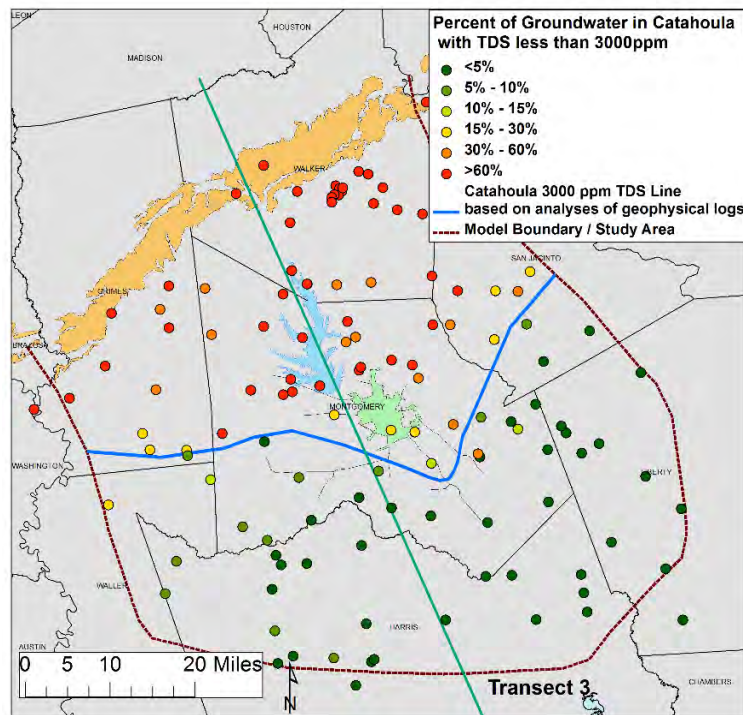


Figure 9-2 Distribution of the percent of the Catahoula Formation in the vicinity of Montgomery County with TDS concentrations below 3,000 ppm based on the analysis of geophysical logs (modified from LGB Guyton and INTERA, 2012).

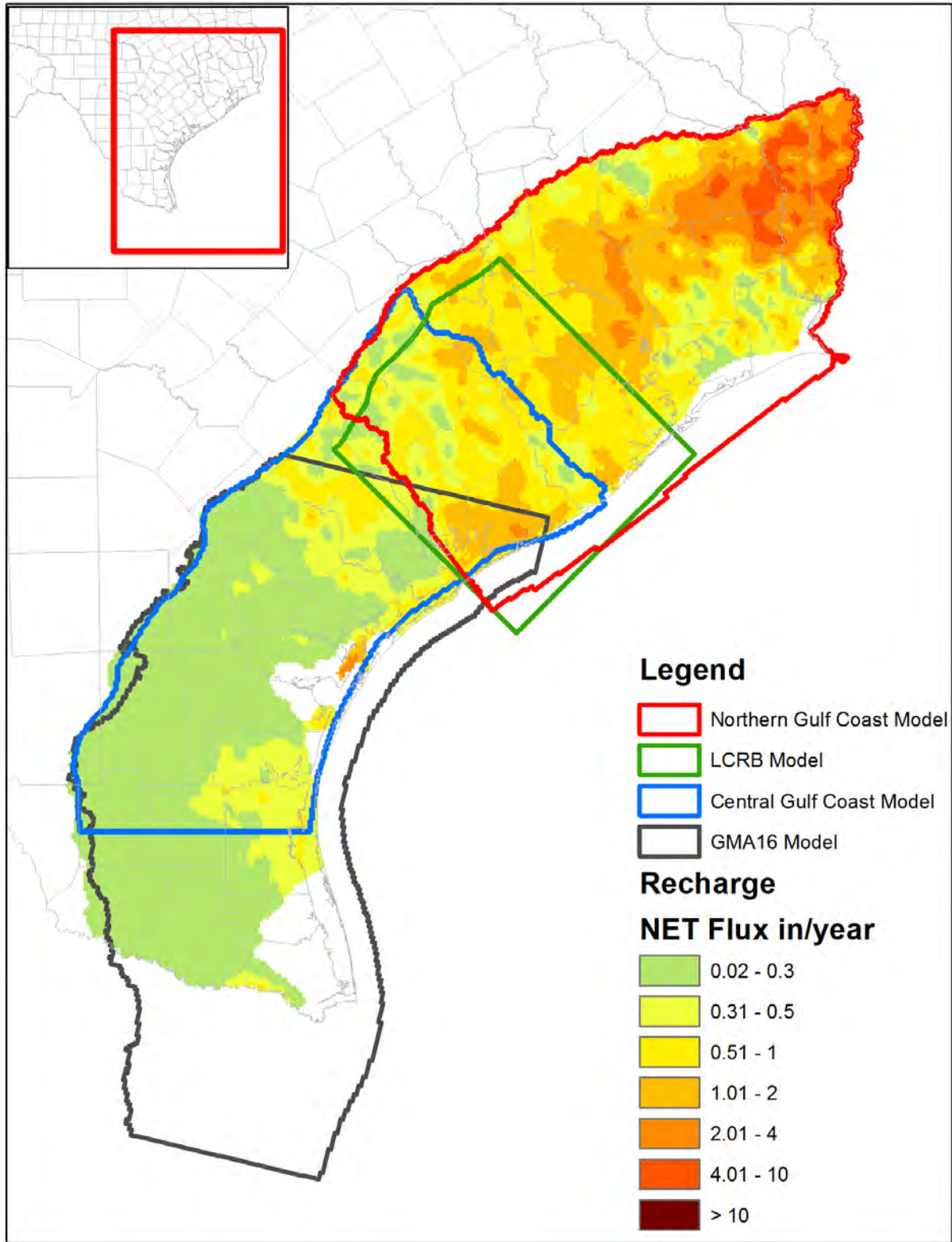


Figure 9-3 Distribution of recharge rates from Scanlon and other (2012) previous shown in Figure 3-4 but replotted to show a different symbology for the recharge rate and to show the location of four groundwater flow models.

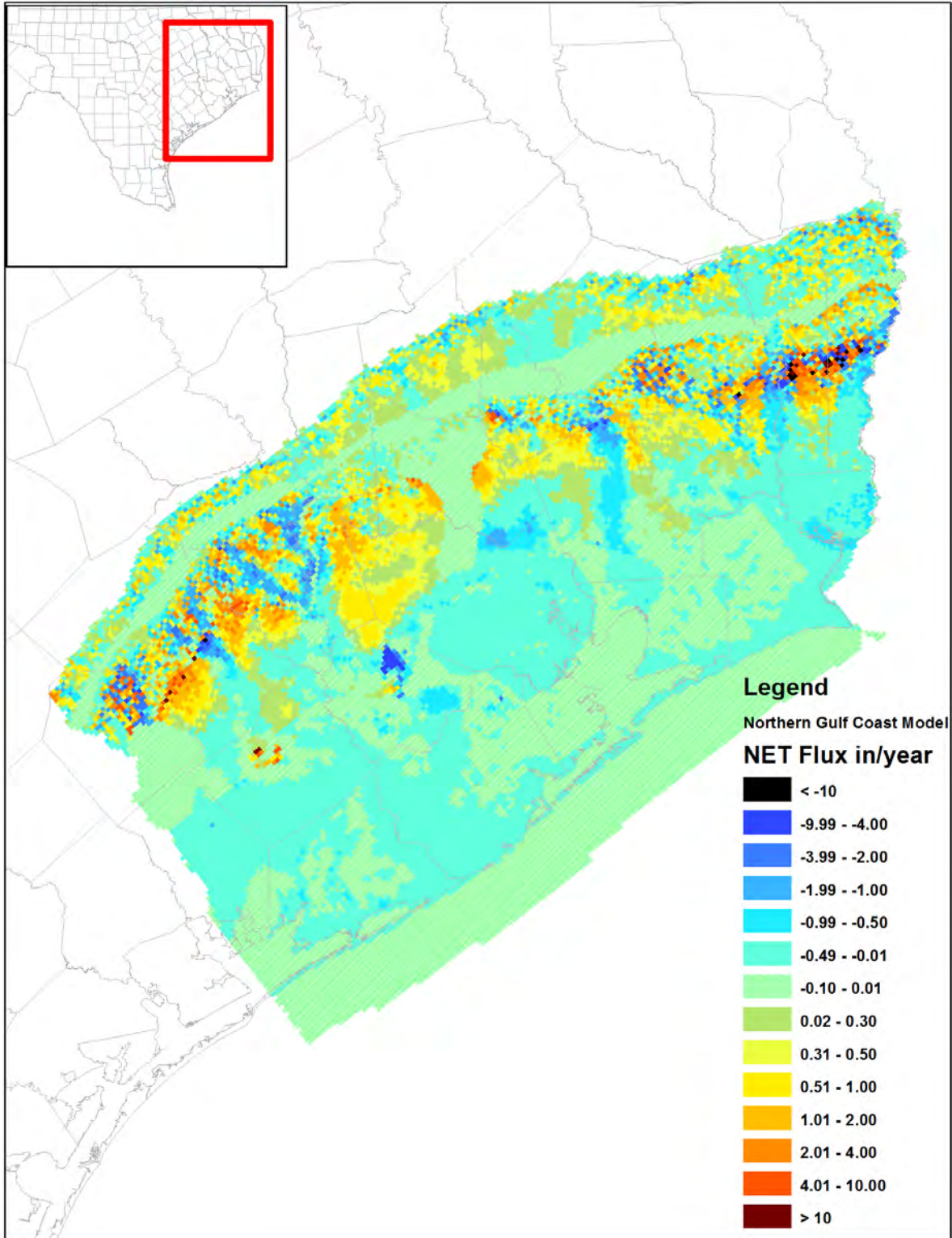


Figure 9-4 Calculation of net flux across the top layer of the Northern Gulf Coast Aquifer System GAM based on the water budget developed for the steady-state condition representing predevelopment (no pumping) conditions. (Note: positive fluxes represent recharge into the aquifer and negative fluxes represent discharge out of the aquifer).

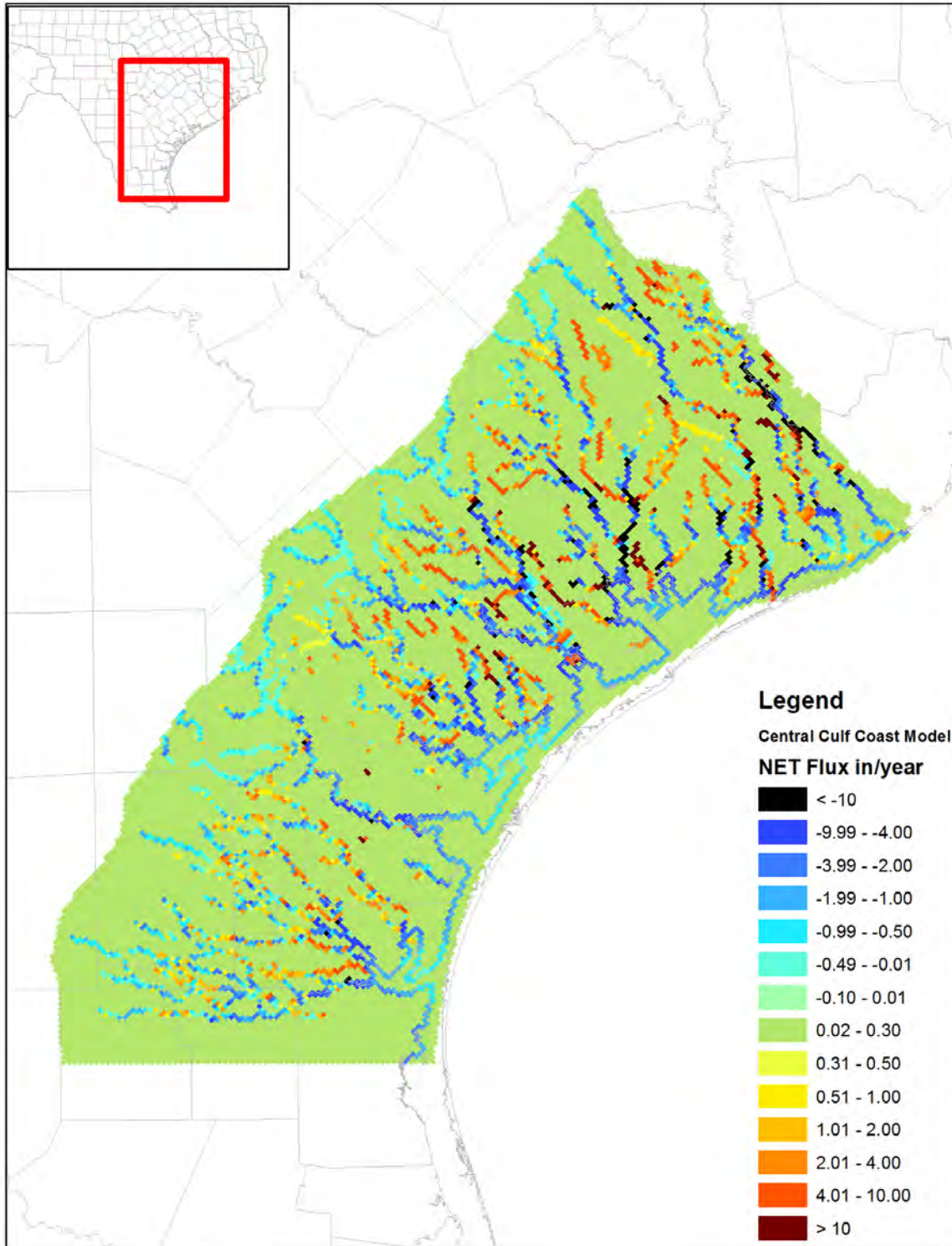


Figure 9-5 Calculation of net flux across the top layer of the Central Gulf Coast Aquifer System GAM based on the water budget developed for the steady-state condition representing predevelopment (no pumping) conditions. (Note: positive fluxes represent recharge into the aquifer and negative fluxes represent discharge out of the aquifer).

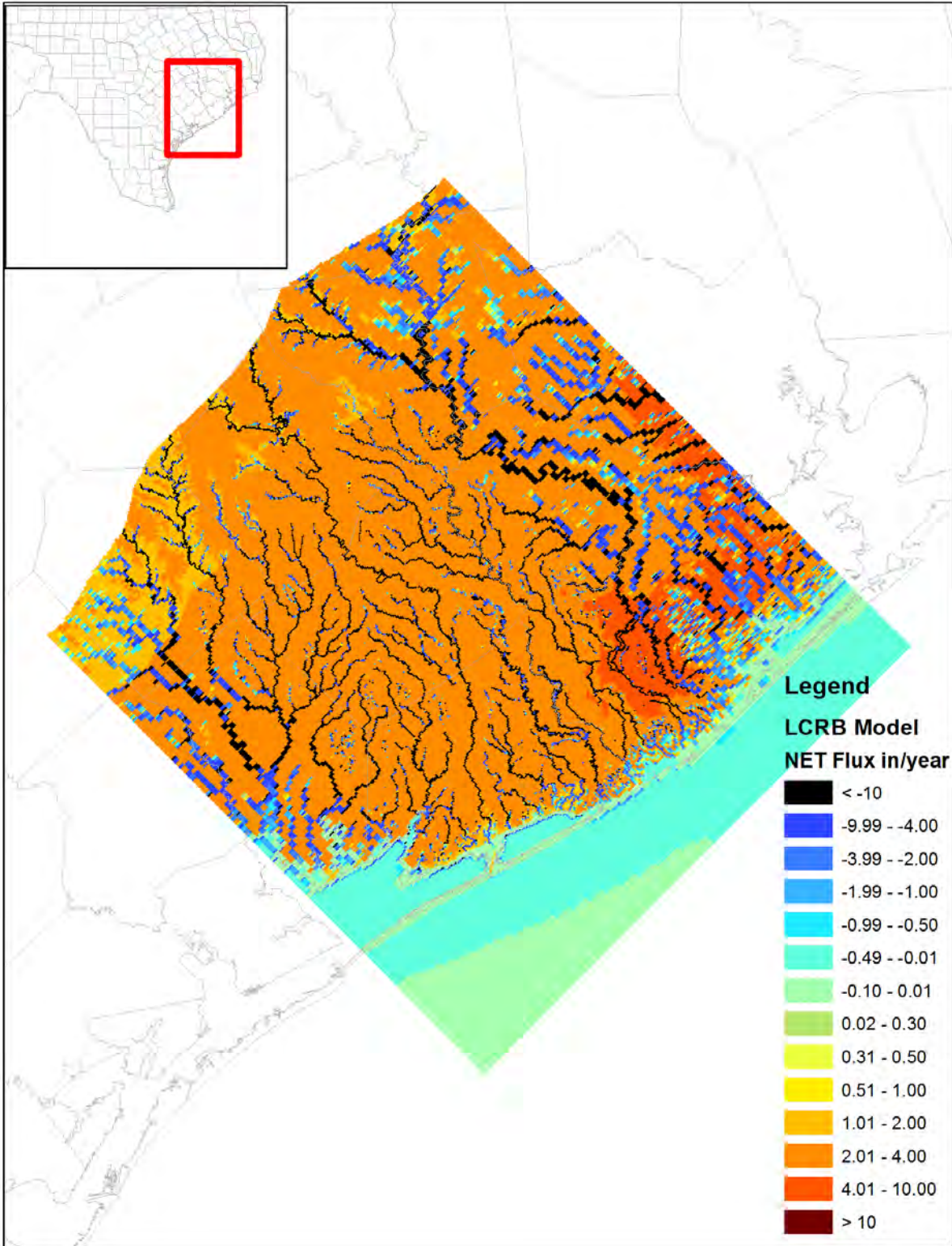


Figure 9-6 Calculation of net flux across the top layer of the LCRB Model based on the water budget developed for the steady-state condition representing predevelopment (no pumping) conditions. (Note: positive fluxes represent recharge into the aquifer and negative fluxes represent discharge out of the aquifer).

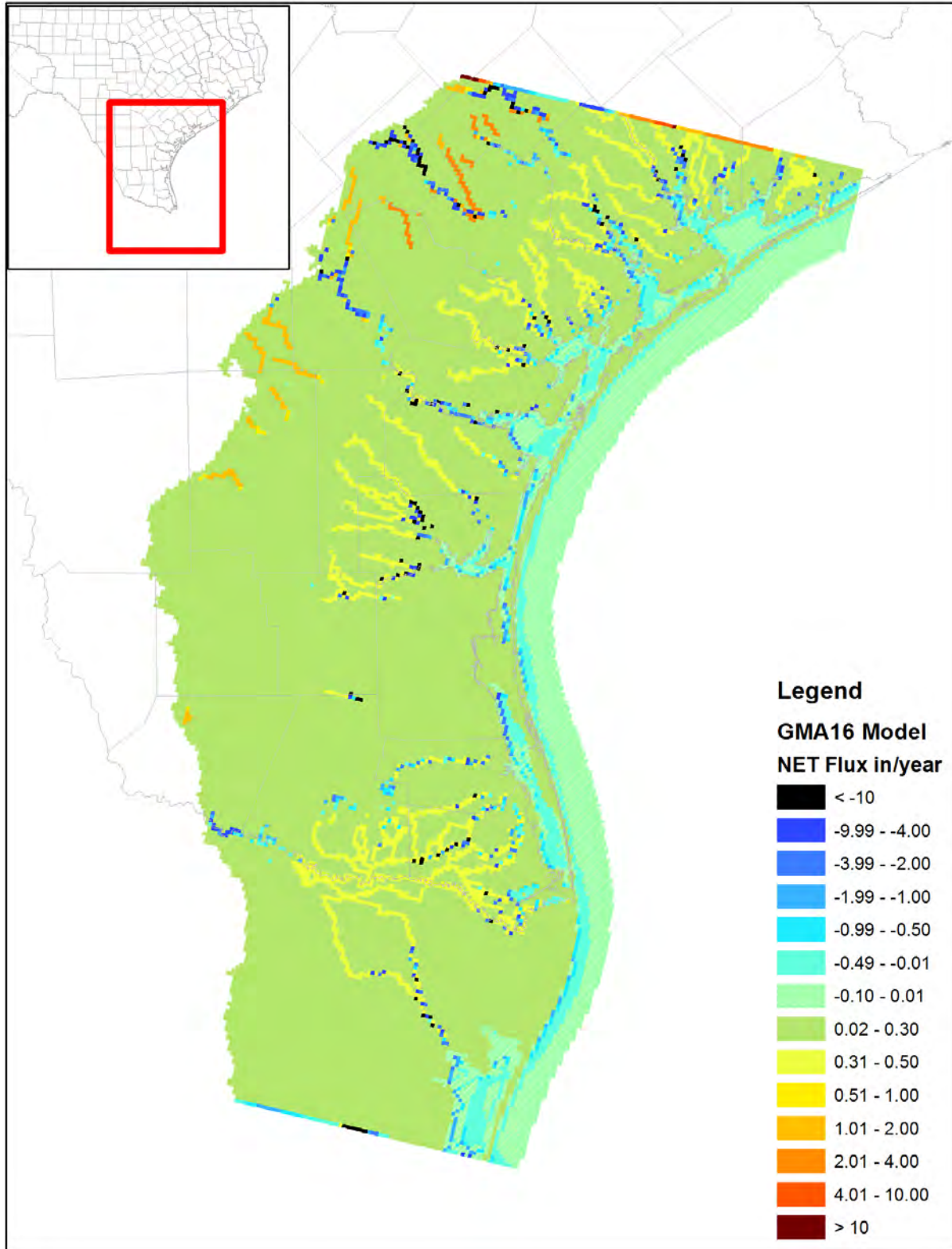


Figure 9-7 Calculation of net flux across the top layer of the GMA 16 AGM based on the water budget developed for the steady-state condition representing predevelopment (no pumping) conditions. (Note: positive fluxes represent recharge into the aquifer and negative fluxes represent discharge out of the aquifer).

Final – Hydrogeochemical Evaluation of the Texas Gulf Coast Aquifer System and
Implications for Developing Groundwater Availability Models

This page intentionally left blank.

10.0 Recommendation

This section lists recommendation for additional work related to this study and the GAM program based on the study findings.

10.1 Water Quality Investigations in the Gulf Coast

The Total Dissolved Solids map (see Figure 6-9) shows that a significant amount of brackish water exists within the Gulf Coast Aquifer System. Within the last decade, brackish groundwater resources have gained considerable attention in the Texas as an alternative water supply. This study identifies and discusses several sources of salinity and elevated TDS in the Gulf Coast. Our study identifies halite dissolution from salt domes, upswelling of brine through growth faults, and the build up of salts in groundwater from high evaporation rates as three of the primary factors that accounts for the brackish resources in the Gulf Coast Aquifer System. Despite our advancement in the understanding of the brackish resources, there are numerous unanswered questions regarding how to quantify and to estimate the TDS associated with brackish groundwater that has not been pumped. Answers to such questions are important to groundwater conservation districts and other agencies interested in developing or managing brackish resources. To help develop these answers, we recommend that TWDB consider the following two projects.

1. Joint analysis of Geophysical Logs and TWDB water quality data – There are literally hundreds of thousands of geophysical logs available in the Gulf Coast Aquifer system. For decades these logs have been used to estimated lithologic and TDS profiles. Our project team recommends that the TWDB explores the benefits of using TWDB extensive water quality data and geophysical logs to help address questions about the nature and extend of brackish water in the Gulf Coast.
2. Additional Investigation into the Sources of Salinity in the Gulf Coast – The recommended investigations would aim to identify and help to characterize the source of elevated TDS throughout the Gulf Coast Aquifer System. Among the goals of these investigations would be to evaluate the relative prevalence of sources of elevated TDS and whether these source of the TDS affects how the TDS in brackish water evolves over time with pumping.

This study shows that a potentially valuable technique for model calibration and evaluation is to compare and evaluate the match between simulated groundwater age from particle tracking and estimated groundwater age from ^{14}C analysis. To help refine and improve this type of evaluation, we recommend that TWDB consider the following two projects.

1. Groundwater Age to Improve Conceptual and Numerical Groundwater Models – The TWDB has assembled an extensive database of ^{14}C data from groundwater samples in Texas aquifers and is currently performing groundwater monitoring of these aquifers. The TWDB is responsible for developing GAMs or AGMs for Texas aquifers. Our project team recommends that the TWDB develops an appropriate strategy for collection additional ^{14}C data to help improve the site conceptual models or GAMs/ AGMs for the Texas aquifers.
2. Correction of Apparent Groundwater Age based on ^{14}C analysis – This report demonstrates that the correction for apparent groundwater age based on ^{14}C analysis can be potentially important. However, a “state-of-the-art” application of NETPATH to perform such correction is expensive and plagued with problems. This report also demonstrates that the relatively simple Pearson Method may be adequate for performing scoping calculations of groundwater age from measured ^{14}C . Our project team recommends that the TWDB investigates the value of developing a simple but standardized “Pearson-type” correction method per aquifer to estimate groundwater ages from the TWDB groundwater ^{14}C data.

10.2 Groundwater Availability Program Guidelines

To help its hydrogeologic consultants produce quality and consistent groundwater models, the TWDB distributes guidelines for the construction, development, and documentation of GAMs. Figure 10-1 shows the table of contents for the guideline the TWDB prepare for the Brazos River Alluvium Aquifer. Based on our evaluation of the very different particle tracks and water budgets generated by the Gulf Coast models for the same Transects, our project team recommends that the TWDB consider expanding the guidelines to help develop numerical model that appropriately reflect the site conceptual model by:

1. Expanding the GAM guideline's Section 3.1.10 Water Quality to include reverse particle tracking to age date the groundwater and then compare the simulate dates from particle tracking to groundwater ages determine from radioactive isotopes such as radiocarbon.
2. Expanding the GAM guideline's Section 3.3 Model Calibration to include documentation of how well the calibrated model represents measured or estimated hydraulic properties of the aquifer; and

10.3 Development of Management Groundwater Models for the Gulf Coast

Our evaluation of the GMAs and AGM used by GMA 14, 15, and 16 in the 2010 joint planning section indicate that there are significant differences in the conceptualization, construction, and calibration among the models. In addition, none of these groundwater models are consistent with the large amount of aquifer characterization information that the TWDB has produced for the Gulf Coast Aquifer System since 2000. This aquifer characterization includes a revised geology and lithology information (Young and others 2010, 2012b), recharge information (Scanlon and others, 2012), and the findings from their report.

During the last decade role and use of TWDB GMAs and AGMs have been increasingly focused on simulating the impacts of pumping on groundwater resource at the county to subcounty scale. The accuracy of these model applications is adversely affected by the lack of updated information in the models. Moreover where the Gulf Coast Aquifer System model's overlap, the different models can and have produced significantly different results. As a result of the major inconsistencies among the different Gulf Coast GMAs and AGM model, our project team recommends that the current GMAs and AGM be replaced with a single model for the entire Gulf Coast Aquifer System. In addition, we suggest that the important findings summarized in Section 9.2 and 9.3 be used to develop a single GAM for the entire Gulf Coast Aquifer System.

Final – Hydrogeochemical Evaluation of the Texas Gulf Coast Aquifer System and
Implications for Developing Groundwater Availability Models

ATTACHMENT 1	1
Groundwater Availability Modeling Program Guidelines	1
Changes from Previous Requests	1
1.0 Introduction	5
2.0 Stakeholder participation	5
3.0 Model development	7
3.1 Conceptual model	7
3.1.1 Physiography and climate	8
3.1.2 Geology	8
3.1.3 Hydrostratigraphy	9
3.1.4 Hydrostratigraphic framework	9
3.1.5 Water levels and regional groundwater flow	9
3.1.6 Recharge	10
3.1.7 Rivers, streams, springs, and reservoirs	10
3.1.8 Hydraulic properties	11
3.1.9 Discharge	11
3.1.10 Water quality	12
3.2 Model architecture	12
3.2.1 Cell size, orientation, layering, and parameter assignment	12
3.2.2 Recharge and surface water	13
3.2.3 Model extents and boundaries	13
3.2.4 Pumping.....	14
3.3 Model calibration	14
3.4 Sensitivity analysis.....	16
4.0 Documentation	17
4.1 Software Requirements	17
4.2 Source information.....	18
4.3 MODFLOW input files	20
4.4 Final reports	21
4.4.1 Report format and figures	21
4.4.2 Report deliverables.....	32
4.4.3 Presentations and web publishing	33
5.0 Project management	33
6.0 Project schedule	34
7.0 References	34
ATTACHMENT 2:.....	36
Data Model for the Groundwater Availability Models	36
1.0 Introduction	36
1.1 Data content and organization	37
1.1.1 Source and derivative geodatabase schema	37
1.1.2 Pumpage geodatabase schema	38
1.1.3 MODFLOW specific data files	38
1.1.4 Model grid feature dataset	38
1.1.5 MODFLOW geodatabase schema	39
1.2 Data documentation	39
1.3 References	39

Figure 10-1 Table of contents from the TWDB groundwater Availability Modeling Program Guidelines for the Brazos River Alluvium Aquifer GAM (TWDB, unpublished correspondence with Cindy Ridgeway).

11.0 References

- Alcala, F.J. and Custodio, E., 2008, Using the Cl/Br ratio as a tracer to identify the origin of salinity in aquifers in Spain and Portugal: *Journal of Hydrology*, vol. 359, p. 189-207.
- Alexander, L.L., and Handschy, J.W., 1998, Fluid flow in a faulted reservoir system: Fault trap analysis for the Block 330 Field, Eugene Island, south addition, offshore Louisiana: *The American Association of Petroleum Geologists Bulletin*, 82, p. 387–411.
- Anderson, R.N., Flemings, P., Losh, S., Austin, J., and Woodhams, R., 1994, Gulf of Mexico growth fault drilled, seen as oil, gas migration pathway: *Oil and Gas Journal*, vol. 92, no. 23, p. 97–104.
- Anthoni, J.F., 2006, <http://www.seafriends.org.nz/oceano/seawater.htm#salinity>.
- Appello, C.A.J, 1994, Cation and proton exchange, pH variations, and carbonate reactions in a freshening aquifer: *Water Resources Research*, v. 30, p. 2793-2805.
- Appello, C.A.J. and Postma, D., 2006, *Geochemistry, groundwater and pollution*: A.A. Balkema Publishers, Leiden, 649p.
- Aravena, R., Wassenaar, L.I., and Barker, J.F., 1995, Distribution and isotopic characterization of methane in a confined aquifer in southern Ontario, Canada: *Journal of Hydrology*, v. 173, p. 51-70.
- Arjen, K., 2006, Salinization above sea level on the Dutch Wadden Islands, *Proceedings of the First SWIM-SWICA Joint Saltwater Intrusion Conference*, Cagliari-Chia, Laguna Italy, September 24-29, p. 147-150.
- ASTM International, 1999, *Guide for Developing Conceptual Site Models for Contaminated Sites*, Designation E 1689-95. ASTM Standards on Determining Subsurface Hydraulic Properties and Groundwater Modeling, Second Edition: Sponsored by ASTM D-18 on Soil and Rock, West Conshohocken, PA.
- Bachman, A.L., 1979, Subsurface disposal of geopressured fluids—Potential geologic and operational problems with recommendations for disposal system testing, In: Dorfman, M.H. and Fisher W.L. (eds.), *Proceedings of the 4th U.S. Gulf Coast geopressured-*

geothermal energy conference—Research and development: The University of Texas at Austin, Center for Energy Studies, 2:972–999.

- Back, W., 1966, Hydrochemical facies and groundwater flow patterns in northern part of the Atlantic Coastal Plain: U.S. Geological Survey Professional Paper 498-A, 42 p.
- Back, W., Hanshaw, B.B., Herman, J.S., Plummer, L.N., Rahn, P.H., Rightmire, C.T., and Rubin, M., 1983, Process and rate of dedolomitization: mass transfer and carbon-14 dating in a regional carbonate aquifer: *Geol. Soc. Am. Bull.*, 94, p. 1415-1429
- Baker, E.T., Jr., 1979, Stratigraphic and hydrogeologic framework of part of the coastal plain of Texas: Texas Department of Water Resources Report 236, 43 p.
- Balsillie, J.H., and Donoghue, J.F., 2004, High resolution sea-level history for the Gulf of Mexico since the last glacial maximum: Florida Geological Survey Report of Investigations no. 103, 66 p.
- Banga, T., Capuano, R.M., and van Nieuwenhuise, D.S., 2002, Fluid flow, stratigraphy and structure in the vicinity of the South Liberty salt dome, Texas: *Gulf Coast Association of Geological Societies Transactions*, v. 52, p. 25–36.
- Barlow, P., 2003, Groundwater in freshwater-saltwater environments of the Atlantic Coast: U.S. Geological Survey Circular 1262, 121p.
- Barlow, P.F. and Reicard, E.G., 2010, Saltwater intrusion in coastal regions of North America: *Hydrogeology Journal*, vol. 18, p. 247-260.
- Bentley, H.W., Phillips, F.M. and Davis, S.N., 1986, Chlorine-36 in the terrestrial environment: Chapter 10: In: Fritz, P., and Fontes, J.-Ch., (Eds.) *Handbook of Environmental Isotope Geochemistry*, vol. 2, The Terrestrial Environment, B. Elsevier, Amsterdam, The Netherlands, p. 427-480.
- Berggren, W.A., Kent, D.V., Swisher, C.C., and Aubry, M.P., 1995, A revised Cenozoic geochronology and chronostratigraphy: *Society of Sedimentary Geology (SEPM) Special Publication 54*, p. 129–212.
- Bethke C.M., 1986, Inverse hydrologic analysis of the distribution and origin of Gulf Coast-type geopressured zones: *J Geophysical Res.*, vol. 91, p. 6535–6545.

- Bethke, C.M. and Johnson, T.M., 2008, Groundwater age and groundwater age dating, *Annual Review of Earth Planetary Sciences*, vol. 36, p. 121-1152.
- Bethke, C.M., Harrison, W.J., Upson, C., Altaner, S.P., 1988, Supercomputer analysis of sedimentary basins: *Science* 239, p. 261–267.
- Billeaud, L.B., Anderson, R.N., Flemings, P.B., and Austin, J., 1994, Active gas and oil migration sought in a growth fault zone: *Petroleum Engineer International*, p. 17–22.
- Bloom, A.L., 1967, Pleistocene shorelines: a new test of isostasy: *Geological Society of America Bulletin* 78, p. 1477–1494.
- Blum, M.D., and Price, D.M., 1998, Quaternary alluvial plain construction in response to glacio-eustatic and climatic controls, *Texas Gulf Coastal Plain: Society of Sedimentary Geology (SEPM) Special Publication No. 59*, p. 31–48.
- Bodenlos, A.J., 1970, Cap-rock development and salt-stock movement, in Kupfer, D. H., editor, *Geology and technology of Gulf Coast salt domes: Baton Rouge, Louisiana, School of Geosciences, Louisiana State University*, p. 73–86.
- Bolt, G.H., and Bruggenwert, M.G., 1978, *Soil Chemistry – Basic elements: Amsterdam: Elsevier*, 281p.
- Bourgeois, F.M., 1997, *Elemental and Stable Isotope Study to Determine the Source of Salt-Water Contamination in the Chicot Aquifer of the Gulf Coast Aquifer System: University of Houston, Houston, Texas, Master’s Thesis*, 313 p.
- Breeuwsma, A., Wosten, J.H.M, Vleeshower, J.J., Van Slobbe, A.M., and Bouma, J., 1986, Derivation of land qualities to asses environmental problems from soil surveys: *Soil Sci. Soc. Am. J.*, vol. 50, p. 186-190.
- Bruce, C.H., 1973, Pressured shale and related sedimentary deformation: mechanisms for development of regional contemporaneous faults: *Am Assoc Petroleum Geol Bull* v. 19, no. 5, p. 878–886.

- Bruno, R.S., and Hanor, J.S., 2003, Large-scale fluid migration driven by salt dissolution, Bay Marchand Dome, offshore Louisiana: *Gulf Coast Association of Geological Societies Transactions*, v. 53, p. 97–107.
- Bryant, W.R., Lugo, J., Cordova, C., and Salvador, A., 1991, Physiography and bathymetry, *in* Salvador, A., ed., *The geology of North America: the Gulf of Mexico basin*, v. J: Boulder, Colorado, Geological Society of America, p. 13–30.
- Butler, J.H., King, D.B., Lobert, J.M., Montzka, S.A., Yvon-Lewis, S.A., Hall, B.D., Warwick, N.J., Mondeel, D.J., Aydin, M., Elkins, J.W., 2007, Oceanic distributions and emissions of short-lived halocarbons: *Global Biogeochemistry Cycles* 21, GB1023. doi: 10.1029/2006GB002732.
- Carr, J.E., Meyer, W.R., Sandeen, W.M., and McLane, I.R., 1985, Digital models for simulation of ground-water hydrology of the Chicot and Evangeline aquifers along the Gulf Coast of Texas: Texas Department of Water Resources, Report 289, 101 p.
- Cartwright, J., Bouroullec, R., James, D., and Johnson, H., 1998, Polycyclic motion history of some Gulf Coast growth faults from high-resolution displacement analysis: *Geology*, vol. 26, p. 819–822.
- Chakraborty, A., 2007, ^{14}C Dating of the Chicot Aquifer Water, Texas Gulf Coast, Evaluation of $\delta^{13}\text{C}$ Correction for Carbon Sources Other than From Calcite Reactions: Thesis, Department of Geosciences, University of Houston, Houston TX.
- Chebotarev, I.I., 1955, Metamorphism of natural waters in the crust of weathering: *Geochim. Cosmochim. Acta*, v. 8, p. 22-28, 137-170.
- Chowdhury, A.H., and Mace, R.E., 2004, Geochemical evolution of groundwater in the Gulf Coast Aquifer of south Texas: in *Proceedings of groundwater flow understanding from the local to the regional scales*, XXXIII Congress International Association of Hydrogeologists and 7th Asociacion Latinoamericana de Hidrologia Subterranea para el Desarrollo, Zacatecas City, Mexico, 4p.

- Chowdhury, A., Wade, S., Mace, R.E., and Ridgeway, C., 2004, Groundwater Availability of the Central Gulf Coast Aquifer System: Numerical Simulations through 1999: Texas Water Development Board, unpublished report.
- Chowdhury, A.H., and Turco, M.J., 2006, Geology of the Gulf Coast aquifer, Texas, *in* R.E. Mace and others, eds., *Aquifers of the Gulf Coast of Texas*: Texas Water Development Board Report 365, p. 23–50.
- Chowdhury, A.H., Boghici, R., and Hopkins, J., 2006, Hydrochemistry, salinity distribution, and trace constituents: implications for salinity sources, geochemical evolution, and flow systems characterization, Gulf Coast Aquifer, Texas: Texas Water Development Board Report 365, p.81-128.
- Chowdhury, A.H., Osting, T., Furnans, J., and Mathew, R., 2010, Groundwater-Surface Water Interaction in the Brazos River Basin: Evidence from Lake Connection History and Chemical and Isotopic Compositions, Report 375. Texas Water Development Board.
- Clark, I.D. and Fritz, P., 1997, *Environmental isotopes in hydrogeology*: CRC Press, Florida, 331p.
- Claypool, G.E., and Kaplan, I.R., 1974, The origin and distribution of methane in marine sediments. *In*. I.R. Kaplan (editor), *Natural Gases in Marine Sediments*. Plenum, New York, N.Y., p. 99-139.
- Clayton, R.N., Friedman, D.L., Garf, T.K., Mayeda, W.F., Meentsk., N.F., Shrimp, 1966, The origin of saline formation waters- 1. Isotopic composition: *Journal of Geophysical Research*, vol. 71, no. 16, p. 3869-3882.
- Coleman, D.D., Liu, C.L., and Riley, K.M. 1988, Microbial methane in the shallow Paleozoic sediments and glacial drift deposits of Illinois, USA: *In*. M. Schoell, *Origin of Methane in the Earth*, *Chem. Geol.*, 71, p. 23-40.
- Conagua, 2007a, *Estadísticas del agua en México: Edición 2007*.
- Conagua, 2007b, Portal on water in México: <http://www.conagua.gob.mx/Conagua/Espaniol/TmpContenido.aspx?id=24002a7d-7cf5-4153-adeb-6e36ce1dff13|SISTEMA>

%20NACIONAL%20DE%20INFORMACIÓN%20DEL%20AGUA|10|0|0|0),
consulted in October 2008.

- Cook, P.G., and Herczeg, A.L., 2000, *Environmental Tracers in Subsurface Hydrology*: Kluwer Academic Publishers, Boston, MA.
- Coplen, T.B., Herczeg, A.L., and Barnes, C., 2000, Isotope engineering—using stable isotopes of the water molecule to solve practical problems, in P.G. Cook and A.L. Herczeg (eds.) in *Environmental tracers in subsurface hydrology*, Kluwer Academic Publishers, p. 79-110.
- Craig, H., 1961, Isotopic variations in meteoric waters: *Science*, vol. 133, p. 1702-1703.
- Crans, W., Mandl, G., and Haremboure, J., 1980, On the theory of growth faulting—A geochemical delta model based on gravity sliding: *Journal of Petroleum Geology*, 2, p. 265–307.
- Cronin, J.G., and Wilson, C.A., 1967, *Groundwater in the flood-plain alluvium of the Brazos River, Whitney Dam to vicinity of Richmond*: Texas Water Development Board Report 41, 206 p.
- Custodio, E., 1987, Hydrogeochemistry and tracers, in Custodio E., *Groundwater problems in coastal areas: Studies and reports in Hydrogeology no. 45*, UNESCO, p. 213-269.
- Davis, S.N., Whittemore, D.O., and Fabryka-Martin, J., 1998, Uses of Cl/Br ratios in studies of potable water: *Groundwater*, vol. 36, p.338-351.
- Deutsch, W.J., 1997, *Groundwater geochemistry: Fundamentals and applications to contamination*: CRC Press, Boca Raton, Florida, 223p.
- Domenico, P.A. 1972, *Concepts and Models in Groundwater Hydrology*: McGraw-Hill, New York.
- Domenico, P.A. and Robbins, G.A., 1985, The displacement of connate waters from aquifers, *Geological Society of America Bulletin*, vol. 96, p. 328-335.
- Domenico, P.A., and Schwartz, F.W., 1990, *Physical and Chemical Hydrogeology*: John Wiley and Sons, New York, 820 p.

- Donoghue, J.F., 2011, Sea level history of the northern Gulf of Mexico Coast and sea level rise scenarios for the near future: *Climatic Change*, vol. 107, p. 17-33.
- Drever, J.I., 1997, *Natural geochemistry of natural waters, surface, and groundwater environments: Second edition*, Prentice Hall, New Jersey, p. 159-174.
- Drever, J.I., 2002, *Natural geochemistry of natural waters, surface, and groundwater environments, Third edition*, Prentice Hall, New Jersey, 436 p.
- Durham Jr., C.O., 1971, A study of the Scotlandville-Denham Springs faults and their effect on school sites. East Baton Rouge Parish, Louisiana: Etco Engineers and Associates Report.
- Durhan J.L., Hogan, J.F., Eastoe, C.J., Hibbs, B., Hutchison, W.R., 2007, Hydrogeologic controls on groundwater recharge and salinization: a geochemical analysis of the northern Hueco Bolson aquifer, Texas, USA: *Hydrogeology Journal*, vol. 16, p. 281-296.
- Dutton, A.R., and Richter, B.C., 1990, Regional geohydrology of the Gulf Coast Aquifer in Matagorda and Wharton counties: Development of a numerical model to estimate the impact of water-management strategies: Contract report prepared for Lower Colorado River Authority, Austin, Texas, under Contract IAC (88-89) 0910, 116 p.
- Dutton, A.R., Smyth, R.C., Nance, H.S., Mullican, J.W., and Gu, Y., 2000, History, regulation, and closure of abandoned centralized and commercial drilling fluid disposal sites in Louisiana, New Mexico, Oklahoma, and Texas: in *Proceedings Groundwater Protection Council Annual Forum*, p. 133-138.
- Dutton, A.S., Nicot, J.P., and Kier, K.S., 2006, Hydrodynamic convergence of hydropressured and geopressured zones, central Texas: *Hydrogeology Journal*, vol. 14, p. 859-867.
- Echols, J.B., Zimmerman, R.K., and Goddard, D.A., 1994, An integrated geochemical-geological approach for determining hydrocarbon generation-migration patterns: Central Gulf Coast Basin: *Gulf Coast Association of Geological Societies*, vol. 44, p. 193–203.
- Edmunds, W.M., Andrews, J.N., Burgess, W.G., Kay, R.L.F., and Lee, D.J., 1984, The evolution of saline and thermal groundwater in Carnmellis granite: *Mineralogical Magazine*, vol. 48, p. 407-424.

- Edmunds, W.M., Carrilla-Rivera, J.J., and Cardona, A., 2002, Geochemical evolution of groundwater beneath Mexico City: *Journal of Hydrology*, vol. 258, p. 1-24.
- Edwards, B.D. and Evans, K.R., 2002, Saltwater Intrusion in Los Angeles Area Coastal Aquifers – the Marine Connection: U.S. Geological Survey Fact Sheet 030-02.
- Emery, K.O., and Garrison, L.E., 1967, Sea levels 7000–20,000 years ago: *Science* 157, p. 684-687.
- Eriksson, E., 1960, The yearly circulation of chloride and sulfur in nature: meteorological, geochemical, and pedological implications: Part II. *Tellus* 12, p. 63–109.
- Esch, W.L., and Hanor, J.S., 1995, Fault and fracture control of fluid and diagenesis around the Iberia Salt Dome, Iberia Parish, Louisiana: *Transactions, Gulf Coast Association of Geological Societies*, vol. 45, p. 181–187.
- Ewing, T.E., 1990, Tectonic map of Texas: University of Texas at Austin, Bureau of Economic Geology, scale 1:750,000, 4 sheets.
- Fisher, W.L., Brown, L.F., McGowen, J.H., and Groat, C.G., 1972, Environmental geologic atlas of the Texas coastal zone—Galveston-Houston area: The University of Texas at Austin, Bureau of Economic Geology, 91 p.
- Fisher, W.L., Brown, L.F., McGowen, J.H., and Groat, C.G., 1973, Environmental geologic atlas of the Texas coastal zone—Beaumont-Port Arthur area: The University of Texas at Austin, Bureau of Economic Geology, 93 p.
- Fogg, G.E., Seni, S.J., and Kreitler, C.W., 1983, Three-dimensional ground-water modeling in depositional systems, Wilcox Group, Oakwood salt dome area, East Texas: The University of Texas at Austin, Bureau of Economic Geology, Report of Investigations No. 133, 55 p.
- Fowler, T., 2011, Natural gas facility in Mont Belvieu explodes (updated): Fuelfix <http://fuelfix.com/blog/2011/09/06/new-pipeline-with-move-ngls-from-panhandle-to-mont-belvieu/>.

- Frank, O.L. and McClymonds, N.E., 1972, Survey of the hydrologic situation on Long Island, N.Y.: in Geological Survey Research 1972 in U.S. Geological Survey Professional Paper 6-27F, 59p.
- Frazier, D.E., 1974, Depositional episodes; Their relationship to the Quaternary stratigraphic framework in the northwestern portion of the Gulf Basin: The University of Texas at Austin, Bureau of Economic Geology Geological Circular 74-1, 28 p.
- Freeze, R.A., and Cherry, J.A., 1979, Groundwater: Prentice-Hall. Inc., New Jersey 604 p.
- Freeze, R.A., and Witherspoon, P.A., 1966, Theoretical analysis of regional groundwater flow. 1. Analytical and numerical solutions to the mathematical model: Water Resources Research, v. 2, no. 4, p. 641-656.
- Freeze, R.A., and Witherspoon, P.A., 1967, Theoretical analysis of regional groundwater flow. 2. Effect of water table configuration and subsurface permeability variation: Water Resources Research, v. 3, no. 2, p. 623-634.
- Freeze, R.A., and Witherspoon, P.A., 1968, Theoretical analysis of regional groundwater flow. 3. Quantitative interpretations: Water Resources Research, v. 4, no. 3, p. 581-590.
- Galloway, W.E., Murphy, T.D., Belcher, R.C., Johnson, B.D., Sutton, S., 1977, Catahoula Formation of the Texas Coastal Plain: Depositional Systems, Composition, Structural Development, Ground-water Flow History, and Uranium Distribution. Bureau of Economic Geology, University of Texas, Austin.
- Galloway, W.E., Hobday, D., and Magara, K., 1982, Frio Formation of the Texas Gulf Coast Plain – depositional systems, structural framework, and hydrocarbon origin, migration, distribution, and exploration potential: BEG Report of Investigations 122, 78 pl.
- Galloway, W.E., Ewing, T.E., Garrett, C.M., Tyler, N., Bebout, D.G., 1983, Atlas of major Texas oil reservoirs: The University of Texas at Austin, Bureau of Economic Geology.
- Galloway, W.E., Jirik, L.A., Morton, R.A., and DuBar, J.R., 1986, Lower Miocene (Fleming) depositional episode of the Texas Coastal Plain and continental shelf: The University of Texas at Austin, Bureau of Economic Geology Report of Investigations No. 150, 50 p.

- Galloway, W.E., 1989, Genetic stratigraphic sequences in basin analysis II: application to northeast Gulf of Mexico Cenozoic basin: American Association of Petroleum Geologists Bulletin, v. 73, p. 143–154.
- Galloway, W.E., Bebout, D.G., Fisher, W.L., Cabrera-Castro, R., Lugo-Rivera, J.E., and Scott, T.M., 1991, Cenozoic, in A. Salvador, ed., The geology of North America: the Gulf of Mexico basin, v. J: Boulder, Colorado, Geological Society of America, p. 245–324.
- Galloway, W.E., Ganey-Curry, P.E., Li, X., and Buffler, R.T., 2000, Cenozoic depositional history of the Gulf of Mexico basin: American Association of Petroleum Geologists Bulletin, v. 84, p. 1743–1774.
- Galloway, W.E., 2005, Gulf of Mexico Basin depositional record of Cenozoic North American drainage basin evolution: International Association Sedimentologists Special Publication 35, p. 409–423.
- Gerber, T.P., Pratson, L.F., Kuehl, S., Walsh, J.P., Alexander, C., and Palmer, A., 2010. The influence of sea level and tectonics on Late Pleistocene through Holocene sediment storage along the high-sediment supply Waipoao continental shelf. Marine Geology. doi:10.1016/j.margeo.2009.10.002
- Glover, R.E., 1959, The pattern of fresh-water flow in a coastal aquifer: J. Geophys. Res., vol. 64, p. 457-459.
- Glynn, P.D., and Plummer, L.N., 2005, Geochemistry and the understanding of ground-water systems: Hydrogeology Journal, vol. 13, p. 263-287.
- Groschen, G.E., 1985, Simulated effects of projected pumping on the availability of freshwater in the Evangeline Aquifer in an area southwest of Corpus Christi, Texas: U.S. Geological Survey Water Resources Investigation Report 85-4182, 103 p.
- Hamlin, H.S., Smith, D.A., and Akhter, M.S., 1988, Hydrogeology of Barbers Hill salt dome, Texas coastal plain: The University of Texas at Austin, Bureau of Economic Geology, Report of Investigations No. 176, 41 p.

- Hamlin, H.S., 2006, Salt domes in the Gulf Coast aquifer, *in* Mace, R.E., and others, eds.,
Aquifers of the Gulf Coast of Texas: Texas Water Development Board Report 365,
p. 217–230.
- Hammond, W.W., Jr., 1969, Ground-Water Resources of Matagorda County, Texas: Texas
Water Development Board Report 91, 163 p.
- Hanor, J.S., 1987, Kilometer scale thermohaline overturn of pore water in the Louisiana Gulf
Coast, *Nature*, vol. 327, p. 501-503.
- Hanor J S, 1994, Origin of saline fluids in sedimentary basins. In: Parnell J (ed) *Geofluids:
origin, migration and Evolution of fluids in sedimentary basins: Geol Soc Spec Publ*,
vol.78, p.51–174.
- Haq, B.U., Hardenbol, J., and Vail, P.R., 1987, Chronology of fluctuating sea levels since the
Triassic: *Science*, vol. 235, p. 1156–1167.
- Harbaugh, A.W., 1990, A computer program for calculating subregional water budgets using
results from the U.S. Geological Survey modular three-dimensional ground-water flow
model: U.S. Geological Survey Open-File Report 90-392, 46 p.
- Harden and Associates, 2002, Availability of brackish groundwater from the Rio Grande
alluvium, Cameron County, Texas: consultant report for the Southmost Regional Water
Authority, 23 p.
- Harrison W.J. and Summa L.L., 1991, Paleohydrology of the Gulf of Mexico basin: *Am J Sci*,
vol. 291, p.109–176.
- Hay, R., 1999, A numerical groundwater flow model of the Gulf Coast Aquifer along the South
Texas Gulf Coast: Texas A&M University—Corpus Christi, M.S. thesis, 47 p.
- HDR Engineering, Inc., 2001, Brazos River alluvium groundwater model and conjunctive use
analysis: HDR Engineering, Inc., File Copy 2002–0152, 27 p.
- Hem, J.D., 1985, Study and interpretation of the chemical characteristics of natural water: U. S.
Geological Survey Water Supply Paper 2254, 249 p.

- Herczeg, A.L. and Edmunds, W.M., 2000, Inorganic ions as tracers, in Environmental tracers in subsurface hydrology, in Cook, P.G., and Herczeg, A.L., (eds.): Kluwer Academic Publishers, p. 31-77.
- Hill, R.T., 1901, Geography and geology of the Black and Grand Prairies, Texas with detailed description of the Cretaceous formations and special reference to artesian waters: U.S. Geological Survey, 21st Annual Report, Washington DC, part 7, 666 p.
- Holzer, T.L., 1984, Ground failure induced by ground water withdrawal from unconsolidated sediment, *in* Holzer, T.L., ed., Man-induced land subsidence: Geological Society of American Review of Engineering Geology, v. 6, p. 67–105.
- Hudak, P.F., and Wachal, D.J., 2001a, Effects of brine injection wells, dry holes, and plugged oil/gas wells on chloride, bromide, and barium concentrations in the Gulf Coast Aquifer, southeast Texas, USA: Environmental Monitoring and Assessment, vol. 72, p. 249-264.
- Hudak, P.F., and Wachal, D.J., 2001b, Oil Production, Agriculture, and Groundwater Quality in the Southeastern Gulf Coast Aquifer, Texas: Environmental Monitoring and Assessment, vol. 72, p. 249-264.
- Hutchison, W.R., Hill, M.E, Anaya, R., Hassan, M., Oliver, W., Jigmond, M., Wade, S, and Aschenbach, E., 2011, Groundwater Management Area 16 Groundwater Flow Model, Unnumbered report: Texas Water Development Board.
- Jenden, P.D., and Kaplan, I.R., 1988, Origin of natural gas in the Sacramento Basin: Am. Assoc. Pet. Geol. Bull., vol. 72.
- Jiménez, B., and Marín, L., 2004, El agua en Mexico vista de la Academia: Academia Mexicana de Ciencias.
- Jones, P.H. and Buford, T.B., 1951, Electric logging applied to ground-water exploration: Geophysics, vol. 16, no. 1, p. 115–139.
- Jorgensen, D.G., 1975, Analog-model studies of ground-water hydrology in the Houston District, Texas: Austin: Texas Water Development Board Report 190, 84 p.

- Jorgensen, D.G., 1977, Salt-water encroachment in aquifers near the Houston Ship Channel, Texas: U.S. Geological Survey Open File Report 76-781, 45 p.
- Kasmarek, M.C., and Strom, E.W., 2002, Hydrogeology and simulation of ground-water flow and land-surface subsidence in the Chicot and Evangeline Aquifers, Houston area, Texas: U.S. Geological Survey Water Resources Investigations Report 02-4022, 61 p.
- Kasmarek, M.C., and Robinson, 2004, Hydrogeology and Simulation of Groundwater Flow and Land-Surface Subsidence in the Northern Part of the Gulf Coast Aquifer System, Texas: United States Geological Society, Scientific Investigation Report 2004-5102.
- Kaufman, W.J., and Orlob, G.T., 1956, Measuring ground water movement with radioactive and chemical tracers: American Water Works Association Journal, v. 48, p. 559-572.
- Kazmann, R.G., 1970, The present and future groundwater supply of the Baton Rouge Area: Louisiana State University, Louisiana Water Resources Research Institute, Bulletin no. 5.
- Kendall, C., and Coplen, T., 2001, Hydrological Processes, vol. 15, p. 1363-1393.
- Khan, A., Mojumder, S.K., Kovats S. and P. Vineis, 2008, Saline contamination of drinking water in Bangladesh: The Lancet, vol. 371, no. 9610, p. 385.
- Klinge, H., Schelkes, K., Rubel, A., Suckow, A., Schildknecht, F., and Ludwig, R., 2002, The saltwater/freshwater regime in the sedimentary cover of the Gorleben salt dome: Transport in Porous Media, v. 47, p. 125–148.
- Knox, P.R., Young, S.C., Galloway, W.E., Baker, Jr., E.T., and Budge, T., 2006, A stratigraphic approach to Chicot and Evangeline aquifer boundaries, central Texas Gulf Coast: Gulf Coast Association of Geological Societies Transaction, v. 56, p. 371-393.
- Knox, P.R., Kelley, V.A., Vreugdenhil, A., Deeds, N. and Seni, S. 2007, Structure of the Yegua-Jackson Aquifer of the Texas Gulf Coastal Plain: INTERA Incorporated, prepared for the Texas Water Development Board.
- Kosters, E.C., Bebout, D.G., Seni, S.J., Garrett, C.M., Brown, Jr., L.F., Hamlin, H.S., Dutton, S.P., Ruppel, S.C., Finley, R.J., Tyler, N., 1989, Atlas of major Texas gas reservoirs: The

- University of Texas at Austin, Bureau of Economic Geology Coast Association of Geological Societies Transactions, v. 56, p. 371–393.
- Kreitler, C.W., 1976, Lineations and faults in the Texas coastal zone: The University of Texas at Austin, Bureau of Economic Geology Report of Investigations No. 85, 32 p.
- Kreitler, C.W., 1979, Ground-Water Hydrology of Depositional Systems: in Galloway, W.E., and others. Depositional and Ground-Water Flow System in the Exploration for Uranium: A Research Colloquium: The University of Texas at Austin, Bureau of Economic Geology, p. 118-176.
- Kreitler, C.W., 1989, Hydrogeology of Sedimentary Basins: Journal of Hydrogeology. vol. 106, p. 29-53.
- Kreitler, C.W., and Richter, B.C., 1986, Hydrochemical Characterization of Saline Aquifers of the Texas Gulf Coast Used for Disposal of Industrial Waste: Prepared for the USEPA by the Bureau of Economic Geology, University of Texas, Austin, TX.
- Kreitler, C.W., Akhter, M.S., Donnelly, A.C., and Wood, W.T., 1988, Hydrogeology of Formations Used for Deep-Well Injection, Texas Gulf Coast: Prepared for the USEPA by the Bureau of Economic Geology, University of Texas, Austin, TX.
- Kreitler, C.W., Guevera, E., Granata, G., and McKalips, D., 1977, Hydrogeology of Gulf Coast aquifers, Houston-Galveston area, Texas: Gulf Coast Association of Geological Societies Transactions, v. 27, p. 72–89.
- Kruskal and Wallis, 1952, Use of ranks in one-criterion variance analysis: Journal of the American Statistical Association, vol. 47, no. 260, p. 583–621.
- Kuecher, G.J., 1995a, The dominant processes responsible for subsidence of coastal wetlands in South Louisiana. In F.B. Barends, F.J.J. Brouwer, F.H. Schroeder (Eds.): The Hague: AHS Publication, Land subsidence, p. 69–81.
- Kuecher, G.J., 1995b, The recognition of active growth faults on the lower deltaic plain of the Mississippi River: Implications for framework modeling of individual delta cycles: Abstracts with Program, Annual Meeting, The Geological Society of America, New Orleans, p. A-214.

- Kuecher, G.J., Roberts, H.H., Thompson, M.D., and Matthews, I., 2001, Evidence for active growth faulting in the Terrebonne delta plain, south Louisiana: implications for wetland loss and vertical migration of petroleum: *Environmental Geosciences*, v. 8, p. 77–94.
- Kuecher, G.J., and Roberts, H.H., 2000, Seismic, electromagnetic, subsidence, and biozonation evidence for active growth faults in south Louisiana. Abstracts with Program: The American Association of Petroleum Geologists, Annual Convention, New Orleans, p. A-81.
- Kyle, R.J., and Price, P.E., 1986, Sulfide mineralization in salt dome cap rocks, in Seni, S.J., and Kyle, J.R., editors, Comparison of cap rocks, mineral resources, and surface features of salt domes in the Houston diapir province: *Geological Society of America, Field Trip Guidebook*, p. 43–63.
- Lambeck, K., Purcell, A., Johnston, P., Nakada, M., Yokoyama, Y., 2003, Water-load definition in the glacio-hydro-isostatic sea-level equation: *Quaternary Science Reviews* 22, p. 309-318.
- Lambert, J., and Aharon P., 2008, Oxygen and Hydrogen Isotope Time-Series Data in the Hydrologic Cycle of the US Gulf Coast: *Gulf Coast Association of Geological Societies Transactions*, v. 58, p. 589-600.
- Land, L.S., Macpherson, G.L., 1992, Origin of saline formation waters, Cenozoic section, Gulf of Mexico sedimentary basin: *Am Assoc Petroleum Geol Bull*, vol. 76, no. 9, p. 1344-1362.
- Larkin, T.J., and Bomar, G.W., 1983, Climatic Atlas of Texas: Texas Water Development Board, Report LP-192, Austin Texas.
- LBG Guyton and INTERA. 2012, Catahoula Aquifer Characterization and Modeling Evaluation in Montgomery County: prepared for the Lone Star Groundwater Conservation District, September 2012.
- LBG-Guyton and Norris Consulting, 2003, Brackish Groundwater Manual for Texas Regional Water Planning Groups: Texas Water Development Board, Austin, Texas.

- Libra, R.D., Hallberg, G.R., and Hoyer, B.E., 1987, Impacts of agricultural chemicals on groundwater quality in Iowa: in *Groundwater Quality and Agricultural Practices* ed. Fairchild, D.M., p. 185-217, Lewis, Chelsea.
- Lindsay, S.V., 2009, Sources of saline water in the Chicot and Evangeline aquifers of Brazoria, Fort Bend, and Wharton counties using multielement hydrochemical analyses: Master's thesis, University of Houston, 107 p.
- Lin, G., and Nunn, J.A., 1997, Evidence for recent migration of geopressed fluids along faults in Eugene Island, Block 330, offshore Louisiana, from estimates of pore water salinity: *Transactions, Gulf Coast Association of Geological Societies*, vol. 47, p. 419–423.
- Losh, S., 1998, Oil migration in a major growth fault: Structural analysis of the Pathfinder core, South Eugene Island Block 330, offshore Louisiana: *The American Association of Petroleum Geologists Bulletin*, 82, p. 1694–1710.
- Losh, S., Eglinton, L., Schoell, M., and Wood, J., 1999, Vertical and lateral fluid flow related to a large growth fault, South Eugene Island Block 330 Field, offshore Louisiana: *The American Association of Petroleum Geologists Bulletin*, vol. 83, no. 2, p. 244–276.
- Loskot, C.L., Sandeen, W.M., and Follett, C.R., 1982, *Ground-Water Resources of Colorado, Lavaca, and Wharton counties, Texas*: Texas Department of Water Resources Report 270, 199 p.
- Martini, A.M., Lynn, M. Walter, and McIntosh, J.C., 2008, Identification of microbial and thermogenic gas components from Upper Devonian black shale cores, Illinois and Michigan basins: *Bulletin of American Association of Petroleum Geologists*, vol. 92, p. 327-339.
- McCaffrey, M.A., Lazar, B., and Holland. H.D., 1987, The evaporation path of seawater and the coprecipitation of Br- and K⁺ with halite: *Jour. Sedimentary Petrology* 57, no. 5
- McDonald, M.G. and Harbaugh, A.W., 1988, A Modular Three-Dimensional Finite Difference Groundwater Flow Model: U.S. Geological Survey Report 83-875, p. 928-937.
- McFarland Jr., E., 1961, Radiocarbon Dating of Late Quaternary Deposits, South Louisiana: *Geological Society of America, Bulletin* 72, p. 129–158.

- McGowen, J.H., Brown, L.F., Jr., Evans, T.J., Fisher, W.L., and Groat, C.G., 1976a,
Environmental geologic atlas of the Texas coastal zone—Bay City-Freeport area: The
University of Texas at Austin, Bureau of Economic Geology, 98 p.
- McGowen, J.H., Brown, L.F., Jr., Evans, T.J., Fisher, W.L., and Groat, C.G., 1976b,
Environmental geologic atlas of the Texas coastal zone—Port Lavaca area: The University
of Texas at Austin, Bureau of Economic Geology, 107 p.
- McMahon P.B., Chapelle, F.H., and Bradley, P.M., 2011, Evolution of redox sources in
groundwater, In Aquatic redox chemistry: American Chemical Society, p. 581-597.
- McManus, K.M., and Hanor, J.S., 1993, Diagenetic evidence for massive evaporite dissolution,
fluid flow, and mass transfer in the Louisiana Gulf Coast: *Geology*, vol. 21, p. 727–730.
- Meisler, H., Leahy, P.P., and Knobel, L.L., 1985, Effect of eustatic sealevel changes on salt-
freshwater relations in the northern Atlantic coastal plain: U.S. Geological Survey Water
Supply Paper 2255, 28. pgs.
- Meisler H., 1989, The occurrence and geochemistry of salty ground water in the northern
Atlantic Coastal Plain: U.S. Geological Survey Professional Paper 1404-D.
- Metz, P.A. and Brindle, D.L., 1996, Potential for water quality degradation of interconnected
aquifers in west-central Florida: U.S. Geological Survey Professional Paper 1403-G,
59p.
- Metz, B., Davidson, O.R., Bosch, P.R., Dave, R., Meyer, L.A., 2007, Contribution of working
group III to the Fourth Assessment Report of the intergovernmental panel on climate
change: Cambridge University Press, NY, 807 p.
- Meyer, W.R. and Carr, J.E., 1979, A Digital Model for the Simulation of Ground-Water
Hydrology in the Houston Area, Texas: Texas Department of Water Resources, LP-103.
- Milne, G.A., Mitrovica, J.X., Schrag, D.P., 2002, Estimating past continental ice volume from
sea-level data: *Quaternary Science Reviews* 21, 361–376.
- Mitchell-Tapping, H.J., 1995, Fault-controlled freshwater lenses within the saline aquifer of
coastal Brevard and Indian River counties, Florida: *Transactions, Gulf Coast Association
of Geological Societies*, vol. 45, p.449–455.

- Morgan, C., and Winner, M.D., 1962, Hydrochemical facies in the 400 foot and 600 foot sands of the Baton Rouge Area, LA: U.S. Geological Survey Prof. Paper 450-B, p. B120-121.
- Morgan, J.P., 1961, Genesis and paleontology of the Mississippi River mudlumps: Louisiana Geological Survey, Baton Rouge. Geological Bulletin, 35.
- Morton, R.A., 1980, Methane entrainment in geopressured aquifers, Texas Gulf Coast: The University of Texas at Austin, Bureau of Economic Geology, 25 p.
- Morton, R.A., Jirik, L.A., and Galloway, W.E., 1988, Middle-Upper Miocene depositional sequences of the Texas Coastal Plain and continental shelf: The University of Texas at Austin, Bureau of Economic Geology Report of Investigations No. 174, 40 p.
- Morton, R.A., and Galloway, W.E., 1991, Depositional, tectonic and eustatic controls on hydrocarbon distribution in divergent margin basins: Cenozoic Gulf of Mexico case history: *Marine Geology*, v. 102, p 239–263.
- Mozley, P. S., and Goodwin, L. B., 1995, Patterns of fault cementation along a Cenozoic normal fault: A record of paleoflow orientations: *Geology*, v. 236, p. 539-542.
- Oden, T.D., 2011, Groundwater Environmental Tracer Data Collected from the Chicot, Evangeline, and Jasper Aquifers in Montgomery County and Adjacent counties, Texas, 2008: U.S. Geological Survey Data Series 590, 65 p.
- Oden, J.H., Oden, T.O., and Szabo, Zoltan, 2010, Groundwater quality of the Gulf Coast aquifer system, Houston, Texas, 2007–08: U.S. Geological Survey Data Series 548, 65 p.
- Oden, J.H., Brown, B.W., and Oden, T.D., 2011, Groundwater quality of the Gulf Coast aquifer system, Houston, Texas, 2010: U.S. Geological Survey Data Series 598.
- Oden, T.D., and Truini, M.T., 2013, Estimated rates of groundwater recharge to the Chicot, Evangeline, and Jasper aquifers by using environmental tracers in Montgomery County and adjacent counties, Texas, 2008 and 2011: Scientific Investigation Report 2013-5024.
- Ophori, D.U., and Tóth, J., 1989, Patterns of groundwater chemistry, Ross Creek Basin, Alberta, Canada: *Ground Water*, vol. 27, no. 1, p. 20-26.

- Osborn S.G. and McIntosh J.C., 2010, Chemical and isotopic tracers of the contribution of microbial gas in Devonian organic-rich shales and reservoir sandstones, northern Appalachian Basin: *Appl Geochem*, vol. 25, p.456–471.
- Osborn, S.G., Vengosh, A., Warner, N.R., and Jackson, R.B., 2011, Methane contamination of drinking water accompanying gas well drilling and hydraulic fracturing: *PNAS*, vol. 1108, p. 8172-8176.
- Pape, J.R., Banner, J.L., Mack, L.E., Musgrove, M., and Guilfoyle, A., 2010, Controls on oxygen isotope variability in precipitation and cave drip waters, central Texas, USA: *Journal of Hydrology*, vol. 285, p. 203-215.
- Pearson, F.J., 1965, Use of C-13/C-12 ratios to correct radiocarbon ages of material initially diluted by limestone: In. *Proceedings of the 6th International Conference on Radiocarbon and Tritium Dating*, Pulman, Washington, p 357.
- Pearson, F.J., and White, D.E., 1967, Carbon-14 ages and flow rates of water n Carrizo Sand, Atascosa County, Texas: *Water Resources Research*, vol., 3, p. 251-261.
- Peltier, W.R., Farrell, W.E., Clark, J.A., 1978, Glacial isostasy and relative sea-level: a global finite element model: *Tectonophysics* 50, p. 81–110.
- Pettijohn, R.A., Weiss, J.S., and Williamson, A.K., 1988, Dissolved-Solides Concentrations and Water Temperatures for Aquifers in the Gulf Cost Systems, South-Central United States: USGS WRI Report 88-4082, map, scale 1:3.500,000. 5 sheets.
- Piper, A.M., 1944, A graphica procedure in geochemical interpretation of water analysis: *America Geophysical Union Trans.*, vol. 25, p. 914-923.
- Plummer, L.N., Jones, B.F., and Tressdell, A.H., 1976, WATEQF – a FORTRAN IV version of WATEQ, a computer code for calculating chemical equilibrium of natural waters: U.S. Geol. Survey, WRI Report 76-13.
- Plummer, L.N., Prestemon, E.C., and Parkhurst, D.L., 1994, An Interactive CODE (NETPATH) For Modeling Net Geochemical Reactions Along A Flow Path Version 2.0: U.S.Geological Survey W.R.I. Report 94-4169, 130 p.

- Plummer, L.N., Bexfield, L.M., Anderholm, S.K., Sanford, W.E., Busenberg, E., 2004a, Geochemical characterization of ground-water flow in the Santa Fe Group aquifer system, Middle Rio Grande Basin, New Mexico: U.S. Geological Survey Water Resources Investigation Report 03-4131, 395 p.
- Plummer, L.N., Bexfield, L.M., Anderholm, S.K., Sanford, W.E., Busenberg, E., 2004b, Hydrochemical tracers in the Middle Rio Grande Basin, USA: 1. Conceptualization of groundwater flow: *Hydrogeology Journal*, vol. 12, p.359–388.
- Plummer, L.N., Sanford, W.E., Bexfield, L.M., Anderholm, S.K., Busenberg, E., 2004c, Using geochemical data and aquifer simulation to characterize recharge and groundwater flow in the Middle Rio Grande Basin, USA. In: Hogan, J.F., Phillips, F.M., Scanlon, B.R. (eds) *Ground-water recharge in a desert environment: the southwestern United States: Am Geophys Union Monograph, Water Science and Application Series*, Washington, D.C., vol. 9, p.185–216.
- Pollock, D.W., 1994, *User's Guide for MODPATH/MODPATH-PLOT, Version 3, A particle tracking post-processing package for MODFLOW, the U.S. Geological Survey finite-difference ground-water flow model*: Reston, VA: U.S. Geological Survey, Open-File Report 94-464.
- Postma, D., Boesen, C., Kristiansen, H. and Larsen, F., 1991, Nitrate reduction in an unconfined sandy aquifer: water chemistry, reduction processes, and geochemical modeling: *Water Resources Research*, vol. 27, p. 2027-2045.
- Railroad Commission of Texas (RCT), 1993. *Statewide Rules for Oil, Gas, and Geothermal Operations*, Oil and Gas Division of RCT, Austin, Texas
- Redfield, A.C., 1967, Postglacial change in sea level in the western north Atlantic Ocean: *Science* 157, 687–692.
- Richter, B.C., and Kreitler, C.W., 1991, *Identification of Sources of Ground-water Salinization Using Geochemical Techniques*, EPA Report/600/2-91/064, US EPA, Ada, OK.
- Richter, B.C., and Kreitler, C.W., 1993, *Geochemical techniques for identifying sources of ground-water salinization*: CRC Press, 258 p.

- Robinove, C.J., Langford, R.H., and Brookhart, J.W., 1958, Saline-water resources of North Dakota: U.S. Geological Survey, Water-Supply Paper 1428, 72 p.
- Roland, H.L., Hill, T.F., Autin, P., Durham Jr., C.O., and Smith, C.G., 1981, The Baton Rouge and Denham Springs-Scotlandville faults: A report prepared for the Louisiana Department of Natural Resources by the Louisiana Geological Survey and Durham Geological Associates Consultants, Baton Rouge.
- Rozanski, K., Araguas-Aragusa, L, and Gonfiantini, R., 1993, Isotopic patterns in modern global precipitation: In: Continental Isotope Indicators of Climate, American Geophysical Union Monograph.
- Sandeen, W.M. and Wesselman, J.B., 1973, Ground-Water Resources of Brazoria County, Texas: Texas Water Development Board, Report 163.
- Sanford W.E., Plummer L.N., McAda D.P., Bexfield L.M., Anderholm S.K., 2004a, Use of environmental tracers to estimate parameters for a predevelopment-ground-water-flow model of the Middle Rio Grande Basin, New Mexico: U.S. Geological Survey Water Resources Investigation Report 03-4286, 102 p.
- Sanford W.E., Plummer L.N., McAda D.P., Bexfield L.M., Anderholm S.K., 2004b, Hydrochemical tracers in the Middle Rio Grande Basin, USA: 2. Calibration of a groundwater model: Hydrogeology Journal, vol. 12, p.:389–407.
- Scanlon, B., Keese, K., Bonal, N, Deeds, N., Kelley, V., and Litvak, M., 2005, Evapotranspiration Estimates with Emphasis on Groundwater Evapotranspiration in Texas: prepared for the Texas Water Development Board.
- Scanlon, B.R., Gates, J.B., Reedy, R.C., Jackson, W.A., Bordovsky, J.P., 2010, Effects of irrigated ecosystem, 2. Quality of soil water and groundwater in the southern High Plains, Texas: Water Resources Research, vol. 46, 14p.
- Scanlon, B.R., Reedy, R., Strassberg, G, Huang, Y., Senay G., 2012, Estimation of Groundwater Recharge to the Gulf Coast Aquifer in Texas, USA: Prepared by the Bureau of Economic Geology, Texas Water Development Board, Austin, TX.

- Schoell, M., 1980, The hydrogen and carbon isotopic composition of methane from natural gases of various origins: *Geochim. Cosmochim. Acta*, 44: 649-661 1.
- Sellards, E.H., Adkins, W.S., and Plummer, F.B., 1932, *The Geology of Texas-Volume I, Stratigraphy*: The University of Texas at Austin, Bureau of Economic Geology, 1007 p.
- Seni, S.J., Kreitler, C.W., Mullican, III, W.F., and Hamlin, H.S., 1984, Utilization of salt domes for chemical-waste disposal: The University of Texas at Austin, Bureau of Economic Geology, report prepared for Texas Department of Water Resources under interagency contract no. IAC (84-85)-1019, 161 p.
- Seni, S.J., and Jackson, M.P.A., 1984, Sedimentary record of Cretaceous and Tertiary salt movement, East Texas basin-Times, rates, and volume of salt flow and their implications for nuclear waste isolation and petroleum exploration: The University of Texas at Austin, Bureau of Economic Geology Report of Investigations No. 139, 89 p.
- Seni, S.J., Collins, E.W., Hamlin, H.S., Mullican, III, W.F., and Smith, D.A., 1985, Phase III— Examination of Texas salt domes as potential sites for permanent storage of toxic chemical waste: The University of Texas at Austin, Bureau of Economic Geology, report prepared for Texas Water Commission under interagency contract no. IAC (84-85)-2203, 310 p.
- Shah, S.D., and Lanning-Rush, J., 2005, Principal faults in the Houston, Texas, metropolitan area: U.S. Geological Survey Scientific Investigation Map 2874.
- Shah, S.D., Houston, N.A., and Braun, C.L., 2007, Hydrogeologic characterization of the Brazos River Alluvial Aquifer, Bosque County to Fort Bend County, Texas: U.S. Geological Survey Scientific Investigations Map 2007-2989, 17 p.
- Sharp, Jr., J.M., Kreitler, C.W., and Lesser, J., 1991, Ground water, *in* A. Salvador, ed., *The geology of North America: the Gulf of Mexico basin*, v. J: Boulder, Colorado, Geological Society of America, p. 529–543.
- Sharp, Jr., J.M., and 12 others, 1988, Diagenetic processes in northwest Gulf Mexico sediments, *in* Chilingarian, G.V., and Wolv, K.H., eds. *Diagenesis II*: Elsevier Science Publishers, p. 43-113.

- Shepard, F.P., 1960, Rise of sea level along the northwest Gulf of Mexico: In: Shepard, F.P., Phleger, F.B., van Andel, T.H. (Eds.), *Recent Sediments: Northwestern Gulf of Mexico*, p. 338–344.
- Simms, A.R., Lambeck, K., Purcell, A., Anderson, J.B., and Rodriguez, A., 2007, Sea-level history of Mexico since the Last Glacial Maximum with implication for melting history of Laurentide Ice Sheet: *Quaternary Science Reviews*, vol. 26, p. 920-940.
- Sprent, J.J., 1987, *The ecology of the nitrogen cycle*: Cambridge University Press, 151p.
- Solis I., 1981, Upper Tertiary and Quaternary depositional systems, Central Coastal Plain, Texas: The University of Texas at Austin, Bureau of Economic Geology Report of Investigations No. 108, 89 p.
- Solomon, S., Thompson, D.W.J., Portmann, R.W., Oltmans, S.J., Thompson, A.M., 2005, On the distribution and variability of ozone in the tropical upper troposphere: implications for tropical deep convection and chemical–dynamical coupling: *Geophysical Research Letters* 32, L23813. doi:10.1029/2005GL024323.
- Sprinkle C.L., 1989, *Geochemistry of the Floridan aquifer system in Florida and in parts of Georgia, South Carolina, and Alabama*: U.S. Geological Survey Professional Paper 1403-I.
- Strom, E., Houston, N., and Garcia, A., 2003, *Selected hydrogeologic datasets for the Jasper Aquifer, Texas*: Reston, VA., United States Geological Survey, Open File Report 2003-299.
- SWIM, 2008, proceedings of SWIM meetings 1 to 19: <http://swim-site.org>.
- Thode, H.G., 1991, Chapter 1 Sulphur Isotopes in Nature and the Environment: An Overview. In *Stable Isotopes in the Assessment of Natural and Anthropogenic Sulphur in the Environment*: Editors Krouse, H.R., and Grinenko, V.A., John Wiley & Sons, Ltd.
- Toth, J., 1962, A theory of groundwater option in small drainage basins in central Alberta, Canada: *Journal of Geophysical Research*, vol. 67, no. 11, p. 4375-4387.

- Toth, J., 1963, A theoretical analysis of groundwater flow in small drainage basins: *Journal of Geophysical Research*, vol. 68, no. 16, p. 4795-4812.
- Toth, J., 1970, A conceptual model of groundwater regime and the hydrogeologic environment: *Journal of Hydrology*, vol. 10, no. 2, p. 164-176.
- Texas Water Development Board, unpublished correspondence with Cindy Ridgeway, Exhibit A
Scope of Work Attachment 1: Groundwater Availability Modeling Program Guidelines.
- Vance, D.B., 1996, Redox reactions in remediation: *Environmental Technology*, vol. 6, p. 24-25.
- Venkatamaran, K., and Uddameri, V., 2011, Impacts of sea level rise caused by climate change on saltwater intrusion into the Gulf Coast Aquifer of south Texas: American Geophysical Union, Fall Meeting, San Francisco, California.
- Verbeek, E.R., 1979, Surface faults in the Gulf Coastal Plain between Victoria and Beaumont, Texas: *Tectonophysics*, v. 52, p. 373–375.
- Verberne, A.M., 1992, Panel says salt water threatens water wells: *The Baton Rouge Advocate*, p. 1.
- Walcott, R.I., 1972, Past sea levels, eustasy and deformation of the Earth: *Quaternary Research* 2, p. 1–14.
- Waples, D.W., 1991, Generation and migration of petroleum from abnormally pressured fluid compartments, a discussion: *The American Association of Petroleum Geologists*, vol. 75, p. 326–327.
- Waterstone Engineering, Inc., and Parsons, Inc., 2003, Groundwater availability of the Central Gulf Coast Aquifer: Numerical simulations to 2050, Central Gulf Coast, Texas: Contract draft report submitted to the Texas Water Development Board, variously paginated.
- Weert, F.V, Gun, J.C.D., and Reckman, J., 2009, Global overview of saline groundwater occurrence and genesis: *International Groundwater Resources Assessment Center Report number GP 2009-1*, 107 p.
- Wesselman, J.B., 1971, Ground-water resources of Chambers and Jefferson counties, Texas: *Texas Water Development Board Report 133*, 173 p.

- Wesselman, J.B., 1972, Ground-water resources of Fort Bend County, Texas: Texas Water Development Board Report 155, 176 p.
- Wesselman, J.B., 1985, Structures, temperatures, pressures and salinities of Cenozoic aquifers of south Texas – map: U.S. Geological Survey Hydrologic Investigations Atlas, H: 654.
- Whittemore, D.O., 1988, Bromide as a tracer in ground-water studies: Geochemistry and analytical determination: Proceedings of Ground Water Geochemistry Conference, Denver, Colorado, National Water Well Association, Dublin, Ohio, p. 339-360.
- Williams, W.D., 1999, Salinization: A major threat to water resources in the arid and semi-arid regions of the world, Lakes and Reservoirs: Research and Management, vol. 4, p. 85-91.
- Williamson A.K., and Grubb, H.F., 2001, Groundwater Flow in the Gulf Coast Aquifer Systems, South-Central United States, Regional Aquifer System Analyses – Gulf Coast Plains: U.S. Geological Survey Professional Paper 1416-F.
- Winker, C.D., 1982, Cenozoic shelf margins, northwestern Gulf of Mexico: Gulf Coast Association of Geological Societies Transactions, vol. 32, p. 427–448.
- Winker, C.D., and Edwards, M.B., 1983, Unstable progradational clastic shelf margins, *in* Stanley, D.J., and Moore, G.T., eds, The shelfbreak; Critical interface on continental margins: SEPM Special Publication 33, p. 139-157.
- Wood, L.A., and Gabrysch, R.K., 1965, Analog model study of groundwater hydrology in the Houston district, Texas, with a section on Design, construction, and use of electric analog models, by E.P. Patten, Jr.: Texas Water Commission Bulletin 6508, 103 p.
- Wood, L.A., Gabrysch, R.K., and Marvin, R., 1963, Reconnaissance investigation of the ground-water resources of the Gulf Coast region, Texas: Texas Water Commission Bulletin 6305, 114 p.
- Young, S.C., and Kelley, V., eds., 2006, A site conceptual model to support the development of a detailed groundwater model for Colorado, Wharton, and Matagorda counties: Prepared by the URS Corporation, Lower Colorado River Authority LSWP Report, Austin, TX.

- Young, S.C., Knox, P., Budge, T., Deeds, N., and Knox, P., 2009, Development of the LCRB Groundwater Flow Model for the Chicot and Evangeline Aquifers in Colorado, Wharton, and Matagorda counties: LSWP Report Prepared by the URS Corporation, prepared for the Lower Colorado River Authority, Austin, TX.
- Young, S.C., Budge, T., Knox, P., Kalboss, R., Baker, E., Hamlin, S., Galloway, B., and Deeds, N., 2010, Hydrostratigraphy of the Gulf Coast Aquifer from the Brazos to the Rio Grande: Unnumbered Report, prepared by URS for the Texas Water Development Board.
- Young, S.C., Ewing, T., Hamlin, S., Baker, E., and Lupton, D., 2012a, Updating the Hydrogeological Framework for the Northern Portion of the Gulf Coast Aquifer: Unnumbered Report, prepared by INTERA for the Texas Water Development Board.
- Young, S.C., Yan, T., and Lupton, D., 2012b, Large-Scale Pumping and Hydraulic Fracturing on the Gulf Coast Aquifer System in DeWitt County: prepared by INTERA for the Pecan Valley Groundwater Conservation District.
- Yvon-Lewis, S.A., Butler, J.H., 2002, Effect of oceanic uptake on atmospheric lifetimes of selected trace gases: *Journal of Geophysical Research*, vol. 107, p. 4414, doi:10.1029/2001JD001267.
- Zimmerman, R.K., 1994, Evidence of wrench faulting in northcentral Louisiana: Louisiana State University, Baton Rouge. *Basin Research Institute Bulletin*, vol. 4, p. 53–61.